Design, synthesis and biological evaluation of novel anti-inflammatory agents

Alexandru Sava

ÉCOLE DOCTORALE
SANTÉ, SCIENCES BIOLOGIQUES ET CHIMIE DU VIVANT
INSTITUT DE CHIMIE ORGANIQUE ET ANALYTIQUE

THÈSE EN COTUTELLE INTERNATIONALE présentée par :

Alexandru SAVA

Soutenue le : **22 octobre 2021**

pour obtenir le grade de :
Docteur de l'Université d'Orléans et de l'Université de Médicine et Pharmacie « Grigore T. POPA » Iasi

Discipline/ Spécialité : Chimie

Design, synthesis and biological evaluation of novel anti-inflammatory agents

THÈSE dirigée par :

Monsieur ROUTIER Sylvain	Professeur, Université d'Orléans
Madame PROFIRE Lenuta	Professeur, Université de Médicine et Pharmacie «Grigore T. Popa », Iasi

RAPPORTEURS :

Monsieur ONIGA Ovidiu	Professeur, Université de Médicine et Pharmacie « IuliuHatieganu », Cluj-Napoca
Monsieur DEMANGE Luc	Professeur, Université Paris Descartes

PRESIDENT DE JURY :

Monsieur DEMANGE Luc	Professeur, Université Paris Descartes

JURY :

Monsieur BURON Frédéric	Maitre de Conférences HDR, Université d'Orléans
Madame LIMBAN Carmen	Professeur, Université de Médicine et Pharmacie «Carol Davila», Bucharest
Monsieur ONIGA Ovidiu	Professeur, Université de Médicine et Pharmacie « Iuliu Hatieganu», Cluj-Napoca
Monsieur DEMANGE Luc	Professeur, Université Paris Descartes
Monsieur ROUTIER Sylvain	Professeur, Université d'Orléans
Madame PROFIRE Lenuta	Professeur, Université de Médicine et Pharmacie «Grigore T. Popa » Iasi

GRIGORE T. POPA UNIVERSITY OF MEDICINE AND PHARMACY IASI
FACULTY OF PHARMACY

UNIVERSITE D'ORLÉANS

PhD THESIS

Design, synthesis and biological evaluation of novel anti-inflammatory agents

PhD Supervisors,
Prof. Dr. Lenuta PROFIRE, PhD
Prof. Dr. Sylvain ROUTIER, PhD

PhD Student,
Alexandru SAVA

2021

Contents

List of abbreviations

5-LOX	5-lipooxygenase
AA	arachidonic acid
ADME-Tox	absorption, distribution, metabolism, excretion and toxicity
AEMPS	the spanish medicines agency
AsA	ascorbic acid
ASP	aspirin
BSA	bovine serum albumin
BTA	benzotriazole
CaM	calmodulin
CCB	clelecoxib
CEAC	vitamin C equivalent antioxidant capacity
cGMP	cyclic monophosphate guanozin
COSY	correlated spectroscopy
COX-1/2	cyclooxygenase-1/2
COXIBs	COX-2 selective drugs
cPLA2	cytosolic phospholipase A2
CV	coefficient of variation
DCF	diclofenac
DPF	docking parameter file
DPPH	2,2-diphenyl-1-picrylhydrazyl radical
EDCI	1-ethyl-3-(3-dimethylaminopropyl)carbodiimide
EGF	epidermal growth factor domain
eNOS	endothelial NO synthase
Eq.	equivalent
ESI	electrospray ion source
EtOAc	ethyl acetate
FLAP	membranary proteins with low molecular mass
FSH	follicle-stimulating hormone
GI	gastrointestinal
GPF	grid parameter file
GSH	L-glutathione
GTP	triphosphate guanosine
Hb	hemoglobin
$HbFe^{2+}$-O_2	oxygenated hemoglobin
HMBC	heteronuclear multiple bond coherence
HOBT	hydroxybenzotriazole
HpETE	hydroperoxy-6-trans-8,11,14-*cis*-eicosatetraenoic acids
HRMS	high resolution mass spectrometry
HSQC	heteronuclear multiple quantum coherence
IND	indomethacin

iNOS	inducible NO synthase
Ki	inhibition effect rate
LCF	ligand coordinate file
LGA	Lamarckian genetic algorithm
LTA_4	leukotriene A_4
LTC_4	leukotriene C_4
LTD_4	leukotriene D_4
LTE_4	leukotriene E_4
LTs	leukotrienes
m.p.	melting point
Mb	myoglobin
MBD	membrane binding domain
$MbFe^{2+}$-O_2	oxygenated myoglobin
MMPs	matrix metalloproteinases
MS	mass spectrometry
NED	N-(1-naphthyl)ethylenediamine
NMR	nuclear magnetic resonance
NO	nitric oxide
NO-IND	nitric oxide-releasing indomethacin
NO-IND-OXDs	nitric oxide-releasing indomethacin derivatives with 1,3,4-oxadiazole scaffold
NO-IND-TXDs	nitric oxide-releasing indomethacin derivatives with 1,3-thiazolidine-4-one scaffold
NONOates	diazeniumdiolates
NO-NSAIDs	nitric oxide release nonsteroidal anti-inflammatory drugs
NOS	nitric oxide synthase
NSAID	nonsteroidal anti-inflammatory drugs
NTG	nitroglycerine
OXD	1,3,4-oxadiazol
PAF	platelet-activating factor
PBS	phosphate buffer solution
PD	Parkinson's disease
PGG2	prostaglandin G2
PGH2	prostaglandin H2
PGHS	prostaglandin endoperoxide H synthase
PGI_2	prostacycline
PGs	prostaglandins
Ph−OH	polyphenols
PLA2	phospholipase A2
PLC	phospholipase C
POX	peroxidase active site
RCF	receptor coordinate file
RMSD	root mean square deviation
ROS	reactive oxygen species

RSD	relative standard deviation
RSNOs	*S*-nitrosothiols
RT	room temperature
sGC	guanylate cyclase
SIRT	sirtuin
SNAP	*S*-nitroso-*N*-acetyl-penicillamine
SNP	sodium nitropruside
SULF	sulfanilamide
TB	tuberculosis
THF	tetrahydrofuran
TLC	thin layer chromatography
TxA_2	thromboxane A_2
TZD	1,3-thiazolidin-4-one
US FDA	United States Food and Drug Administration
ΔG	Gibbs free energies

Acknowledgements

I take this opportunity to express my gratitude to the people who were essential in the successful achievement of this thesis.

Foremost, I am extremely grateful to my PhD supervisors Professor Lenuta PROFIRE and Professor Sylvain ROUTIER for their support, advices, valuable comments and suggestions all over this period. Their generous guidance and encouragement were the reason why I was able to be deeply involved in the subject and to overcome the problems encountered during the thesis. They were always acting professionally, but at the same time offering a family atmosphere that made the work in the laboratory even more interesting. Words can never be enough to thank your kindness and also for the exceptional human qualities with which they have surrounded me and which I will always keep as benchmarks of conduct in life.

I am hugely indebted to Frederic BURON, Associated Professor, HDR, at Institute of Organic and Analytical Chemistry (ICOA) from University of Orléans and from French National Center for Scientific Research (CNRS), for trust, understanding and not least for scientific support.. He was an essential part of my success in this thesis being also a big source of motivation and ideas.

Furthermore, I would like to express my deepest appreciation to the honorable members of thesis committee for the honor they have done to me, accepting to be in my committee of the thesis and for the deep reviewing and correction.

Also, I would like to express my deepest appreciation to Prof. Anca MIRON, Associated Professor Dan LUPASCU and Lecturer Ioana Vasincu for accepting to be in the thesis follow-up committee where they guided and encouraged me all over my thesis.

In addition, I would also like to extend my gratitude to Rodica CUCIUREANU, Professor at Faculty of Pharmacy, Department of Environmental and Food Chemistry for the advices and support provided in the carried out research.

I express my gratitude to the management research team of the international grants PN III Program, Subprogram 3.1. Bilateral/Multilateral, AUFRo Module - "Synthesis of bioactive molecules with anti-inflammatory action, BioChemInflam", project no. 28 AUF/01.03.2019, 2019-2020 (Partners: University of Orleans, ICOA, France; University of Medicine and Pharmacy "N. Testemiteanu", Chisinau, Moldavia) and Bilateral research Project Romania-France, within Europen and International Cooperation Program - "Inovative strategy for Alzheimer disease: targeting neuroinflammation and DYRK/CLK kinases", project no. 93BM, 2017-2018, for scientific determination and financial support. This work was also partially supported by the Grigore T. Popa University of Medicine and Pharmacy, Iasi, Young Researcher project, grant no. 6985/2020.

Special thanks to Dr. Sandra CONSTANTIN and Dr. Cosmin OSTACHE for their unwavering support, encouragement and continuous caring given to me.

Thanks should also go to my friends in the laboratory of ICOA for their practical suggestions, constructive advices and for all the wonderful moments that we spent together outside the lab.

I would like to extend my sincere thanks to Professor Gladiola TANTARU, Professor Nela BIBIRE, Professor Mihai APOSTU, Lecturer Alina PANAINTE and Lecturer Madalina VIERIU from Department of Analitical Chemistry for their confidence, support and understanding given to me in all this period.

Particular thanks go to the collective from Department of Pharmaceutical Chemistry for its unwavering guidance, valuable advices and unconditional help.

Last but not the least, I would like to thank my family for supporting me spiritually throughout writing this thesis and in my life in general.

Finally, I would like to thank a great woman that influenced me all the time and that was near me in every step I made. I would not have continued without her support. Thank you for every small thing that you made to me, for every encouragement. Simply, thank you my wife, ELISABETA.

Abstract (Résumé)

ÉTAT DE L'ART

Chapitre 1 *L'inflammation*

L'inflammation est une réaction de défense (non spécifique et locale) des organismes vivants avancés à toute blessure causée par un traumatisme, des toxines microbiennes ou des produits chimiques nocifs [6,7]. Cette réponse vise à inactiver ou à détruire les organismes envahisseurs, à éliminer les irritants et à préparer le terrain pour la réparation des tissus [8,9]. Étant donné que les composants essentiels du processus inflammatoire se trouvent dans la circulation sanguine, cette réaction ne se produit que dans les tissus vasculaires. Elle n'est pas spécifique car elle se manifeste de manière identique, indépendamment de l'étiologie du processus inflammatoire et de la nature aiguë ou chronique de l'inflammation [10]. Il s'agit d'un processus complexe qui consiste en des réactions immunologiques et non immunologiques [11].

Les inducteurs de l'inflammation déclenchent la production de plusieurs médiateurs inflammatoires, qui à leur tour endommagent la fonctionnalité de nombreux tissus et organes d'une manière qui leur permet de s'adapter aux conditions indiquées par les inducteurs particuliers de l'inflammation. Ceux-ci constituent le réseau chimique de la réponse inflammatoire et entraînent des aspects cliniques et pathologiques de l'inflammation.

Essentiellement, l'inflammation reste une réponse physiologique cruciale pour le corps humain à tout type d'agression et une réponse adaptative pour restaurer l'homéostasie [12].

Lorsque l'inflammation persiste pendant une longue période, maintenant le corps dans un état d'alerte constant, elle peut devenir chronique, avec un impact négatif sur les tissus et les organes [13]. Les conséquences cliniques des dommages inflammatoires chroniques peuvent être graves et inclure un risque accru de nombreuses maladies chroniques telles que: la polyarthrite rhumatoïde [14], les maladies inflammatoires de l'intestin [15], les troubles métaboliques (diabète sucré et obésité) [16-18], les troubles cardiovasculaires (cardiopathie ischémique, athérosclérose) [19,20], les maladies neurodégénératives (maladie de Parkinson et d'Alzheimer) [21-23] et le cancer [24]; bon nombre de ces affections mettent la vie en danger [25,26].

L'inflammation chronique est étroitement liée à la pathogenèse des maladies inflammatoires qu'il devient difficile d'identifier à la fois la cause et l'effet de ces troubles. Par exemple, l'inflammation est causée par l'obésité, tandis que l'inflammation chronique peut conduire au diabète associé à l'obésité en partie à cause de la résistance à l'insuline.

Les maladies inflammatoires sont parmi les causes les plus fréquentes de maladie chronique dans le monde. Le coût croissant des soins de santé peut être principalement dû à la gravité et à la complexité des troubles inflammatoires [12].

Les médiateurs inflammatoires comprennent une variété de molécules synthétisées (principalement par les cellules de défense immunitaire) qui agissent sur les vaisseaux sanguins et / ou les cellules pour favoriser une réponse inflammatoire [27].

Les médiateurs chimiques libérés qui varient en fonction de leurs propriétés biochimiques comprennent: (i) les amines vasoactives (histamine et sérotonine); ii) peptides vasoactifs (substance P); iii) fragments de composants du complément (anaphylatoxines); iv) médiateurs lipidiques (eicosanoïdes et facteurs d'activation plaquettaire); v) cytokines; vi) les chimiokines; vii) enzymes protéolytiques; (viii) espèces réactives de l'oxygène et (ix) oxyde nitrique [7,25,28–30].

L'inhibition de la cascade d'acide arachidonique est l'une des stratégies les plus utilisées pour le traitement des maladies inflammatoires (Fig. 1.1). L'acide arachidonique (AA, acide 5,8,11,14-eicostétraénoïque, ω-6) est l'acide gras polyinsaturé le plus abondant dans la couche phospholipidique de la membrane cellulaire qui est libéré directement par une acyl hydrolase (phospholipase A2, PLA2) ou indirectement par la phospholipase C (PLC) [5,6]. L'AA est métabolisé pour former des eicosanoïdes soit par la voie cyclooxygénase (COX-1 et COX-2), lorsque des prostanoïdes cycliques (c'est-à-dire les prostaglandines (PG), la prostacycline (PGI2) et les thromboxanes (TxA2)) sont générés, soit par la voie lipoxygénase, qui génèrent des leucotriènes à chaîne linéaire (LTC4, LTD4, LTE4) et des lipoxines [6,31]. Les enzymes de cette cascade sont bloquées directement par les AINS et les coxibes et indirectement par les glucocorticoïdes.

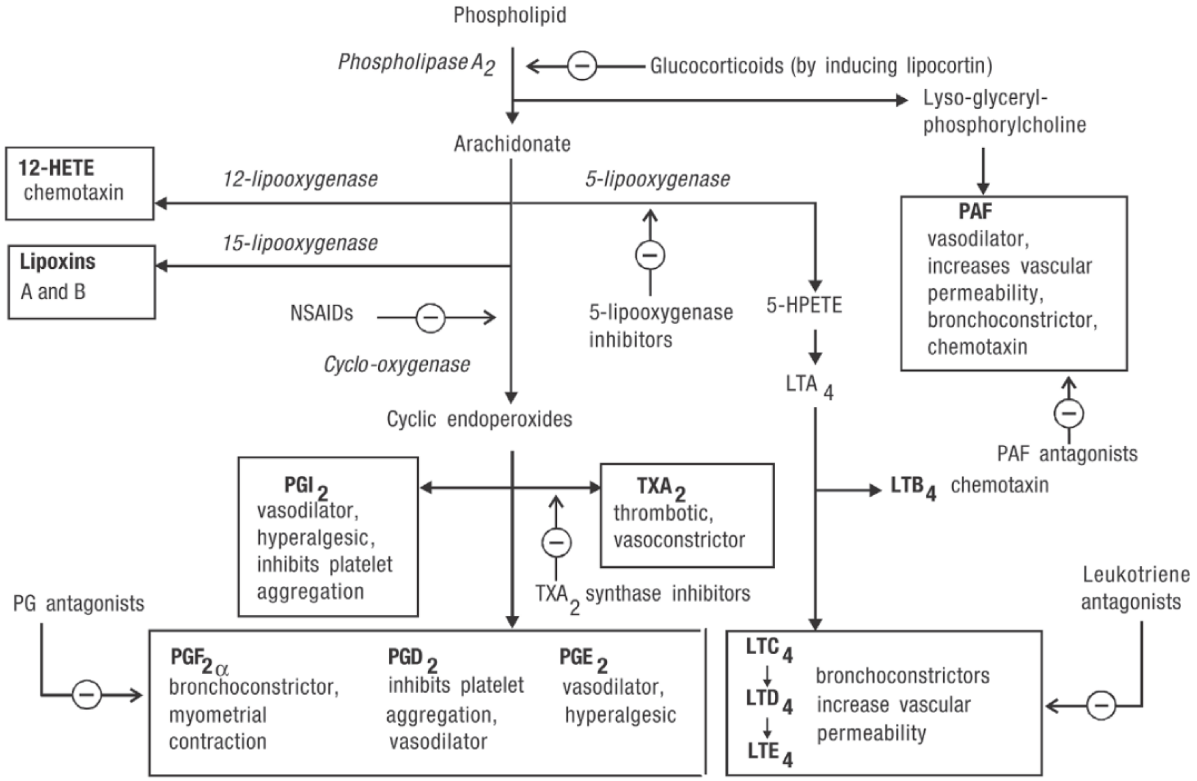

Fig. 1.1. La voie de l'acide arachidonique (adaptée après [6]).

En bref, l'inflammation est connue comme une réponse physiologique importante pour le corps humain à tout type d'agression et est également impliquée dans la pathogenèse de nombreuses maladies chroniques telles que les troubles métaboliques, neurodégénératifs, cardiovasculaires et le cancer. Afin d'identifier des cibles spécifiques pour une intervention thérapeutique, ont été signalés une variété de mécanismes inflammatoires sous-jacents.

Par exemple, le facteur de nécrose tumorale α (TNFα) est une cytokine pro-inflammatoire impliquée dans la pathogenèse de maladies inflammatoires systémiques telles que la polyarthrite rhumatoïde, la spondylarthrite ankylosante, le psoriasis ainsi que les

affections inflammatoires de l'intestin par activation intracellulaire du facteur nucléaire kappa-B (NF-kB), des caspazes et de la protéine kinase activée par le mitogène (MAPK)[89].

Dans les années 1990, le traitement de la polyarthrite rhumatoïde a été révolutionné par le développement de la thérapie à base de protéines. Le succès de protéines injectables telles que l'étanercept (Enbrel®), l'infliximab (Remicade®) et l'adalimumab (Humira®) a donné une nouvelle dimension au traitement anti-inflammatoire. Un traitement à long terme avec ces protéines pourrait avoir des effets secondaires tels que la tuberculose latente, des effets cardiovasculaires nocifs ou un risque accru de développer un cancer. Dans le même temps, le traitement anti-TNF implique des coûts élevés et une faible observance de la part du patient [4].

Par conséquent, une meilleure compréhension des mécanismes moléculaires des voies inflammatoires contribuera sans aucun doute à améliorer la prévention et le traitement des maladies inflammatoires.

Chapitre 2 *L'indométacine et ses dérivés*

L'indométacine (acide 1-(4-chlorobenzoyl)-5-méthoxy-2-méthyl-1H-indol-acétique) (6, IND) a été découverte par Rahway (1963) de Merk&Co (SUA) Company et a été approuvée pour son utilisation thérapeutique en 1965 (Fig. 2.1).

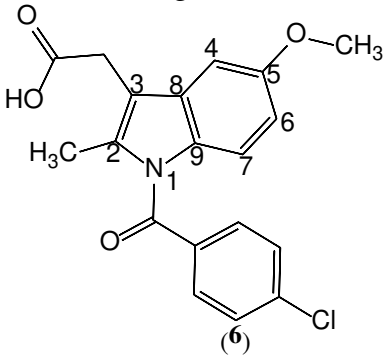

(**6**)

Fig. 2.1. La structure d'indomethacin.

L'IND est le dérivé de l'acide indole-acétique le plus connu et le plus testé [90], restant l'un des AINS les plus pertinents utilisés dans le monde pour le traitement de la polyarthrite rhumatoïde aiguë et chronique et d'autres maladies rhumatismales inflammatoires, des épisodes de goutte aiguë et des douleurs musculo-squelettiques aiguës [91,92]. En raison de sa puissance, son efficacité clinique est comparable, ou parfois supérieure à tout autre AINS. Comme d'autres AINS, la plupart de ses effets toxiques et thérapeutiques sont dus à l'inhibition de la synthèse des prostaglandines et pour cette raison, les effets secondaires limitent inévitablement son utilisation.

Il a été documenté que l'utilisation clinique à long terme de l'IND est responsable d'un large éventail d'effets secondaires, y compris l'irritation gastro-intestinale (GI), les saignements et les ulcérations, les troubles digestifs (nausées, vomissements, douleurs abdominales, diarrhée ou constipation), l'anxiété accrue, les maux de tête, les étourdissements, l'œdème périphérique, l'hypertension artérielle, la tachycardie, le dysfonctionnement des reins et du foie, les réactions allergiques et anaphylactiques [91,93].

Une enquête documentaire a révélé que différentes stratégies sont rapportées pour améliorer le profil d'innocuité des AINS: (i) développement d'inhibiteurs sélectifs de la COX-2; ii) la co-administration d'un agent protecteur IG; (iii) ainsi que le développement d'AINS à libération d'oxyde nitrique (NO-AINS). Chaque stratégie présente un certain

nombre d'avantages et de limites. Par exemple, les médicaments sélectifs COX-2 peuvent résoudre les complications gastro-intestinales, mais peuvent induire de graves effets secondaires cardiovasculaires. Les NO-AINS suppriment l'inflammation aussi efficacement que les AINS parents, mais la production de NO est obtenue par un mécanisme dépendant du thiol, contribuant à la tolérance aux nitrates. En outre, l'observance du patient est réduite dans la stratégie de combinaison de médicaments.

Pour résoudre les problèmes d'innocuité et d'efficacité liés à l'IND, il a été rapporté différentes approches pour améliorer les propriétés physicochimiques, pour réduire les effets secondaires par des stratégies additives ou synergiques, pour améliorer le profil biopharmaceutique, pour optimiser la voie d'administration ou par une administration ciblée.

Sur la base des données susmentionnées, nous pouvons conclure que l'IND est un échafaudage polyvalent dont les changements structurels peuvent être développés composés avec un profil pharmaco-toxycologique amélioré.

De plus, l'anneau indole est un groupe de pharmacophores très important dans les études de découverte de médicaments générant des composés ayant de nombreuses applications et utilisations thérapeutiques. Pour des utilisations thérapeutiques, plusieurs médicaments commerciaux à base d'indole ayant été approuvés avec une application dans les anticancéreux, les antihypertenseurs, les antidépresseurs, les anti-VIH, les agonistes opioïdes ainsi que dans le traitement analgésique [117].

Chapitre 3 *Dérivés de thiazolidine-4-one à potentiel thérapeutique*

L'échafaudage 1,3-thiazolidine-4-one sert de noyau à de nombreux composés synthétiques d'un grand intérêt en chimie médicinale [118]. Cet échafaudage est un composant structurel de divers produits naturels, comme la thiamine (vitamine B1), l'acidomycine (isolée des souches de Strepomyces) [119 120] et de nombreux produits métaboliques (cyclopeptides cytotoxiques) de champignons et d'animaux marins primitifs [121]. Plusieurs médicaments à base de thiazolidine-4-one tels que la ralitoline (17) (anticonvulsivant), l'étozoline (18) (diurétique de l'anse), l'epalréstat (19) (un inhibiteur de l'aldose réductase pour le traitement de la neuropathie périphérique diabétique) et la pioglitazone (20) (médicament antidiabétique oral) ont déjà été approuvés pour un usage thérapeutique (Fig. 3.1). La littérature rapporte pour l'échafaudage de thiazolidine-4-one d'autres effets biologiques importants tels que les effets anti-inflammatoires, antioxydants, antagonistes du facteur d'activation plaquettaire (PAF), inhibition de la cyclooxygénase (COX), antagoniste du facteur de nécrose tumorale ainsi que des effets anticancéreux, anticonvulsivants, antimicrobiens, antiviraux et anti-VIH [122-129].

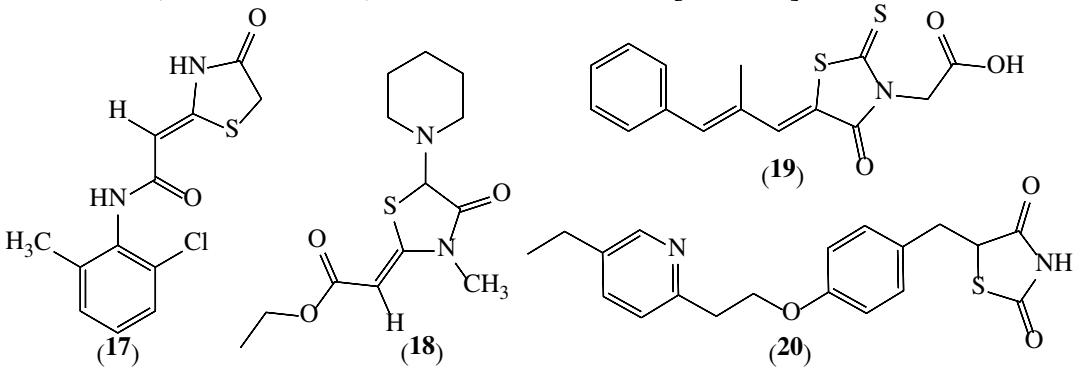

Fig. 3.1. Representative drugs containing the thiazolidin-4-one core.

Les nouveaux dérivés avec l'échafaudage thiazolidine-4-one présentent une pléthore d'activités prometteuses en raison de la chimie de l'hétérocycle et de l'interaction des substituants pharmacophoriques avec les différentes cibles biologiques.

Les thiazolidines restent un échafaudage polyvalent et la puissance des composés synthétisés dépend de la nature et de la position des substituants qui y sont attachés. Ainsi, par des études d'amarrage moléculaire ainsi que des études de relation d'activité structurelle, il a été rapporté de nouveaux composés avec un meilleur profil pharmacologique et avec une utilisation thérapeutique prometteuse.

Chapitre 4 *Dérivés d'oxadiazole ayant un potentiel thérapeutique*

L'utilisation de l'échafaudage d'oxadiazole comme noyau important pour de nombreux médicaments est basée sur plusieurs avantages [173-177]: (i) c'est une partie essentielle du pharmacophore en contribuant favorablement à la liaison au ligand; ii) il agit comme un agent de liaison aromatique plat pour fournir l'orientation appropriée de la molécule; iii) il induit une stabilité métabolique, une solubilité dans l'eau et une lipophilie plus faible; (iv) il peut facilement moduler chimiquement les composés contenant du carbonyle tels que les amides, les carbamates, les esters et les esters hydoxamiques.

Selon les données de la littérature, les composés contenant le noyau d'oxadiazole ont des effets biologiques importants tels que anti-inflammatoire [177-179], antioxydant [180,181], antidiabétique [182], anticonvulsivant [183], anticancéreux [184], antituberculeux [185,186], antiviral [187], antidépresseur [188]. Pour un usage thérapeutique, plusieurs médicaments commerciaux à base d'oxadiazole ont déjà été approuvés tels que: furamizole (forte activité antibactérienne, un antibiotique) (47), butalamine (un vasodilatateur) (48), oxolamine (un antitussif) (55), pleconaril (un antiviral) (50), fasiplon (un médicament anxiolitique non benzodiazépine) (52), raltégravir (un médicament antirétroviral pour le traitement de l'infection par le VIH) (51), nésapidil (comme anti-arrhytmique) (54), zibotentan (comme anticancéreux) (53) ainsi que tiodazosine (comme antihypertenseur) (49) (Fig.4.1.). Dans la nature, l'échafaudage d'oxadiazole a été signalé dans l'acide quisqualique (de Quiqualis fructus, agoniste puissant du récepteur du glutamate de sous-type (AMPA)) et les phidianidines A et B (d'organismes marins primitifs, cytotoxicité élevée contre les lignées cellulaires de mammifères tumoraux) [189,190].

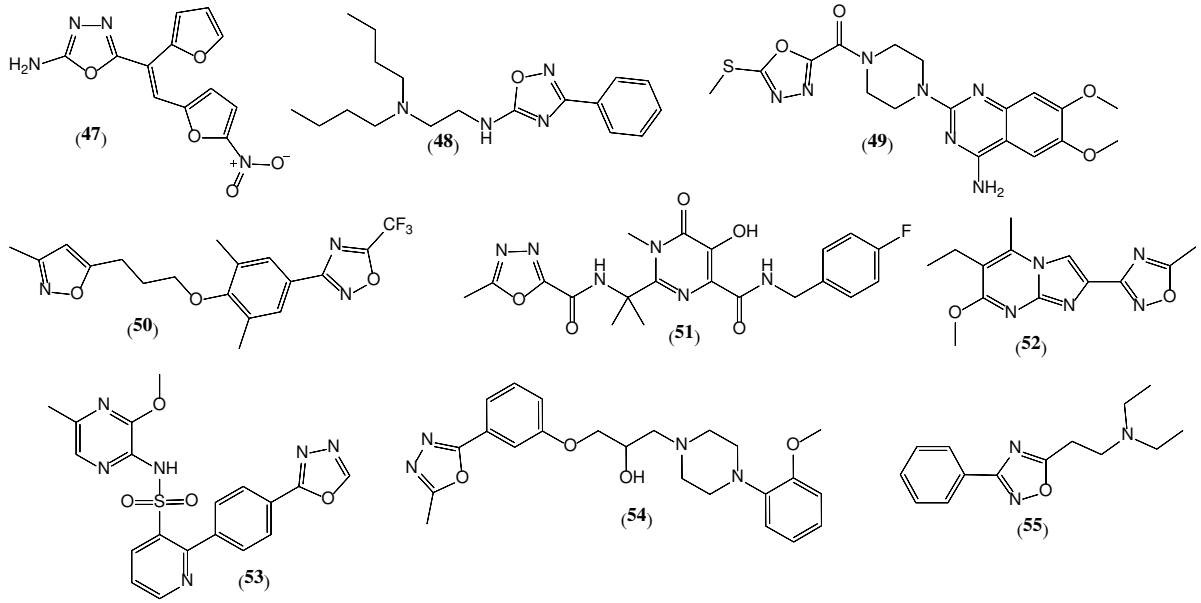

Fig. 4.1. Médicaments représentatifs contenant le noyau d'oxadiazole.

Sur la base des résultats présentés dans la littérature, nous pouvons conclure que les 2,5-disubstitués-1,3,4-oxadiazoles sont les composés les plus puissants avec un large profil d'activité biologique et des propriétés pharmacocinétiques améliorées.

En se référant à la relation structure-activité, en termes de sélectivité des dérivés du 1,3,4-oxadiazole pour les isoenzymes de la COX, on peut apprécier ce qui suit [173]:

- la présence d'un groupe de retrait d'électrons sur le cycle phényle peut améliorer la sélectivité de la COX-2, par rapport aux groupes donneurs d'électrons, qui ont un effet inverse. De plus, la présence de p-Cl, de p-NO2 ou de p-tert-butyle augmente également l'inhibition de la COX-2;
- la sélectivité de la COX-2 est diminuée par le remplacement du cycle phényle par le noyau pyridine ;
- -la sélectivité de la COX-2 est augmentée par conversion du groupe méthylthio (SCH3) en groupe méthylsulfonyle (SO2CH3) ;
- -N-acétylation de l'atome d'azote du noyau d'oxadiazole n'affectent pas significativement la sélectivité de la COX.

Chapitre 5 *Oxyde nitrique et médicaments libérant de l'oxyde nitrique*

Les oxydes nitriques (NOx) sont utilisés depuis l'Antiquité. Les archives historiques indiquent que les Phéniciens, les Romains et les Grecs anciens conservaient la viande en utilisant du nitrate de calcium en raison de ses propriétés antibactériennes [231-233]. De nos jours, la législation sanitaire n'autorise l'utilisation des nitrates et des nitrites, en tant qu'additifs alimentaires, pour la conservation des préparations de viande, qu'en maintenant des limites bien définies [234]. Le nitrate de potassium (E252, salpêtre indien), le nitrate de sodium (E251) et le nitrite de potassium (E249) sont les additifs alimentaires les plus largement utilisés car ils maintiennent la couleur spécifique des préparations de viande, retardent leur brunissement, réduisent la croissance des bactéries et détruisent les spores botuliques. L'utilisation de nitrites dans la viande peut avoir des effets toxiques directs (tels que la formation de méthémoglobine) et indirects (formation de nitrosamines à action cancérogène et mutagénique).

Les premières indications médicales ont été enregistrées dans le Soutra du Diamant (868 après JC), qui est considéré comme le plus ancien texte imprimé décrivant les pratiques médicales chinoises. Il a été noté que pour le traitement de l'angine de poitrine, il est recommandé de placer sous la langue quelques cristaux de salpêtre indien [231,235].

La découverte du rôle du NO dans les processus physiologiques et pathologiques dans le corps humain a suscité un grand intérêt de la part des chercheurs, révolutionnant de nombreux aspects de la physiologie cellulaire. Par conséquent, malgré sa simplicité structurelle, le NO a une chimie complexe, fournissant au radical libre une action biologique étendue et variée dans la régulation d'un large éventail de processus physiopathologiques / physiologiques.

L'usage thérapeutique est limité par sa courte durée de vie, son instabilité pendant le stockage et son potentiel toxique. Au vu de tout cela, il a été rapporté la synthèse des donneurs de NO afin de stabiliser ce radical, jusqu'à ce qu'il soit nécessaire de le libérer.

Certainement, le potentiel de la thérapie au nitrate deviendra une nouvelle approche thérapeutique réussie une fois que vous aurez pleinement compris la libération cinétique et la toxicité à long terme du NO de chaque médicament et la capacité de cibler avec précision la libération de NO dans un organe ou un tissu spécifique.

CONTRIBUTIONS PERSSONELLES

Chapitre 6 *La motivation, les hypothèses de travail et les objectifs de la recherche personnelle*

Les stratégies pharmacologiques pour supprimer l'inflammation sont axées sur les agonistes du récepteur des glucocorticoïdes (glucocorticoïdes), l'inhibition de la cascade d'acide arachidonique (AINS) et sur le blocage de la signalisation des cytokines pro-inflammatoires (médicaments ciblant le facteur de nécrose tumorale – TNFα et la signalisation de l'interleukine IL-1) [277].

Les AINS sont des médicaments ayant des propriétés thérapeutiques analgésiques, anti-inflammatoires et antipyrétiques courantes. Ils inhibent la COX dans une grande variété de systèmes, allant de la synthèse enzymatique microsomale à différentes cellules et tissus. Par conséquent, l'inhibition de la COX est devenue le principal mécanisme d'action des ADNA, qui est responsable des effets thérapeutiques et secondaires de ces médicaments [278]. Il existe plusieurs structures chimiques différentes pour les AINS et leurs caractéristiques importantes sont le profil pharmacocinétique, la puissance et l'équilibre de leur affinité pour les isoenzymes COX (COX-1 et COX-2, en particulier). Cet équilibre affectera les effets finaux des médicaments et leur profil d'innocuité [277,279]. Les AINS non sélectifs classiques, qui inhibent non spécifiquement la COX-1 et la COX-2 (par exemple l'indométacine), contrecarrent l'inflammation, la fièvre et la douleur. Il est important de noter que sous une utilisation à long terme, au cours de la maladie chronique, ces médicaments induisent des effets secondaires graves, principalement des lésions gastro-intestinales et une irritation rénale. D'autre part, les médicaments sélectifs de la COX-2 (COXIB), bien que capables de résoudre les effets secondaires gastro-intestinaux, ont malheureusement été associés à une augmentation significative du risque cardiovasculaire, en particulier en cas d'utilisation à long terme, apparemment en raison d'un déséquilibre de PGI2 antithrombotique et vasodilatateur et de thromboxane pro-thrombotique (TxA2).

En bref, malgré les avantages cliniques des AINS par l'inhibition non sélective de la COX ou par l'inhibition relative de la COX-1 et de la COX-2, leur utilisation à long terme augmente l'incidence des effets secondaires (réactions cutanées gastro-intestinales, rénales, allergiques, risque accru de syndromes coronariens aigus, saignements) [278,279].

Les médicaments classiques ont été conçus dans le but de cibler une seule entité biologique (une cible) avec une sélectivité élevée, afin d'éviter tout effet indésirable en manquant de cibler d'autres cibles biologiques (hors cible). Une telle approche « une cible, une maladie » a conduit au développement de plusieurs médicaments précieux (par exemple, des inhibiteurs de la COX, utilisés pour le traitement de l'inflammation, de la fièvre et de la douleur).

On sait qu'une seule perturbation dans la physiologie de la cellule (voie de signalisation ou métabolisme) entraîne souvent une cascade d'effets complexes. Cependant, une seule modification au cours de la chaîne d'événements ne suffit pas à rétablir l'équilibre initial dans la cellule.

Pour améliorer l'efficacité clinique des AINS, deux stratégies de plateforme émergent actuellement. Le premier est la combinaison de médicaments, afin de réduire les effets secondaires des AINS et la deuxième stratégie suppose qu'un seul composé peut atteindre plusieurs cibles (un seul médicament-plusieurs cibles).

Les AINS-NO sont une nouvelle classe d'anti-inflammatoires développés dans le but de réduire les ulcérations gastriques par la libération de NO. Par la suite, la même stratégie de liaison a été appliquée aux inhibiteurs sélectifs de la COX-2 (COXIB) pour contrer les événements cardiaques indésirables. Le naproxcinod (nitronaproxène) a été le seul AINS-NO

jusqu'à présent, largement étudié dans le cadre d'essais cliniques, mais n'a pas réussi à obtenir l'approbation de la FDA américaine en raison du manque d'études contrôlées à long terme [285].

Les inhibiteurs doubles de la COX-2 et de la 5-LOX sont censés posséder une plus grande efficacité avec des effets secondaires réduits des inhibiteurs sélectifs de la COX-2. C'est la stratégie la plus adaptée pour offrir non seulement un profil anti-inflammatoire amélioré, mais aussi une sécurité accrue pour les AINS traditionnels. Par exemple, la licofelone (ML3000), dans les essais précliniques et cliniques, a montré un effet anti-inflammatoire comparable aux AINS conventionnels, mais la sécurité gastro-intestinale a été améliorée. À l'heure actuelle, il est testé en phase III pour le traitement de l'arthrose afin de confirmer la raison d'être de la conception et de l'application prévue [286].

La littérature nous donne de nombreuses preuves qui soutiennent qu'un médicament, qui agit sur plusieurs cibles thérapeutiques peut influencer subtilement l'activité de nombreuses enzymes. Ainsi, il est possible de développer de nouvelles stratégies thérapeutiques plus complexes et efficaces pour établir l'homéostasie cellulaire.

Par conséquent, la double inhibition des voies COX/LOX et l'augmentation du taux de NO sur le site inflammatoire peuvent constituer une nouvelle approche thérapeutique dans le cas des maladies inflammatoires.

L'objectif de la recherche doctorale était de prouver l'amélioration du profil pharmacologique et d'innocuité de certains nouveaux donneurs d'oxyde nitrique d'indométacine (donneurs d'indométacine-NO) qui ont été développés en tant que nouvelle stratégie thérapeutique multi-cibles, capable d'inhiber les voies de COX et de libérer du NO dans le milieu gastrique.

Chapitre 7 *Synthèse et caractérisation de nouveaux dérivés d'indométacine libérant de l'oxyde nitrique*

La stratégie de synthèse des dérivés proposés de l'indométacine libérant de l'oxyde nitrique (NO-IND) (9a-s; 11a-m, t-v) (Fig. 7.1) est conçue conformément à l'analyse des critères rétrosynthétiques, qui comprend le plus petit nombre possible d'interconversions et implique l'association de 3 échafaudages, comme suit:

- ✓ un échafaudage indol (indométacine) (IND, synthon A);
- ✓ un échafaudage de 1,3-thiazolidin-4-one (TZD, synthon B) ou de 1,3,4-oxadiazol-2-thiol (OXD, synthon C);
- ✓ ester de nitrate donneur d'oxyde nitrique (NO) relié à un agent de liaison aromatique, substitué

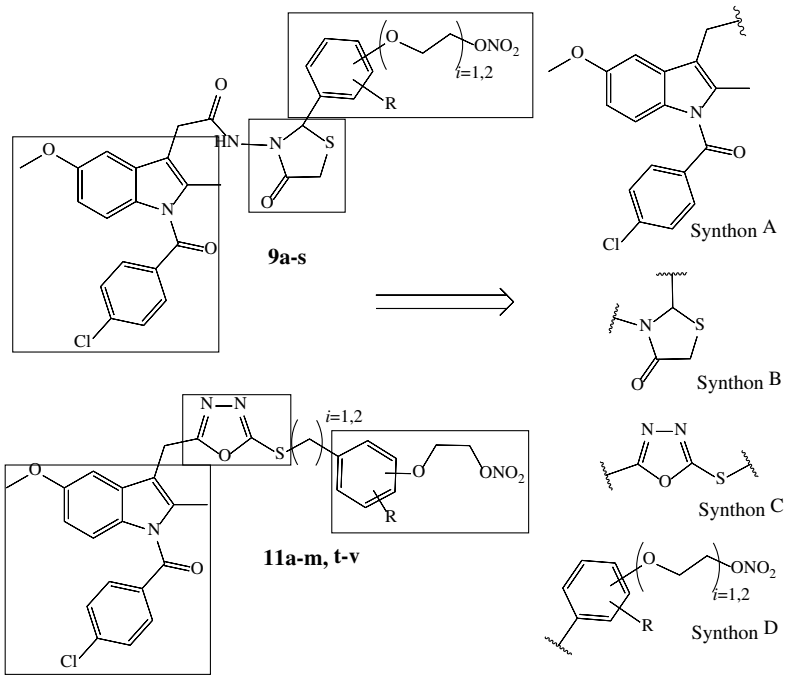

Fig. 7.1. La structure des dérivés NO-IND conçus.

Pour obtenir les composés conçus, une synthèse de type convergent, qui comporte plusieurs étapes, a été appliquée

- ✓ synthèse de liants donneurs de NO, par réaction de métathèse de divers halogénures phénoxy-alkylés primaires avec du nitrate d'argent;
- ✓ synthèse de l'hydrazide d'indométacine par une réaction de couplage peptidique;
- ✓ synthèse de dérivés d'indométacine hydrazone par réaction de l'hydrazide d'indométacine avec des dérivés benzaldéhydes d'ester de nitrate;
- ✓ synthèse des dérivés d'indométacine libérant de l'oxyde nitrique contenant un échafaudage 1,3-thiazolidine-4-one (NO-IND-TZDs) par réaction de dérivés d'hydrazone indométacine avec l'acide mercaptoacétique, en utilisant une réaction d'annelation;
- ✓ synthèse de dérivés d'indométacine libérant de l'oxyde nitrique contenant un échafaudage de 1,3,4-oxadiazole (NO-IND-OXDs) par alkylation de dérivés d'indométacine-oxadiazole (IND-OXD) avec des nitrates de (halidealkyl)phénoxy.

Le schéma général de synthèse des nouveaux dérivés d'indométacine libérant de l'oxyde nitrique est présenté à la figure 7.2.

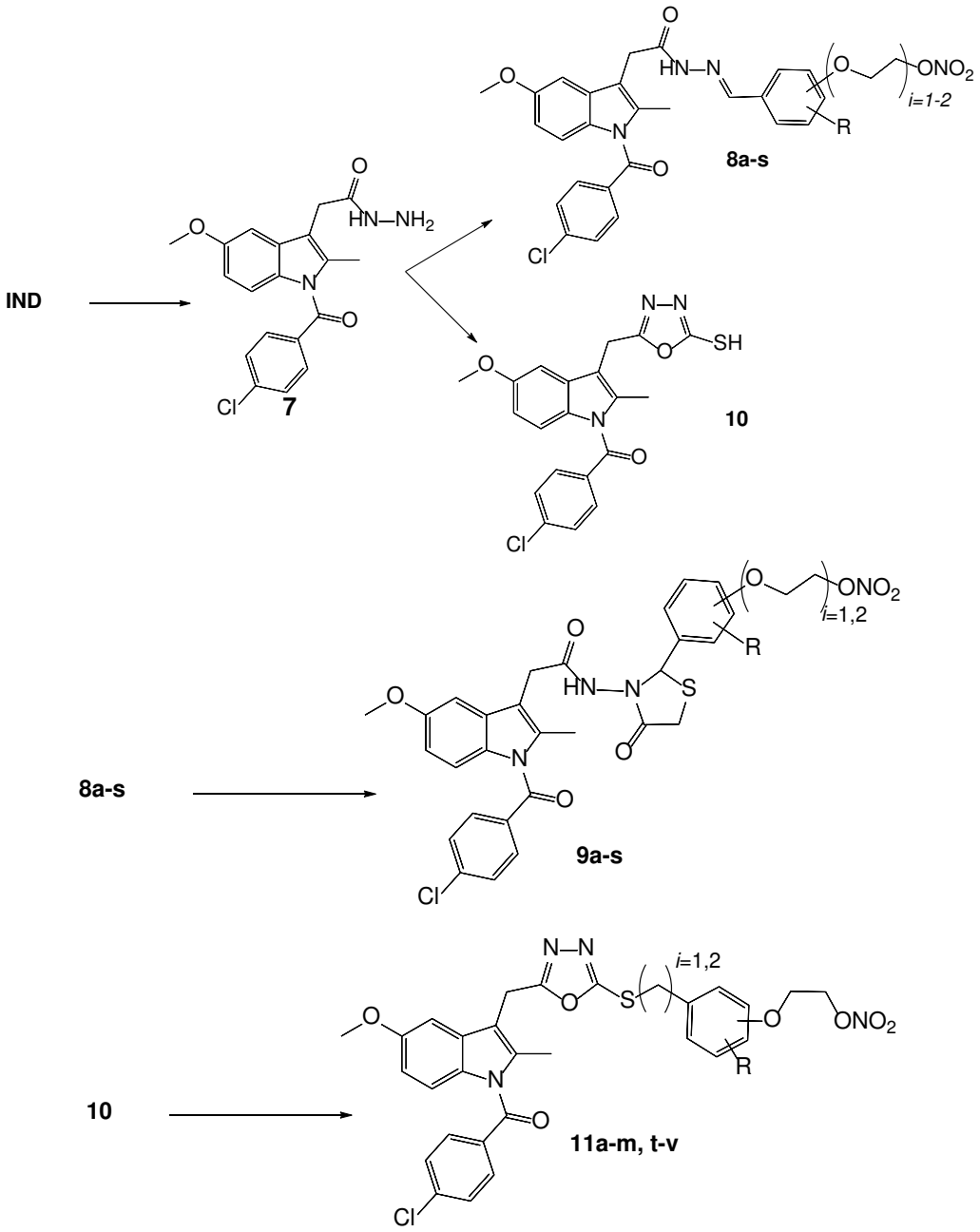

Fig. 7.2. Le schéma général de la synthèse des dérivés NO-IND.

Dans cette étude, un certain nombre de 144 composés ont été synthétisés, dont 109 composés intermédiaires et 35 composés finaux (NO-IND-TZD et NO-IND-OXD). La synthèse a été réalisée en plusieurs étapes : (i) synthèse de liants donneurs de NO, qui impliquait la synthèse de dérivés halogénures-alcoxy-benzaldéhyde (2a-s, t, u), de dérivés benzaldéhyde d'ester de nitrate (3a-s), d'alcool (bromoéthoxy)aromatique (4a-m, t-v), de dérivés de nitrate de (hydroxyalkyl)phénoxy (5a-m, t-v) et de dérivés de nitrate de (halidéalkyl)phénoxy (6a-m, t-v); ii) la synthèse des dérivés de l'indométacine libérant de l'oxyde nitrique contenant un échafaudage 1,3-thiazolidine-4-one (NO-IND-TZDs, 9a-s), qui a impliqué la synthèse de l'hydrazide d'indométacine (7) et des hydrazones d'indométacine varius (8a-s) et (iii) la synthèse des dérivés de l'indométacine libérant de l'oxyde nitrique contenant un échafaudage de 1,3,4-oxadiazole (NO-IND-OXDs, 11a-m, t-v), qui a impliqué la synthèse du dérivé indométacine-oxadiazole (IND-OXD, 10).

La structure chimique de tous les dérivés synthétisés (intermédiaires et finales) a été prouvée par RMN (RMN 1H, RMN 13C, (1H,13C)-HSQC) et analyse spectroscopique de masse (HRMS) qui confirment la synthèse conçue.

Chapitre 8 *Étude de doking pour les nouveaux dérivés d'indométacine libérant de l'oxyde nitrique*

L'amarrage informatique est largement utilisé pour étudier les interactions ligand-protéine et pour le développement et la découverte de médicaments [370,371]. Cette technique de calcul rapide commence par une cible de structure connue (une structure cristallographique d'une enzyme d'intérêt médicinal). L'amarrage est utilisé pour prédire l'affinité de liaison d'un ligand contre la macromolécule cible, en fonction de leurs interactions ioniques et hydrophobes dans des conditions physiologiques simulées [371,372]. Alors que les expériences d'amarrage unique sont utiles pour explorer la fonction de la cible [373], le criblage virtuel utilise des algorithmes et des modèles informatiques afin d'identifier et d'optimiser les composés de frappe et de plomb [372]. Le criblage virtuel est basé sur une vaste bibliothèque de composés qui sont ancrés et classés et peuvent être utilisés pour l'identification des nouvelles molécules bioactives pour le développement de médicaments [373,374]. Les techniques in silico utilisées pour la conception de médicaments sont devenues des méthodes économiques, fiables, rentables et rapides, tout en nécessitant moins de main-d'œuvre [370,371].

Sur la base des résultats obtenus, nous pouvons dire que les dérivés synthétisés de l'indométacine libérant de l'oxyde nitrique, avec un échafaudage de 1,3-thiazolidine-4-one (NO-IND-TZDs, 9a-s) et un échafaudage de 1,3,4-oxadiazole (NO-IND-OXDs, 11a-m, t-v) ont les prémisses théoriques pour être des agents anti-inflammatoires prometteurs. De plus, on sait que l'hybridation de différentes molécules pharmacophoriques entraînerait un effet synergique sur leur activité anti-inflammatoire, en particulier la capacité à inhiber la COX.

Sur la base des valeurs de l'indice de sélectivité des isoenzymes COX, on apprécie que les NO-IND-TZD (9a-s) soient sélectives en COX-1, sauf 9l, qui est sélective en COX-2, avec un indice de sélectivité amélioré, en référence à l'IND et au DCF.

En ce qui concerne les NO-IND-OXD (11a-m, t-v), il a été noté qu'ils sont sélectifs en COX-2 avec un indice sélectif amélioré en référence avec l'IND et le DCF, à l'exception des 11m, 11d et 11g qui sont sélectifs de la COX-1. En outre, il a été observé que les composés 11l, 11u et 11k sont plus sélectifs en COX-2 en référence avec CCB.

Nos résultats sont en accord avec la littérature qui a rapporté que le remplacement du groupe acide carboxylique libre des AINS conventionnels par différents hétérocycles comme le 1,3,4-oxadiazole 1,3-thiazolidine-4-one peut fournir de nouveaux médicaments avec une activité anti-inflammatoire accrue, une efficacité améliorée et avec moins d'effets secondaires, réduisant le potentiel ulérogène [140,194,385].

Chapitre 9 *Étude in silico ADME-Tox*

L'étude ADME-Tox (Absorption, Distribution, Metabolism, Excretion and Toxicity) offre des données importantes pour prédire les propriétés pharmacologiques et toxicologiques de nouveaux candidats, au cours du processus de découverte du médicament [386-388].

En bref, le profil ADME-Tox prédit pour les NO-IND-TZD (9a-s) et NO-IND-OXD (11a-m, t-v) comprenait des propriétés physico-chimiques et ADME optimales pour l'administration orale, une bonne absorption dans l'intestin grêle, une faible fraction non liée et une mauvaise distribution au cerveau. En ce qui concerne le métabolisme, les composés

testés n'inhibent pas le CYP2D6, qui est déterminant dans les processus de biotransformation et pourrait avoir un certain degré d'hépatotoxicité.

Enfin, le profil ADME-Tox des composés testés a montré que les composés conçus proposés sont généralement considérés comme ayant des propriétés physico-chimiques et ADME optimales pour l'administration orale.

Chapitre 10 *Évaluation biologique des nouveaux dérivés de l'indométacine libérant de l'oxyde nitrique*

Les dérivés synthétisés de l'indométacine libérant de l'oxyde nitrique, avec un échafaudage de 1,3-thiazolidine-4-one (NO-IND-TZDs, 9a-s) et d'un échafaudage de 1,3,4-oxadiazole (NO-IND-OXDs, 11a-m, t-v), ont été évalués biologiquement en termes d'effet antioxydant et anti-inflammatoire ainsi que de capacité de libération d'oxyde nitrique.

L'activité de piégeage des radicaux libres des nouveaux NO-IND-TZD (9a-s) et NO-IND-OXD (11a-m, t-v) a été évaluée à l'aide du test du radical 2,2-diphényl-1-picrylhydrazyl (DPPH) avec une légère modification [398–400]. L'IND et l'aspirine (ASP), en tant que médicaments de référence, et la vitamine C, en tant qu'antioxydant standard, ont été utilisés dans le test.

Sur la base des résultats de piégeage radicalaire DPPH, on peut apprécier que la présence d'échafaudages thiazolidine-4-one et 1,3,4-oxadiazole avait une influence favorable sur le potentiel antioxydant, tous les composés testés étant plus actifs que le composé parent IND.

Le test de Mizushima est le test le plus couramment cité dans la littérature pour prédire les pouvoirs anti-inflammatoires des médicaments. Il s'agit d'un essai néphélométrique basé sur la dénaturation thermique de l'albumine sérique bovine (BSA), qui assure une corrélation significative entre les effets anti-inflammatoires in vitro et in vivo [412].

Nos recherches ont révélé que le remplacement du groupe carboxyle de l'IND par la fraction thiazolidine-4-one ou 1,3,4-oxadiazole améliore les interactions médicament-protéine. Ces effets mesurables ont été signalés [426] comme une mesure pour la prédiction des propriétés anti-inflammatoires des différents composés. Ces résultats sont en accord avec les précédents résultats in silico qui ont montré que le composé synthétisé promet d'avoir des propriétés anti-inflammatoires significatives.

Pour évaluer la libération d'oxyde nitrique, les AINS-NO nouvellement synthétisés (9a-s, 11a-m, t-v) ont été soumis à une méthode colorimétrique Griess modifiée [427,428], basée sur la décomposition de la fraction ester de nitrate en présence de composés à base de Hg^{2+} et de thiol.

Les composés synthétisés peuvent être une entité chimique entièrement nouvelle qui assure une inhibition équilibrée des enzymes COX tout en étant plus sûr en termes d'effets secondaires gastro-intestinaux et de don d'oxyde nitrique sur les sites d'inflammation à la concentration sous-micromolaire physiologique de NO décrite dans la littérature.

Chapitre 11 *Conclusions generales*

Dans le contexte actuel de progrès scientifique dans le domaine de la découverte de nouveaux composés à potentiel thérapeutique, les recherches menées dans le cadre de la thèse de doctorat apportent des contributions originales au développement de nouvelles stratégies thérapeutiques pour les maladies inflammatoires. La recherche visait à développer de nouveaux donneurs d'oxyde nitrique d'indométacine en tant que stratégie multi-cible, capable d'améliorer le profil pharmacologique et d'innocuité du composé parent.

Les objectifs poursuivis tout au long des travaux, tels que la conception et la synthèse de nouveaux dérivés d'indométacine libérant de l'oxyde nitrique avec respectivement 1,3-thiazolidine-4-one et 1,3,4-oxadiazole, ainsi que l'évaluation biologique en termes de sélectivité de l'inhibition de la COX, d'effet anti-inflammatoire, d'effet antioxydant et de leur capacité à libérer du NO, peuvent être considérés comme remplis

Dans ce qui suit sont présentées les principales conclusions des études menées sur les nouveaux dérivés de l'indométacine qui font l'objet de cette thèse.

La synthèse réalisée dans cette étude a abouti à l'obtention de 144 composés (109 intermédiaires et 35 finaux) appartenant aux séries suivantes : (i) liants donneurs de NO (3a-s et 6a-m,t-v) ; ii) hydrazide d'indométacine (7); iii) dérivé de l'indométacine hydrazone (8a-s); iv) Dérivé IND-OXD (10); v) dérivés d'indométacine libérant de l'oxyde nitrique contenant un échafaudage de 1,3-thiazolidine-4-one (NO-IND-TZDs) (9a-s) et vi) dérivés d'indométacine libérant de l'oxyde nitrique contenant un échafaudage de 1,3,4-oxadiazole (NO-IND-OXDs) (11a-m,t-v).

Pour étudier la sélectivité des isoenzymes COX des nouveaux dérivés finaux d'indométacine libérant de l'oxyde nitrique, avec un échafaudage de 1,3-thiazolidine-4-one (NO-IND-TZDs, 9a-s) et 1,3,4-oxadiazole (NO-IND-OXDs, 11a-m, t-v), une analyse moléculaire de l'amarrage a été effectuée. Sur la base des résultats obtenus, nous pouvons conclure que le composé conçu peut être un puissant inhibiteur de la COX-2 et avoir les prémisses théoriques pour être des agents anti-inflammatoires prometteurs.

Afin de prédire les propriétés pharmacologiques et toxicologiques des nouveaux dérivés finaux de l'indométacine libérant de l'oxyde nitrique, une étude ADME-Tox a été réalisée. On a noté des propriétés physico-chimiques optimales et un profil pharmacocinétique favorable avec une bonne absorption dans l'intestin grêle et une mauvaise distribution au cerveau. Les descripteurs de toxicité ont révélé que les composés testés pouvaient être hépatotoxiques, mais de nombreuses études, y compris in vivo, doivent être réalisées afin de le confirmer. Le profil ADME-Tox a recommandé le composé développé pour l'administration orale.

L'activité de piégeage des radicaux libres des nouveaux NO-IND-TZDs et NO-IND-OXDs a été évaluée à l'aide d'une méthode colorimétrique basée sur la capacité des composés antioxydants à piéger le radical DPPH. Les résultats ont révélé que la présence d'échafaudages thiazolidine-4-one et 1,3,4-oxadiazole influence un potentiel antioxydant favorable, tous les composés testés étant environ 20 fois plus actifs que les médicaments de référence (IND, ASP)

L'effet anti-inflammatoire a été prédit par dénaturation thermique de l'albumine sérique bovine. Il a été noté que les NO-IND-OXD augmentent significativement l'effet de dénaturation que les NO-IND-TZD, et tous se sont révélés plus actifs que les médicaments de référence (IND et ASP). Ces résultats sont en accord avec les résultats d'amarrage moléculaire précédents qui ont montré que le remplacement du groupe carboxyle de l'IND par la fraction thiazolidine-4-one ou 1,3,4-oxadiazole améliore significativement les propriétés anti-inflammatoires.

La capacité de libération de NO des composés synthétisés a été évaluée par un test de Griess colorimétrique modifié pour simuler de manière appropriée les conditions corporelles. Les résultats ont révélé que la quantité de NO libérée par les composés testés était fortement favorisée par la position méta (3-oxy-éthyle) et ortho (2-oxy-éthyle) de la fraction ester nitrate et par la présence des groupes de retrait d'électrons (Cl, Br, NO2) sur le cycle aromatique. De plus, la présence d'un groupement 1,3,4-oxadiazole augmente significativement la quantité de NO libérée par rapport à la présence de fraction thiazolidine-4-one, étant comparable au SNP comme médicament de référence. Dans les conditions de travail, il peut apprécier que la majorité des composés libèrent de 4,4 à 14,7 plus de NO que les médicaments de référence NTG.

Les résultats obtenus ont permis de démontrer que les composés synthétisés présentaient des résultats encourageants basés sur une stratégie multi-cibles ayant une activité anti-inflammatoire, antioxydante et de libération d'oxyde nitrique par rapport aux médicaments de référence. En outre, les résultats de notre étude nous encouragent fortement à comprendre que les effets supplémentaires des composés synthétisés peuvent réduire les effets secondaires de l'utilisation de l'indométacine.

Chapitre 12 *Éléments d'originalité et perspectives de recherche*

Les recherches effectuées dans le cadre de la thèse de doctorat visaient la conception, la synthèse et la caractérisation biologique de certains nouveaux donneurs d'oxyde nitrique indométacine, en tant que nouvelle stratégie thérapeutique multi-cibles.

La nouveauté majeure de cette recherche réside dans la conception originale des dérivés développés de l'indométacine, qui contiennent trois éléments pharmacophores: (i) une structure indol, (ii) un échafaudage de 1,3-thiazolidine-4-one/1,3,4-oxadiazole et (iii) un ester de nitrate donneur d'oxyde nitrique, chacun d'eux ayant des effets biologiques importants prouvés.

L'indométacine est l'un des AINS les plus pertinents utilisés dans le monde pour le traitement de la polyarthrite rhumatoïde aiguë et chronique et d'autres maladies rhumatismales inflammatoires, mais son utilisation clinique à long terme est associée à des effets secondaires graves, en particulier au niveau gastro-intestinal

La 1,3-thiazolidine-4-one et la 1,3,4-oxadizole, respectivement, sont des échafaudages importants associés à des effets biologiques bénéfiques comme effets anti-inflammatoires, antioxydants, anticancéreux, anticonvulsivants, antimicrobiens, antiviraux et anti-VIH.

L'oxyde nitrique est une molécule endogène remarquable qui joue un rôle clé dans une grande variété de processus physiologiques et physiopathologiques, tels que l'inflammation, la vasodilatation, l'adhésion plaquettaire, la neurotransmission thrombose, la communication neuronale et la cicatrisation des plaies

Sur la base de la stratégie conçue, 35 nouveaux AINS originaux libérant de l'oxyde nitrique (19 NO-IND-TZD et 16 NO-IND-OXD) ont été synthétisés. Aussi, on a obtenu 98 intermédiaires molécules organiques, qui ne sont pas cités dans la littérature, à partir d'un montant total de 109 intermédiaires.

De plus, pour obtenir l'hydrazide indométacine, qui était un dérivé intermédiaire important, on a développé une méthode de synthèse plus efficace qui s'est avérée rapide, pratique, se déroule dans des conditions douces et adaptée à une préparation à grande échelle, par rapport aux méthodes citées dans la littérature.

Les résultats obtenus par évaluation computationnelle et biologique ont permis de démontrer que les nouveaux dérivés de l'indométacine présentaient des résultats prometteurs dans certains des effets évalués par rapport aux médicaments de référence.

Cela nous encourage à conclure que les composés multi-cibles conçus ont une activité anti-inflammatoire, antioxydante et libératrice d'oxyde nitrique, respectivement. Ainsi, l'unité 1,3-thiazoldine-4-one ou 1,3,4-oxadiazole liée à un squelette contenant un précurseur d'oxyde nitrique semble jouer un rôle de bioisoster couramment utilisé dans la chimie médicinale moderne.

STATE OF THE ART

Chapter 1

Inflammation

1.1. Introduction

Brief history. Medicines to relieve pain, fever and inflammation have been known for centuries [1], and the history of the anti-inflammatory drugs is an impressive example of the success of research in the development of new therapeutic agents. Thus, the chemical advances from modern age leads to development of the nonsteroidal anti-inflammatory drugs (NSAIDs). It is known two stages of NSAID drug discovery: a *pre-prostaglandin period* (up to the 1970's) and a modern stage of *the screening* in the drug-discovery process [2–4]. The first commercial drug was developed empirically after screening on laboratory animals for anti-inflammatory, analgesic and antipyretic activities. So the aspirin (acetylsalicylic acid) was introduced to the market by Bayer Company in 1899. In the following decades, other antipyretic, analgesic and anti-inflammatory compounds were synthesized and marked: phenylbutazone (4-butyl-1,2-diphenylpirazolidin-3,5-diona) in 1949, indomethacin (acid 1-(4-chlorobenzoyl)-5-methoxy-2-methyl-1*H*-indol-acetic) in 1963 and ibuprofen in 1969.

In medicinal chemistry, the possibility to develop more safer anti-inflammatory therapies was changed by John Vane which discovered that the aspirin, indomethacin and sodium salt of salicylic acid cause a decrease in the synthesis of prostaglandins (dose function) in liver tissue [2,4,5]. Moreover, the use of NSAIDs in treating various inflammatory conditions such as rheumatoid arthritis and acute musculoskeletal pain validated the inhibition of the cyclooxygenase (COX) as a highly suitable target in the anti-inflammatory therapies.

The inflammation is a defense reaction (non-specific and local) of advanced living organisms to any injury that is caused by trauma, microbial toxins or harmful chemicals [6,7]. This response is intended to inactivate or destroy the invading organisms, remove irritants and set the stage for tissue repair [8,9]. Since the essential components of the inflammatory process are found in the blood stream, this reaction occurs only in vascular tissues. It is nonspecific because it manifests itself identically, regardless of the etiology of the inflammatory process and the acute or chronic nature of inflammation [10]. It involves a complex process which consists of immunological and non-immunological reactions [11].

Inducers of inflammation trigger the production of several inflammatory mediators, which in turn injury the functionality of many tissues and organs in a way that allows them to adapt to the conditions indicated by the particular inducers of inflammation. These constitute the chemical network of the inflammatory response and result in clinical and pathological aspects of inflammation.

In essence, the inflammation remains a crucial physiological response for the human body to any kind of aggression and an adaptive response for restoring homeostasis [12].

When inflammation persists for a long time, holding the body in a constant state of alert, it may become chronically, with a negative impact on tissue and organs [13]. The clinical consequences of chronic inflammation-driven damage can be severe and include increased risk of many chronic diseases such as: rheumatoid arthritis [14], inflammatory bowel disease [15], metabolic disorders (diabetes mellitus and obesity) [16–18], cardiovascular disorders (ischemic heart disease, atherosclerosis) [19,20], neurodegenerative diseases (Parkinson's and Alzheimer's disease) [21–23] and cancer [24]; many of these conditions being life-threatening [25,26].

Chronic inflammation is tightly linked to the pathogenesis of inflammatory diseases that it becomes difficult to identify both cause and effect of these disorders. For example, inflammation is caused by obesity, whereas chronic inflammation can lead to obesity-associated diabetes partly because of insulin resistance.

Inflammatory diseases are among the commonest cause of chronic ill-health globally. The mounting cost of healthcare may be dominantly due to the severity and complexity of inflammatory disorders [12].

1.2. The inflammatory mediators and intracellular signaling pathways

The inflammatory mediators include a variety of synthesized molecules (by immune defense cells principally) that act on blood vessels and/or cells to promote an inflammatory response [27].

The released chemical mediators which vary according to their biochemical properties include: (i) vasoactive amines (histamine and serotonin); (ii) vasoactive peptides (substance P); (iii) fragments of complement components (anaphylatoxins); (iv) lipid mediators (eicosanoids and platelet-activating factors); (v) cytokines; (vi) chemokines; (vii) proteolytic enzymes; (viii) reactive oxygen species and (ix) nitric oxide [7,25,28–30].

The inhibition of the arachidonic acid cascade is one of the most used strategies for the treatment of the inflammatory diseases (Fig. 1.1). Arachidonic acid (AA, acid 5,8,11,14-eicosatetraenoic, ω-6) is the most abundant polyunsaturated fatty acid in the phospholipidic layer of the cell membrane which is released directly by an acyl hydrolase (phospholipase A2, PLA2) or indirectly by phospholipase C (PLC) [5,6]. AA is metabolized to form ***eicosanoids*** either by cyclooxygenase pathway (COX-1 and COX-2), when cyclic *prostanoids* (i.e. prostaglandins (PGs), prostacycline (PGI_2) and thromboxanes (TxA_2)) are generated, or by lipoxygenase way, which generate linear chain *leukotrienes* (LTC_4, LTD_4, LTE_4) and *lipoxins* [6,31]. The enzymes of this cascade are blocked directly by NSAIDs and coxibe and indirectly by glucocorticoids.

1.2.1. Prostaglandin endoperoxide H synthase (COX) pathway

Increased knowledge of the prostaglandin endoperoxide H synthase (PGHS) pathway contributes to understanding the structural determinants of the PGHS function and substrate binding, helping to efficiently target the inflammatory process. PGHS exists as two isoforms, namely PGHS-1 and PGHS-2, also known as COX-1 and COX-2, respectively [32].

COX-1 and COX-2 are bifunctional isenzymes which catalyze the transformation of unsaturated fatty acids such as AA, dihomo-γ-linolenic acid and eicosapentaenoic acid which are released by phospholipases A2, C or D from the phospholipid layer of the cell membrane [5,31,33,34]. The metabolism of AA consists of two sequential reactions: the double dioxygenation of AA to prostaglandin G2 (PGG2) and the reduction of PGG2 to PGH2 (Fig.

1.2). Oxygenation of AA is carried out in the distinct COX active site, which is mechanistically coupled with peroxidase active sites where the reduction of PGH2 takes place. PGH2 is very unstable and have not pharmacological activity. After diffuses from COX proteins it is transformed to prostaglandins (PGE2, PGD2, PGF2R, PGI2) and thromboxane A2 (TxA2) [5,33,35].

COX-1 is a constitutive form and is expressed in most human organs and tissues. It is responsible for the maintenance of internal homeostasis by participating in general body processes, such as cytoprotection of the gastric mucosa, inhibition of hydrochloric acid gastric secretion, increasing the mucus secretion, platelet aggregation, vascular smooth muscle functioning and regulation of the glomerular filtration and the renal blood flow [34].

On the other hand, COX-2 enzyme is inducible and specific to some type of cells and tissues and usually remains undetected in healthy tissues and organs. In adults, it is found only in the central nervous system, kidneys, vesicles and placenta, whereas in the foetus, it occurs in heart, kidneys, lungs, and skin. Increase of its level of expression is caused by various proinflammatory agents which are involved in inflammation, pain, fever, tumor, Alzheimer's disease or osteoarthritis [34,36].

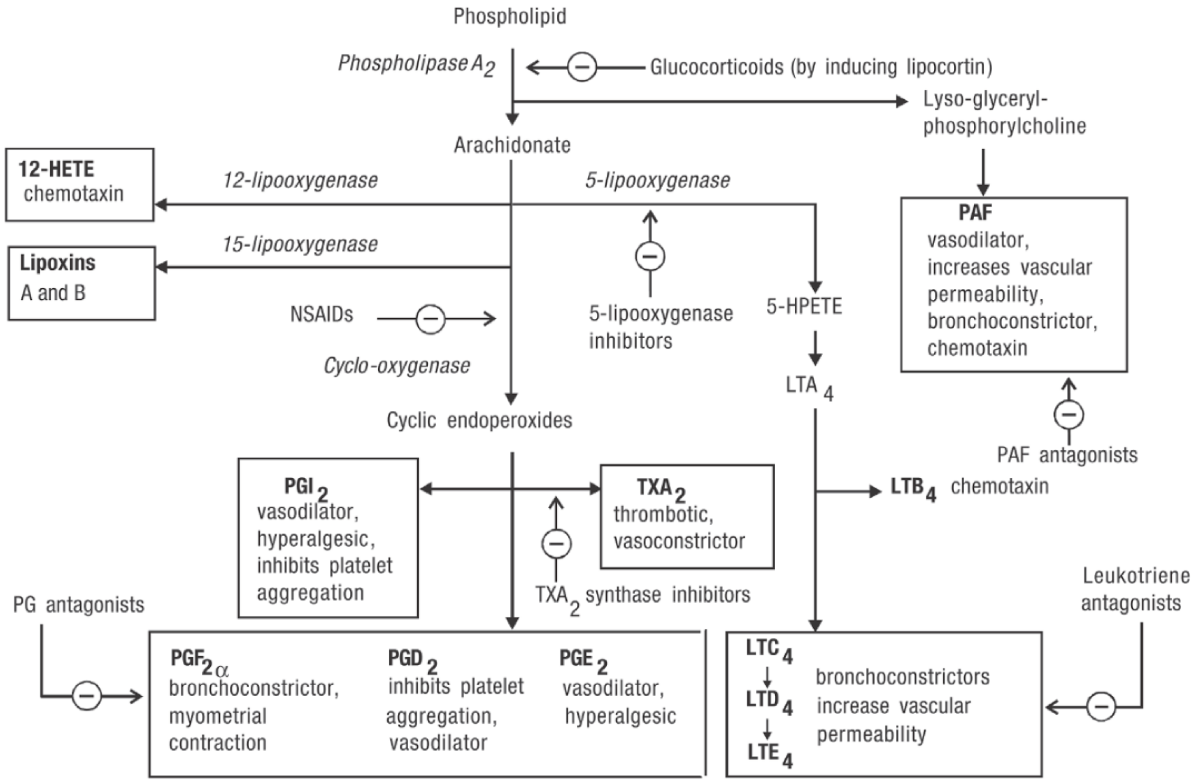

Fig. 1.1. The arachidonic acid pathway (adapted after [6]).

Both of the COX isoenzymes are located in the lumen of the endoplasmatic reticulum and nuclear membrane but the COX-2 is more concentrated in the nucleus. Structurally, COX is a homodimer stabilized by hydrophobic interactions, hydrogen bonds and electrolyte bridges. This form ensures its structural integrity and catalytic activity. COX-1 contains 576 units of amino acids while COX-2 contains 587 amino acids, the two isoenzymes having 60-65% identical sequences [37–39].

Each COX monomer has three structural domains [5,40,41]: the epidermal growth factor domain (EGF) at the *N*-terminus, the neighboring membrane binding domain (MBD) and the catalytic domain comprising which comprises ~80% of the enzyme (*C*-terminus) (Fig.

1.3). The peroxidase (POX) and cyclooxygenase (COX) active site are located in the catalytic domain on opposite each other with the prosthetic heme positioned at the base of the POX.

The catalytic domain and EGF are involved in dimer interface interaction and place the two MBD on the same face of the homodimer about 25 Å distance. The EGF form a substantial portion of the dimer interface which presents the disulfide bonds essential for folding and for holding the monomers together [42–44].

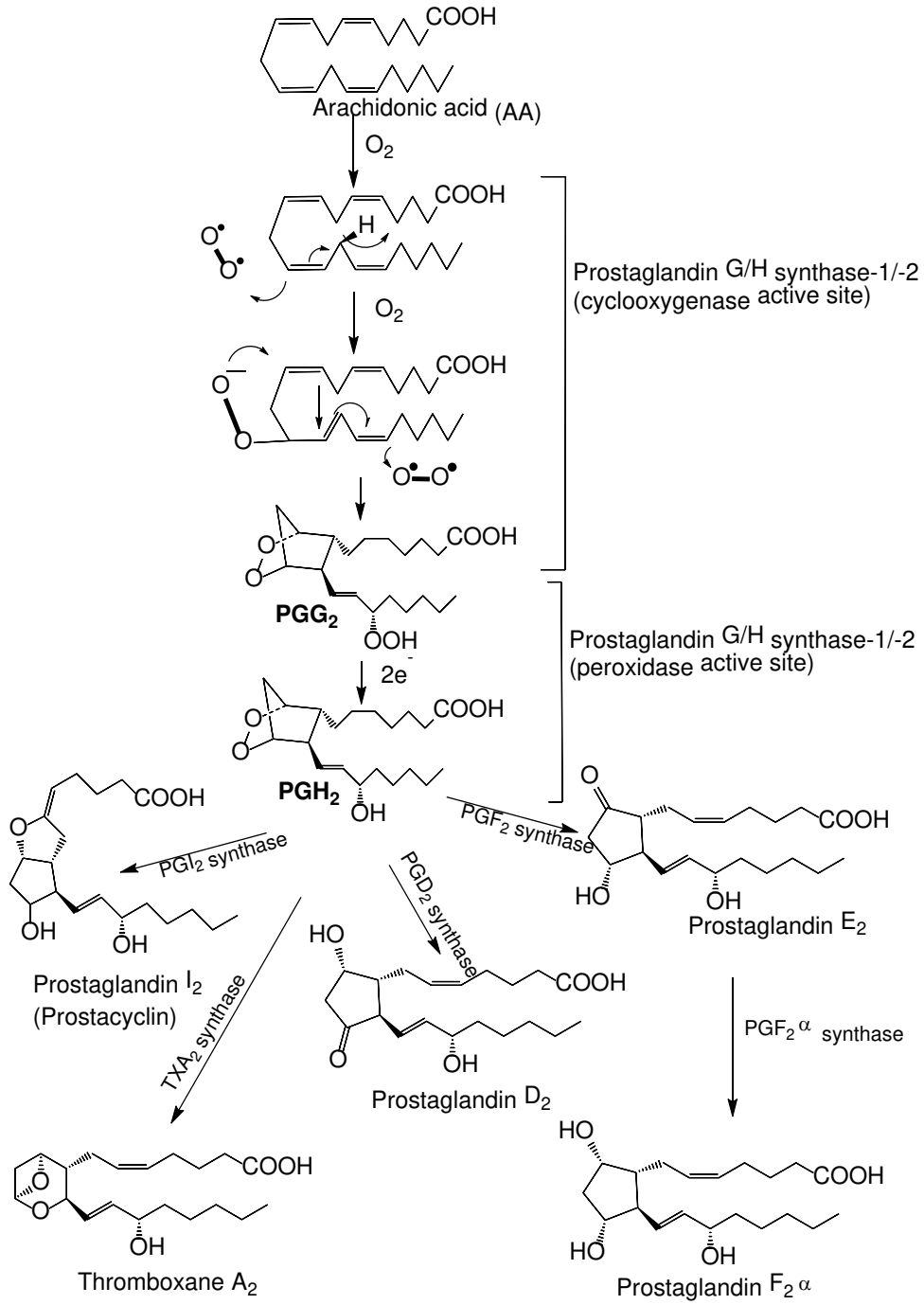

Fig. 1.2. The cyclooxygenase pathway (adapted after [33–35]).

The MBD contains four short amphipathic α helices. The three helices A-C lie in the same plane, while the last helix (helix D) projects up into the catalytic domain. The aromatic and hydrophobic residues from MBD create a hydrophobic surface favoring interactions with

one face of the lipid bilayer on the endoplasmic reticulum lumen and the nuclear membrane. This structure creates an entrance to the COX binding pocket and allows access for fatty acid substrates, arachidonic acid, O_2 and NSAIDs [45].

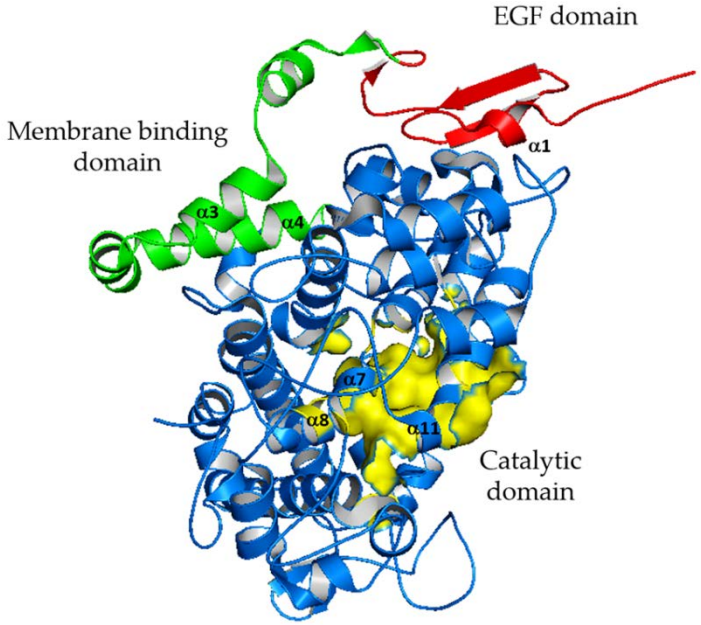

Fig. 1.3. The structural representation of COX-2 folding (adapted after [37]).

The globular catalytic domain represents the bulkiest part of the COX monomers representing the NSAID target or binding substrate site. The COX active site is a hydrophobic channel that is extended from the MBD into the core of the globular catalytic domain. At the interface between MBD and catalytic domain there is a narrow constriction composed of three charged amino acids (Arg120, Tyr355 and Glu524) which is the gateway to the active center. At the apex of the channel, both isozymes have two important amino acids Ser530 and Tyr385. Ser530 is the amino acid targeted by different NSAIDs and influences the COX stereochemistry in prostaglandins synthesis. The catalytic residue Tyr385 is located at the top of the channel and is involved in the hydroperoxidase activity [35,38] (Fig. 1.4).

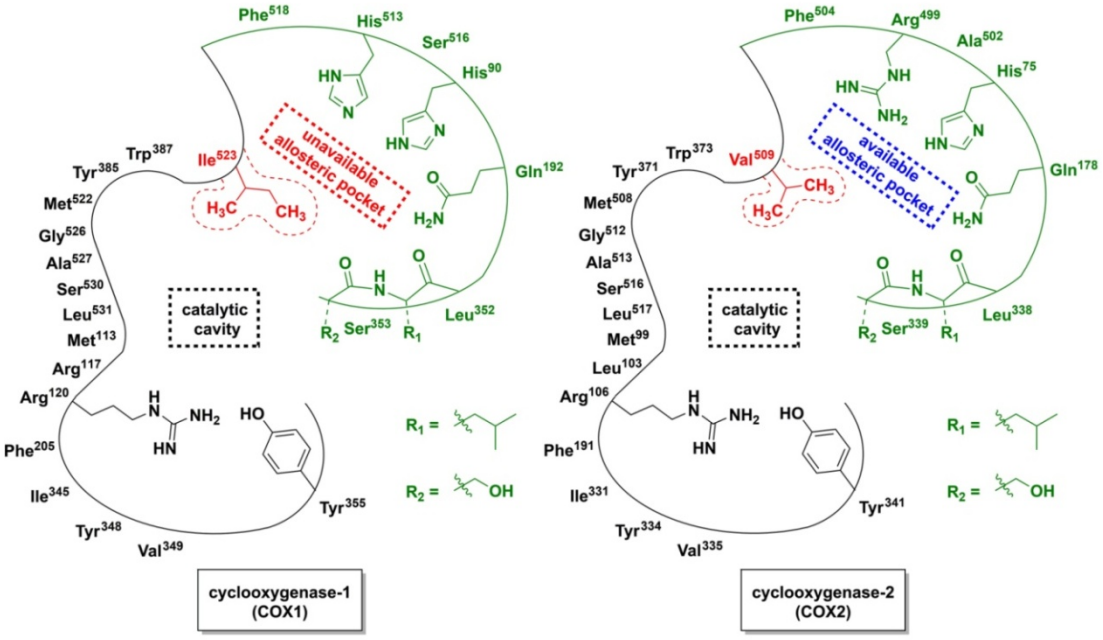

Fig. 1.4. The two dimensional active site of COX-1 and COX-2 (adapted after [45]).

The main difference between the active sites of both COX isoenzymes is the replacement of Ile (Ile434 and Ile523) in COX-1 by less bulky amino acid Val (Val434 and Val523) in COX-2. The loss of a single methyl group (Ile *vs.* Val) is sufficient to open a secondary internal hydrophobic side pocket in COX-2 that enlarging the volume of the active site by approximately 25% and giving access to Arg513 replaced in COX-1 by a His513 [5,31,35].

Tradidional NSAIDs, such as aspirin, flurbiprofen and indomethacin, act on the COX enzyme competing with AA for the active site [46–48]. AA is bound by COX adopting an extended L-shaped conformation (Fig. 1.5). The carboxyl group (C1) of AA interacts with the guanidinium group of Arg120 and makes a hydrogen bond with the phenolic oxygen of Tyr355. The carbons between C7 to C14 form an S shape surrounding side chain of Ser530. The two hydrogen attached to the sp^3-hybridized C13 are close to the phenolic oxygen of Tyr385 resulting in *S*-chirality center (pro-S hydrogen). Therefore, Tyr385 promotes the radicalic transformation of AA in further intermediaries. The ω end of AA (C14 through C20) is oriented at the top of the hydrophobic channel binding in a *cul-de-sac* along helices 6 (residues 325 to 353) and helices 17 (residues 520 to 535). In this arrangement the most majority of interactions between the substrate and the enzyme are van der Waals interactions. The Gly533 mutation at the top of the hydrophobic channel isolates the channel and prevents oxygenation of AA, but not of shorter-chain fatty acids.

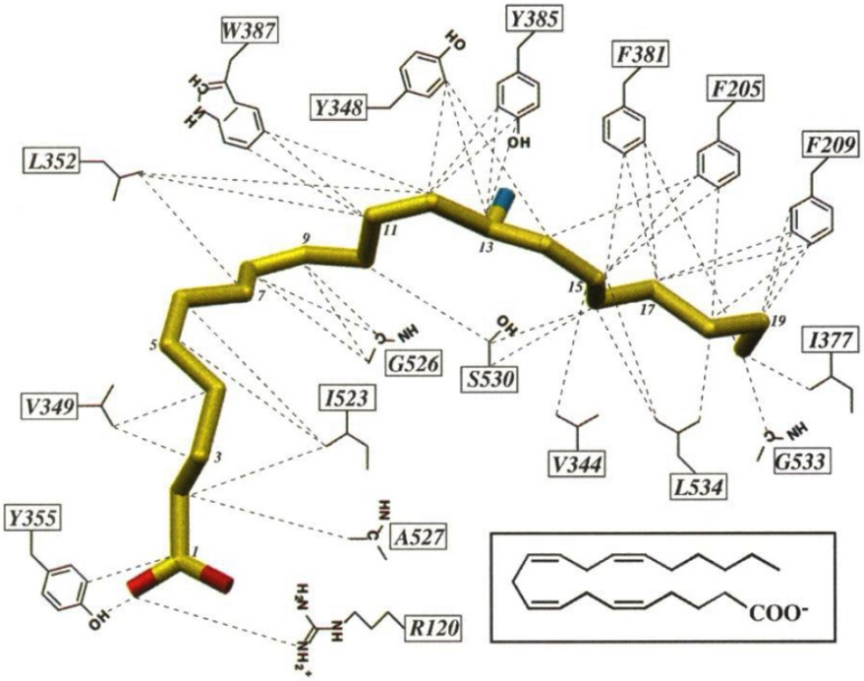

Fig. 1.5. The schematic representation of AA interaction with COX channel residues (adapted after [46]).

Flurbiprofen exhibits strong interaction with the binding pocket of the COX enzymes due to the carboxyl group, which forms a salt bridge with the guanidinium group of Arg120 and a hydrogen bond with Tyr355 from narrow site. The distal aromatic ring forms van der Waals interactions with Gly526 and Ala527 blocking the access to Tyr385 and with Ser530. The fluorophenyl ring makes close contacts (Van der Walls) with Val349 and Ala527 from COX-2. Also, fluoride interacts in COX-1 with Ile-523, but no interaction was observed with Val523 from COX-2 [49,50].

Aspirin has a unique therapeutic action and irreversibly inhibit COX-1 and COX-2 activity through the acetylation of the hydroxyl group of Ser-530 [41,51].

Indomethacin binds deeply to the active center of COX isoenzymes. The *p*-chlorobenzoyl group is deeply oriented in the hydrophobic channel and is stabilized by hydrophobic interactions with Phe381, Leu384, Tyr385 and Trp387. The benzoyl oxygen interacts with Ser530 and Val349 whereas the 4-bromobenzyl analogue (without benzoyl oxygen) enhances the COX-2 selectivity compared with indomethacin, which suggests that, the benzoyl oxygen increase COX-1 affinity. The carboxyl group of indomethacin forms a salt bridge with the guanidinium group of Arg120 and a hydrogen bond interaction with Tyr355 at the constriction site. The *O*-methoxy group interacts with the amino acids from inside of the COX-2 extra cavity delimited by Tyr355, Val523 and Ser353. The six member indolic ring, which interact with Val349 and the 2-methyl group, is oriented in a small hydrophobic pocket formed by Ala527, Ser530 and Leu531. These interactions are critical for the time dependence of COX inhibition by indomethacin. The indomethacin esterification does not influence its enzymatic kinetics, but this structural change makes the interaction with the hydrophobic channel less stable [5,52–54].

1.2.2. 5-Lipooxygenase pathway

5-Lipooxygenase (5-LOX) is part of a family of *lipid peroxidation enzymes* and is found in both plant and animal organisms. The LOX family contains cytosolic enzymes involved in oxygenation of the polyenic chain of fatty acids with the formation of corresponding hydroxyperoxides. Doubles bonds should have a *cis* conformation and be separated by a methylene group. The incorporation of molecular oxygen into AA substrate leads to the formation of the hydroperoxy-6-trans-8,11,14-cis-eicosatetraenoic acids family (HpETE). In the active site of LOX enzymes there is a nonheme iron atom which acts as an electron donor or acceptor during catalysis. The LOX is inactive for Fe^{2+} state and being active for Fe^{3+} [55,56].

In human body LOXs are classified as 5-,12- and 15-LOX based on regio specific incorporation of molecular oxygen on AA, generating 5-, 12- and 15-HpETE respectively. Platelets also contain only 15-LOX isoforms while leukocytes contain both 5-LOX and 12-LOX. In plants were identified 9- and 13-LOXs which incorporate oxygen on linoleic or α–linolenic acids on position 9 and 13 respectively [47].

5-LOX catalyzes incorporation of molecular oxygen into liberated AA giving 5-HpETE as well as the subsequent dehydration process with the formation of LTA_4 (Fig. 1.6). The latter unstable endoperoxide can be converted under the action of LTA_4-hydrolase (a zinc bound epoxide hydrolase) into a dihydroxyacid (LTB_4) or by conjugation with glutathione to LTC_4. By successively removing a remainder of glutamic acid and glycine from LTC_4 (under the action of a γ-glutamyl-transferase and a dipeptidase, respectively) LTD_4 and LTE_4 are obtained. LTC_4, LTD_4 and LTE_4 are also called cysteinil- or peptido-leukotriene [55,57–59].

Unlike prostanoids, leukotrinenes (LTs) are produced almost exclusively by inflammatory cells. However, while 5-LOX is expressed in myeloid cells, LTA_4 hydrolase and LTC_4 synthase are more widely distributed throughout the body: LTA_4 hydrolase is presented at intestinal level, spleen, lung, kidney and erythrocytes while LTC_4 synthase in mastocyte cells, basophils, eosinophils, endothelial cells and platelets [6,60]. LTs are paracrine hormones and express a wide spectrum of biological activities, mediated by specific receptors paired with protein G.

LTB4 is a potent chemotactic agent for inflammatory cells such as neutrophils, macrophages and eosinophils. It is involved in leukocyte migration towards inflammatory

sites and it plays an important role in immune reactions by enhancing the release of proinflammatory cytokines by macrophages and lymphocytes [31].

Cysteinyl-LTs (LTC_4, LTD_4 and LTE_4) are potent constrictors of smooth muscles (100-1000 times more potent as histamine), leading to important broncho constriction. They also stimulate mucus secretion and play an important role in bronchial smooth muscle cells proliferation. In the micro-vascular system, by contracting endothelial cells, they increase the vascular permeability and lead to edema, due to plasma extravasations. Furthermore, they present chemo attractive properties for eosinophils. In regard to these potent biological activities, LTs have been recognized to be important mediators of numerous inflammatory diseases and allergic disorders such as rheumatoid arthritis, inflammatory bowel disease, ulcerative colitis, asthma, psoriasis and allergic rhinitis [31,57,61,62].

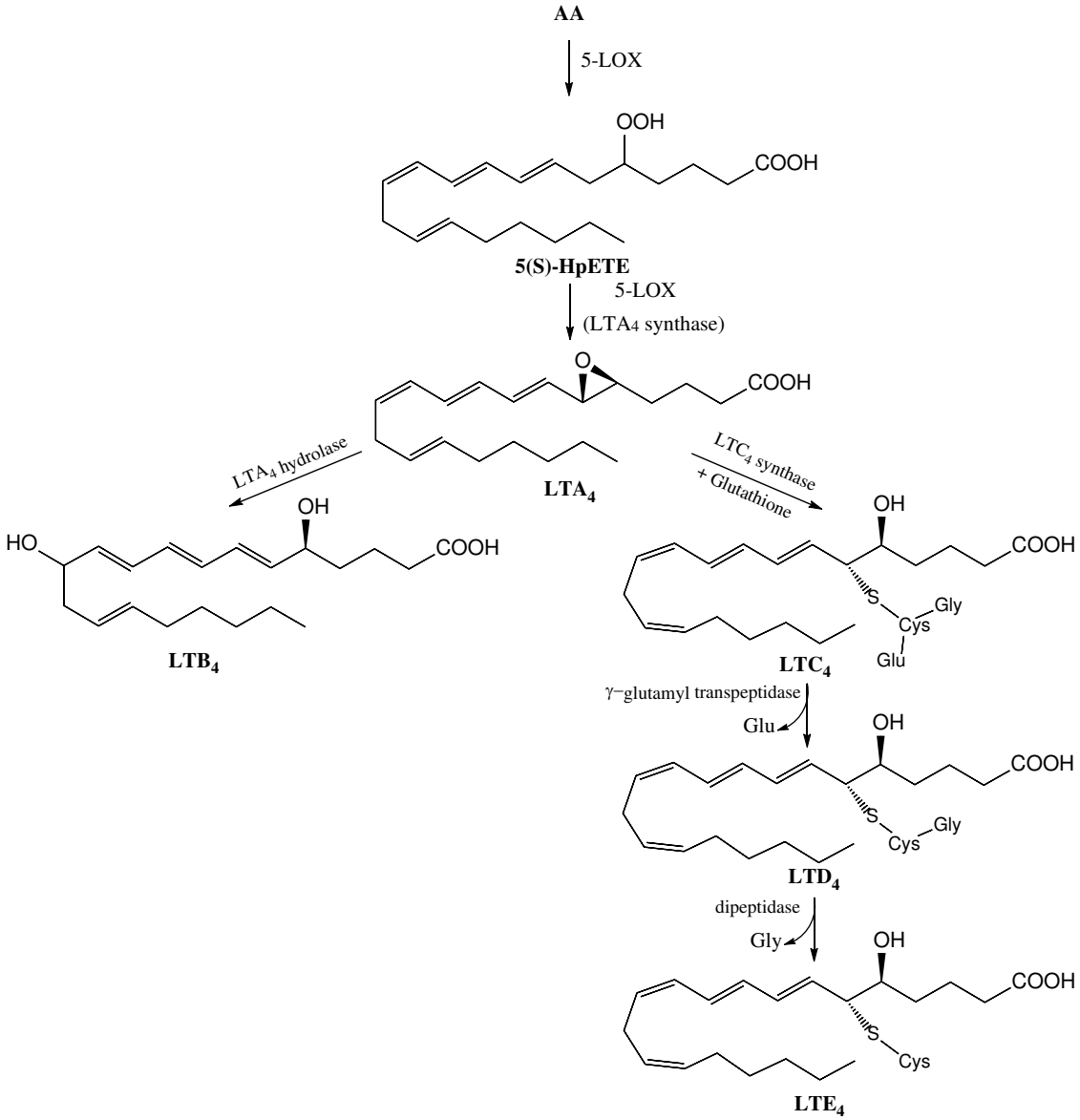

Fig. 1.6. The leukotrinene pathway biosynthesis (adapted after [55]).

Structurally, 5-LOX is a monomer containing about 673 amino acids forming two units: a short *N*-terminal domain (a field that presents itself as a barrel in which each sheet is twisted in the form of a spiral) and a large *C*-terminal domain, consisting of α-helixes. This area

represents the active center of the enzyme with a non-hemic iron atom. In most cells, 5-LOX is located in cytosol, only in a few cases it can be found in the nucleus. This isoform is activated by Ca^{2+} which binds reversibely the *N*-terminal domain. The enzyme can also be activated by ATP in the presence of Ca^{2+} (co stimulation effect), lipid hydroperoxides and phosphatidylcholine. Once the cell is activated and intracellular penetration of Ca^{2+} occurs, 5-LOX (regardless of its location) is translocated at the nuclear level. After which it interacts with membranary proteins with low molecular mass (FLAP), involved in AA transfer to 5-LOX. This interaction between the enzyme and FLAP is crucial stage for the biosynthesis of LTs [62–67].

Considering the pro-inflammatory properties of LTB4 and the multiple activities of cysteinil-LTs, the modulation of this pathway represents a real interest in the treatment of numerous allergic, inflammatory and asthma conditions [68,69]. In order to influence the cellular LTs synthesis were proposed several strategies for inhibition of the 5-LOX pathway, that can be basically pursued [70,71]: inhibition of cytosolic phospholipase A2 (cPLA2), inhibitors of FLAP and of 5-LOX.

Suppression of $cPLA_2$ by glucocorticoids [72] and varespladib (**1**) (Fig. 1.7) [73,74] would reduce the availability of AA for eicosanoids formation. However, they were not reported improved efficiency in clinical studies.

FLAP inhibitors prevent 5-LOX interaction with FLAP which is necessary for the activation of 5-LOX and AA substrate transfer. Such compounds are efficient in intact cells when LTs products are formed from endogenously synthesized AA. Today there are some compounds which are in phases 1-3 development status [75].

Direct inhibition of 5-LOX involves either antioxidant mechanism or interaction with the non-heme iron enzymatic moiety. Antioxidant compounds can interact with 5-LOX peroxidase function blocking LTs formation. Compounds developed have been found to have unacceptable toxicity for clinical development [76].

The most widely used iron chelators are hydroxamic acid (R-CO-NH-OH) and *N*-hydroxyurea (R-N(OH)-CO-NH-R). Zileuton (**2**) (Fig. 1.7) is the first 5-LOX inhibitor introduced into the therapeutic for the treatment of bronchial asthma. However, the therapeutic potential in inflammatory bowel disease, in allergic rhinitis, rheumatoid arthritis was found to have low efficiency.

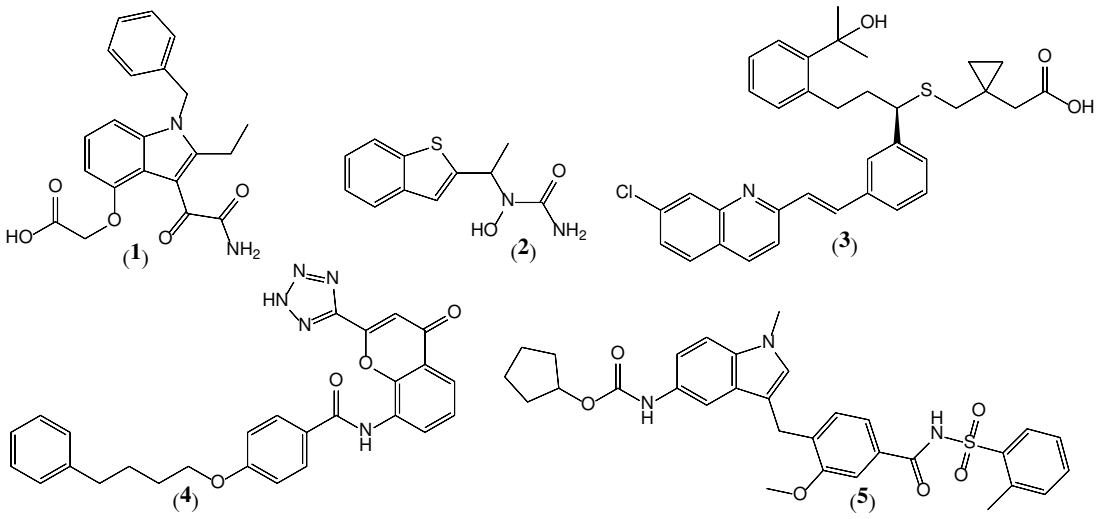

Fig. 1.7. Representative drugs used for inhibition of 5-LOX pathway.

Although intensive efforts have been made to develop inhibitory compounds of LTs biosynthesis, results are still expected.

The design of antagonists for leukotriene receptor was more fruitful by bringing three compounds to market: montelukast (**3**), pranlukast (**4**) and zafirlukast (**5**) (Fig. 1.7). All these compounds, although effective in treating asthma, are ineffective as monotherapy for inflammatory conditions. Therefore, a promising approach consists in dual COX-2 and 5-LOX inhibition.

1.2.3. Reactive oxygen species

Reactive oxygen species (ROS) are highly reactive chemical entities derived from molecular oxygen (molecules or molecular fragments) that exhibit one or more unpaired electrons. ROS include superoxide anion ($O_2^{-\bullet}$), hydroxyl radical ($HO^{\bullet}$), hydrogen peroxide (H_2O_2), nitric oxide (NO), hypochlorous acid (HOCl) and singlet oxygen ($^1[O_2]$) [77,78].

The increase of ROS synthesis can be both endogenous and exogenous. Endogenous increase occurs in inflammatory and infectious processes, neoplasms, activation of immune cells, aging and intense physical exercise. By exposure to pollutants, heavy metals, pesticides, cigarette smoke, ultraviolet or ionizing radiation, some medicinal molecules (cyclosporin, tacrolimus) or food (smoked meat, fats), an exogenous increase in the formation of ROS occurs [79–81].

At low concentration, ROS act as important mediators involved in regulation of mitogenic response, in antimicrobial defense and in intracellular signaling [82–84]. ROS being also signaling molecules, play an important role in the initiation, progression, and resolution of the inflammatory response. The ROS overproduction by polymorphonuclear neutrophils at the inflammation site causes endothelial dysfunction (increase vascular permeability and leukocyte extravasation, phagocytosis, angiogenesis) and tissue injury [82,85]. Moreover, the exceeding the cellular neutralization capacity of ROS, with the appearance of oxidative stress, leads to damage to cellular structures: cell membrane or membranes of cellular organelles, proteins, lipids and nucleic acids. Disruption of physiological redox signaling and damage of cellular structures, can contribute to the development of chronic diseases such as diabetes mellitus, obesity, cardiovascular, renal and neurodegenerative diseases [80,83,86].

Endogenous antioxidant defense consists of numerous enzyme systems, such as superoxide dismutase, catalase, glutathione peroxidase and non-enzymatic, including glutathione, alpha lipoic acid, ferritin, uric acid, bilirubin, coenzyme Q [87]. Exogenous antioxidants support endogenous ones, either being of food origin or administered as dietary supplements.

By interaction of immune system cells with endogenous and exogenous inductors of inflammation results in generation ROS and stimulation of the chemokines biosynthesis and pro-inflammatory cytokines. These activate some specific cellular signaling pathways, increasing the oxidative stress. Thus, an inflammation cycle-oxidative stress is formed enhancing the injury effects [88].

To counteract the destructive effects of ROS, a sustained activity of antioxidants and DNA restoration mechanisms are necessary. In the case of chronic inflammation, due to the depletion of antioxidants, damage to cellular structures can be marked, with increased risk of developing chronic diseases.

1.3. Conclussions

Briefly, the inflammation is known as an important physiological response for the human body to any kind of aggression and also is involved in pathogenesis of many chronic diseases such as metabolic, neurodegenerative, cardiovascular disorders and cancer. In order, to identify specific targets for therapeutic intervention, were reported a variety of underlying inflammatory mechanisms.

For example, the tumor necrosis factor α (TNF_{α}) is a pro-inflammatory cytokine involved in the pathogenesis of systemic inflammatory conditions such as rheumatoid arthritis, ankylosing spondylitis, psoriasis as well as inflammatory bowel conditions by intracellular activation of nuclear factor kappa-B (NF-kB), caspazes and mitogen-activated protein kinase (MAPK)[89].

In the 1990s the treatment of rheumatoid arthritis was revolutionized by the development of protein-based therapy. The success of injectable proteins such as etanercept (Enbrel®), infliximab (Remicade®) and adalimumab (Humira®) gave a new dimension to anti-inflammatory therapy. Long-term therapy with these proteins could have side effects such as latent tuberculosis, harmful cardiovascular effects, or increased risk of developing cancer. At the same time, anti TNF therapy involves high costs and low compliance on the part of the patient [4].

Therefore, a better understanding of molecular mechanisms of inflammatory pathways will undoubtedly contribute to improve the prevention and treatment of inflammatory diseases.

Chapter 2

Indomethacin and its derivatives

2.1. Chemistry and pharmaco-toxicological profile

Indomethacin (1-(4-chlorobenzoyl)-5-methoxy-2-methyl-1*H*-indol-acetic acid) (**6, IND**) was discovered by Rahway (1963) from Merk&Co (SUA) Company and has been approved for its therapeutic use in1965 (Fig. 2.1).

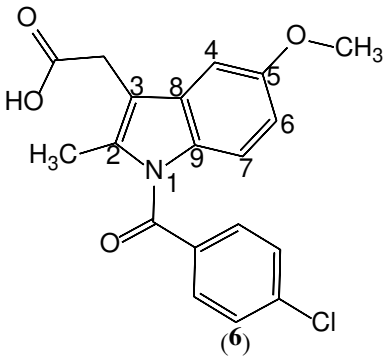

(**6**)

Fig. 2.1. Indomethacin structure.

IND is the best-known and the most thoroughly tested indole-acetic acid derivative [90], remaining one of the most relevant NSAIDs used worldwide for the treatment of acute and chronic rheumatoid arthritis and other inflammatory rheumatic diseases, episodes of acute gout and acute musculoskeletal pain [91,92]. Due to its potency, its clinical efficacy is comparable, or sometimes higher to any other NSAIDs. Like other NSAIDs, most of its toxic and therapeutic effects are due to inhibition of prostaglandin synthesis and for this reason the side effects inevitably limit its use.

It was documented that long-term clinical use of IND is responsible for a wide range of side effects including gastrointestinal (GI) irritation, bleeding and ulceration, digestive disorders (nausea, vomiting, abdominal pain, diarrhea or constipation), increased anxiety, headache, dizziness, peripheral edema, arterial hypertension, tachycardia, kidney and liver dysfunction, allergic and anaphylactic reactions [91,93].

The incidence of IND's adverse events have a higher prevalence at patients with multiple, co-existing chronic conditions and which commonly have more prescribed drugs. Indomethacin can interact with several other medications causing seriously side effects. For instance, IND potentiates the effect of anticoagulants and anti-platelet drugs, increased plasma digoxin concentrations, induces renal insufficiency and severe metabolic acidosis at patients with diabetes mellitus who take metformin, reduces the effect of diuretics and causes impairment of renal function and hyperkalemia, in association with angiotensin converting enzyme inhibitors (lisinopril). Moreover, it was reported a cross reactivity with aspirin reducing its absorption [90].

Gastrotoxicity is the main adverse effect of IND and symptoms range from abdominal discomfort to ulcer penetration and perforation. It is known that the GI mucosal injury of NSAIDs is caused by several different mechanisms. The first mechanism is represented by the direct contact effect, which is attributed to the carboxyl group causing local irritation upon oral administration. On the other way, NSAIDs can act by an ion-trapping mechanism in mucosal cell enabling back diffusion of H^+ from the lumen into the mucosa. The COX-1 inhibition represents another possible mechanism by local inhibition of prostaglandin synthesis in the GI tract [94,95].

Literature survey revealed that are reported different strategies to improve the safety profile of NSAIDs: (i) development of selective COX-2 inhibitors; (ii) co administration of a GI protective agents; (iii) as well as development of nitric oxide release NSAIDs (NO-NSAIDs). Each strategy has a number of advantages and limitations. For example, COX-2 selective drugs can resolve the GI complications but can induce serious cardiovascular side effects. NO-NSAIDs suppress inflammation as effectively as the parent NSAIDs but NO production is achieved through a mechanism thiol dependent, contributing to nitrate tolerance. Also, the patient compliance is reduced in drug combination strategy.

To address safety and efficacy issues related to IND, it were reported different approaches to improve the physicochemical properties, to reduce side effects by additive or synergistic strategies, to enhance the biopharmaceutical profile, to optimize of route of administration or by targeted delivering.

2.2. Chemical modulation of Indomethacin

By replacing the 4-chlorobenzoyl group of IND with a 4-bromobenzyl, were obtained potent and selective COX-2 inhibitors [96,97]. Studies have shown that the presence of the *N*-phenyl or *N*-benzyl on the indole core is essential for the anti-inflammatory and analgesic effect [98]. Removal of the 2-methyl ($-CH_3$) group from the indole scaffold generates the inactive compounds [99]. So, the methyl group is indispensable for fixing the IND molecule in the hydrophobic channel of COX [96]. The presence of a methoxy ($-OCH_3$) or oxo-methylene group ($-OCH_2-$) at position 5 of indole is also indispensable for maintaining the anti-inflammatory activity [98]. The esterification of the carboxyl group generates highly selective COX-2 inhibitors and eliminates the GI side effects of the parent compound [99].

In order to improve the pharmaco-toxicological profile of IND, it was reported the synthesis and biological evaluation of a series of *morpholinoalkyl esters* (Fig. 2.2). Noteworthy, based on *in vitro* and *in vivo* assay, the designed compounds showed some advantages than parent compound. These prodrugs were freely soluble (2000-fold over the IND), more lipophilic (in neutral or basic media) than IND and stable enough in simulated gastric fluid to be absorbed intact. The oral absorption was also significantly increased in experimental animals as compared to parent drug. Regarding to the GI toxicity, the prodrugs were significantly less irritating than IND in terms of the severity of gastric mucosal injury. So, the IND's morpholinoalkyl esters (**7**) represent promising useful derivatives with improved pharmacological profile [100].

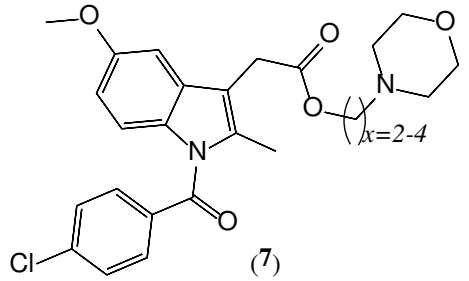

(**7**)

Fig. 2.2. The structure of the morpholinoalkyl esters of indomethacin.

At the same time, it was observed that aliphatic esters with linear chain and with large numbers of carbon atoms enhance COX selectivity, but by branching and inserting functional groups, this effect is diminished. The potency and selectivity on COX-2 isoenzyme can be also significantly enhanced by aromatic esters synthesis, by elongation of distance between the ester oxygen and the aromatic ring and by substitution of the aromatic ring [99]. To preserve the anti-inflammatory activity it was reported that a hydrophobic chain should be used for esterification, because the presence of polar groups prevent penetration to the hydrophobic pocket site of COX. In addition, the shielding of the carboxylic group in an ester can reduce the ulcerogenic activity [101].

Moreover, a series of amide derivatives of IND were showed appreciable anti-inflammatory effect. It was noted, that the *N*-methyl amide displayed selective COX-2 inhibition. By increasing the amidic group radical to the octyl, the maximum effect is obtained, which is also maintained in the case of aliphatic chain branching. At the same time, the *L*-enantiomers were much more potent than the corresponding *D*-enantiomers. The most potent and selective COX-2 inhibitors were found to be the aromatic amides containing the 4-fluoro, 4-methylthio or 3-pyridinyl substituents. The secondary amides exhibit anti-inflammatory action, while the corresponding tertiary amides showed no significant inhibition of either COX isoenzymes. This suggests that amide nitrogen forms a hydrogen bond with the important amino acids from narrow constriction of COX isoenzymes (Tyr355 or Glu524) [99].

These observations are consistent with the model proposed by *Kalgutkar et al.* [97] with regard to the binding of esters and amides on COX-2 active site pocket. The IND nucleus is located inside of the active pocket of COX and the ester and amide group, respectively, interacts with amino acids from entrance at the active site, under the narrow constriction in the COX's membrane binding domain. Ser530, at the apex of the channel, is targeted by oxygen from the 4-chlorobenzoic moiety and the oxygen from the carboxyl group interacts with Arg120. These prodrugs enhance the COX-2 potency and selectivity due to bulky ester/amide functional groups which cannot take a suitable steric conformation in the COX-1 binding pocket due to its reduced volume [99].

Briefly, the applications of prodrugs approaches improve the pharmacokinetics parameters, decrease in gastric toxicity and improvement of chemical properties [94,95]. Temporarily inactive prodrugs block acidic grouping until absorption and release the active compound (IND) in the bloodstream after absorption.

A series of mutual prodrugs of IND (**8**) (Fig. 2.3) with naturally occurring antioxidants (eugenol, hesperetin, thymol, menthol, umbeliferone) showed an analgesic and anti-inflammatory activity far superior to physical mixtures between IND and corresponding antioxidants, significantly reducing the ulcerogenic effect [102,103].

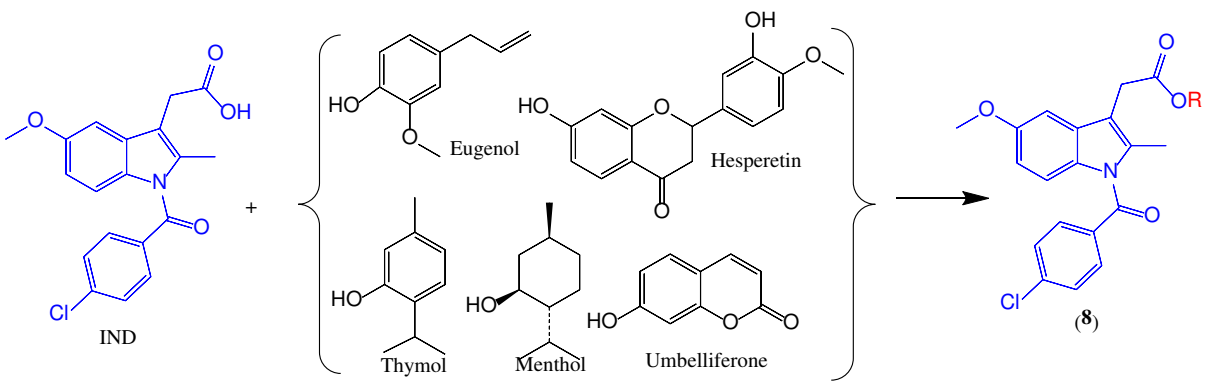

Fig. 2.3. The prodrug structures of indomethacin, with naturally occurring antioxidants.

By amidation of the carboxyl group of IND with *L*-cysteine ethyl ester, it was obtained a new prodrug with increased anti-inflammatory activity, reduced GI toxicity, antioxidant properties but with decreased hypocholesterolemic potency than parent NSAID [104].

An IND-lecitin conjugate was also synthesized in order to obtain a controlled release profile of the free drug in the systemic blood circulation. It was proved that the phospholipid-drug conjugate can release the free drug into the GI tract by PLA2 enzymes [105].

In order to overcome the gastric toxicity of IND it was reported a new approach which involves the block of acidic functionality and the decrease of gastric secretions and of motility [106]. By synthesis of *N*,*N*-disubstituted aminoethanol ester derivatives of IND (**9**) (Fig. 2.4) it was obtained derivatives which showed: (i) stability in aqueous solution, (ii) rapid hydrolysis in human plasma, (iii) anticholinergic action at the GI level, (iv) maintaining the anti-inflammatory and analgesic properties of IND and (v) inhibition of IND-induced GI irritation.

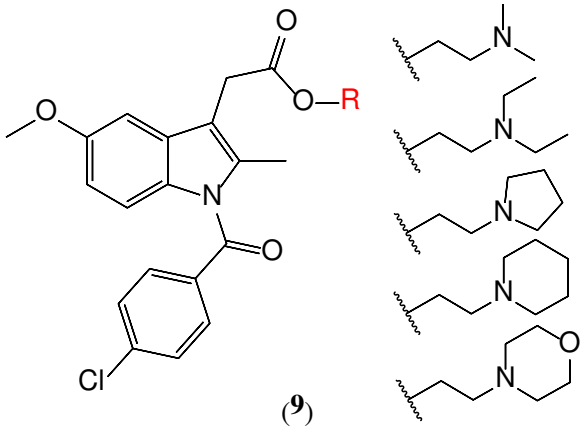

(**9**)

Fig. 2.4. *N*,*N*-disubstituted aminoethanol ester derivatives of indomethacin.

A novel series of IND analogs were synthesized by replacement of the 4-chlorobenzoyl group with a 5-LOX pharmacophore (*N*-difluoromethyl-1,2-dihydropyrid-2-one moiety), attached by a C=O (**10**) or $-CH_2-$ (**11**) linker to the indole *N*-position (Fig. 2.5) [107]. The structure-activity data acquired indicated that this approach is not suitable for the design of IND analogs as effective antiinflammatory agents that act by inhibition of the COX-2 and/or 5-LOX pathway.

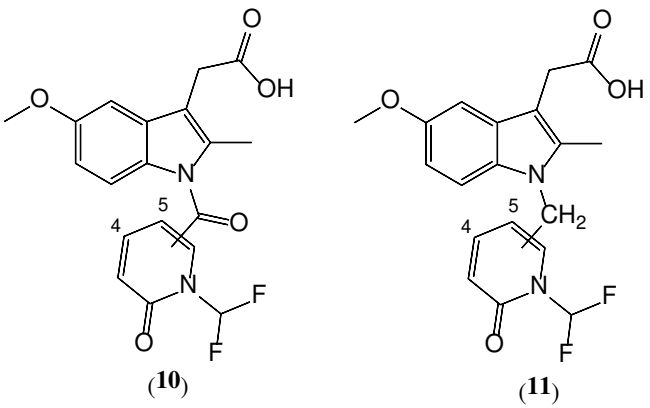

(**10**) (**11**)

Fig. 2.5. Indomethacin analogs containing a *N*-difluoromethyl-1,2-dihydropyrid-2-one-4- or 5-carbonyl moiety (**10**) and *N*-difluoromethyl-1,2-dihydropyrid-2-one-4- or 5-ylmethyl moiety (**11**).

It is know that the methyl group at the *C-2* position of IND forms a strong hydrophobic binding interaction with Val349, Ala527, Ser530 and Leu531 residues from hydrophobic pocket of COX isoenzymes. Based on these findings it was reported the synthesis and biochemical evaluation of a fluorinated analogue of IND bearing a lipophilic 3,3,3-trifluoroprop-1-enyl group at its *C-2* position (**12**) (Fig. 2.6) [108]. It was noted that this alkenyl derivative exhibited higher inhibitory activity and selectivity towards COX-2 than IND and 2-CF_3-IND analog (**13**) (Fig. 2.6) due to a significant increase in Van der Waals interactions [109].

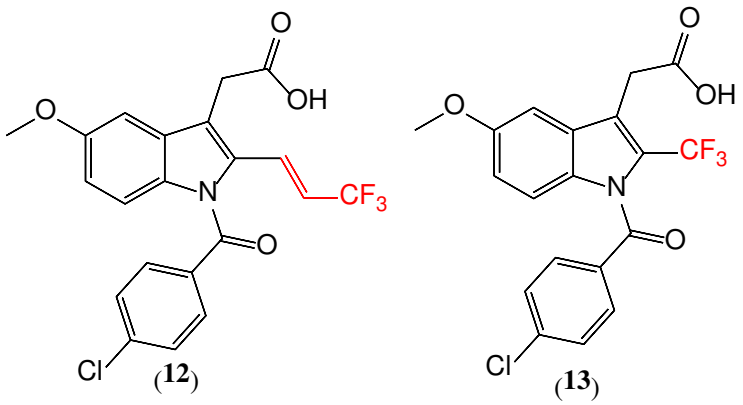

Fig. 2.6. The structure of Indomethacin analogues bearing a 3,3,3-trifluoroprop-1-enyl (**12**) and a 2-CF_3 group (**13**) at its 2-position.

To improve the IND selectivity against COX-2 it was reported a new strategy [110] that involved: (i) elimination of carboxyl group to reduce the possibility of the inhibitor forming a salt bridge with Arg120 and, ultimately, to prevent COX-1 inhibition; (ii) ring extension of IND for reducing the possibility of analogs to remain fixing into the narrow hydrophobic tunnel of COX-1 and (iii) introduction of methyl-sulfonyl group to enhance the interaction of analogs with the polar side pocket, which is essential for COX-2 inhibition (Fig. 2.7). The biological activity results of the new analog (**14**) revealed the success of the approach provides. It was obtained a significant improved activity against COX-2 with superior potency to celecoxib. In addition, it was reported a high safety against gastric ulceration than IND and being so close to celecoxib.

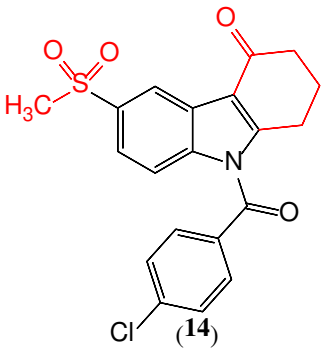

Fig. 2.7. Ring extended analog of indomethacin.

By synthesis of a novel series of aryl carboximidamides starting from IND (IND−CO−O−N=C(NH_2)−R) were obtained devoid compounds of any obvious cytotoxicity and which suppressed the overproduction of PGE2 and NO [92].

It was also documented that IND presents preventive chemotherapeutic effect on different animal model and can exhibit important general anti-cancer activity against a wide

range of cancer cells [111,112]. Its antiproliferative effects include different mechanisms, such as induction of apoptosis and improvement if immune response [113,114]. Moreover, by conjugation of three moieties such as IND, a diethyl phosphate group and a linker, a phosphor-tyrosol-IND derivative (**15**) was synthesized (Fig. 2.8), which possess potent anticancer efficacy in preclinical model of human colon cancer and is 30 fold more potent than IND in the inhibition of cancer cells growth [115]. Based on the structure activity relationship data, recently it was reported the synthesis of new IND analogs (**16**) (Fig. 2.8) which exhibited cytotoxic activity compared to 5-fluorouracil, as reference standard [116]. It was concluded that the replacing of carboxylic group with bulkier lipophlilic functionalities can enhance the cell grow inhibition.

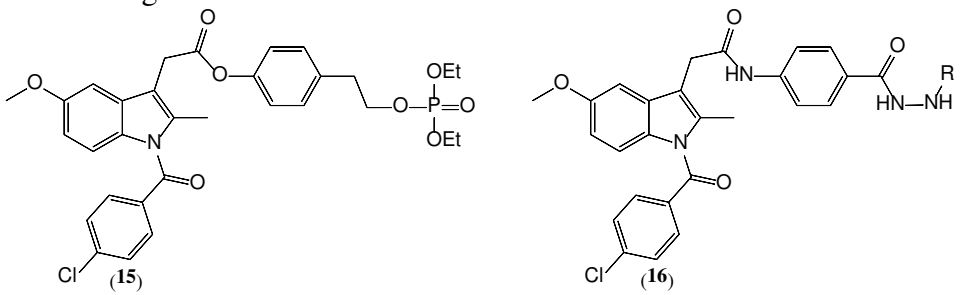

Fig. 2.8. General structure of anticancer analogs of indomethacin.

2.3. Conclussions

Based on the aforementioned data we can conclude that the IND is a versatile scaffold by whose structural changes can be developed compounds with improved pharmaco-toxycological profile.

Moreover, indole ring is a very important pharmacophore group in drug discovery studies generating compounds with numerous applications and therapeutic uses. For therapeutic uses there were already been approved several commercial indole based drugs with application in anticancer, antihypertensive, antidepressant, anti-HIV, opioid agonist as well as in analgesic therapy [117].

Chapter 3

Thiazolidine-4-one derivatives with therapeutic potential

The 1,3-thiazolidine-4-one scaffold serve as a core for many synthetic compounds of great interest in medicinal chemistry [118]. This scaffold is a structural component of various natural products, like thiamine (vitamin B_1), acidomycin (isolated from *Strepomyces* strains) [119,120] and many metabolic products (cytotoxic cyclopeptides) of fungi and primitive marine animals [121]. Several thiazolidine-4-one based drugs such as ralitoline (**17**) (anticonvulsant), etozoline (**18**) (loop diuretic), epalrestat (**19**) (an aldose reductase inhibitor for the treatment of diabetic peripheral neuropathy) and pioglitazone (**20**) (oral anti-diabetic drug) have already been approved for therapeutic use (Fig. 3.1). The literature reports for thiazolidine-4-one scaffold other important biological effects such as anti-inflammatory, antioxidant, platelet-activating factor (PAF) antagonist, cyclooxygenase (COX) inhibition, tumor necrosis factor antagonist as well as anticancer, anticonvulsant, antimicrobial, antiviral and anti HIV effects [122–129].

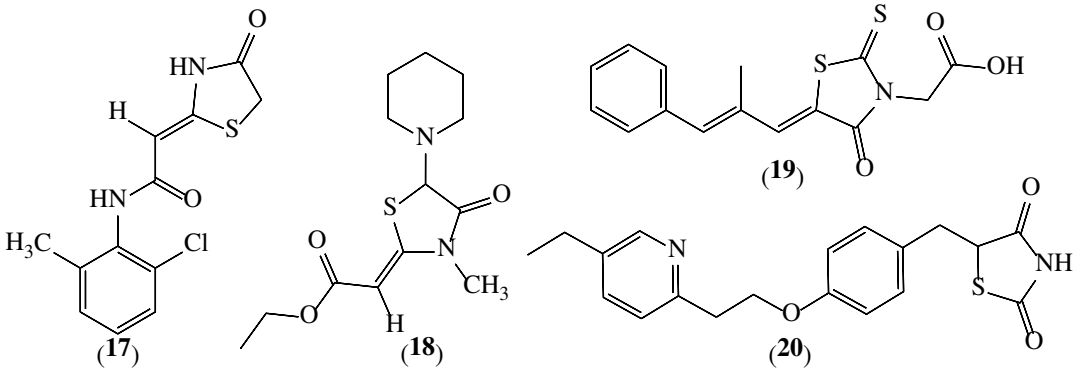

Fig. 3.1. Representative drugs containing the thiazolidin-4-one core.

3.1. Chemistry

The thiazolidinones are five-membered heterocycles containing two hetero-atoms; a sulfur atom in position 1 and a nitrogen atom in position 3 as well as a carbonyl group located at the 1st, 3rd or 4th position, respectively [120,130–132]. For thiazolidine-4-one the carbonyl group is unreactive and the subtituents present in the 3 and 5 positions may vary without affecting the chemical properties of this moiety. On the other hand a group attached to the carbon atom in the 2 position exerts the greatest difference in structure and properties enhancing biologically activity. The 2,3-disubstitued thiazolidine-4-one derivatives (such us 2-aryl-3-(2-pyridyl)-thiazolidine-4-ones) present optical activity and the preferred configuration is hat in which 2 protons of C-2 and C-5 are in *cis* diequatorial conformation

and due to the phenyl group which take the axial orientation avoiding the steric crowding with pyridyl group (Fig. 3.2) [131,133–135].

The unsubstituted thiazolidine-4-ones are rather soluble in water, whereas the introduction of an aryl or an alkyl substituent decreases significantly the water solubility. Also, unsubstitued derivatives are solids and the attachment of radicals on nitrogen lowers the melting points [131,133].

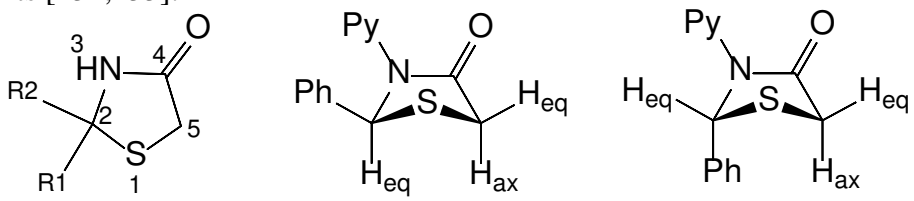

Fig. 3.2. The structure and stereochemistry of thiazolidine-4-one heterocycles.

3.2. Biological effects of thiazolidine-4-one derivatives

The thiazolidine-4-one scaffold serves as core for many synthetic compounds of great interest in medicinal chemistry. Its use may be owed to the simplicity of the synthetic methodologies, maneuverability, versatility and stereochemical orientation giving a complete range of novel derivatives (Table 3.1) [127].

Table 3.1. Structure-activity relationships displaying by different substituents, at various positions, of thiazolidine-4-one moiety, for different biological activities.

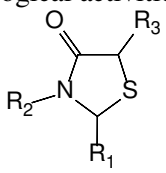

Effects	R_1	R_2	R_3
Anti-inflammatory and analgesic	dialkyl, substituted aryl or heteroaryl	substituted aryl or heteroaryl	unsubstituted, substituted benzylidene
Antitumor/anticancer	substituted aryl, *N*-substituted imine	unsubstituted, substituted aryl	unsubstituted,substituted arylidene or benzylidene
Antimicrobial	substituted aryl or hydrazinyl	substituted aryl or heteroaryl linked via amido	unsubstituted, substituted benzylidene, short alkyl group
Antitubercular	substituted aryl	unsubstituted, substituted benzamido or phenylamino	unsubstituted, short alkyl
Antidiabetic	substituted aryl	substituted aryl, aryl or benzyl amido	unsubstituted, short alkyl
Antiparkinsonian	substituted aryl or heteroaryl	azetidine, substituted amine or amido	unsubstituted
Anticonvulsant	unsubstituted, substituted aryl, imine	unsubstituted, substituted aryl	unsubstituted, substituted aryl or benzylidene
Antiviral	substituted aryl or hydrazinyl	substituted aryl or heteroaryl	unsubstituted, methyl

3.2.1. Anti-inflammatory and analgesic effects

Thiazolidine-4-one is an important pharmacodynamic heterocyclic nucleus, which when alone or when incorporated into different heterocyclic templates, has been reported to possess potent anti-inflammatory effects. As it known, the selective COX-2 inhibitors, such as rofecoxib, valdecoxib and celecoxib, are associated with serious cardiovascular events. In this context, constant efforts are being made to design new COX-2 inhibitors and multi-targeting drugs in order to obtain high selectivity to COX izoenzymes and to get positive effects on the cardiovascular system that means reduced cardiotoxicity.

In this direction were reported the design and synthesis of some new selective COX-2 inhibitors of the type of diarylheterocyclic inhibitors whith thiazolidine-4-one as central heterocyclic core (Fig. 3.3).

The compound **(22)** and bisthiazoldinones derivatives (**23**) showed a good anti-inflammatory activity and were less ulcerogenic than reference drug celecoxib (**21**) [127,136]. By, structure activity relationship studies it was designed new analogs of coxibs: 2-substituted-1,3-thiazolidine-4-one benzenesulfonamide (**24**) and 2-aryl-5-methyl-4-thiazolidine-4-one amino benzensulonamide (**25**). They showed comparable inhibitory activity against COX-1 and COX-2 with celecoxib. The literature reports showed that the 1,3-thiazolidine-4-one central core of the selective COX-2 inhibitors has the least contribution in interaction with the hydrophobic active site of COX-2 enzyme. Instead, the central core is responsible for projections of the two pharmacophore aromatic rings in the proper orientation for an efficient binding. Moreover, the heterocyclic core enhances the lipophilicity of desired compound and thus favoring the strong attachment into the lipophilic active site of COX [118,133,137–139].

Based on biological activities of indole and thiazolidine-4-ones moieties, novel anti-inflammatory drugs (**26**) were designed and synthesized, which showed better pharmacological profile than reference drugs [140].

The biological evaluation of hybrid molecules (**27**), containing a classical NSAID (ibuprofen) and thiazolidine-4-one scaffold showed a good anti-inflammatory and analgesic effect and also a safer profile compared with ibuprofen [141].

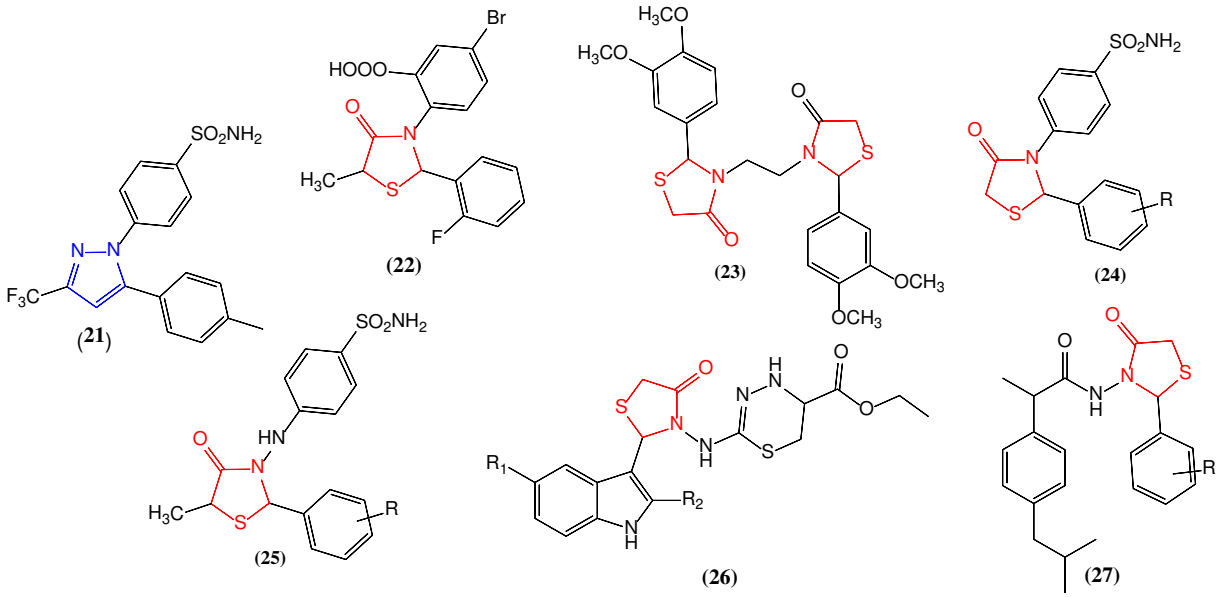

Fig. 3.3. Thiazolidinone derivatives with anti-inflammatory effects.

3.2.2. Anticancer effects

Cancer represents one of the main causes of mortality in developed countries. Despite the recent advances recorded for therapeutic strategies, which are based on surgical resection and/or chemotherapy, the outlook for patients remains poor.

The increasing diversity of small molecule libraries is an important source for the discovery of new and safer drug candidates, improving the management of cancer disease (Fig. 3.4).

A review of current literature revealed that 2,3-disubstituted-1,3-thiazolidine-4-ones (**28**) (Fig. 3.4) has been reported for their antiproliferative activity inducing cell cycle arrest and apoptosis in human renal adenocarcinoma cells (769-P) in a dose-dependent manner [142] and agains leukemia cell lines [131]. Also, it was noted that 2,5-disubstituted-1,3-thiazolidine-4-ones had antiproliferative activity in human colon adenocarcinoma cells (HT29), human colon cancer cell lines, human gastric cancer cell line and sarcoma-derived cells [143,144]. The 5-enamine-thiazolidine-4-one derivatives (**29**) were demonstrated to induce growth inhibition of all 59 human tumor cell lines [145].

Among thiazolidinone derivatives, the 3,5-disubstituted-thiazolidine-2,4-dione analogs (**30**) are one of the most promising groups in anticancer drug discovery, effectively inhibiting the growth of U937 cells (human myeloid leukaemia *cell* line) mediated through the inhibition of the Raf/MEK/ERK and PI3K/Akt signaling pathway. In turn, benzylidene-thiazolidine-2,4-dione derivatives (**31**) displayed selective cytotoxic and genotoxic activity on human lung carcinoma, breast adenocarcinoma, leukemia and colon adenocarcinoma without affecting the normal cells [146]. The 2,3,5-trisubstituted derivatives showed to induce cell growth arrest and significant cytotoxicity towards human lung and human breast cancer cultures [147].

The screening of novel 3-indolyl-thiazolidine-4-one derivatives (**32**) against breast carcinoma (MCF7) and cervix carcinoma cell line (HELA) showed significant antitumor activity against both types of carcinoma cell, compared with 5-florouracil and doxorubicin used as reference drugs [138,148]. Also, a novel series of thiazolidine-4-one with indolyl-2-one moiety (**33**) demonstrated excellent cytotoxic activities against different cancer cell line such us HT-29 (human colon cancer), MDA-MB-231 (human breast cancer) and H460 (human lung cancer). SAR studies revealed that the introduction of indolyl-2-one structure at the *C-2* position of the thiazolidine-4-one hetrocycle enhanced their antitumor activities. The side chain from the *N-3* position of the thiazolidine-4-one scaffold also enhance antitumor potency and improve the solubility and bioavailability of designed compounds [149].

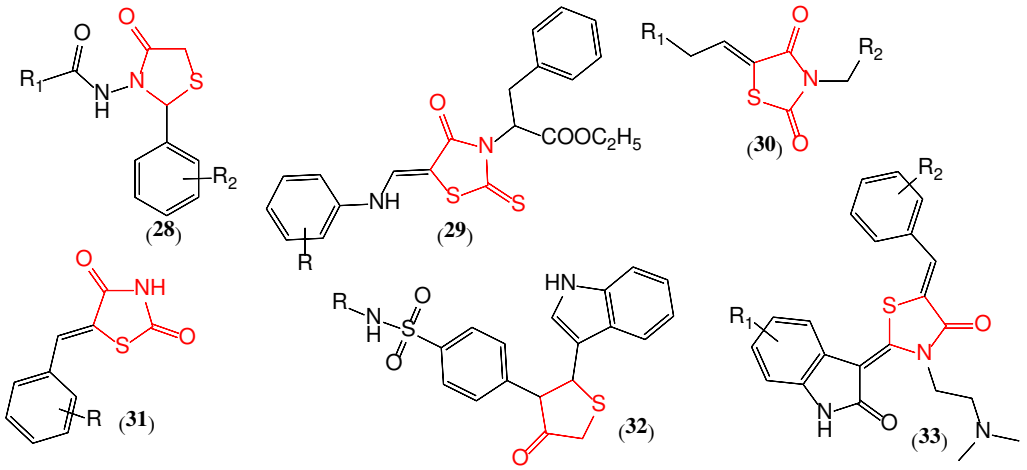

Fig. 3.4. Thiazolidinone derivatives with anticancer effects.

3.2.3. Antiparkinsonian effects

Parkinson's disease (PD) is a condition characterized by brain damage that causes an important degree of disability in evolution. Parkinson's disease is caused by the destruction in the brain of dopamine-producing neurons. Symptoms of Parkinson's disease become more and more evident as the disease progresses and are largely related to limb tremor, movement stiffness and generally slowing and motor difficulty. Exact etiology of Parkinson's has not yet been established, despite massive efforts at scientific and medical research. The incidence of the disease increases with age and most often occurs between 50 and 70 years of age, but about 4% of patients are diagnosed before the age of 50 [150].

According to national statistics there are about 70,000 people diagnosed with Parkinson's disease in Romania. However, the number of patients may be much higher, as many people suffering from this disease are undiagnosed.

The complexity of Parkinson's disease, especially in the advanced stages, represents a significant clinical, human and economic burden and the literature revealed a great interest of researchers towards increasing the quality of life of these patients and providing a realistic perspective on the problem.

For example, in a newly report from 2020 where showed by *in silico* assay that the thiazolidine-4-one derivatives bearing 1,3,4-oxadiazole moiety (**34**) revealed a stronger interaction than the standard drug at active site of Sirtuin (SIRT) 3 [151]. SIRT3 is a major mitochondrial deacetylase that has a potential therapeutic role in neuro-degenerative disease (Fig. 3.5) [152].

Also, 5-benzylidene-thiazolidinone derivatives (**35**) presented effectively improved locomotor ability in the 1-methyl-4-phenyl-1,2,3,6-tetrahydropyridine (MPTP) mice model. The molecular mechanism against MPTP neurotoxicity was explained by improving the mitochondrial dysfunction which can be a therapeutic pathway to delay the common neurodegenerative progression associated with Parkinson's disease [153].

It was showed that the substitution of thiazolidine-4-one with naphthalene scaffold (**36**) enhance significantly the anti-Parkionson's activity, protecting the diseased brain of 6-OHDA lesioned rat's model [154].

Moreover, a new series of indole derivatives which have incorporated the thiazolidine-4-one moiety (**37**) showed significantly improved anti-Parkinson's activity, such as tremor, rigidity and hypokinesia [155].

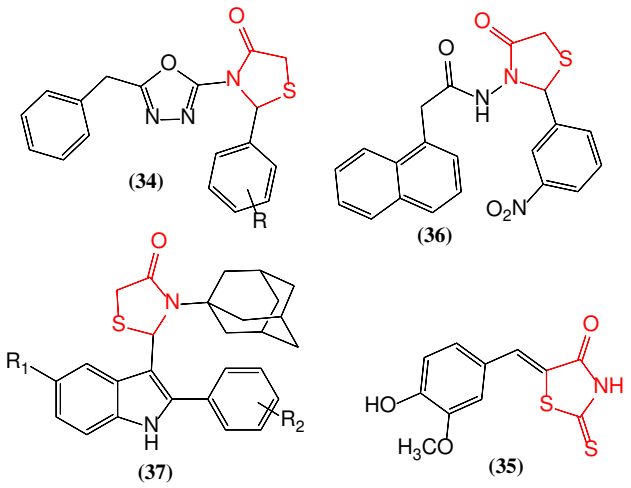

Fig. 3.5. Thiazolidinone derivatives with antiparkinsonian effects.

3.2.4. Antitubercular effects

Tuberculosis (TB) is an airborne contagious infection disease, which has a chronic evolution. In many low-income and middle-income countries, untreated or improperly treated tuberculosis continues to be a major cause of morbidity and mortality and drug-resistant. TB is a major concern in many settings. The most commonly affected are the adult population in the most productive years of life (more 25 years of age), thus having economic and social consequence [156].

For example, in Romania was reported a favorable evolution by decreasing the tuberculosis incidence with 27.9% from 1995 to 2016. Nevertheless, tuberculosis is still remaining a major public health problem in the country, with an incidence rates higher than those of other EU countries [157,158].

Due to the complexity of the tuberculosis pathology in the literature were reported many strategies in searching for new antitubercular drugs (Fig. 3.6) [159,160].

It was reported that the thiazolidindiones spiro-fused to indolyl-2-ones (**38**) can be a new class of potent and selective inhibitors of *Mycobacterium tuberculosis* protein tyrosine phosphatase B. Also, slight structural modification of this scaffold led to significantly improved pharmacokinetic profile in terms of increased compound solubility and cell permeability [161].

Literature survey revealed that the presence of 5-acetylthiazolylimino on the 2 position and of benzyliden subtituent at *C-5* position of the thiazolidine-4-one scaffold (**39**) represented a successful strategy to obtain potent antitubercular agents with broad spectrum antibacterial and antifungal activities, comparable to the reference drugs such as isonicotinylhydrazide, ciprofloxacin and amphotericin B [162]. In turn, the presence of methyl in *C-5* position and a substituted aryl moiety in *C-2* position of thiazolidine-4-one scaffold (**40**) was considered another strategy to obtain a lead antimycobacterial compound [163].

Moreover, it was demonstrated that thiazolidine-4-one derivatives (**41**) are better than thiazole derivatives for their biological properties. A stereospecific synthesized derivatives from thiazolidinone scaffold exhibited two fold enhanced antimycobacterial potency than rifampicin. Among the synthetised derivatives also examined for their antibacterial effectiveness, the thiazolidinones bearing compounds elicited again better biological response than corresponding thiazole derivatives. Likewise, antimicrobial assay pointed out that the thiazolidineones showed enhanced potency than ciprofolxacin and amphotericin B against *Staphylococcus aureus*, *Rhizopus sp* and *Klebsiella pneumonia* [164].

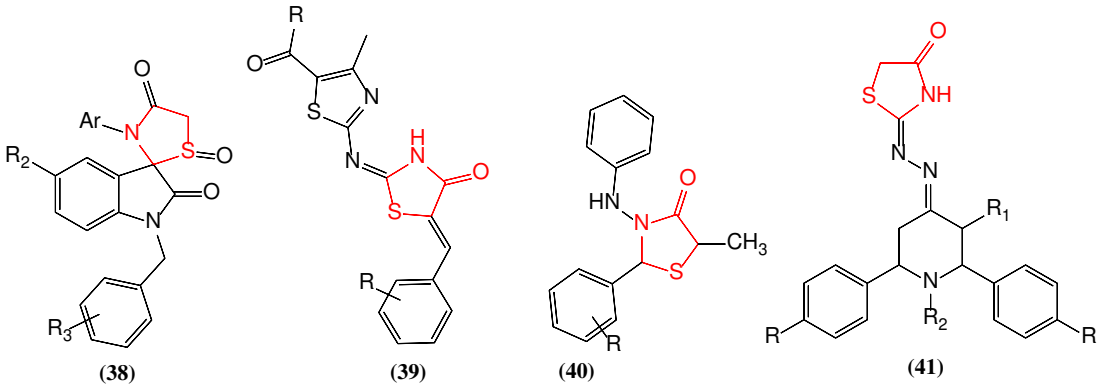

Fig. 3.6. Thiazolidinone derivatives with antitubercular effects.

3.2.5. Miscellaneous effects

Recent publications showed that the thiazolidine-4-one derivatives form a new class of matrix metalloproteinases (MMPs) inhibitors in tissue damage. The MMPs are a large family of zinc endopeptidases that have been implicated in a wide variety of biological processes (tissue repair and remodulation, cellular differentiation, embryogenesis, angiogenesis, ovulation) and pathological conditions such as atherosclerosis, cancer, brain degenerative diseases, liver cirrhosis, atherosclerosis, varicose veins [165,166]. Increased levels of these enzymes, that are responsible for extracellular matrix maintenance, have been observed in the cartilage of patients with osteoarthritis being correlated with the severity of the disease. It was proved that the thiazolidine-4-one scaffold forms the most potent MMP-13 inhibitors (**42**), as novel clinical inhibitors of cartilage degradation, with application for the treatment of osteoarthritis [167]. Moreover, it was reported that the compounds which bearing a 4-carboxyphenyl substituent at position *C-2* of the thiazolidine-4-one ring (**43**) are stronger inhibitors of MMP-9 reducing the NF-kB levels (Fig.3.7) [168].

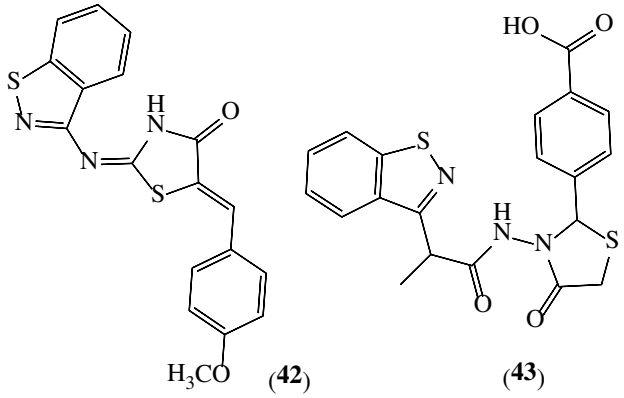

Fig. 3.7. Thiazolidinone derivatives with matrix metalloproteinases inhibition effects.

Likewise, thiazolidinone scaffold serves as core for carbonic anhydrase inhibitors. Carbonic anhydrase is an enzyme which is founded in red blood cells, pancreatic cell, gastric mucosa and renal tubules, catalyzing interconversion of carbon dioxide and carbonic acid [169,170]. New aminoindane thiazolidin-4-one derivatives (**44**) (Fig. 3.8) proved a potent inhibition activity against carbonic anhydrase I and II. The hydrophobic part (indamine moiety) is able to approach to the active side of the enzyme and the thiazolidinone ring (hydrophilic part of molecule) interacts with zinc and hydroxide from catalytically active site. These designed compounds serve as core for developing of new drugs candidates for the treatment of glaucoma, gastric duodenal ulcers, osteoporosis and neurological disorders [171].

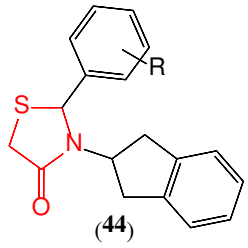

Fig. 3.8. Thiazolidinone derivative with carbonic anhydrase inhibition effects.

The follicle-stimulating hormone (FSH) is involved in ovulation and is an important target for development of novel reproductive therapies. The orally drugs antagonists of FSH can represent a new class of non-steroidal contraceptive drugs. Thiazolidinone core is a flexible and versatile moiety for development of new compounds for modulation of FSH receptor activity [131]. The pharmacological properties of thiazolidinone-containing compounds showed that minor modification to the core thiazolidine ring, at either an aryl group at position *N-3* or an acetic acid amide chain at position *C-5* resulted in differing pharmacological profiles to the parent compound, acting as FSHR antagonists (**45**) or FSHR agonists (**46**) (Fig. 3.9) [172].

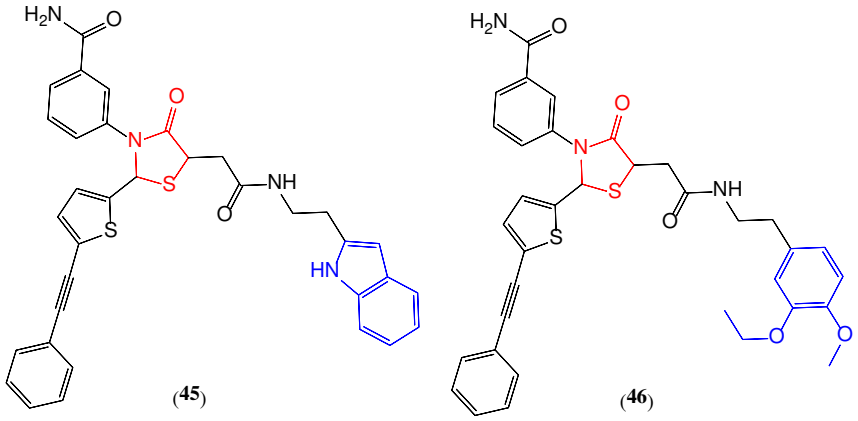

Fig. 3.9. Thiazolidinone derivatives as FSHR antagonists and agonists, respectively.

3.3. Conclusions

The new derivatives with thiazolidine-4-one scaffold exhibit a plethora of promising activities due to the chemistry of the heterocycle and to the interaction of the pharmacophoric substituents with the different biological targets.

Thiazolidine-ones remain a versatile scaffold and the potency of the synthesized compounds depends upon the nature and position of the substituents attached onto it. So, by molecular docking studies as well as the structural activity relationship studies it was reported new compounds with a better pharmacological profile and with a promising therapeutic use.

Chapter 4

Oxadiazole derivatives with therapeutic potential

The use of oxadiazole scaffold as important core for many drugs is based on several advantages [173–177]: (i) it is an essential part of the pharmacophore by favorably contributing to ligand binding; (ii) it acts as a flat aromatic linker to provide the appropriate orientation of the molecule; (iii) it induces metabolic stability, water solubility and lower lipophilicity; (iv) it can easy chemical modulates the carbonyl containing compounds such as amides, carbamates, esters and hydoxamic esters.

According to the literature data, the compounds containing the oxadiazole core have important biological effects such as anti-inflammatory [177–179], antioxidant [180,181], antidiabetic [182], anticonvulsant [183], anticancer [184], anti-tubercular [185,186], antiviral [187], antidepressant [188]. For therapeutic use there were already been approved several commercial oxadiazole based drugs such as: furamizole (strong antibacterial activity, an antibiotic) (**47**), butalamine (a vasodilator) (**48**), oxolamine (a cough suppressant) (**55**), pleconaril (an antiviral) (**50**), fasiplon (a non benzodiazepine anxiolitic drug) (**52**), raltegravir (an antiretroviral drug for the treatment of HIV infection) (**51**), nesapidil (as anti-arrhytmic) (**54**), zibotentan (as anticancer) (**53**) as well as tiodazosin (as anti-hypertensive) (**49**) (Fig.4.1.). In nature, the oxadiazole scaffold has been reported to occur in quisqualic acid (from *Quiqualis fructus*, strong agonist of (AMPA)-subtype glutamate receptor) and phidianidines A and B (from primitive marine organisms, high cytotoxicity against tumor mammalian cell lines) [189,190].

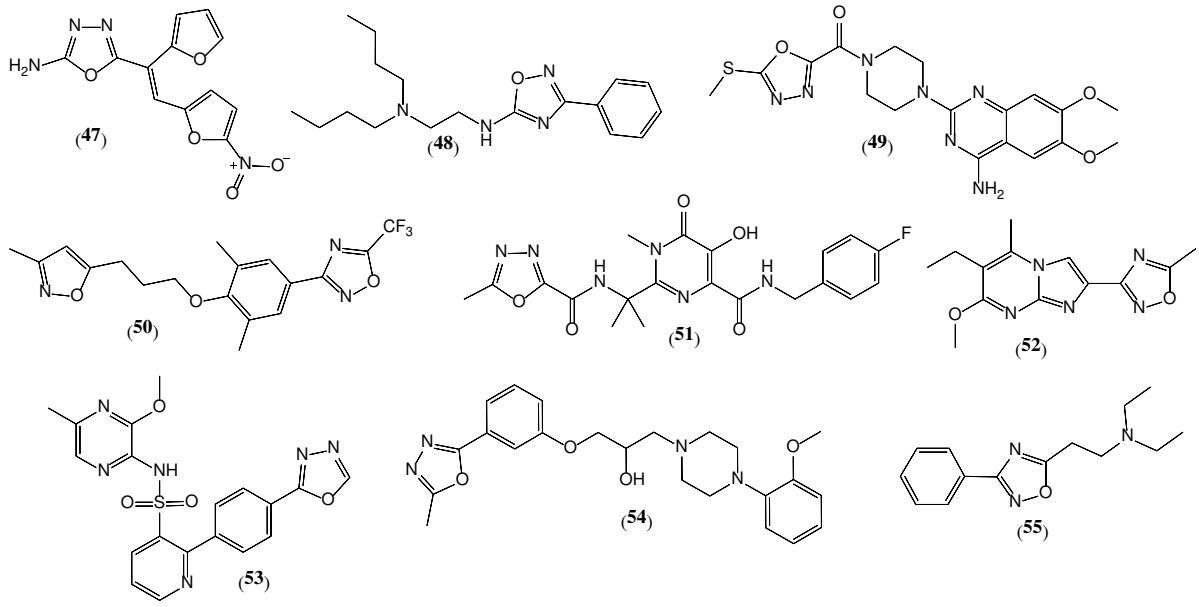

Fig. 4.1. Representative drugs that containing the oxadiazole core.

4.1. Chemistry

Oxadiazole is a heterocyclic scaffold which contains two nitrogen and one oxygen atom in a five member ring with two double bonds. Depending on the nitrogen position in the ring have been identified four different isomers such as 1,2,3-oxadiazole (**56**), 1,2,4-oxadiazole (**57**), 1,2,5-oxadiazole (**58**) and 1,3,4-oxadiazole (**59**) (Fig. 4.2). Oxadiazole rings have a conjugated diene character and a reduced aromaticity due to the presence of two nitrogens. Also, oxadiazoles display hydrogen bond acceptor properties [173,175,191].

Among the different isomers, 1,3,4-regioisomer showed an improved lipophilicity profile favoring ADMET properties of designed compounds. Moreover, it proved a plethora of pharmacological properties as reported in the literature. It was considered that the presence of toxophoric −O−C=N− linkage and the weak base characteristic may be responsible for its potent biological activities [189,192–194].

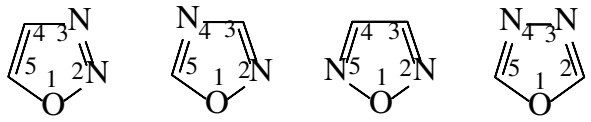

(**56**) (**57**) (**58**) (**59**)

Fig. 4.2. Chemical structure of oxadiazole isomers.

4.2. Biological activity of 1,3,4-oxadiazole derivatives

4.2.1. Anti-inflammatory and analgesic effects

A literature survey, noted that the replacement of the free carboxylic acid group of conventional NSAIDs with 1,3,4-oxadiazole heterocycle may provide new drugs with increased anti-inflammatory effects. This chemical modification resulted in the conversion of NSAIDs into balanced dual inhibitors of COX and 5-LOX, with an improved efficiency and with fewer side effects, reducing ulerogenic potential [179,194].

Moreover, it is know that the hybridization of different pharmacophoric molecule would result in a synergistic effect, especially on their ability to inhibit COX (Fig. 4.3). For example, the Mannich base-type hybrid compounds (**60**) containing an arylpiperazine moiety (analgesic and anti-inflammatory activity), 1,3,4-oxadiazole ring and pyridothiazine-1,1-dioxide core (analgesic activity) showed an improved anti-inflammatory effect by preferential binding to the hydrophobic pocket of COX-2 [177].

Chemoprevention strategy involves non-cytotoxic anti-inflammatory drugs used to inhibit or reverse development and malignization of precancerous cells. According to this clinical observation [195], it was reported the development of new class of low toxic anti-inflammatory derivatives consisting of amino acid - linked betulonic acid - oxadiazole conjugates (**61**) [196]. Usually, the conventional NSAIDs are used in cancer treatment as potent chemopreventive medicine, but their long-term administration increase the incidence of side effects (gastrointestinal, cardiovascular toxicity). Therefore, the combination of low toxic betulonic acid, known as multitarget drug, with 1,3,4-oxadiazole and different ω-amino acid leads to enhanced anti-inflammatory activity with reduced cytotoxic properties of the conjugates by NF-kB and Nrf2 pathways.

The 1,3,4-oxadiazole/oxime hybrids (**62**) were proved to be potent anti-inflammatory drugs and gastric safer, due to NO released from oxime grupe. The anti-inflammatory effects of these developed compounds were proved using carrageenan-induced paw edema model, in rats [197,198].

Literature survey revealed that the attachment of indolyl (**63**) or coumarin (**64**) scaffold to oxadiazole ring enhanced the anti-inflammatory and analgesic activity than indomethacin, used as reference drugs [199,200].

Another cited approach used to develop safer anti-inflammatory drug consists of the association of 1,3,4 oxadiazole ring with benzothiazole scaffold (**65**) [201,202]. It was proved that the design compounds have promising anti-inflammatory activity. The compounds exhibited a higher affinity to inhibit COX-2 enzyme than COX-1 and a significant edema inhibition in comparison with indomethacin used as reference drug. Also, the radical scavenging assay indicated that the 1,3,4-oxadiazole derivatives exhibited significant radical scavenging property in comparison to the reference drug, ascorbic acid. Moreover, the oxadiazole moiety in association with benzoxazole can exhibit considerable antithrombotic activity due to the inhibition of factor Xa [203].

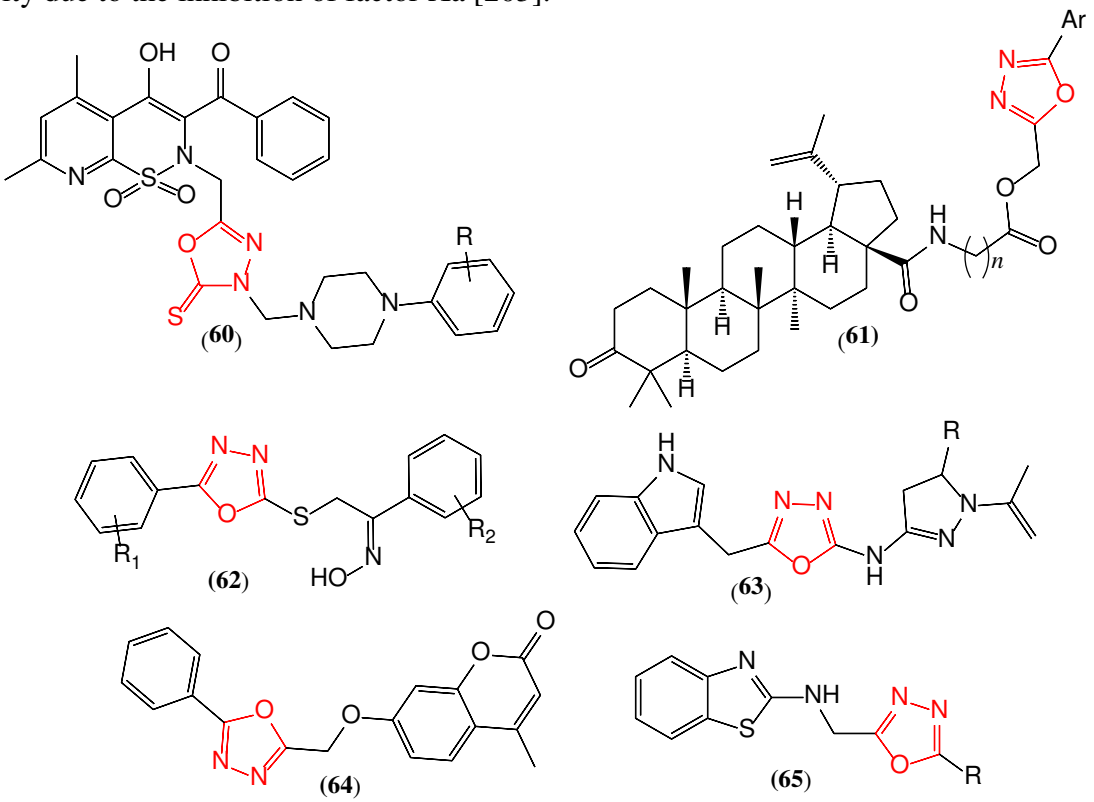

Fig. 4.3. 1,3,4-Oxadiazole derivatives with anti-inflammatory effects.

4.2.2. Antidiabetic effects

Diabetes mellitus is a chronic and progressive metabolic disorder characterized by increased levels of blood glucose due to impaired insulin secretion or liver/peripheral insulin resistance [204,205]. The latest tendency in anti-diabetic research showed an increased interest of molecular hybridization for the medicinal drug development, based on the combination of two or more pharmacophoric moieties of different biologically active substances to make a new potent hybrid molecule with enhanced efficiency (Fig. 4.4). In view of the aforementioned strategy, it was reported the new potential antidiabetic hybrid compounds which incorporate three distinct heterocyclic rings with several biological applications. So, by incorporation of benzohiazole, oxadiazole and thiazolidin-4-one heterocyclic ring systems in a single molecule resulted new hybrids (**66**) which proved antihyperglycemic effect, when administrated orally, better than pioglitazone, as standard drug. Also, the compounds showed higher inhibition of α-glucosidase (pathway widely used

in the treatment of patients with type II diabetes) when compared to the acarbose standard [182,206].

In the continuous attempt to mitigate the diabetes challenge it was found that the association between 1,3,4-oxadiazole and 6-methyl pyridine moiety (**67**) showed good inhibition of α-amylase and α-glucosidase [207].

Other potent α-glucosidase inhibitors reported are compounds based on indole and oxadiazole scaffold with *N*-substituted acetamides (**68**). Furthermore, these hybrid compounds showed low toxicity towards red blood cell membrane [208].

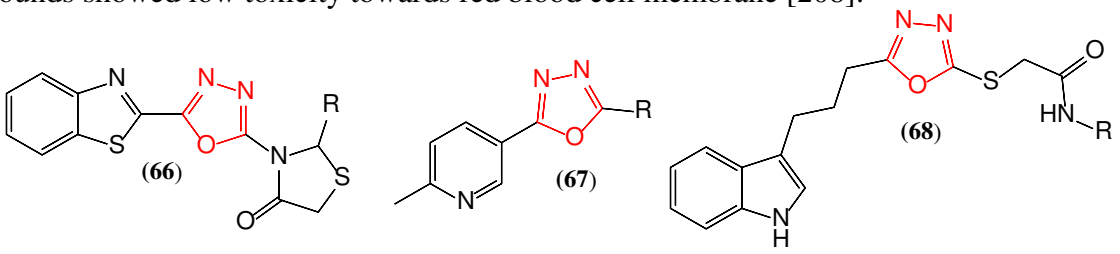

Fig. 4.4. 1,3,4-Oxadiazole derivatives with antidiabetic effects.

4.2.3. Anticonvulsant effects

The epilepsy is the second most common neurological disorder, which affects people all around the world of different ages, races, social classes and geographical location [209,210]. The etiology of seizures in epilepsy can be an injury to the brain, genetically, but most of the time, it is idiopathic [211].

1,3,4-oxadiazole has been found to be potent anticonvulsant pharmacophore (Fig. 4.5). It was reported that the introduction of different substituted benzene ring on the *C-5* position and a 4-methoxy aniline group in the 2 position of the 1,3,4 oxadiazole ring (**69**), the anticonvulsant activity was considerably increased against maximal electroshock seizure [212].

For rational design of new benzodiazepine receptor agonists with enhanced selectivity, safety and efficacy, various models were reported, which do not contain the benzododiazepine nucleus. So, it was showed that a simple non rigid structure of 2-amino-5-substituted-phenoxybenzyl-1,3,4-oxadiazole (**70**) have high receptor binding affinity on GABA/BZD receptor complex. Also, it was note a significantly increase pentylenetetrazole induced seizure threshold [213].

To allow penetration through the blood brain barrier, is was developed novel antiepileptic agents by attaching an substituted 1,3,4-oxadiazole heterocyclic core to secondary amine of nipecotic acid The developed derivatives (**71**) elicited antiepileptic effect comparable with tiagabine. Also, for these compounds it was noted a synergistic antidepressant effect, devoid of neurotoxicity and they exhibited also a good renal and hepatic safety profile, after prolong use [214].

Other effective anticonvulsant activity, by electroshock method, was reported for compounds with 2-mercapto-1,3,4 oxadiazol core [215].

In order to obtain anticonvulsant compounds with lipophilic character the oxadiazol core was coupled with benzoxazole moiety [216]. The biological screening of developed compounds (**72**) revealed anticonvulsant activity comparable to phenytoin and carbamazepine and they showed no neurotoxicity in the rotarod test.

Based on conformational studies of the current anticonvulsivant drugs, new compounds (**73**) were developed following four binding site hypotheses: (i) the presence of 5-substituted-phenyl-1,3,4-oxadiazol moiety, as hydrophobic site; (ii) urea, as hydrogen bonding site; (iii) *N*-amine, as electron donor system and (iv) another hydrophobic distal hydrocarbon moiety, which is responsible for controlling the pharmacokinetic properties of the anticonvulsant

compounds. The biological assay revealed that the compounds inhibited or attenuated seizures by promoting GABAergic neurotransmission [217].

Taking in consideration the anticonvulsant properties of oxadiazole and phenytoin, a well established antiepileptic drug, new hybrids (**74**) were synthesized and evaluated as anticonvulsant agents [218]. Preliminary screening revealed an important biological activity for tested compounds, indicating their possible efficacy in protection against generalized seizures of the tonic-clonic type. Furthermore, all of the compounds showed no significant neurotoxic effect.

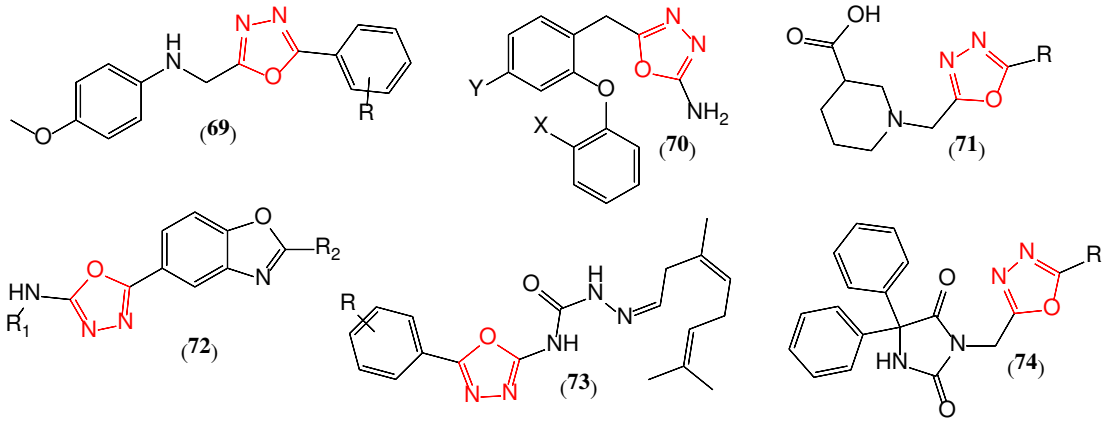

Fig. 4.5. 1,3,4-Oxadiazole derivatives with anticonvulsant effects.

4.2.4. Antioxidant effects

Reactive oxygen species (ROS) are normally formed normally in the body as products of cellular metabolism and participate in many physiological pathways. The regulation of ROS's production is controlled by endogenous antioxidant systems, such as superoxide dismutase, catalase and glutathione peroxidase, as well as exogenous antioxidants. Oxidative stress toxicity occurs because of overproduction of ROS causing significant damage of biological macromolecules, which are involved in physiological process. Thus, the rise of oxidative stress may result in structural and functional damage of cells, tissue and organs contributing to various health disorders such as cancer, diabetes, aging, heart diseases, rheumatoid arthritis and neurodegenerative disorders [219–221].

The therapeutic antioxidants, due to their ability to prevent or slow down cell damage and inhibit oxidative stress, are gaining increasing importance and interest from researchers. Due to the antioxidant potential of the 1,3,4-oxadiazole cycle, many researchers have focused their studies on the synthesis of compounds incorporating this heterocycle (Fig. 4.6).

Literature revealed that the 1,3,4-oxadiazole derivatives containing phenolic moieties (**75**) showed significant 2,2-diphenyl-1-picrylhydrazyl radical (DPPH) scavenging activity in comparison with ascorbic acid and nordihydroguaiaretic acid (as reference drugs) as a result of participation of both aromatic rings and heterocyclic ring [222]. Also, it was reported that the novel coumarin-oxadiazole hybrids (**76**) showed good to moderate antioxidant activity as compared to ascorbic acid as standard drug [223].

A series of bisoxadiazole derivatives (**77**) provided to have a very high antioxidant activity in ferric reducing antioxidant power and DPPH tests, compared to Trolox standard [224].

Considering the importance of the organochalcogen compound as bioactive molecule, it was reported a simple and efficient methodology for synthesis of substituted 1,3,4-oxadiazole derivatives containing selenium and sulfur as chalcogen substituents [225]. The free radical scavenging activity of newly compounds was evaluated using DPPH and phosphor-

molybdenum assays. The results revealed that the organosulfur analogues (**78**) have the higher antioxidant property than the standard butylated hydroxytoluene.

Furthermore, after a careful research in the literature, it was found that 2,5-disubstitued 1,3,4-oxadiazole derivatives represent the most promising strategy to obtain leading compound with antioxidant potential. This class of compounds includes substituted bis(1,3,4-oxadiazoles) (**79**) [226], 1,3,4-oxadiazole thieno [2,3-*d*]pyrimidines (**80**) [227], sulfonamide-methane-1,3,4-oxadiazoles (**81**) [228], 1,3,4-oxadiazoles containing 3-fluoro-4-methoxy-phenyl moiety (**82**) [229], 2-benzoylamino-5-hetaryl-1,3,4-oxadiazoles (**83**) [230] and 1,3,4-oxadiazoles containing benzoxazole scaffold (**84**) [203].

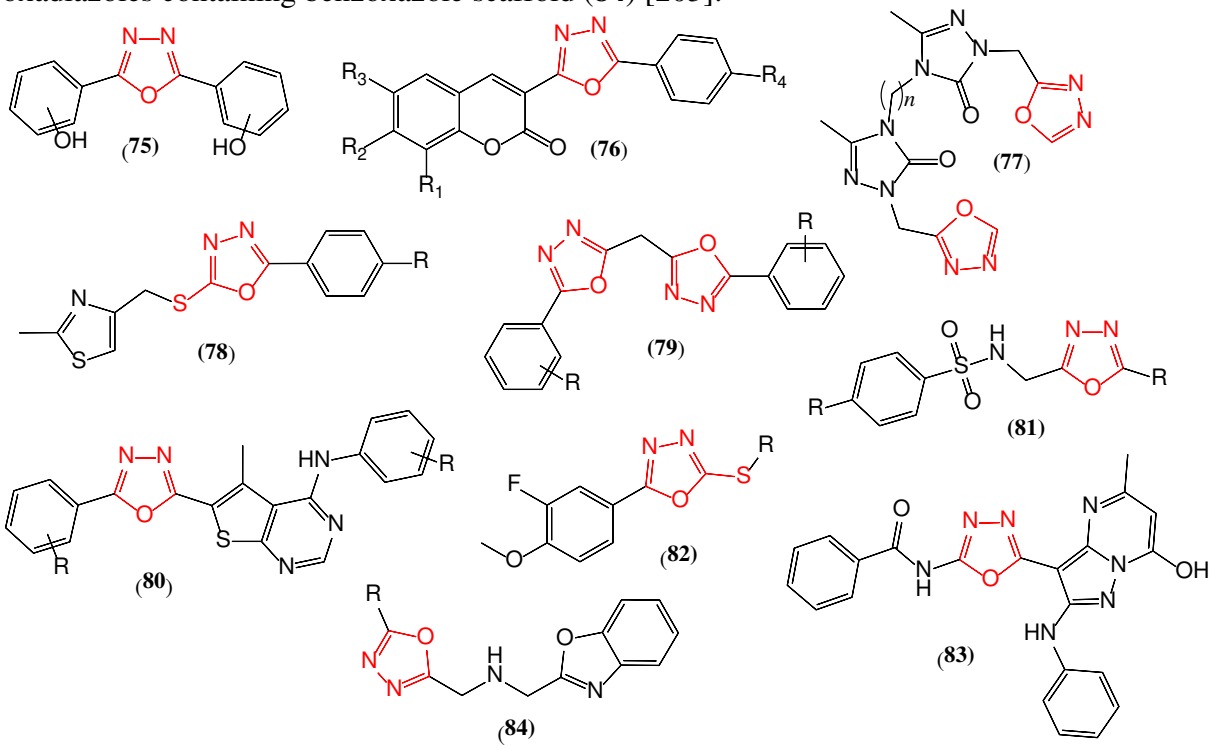

Fig. 4.6. 1,3,4-Oxadiazole derivatives with antioxidant effects.

4.3. Conclusions

Based on the results presented in the literature we can conclude that 2,5-disubstituted-1,3,4-oxadiazoles are the most potent compounds with a broad biological activity profile and improved pharmacokinetic properties.

Referring to the structure-activity relationship, in terms of the selectivity of 1,3,4-oxadiazole derivatives for COX isoenzymes, it can appreciate the following [173]:

- the presence of electron withdrawing group on phenyl ring can enhance COX-2 selectivity, compared with electron donating groups, that have a reverse effect. Moreover, the presence of *p*-Cl, *p*-NO_2 or *p*-tert-butyl also increase the COX-2 inhibition;

- COX-2 selectivity is decreased by the replacement of the phenyl ring with pyridine core;

-the COX-2 selectivity is increased by conversion of methylthio group (SCH_3) to the methyl sulfonyl group (SO_2CH_3);

-*N*-acetylation of the nitrogen atom of the oxadiazole core do not significantly affect the COX selectivity.

Chapter 5

Nitric oxide and nitric oxide releasing drugs

Nitric oxides (NO_x) have been used since ancient times. Historical records state that the Phoenicians, Romans and ancient Greeks preserved meat by using calcium nitrate due to its antibacterial properties [231–233]. Nowadays, health legislation allows the use of nitrates and nitrites, as food additives, for the preservation of meat preparations, only by maintaining well-defined limits [234]. Potassium nitrate (E252, Indian Saltpetre), sodium nitrate (E251) and potassium nitrite (E249) are the most widely used food additives as they maintain the specific color of meat preparations, delay their browning, reduce the growth of bacteria and destroy botulinum spores. The use of nitrites in meat may have direct toxic effects (such as methemoglobin formation) and indirect toxic effects (formation of nitrosamines with carcinogenic and mutagenic action).

The first medical indications were recorded in the *Diamond Sutra* (868 AD), which is considered as the oldest printed text describing Chinese medical practices. It was noted that for the treatment of angina is recommended to place under the tongue a few crystals of Indian Saltpetre [231,235].

5.1. Nitric oxide chemistry

NO is a diatomic free radical, consisting of a nitrogen atom and an oxygen atom. It is one of the smallest diatomic molecules containing a unpaired electron in its antibonding π orbital, but which remains uncharged (Fig. 5.1) [236–240]. Although NO has an unpaired electron it does not react to form a dimmer but reacts with other reactive species with harmful potential such as superoxide ion, nitrite or radical carbon/sulphur/oxygen atoms [240,241].

NO is a highly reactive molecule, with a half-life which depends on many factors [241]. For example, at a low concentration (<1 μmol L^{-1}), NO has a half-life from several minutes to one hour and thus may diffuse through multiple cell layers or over longer distances in intercellular spaces. At a high concentration, NO has a shorter half-life of the order of seconds. In addition, the half-life also depends on the local concentration in oxygen, hydrogen peroxide, protein, hemoprotein, copper or iron, cysteine and ascorbic acid [236,242]. Different NO concentrations within the same cell, variable half-life and high diffusion are attributes that make NO a paracrine-signal molecule (between close cells) and autocrine (in one cell). The NO's lipophilic character represents another significant factor in its role as messenger. High lipophilia, nonpolar character, low basicity and its small size allow the penetration and accumulation of NO in cells. Another important property is its passive transport through biological membranes.

The orbitals of the oxygen atom are lower in energy than the orbitals of the nitrogen atom. Molecular connecting orbitals are also energetically closer to the contributing orbital of oxygen than the contributing orbital of nitrogen and each antibonding orbital has an energy level closer to the contributing orbitals of nitrogen than to those of oxygen. The consequence of these energy differences makes the molecular orbital asymmetrical by the greater contribution of oxygen. Overall, the diagram shows eight electrons in the bonding orbitals and three electrons in the antibonding orbitals, so that the distribution of electrons is polarized

toward oxygen, as expected only by comparing the electronegativities between N and O atoms. Since there are eight electrons in the bonding orbitals and three electrons in the antibonding orbitals, it means that NO has 2½ bond order. The presence of the unpaired electron makes this molecule considered a molecular radical. As there is not possible to represent half of a bond in valence bond terms, NO is usually represented with a double bond, represented 4 bonding electrons. The remaining seven electrons can be shown as three lone pairs and one unpaired electron was represented on nitrogen atom.

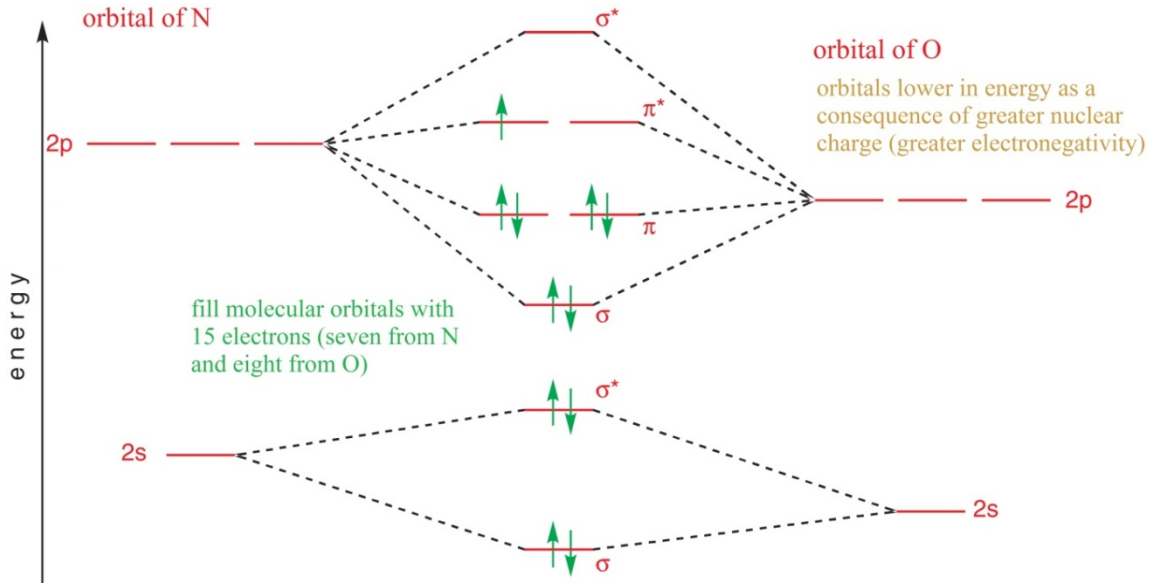

Fig. 5.1. Molecular orbital diagram for NO (adapted after [239]).

5.1.1. The reaction of NO with oxygen species

One of the most important reactions of NO is its oxidation when, in aqueous solution, NO is oxidized by O_2 to N_2O_3 (dinitrogen trioxide) and the latter dissolves in water with the formation of nitrite ion (NO_2^-) (Fig. 5.1). If NO oxidation is carried out in the air, NO_2 can dimerize with the formation of N_2O_4 and by dissolving in water leads to the generation of nitrite (NO_2^-) and nitrate (NO_3^-) ions. Nitric oxides like NO_2 and N_2O_3, can concentrate itself in hydrophobic area of cells exerting their toxic effects: N_2O_3 enhance nitrosative stress and NO_2 promote formation of toxic peroxonitrite radical ($ONOO^-$) [231,241,242].

$$2\ NO + O_2 \longrightarrow 2\ NO_2$$
$$NO + NO_2 \longrightarrow N_2O_3$$
$$N_2O_3 + H_2O \longrightarrow 2\ NO_2^- + 2\ H^+$$

Fig. 5.1. The oxidation reaction of NO.

Also, NO reacts spontaneously with superoxide radical (O_2^-) forming peroxonitrite radical ($ONOO^-$) (Fig. 5.2). At physiological pH, $ONOO^-$ is found in the form of peroxinitros acid (HOONO, pKa = 6.5) which rapidly (half-life 1 sec) decomposes to the highly reactive hydroxyl radical whereas at pH = 9 it decomposes at oxygen and nitrite anion [236,243].

$$NO + O_2^- \longrightarrow ONOO^-$$
$$ONOO^- + H^+ \longrightarrow HOONO \longrightarrow HO^- + NO_2^-$$

Fig. 5.2. The reaction of NO with superoxide radical.

Peroxonitrite radical further interacts with biological targets by oxidation of thiol group from amino acids. Moreover it is responsible for protein tyrosine nitration and lipid peroxidation [236,241].

5.1.2. The reaction of NO with heme proteins

Heme proteins play an important role in the chemistry and physiological signalling process of NO, due to its ability to make coordinate bonds with iron from the prosthetic group [244]. The NO binding on Fe^{2+} involves two interactions: (i) a σ bond can be formed by donating the unpaired electron from the NO to an *d* orbital of the metal or (ii) a link π that can be formed by the overlap between the orbital π of the antibonding orbital of the NO with an *d* orbital of the metal with close symmetry [244–246].

An example of this interaction is the activation of *guanylate cyclase (*sGC*)* by NO. This enzyme contains a prosthetic part consisting of an iron atom that is bond to a histidine and also to the four nitrogen atoms of the porphyrin system in a pentacoordinate bond system. When interaction with NO occurs, the iron-histidine bond is broken with the formation of a new Fe−NO coordinate bond. The iron atom being above the porphyrin plane allows the interaction with triphosphate guanosine (GTP) in the formed cavity with the cyclic monophosphate guanozin (cGMP) (Fig. 5.3) [247]. Important to note is that NO is the only biological ligand capable of performing this type of chemistry that allows signaling specificity for NO, as an exclusive activator of the sGC.

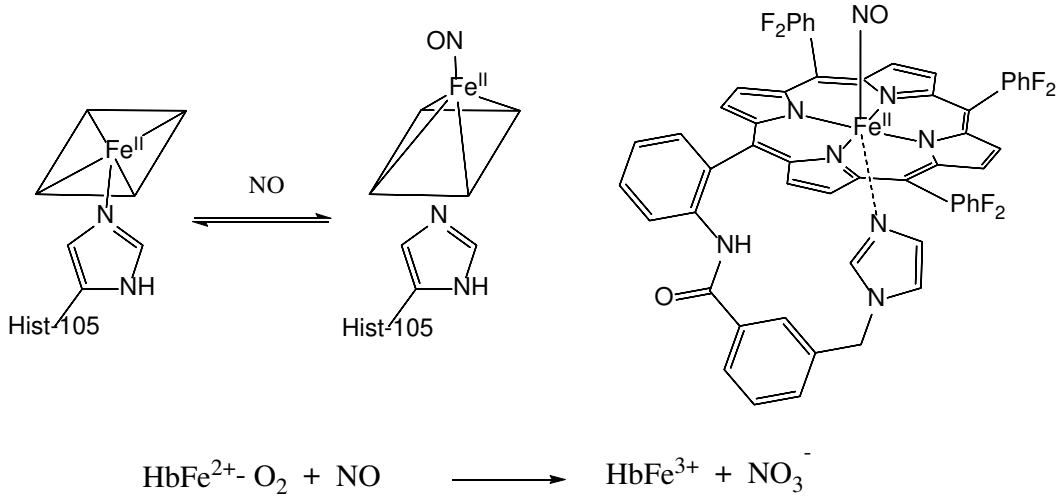

$$HbFe^{2+}\text{-}O_2 + NO \longrightarrow HbFe^{3+} + NO_3^-$$

Fig. 5.3. The reaction of NO with heme proteins.

Under physiological condition, both the hemoglobin (Hb) and myoglobin (Mb) bind the molecular oxygen forming the corresponding oxygenated ferrous forms ($HbFe^{2+}$-O_2 and $MbFe^{2+}$-O_2 respectively). In the presence of NO occurs an extremely fast NO dioxygenation reaction forming the corresponding ferric forms (methemoglobin and metmyoglobin) which inactivate of NO in human pathophysiology. (Fig. 5.3) [244,248].

5.1.3. The reaction of NO with thiol group

Dinitrogen trioxide (N_2O_3) formed by oxidation of NO can react with thiol group of peptides and proteins (RS^-) forming *S*-nitrosothiols (RS-NO), also known as thionitrites [249,250]. RSNOs allow the transportation and storage of NO in biological fluids playing important roles in several physiological functions (vasodilatation, antiplatelet aggregation,

antimicrobial) and physiopathological events (neurodegenerative diseases, apoptosis, cancer, asthma, chronic obstructive pulmonary disease, preeclampsia and diabetes).

Moreover, *S*-nitrosation reaction occurs in proteins in which the thiol is an important group for activity of glyceraldehyde-3-phosphate dehydrogenase, creatine kinase or glutathione reductase [251] (Fig. 5.4).

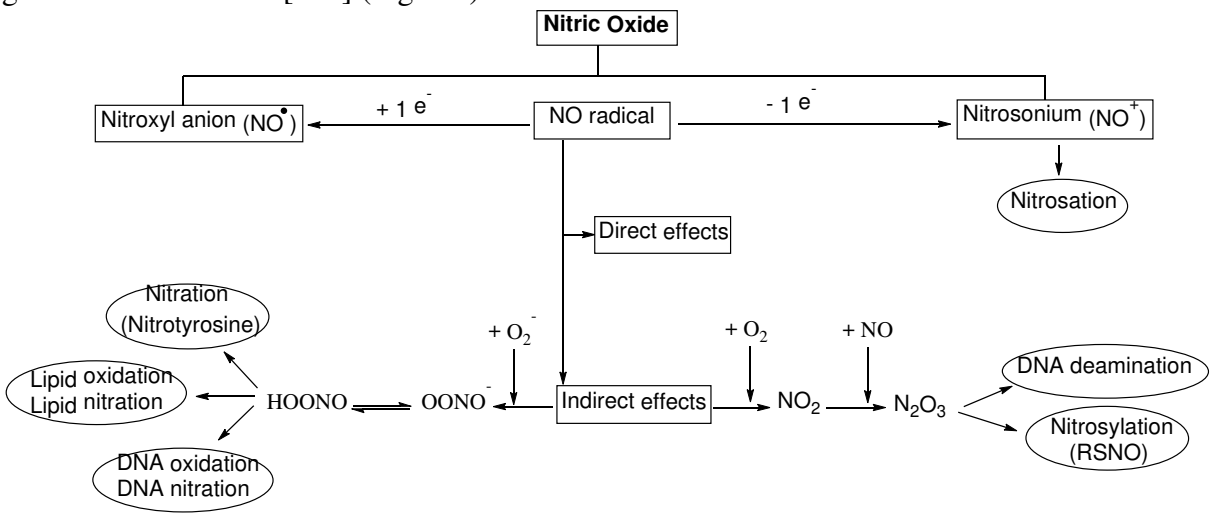

Fig 5.4. The nitric oxide chemistry (adapted after [252]).

5.2. The endogenous synthesis of NO

Synthesis of NO in biological systems involves enzyimatically or non-enzymatically pathways.

5.2.1. The enzymatic synthesis of NO

NO is mainly produced in mammalians cells through conversion of *L*-arginine to *L*-citroline by nitric oxide synthase (NOS) mediated [236,241,247,253].

In mammals, three NOS isoforms (neuronal, inducible and endothelial) have been identified and each type is characteristic of particular physiological processes [6,254].

Neuronal NO synthase (nNOS) is mainly distributed in brain being involved in the modulation of neural physiology functions (neurotransmission, neuronal development, regeneration, synaptic plasticity and gene expression regulation) as well as in the neuronal disorders caused by NO overproduction. Moreover, nNOS expression has been detected at the level of myocardium, skeletal muscle, myometer and in certain smooth muscle cells [255,256].

Inducible NO synthase (iNOS) was isolated from macrophages and its expression can be induced in a wide range of cells and tissues by proinflammatory cytokines. The high amounts of NO produced by iNOS have antimicrobial, antiviral and antitumor actions. However, aberrant iNOS induction may have detrimental consequences being involved in development of human diseases such as arthritis, multiple sclerosis, asthma, colitis, neurodegenerative diseases, psoriasis, tumor development, septic shock or transplant rejection. Besides the immune properties, iNOS-derived NO has hepatoprotective action and also is involved in wound healing [257].

Endothelial NO synthase (eNOS) is the main source of NO in the vascular endothelium. NO is the main vasoprotector molecule by vasodilatator and anti atherosclerotic activities, as well as by inhibition of platelet aggregation, of smooth muscle cell proliferation and of

leukocyte adhesion. The decreasing of NO synthesis was associated with arterial hypertension, hypercholesterolemia, smoking and diabetes mellitus [258,259].

NOS isoenzymes can be divided into calcium independent such as iNOS and calcium dependent such as nNOS and eNOS but all NOS enzymes bind to calmodulin (CaM) which is required to fully activate the enzyme. CaM serves as a Ca^{2+} sensor and for activation of nNOS and eNOS is neded a high calcium concentration (200-400 nM) while in iNOS, CaM binds to calcium at extremely low concentrations (less 40 nM) [260,261].

5.2.2. The non-enzymatic synthesis of NO

The nitrates and nitrites are generally known as undesirable residues (pollutants) of the food chain, which exert a carcinogenic potential, but also as marchers of endogenous NO metabolism (oxidative end product). However, it was reported that nitrate can be recycled *in vivo* to form nitrite and then NO and other active nitrogen oxides. This is an important alternative source of NO especially in hypoxic conditions where the classical oxygen-dependent L-aginine/NOS system is dysfunctional [253,262–264].

Bioactivation of NO_3^-, from food or endogenous sources, requires firstly reduction to NO_2^-. This conversion is mainly carried out by commensal bacteria (*Staphylococcus* spp., *Streptococcus* spp. *Rothia* spp., *Veillonella* spp) on the gastrointestinal tract or on the surfaces of the mucous membranes (Fig. 5.5).

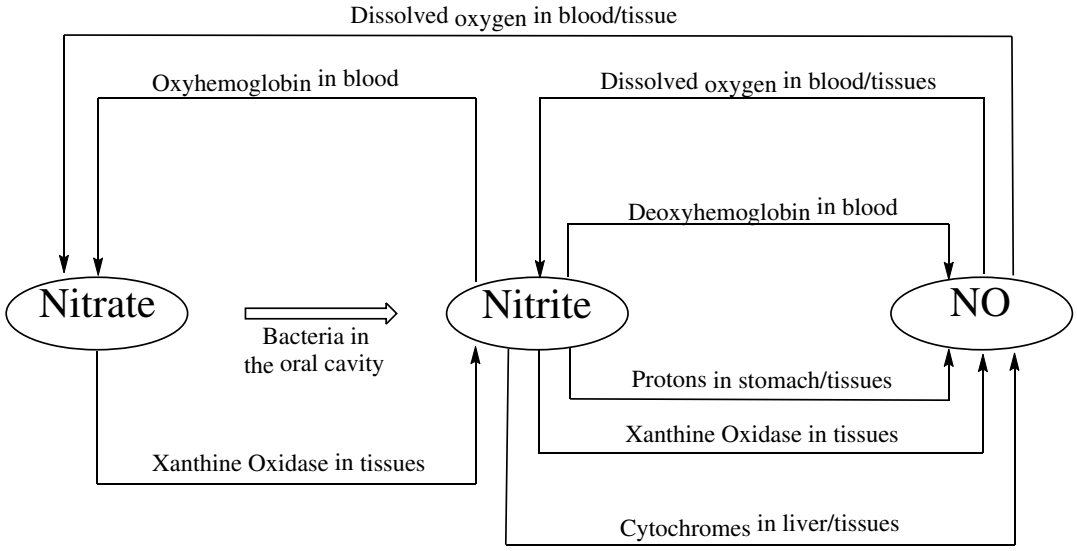

Fig. 5.5. The synthesis of NO by reduction of nitrate and nitrite (adapted after [263]).

Once NO_2^- is formed, the body has numerous mechanisms to reduce it to NO by hemoglobin, myoglobin, xanthin-oxido-reductase, eNOS, carbonic anhydrase, ascorbate, polyphenols enzymes [233,262,265].

It was reported a high concentration of NO on the stomach due to the acidic pH at this level and the high level of NO_2^- from saliva. Under acidic condition (pH = 1.5 – 3.5) the nitrite forms nitrous acid (pKa = 3.4), which is rapidly dissociates to N_2O_3 and water. Subsequently dinitrogen trioxide undergoes hemolytic cleavage to give NO and nitrogen dioxide (Fig. 5.6).

$$NO_2^- + H^+ \longrightarrow HNO_2$$
$$2\,HNO_2 \longrightarrow N_2O_3 + H_2O$$
$$N_2O_3 \longrightarrow NO_2 + NO$$

Fig. 5.6. The synthesis of NO by reduction of nitrite under acidic pH conditions.

At this gastric level, NO enhances the gastric protection. Moreover, the NO production protects against pathogenic organisms ingested with food. For example *Candida albicans* and *Escherichia coli* are much more sensitive to the concomitant action of NO and gastric acid than only to the action of hydrochloric acid [242].

The reduction of nitrite to NO in the presence of protons is greatly improved by compounds such ascorbic acid (vitamine C, AsA) and polyphenols (Ph−OH) (Fig. 5.7). In the presence of AsA, amount of nitrous acid is reduced to NO without obtaining N_2O_3 as final product. Most vegetables contain large amounts of AsA and polyphenols beside to nitrite. Moreover, the gastric mucosa actively secretes AsA. Therefore, vegetable intake ensures a very effective reduction of nitrite to NO [241].

$$2\,HNO_2 + AsA \longrightarrow 2\,NO + dehydroAsA + H_2O$$

$$HNO_2 + Ph\text{-}OH \longrightarrow 2\,NO + Ph{=}O + H_2O$$

Fig. 5.7. The synthesis of NO by reduction of nitrite under action of natural antioxidants.

5.3. The biological effects of NO

The discovery of endogenous NO synthesis in mammals and its remarkable biologic actions has led to the enrichment of biomedical knowledge in order to develop new therapeutic approaches. The research has been extensive on other organisms and it has been found that systems involving NO have been identified also in various invertebrates, plants and prokaryotes.

In 1992, NO was proclaimed "molecule of the year", marking the start of a new era in biomedicine, an area that began the study of free radicals and the discovery of new gases with biological roles [231].

Nowadays, NO is considered: (i) a "poisonous", harmful radical, which causes chemical damage to cellular proteins, lipids and DNA (inducing apoptosis and leading to necrosis or elimination of pathogenic cells), but also (ii) an important signal molecule which has a key role in a wide variety of biological processes such as immune defenses, inflammation, neurotransmission, vasodilatation, platelet adhesion, thrombosis and wound healing [254,266,267].

In the cardiovascular system, NO is released by endothelial cells and causes relaxation of smooth vascular muscle cells, thus increasing the flow of arterial blood. In the nervous system, NO is a neurotransmitter with role in the transmission of intercellular signal. Over-production of NO induces cell death and loss of neurons. Phagocyte immune cells also produce NO that they use as a weapon against cellular pathogens.

This molecule is also essential for establishing symbiotic relationships between prokaryotic and eukaryotic cells, in developing bacterial resistance to antibiotics, cellular adaptation to hypoxia in various organisms or fusion of gametes. Of biomedical importance is the overproduction of NO that occurs in certain inflammatory reactions, autoimmune conditions, cellular degeneration and in the case of ischemic lesions. Thus, the reduction of NO production becomes a therapeutic approach in the medical intervention of several pathologies. But, lack of NO synthesis leads to various conditions including compromise of defense against pathogens, endothelial dysfunction, atherosclerosis, cardiac events, hereditary motor disorders and muscular dystrophy [231,242,258].

NO is also intimately involved in regulating all aspects of our lives from waking, digestion, sexual function, perception of pain and pleasure, memory recall and sleeping [266,268]. Moreover, NO is known to have a protective effect on the gastrointestinal tract, based on its properties to stimulate gastric mucus secretion, to increase the mucosal blood flow and to inhibit the leukocyte adherence to vascular endothelium [254,269,270].

From an overview of the research undertaken, perhaps one of the deepest conclusions is that through millions of years of efficient evolution and selection, nature has the amazing ability to exploit in its beneficial even the most poisonous (harmful) molecules.

5.4. Nitric oxide releasing drugs

Nitric oxide is a very instable gas and nevertheless NO inhalation (in a blend of 0.8% NO and 99.2% nitrogen) is used in particular applications for treatment of pulmonary hypertension in adults and in neonates [271].

Most common pharmacological approaches consist in the use of NO donor drugs which are employed to ensure the stable delivery of NO for its vascular and hemodynamic effects. Their long-term use has been limited by the development of nitrate tolerance and toxicity issues [272–274].

The organic nitrates/nitrites are the most used NO donor drugs in the treatment of ischaemic syndromes related to cardiovascular diseases by coronary vasodilatation effect.

They have been used in the treatment of angina long before the role of NO on the cardiovascular system has been recognized [242]. Therefore, Brunton *et al.* recommended the isoamyl nitrite (**85**) (the first vasodilator), for the treatment of the heart diseases as well as angina pectoris [275]. Also, in 1879 Murrell was one of the first which recognized the clinical benefits of glyceryl trinitrate (**86**) (nitroglycerin) for the management of patients with angina pectoris (Fig 5.8) [231,276].

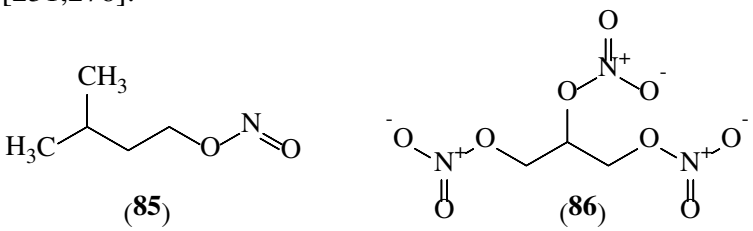

(**85**) (**86**)

Fig. 5.8. The first nitric oxide releasing drugs.

At the beginning of the 20th century it was known that NO was an important component of polluted air being considered a poisonous gas and the possibility of its internal use was never taken into account [242].

After the 1970s, numerous researches were carried out to establish the biological implications of NO. An important step was the conclusions of Ignarro *et al.* which in 1979 demonstrated that the NO donor products (sodium nitropruside and nitrosamines) induce the relaxation of the smooth vascular muscles and inhibition of platelet aggregation by the activation of guanylate cyclase [232].

The representative drugs of organic nitrates are nitroglycerin, isoamyl nitrite, isosorbide mononitrate (**86**), isosorbide dinitrate (**87**), nicorandil (**88**) si Nipradilol (**89**). (Fig. 5.9).

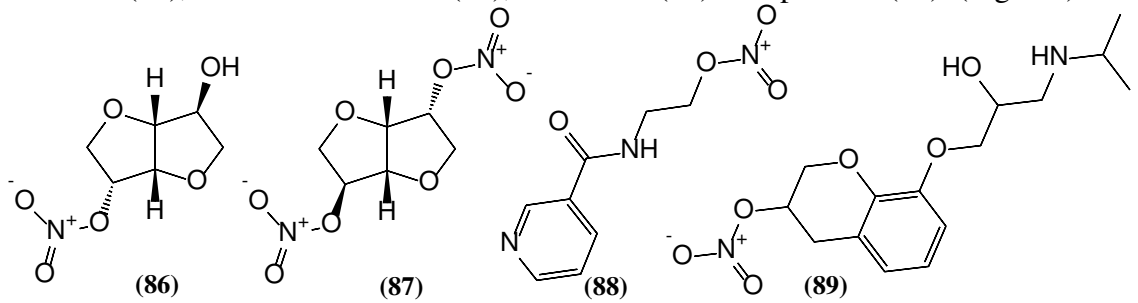

(**86**) (**87**) (**88**) (**89**)

Fig. 5.9. The structure of some organic nitrates with therapeutic use.

These products are quickly absorbed through the oral cavity and release NO by enzymatic hydrolysis. Long term uses of nitrate vasodilatators induce tachyphylaxis (by nitrate tolerance) as well as oxidative stress, endotehelial and cardiac autonomic dysfunctions as aggressive side effects. The nitrate tolerance depends by the type of nitrate and used doses. The nitrate tolerance could be reduced also by slow release of NO. Another approach consists of the supplementation of nitrate treatment with antioxidants for reducing the oxidative stress.

Diazeniumdiolates (NONOates) (Fig. 5.10) are another class of NO donors which present specific characteristics such as: (i) spontaneous decomposition in solution by first-order kinetics and (ii) amount of NO released is solely dependent only on the structure of the nucleophile, on pH and temperature but is not influenced by biological tissues and reducing agents. Moreover, these products do not develop tolerance due to that NO release is not influenced by the biological factors. At present, despite its many above mentioned advantages, diazoniumdiolate derivatives are not yet approved for clinical use but represent potential therapeutic candidates.. Some examples of NONOates are spermine –NONOate (**90**), dietyhylamineNONOate (**91**), V-PYPRO/NO (**92**)

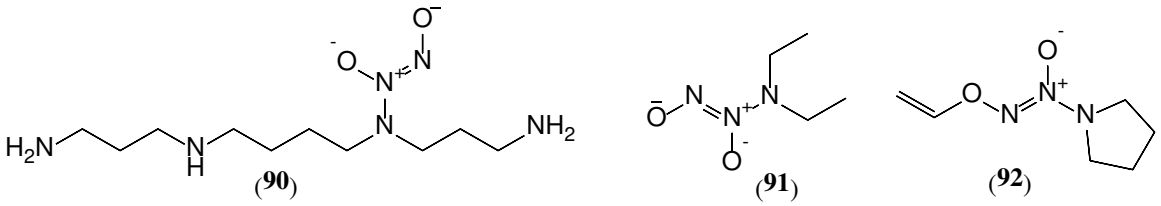

Fig. 5.10. The structure of some diazeniumdiolates.

S-Nitrosothiols (RSNO) do not have the drawbacks of the classic organic nitrates such as drug tolerance and oxidative stress induction and also, do not release NO spontaneously (Fig. 5.11.). The rate of NO release from RSNOs is influenced by transition metals (such as Cu^{+}), reducing agents (ascorbic acid), enzymes (superoxide dismutase, protein disulfide isomerase), ultraviolet light, heat, pH and the structure of the compounds (the nature and property of the substitutive R group). Endogenous *S*-nitroso-gluthation (**93**) *S*-nitrosoalbumin and *S*-nitrosoacetylcysteine (**94**) are distributed in plasma, red blood cells and tissue at different concentrations. Moreover, *S*-nitrosothiols have shown a good therapeutic efficacy as antiaggregating agents, as well as antimicrobial and antineoplastic agents, in experimental conditions. At last, RSNO hybrids such as captopril−SNO (**95**), diclofenac−SNO (**96**), tissue plasminogen activator−SNO, ameliorate the efficacy of the parent drug in their specific indications.

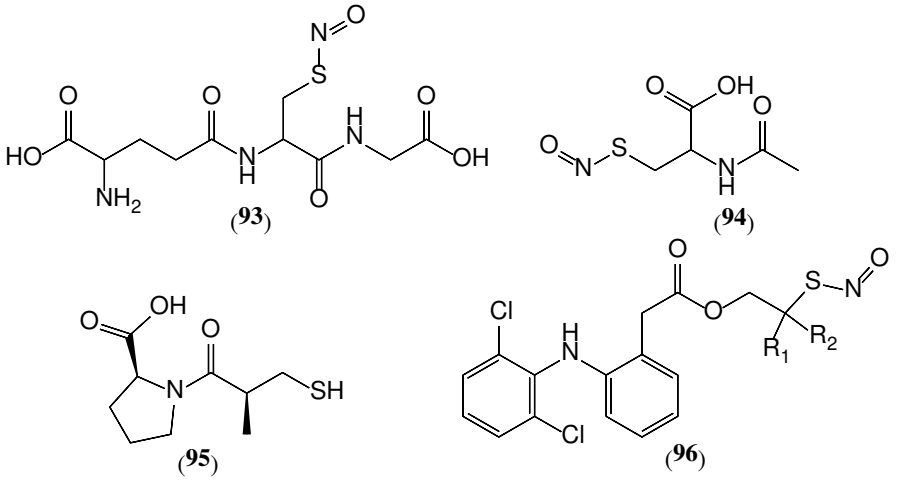

Fig. 5.11. The structure of some *S*-nitrosothiols.

Metal nitrosyl compounds are complexes that contain NO ligand which form strong coordinate bond with metal cation. Under light irradiation, one electron is promoted from the π orbital of the metal ion to the π anti-bond orbital of NO which occurs in a rapid release of NO. The most used metal NO donors have Ru or Fe as the metal center (Fig. 5. 12). Sodium nitroprusside (**97**) is a medicine used in management of acute hypertension being a potent vasodilator. It exerts its action reacting with sulfhydryl groups on erythrocytes and other proteins to produce NO. Moreover, it needs to be administered only intravenous in dextrose 5% in water and protected from light al the times.

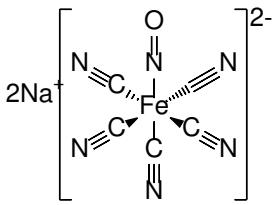

(**97**)

Fig. 5.12. The structure of sodium nitroprosside.

In order to enlarge the potential therapeutic spectrum of classical drugs, it was reported the synthesis of *pharmacodinamic hybrids* which have the characteristics of parent drugs together with those of NO.

For example, the rationale design of NO releasing steroids such as NO-hydrocortisone and NO-prednisolone was leading to the production of new compounds which ameliorated the bone demineralization. Moreover, the NO releasing NSAIDs, obtained by linking an NO-releasing moiety to different NSAIDs by means of a spacer molecule, showed to lack gastrointestinal toxicity of original NSAIDs. By large number of pharmacological studies reported, these hybrid drugs could be recommended for treating different disorder where inflammation is involved (rheumatoid disease, neuroinflammatory disease, cancer, diabetes mellitus, different pain syndromes).

5.5. Conclusions

The discovery of the role of NO in physiological and pathological process in the human body has stimulated great interest form researchers, revolutionizing many aspects of cell physiology. Therefore, despite its structural simplicity, NO has a complex chemistry, providing the free radical with extensive and varied biological action in regulation of a wide range of patho/physiological processes.

The therapeutic use is limited by its short lifespan, instability during storage and its toxic potential. In view of all these, it was reported the synthesis of NO donors in order to to stabilize this radical, until it is necessary to release it.

Definitely, the potential of nitrate therapy will become a successful new therapeutic approach once with full understanding of the kinetic release and long term toxicity of NO from each drug and of the ability to accurately target NO release to a specific organ or tissue.

PERSONAL CONTRIBUTIONS

Chapter 6

The motivation, working hypotheses and objectives of the personal research

Pharmacological strategies to suppress inflammation are focused on agonists of the glucocorticoid receptor (glucocorticoids), inhibition of the arachidonic acid cascade (NSAIDs) and on the blockade of pro-inflammatory cytokine signaling (drugs targeting tumor necrosis factor–TNFα, and interleukin IL−1 signaling) [277].

NSAIDs are drugs with common analgesic, anti-inflammatory, and anti-pyretic therapeutic properties. They inhibit COX in a wide variety of systems, ranging from microsomal enzyme synthesis to different cells and tissues. Therefore, COX inhibition has become the main action mechanism of NSADs, that is responsible for both the therapeutic and side effects of these drugs [278]. There are several different chemical structures for NSAIDs and their important characteristics are the pharmacokinetic profile, the potency and the balance of their affinity for the COX isoenzymes (COX-1 and COX-2, expecially). This balance will affect the final effects of the drugs and their safety profile [277,279]. The classical nonselective NSAIDs, that nonspecifically inhibit both COX-1 and COX-2 (e.g. indomethacin), counteracts inflammation, fever and pain. It is important to note that under long-term use, during the chronic disease, these drugs induce severe side effects, mainly gastrointestinal injury and renal irritation. On the other hand, the COX-2 selective drugs (COXIBs) although can resolve the gastrointestinal side effects, unfortunately were associated with a significantly increased of cardiovascular risk, especially under long-term use, apparently owing to an imbalance of antithrombotic and vasodilatory PGI2 and pro-thrombotic thromboxane (TxA2).

Briefly, despite the clinical benefits of NSAIDs through nonselective COX inhibition or to the relative COX-1 and COX-2 inhibition, long term use of them increase the incidence of side effects (gastrointestinal, renal, allergic skin reactions, increased risk of acute coronary syndromes, bleeding) [278,279].

A study from 2016, conducted as part of the EU funded Safety of non-steroidal anti-inflammatory drugs (SOS) project, assayed the cardiovascular safety of NSAIDs and estimated the risk of hospital admission for heart failure as results of NSAIDs use [280]. This study used electronic longitudinal patient records from seven databases from Germany, Italy, Netherlands and UK. The overall study period was from 1999 to 2012. They found that current use of any NSAID was associated with a 19% increase risk of hospital admission for heart failure compared with past use. This risk was proved for seven traditional NSAIDs (diclofenac, ibuprofen, indomethacin, ketorolac, naproxen, nimesulide, and piroxicam) and two COX-2 inhibitors (etoricoxib and rofecoxib). Additionally, the study revealed that the

increased risk of heart failure also affected patients without prior outpatient diagnosis or secondary hospital diagnosis heart failure. There is also an increasing dose dependent risk of heart failure for most individual NSAIDs. Odds ratios ranged from 1.16 for naproxen to 1.83 for ketorolac. Risk of heart failure doubled for diclofenac, etoricoxib, indomethacin, piroxicam, and rofecoxib used at very high doses (≥ 2 defined daily dose equivalents). Even medium doses (0.9-1.2 defined daily dose equivalents) of indomethacin and etoricoxib increased the risk of hospital admission for heart failure.

About gastroduodenal ulcer rate there are evidence that it range from 5% to 80% in short-term endoscopy studies and from 15% to 40% in long term users [281].

A study conducted in Portugal in 2015 revealed that the most widely used over-the-counter drugs were ibuprofen and diclofenac and that the duration of treatment was less than a week in 80% of cases [282].

The Spanish Medicines Agency (AEMPS) published in 2014 a report on the use of prescription NSAIDs in Spain between 2000 and 2012. The AEMPS reported a 26.5% increase in the use of NSAIDs in the study period. The most widely used NSAID was ibuprofen, followed by diclofenac [283].

Several studies have looked at the utilization of NSAIDs in France using field studies, clinical trials or the national claims and dispensing databases. They found that there are 5 main user population [279]:

- 3-4% of all NSAID users there are patients with chronic inflammatory disease, who used NSAIDs just about every day; the mean age is 54.4;
- 13% of users suffer from the osteoarthritis; duration of prescription varies between 1 to 6 mounth; the mean age is 66;
- 30% of users suffer from back pain; the mean prescription is 15 days and the mean age is 52;
- 15% of users have osteoarticulare symptoms; the mean prescription is 13 days and the mean age is 49;
- non rheumatic indications (such us flu symptoms, headache, toothache or menstrual pain) represent 36% of users with a mean age of 43 and a prescription duration of 8.8 days.

Classical drugs have been designed with the aim of targeting a single biological entity (one target) with high selectivity, to avoid any unwanted effects through missing targeting other biological targets (off-target). Such a "one-target-one-disease" approach led to the development of several valuable drugs (e.g. inhibitors of COX, used for the therapy of inflammation, fever and pain).

It is know that a single disturbance in the physiology of the cell (signaling pathway or metabolism) it often results in a cascade of complex effects. However, a single modification during the events chain it is not enough to reestablish the initial equilibrium in the cell.

To improve clinical efficacy of NSAIDS, two platform strategies are currently emerging.

The first one is drug combination, in order to reduce the side effects of NSAIDs. For exemple, NSAIDs-induced gastroduodenal ulcers can be prevented by using of GI protective agents like misoprostol, H_2 receptor antagonists or proton pump inhibitors. This strategy is used in aproximatively 20% of elderly patients [284]. Intake of acetylsalicylic acid (aspirin) together with paracetamol (acetaminophen) and caffeine apparently relieves pain more efficiently than the single drugs. However, there are three major drawbacks for this combination. First, patient compliance is reduced when multiple medications are prescribed, especially for the treatment of asymptomatic and chronic diseases. Second, only explicit key targets associated with the respective disease are exploited but not the majority of disease-

relevant signaling pathways. Thus, potential synergistic effects of inhibiting multiple pathways, perhaps only moderately to readjust homeostasis remain unrevealed. Third, very complex pharmacokinetics might result, which make extensive clinical trials necessary to estimate benefit, side-effects and potential drug–drug interactions. Although the compliance issue can be resolved by combining individual drugs in a single pill (multi-component drugs), the others drawbacks remain. In addition, although the benefits of interfering with multiple targets are unquestioned for complex diseases like inflammation, the poly-pharmacological strategy remains a matter of dispute.

The second strategy assumes that a single compound can hit multiple targets (single drug-multiple targets). Referring to this strategy, the development of NSAIDs involved an interesting evolution from nonselective agents for COX (e.g. indomethacin) to selective COX-2 inhibitors (e.g. celecoxib) and finally designing multi-targeting agents to develop new classes of safer NSAIDs such as nitric oxide donating nonsteroidal anti-inflammatory drugs (NO-NSAIDs), dual inhibitors of COX-2 and 5-LOX.

NO-NSAIDs are a new class of anti-inflammatory drugs developed with the aim to reduce gastric-ulcerations through releasing of NO. Afterward, the same linking strategy was applied to selective COX-2 inhibitors (COXIBs) to counteract the adverse cardiac events. Naproxcinod (nitronaproxen) has been the only NO-NSAID so far, extensively investigated in clinical trials, however failed to gain approval by US FDA due to lack of long-term controlled studies [285].

Dual COX-2 and 5-LOX inhibitors supposed to possess greater efficacy with reduced side effects of selective COX-2 inhibitors. This is the most adapted strategy to offer not only improved anti-inflammatory profile but also enhanced safety for traditional NSAIDs. For example, licofelone (ML3000), in preclinical and in clinical trials, showed an anti-inflammatory effect comparable with conventional NSAIDs, but the gastrointestinal safety was improved. Currently, it is tested in phase III for treatment of osteoarthritis for confirming the rationale behind the intended design and application [286].

Literature gives us many proofs that sustain that a drug, which operates on several therapeutic targets can subtly influence the activity of many enzymes. Such, it is possible to develop new therapeutic strategies which are more complex and efficient for establish the cell homeostasis.

Therefore, the dual inhibition of COX/LOX pathways and increase of NO level on the inflammatory site may be a new therapeutic approach in the case of inflammatory diseases.

The goal of the doctoral research was to prove the improved pharmacological and safety profile of some new indomethacin nitric oxide donors (indometacin-NO donors) which were developed as new therapeutic multi-targets strategy, able to inhibit COX pathways and to release NO in the gastric medium.

More specific, the main objectives of the research were the design and synthesis of some new nitric oxide-releasing indomethacin derivatives with 1,3-thiazolidine-4-one and 1,3,4-oxadiazole scaffold, respectively, as well as biological evaluation in terms of COX isoenzyme inhibition selectivity, anti-inflammatory and antioxidant effects and also their capacity to release NO.

The arguments that justify the importance of this research are the followings:

- the inflammation is a complex patho/physiological process which is responsible for many widespread diseases, such as rheumatoid arthritis, osteoarthritis, atherosclerosis, diabetes, neurodegeneration, allergy, infection and cancer. Drug development during the past decades made efforts to obtain potent and specific drugs focusing on a limited number of key targets considered crucial for disease.

Unsatisfactory safety and efficacy profiles of them need the development of ***multi-target agents*** to treat complex inflammatory diseases.

- the multi-target strategy (single drug–multiple targets), which is based on rationale design of new chemical entities as new anti-inflammatory potential drugs, is able to hit multiple targets (polypharmacolgy) in order to enhance efficacy and/or improve safety profile of classical drugs. This approach could be subject for ***technogical transfer*** to pharmaceutical companies interested to develop new innovative drugs.

The design of the indomethacin-NO donors was based on *in silico* studies (quantitative structure-activity relationship), using computational methods. Ligand-based computational methods are able to determine essential structural features for a set of bioactive ligands and indentify the structure of the potential lead molecule. These computational approaches that combine ligand and structure activity relationship methods provide the most comprehensive information about drug-target interaction and significantly increase the success rate of the rational drug design.

The related activities of the research were the following:

- the design and synthesis of some new nitric oxide-releasing indomethacin derivatives with 1,3-thiazolidine-4-one scaffold (NO-IND-TXDs);
- the design and synthesis of some new nitric oxide-releasing indomethacin derivatives with 1,3,4-oxadiazole scaffold (NO-IND-OXDs);
- nuclear magnetic resonance (^{1}H NMR, ^{13}C NMR, ^{1}H,^{13}C-HSQC) and mass spectroscopy (HRMS) analysis, to prove the chemical structure of all synthesized derivatives (intermediary and final);
- *in silico* docking study for interaction between novel nitric oxide-releasing indomethacin derivatives and COX isoenzymes;
- *in silico* ADME-Tox study to predict the pharmacokinetic and toxicity profile of the synthesized compounds;
- *in vitro* anti-inflammatory activity evaluation, based on the study of the interaction of nitric oxide-releasing indomethacin derivatives with non enzymatic protein, in order to evaluated the protection against protein denaturation;
- *in vitro* antioxidant activity evaluation based on 2.2-diphenil-1-picrylhydrazyl (DPPH) radical scavenging assay;
- *in vitro* nitric oxide release assay using a modified Griess colorimetric method.

Chapter 7

Synthesis and characterization of novel nitric oxide-releasing indomethacin derivatives

The synthesis strategy for proposed nitric oxide-releasing indomethacin (NO-IND) derivatives (**9a-s; 11a-m, t-v**) (Fig. 7.1) is designed in accordance with the retrosynthetic criteria analysis, which includes the lowest possible number of interconversions and involves the association of 3 scaffolds, as follows:

- ✓ an indol scafffold (indomethacin) (IND, synthon A);
- ✓ an 1,3-thiazolidin-4-one (TZD, synthon B) or 1,3,4-oxadiazol-2-thiol (OXD, synthon C) scaffolds;
- ✓ a nitric oxide (NO) donor nitrate ester connected to an aromatic linker, substituted with different electron-withdrawing and electron-donating groups (synthon D).

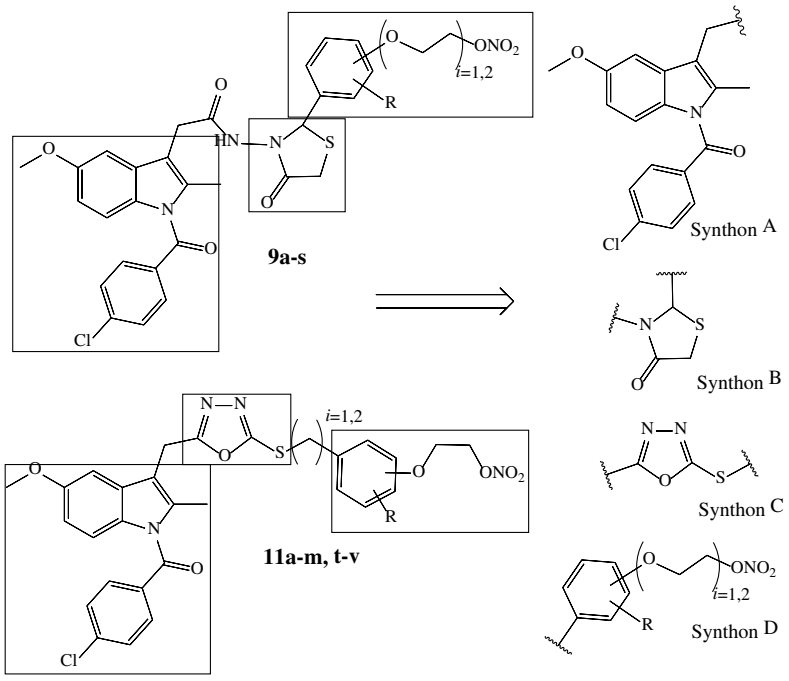

Fig. 7.1. The structure of the designed NO-IND derivatives.

To obtain the designed compounds, a convergent type synthesis, which involves several steps, was applied:

- ✓ synthesis of NO-donor linkers, by the metathesis reaction of various primary phenoxy-alkyl halides with silver nitrate;
- ✓ synthesis of indomethacin hydrazide by a peptide coupling reaction;
- ✓ synthesis of indomethacin hydrazone derivatives by reaction of indomethacin hydrazide with nitrate ester benzaldehyde derivatives;

- ✓ synthesis of the nitric oxide-releasing indomethacin derivatives containing a 1,3-thiazolidin-4-one scaffold (NO-IND-TZDs) by reaction of indomethacin hydrazone derivatives with mercaptoacetic acid, using an annelation reaction;
- ✓ synthesis of nitric oxide-releasing indomethacin derivatives containing a 1,3,4-oxadiazole scaffold (NO-IND-OXDs) by alkylation of indomethacin-oxadiazole derivative (IND-OXD) with (halidealkyl)phenoxy nitrates.

The general scheme for synthesis of the novel nitric oxide-releasing indomethacin derivatives is presenting in Fig. 7.2.

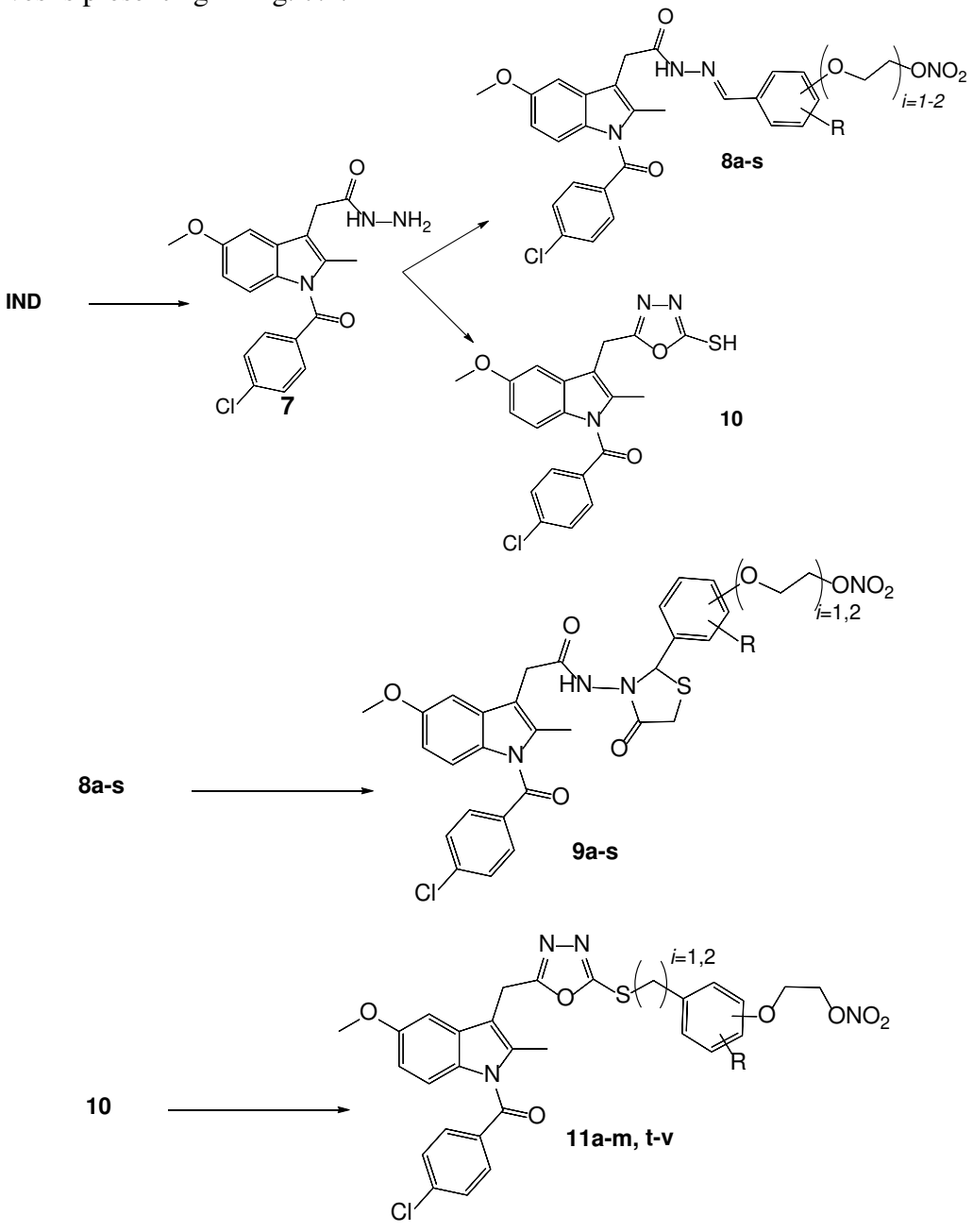

Fig. 7.2. The general scheme of the synthesis of NO-IND derivatives.

7.1. Materials and methods

All solvents used for chemical synthesis were of analytical grade or HPLC *p.a*. quality unless otherwise stated. The anhydrous solvents needed for certain reactions have been distilled or dried according to standard procedures prior to use: dichloromethane has been distilled under P_2O_5 and acetonitrile has been dried on cartridge by a GT S100 station.

The progress of the reaction and purity of synthesized compounds were monitored by thin layer chromatography (TLC), using 2×5 cm pre-coated silicagel 60 F254 aluminum plate (Merck) and UV lamp exposure at 254 nm. Column chromatography purifications are performed on silicagel 60 (0.063−0.200 mm, Merk) or on C18 AIT 40-60 m silicagel.

The ^{1}H NMR (250 MHz or 400 MHz), ^{13}C NMR (63 MHz or 101 MHz) and 19F NMR (376 MHz) spectra were recorded on Bruker Avance DPX250 (250, 131 MHz) or Bruker Avance II (400 MHz) spectrometer. Chemical shifts (δ H, δ C) and coupling constant values (*J*) are given in *ppm* and *Hz*, respectively. An internal standard of tetramethylsilane (TMS, δ H = 0, δ C = 0) in $CDCl_3$ and DMSO-d6 was used. The multiplicity of signals is represented as follows: singlet (s), doublet (d), doublet of doublets (dd), doublet of doublets of doublets (ddd), triplet (t), triplet of doublets (dt), quartet (q), hexuplet (h), multiplet (m). Chemical displacements for hydrogen and carbon atoms have also been confirmed by 2D-RMN experiments: gCOSY (gradient-selected Correlation Spectroscopy), gHMBC (gradient-selected Heteronuclear Multiple Bond Coherence), gHMQC (gradient-selected Heteronuclear Multiple Quantum Coherence).

High resolution mass spectrometry (HRMS) has been made on a Bruker maXis mass spectrometer within the "Research Federation" platform between ICOA and CBM (FR2708). The samples were ionized by electrospray ion source (ESI), using N_2 for nebulization (pressure of 0.6 bar) and drying (flow of 7 L/min, temperature of 200 °C). The capillary potential was set at 4500 V and collision cell RF at 1800.0 Vpp. The ion polarities were positive and were analyzed using scanning range between 50–2500*m/z*. Melting points (m.p.) were measured on a Kofler heating bench.

The results obtained, based on the applied spectral analyses, have confirmed the structure of the new compounds and the intermediates used and implicitly the performed syntheses.

7.1.1. Synthesis of NO-donor linkers

In order to ensure appropriate conjugation between various NO-donor linkers and IND, the nitrate ester moiety was inserted into different substituted phenoxy-alkyl structures which posses a carbonyl or a benzyl halide function, suitable for final synthesis stage of the desired nitric oxide-releasing indomethacin (NO-IND) derivatives.

7.1.1.1. Procedure for the synthesis of the halide-alcoxy-benzaldehyde derivatives

To a solution of hydroxyl-benzaldehydes (**1a-p, t, u)** (1.0 Eq.) in acetonitrile (150 mL), 1,2-dibromoethane or bis(2-chloroethyl)ether (10.0 Eq.) and potassium carbonate (2.0 Eq.) were added, according to the method reported in the literature [287–289], which was adapted to our synthesis in terms of the ratio of reagents, solvent, time of reaction, purification method. The mixture was stirred overnight under reflux and progress of reaction was monitored by TLC. After cooling to room temperature, distilled water (4 × 50 mL) was added and the mixture was extracted with diethyl ether (50 mL). The combined organic layers were washed with brine (50 mL), dried over anhydrous magnesium sulfate and concentrated under reduced pressure. The crude products were purified by flash chromatography (silicagel, petroleum ether/ethyl acetate) to give the pure products (**2a-s, t, u**).

7.1.1.2. Procedure for the synthesis of the nitrate ester benzaldehyde derivatives

To a solution of the appropriate halide-alcoxy-benzaldehyde derivatives (**2a-s**) (1.0 Eq.), in acetonitrile (50 mL), silver nitrate (1.5 Eq.) was added and the mixture was stirred under reflux and darkness for approximately 12 h, according to the method reported in the literature [290–292], which was adapted to our synthesis in terms of the ratio of reagents, solvent, time of reaction, purification method. Then brine was added to precipitate the excess of silver nitrate. After filtration, the mixture was extracted with diethyl ether (2 × 50 mL). The combined organic layers were washed with water (50 mL) and brine (50 mL), dried over anhydrous magnesium sulfate, filtered and concentrated under reduced pressure. The crude products were purified by flash chromatography (silicagel, petroleum ether/ethyl acetate) to give the pure products (**3a-s)**.

7.1.1.3. Procedure for the synthesis of the (bromoethoxy)aromatic alcohol derivatives

To a solution of appropriate benzaldehyde (**2a-m, t, u)** (1.0 Eq.), in dry THF (30 mL), sodium borohydride (1.1 Eq.) was added at 0°C and the mixture was stirred at room temperature for 12-24 h, according to the method reported in the literature [293–296]. Then, the excess of sodium borohydride was quenched by addition of 1M HCl and the organic mixture was extracted with EtOAc (2 x 30 mL). The combined organic layers were washed with water and brine, dried over anhydrous magnesium sulfate, filtered and concentrated under reduced pressure. To obtain 2-(4-(2-bromoethoxy)phenyl)ethanol (**4v)**, 4-(2-hydroxyethyl) phenol (**1v)** (1.0 Eq.) was reacted with 1,2-dibromoethane (10.0 Eq.) in CH_3CN (50 mL for 15 mmol scale) in presence of potassium carbonate (2.0 Eq.). The resulting mixture was heated to reflux for 20 h. After cooling to room temperature, distilled water (100 mL) was added and the crude product was extracted with diethyl ether (3 × 50 mL). The combined organic layers were washed with distilled water (50 mL), brine (50 mL) and dried over anhydrous magnesium sulfate.The crude products were purified by column chromatography on silicagel with petroleum ether/ EtOAc or CH_2Cl_2/CH_3OH to give the pure compounds **4a-m, t-v**.

7.1.1.4. Procedure for the synthesis of the (hydroxyalkyl)phenoxy nitrate derivatives

To a solution of the appropriate (bromoethoxy)aromatic alcohol derivatives (**4a-m, t-v)** (1.0 Eq.), in acetonitrile (50 mL for 10 mmol scale), silver nitrate (1.5 Eq.) was added. The mixture was stirred under reflux and darkness for approximately 12 h, according to the methods reported in the literature [54,291,292,297–301], which were adapted to our synthesis in terms of the ratio of reagents, solvent, time of reaction, purification method. At the end of reaction, brine was added to precipitate the excess of silver nitrate. After filtration through celite, the mixture was extracted with diethyl ether (2 × 50 mL). The combined organic layers were washed with distilled water (50 mL) and brine (50 mL), dried over anhydrous magnesium sulfate, filtered and concentrated under reduced pressure. The crude products were purified by flash chromatography (silicagel, petroleum ether/EtOAc) to give the pure products **5a-m, t-v**.

7.1.1.5. Procedure for the synthesis of the (halidealkyl)phenoxy nitrate derivatives

To a stirred solution of the appropriate (hydroxyalkyl)phenoxy nitrate derivatives (**5a-m**, **t**, **u)** (1.0 Eq.) in dry CH_2Cl_2 (35 mL for 7 mmol scale), 10 mL solution of thionyl chloride (1.2 Eq.) and benzotriazole (BTA, 1.2 Eq.) in dry CH_2Cl_2, were slowly added, into small portions, according to the methods reported in the literature [302,303], which were adapted to

our synthesis in terms of the ratio of reagents, solvent, time of reaction, purification method. Before the reaction is complete, benzotriazole hydrochloride started separating out as a solid. Reaction mixture was stirred further for 20-30 min and after that the solid was filtered off. The filtrate was successively washed with distilled water (2 × 50 mL) and brine (50 mL). The combined organic layers were dried over anhydrous magnesium sulfate, filtered and concentrated under reduced pressure to get a crude product, that was purified by flash chromatography (silicagel, petroleum ether/ EtOAc) to give the pure products **(6a-m, t, u).**

To obtain 2-(4-(2-iodooethyl)phenoxy)ethyl nitrate (**6v)**, to a solution of (hydroxyethyl)phenoxy)ethyl nitrate (**5v)** (1.0 Eq.) in CH_2Cl_2 (30 mL), imidazole (1.3 Eq.), triphenylphosphine (PPh_3, 1.3 Eq.) and iodine (1.3 Eq.) were sequentially added at 0°C, according to the method descried in the literature [304–306]. The resulted mixture was stirred at room temperature for 6 h and reaction was quenched by addition of 10 mL of saturated aqueous $Na_2S_2O_3$ solution. The organic layer was separated and washed with water (2 × 50 mL) and brine (50 mL). The combined organic layers were dried over anhydrous magnesium sulfate and the solvent was removed under reduced pressure. The crude product was purified by flash column chromatography to give the pure product.

7.1.2. Procedure for the synthesis of 2-(1-(4-chlorobenzoyl)-5-methoxy-2-methyl-1*H*-indol-3-yl)acetohydrazide

Method 1. To a solution of IND (1.0 Eq., 0.57 mmol) in absolute ethanol (10 mL), H_2SO_4 (1.0 Eq., 30 μL, 96%) was added and the resulting mixture was heated at reflux for 6 h. The progress of the reaction was monitored by TLC using CH_2Cl_2/MeOH (9.9/0.1) as eluent. After cooling to room temperature a saturated solution of $NaHCO_3$ (5 mL) and distilled water (4 × 20 mL) were added and the mixture was extracted with AcOEt (2 × 20 mL). The combined organic layers were washed with brine (20 mL), dried over anhydrous magnesium sulfate and concentrated under reduced pressure. The resulted IND ester was purified by flash chromatography (silicagel, petroleum ether/ethyl acetate) to get 0.14 g of the final product as white solid in 63% yield. Then, to a solution of IND ester in absolute ethanol, hydrazine hydrate (1.5 Eq.) was added and the mixture was stirring at reflux for 5 h. The progress of the reaction was monitored by TLC using petroleum ether/AcOEt (6/4) as eluent and was observed an intense degradation which made no possible to isolate the desired hydrazide

Method 2. To a suspension of IND (1.0 Eq., 45.5 mmol) in acetonitrile (300 mL), hydroxybenzotriazole (HOBt, 1.1 Eq., 54.6 mmol) and 1-ethyl-3-(3-dimethylaminopropyl) carbodiimide (EDC, 1.0 Eq., 54.6 mmol) were added and the mixture was stirred at room temperature for 3 h, according to the method reported in the literature [307,308], which was adapted to our synthesis in terms of the ratio of reagents, solvent, time of reaction, purification method. The resulting mixture was then slowly added drop wise, at 0-5°C, to solution of hydrazine (2.0 Eq., 91 mmol) and cyclohexene (1 mL) in acetonitrile (200 mL). The mixture was kept at this temperature for 1 h and then was diluted with distilled water (500 mL), when indomethacin hydrazide (**7)** is formed, which was collected by filtration.

7.1.3. Procedure for the synthesis of the indomethacin hydrazone derivatives

To a suspension of indomethacin hydrazide (**7**, 1.0 Eq.) in absolute ethanol, the corresponding nitrate ester benzaldehyde (**3a-s,** 1.1 Eq.) was added in presence of catalytic amount of hydrochloric acid. The mixture was stirred for 12 h under reflux when an extensive precipitated was formed. After cooling at room temperature, the precipitate was collected by filtration, washed with cold water (80 mL), ethyl ether (30 mL), dried over anhydrous magnesium sulfate, filtered and concentrated under reduced pressure.

7.1.4. Procedure for the synthesis of the nitric oxide-releasing indomethacin derivatives with 1,3-thiazolidine-4-one scaffold

To a suspension of indomethacin hydrazone derivatives (**8a-s**) (1.0 Eq.) in dry toluene (80 mL), mercaptoacetic acid (1.5 Eq.) was added in presence of few amount of anhydrous magnesium sulfate (2-3 g), using a Dean Stark equipment and applying a modified method [124,309,310]. The mixture was stirred for 14 h at 110°C, after that was cooled at room temperature and the solvent was removed under reduced pressure. The residue was taken up with ethyl acetate (30 mL), filtered and the filtrate was successively washed with a diluted aqueous solution of sodium bicarbonate (20 mL), water and finally with brine. The combined organic layers were dried over anhydrous magnesium sulfate and solvent was removed under reduced pressure to get a crude product that was purified by column chromatography (silicagel, petroleum ether/ethyl acetate or acetonitrile/toluene) to give the pure products (**9a-s**).

7.1.5. Procedure for the synthesis of (4-chlorobenzoyl)-5-methoxy-2-methyl-1H-indol-3-yl)methyl)-2-mercapto-1,3,4-oxadiazole

To a suspension of indomethacin hydrazide (**7**) (1.0 Eq.) in CH_3CN (150 mL for 12 mmol scale), Et_3N (2.0 Eq.) and CS_2 (2.0 Eq.) were slowly added, into small portions, according to the method reported in the literature [311–314], which was adapted to our synthesis in terms of the ratio of reagents, solvent, time of reaction and purification method. The mixture was stirred for 3 h under reflux till hydrogen sulfide formation was stopped. After cooling at room temperature, the solvent was removed under reduced pressure and the residue was dissolved in EtOAc (40 mL) and acidified with aqueous diluted HCl 0.5M solution (10 mL). The organic layer was separated and was successively washed with distilled water (3 × 50 mL) and finally with brine (50 mL). The combined organic layers were dried over anhydrous magnesium sulfate, filtered and concentrated under reduced pressure. The crude product was purified by column chromatography to give the pure IND-OXD derivative.

7.1.6. Procedure for the synthesis of the nitric oxide-releasing indomethacin derivatives with 1,3,4-oxadiazole scaffold

To a suspension of (4-chlorobenzoyl)-5-methoxy-2-methyl-1*H*-indol-3-yl)methyl)-2-mercapto-1,3,4-oxadiazole (**10**) (1.0 Eq.) in acetonitrile (70 mL for 4 mmol scale), the corresponding (halidealkyl)phenoxy nitrates (**6a-m, t-v**) (1.1 Eq.) were added in one portion followed by Et_3N drop wise adding (1.5 Eq.), according to the method reported in the literature, which was adapted to our synthesis in terms of the ratio of reagents, solvent, time of reaction and purification method [315,316]. The mixture was stirred at room temperature for 3-6 h upon reaction completion (as monitored by TLC) and then the solvent was removed under reduced pressure. The residue was taken up with EtOAc (50 mL) and successively washed with distilled water (2 × 50 mL) and finally with brine (50 mL). The combined organic layers were dried over anhydrous magnesium sulfate and solvent was removed under reduced pressure to get crude products that were purified by flash column chromatography to give the pure products (**11a-m, t-v**).

7.2. Results and discussions

7.2.1. Synthesis of nitric-oxide releasing indomethacin derivatives

7.2.1.1. Synthesis of NO-donor linkers

Nitrate esters represent an important functional group which confers unique biological properties to NO donor drugs by releasing of nitric oxide in biological media [317–319]. The preparation of organic nitrate esters is generally accomplished by esterification of the appropriate alcohols or by substitution of reactive alkyl halides with silver nitrate [320]. Usually, the alcohols and polyols can be converted into the corresponding nitrate esters by *O*-nitration either with a mixture of nitric and sulfuric acids or only nitric acid [321–323]. The esterification is normally carried out in an ice bath, by slow addition of the alcohol to the carboxylic acid, mixed with a small amount of urea or urea nitrate to destroy any nitrous acid formed. To avoid the undesirable side reactions by oxidation of the alcohols is also necessary an adequate stirring and careful control of temperature. The nitrate esters, which are formed rapidly, are separated from excess of acid either by careful distillation or by pouring the reaction mixture into cold water. Using this procedure, different primary and secondary nitrates were obtained in good yield [324,325].

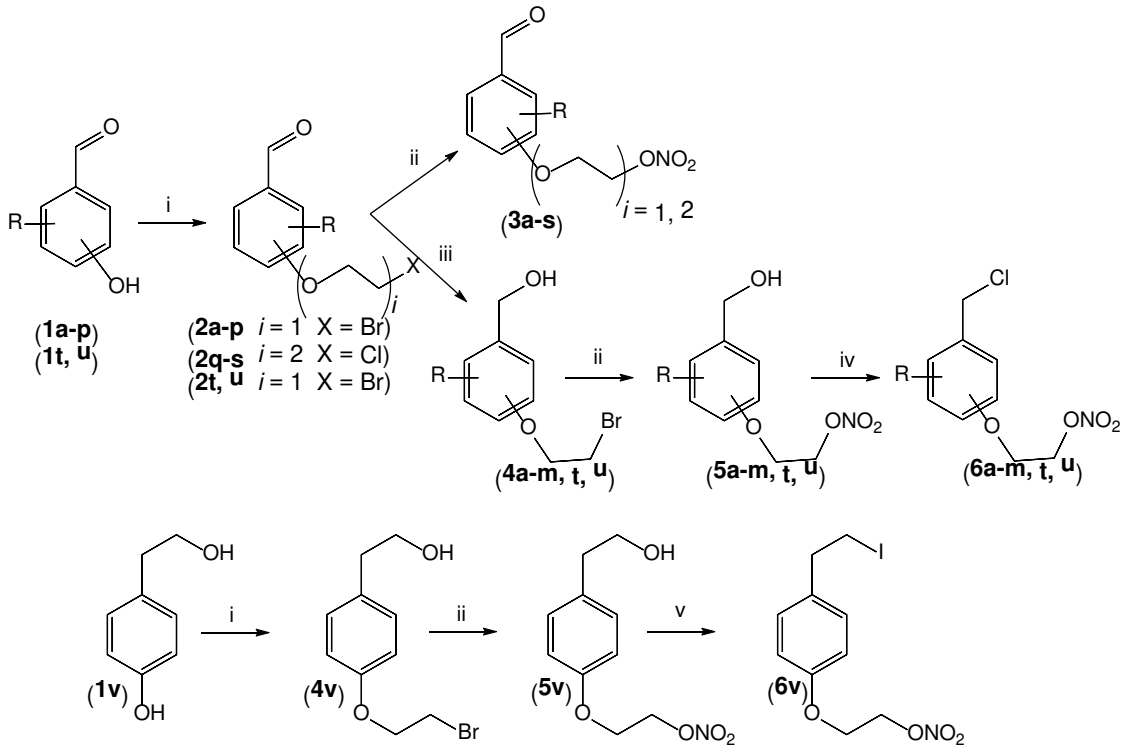

Fig. 7.3. The synthesis of the nitrate ester linkers: nitrate ester benzaldehydes (**3a-s**) and nitrate ester benzyl halide (**6a-m, t-v**), respectively. Reagents and conditions: (i) $C_2H_4Br_2/(CH_2CH_2Cl)_2O$, K_2CO_3/CH_3CN, 95°C, 18–26 h, (ii) $AgNO_3/CH_3CN$, 95°C, 8–12 h (iii) $NaBH_4$/THF, RT, 12–24 h, (iv) $SOCl_2$, BTA/ dry CH_2Cl_2, RT, 20–30 min, (v) imidazole, PPh_3, I_2/ CH_2Cl_2, RT, 6h.

This method is potentially very dangerous, need to elaborate safety precaution and is not suitable for large scale preparation due to highly acidic conditions with a strong oxidizing agent in contact with an organic solvent.

A safer method for preparation of nitrate esters is the metathesis reaction of organic halides with silver nitrate in organic solvent [326–331]. The reaction can be carried out by

stirring of powdered silver nitrate with alkyl halide, either in homogenous (acetonitrile or glacial acetic acid) or in heterogenous (benzene, diethyl ether, nitromethane and nitrobenzene) conditions. As alkyl halides could be used primary and secondary alkyl iodine or bromide as well as alkyl chloride of the tertiary, allylic or benzylic type, which react rapidly with silver nitrate, at room temperature or slightly higher. So, this method involves mild conditions and can be very useful for preparation of alkyl nitrates.

In order to ensure appropriate conjugation between NO-donor linker and indomethacin, the nitrate ester moiety was inserted into different substituted phenoxy-alkyl structures which posses a carbonyl or a benzyl halide function, suitable for final stage synthesis of the desired NO-IND derivatives.

So, in our study, two type of nitrate ester linkers: nitrate ester benzaldehyde derivatives (**3a-s**) and (halidealkyl)phenoxy nitrate derivatives (**6a-m, t-v**), respectively, were synthesized (Fig. 7.3).

The intermediate *halide-alcoxy-benzaldehyde derivatives* (**2a-s, t, u)** were prepared by SN2 Williamson ether synthesis method using a hydroxyl benzaldehides as phenoxide which are strong nucleophiles and strong bases. To avoid the dimerization, the 1,2-dibromoethane or bis(2-chloroethyl)ether (excellent electroplile) were used in exces. After flash chromatography purification the desired compound (**2a-s, t, u)** were obtained in good yields, which ranged between 80 and 95%. Their main physico-chemical and spectral characteristics (^{1}H NMR, ^{13}C NMR, MS) are presented in Table 7.1.

Table 7.1. The identification characteristics (^{1}H NMR, ^{13}C NMR, MS, R_f) of the halide-alcoxy-benzaldehyde derivatives (**2a-s**, **t**, **u**).

Cpd.	The identification characteristics (^{1}H NMR, ^{13}C NMR, MS, R_f)
2a	*4-(2-Bromoethoxy)benzaldehyde* was obtained from 4-hydroxybenzaldehyde (**1a**)as a yellow oil in 96% yield. ^{1}H NMR (400 MHz, DMSO-d_6) δ = 3.77 – 3.90 (m, 2H), 4.39 – 4.49 (m, 2H), 7.16 (d, *J* = 8.7 Hz, 2H), 7.88 (d, *J* = 8.7 Hz, 2H), 9.88 (s, 1H). ^{13}C NMR (101 MHz, DMSO-d_6) δ = 31.5 (CH_2), 68.5 (CH_2), 115.5 ($2CH_{Ar}$), 130.4 (C_q), 132.2 ($2CH_{Ar}$), 163.2 (C_q), 191.7 (C = O); HRMS (ESI-MS) *m/z* calcd for $C_9H_{10}BrO_2$ $[M+H]^+$: 228.9864, found: 228.9859; Rf (petroleum ether/EtOAc = 6/4) 0.68.
2b	*4-(2-Bromoethoxy)-3-fluorobenzaldehyde* was obtained from 3-fluoro-4-hydroxy-benzaldehyde (**1b**) as a white solid in 91% yield, m.p. 61-63°C. ^{1}H NMR (400 MHz, DMSO-d_6) δ = 3.87 (dd, *J* = 6.0 HZ, 4.7 Hz, 2H), 4.53 (dd, *J* = 6.1 Hz, 4.7 Hz, 2H), 7.41 (t, *J* = 8.3 Hz, 1H), 7.71 (dd, *J* = 11.3 Hz, 2.0 Hz, 1H), 7.77 (ddd, *J* = 8.3 Hz, 2.0 Hz, 1.0 Hz, 1H), 9.87 (d, *J*= 2.0 Hz, 1H). ^{13}C NMR (101 MHz, DMSO-d_6) δ = 30.7 (CH_2), 69.0 (CH_2), 114.9 (d, *J* = 1.7 Hz, CH_{Ar}), 115.4 (d, *J* = 18.4 Hz, CH_{Ar}), 128.2 (d, *J* = 3.1 Hz, CH_{Ar}), 130.1 (d, *J* = 5.0 Hz, C_q), 151.0 (d, *J* = 10.7 Hz, C_q), 151.5 (d, *J* = 247.3 Hz, C_qF), 190.8 (d, *J* = 2.2 Hz, C = O). ^{19}F NMR (376 MHz, DMSO-d_6) δ = -133.32 (ddd, *J* = 10.9 Hz, 8.3 Hz, 2.1 Hz); HRMS (ESI-MS) *m/z* calcd for $C_9H_9BrFO_2$ $[M+H]^+$: 246.9770, found: 246.9764; Rf (petroleum ether/EtOAc = 7/3) 0.65.

Cpd.	The identification characteristics (^{1}H NMR, ^{13}C NMR, MS, R_f)
2c	*4-(2-Bromoethoxy)-3-chlorobenzaldehyde* was obtained from 3-chloro-4-hydroxy-benzaldehyde (**1c**) as a white solid in 95% yield, m.p. 62-64 °C.^{1}H NMR (400 MHz, DMSO-d_6) δ= 3.82 - 3.92 (m, 2H), 4.50 - 4.59 (m, 2H), 7.38 (d, *J* = 8.5 Hz, 1H), 7.89 (dd, *J* = 8.5 Hz, 2.0 Hz, 1H), 7.97 (d, *J* = 2.0 Hz, 1H), 9.88 (s, 1H). ^{13}C NMR (101 MHz, DMSO-d_6) δ = 30.6 (CH_2), 69.1 (CH_2), 114.0 (CH_{Ar}), 122.3 (C_q), 130.4 (C_q), 130.6 (CH_{Ar}), 130.8 (CH_{Ar}), 157.9 (C_q), 190.7 (C = O). HRMS (ESI-MS) *m/z* calcd for $C_9H_9BrClO_2$ $[M+H]^+$: 262.9474, found: 262.9469; Rf (petroleum ether/EtOAc = 5/5) 0.74.
2d	*4-(2-Bromoethoxy)-3-methoxybenzaldehyde* ***(2d)*** was obtained from 4-hydroxy-3-methoxybenzaldehyde (**1d**) as white *needle*-shaped *crystals* in 86% yield, m.p. 66-68 °C. ^{1}H NMR (400 MHz, DMSO-d_6) δ =3.84 (dd, *J* = 6.0 Hz, 4.9 Hz, 2H), 3.85 (s, 3H), 4.43 (dd, *J* = 6.1 Hz, 4.8 Hz, 2H), 7.20 (d, *J* = 8.2 Hz, 1H), 7.42 (d, *J* = 2.0 Hz, 1H), 7.54 (dd, *J* = 8.2 Hz, 2.0 Hz, 1H), 9.85 (s, 1H). ^{13}C NMR (101 MHz, DMSO-d_6) δ =30.9 (CH_2), 55.6 (CH_3), 68.6 (CH_2), 110.0 (CH_{Ar}), 112.6 (CH_{Ar}), 125.9 (CH_{Ar}), 130.1 (C_q), 149.2 (C_q), 152.7 ($3C_q$), 191.5 (C = O); HRMS (ESI-MS) *m/z* calcd for $C_{10}H_{12}BrO_3$ $[M+H]^+$: 258.9970, found: 258.9964; Rf (petroleum ether/EtOAc =6/4) 0.55.
2e	*4-(2-Bromoethoxy)-3-ethoxybenzaldehyde* ***(2e)*** was obtained from 3-ethoxy-4-hydroxybenzaldehyde (**1e**) as yellowish white *needle*-shaped *crystals* in 65% yield, m.p. 65-67 °C. ^{1}H NMR (400 MHz, DMSO-d_6) δ =1.35 (t, *J* = 6.9 Hz, 3H), 3.83 (dd, *J* = 6.1 Hz, 5.0 Hz, 2H), 4.12 (q, *J* = 6.9 Hz, 2H), 4.43 (dd, *J* = 6.1 Hz, 5.0 Hz, 2H), 7.20 (d, *J* = 8.3 Hz, 1H), 7.41 (d, *J* = 1.9 Hz, 1H), 7.53 (dd, *J* = 8.2 Hz, 1.9 Hz, 1H), 9.84 (s, 1H). ^{13}C NMR (101 MHz, DMSO-d_6) δ =14.6 (CH_3), 30.9 (CH_2), 64.1 (CH_2), 68.6 (CH_2), 111.7 (CH_{Ar}), 113.2 (CH_{Ar}), 125.6 (CH_{Ar}), 130.2 (C_q), 148.5 (C_q), 153.0 (C_q), 191.4 (C = O); HRMS (ESI-MS) *m/z* calcd for $C_{11}H_{14}BrO_3$ $[M-H]^+$: 273.0126 found: 272.0121; Rf (petroleum ether/EtOAc =6/4) 0.55.
2f	*4-(2-Bromoethoxy)-3-nitrobenzaldehyde* ***(2f)*** was obtained from 4-hydroxy-3-nitrobenzaldehyde (**1f**) as greenish yellow solid in 85% yield, m.p. 68-70 °C. ^{1}H NMR (400 MHz, DMSO-d_6) δ =3.80 - 3.88 (m, 2H), 4.60 - 4.68 (m, 2H), 7.59 (d, *J* = 8.7 Hz, 1H), 8.18 (dd, *J* = 8.7 Hz, 2.0 Hz, 1H), 8.43 (d, *J* = 2.0 Hz, 1H), 9.96 (s, 1H). ^{13}C NMR (101 MHz, DMSO-d_6) δ =30.3 (CH_2), 69.8 (CH_2), 115.8 (CH_{Ar}), 126.3 (CH_{Ar}), 129.1 (C_q), 134.8 (CH_{Ar}), 139.6 (C_q), 154.6 (C_q), 190.4 (C = O); HRMS (ESI-MS) *m/z* calcd for $C_9H_9BrNO_4$ $[M+H]^+$: 273.9715, found: 273.909; Rf (petroleum ether/EtOAc =7/3) 0.70.
2g	*4-(2-Bromoethoxy)-3,5-dimethoxybenzaldehyde* ***(2g)*** was obtained from 4-hydroxy-3,5-dimethoxybenzaldehyde (**1g**) as white solid in 95% yield, m.p. 64-66 °C. ^{1}H NMR (400 MHz, DMSO-d_6) δ =3.69 (t, *J* = 5.9 Hz, 2H), 3.87 (s, 6H), 4.27 (t, *J* = 5.9 Hz, 2H), 7.27 (s, 2H), 9.89 (s, 1H). ^{13}C NMR (101 MHz, DMSO-d_6) δ =31.6 (CH_2), 56.2 ($2CH_3$), 72.4 (CH_2), 106.7 ($2CH_{AR}$), 131.9 (C_q), 141.2 (C_q), 153.2 ($2C_q$), 191.9 (C = O); HRMS (ESI-MS) *m/z* calcd for $C_{11}H_{14}BrO_4$ $[M+H]^+$: 289.0075, found: 289.0070; Rf (petroleum ether/ EtOAc =7/3) 0.50.
2h	*4-(2-Bromoethoxy)-3,5-dichlorobenzaldehyde* ***(2h)*** was obtained from 3,5-dichloro-4-hydroxybenzaldehyde (**1h**) as white solid in 95% yield, m.p. 67-69 °C. ^{1}H NMR (400 MHz, DMSO-d_6) δ =3.76 -3.92 (m, 2H), 4.35 - 4.49 (m, 2H), 8.0 (s, 2H), 9.91 (s, 1H).^{13}C NMR (101 MHz, DMSO-d_6) δ =31.2 (CH_2), 73.4 (CH_2), 129.4 ($2C_q$), 130.0 ($2CH_{Ar}$), 133.6 (C_q), 154.7 (C_q), 190.2 (C = O); HRMS (ESI-MS) *m/z* calcd for $C_9H_8BrCl_2O_2$ $[M+H]^+$: 296.9085, found: 296.9079; Rf (petroleum ether/EtOAc =8/2) 0.66.

Cpd.	The identification characteristics (^{1}H NMR, ^{13}C NMR, MS, R_f)
2i	*3-(2-Bromoethoxy)benzaldehyde **(2i)*** was obtained from 3-hydroxybenzaldehyde (**1i**) as a colorless oil in 91% yield. ^{1}H NMR (400 MHz, DMSO-d_6) δ =3.76 – 3.90 (m, 2H), 4.32 – 4.47 (m, 2H), 7.26 - 7.33 (m, 1H), 7.44 (d, *J* = 2.7 Hz, 1H), 7.49 - 7.56 (m, 2H), 9.97 (s, 1H). ^{13}C NMR (101 MHz, DMSO-d_6) δ =31.1 (CH_2), 68.0 (CH_2), 114.0 (CH_{Ar}), 121.4 (CH_{Ar}), 122.7 (CH_{Ar}), 130.4 (CH_{AR}), 137.6 (C_q), 158.4 (C_q), 192.7 (C = O); HRMS (ESI-MS) *m/z* calcd for $C_9H_{10}BrO_2$ $[M+H]^+$: 228.9864, found: 228.9859; Rf (petroleum ether/EtOAc =7/3) 0.57.
2j	*3-(2-Bromoethoxy)-4-methoxybenzaldehyde **(2j)*** was obtained from 3-hydroxy-4-methoxybenzaldehyde (**1j**) as white solid in 88% yield, m.p. 64-66 °C. ^{1}H NMR (400 MHz, DMSO-d_6) δ =3.74 - 3.85 (m, 2H), 3.89 (s, 3H), 4.31 - 4.44 (m, 2H), 7.19 (d, *J* = 8.3 Hz, 1H), 7.41 (d, *J* = 1.9 Hz, 1H), 7.58 (dd, *J* = 8.3 Hz, 1.9 Hz, 1H), 9.83 (s, 1H). ^{13}C NMR (101 MHz, DMSO-d_6) δ =31.1 (CH_2), 56.0 (CH_3), 68.6 (CH_2), 111.6 (CH_{Ar}), 111.8 (CH_{Ar}), 126.4 (CH_{Ar}), 129.6 (C_q), 147.7 (C_q), 154.4 (C_q), 191.3 (C = O); HRMS (ESI-MS) *m/z* calcd for $C_{10}H_{12}BrO_3$ $[M+H]^+$: 258.9970, found: 258.9964; Rf (petroleum ether/EtOAc =5/5) 0.64.
2k	*3-(2-Bromoethoxy)-4-nitrobenzaldehyde **(2k)*** was obtained from 3-hydroxy-4-nitrobenzaldehyde (**1k**) as brown solid in 80% yield, m.p. 69-71 °C. ^{1}H NMR (400 MHz, DMSO-d_6) δ =3.76 -3.88 (m, 2H), 4.54 - 4.70 (m, 2H), 7.68 (dd, *J* = 8.2 Hz, 1.5 Hz, 1H), 7.86 (d, *J* = 1.5 Hz, 1H), 8.07 (d, *J* = 8.2 Hz, 1H), 10.06 (s, 1H). ^{13}C NMR (101 MHz, DMSO-d_6), δ =30.5 (CH2), 69.5 (CH2), 115.6 (CHAr), 122.2 (CHAr), 125.4 (CHAr), 139.5 (Cq), 143.1 (Cq), 150.4 (Cq), 191.9 (C = O); HRMS (ESI-MS) m/z calcd for C9H9BrNO4 [M+H]+: 273.9715, found: 273.9709; Rf (petroleum ether/EtOAc =4/4) 0.65.
2l	*2-Bromo-3-(2-bromoethoxy)-4-methoxybenzaldehyde **(2l)*** was obtained from 2-bromo-3-hydroxy-4-methoxybenzaldehyde (**1l**) as a white solid in 90% yield, m.p. 70-72 °C. ^{1}H NMR (400 MHz, DMSO-d_6) δ =3.79 (t, *J* = 5.8Hz, 2H), 3.94 (s, 3H), 4.29 (t, *J* = 5.8 Hz, 2H), 7.27 (dd, *J* = 8.7 Hz, 0.8 Hz, 1H), 7.68 (d, *J* = 8.7 Hz, 1H), 10.10 (d, *J* = 0.8 Hz, 1H). ^{13}C NMR (101 MHz, DMSO-d_6) δ =31.4 (CH_2), 56.6 (CH_3), 72.5 (CH_2), 112.2 (CH_{Ar}), 121.4 (C_q), 126.7 (C_q), 126.9 (CH_{Ar}), 144.3 (C_q), 158.1 (C_q), 190.4 (C = O); HRMS (ESI-MS) *m/z* calcd for $C_{10}H_{11}Br_2O_3$ $[M+H]^+$: 338.9054, found: 338.9049; Rf (petroleum ether/EtOAc =6/4) 0.66.
2m	*2-(2-Bromoethoxy)benzaldehyde **(2m)*** was obtained from 2-hydroxybenzaldehyde (**1m**) as a greenish yellow oil in 92% yield. ^{1}H NMR (400 MHz, DMSO-d_6) δ =3.82 - 3.93 (m, 2H), 4.42 - 4.54 (m, 2H), 7.11 (ddt, *J* = 7.3 Hz, 0.9 Hz, 1H), 7.26 (ddd, *J* = 8.4 Hz, 0.9 Hz, 0.5 Hz, 1H), 7.61 - 7.75 (m, 2H), 10.45 (s, 1H). ^{13}C NMR (101 MHz, DMSO-d_6) δ =31.3 (CH_2), 68.5 (CH_2), 114.1 (CH_{Ar}), 121.3 (CH_{Ar}), 124.5 (C_q), 127.4 (CH_{Ar}), 136.4 (CH_{Ar}), 160.4 (C_q), 189.1 (C = O); HRMS (ESI-MS) *m/z* calcd for $C_9H_{10}BrO_2$ $[M+H]^+$: 228.9864, found: 228.9859; Rf (petroleum ether/EtOAc =7.5/2.5) 0.56.
2n	*3-Bromo-4-(2-bromoethoxy)benzaldehyde **(2n)*** was obtained from 3-bromo-4-hydroxybenzaldehyde (**1n**) as a white solid in 86% yield, m.p. 64-66 °C. ^{1}H NMR (400 MHz, DMSO-d_6) δ =3.82 - 3.90 (m, 2H), 4.50 - 4.58 (m, 2H), 7.33 (d, *J* = 8.5 Hz, 1H), 7.91 (dd, *J* = 8.5 Hz, 2.0 Hz, 1H), 8.11 (d, *J* = 2.0 Hz, 1H), 9.86 (s, 1H). ^{13}C NMR (101 MHz, DMSO-d_6) δ =30.6 (CH_2), 69.2 (CH_2), 111.7 (C_q), 113.8 (CH_{Ar}), 130.9 (C_q), 131.1 (CH_{Ar}), 134.1 (CH_{Ar}), 158.8 (C_q), 190.5 (C = O); HRMS (ESI-MS) *m/z* calcd for $C_9H_9Br_2O_2$ $[M+H]^+$: 308.8949, found: 308.8943; Rf (petroleum ether/EtOAc =6/4) 0.57.

Cpd.	The identification characteristics (^{1}H NMR, ^{13}C NMR, MS, R_f)
2o	*5-(2-Bromoethoxy)-2-nitrobenzaldehyde* ***(2o)*** was obtained from 5-hydroxy-2-nitrobenzaldehyde (**1o**) as green solid in 86% yield, m.p. 67-69 °C. ^{1}H NMR (400 MHz, DMSO-d_6) δ =3.81 - 3.89 (m, 2H), 4.51 - 4.62 (m, 2H), 7.29 (d, *J* = 2.8 Hz, 1H), 7.40 (dd, *J* = 9.0 Hz, 2.9 Hz, 1H), 8.19 (d, *J* = 9.0 Hz, 1H), 10.29 (s, 1H). ^{13}C NMR (101 MHz, DMSO-d_6) δ =30.8 (CH_2), 68.9 (CH_2), 114.3 (CH_{Ar}), 118.7 (CH_{Ar}), 127.3 (CH_{Ar}), 134.2 (C_q), 142.1 (C_q), 162.1 (C_q), 189.8 (C = O); HRMS (ESI-MS) *m/z* calcd for $C_9H_9BrNO_4$ $[M+H]^+$: 273.9715, found: 273.9709; Rf (petroleum ether/EtOAc =6/4) 0.65.
2p	*4-(2-Bromoethoxy)-3-chloro-5-methoxybenzaldehyde* ***(2p)*** was obtained from 3-chloro-4-hydroxy-5-methoxybenzaldehyde (**1p**) as white *needle*-shaped *crystals* in 86% yield, m.p. 65-67 °C. ^{1}H NMR (400 MHz, DMSO-d_6) δ =3.67 – 3.83 (m, 2H), 3.92 (s, 3H), 4.30 – 4.49 (m, 2H), 7.52 (d, *J* = 1.8 Hz, 1H), 7.65 (d, *J* = 1.8 Hz, 1H), 9.89 (s, 1H). ^{13}C NMR (101 MHz, DMSO-d_6) δ =31.6 (CH_2), 56.4 (CH_3), 72.9 (CH_2), 111.1 (CH_{Ar}), 124.1 (CH_{Ar}), 127.6 (C_q), 132.6 (C_q), 148.2 (C_q), 153.6 (C_q), 191.1 (C = O); HRMS (ESI-MS) *m/z* calcd for $C_{10}H_{11}BrClO_3$ $[M+H]^+$: 292.9580, found: 292.9575; Rf (petroleum ether/EtOAc =6/4) 0.64.
2q	*4-(2-(2-Chloroethoxy)ethoxy)benzaldehyde* ***(2q)*** was obtained from 4-hydroxy-benzaldehyde (**1a**) and bis(2-chloroethyl)ether as a fine white needle crystals in 79% yield, m.p. 65-67 °C. ^{1}H NMR (400 MHz, DMSO-d_6) δ =3.74 (s, 4H), 3.77 - 3.88 (m, 2H), 4.16 - 4.29 (m, 2H), 7.08 - 7.17 (m, 2H), 7.79 - 7.91 (m, 2H), 9.87 (s, 1H). ^{13}C NMR (101 MHz, DMSO-d_6) δ =43.5 (CH_2), 67.6 (CH_2), 68.6 (CH_2), 70.6 (CH_2), 114.9 ($2CH_{Ar}$), 129.7 (C_q), 131.8 ($2CH_{AR}$), 163.4 (C_q), 191.3 (C = O); HRMS (ESI-MS) *m/z* calcd for $C_{11}H_{14}ClO_3$ $[M+H]^+$: 229.0631, found: 229.0626; Rf (petroleum ether/EtOAc =6/4) 0.50.
2r	*4-(2-(2-Chloroethoxy)ethoxy)-3-methoxybenzaldehyde* **(2r)** was obtained from 4-hydroxy-3-methoxybenzaldehyde (**1d**) and bis(2-chloroethyl)ether as a fine white needle crystals in 88% yield, m.p. 64-66 °C. ^{1}H NMR (250 MHz, DMSO-d_6) δ =3.64 - 3.80 (m, 4H), 3.78 - 3.89 (m, 5H), 4.15 - 4.28 (m, 2H), 7.18 (d, *J* = 8.7 Hz, 1H), 7.40 (d, *J* = 1.9 Hz, 1H), 7.53 (dd, *J* = 8.3Hz, 1.9 Hz, 1H), 9.84 (s, 1H).13C NMR (101 MHz, DMSO-d6) δ =43.5 (CH2), 55.6 (CH3), 68.1 (CH2), 68.6 (CH2), 70.7 (CH2), 109.8 (CHAr), 112.3 (CHAr), 125.9 (CHAr), 129.8 (Cq), 149.2 (Cq), 153.4 (Cq), 191.3 (C = O); HRMS (ESI-MS) m/z calcd for C12H16ClO4 [M+H]+: 259.0737, found: 259.0732; Rf (petroleum ether/EtOAc =5/5) 0.46.
2s	*4-(2-(2-Chloroethoxy)ethoxy)-3-ethoxybenzaldehyde* ***(2s)*** was obtained from 3-ethoxy 4-hydroxybenzaldehyde (**1e**) and bis(2-chloroethyl)ether as a fine white needle crystals in 83% yield, m.p. 64-66 °C.^{1}H NMR (250 MHz, DMSO-d_6) δ =1.35 (t, *J* = 6.9 Hz, 3H), 3.68 -3.81 (m, 4H), 3.81 - 3.88 (m, 2H), 4.10 (q, *J* = 6.9 Hz, 2H), 4.17 -4.27 (m, 2H), 7.19 (d, *J* = 8.3 Hz, 1H), 7.39 (d, *J* = 1.9 Hz, 1H), 7.52 (dd, *J* = 8.3 Hz, 1.9 Hz, 1H), 9.83 (s, 1H). ^{13}C NMR (101 MHz, DMSO-d_6) δ =14.6 (CH_3), 43.5 (CH_2), 63.9 (CH_2), 68.3 (CH_2), 68.6 (CH_2), 70.8 (CH_2), 111.2 (CH_{Ar}), 112.6 (CH_{Ar}), 125.7 (CH_{Ar}), 129.8 (C_q), 148.5 (C_q), 153.6 (C_q), 191.4 (C = O); HRMS (ESI-MS) *m/z* calcd for $C_{13}H_{18}ClO_4$ $[M+H]^+$: 273.0894, found: 273.0888, Rf (petroleum ether/EtOAc =4/6) 0.66.

Cpd.	The identification characteristics (^{1}H NMR, ^{13}C NMR, MS, R_f)
2t	*5-Bromo-2-(2-bromoethoxy)benzaldehyde*(***2t***) was obtained from 5-bromo-2-hydroxybenzaldehyde (**1t**) as white solid in 88% yield, m.p. 61-63 °C. ^{1}H NMR (400 MHz, DMSO-d_6) δ = 3.82 – 3.91 (m, 2H), 4.45 – 4.54 (m, 2H), 7.26 (d, *J* =8.9 Hz, 1H), 7.74 (d, *J* =2.7 Hz, 1H), 7.81 (dd, *J* =8.9 Hz, 2.7 Hz, 1H), 10.34 (s, 1H). ^{13}C NMR (101 MHz, DMSO-d_6) δ = 31.1 (CH_2), 69.0 (CH_2), 113.1 (C_q), 117.0 (CH_{Ar}), 126.0 (C_q), 129.6 (CH_{Ar}), 138.5 (CH_{Ar}), 159.4 (C_q), 187.9 (C = O); HRMS (ESI-MS) *m/z* calcd for $C_9H_9Br_2O_2$ $[M+H]^+$: 308.8949, found: 308.8943; Rf (petroleum ether/ EtOAc = 8/2) 0.68.
2u	*3-(2-Bromoethoxy)-2-chloro-4-methoxybenzaldehyde* ***(2u)*** was obtained from 2-chloro-3-hydroxy-4-methoxybenzaldehyde **(1u)** as a white solid in 95% yield, m.p. 70-72 °C. ^{1}H NMR (400 MHz, DMSO-d_6) δ = 3.77 (t, *J* = 5.7 Hz, 2H), 3.94 (s, 3H), 4.30 (t, *J* = 5.7 Hz, 2H), 7.25 (dd, *J* = 8.8 Hz, 0.7 Hz, 1H), 7.69 (d, *J* = 8.7 Hz, 1H), 10.19 (d, *J* =0.7 Hz, 1H). ^{13}C NMR (101 MHz, DMSO-d_6) δ = 31.4 (CH_2), 56.6 (CH_3), 72.6 (CH_2) , 111.6 (CH_{Ar}), 125.6 (C_q) , 126.4 (CH_{Ar}) , 130.5 (C_q), 143.3 (C_q), 158.2 (C_q), 188.5 (C = O);HRMS (ESI-MS) *m/z* calcd for .$C_{10}H_{11}BrClO_3$ $[M+H]^+$: 292.9580, found: 292.9575. Rf (Petroleum Ether/EtOAc =7/3) 0.61

By reaction of primary *halide-alcoxy-benzaldehyde derivatives* (**2a-s**) with silver nitrate in acetonitrile the corresponding *nitrate ester benzaldehyde derivatives* (**3a-s**) were obtained in good yields, which ranged between 85 and 99%. High yields could be explained by the relatively high solubility of silver nitrate in acetonitrile which resulted in homogenous reaction mixture. Their main physico-chemical and spectral characteristics (^{1}H NMR, ^{13}C NMR, MS) are presented in Table 7.2.

Table 7.2. The identification characteristics (^{1}H NMR, ^{13}C NMR, MS, R_f) of the halide-alcoxy-benzaldehyde derivatives (**3a-s**).

Cpd.	The identification characteristics (^{1}H NMR, ^{13}C NMR, MS, R_f)
3a	*2-(4-Formylphenoxy)ethyl nitrate* was obtained from 4-(2-bromoethoxy) benzaldehyde (**2a)** as yellow oil in 95% yield. ^{1}H NMR (400 MHz, DMSO-d_6) δ = 4.39 - 4.50 (m, 2H), 4.88 - 4.95 (m, 2H), 7.11 - 7.20 (m, 2H), 7.84 - 7.93 (m, 2H), 9.88 (s, 1H). ^{13}C NMR (101 MHz, DMSO-d_6) δ = 64.5 (CH_2), 71.7 (CH_2), 115.0 ($2CH_{Ar}$), 130.1 (C_q), 131.8 ($2CH_{Ar}$), 162.7 (C_q), 191.3(C = O); HRMS (ESI-MS) *m/z* calcd for $C_9H_{10}NO_5$ $[M+H]^+$: 212.0559, found: 212.0554; Rf (petroleum ether/EtOAc = 6/4) 0.42.
3b	*2-(2-Fluoro-4-formylphenoxy)ethyl nitrate*was obtained from 4-(2-bromoethoxy)-3-fluoro-benzaldehyde (**2b)** as borrow oil in 99% yield. ^{1}H NMR (400 MHz, DMSO-d_6) δ = 4.46 - 4.61 (m, 2H), 4.86 - 5.03 (m, 2H), 7.43 (t, *J* = 8.3 Hz, 1H), 7.71 (dd, *J* = 11.3 Hz, 1.9 Hz, 1H), 7.78 (ddd, *J* = 8.3 Hz, 1.9 Hz, 1.0 Hz, 1H), 9.87 (d, *J* = 2.1 Hz, 1H). ^{13}C NMR (101 MHz, DMSO-d6) δ= 65.6 (CH_2), 71.5 (CH_2), 114.8 (d, *J* = 1.6 Hz, CH_{Ar}), 115.4 (d, *J* = 18.2 Hz, CH_{Ar}), 128.2 (d, *J* = 3.2 Hz, CH_{Ar}), 130.2 (d, *J* = 5.0 Hz, C_q), 151.0 (d, *J* = 10.7 Hz, C_q), 151.6 (d, *J* = 247.4 Hz, C_qF), 190.8 (d, *J* = 2.1 Hz, C =O). ^{19}F NMR (376 MHz, DMSO-d_6) δ = -133.32 (ddd, *J* = 10.9 Hz, 8.3 Hz, 2.1 Hz); HRMS (ESI-MS) m/z calcd for C9H9FNO5 $[M+H]^+$: 230.0465, found: 230.0459; Rf (petroleum ether/EtOAc = 5/5) 0.45.

Cpd.	The identification characteristics (^{1}H NMR, ^{13}C NMR, MS, R_f)
3c	*2-(2-Chloro-4-formylphenoxy)ethyl nitrate* was obtained from 4-(2-bromoethoxy)-3-chloro-benzaldehyde (**2c)** as pale yellow solid in 85% yield, m.p. 58-60 °C. ^{1}H NMR (400 MHz, DMSO-d_6) δ = 4.51 - 4.58 (m, 2H), 4.91 - 5.00 (m, 2H), 7.40 (d, *J* = 8.5 Hz, 1H), 7.89 (dd, *J* = 8.5Hz, 2.0 Hz, 1H), 7.96 (d, *J* = 2.0 Hz, 1H), 9.87 (s, 1H). ^{13}C NMR (101 MHz, DMSO-d_6) δ = 65.8 (CH_2), 71.3 (CH_2), 113.9 (CH_{Ar}), 122.3 (C_q), 130.5 (C_q), 130.6 (CH_{Ar}), 130.7 (CH_{Ar}), 157.8 (C_q), 190.7 (C = O); HRMS (ESI-MS) *m/z* calcd for $C_9H_9ClNO_5$ $[M+H]^+$: 246.0169, found: 246.0164; Rf (petroleum ether/EtOAc = 4/6) 0.68
3d	*2-(4-Formyl-2-methoxyphenoxy)ethyl nitrate **(3d)*** was obtained from 4-(2-bromoethoxy)-3-methoxybenzaldehyde (**2d**) as yellow oil in 99% yield. ^{1}H NMR (400 MHz, DMSO-d_6) δ =3.84 (s, 3H), 4.39 - 4.46 (m, 2H), 4.88 - 4.95 (m, 2H), 7.22 (d, *J* = 8.3 Hz, 1H), 7.42 (d, *J* = 1.9 Hz, 1H), 7.55 (dd, *J* = 8.3 Hz, 1.9 Hz, 1H), 9.85 (s, 1H). ^{13}C NMR (101 MHz, DMSO-d_6) δ =55.6 (CH_3), 65.0 (CH_2), 71.7 (CH_2), 109.9 (CH_{Ar}), 112.5 (CH_{Ar}), 125.8 (CH_{Ar}), 130.2 (C_q), 149.2 (C_q), 152.6 (C_q), 191.5 (C = O); HRMS (ESI-MS) *m/z* calcd for $C_{10}H_{12}NO_6$ $[M+H]^+$: 242.0665, found: 242.0659; Rf (petroleum ether/EtOAc =6/4) 0.43.
3e	*2-(2-Ethoxy-4-formylphenoxy)ethyl nitrate **(3e)*** was obtained from 4-(2-bromoethoxy)-3-ethoxybenzaldehyde (**2e**) as yellow oil in 92% yield ^{1}H NMR (400 MHz, DMSO-d_6) δ =1.34 (t, *J* = 6.9 Hz, 3H), 4.09 (q, *J* = 6.9 Hz, 2H), 4.39 - 4.46 (m, 2H), 4.89 - 4.96 (m, 2H), 7.21 (d, *J* = 8.3 Hz, 1H), 7.40 (d, *J* = 1.9 Hz, 1H), 7.53 (dd, *J* = 8.2 Hz, 1.9 Hz, 1H), 9.84 (s, 1H). ^{13}C NMR (101 MHz, DMSO-d_6) δ =14.5 (CH_3), 64.0 (CH_2), 65.2 (CH_2), 71.6 (CH_2), 111.4 (CH_{Ar}), 113.1 (CH_{Ar}), 125.5 (CH_{Ar}), 130.3 (C_q), 148.5 (C_q), 152.8 (C_q), 191.4 (C = O); HRMS (ESI-MS) *m/z* calcd for $C_{11}H_{14}NO_6$ $[M+H]^+$: 256.0821, found: 256.0816; Rf (petroleum ether/EtOAc =6/4) 0.52.
3f	*2-(4-Formyl-2-nitrophenoxy)ethyl nitrate* **(3f)** was obtained from 4-(2-bromoethoxy)-3-nitrobenzaldehyde (**2f**) as pale yellow solid in 60% yield, m.p. 55-57 °C. ^{1}H NMR (400 MHz, DMSO-d_6) δ =4.59 - 4.70 (m, 2H), 4.89 - 5.00 (m, 2H), 7.61 (d, *J* = 8.7 Hz, 1H), 8.19 (dd, *J* = 8.7 Hz, 2.0 Hz, 1H), 8.43 (d, *J* = 2.0 Hz, 1H), 9.96 (s, 1H). ^{13}C NMR (101 MHz, DMSO-d_6) δ =66.6 (CH_2), 71.1 (CH_2), 115.8 (CH_{Ar}), 126.4 (CH_{Ar}), 129.2 (C_q), 134.9 (CH_{AR}), 139.6 (C_q), 154.7 (C_q), 190.4 (C = O); HRMS (ESI-MS) *m/z* calcd for $C_9H_9N_2O_7$ $[M+H]^+$: 257.0410, found: 257.0404; Rf (petroleum ether/EtOAc =3/7) 0.57.
3g	*2-(4-Formyl-2,6-dimethoxyphenoxy)ethyl nitrate **(3g)*** was obtained from 4-(2-bromo-ethoxy)-3,5-dimethoxybenzaldehyde (**2h**) as pale yellow solid in 92% yield, m.p. 52-54 °C. ^{1}H NMR (400 MHz, DMSO-d_6) δ =3.85 (s, 6H), 4.18 - 4.35 (m, 2H), 4.70 - 4.87 (m, 2H), 7.26 (s, 2H), 9.89 (s, 1H). ^{13}C NMR (101 MHz, DMSO-d_6) δ =56.1 ($2CH_3$), 68.7 (CH_2), 72.8 (CH_2), 106.6 ($2CH_{Ar}$), 132.1(C_q), 141.0 (C_q), 153.3 ($2C_q$), 191.9 (C = O); HRMS (ESI-MS) *m/z* calcd for $C_{11}H_{14}NO_7$ $[M+H]^+$: 272.0770, found: 272.0765; Rf (petroleum ether/EtOAc =2/8) 0.20.
3h	*2-(2,6-Dichloro-4-formylphenoxy)ethyl nitrate **(3h)*** was obtained from 4-(2-bromo-ethoxy)-3,5-dichlorobenzaldehyde (**2h**) as white solid in 54% yield, m.p. 49-51 °C. ^{1}H NMR (250 MHz, DMSO-d_6) δ =4.33 - 4.55 (m, 2H), 4.79 - 5.04 (m, 2H), 8.02 (s, 2H), 9.91 (s, 1H). ^{13}C NMR (101 MHz, DMSO-d_6) δ =68.5 (CH_2), 72.4 (CH_2), 129.4 ($2C_q$), 130.0 ($2CH_{Ar}$), 133.6 (C_q), 154.7 (C_q), 190.2 (C = O); HRMS (ESI-MS) *m/z* calcd for $C_9H_8Cl_2NO_5$ $[M+H]^+$: 279.9780, found: 279.9775; Rf (petroleum ether/EtOAc =8/2) 0.52.

Cpd.	The identification characteristics (^{1}H NMR, ^{13}C NMR, MS, R_f)
3i	*2-(3-Formylphenoxy)ethyl nitrate* ***(3i)*** was obtained from 3-(2-bromoethoxy)benzaldehyde (**2i**) as yellow oil in 86% yield. ^{1}H NMR (400 MHz, DMSO-d_6) δ =4.33 - 4.44 (m, 2H), 4.86 - 4.95 (m, 2H), 7.25 - 7.35 (m, 1H), 7.39 - 7.49 (m, 1H), 7.48 - 7.61 (m, 2H), 9.97 (s, 1H). ^{13}C NMR (101 MHz, DMSO-d6) δ =64.3 (CH2), 71.8 (CH2), 113.8 (CHAr), 121.4 (CHAr), 122.9 (CHAr), 130.4 (CH_{Ar}), 137.7 (Cq), 158.4 (Cq), 192.8 (C = O); HRMS (ESI-MS) m/z calcd for C9H10NO5 [M+H]+: 212.0559, found: 211.0554; Rf (petroleum ether/EtOAc =8/2) 0.38.
3j	*2-(5-Formyl-2-methoxyphenoxy)ethyl nitrate* ***(3j)*** was obtained from 3-(2-bromo-ethoxy)-4-methoxybenzaldehyde (**2j**) as pale yellow solid in 87% yield, m.p. 50-52 °C. ^{1}H NMR (400 MHz, DMSO-d_6) δ =3.88 (s, 3H), 4.34 - 4.41 (m, 2H), 4.87 - 4.94 (m, 2H), 7.20 (d, *J* = 8.3 Hz, 1H), 7.44 (d, *J* = 1.9 Hz, 1H), 7.60 (dd, *J* = 8.3 Hz, 1.9 Hz, 1H), 9.84 (s, 1H). ^{13}C NMR (101 MHz, DMSO-d_6) δ =56.0 (CH_3), 65.0 (CH_2), 71.8 (CH_2), 111.5 (CH_{Ar}), 111.7 (CH_{Ar}), 126.6 (CH_{Ar}), 129.6 (C_q), 147.6 (C_q), 154.4 (C_q), 191.3 (C = O); HRMS (ESI-MS) *m/z* calcd for $C_{10}H_{12}NO_6$ $[M+H]^+$: 242.0665, found: 241.0660. Rf (petroleum ether/EtOAc =7/3) 0.35.
3k	*2-(5-Formyl-2-nitrophenoxy)ethyl nitrate* ***(3k)*** was obtained from 3-(2-bromoethoxy)-4-nitrobenzaldehyde (**2k)** as orange solid in 99% yield, m.p. 56-58 °C. ^{1}H NMR (400 MHz, DMSO-d_6) δ =4.58 - 4.65 (m, 2H), 4.89 - 4.96 (m, 2H), 7.70 (dd, *J* = 8.2 Hz, 1.2 Hz, 1H), 7.87 (d, *J* = 1.3 Hz, 1H), 8.08 (d, *J* = 8.2 Hz, 1H), 10.07 (s, 1H). ^{13}C NMR (101 MHz, DMSO-d_6) δ =66.3 (CH_2), 71.2 (CH_2), 115.3 (CH_{Ar}), 122.4 (CH_{Ar}), 125.5 (CH_{Ar}), 139.5 (C_q), 143.0 (C_q), 150.5 (C_q), 192.0 (C = O); HRMS (ESI-MS) *m/z* calcd for $C_9H_9N_2O_7$ $[M+H]^+$: 257.0410, found: 257.0406. Rf (petroleum ether/EtOAc =5/5) 0.58.
3l	*2-(2-Bromo-3-formyl-6-methoxyphenoxy)ethyl nitrate* ***(3l)*** was obtained from 2-bromo-3-(2-bromoethoxy)-4-methoxybenzaldehyde (**2l**) as brown solid in 99% yield, m.p. 66-68 °C. ^{1}H NMR (400 MHz, DMSO-d_6) δ =3.93 (s, 3H), 4.25 - 4.34 (m, 2H), 4.80 - 4.92 (m, 2H), 7.29 (dd, *J* = 8.7 Hz, 0.7 Hz, 1H), 7.69 (d, *J* = 8.7 Hz, 1H), 10.10 (d, *J* = 0.7 Hz, 1H). ^{13}C NMR (101 MHz, DMSO-d_6) δ =56.7 (CH_3), 68.8 (CH_2), 72.7 (CH_2), 112.2 (CH_{Ar}), 121.3 (C_q), 126.7 (C_q), 127.1 (CH_{Ar}), 144.3 (C_q), 158.1 (C_q), 190.3 (C = O); HRMS (ESI-MS) *m/z* calcd for $C_{10}H_{11}BrNO_6$ $[M+H]^+$: 319.9770, found: 319.9765; Rf (petroleum ether/EtOAc =7/3) 0.38.
3m	*2-(2-Formylphenoxy)ethyl nitrate* ***(3m)*** was obtained from 2-(2-bromoethoxy)benzaldehyde (**2m**) as yellow oil in 83% yield. ^{1}H NMR (250 MHz, DMSO-d_6) δ =4.40 - 4.54 (m, 2H), 4.92 - 5.05 (m, 2H), 7.09 (tt, *J* = 7.5 Hz, 0.9 Hz, 1H), 7.18 - 7.30 (m, 1H), 7.58 - 7.66 (m, 1H), 7.66 - 7.76 (m, 1H), 10.36 (d, *J* = 0.8 Hz, 1H). ^{13}C NMR (101 MHz, DMSO-d_6) δ =66.5 (CH_2), 71.3 (CH_2), 114.1 (CH_{Ar}), 121.3 (CH_{Ar}), 124.5 (C_q), 127.4 (CH_{Ar}), 136.4 (CH_{AR}), 160.4 (C_q), 189.1 (C = O); HRMS (ESI-MS) *m/z* calcd for $C_9H_{10}NO_5$ $[M+H]^+$: 212.0559, found: 211.0553; Rf (petroleum ether/EtOAc =8/2) 0.21.
3n	*2-(2-Bromo-4-formylphenoxy)ethyl nitrate* ***(3n)*** was obtained from 3-bromo-4-(2-bromo-ethoxy)benzaldehyde (**2n**) as yellow oil in 85% yield ^{1}H NMR (400 MHz, DMSO-d_6) δ =4.50 - 4.57 (m, 2H), 4.90 - 5.00 (m, 2H), 7.35 (d, *J* = 8.6 Hz, 1H), 7.92 (dd, *J* = 8.5 Hz, 2.0 Hz, 1H), 8.10 (d, *J* = 2.0 Hz, 1H), 9.86 (s, 1H). ^{13}C NMR (101 MHz, DMSO-d_6) δ =65.9 (CH_2), 71.3 (CH_2), 111.6 (C_q), 113.8 (CH_{Ar}), 130.9 (C_q), 131.0 (CH_{Ar}), 134.0 (CH_{Ar}), 158.7 (C_q), 190.5 (C = O); HRMS (ESI-MS) *m/z* calcd for $C_9H_9BrNO_5$ $[M+H]^+$: 289.9664, found: 289.9659; Rf (petroleum ether/EtOAc =7/3) 0.23.

Cpd.	The identification characteristics (^{1}H NMR, ^{13}C NMR, MS, R_f)
3o	*2-(3-Formyl-4-nitrophenoxy)ethyl nitrate* ***(3o)*** was obtained from 5-(2-bromoethoxy)-2-nitrobenzaldehyde (**2o**) as brown solid in 99% yield, m.p. 52-54 °C. ^{1}H NMR (400 MHz, DMSO-d_6) δ =4.46 - 4.62 (m, 2H), 4.85 - 5.01 (m, 2H), 7.30 (d, *J* = 2.9 Hz, 1H), 7.40 (dd, *J* = 9.0 Hz, 2.9 Hz, 1H), 8.19 (d, *J* = 9.0 Hz, 1H), 10.29 (s, 1H). ^{13}C NMR (101 MHz, DMSO-d_6) δ =65.4 (CH_2), 71.5 (CH_2), 114.2 (CH_{Ar}), 118.8 (CH_{Ar}), 127.2 (CH_{Ar}), 134.2 (C_q), 142.2 (C_q), 162.0 (C_q), 189.8 (C = O); HRMS (ESI-MS) *m/z* calcd for $C_9H_9N_2O_7$ $[M+H]^+$: 257.0410, found: 257.0404; Rf (petroleum ether/EtOAc =7/3) 0.40.
3p	*2-(2-Chloro-4-formyl-6-methoxyphenoxy)ethyl nitrate* ***(3p)*** was obtained from 4-(2-bromoethoxy)-3-chloro-5-methoxybenzaldehyde (**2p**) as borrow oil in 98% yield. ^{1}H NMR (400 MHz, DMSO-d_6) δ =3.91 (s, 3H), 4.33 - 4.45 (m, 2H), 4.79 - 4.90 (m, 2H), 7.52 (d, *J* =1.8 Hz, 1H), 7.64 (d, *J* = 1.8 Hz, 1H), 9.89 (s, 1H). ^{13}C NMR (101 MHz, DMSO-d_6) δ =56.4 (CH_3), 69.2 (CH_2), 72.7 (CH_2), 111.1 (CH_{Ar}), 124.0 (CH_{Ar}), 127.6 (C_q), 132.8 (C_q), 148.0 (C_q), 153.6 (C_q), 191.0 (C = O); HRMS (ESI-MS) *m/z* calcd for $C_{10}H_{11}ClNO_6$ $[M+H]^+$: 276.0275, found: 276.0270; Rf (petroleum ether/EtOAc =6/4) 0.55.
3q	*2-(2-(4-Formylphenoxy)ethoxy)ethyl nitrate* ***(3q)*** was obtained from 4-(2-(2-chloroethoxy)ethoxy)benzaldehyde (**2a**) as yellow *needle*-shaped *crystals* in 86% yield, m.p. 51-53 °C. ^{1}H NMR (400 MHz, DMSO-d_6) δ =3.69 - 3.89 (m, 4H), 4.13 - 4.28 (m, 2H), 4.60 - 4.76 (m, 2H), 7.08 - 7.18 (m, 2H), 7.79 - 7.93 (m, 2H), 9.87 (s, 1H). ^{13}C NMR (101 MHz, DMSO-d_6) δ =66.6 (CH_2), 67.6 (CH_2), 68.7 (CH_2), 72.9 (CH_2), 115.0 ($2CH_{Ar}$), 129.7 (C_q), 131.8 ($2CH_{Ar}$), 163.4(C_q), 191.3 (C = O); HRMS (ESI-MS) *m/z* calcd for $C_{11}H_{14}NO_6$ $[M+H]^+$: 256.0821, found: 256.0816; Rf (petroleum ether/EtOAc =4/6) 0.58.
3r	*2-(2-(4-Formyl-2-methoxyphenoxy)ethoxy)ethyl nitrate* ***(3r)*** was obtained from 4-(2-(2-chloroethoxy)ethoxy)-3-methoxybenzaldehyde (**2d**) as brown oil in 86% yield. ^{1}H NMR (400 MHz, DMSO-d_6) δ =3.71 - 3.87 (m, 7H), 4.15 - 4.27 (m, 2H), 4.63 - 4.74 (m, 2H), 7.18 (d, *J* = 8.3 Hz, 1H), 7.40 (d, *J* = 1.9 Hz, 1H), 7.53 (dd, *J* = 8.3 Hz, 1.9 Hz, 1H), 9.84 (s, 1H). ^{13}C NMR (101 MHz, DMSO-d_6) δ =55.5 (CH_3), 66.6 (CH_2), 68.0 (CH_2), 68.7 (CH_2), 72.9 (CH_2), 109.7 (CH_{Ar}), 112.2 (CH_{Ar}), 125.9 (CH_{Ar}), 129.8 (C_q), 149.2 (C_q), 153.3 (C_q), 191.3 (C = O); HRMS (ESI-MS) *m/z* calcd for $C_{12}H_{16}NO_7$ $[M+H]^+$: 286.0927, found: 286.0921; Rf (petroleum ether/EtOAc =4/6) 0.59.
3s	*2-(2-(2-Ethoxy-4-formylphenoxy)ethoxy)ethyl nitrate* ***(3s)*** was obtained from 4-(2-(2-chloroethoxy)ethoxy)-3-ethoxybenzaldehyde (**2e**) as brown solid in 60% yield, m.p. 55-57 °C. ^{1}H NMR (400 MHz, DMSO-d_6) δ =1.35 (t, *J* = 6.9 Hz, 3H), 3.77 - 3.88 (m, 4H), 4.10 (q, *J* = 6.9Hz, 2H), 4.16 -4.28 (m, 2H), 4.63 - 4.74 (m, 2H), 7.18 (d, *J* = 8.2 Hz, 1H), 7.39 (d, *J* = 1.9 Hz, 1H), 7.52 (dd, *J* = 8.2 Hz, 1.9 Hz, 1H), 9.83 (s, 1H). ^{13}C NMR (101 MHz, DMSO-d_6) δ =14.5 (CH_3), 63.9 (CH_2), 66.7 (CH_2), 68.2 (CH_2), 68.7 (CH_2), 72.9 (CH_2), 111.2 (CH_{Ar}), 112.6 (CH_{Ar}), 125.7 (CH_{Ar}), 129.8 (C_q), 148.4 (C_q), 153.5 (C_q), 191.4 (C = O); HRMS (ESI-MS) *m/z* calcd for $C_{13}H_{18}NO_7$ $[M+H]^+$: 300.1083, found: 300.1078; Rf (petroleum ether/EtOAc =4/6) 0.62.

The reduction of *halide-alcoxy-benzaldehyde derivatives* (**2a-s**, **t**, **u)** with sodium borohydride was leading to synthesis of desired *(bromoethoxy)aromatic alcohol derivatives* (**4a-m**, **t**, **u**) in a good yields, which ranged between 86 and 99%. This method offers significant advantages like mild reaction conditions and easy isolation (simple neutralization

and extraction) of the product. Their main physico-chemical and spectral characteristics (^{1}H NMR, ^{13}C NMR, MS) are presented in Table 7.3.

Table 7.3. The identification characteristics (^{1}H NMR, ^{13}C NMR, MS, R_f) of the halide-alcoxy-benzaldehyde derivatives (**4a-m**, **t-v**).

Cpd.	The identification characteristics (^{1}H NMR, ^{13}C NMR, MS, R_f)
4a	*(4-(2-Bromoethoxy)phenyl)methanol*was obtained from 4-(2-bromoethoxy) benzaldehyde (**2a)** as white solid, yield 95%, m.p. 73–75°C; ^{1}H NMR (250 MHz, DMSO-d_6) δ = 3.68–3.80 (m, 2H), 4.18–4.30 (m, 2H), 4.37 (d, *J* = 5.7 Hz, 2H), 5.01 (t, *J* = 5.7 Hz, 1H), 6.81–6.93 (m, 2H), 7.13–7.25 (m, 2H); ^{13}C NMR (101 MHz, DMSO-d_6) δ = 31.5 (CH_2), 62.5 (CH_2OH), 67.7 (CH_2), 114.3 ($2CH_{Ar}$), 127.9 ($2CH_{Ar}$), 135.1 (C_q), 156.8 (C_q); HRMS (ESI-MS) *m/z* calcd for $C_9H_{11}BrNaO_2$ $[M+Na]^+$: 252.9840, found: 252.9835; Rf (CH_2Cl_2/CH_3OH = 9.8/0.2) 0.53.
4b	*(4-(2-Bromoethoxy)-3-fluorophenyl)methanol*was obtained from4-(2-bromoethoxy)-3-fluorobenzaldehyde (**2b)** as pale yellow oil, yield 93%; ^{1}H NMR (250 MHz, DMSO-d_6) δ = 3.76–3.84 (m, 2H), 4.32–4.40 (m, 2H), 4.42 (dd, *J* = 5.7 Hz, 0.7 Hz, 2H), 5.19 (t, *J* = 5.7 Hz, 1H), 7.00–7.22 (m, 3H); ^{13}C NMR (101 MHz, DMSO-d_6) δ = 31.2 (CH_2), 61.9 (CH_2OH), 69.0 (CH_2), 114.2 (d, *J* = 18.2 Hz, CH_{Ar}), 115.3 (d, *J* = 1.9 Hz, CH_{Ar}), 122.4 (d, *J* = 3.4 Hz, CH_{Ar}), 136.6 (d, *J* = 5.6 Hz, C_q), 144.3 (d, *J* = 10.9 Hz, C_q), 151.6 (d, *J* = 243.9 Hz, C_qF); ^{19}F NMR (376 MHz, DMSO-d_6) δ = -134.7 (dd, *J* = 12.5 Hz, 8.6 Hz); HRMS (ESI-MS) *m/z* calcd for $C_9H_{10}BrFNaO_2$ $[M+Na]^+$: 270.9746, found: 270.9740; Rf (CH_2Cl_2/CH_3OH = 9.8/0.2) 0.61.
4c	*(4-(2-Bromoethoxy)-3-chlorophenyl)methanol* was obtained from 4-(2-bromoethoxy)-3-chlorobenzaldehyde (**2c)** as pale yellow oil, yield 97%; ^{1}H NMR (400 MHz, DMSO-d_6) δ = 3.75–3.83 (m, 2H), 4.35–4.40 (m, 2H), 4.42 (d, *J* = 5.8 Hz, 2H), 5.19 (t, *J* = 5.8 Hz, 1H), 7.11 (d, *J* = 8.4 Hz, 1H), 7.22 (dd, *J* = 8.4 Hz, 2.0 Hz, 1H), 7.37 (d, *J* = 2.1 Hz, 1H); ^{13}C NMR (101 MHz, DMSO-d_6) δ = 31.0 (CH_2), 61.8 (CH_2OH), 68.8 (CH_2), 114.1 (CH_{Ar}), 121.2 (C_q), 126.3 (CH_{Ar}), 128.1 (CH_{Ar}), 136.6 (C_q), 152.0 (C_q). HRMS (ESI-MS) *m/z* calcd for $C_9H_{10}BrClNaO_2$ $[M+Na]^+$: 286.9450, found: 286.9835; Rf (petroleum ether/EtOAc = 5/5) 0.58.
4d	*(4-(2-Bromoethoxy)-3-methoxyphenyl)methanol* was obtained from 4-(2-bromoethoxy)-3-methoxybenzaldehyde (**2d**)as white solid, yield 91%; m.p. 68-70 °C, ^{1}H NMR (250 MHz, DMSO-d_6) δ = 3.70–3.82 (m, 2H), 3.77 (s, 3H), 4.26 (m, 2H), 4.42 (d, *J* = 5.7 Hz, 2H), 5.08 (t, *J* = 5.7 Hz, 1H), 6.81 (ddt, *J* = 8.1 Hz, 1.9 Hz, 0.72, 1H), 6.92 (d, *J* = 8.1 Hz, 1H), 6.95 (d, *J* = 1.9 Hz, 1H); ^{13}C NMR (101 MHz, DMSO-d_6) δ = 31.5 (CH_2), 55.5 (CH_3), 62.7 (CH_2OH), 69.0 (CH_2), 111.1 (CH_{Ar}), 114.2 (CH_{Ar}), 118.6 (CH_{Ar}), 136.3 (C_q), 146.0 (C_q), 149.1 (C_q);. HRMS (ESI-MS) *m/z* calcd for $C_{10}H_{13}BrNaO_3$ $[M+Na]^+$: 282.9946, found: 282.9940 ; Rf (petroleum ether/EtOAc = 3/7) 0.53.
4e	*(4-(2-Bromoethoxy)-3-ethoxyphenyl)methanol* was obtained from 4-(2-bromoethoxy)-3-ethoxybenzaldehyde (**2e**) as white solid, yield 93%, m.p. 53–55°C; ^{1}H NMR (250 MHz, DMSO-d_6) δ = 1.32 (t, *J* = 6.9 Hz, 3H), 3.75 (dd, *J* = 6.0 Hz, 5.2 Hz, 2H), 4.03 (q, *J* = 6.9 Hz, 2H), 4.27 (t, *J* = 6.0 Hz, 5.22 Hz, 2H), 4.41 (d, *J* = 5.7 Hz, 0.6 Hz, 2H), 5.07 (t, *J* = 5.7 Hz, 1H), 6.81 (ddt, *J* = 8.0 Hz, 1.8 Hz, 0.6 Hz, 1H), 6.89–6.96 (m, 2H); ^{13}C NMR (101 MHz, DMSO-d_6) δ = 14.8 (CH_3), 31.5 (CH_2), 62.6 (CH_2OH), 64.0 (CH_2), 69.2 (CH_2), 112.8 (CH_{Ar}), 115.1 (CH_{Ar}), 118.8 (CH_{Ar}), 136.5 (C_q), 146.4 (C_q), 148.5 (C_q); HRMS (ESI-MS) *m/z* calcd for $C_{11}H_{15}BrNaO_3$ $[M+Na]^+$: 297.0102, found: 297.0096; Rf (petroleum ether/EtOAc = 3/7) 0.55.

Cpd.	The identification characteristics (^{1}H NMR, ^{13}C NMR, MS, R_f)
4f	*(4-(2-Bromoethoxy)-3-nitrophenyl)methanol* was obtained from 4-(2-bromoethoxy)-3-nitrobenzaldehyde (**2f**) as brown oil, yield 86%; ^{1}H NMR (400 MHz, DMSO-d_6) δ = 3.72–3.84 (m, 2H), 4.41–4.56 (m, 4H), 5.35 (t, *J* = 5.7 Hz, 1H), 7.34 (d, *J* = 8.7 Hz, 1H), 7.57 (dd, *J* = 8.6 Hz, 2.1 Hz, 1H), 7.79 (d, *J* =2.1 Hz, 1H); ^{13}C NMR (101 MHz, DMSO-d_6) δ = 30.7 (CH_2), 61.4 (CH_2OH), 69.4 (CH_2), 115.4 (CH_{Ar}), 122.6 (CH_{Ar}), 132.2 (CH_{Ar}), 135.9 (C_q), 139.4 (C_q), 149.3 (C_q); HRMS (ESI-MS) *m/z* calcd for $C_9H_{11}BrNO_4$ $[M+H]^+$: 275.9871, found: 275.9865; Rf (petroleum ether/EtOAc = 4/6) 0.56.
4g	*(4-(2-Bromoethoxy)-3,5-dimethoxyphenyl)methanol* was obtained from 4-(2-bromoethoxy)-3,5-dimethoxybenzaldehyde (**2g**)as white solid, yield 96%, m.p. 71–73 °C; ^{1}H NMR (400 MHz, DMSO-d_6) δ = 3.64 (td, *J* = 6.2 Hz, 1.3 Hz, 2H), 3.77 (d, *J* = 1.3 Hz, 6H), 4.11 (td, *J* = 6.2 Hz, 1.3 Hz, 2H), 4.44 (d, *J* = 5.6 Hz, 2H), 5.16 (td, *J* = 5.7 Hz, 1.3 Hz, 1H), 6.64 (s, 2H); ^{13}C NMR (101 MHz, DMSO-d_6) δ = 31.6 (CH_2), 55.9 ($2CH_3$), 62.9 (CH_2OH), 72.3 (CH_2), 103.4 ($2CH_{Ar}$), 134.4 (C_q), 138.7 (C_q), 152.6 ($2C_q$); HRMS (ESI-MS) *m/z* calcd for $C_{11}H_{15}BrNaO_4$ $[M+H]^+$: 291.0232, found: 291.0228; Rf (petroleum ether/EtOAc = 2/8) 0.50.
4h	*(4-(2-Bromoethoxy)-3,5-dichlorophenyl)methanol*was obtained from 4-(2-bromoethoxy)-3,5-dichlorobenzaldehyde (**2h**) as white solid, yield 96%, m.p. 65–67 °C; ^{1}H NMR (250 MHz, DMSO-d_6) δ = 3.72–3.86 (m, 2H), 4.18–4.34 (m, 2H), 4.46 (d, *J* = 5.8 Hz, 2H), 5.40 (t, *J* = 5.8 Hz, 1H), 7.40 (s, 2H); ^{13}C NMR (101 MHz, DMSO-d_6) δ = 31.2 (CH_2), 61.3 (CH_2OH), 72.9 (CH_2), 126.8 ($2CH_{Ar}$), 128.0 (C_q), 141.3 (C_q), 148.5 (C_q); HRMS (ESI-MS) *m/z* calcd for $C_9H_9BrCl_2NaO_2$ $[M+Na]^+$: 320.9061, found: 320.9055; Rf (CH_2Cl_2/CH_3OH= 9.8/0.2) 0.64.
4i	*(3-(2-Bromoethoxy)phenyl)methanol* was obtained from 3-(2-bromoethoxy benzaldehyde (**2i**) as colorless oil, yield 90%; ^{1}H NMR (250 MHz, DMSO-d_6) δ = 3.70–3.87 (m, 2H), 4.16–4.34 (m, 2H), 4.48 (d, *J* = 5.8 Hz, 2H), 5.17 (t, *J* = 5.8 Hz, 1H), 6.76–6.86 (m, 1H), 6.86–6.96 (m, 2H), 7.24 (t, *J* = 8.0 Hz, 1H); ^{13}C NMR (101 MHz, DMSO-d_6) δ = 31.5 (CH_2), 62.7 (CH_2OH), 67.6 (CH_2), 112.5 (CH_{Ar}), 112.8 (CH_{Ar}), 119.0 (CH_{Ar}), 129.2 (CH_{Ar}), 144.4 (C_q), 157.9 (C_q); HRMS (ESI-MS) *m/z* calcd for $C_9H_{11}BrNaO_2$ $[M+Na]^+$: 252.9840, found: 252.9834; Rf (petroleum ether/EtOAc = 5/5) 0.58.
4j	*(3-(2-Bromoethoxy)-4-methoxyphenyl)methanol* was obtained from 3-(2-bromoethoxy)-4-methoxybenzaldehyde (**2j)** as colorless oil, yield 91%; ^{1}H NMR (250 MHz, DMSO-d_6) δ = 3.75 (s, 3H), 3.63–3.90 (m, 2H), 4.27 (dd, *J* = 6.1 Hz, 5.1 Hz, 2H), 4.40 (d, *J* = 5.7 Hz, 2H), 5.05 (t, *J* = 5.7 Hz, 1H), 6.84–6.90 (m, 1H), 6.91 (s, 1H), 6.92–6.96 (m, 1H); ^{13}C NMR (101 MHz, DMSO-d_6) δ = 31.4 (CH_2), 55.7 (CH_3), 62.6 (CH_2OH), 68.7 (CH_2), 112.2 (CH_{Ar}), 112.9 (CH_{Ar}), 119.6 (CH_{Ar}), 135.2 (C_q), 147.1 (C_q), 148.0 (C_q); HRMS (ESI-MS) *m/z* calcd for $C_{10}H_{13}BrNaO_3$ $[M+Na]^+$: 282.9946, found: 282.9937; Rf (petroleum ether/EtOAc = 3/7) 0.64.
4k	*(3-(2-Bromoethoxy)-4-nitrophenyl)methanol*was obtained from 3-(2-bromoethoxy)-4-nitro-benzaldehyde (**2k**)as greenish yellow oil, yield 97%; ^{1}H NMR (250 MHz, DMSO-d_6) δ = 3.75–3.86 (m, 2H), 4.44–4.53 (m, 2H), 4.57 (d, *J* = 5.7 Hz, 2H), 5.48 (t, *J* = 5.7 Hz, 1H), 7.09 (ddt, *J* = 8.3 Hz, 1.5 Hz, 0.8 Hz, 1H), 7.23–7.34 (m, 1H), 7.86 (d, *J* = 8.3 Hz, 1H); ^{13}C NMR (101 MHz, DMSO-d_6) δ = 30.7 (CH_2), 62.0 (CH_2OH), 69.2 (CH_2), 112.6 (CH_{Ar}), 118.4 (CH_{Ar}), 125.1 (CH_{Ar}), 138.0 (C_q), 150.3 (C_q), 150.7 (C_q); HRMS (ESI-MS) *m/z* calcd for $C_9H_{11}BrNO_4$ $[M+H]^+$: 275.9871, found: 275.9866; Rf (petroleum ether/EtOAc = 3/7) 0.54.

Cpd.	The identification characteristics (^{1}H NMR, ^{13}C NMR, MS, R_f)
4l	*(2-Bromo-3-(2-bromoethoxy)-4-methoxyphenyl)methanol* was obtained from 2-bromo-3-(2-bromoethoxy)-4-methoxybenzaldehyde (**2l**)as white solid, yield 99%, m.p. 68–70°C; ^{1}H NMR (250 MHz, DMSO-d_6) δ = 3.75 (dd, *J* = 6.2 Hz, 5.6 Hz, 2H), 3.82 (s, 3H), 4.23 (dd, *J* = 6.2 Hz, 5.6 Hz, 2H), 4.45 (dd, *J* = 5.6 Hz, 0.9 Hz, 2H), 5.29 (t, *J* = 5.6 Hz, 1H), 7.10 (d, *J* = 8.6 Hz, 1H), 7.24 (dt, *J* = 8.5 Hz, 0.8 Hz, 1H); ^{13}C NMR (101 MHz, DMSO-d_6) δ = 31.5 (CH_2), 56.2 (CH_3), 62.5 (CH_2OH), 72.3 (CH_2), 111.8 (CH_{Ar}), 116.4 (C_q), 123.3 (CH_{Ar}), 133.7 (C_q), 143.9 (C_q), 151.7 (C_q); HRMS (ESI-MS) *m/z* calcd for $C_{10}H_{12}Br_2NaO_3$ $[M+Na]^+$: 360.9051, found: 360.9039; Rf (petroleum ether/EtOAc = 3/7) 0.63.
4m	*(2-(2-Bromoethoxy)phenyl)methanol*was obtained from 2-(2-bromoethoxy)benzaldehyde (**2m**) as pale yellow oil, yield 88%; ^{1}H NMR (250 MHz, DMSO-d_6) δ = 3.72–3.87 (m, 2H), 4.24–4.38 (m, 2H), 4.56 (dd, *J* = 5.5 Hz, 0.8 Hz, 2H), 4.97 (t, *J* = 5.6 Hz, 1H), 6.88–7.02 (m, 2H), 7.20 (dddt, *J* = 8.1 Hz, 7.5 Hz, 1.8 Hz, 0.6 Hz, 1H), 7.40 (dddd, *J* = 7.4 Hz, 1.9 Hz, 1.0 Hz, 0.6 Hz, 1H; ^{13}C NMR (101 MHz, DMSO-d_6) δ = 31.8 (CH_2), 57.7 (CH_2OH), 67.9 (CH_2), 111.5 (CH_{Ar}), 120.7 (CH_{Ar}), 126.9 (CH_{Ar}), 127.5 (CH_{Ar}), 130.9 (C_q), 154.5 (C_q); HRMS (ESI-MS) *m/z* calcd for $C_9H_{11}BrNaO_2$ $[M+Na]^+$: 252.9840, found: 252.9834; Rf (petroleum ether/EtOAc = 5/5) 0.49.
4t	*(5-Bromo-2-(2-bromoethoxy)phenyl)methanol*was obtained from 5-bromo-2-(2-bromo-ethoxy)benzaldehyde (**2t**) as pale yellow oil, yield 89%; ^{1}H NMR (250 MHz, DMSO-d_6) δ = 3.74–3.84 (m, 2H), 4.26–4.36 (m, 2H), 4.53 (dt, *J* = 5.67 Hz, 0.85 Hz, 2H), 5.19 (t, *J* = 5.6 Hz, 1H), 6.93 (d, *J* = 8.6 Hz, 1H), 7.36 (ddt, *J* = 8.6 Hz, 2.6 Hz, 0.7 Hz, 1H), 7.50 (dt, *J* = 2.6 Hz, 0.9 Hz, 1H); ^{13}C NMR (101 MHz, DMSO-d_6) δ = 31.5 (CH_2), 57.3 (CH_2OH), 68.1 (CH_2), 112.5 (C_q), 113.8 (CH_{Ar}), 129.1 (CH_{Ar}), 129.8 (CH_{Ar}), 133.7 (C_q), 153.6 (C_q); HRMS (ESI-MS) *m/z* calcd for $C_9H_{10}Br_2NaO_2$ $[M+Na]^+$: 330.8945, found: 330.8953; Rf (petroleum ether/EtOAc = 5/5) 0.47.
4u	*(3-(2-Bromoethoxy)-2-chloro-4-methoxyphenyl)methanol* was obtained from 3-(2-bromo-ethoxy)-2-chloro-4-methoxybenzaldehyde (**2u**) as white solid, yield 99%, m.p. 76–78°C; ^{1}H NMR (400 MHz, DMSO-d_6) δ = 3.73 (t, *J* = 5.8 Hz, 2H), 3.82 (s, 3H), 4.24 (t, *J* = 5.8 Hz, 2H), 4.48 (d, *J* = 5.0 Hz, 2H), 5.24 (t, *J* = 5.6 Hz, 1H), 7.05 (d, *J* = 8.6 Hz, 1H), 7.23 (t, *J* = 8.5 Hz, 0.9 Hz, 1H); ^{13}C NMR (101 MHz, DMSO-d_6) δ = 31.5 (CH_2), 56.1 (CH_3), 60.2(CH_2OH), 72.4 (CH_2), 111.2 (CH_{Ar}), 123.1 (CH_{Ar}), 125.2 (C_q), 132.3 (C_q), 142.9 (C_q), 151.9 (C_q); HRMS (ESI-MS) *m/z* calcd for $C_{10}H_{12}BrClNaO_3$ $[M+Na]^+$: 316.9556, found: 316.9552; Rf (petroleum ether/EtOAc = 3/7) 0.66.
4v	*2-(4-(2-Bromoethoxy)phenyl)ethanol* was obtained from 4-(2-hydroxyethyl)phenol (**1v**) as white needle crystals, yield 82%, m.p. 65–68 °C;^{1}H NMR (250 MHz, DMSO-d_6) δ = 2.65 (t, *J* =7.1 Hz, 2H), 3.55 (td, *J* = 7.1 Hz, 5.2 Hz, 2H), 3.72–3.83 (m, 2H), 4.21–4.33 (m, 2H), 4.58 (t, *J* = 5.2 Hz, 1H), 6.79–6.93 (m, 2H), 7.06–7.23 (m, 2H); ^{13}C NMR (101 MHz, DMSO-d_6) δ = 31.5 (CH_2), 38.1 (CH_2), 62.4 (CH_2OH), 67.7 (CH_2), 114.4 ($2CH_{Ar}$), 129.8 ($2CH_{Ar}$), 132.0 (C_q), 156.2 (C_q); HRMS (ESI-MS) *m/z* calcd for $C_{10}H_{14}BrO_2$ $[M+H]^+$: 245.0177, found: 245.0171; Rf (petroleum ether/ EtOAc = 3/7) 0.60.

By the metathesis reaction of the *(bromoethoxy)aromatic alcohol derivatives* (**4a-m**, **t-v**) with silver nitrate in acetonitrile, the corresponding *(hydroxyalkyl)phenoxy nitrate derivatives* (**5a-m**, **t-v**) were obtained in high yields, which ranged between 89% and 99%.

Their main physico-chemical and spectral characteristics (^{1}H NMR, ^{13}C NMR, MS) are presented in Table 7.4.

Table 7.4. The identification characteristics (^{1}H NMR, ^{13}C NMR, MS, R_f) of the (hydroxyalkyl)phenoxy nitrate derivatives (**5a-m**, **t, u**).

Cpd.	The identification characteristics (^{1}H NMR, ^{13}C NMR, MS, R_f)
5a	*2-(4-(Hydroxymethyl)phenoxy)ethyl nitrate* wasobtained from (4-(2-bromoethoxy)phenyl) methanol **(4a)** as white solid, yield 97%, m.p. 55–57 °C; ^{1}H NMR (250 MHz, DMSO-d_6) δ = 4.23–4.34 (m, 2H), 4.42 (d, *J* = 5.6 Hz, 2H), 4.81–4.91 (m, 2H), 5.05 (t, *J* = 5.6 Hz, 1H), 6.79–6.98 (m, 2H), 7.15–7.31 (m, 2H); ^{13}C NMR (101 MHz, DMSO-d_6) δ = 62.5 (CH_2OH), 64.0 (CH_2), 72.1 (CH_2), 114.1 ($2CH_{Ar}$), 127.9 ($2CH_{Ar}$), 135.2 (C_q), 156.7 (C_q); HRMS (ESI-MS) *m/z* calcd for $C_9H_{11}NNaO_5$ $[M+Na]^+$: 236.0535, found: 236.0526; Rf (petroleum ether/EtOAc = 6/4) 0.62.
5b	*2-(2-Fluoro-4-(hydroxymethyl)phenoxy)ethyl nitrate* was obtained from (4-(2-bromoethoxy)-3-fluorophenyl)methanol (**4b**) as greenish yellow oil, yield 95%; ^{1}H NMR (400 MHz, DMSO-d_6) δ = 4.33–4.39 (m, 2H), 4.42 (d, *J* = 5.6 Hz, 2H), 4.84–4.94 (m, 2H), 5.19 (t, *J* = 5.7Hz, 1H), 7.03–7.09 (m, 1H), 7.11–7.18 (m, 2H); ^{13}C NMR (101 MHz, DMSO-d_6) δ = 61.9 (CH_2OH), 65.4 (CH_2), 71.9 (CH_2), 114.2 (d, *J* = 18.0 Hz, CH_{Ar}), 115.1 (d, *J* = 1.8 Hz, CH_{Ar}), 122.4 (d, *J* = 3.5 Hz, CH_{Ar}), 136.7 (d, *J* = 5.5 Hz, C_q), 144.2 (d, *J* = 10.7 Hz, C_q), 151.5 (d, *J* = 243.9 Hz, C_qF); ^{19}F NMR (376 MHz, DMSO-d_6) δ = -134.94 (dd, *J* = 12.1 Hz, 8.3 Hz); HR.MS (ESI-MS) *m/z* calcd for $C_9H_{10}FNNaO_5$ $[M+Na]^+$: 254.0441, found: 254.0436; Rf (CH_2Cl_2/CH_3OH = 9.8/0.2) 0.66.
5c	*2-(2-Chloro-4-(hydroxymethyl)phenoxy)ethyl nitrate* was obtained from (4-(2-bromoethoxy)-3-chlorophenyl)methanol **(4c)** as orange oil, yield 97%; ^{1}H NMR (400 MHz, DMSO-d_6) δ = 4.33–4.39 (m, 2H), 4.42 (d, *J* = 5.8 Hz, 2H), 4.85–4.95 (m, 2H), 5.20 (t, *J* = 5.8 Hz, 1H), 7.14 (d, *J* = 8.4 Hz, 1H), 7.23 (dd, *J* = 8.4 Hz, 2.0 Hz, 1H), 7.36 (d, *J* = 2.0 Hz, 1H); ^{13}C NMR (101 MHz, DMSO-d_6) δ = 61.8 (CH_2OH), 65.4 (CH_2), 71.7 (CH_2), 114.0 (CH_{Ar}), 121.2 (C_q), 126.3 (CH_{Ar}), 128.1 (CH_{Ar}), 136.7 (C_q), 151.9 (C_q); HRMS (ESI-MS) *m/z* calcd for $C_9H_{10}ClNNaO_5$ $[M+Na]^+$: 270.0145, found: 270.0140; Rf (CH_2Cl_2/CH_3OH = 9.8/0.2) 0.63.
5d	*2-(4-(hydroxymethyl)-2-methoxyphenoxy)ethyl nitrate*was obtained from (4-(2-bromoethoxy) -3-methoxyphenyl)methanol **(4d)** as brown solid, yield 99%, m.p. 51–52 °C; ^{1}H NMR (250 MHz, DMSO-d_6) δ = 3.75 (s, 3H), 4.17–4.31 (m, 2H), 4.42 (d, *J* = 5.5 Hz, 2H), 4.78–4.91 (m, 2H), 5.09 (t, *J* = 5.6 Hz, 1H), 6.81 (ddt, *J* = 8.0 Hz, 1.9 Hz, 0.7 Hz, 1H), 6.87–7.00 (m, 2H);13C NMR (101 MHz, DMSO-d6) δ = 55.4 (CH3), 62.7 (CH2OH), 65.2 (CH2), 72.2 (CH2), 110.9 (CHAr), 114.0 (CHAr), 118.5 (CHAr), 136.4 (Cq), 146.0 (Cq), 149.0 (Cq); HRMS (ESI-MS) m/z calcd for C10H13NNaO6 [M+Na]+: 266.0641, found: 266.0632; Rf (petroleum ether/EtOAc = 6/4) 0.55.

Cpd.	The identification characteristics (^{1}H NMR, ^{13}C NMR, MS, R_f)
5e	*2-(2-Ethoxy-4-(hydroxymethyl)phenoxy)ethyl nitrate* was obtained from (4-(2-bromoethoxy)-3-ethoxyphenyl)methanol **(4e)** as greenish yellow solid, yield 99%, m.p. 57–59 °C; ^{1}H NMR (250 MHz, DMSO-d_6) δ = 1.31 (t, *J* = 6.98 Hz, 3H), 4.01 (q, *J* = 6.96 Hz, 2H), 4.17–4.29 (m, 2H), 4.41 (d, *J* = 5.1 Hz, 2H), 4.76–4.91 (m, 2H), 5.08 (t, *J* = 5.6 Hz, 1H), 6.81 (ddt, *J* = 8.1 Hz, 1.9 Hz, 0.7 Hz, 1H), 6.94 (d, *J* = 8.1 Hz, 1H), 6.94 (d, *J* = 1.9 Hz, 1H); ^{13}C NMR (101 MHz, DMSO-d_6) δ = 14.7 (CH_3), 62.7 (CH_2OH), 63.8 (CH_2), 65.7 (CH_2), 72.2 (CH_2), 112.4 (CH_{Ar}), 114.9 (CH_{Ar}), 118.7 (CH_{Ar}), 136.6 (C_q), 146.3 (C_q), 148.5 (C_q); HRMS (ESI-MS) *m/z* calcd for $C_{11}H_{15}NNaO_6$ $[M+Na]^+$: 280.0797, found: 280.0794; Rf (petroleum ether/EtOAc = 6/4) 0.48.
5f	*2-(4-(Hydroxymethyl)-2-nitrophenoxy)ethyl nitrate* was obtained from(4-(2-bromoethoxy)-3-nitrophenyl)methanol **(4f)** as brown greenish yellow solid, yield 95%, m.p. 56–58 °C; ^{1}H NMR (400 MHz, DMSO-d_6) δ = 4.44–4.53 (m, 4H), 4.86–4.93 (m, 2H), 5.36 (t, *J* = 5.7 Hz, 1H), 7.36 (d, *J* = 8.6 Hz, 1H), 7.59 (dd, *J* = 8.6 Hz, 2.1 Hz, 1H), 7.80 (d, *J* = 2.1 Hz, 1H); ^{13}C NMR (101 MHz, DMSO-d_6) δ = 61.4 (CH_2OH), 66.1 (CH_2), 71.4 (CH_2), 115.4 (CH_{Ar}), 122.7 (CH_{Ar}), 132.3 (CH_{Ar}), 136.0 (C_q), 139.3 (C_q), 149.3 (C_q); HRMS (ESI-MS) *m/z* calcd for $C_9H_{10}N_2NaO_7$ $[M+Na]^+$: 281.0386, found: 281.0381; Rf (CH_2Cl_2/CH_3OH = 9.8/0.2) 0.52.
5g	*2-(4-(Hydroxymethyl)-2,6-dimethoxyphenoxy)ethyl nitrate* was obtained from(4-(2-bromo-ethoxy)-3,5-dimethoxyphenyl)methanol **(4g)** asgreenish yellow solid, yield 99%, m.p. 56–58 °C; ^{1}H NMR (250 MHz, DMSO-d_6) δ = 3.74 (s, 6H), 4.04–4.15 (m, 2H), 4.43 (dt, *J* = 5.8 Hz, 0.6 Hz, 2H), 4.67–4.78 (m, 2H), 5.17 (t, *J* = 5.8 Hz, 1H), 6.63 (d, *J* = 0.6 Hz, 2H);^{13}C NMR (101 MHz, DMSO-d_6) δ = 55.8 ($2CH_3$), 62.9 (CH_2OH), 68.4 (CH_2), 72.9 (CH_2), 103.3 ($2CH_{Ar}$), 134.2 (C_q), 138.9 (C_q), 152.6 ($2C_q$); HRMS (ESI-MS) *m/z* calcd for $C_{11}H_{16}NO_7$ $[M+H]^+$: 274.0927, found: 274.0922; Rf (petroleum ether/EtOAc = 7/3) 0.43.
5h	*2-(2,6-Dichloro-4-(hydroxymethyl)phenoxy)ethyl nitrate* was obtained from 4-(2-bromo ethoxy)-3,5-dichlorophenyl)methanol **(4h)** as greenish yellow oil, yield 99%; ^{1}H NMR (250 MHz, DMSO-d_6) δ = 4.20–4.34 (m, 2H), 4.46 (dt, *J* = 5.8 Hz, 0.8 Hz, 2H), 4.78–4.94 (m, 2H), 5.40 (t, *J* = 5.8 Hz, 1H), 7.41 (t, *J* = 0.8 Hz 2H); ^{13}C NMR (101 MHz, DMSO-d_6) δ = 61.2 (CH_2OH), 69.4 (CH_2), 72.5 (CH_2), 126.8 ($2CH_{Ar}$), 127.9 ($2C_q$), 141.4 (C_q), 148.4 (C_q); HRMS (ESI-MS) *m/z* calcd for $C_9H_9Cl_2NNaO_5$ $[M+Na]^+$: 303.9755, found: 303.9747; Rf (CH_2Cl_2/CH_3OH = 9.8/0.2) 0.53.
5i	*2-(3-(Hydroxymethyl)phenoxy)ethyl nitrate* was obtained from (3-(2-bromoethoxy)phenyl) methanol **(4i)** as colorless oil, yield 89%; ^{1}H NMR (250 MHz, DMSO-d_6) δ = 4.16–4.34 (m, 2H), 4.48 (d, *J* = 5.8 Hz, 2H), 4.81–4.90 (m, 2H), 5.17 (t, *J* = 5.8 Hz, 1H), 6.76–6.86 (m, 1H), 6.86–6.96 (m, 2H), 7.24 (t, *J* =8.0 Hz, 1H); ^{13}C NMR (101 MHz, DMSO-d_6) δ = 62.8 (CH_2OH), 67.6 (CH_2), 72.1 (CH_2),112.5 (CH_{Ar}), 112.8 (CH_{Ar}), 119.0 (CH_{Ar}), 129.2 (CH_{Ar}), 144.4 (C_q), 157.9 (C_q); HRMS (ESI-MS) *m/z* calcd for $C_9H_{11}NNaO_5$ $[M+Na]^+$: 236.0535, found: 236.0529; Rf (CH_2Cl_2/CH_3OH = 9.6/0.4) 0.39.
5j	*2-(5-(Hydroxymethyl)-2-methoxyphenoxy)ethyl nitrate* was obtained from (3-(2-bromoethoxy) -4-methoxyphenyl)methanol (4j) asyellow solid, yield 80%, m.p. 51–53 °C; ^{1}H NMR (250 MHz, DMSO-d_6) δ = 3.74 (s, 3H), 4.21–4.30 (m, 2H), 4.41 (d, *J* = 5.7 Hz, 2H), 4.81–4.90 (m, 2H), 5.06 (t, *J* = 5.7 Hz, 1H), 6.82–6.98 (m, 3H); ^{13}C NMR (101 MHz, DMSO-d_6) δ = 55.6 (CH_3), 62.6 (CH_2OH), 65.0 (CH_2), 72.1 (CH_2), 112.0 (CH_{Ar}), 112.8 (CH_{Ar}), 119.7 (CH_{Ar}), 135.1 (C_q), 147.0 (C_q), 148.0 (C_q); HRMS (ESI-MS) *m/z* calcd for $C_{10}H_{13}NNaO_6$ $[M+Na]^+$: 266.0641, found: 266.0635 ; Rf (petroleum ether/EtOAc = 7/3) 0.63.

Cpd.	The identification characteristics (^{1}H NMR, ^{13}C NMR, MS, R_f)
5k	*2-(5-(Hydroxymethyl)-2-nitrophenoxy)ethyl nitrate* was obtained from (3-(2-bromoethoxy)-4-nitrophenyl)methanol **(4k)** as brown oil, yield 94%; ^{1}H NMR (250 MHz, DMSO-d_6) δ = 4.43–4.53 (m, 2H), 4.58 (d, *J* = 5.7 Hz, 2H), 4.85–4.96 (m, 2H), 5.49 (t, *J* = 5.7 Hz, 1H), 7.10 (ddt, *J* = 8.3 Hz, 1.5 Hz, 0.7 Hz, 1H), 7.28–7.33 (m, 1H), 7.87 (d, *J* = 8.3 Hz, 1H); ^{13}C NMR (101 MHz, DMSO-d_6) δ = 62.0 (CH_2OH), 65.9 (CH_2), 71.3 (CH_2), 112.5 (CH_{Ar}), 118.5 (CH_{Ar}), 125.1 (CH_{Ar}), 137.9 (C_q), 150.4 (C_q), 150.7 (C_q); HRMS (ESI-MS) *m/z* calcd for $C_9H_{10}N_2NaO_7$ $[M+Na]^+$: 281.0386, found: 281.0380; Rf (CH_2Cl_2/CH_3OH = 9.6/0.4) 0.53.
5l	*2-(2-Bromo-3-(hydroxymethyl)-6-methoxyphenoxy)ethyl nitrate* was obtained from (2-bromo-3-(2-bromoethoxy)-4-methoxyphenyl)methanol (**4l**): as white solid, yield 92%, m.p. 58–60 °C; ^{1}H NMR (400 MHz, DMSO-d_6) δ = 3.81 (s, 3H), 4.16–4.25 (m, 2H), 4.44 (dd, *J* = 5.6 Hz, 0.8 Hz, 2H), 4.76–4.87 (m, 2H), 5.29 (t, *J* = 5.6 Hz, 1H), 7.10 (d, *J* = 8.5 Hz, 1H), 7.25 (dt, *J* = 8.5 Hz, 0.8 Hz, 1H); ^{13}C NMR (101 MHz, DMSO-d_6) δ = 56.0 (CH_3), 62.5 (CH_2OH), 68.6 (CH_2), 72.7 (CH_2), 111.8 (CH_{Ar}), 116.4 (C_q), 123.4 (CH_{Ar}), 133.7 (C_q), 143.8 (C_q), 151.7 (C_q); HRMS (ESI-MS) *m/z* calcd for $C_{10}H_{12}BrNNaO_6$ $[M+Na]^+$: 343.9746, found: 343.9737; Rf (CH_2Cl_2/CH_3OH = 9.6/0.4) 0.56.
5m	*2-(2-(Hydroxymethyl)phenoxy)ethyl nitrate* was obtained from(2-(2-bromoethoxy)phenyl) methanol **(4m)** as orange oil, yield 93%; ^{1}H NMR (400 MHz, DMSO-d_6) δ = 4.25–4.31 (m, 2H), 4.47 (d, *J* = 5.6 Hz, 2H), 4.86–4.92 (m, 2H), 4.98 (t, *J* = 5.6 Hz, 1H), 6.97 (t, *J* = 7.4 Hz, 2H), 7.21 (td, *J* = 7.8 Hz, 1.8 Hz, 1H), 7.39 (dd, *J* = 7.1 Hz, 1.2 Hz, 1H); ^{13}C NMR (101 MHz, DMSO-d_6) δ = 57.6 (CH_2OH), 64.4 (CH_2), 72.0 (CH_2), 111.4 (CH_{Ar}), 120.8 (CH_{Ar}), 127.0 (CH_{Ar}), 127.5 (CH_{Ar}), 130.7 (C_q), 154.5 (C_q); HRMS (ESI-MS) *m/z* calcd for $C_9H_{11}NNaO_5$ $[M+Na]^+$: 236.0535, found: 236.0530; Rf (CH_2Cl_2/CH_3OH = 9.6/0.4) 0.62.
5t	*2-(4-Bromo-2-(hydroxymethyl)phenoxy)ethyl nitrate* was obtained from (5-bromo-2-(2-bromoethoxy)phenyl)methanol **(4t)** as greenish yellow oil, yield 95%; ^{1}H NMR (250 MHz, DMSO-d_6) δ = 4.26–4.34 (m, 2H), 4.45 (dt, *J* = 5.6 Hz, 0.8 Hz, 2H), 4.85–4.92 (m, 2H), 5.19 (t, *J* = 5.6 Hz, 1H), 6.95 (d, *J* = 8.7 Hz, 1H), 7.38 (ddt, *J* = 8.7 Hz, 2.6 Hz, 0.7 Hz, 1H), 7.49 (dt, *J* = 2.6 Hz, 0.9 Hz, 1H); ^{13}C NMR (101 MHz, DMSO-d_6) δ = 57.2 (CH_2OH), 64.8 (CH_2), 71.8 (CH_2), 112.6 (C_q), 113.7 (CH_{Ar}), 129.2 (CH_{Ar}), 129.9 (CH_{Ar}), 133.6 (C_q), 153.7 (C_q); HRMS (ESI-MS) *m/z* calcd for $C_9H_{10}BrNNaO_5$ $[M+Na]^+$: 313.9640, found: 313.9634; Rf (CH_2Cl_2/CH_3OH = 9.6/0.4) 0.55.
5u	*2-(2-Chloro-3-(hydroxymethyl)-6-methoxyphenoxy)ethyl nitrate* was obtained from (3-(2-bromoethoxy)-2-chloro-4-methoxyphenyl)methanol (**4u**) as white solid, yield 91%, m.p. 57–59 °C; ^{1}H NMR (400 MHz, DMSO-d_6) δ = 3.80 (s, 3H), 4.15–4.29 (m, 2H), 4.48 (dd, *J* = 5.6 Hz, 0.8 Hz, 2H), 4.75–4.90 (m, 2H), 5.25 (t, *J* = 5.6 Hz, 1H), 7.06 (d, *J* = 8.6 Hz, 1H), 7.24 (dt, *J* = 8.7 Hz, 0.9 Hz, 1H); ^{13}C NMR (101 MHz, DMSO-d_6) δ = 56.0 (CH_3), 60.2 (CH_2OH), 68.7 (CH_2), 72.7 (CH_2), 111.1 (CH_{Ar}), 123.2 (CH_{Ar}), 125.2 (C_q), 132.3 (C_q), 142.8 (C_q), 151.9 (C_q); HRMS (ESI-MS) *m/z* calcd for $C_{10}H_{12}ClNNaO_6$ $[M+Na]^+$: 300.0251, found: 300.0246; Rf (CH_2Cl_2/CH_3OH = 9.6/0.4) 0.55.

Cpd.	The identification characteristics (^{1}H NMR, ^{13}C NMR, MS, R_f)
5v	*2-(4-(2-Hydroxyethyl)phenoxy)ethyl nitrate* (***5v***) was obtained from 2-(4-(2-bromoethoxy) phenyl)ethanol (**4v**) as white solid, yield 98%, m.p. 53–55 °C; ^{1}H NMR (250 MHz, DMSO-d_6) δ = 2.65 (t, *J* = 7.1 Hz, 2H), 3.55 (td, *J* = 7.1 Hz, 5.2 Hz, 2H), 4.21–4.31 (m, 2H), 4.58 (t, *J* = 5.2 Hz, 1H), 4.82–4.89 (m, 2H), 6.82–6.90 (m, 2H), 7.08–7.18 (m, 2H); ^{13}C NMR (101 MHz, DMSO-d_6) δ = 38.1 (CH_2), 62.4 (CH_2OH), 64.0 (CH_2), 72.1 (CH_2), 114.2 ($2CH_{Ar}$), 129.9 ($2CH_{Ar}$), 132.1 (C_q), 156.1 (C_q); HRMS (ESI-MS) *m/z* calcd for $C_{10}H_{13}NNaO_5$ $[M+Na]^+$: 250.0691, found: 250.0697; Rf (petroleum ether/EtOAc = 6/4) 0.63.

Common methods for conversion of alcohols to the corresponding alkyl chloride involve activation of hydroxyl group before treatment with a chlorination agent such as thionyl chloride, *phosphorus trichloride* and phosphorous pentachloride [302]. In the present study thionyl chloride, in combination with benzotryazole, was used, the last one having some favorable features. It is amphoteric compound, beeing a mild base as well as acid, and can be removed from the mixture reaction by acid or alkali wash. Moreover it is a good leaving group and his hydrochloride salt is insoluble in organic solvents like CH_2Cl_2. These are important advantages in reference with commonly used bases like pyridine and triethylamine.

Appling this method, the desired *(halidealkyl)phenoxy nitrate derivatives* (**6a-m, t, u**) were obtained at room temperature in good yileds, which ranged between 83% and 99%. Their main physico-chemical and spectral characteristics (^{1}H NMR, ^{13}C NMR, MS) are presented in Table 7.5.

Table 7.5. The identification characteristics (^{1}H NMR, ^{13}C NMR, MS, R_f) of the (halidealkyl)phenoxy nitrate derivatives (**6a-m**, **t-v**).

Cpd.	The Identificationcharacteristics (^{1}H NMR, ^{13}C NMR, MS, R_f)
6a	*2-(4-(Chloromethyl)phenoxy)ethyl nitrate* was obtained from 2-(4-(hydroxymethyl)phenoxy) ethyl nitrate (**5a**) as yellow oil, yield 99%; ^{1}H NMR (400 MHz, DMSO-d_6) δ = 4.28–4.36 (m, 2H), 4.73 (s, 2H), 4.85–4.93 (m, 2H), 6.97 (d, *J* = 8.2 Hz, 2H), 7.38 (d, *J* = 8.2 Hz, 2H); ^{13}C NMR (101 MHz, DMSO-d_6) δ = 46.1 (CH_2), 64.0 (CH_2), 72.0 (CH_2), 114.6 ($2CH_{Ar}$), 130.3 (C_q), 130.4 ($2CH_{Ar}$), 157.8 (C_q); HRMS (ESI-MS) *m/z* calcd for $C_9H_{10}ClNNaO_4$ $[M+Na]^+$: 254.0196, found: 254.0185; Rf (petroleum ether/EtOAc = 7/3) 0.69.
6b	*2-(4-(Chloromethyl)-2-fluorophenoxy)ethyl nitrate* was obtained from 2-(2-fluoro-4-(hydroxyllmethyl)phenoxy)ethyl nitrate **(5b)** aspale yellow oil, yield 97%; ^{1}H NMR (400 MHz, DMSO-d_6) δ = 4.36–4.43 (m, 2H), 4.72 (s, 2H), 4.86–4.93 (m, 2H), 7.16–7.26 (m, 2H), 7.33 (dd, *J* = 12.3 Hz, 1.7 Hz, 1H); ^{13}C NMR (101 MHz, DMSO-d_6) δ = 45.3 (CH_2), 65.3 (CH_2), 71.7 (CH_2), 115.2 (d, *J* = 1.9 Hz, CH_{Ar}), 116.7 (d, *J* = 18.7 Hz, CH_{Ar}), 125.5 (d, *J* = 3.5 Hz, CH_{Ar}), 131.3 (d, *J* = 6.6 Hz, C_q), 145.7 (d, *J* = 10.6 Hz, C_q), 151.19 (d, *J* = 244.7 Hz, C_qF); ^{19}F NMR (376 MHz, DMSO-d_6) δ = -134.2 (dd, *J* = 12.3 Hz, 7.5 Hz); HRMS (ESI-MS) *m/z* calcd for $C_9H_9ClFNNaO_4$ $[M+Na]^+$: 272.0102, found: 272.0096; Rf (petroleum ether/EtOAc = 7/3) 0.69.

Cpd.	The Identificationcharacteristics (^{1}H NMR, ^{13}C NMR, MS, R_f)
6c	*2-(2-Chloro-4-(chloromethyl)phenoxy)ethyl nitrate* was obtained from 2-(2-chloro-4-(hydroxylmethyl)phenoxy)ethyl nitrate (**5c**) as white solid, yield 95%, m.p. 52–54 °C; ^{1}H NMR (400 MHz, DMSO-d_6) δ = 4.38–4.46 (m, 2H), 4.73 (s, 2H), 4.89–4.95 (m, 2H), 7.19 (d, *J* = 8.5 Hz, 1H), 7.39 (dd, *J* = 8.5 Hz, 2.2 Hz, 1H), 7.54 (d, *J* = 2.1 Hz, 1H); ^{13}C NMR (101 MHz, DMSO-d_6) δ = 45.1 (CH_2), 65.4 (CH_2), 71.6 (CH_2), 114.1 (CH_{Ar}), 121.3 (C_q), 129.0 (CH_{Ar}), 130.5 (CH_{Ar}), 131.7 (C_q), 153.1 (C_q); HRMS (ESI-MS) *m/z* calcd for $C_9H_9Cl_2NNaO_4$ $[M+Na]^+$: 287.9806, found: 287.9798; Rf (petroleum ether/EtOAc = 7/3) 0.65.
6d	*2-(4-(Chloromethyl)-2-methoxyphenoxy)ethyl nitrate* was obtained from 2-(4-(hydroxyl-methyl)-2-methoxyphenoxy)ethyl nitrate **(5d)** as white solid, yield 85%, m.p. 54–56 °C; ^{1}H NMR (250 MHz, DMSO-d_6) δ = 3.77 (s, 3H), 4.20–4.35 (m, 2H), 4.71 (s, 2H), 4.80–4.91 (m, 2H), 6.96–6.99 (m, 2H), 7.07 (s, 1H); ^{13}C NMR (101 MHz, DMSO-d_6) δ = 46.5 (CH_2), 55.6 (CH_3), 65.0 (CH_2), 72.0 (CH_2), 112.9 (CH_{Ar}), 113.7 (CH_{Ar}), 121.4 (CH_{Ar}), 131.0 (C_q), 147.3 (C_q), 149.0 (C_q). HRMS (ESI-MS) *m/z* calcd for $C_{10}H_{12}ClNNaO_5$ $[M+Na]^+$: 284.0302, found: 284.0299; Rf (petroleum ether/EtOAc = 5/5) 0.76.
6e	*2-(4-(Chloromethyl)-2-ethoxyphenoxy)ethyl nitrate* was obtained from2-(2-ethoxy-4-(hydroxylmethyl)phenoxy)ethyl nitrate **(5e)** as white solid, yield 84%, m.p. 57–60 °C; ^{1}H NMR (250 MHz, DMSO-d_6) δ = 1.32 (t, *J* = 6.9 Hz, 3H), 4.02 (q, *J* = 6.9 Hz, 2H), 4.24–4.33 (m, 2H), 4.70 (s, 2H), 4.81–4.92 (m, 2H), 6.95–6.99 (m, 2H), 7.06 (d, *J* = 1.7 Hz, 0.6 Hz, 1H); ^{13}C NMR (101 MHz, DMSO-d_6) δ = 14.6 (CH_3), 46.4 (CH_2), 63.9 (CH_2), 65.4 (CH_2), 72.0 (CH_2), 114.4 (CH_{Ar}), 114.5 (CH_{Ar}), 121.5 (CH_{Ar}), 131.2 (C_q), 147.6 (C_q), 148.4 (C_q); HRMS (ESI-MS) *m/z* calcd for $C_{11}H_{14}ClNNaO_5$ $[M+Na]^+$: 298.0458, found: 298.0456; Rf (petroleum ether/EtOAc = 7/3) 0.72.
6f	*2-(4-(Chloromethyl)-2-nitrophenoxy)ethyl nitrate* was obtained from2-(4-(hydroxymethyl)-2-nitrophenoxy)ethyl nitrate **(5f)** as greenish yellow solid, yield 90%, m.p. 56–58 °C; ^{1}H NMR (400 MHz, DMSO-d_6) δ = 4.49–4.55 (m, 2H), 4.81 (s, 2H), 4.86–4.94 (m, 2H), 7.42 (d, *J* = 8.7 Hz, 1H), 7.74 (dd, *J* = 8.7 Hz, 2.3 Hz, 1H), 8.00 (d, *J* = 2.3 Hz, 1H); ^{13}C NMR (101 MHz, DMSO-d_6) δ = 44.4 (CH_2), 66.1 (CH_2), 71.3 (CH_2), 115.8 (CH_{Ar}), 125.3 (CH_{Ar}), 131.0 (C_q), 133.0 (CH_{Ar}), 139.2 (C_q), 150.4 (C_q); HRMS (ESI-MS) *m/z* calcd for $C_9H_9ClN_2NaO_6$ $[M+Na]^+$: 299.0047, found: 299.0044; Rf (CH_2Cl_2) 0.70.
6g	*2-(4-(Chloromethyl)-2,6-dimethoxyphenoxy)ethyl nitrate* was obtained from 2-(4-(hydroxymethyl)-2,6-dimethoxyphenoxy)ethyl nitrate (**5*g***) as white solid, yield 86%, m.p. 59–61 °C; ^{1}H NMR (400 MHz, DMSO-d_6) δ = 3.76 (s, 6H), 4.09–4.17 (m, 2H), 4.70 (s, 2H), 4.72–4.78 (m, 2H), 6.78 (s, 2H); ^{13}C NMR (101 MHz, DMSO-d_6) δ = 46.6 (CH_2), 55.9 ($2CH_3$), 68.5 (CH_2), 72.9 (CH_2), 106.1 ($2CH_{Ar}$), 133.6 (C_q), 135.6 (C_q), 152.7 ($2C_q$); HRMS (ESI-MS) *m/z* calcd for $C_{11}H_{15}ClNO_6$ $[M+H]^+$: 292.0588, found: 292.0580; Rf (petroleum ether/EtOAc = 7/3) 0.61.
6h	*2-(2,6-Dichloro-4-(chloromethyl)phenoxy)ethyl nitrate* was obtained from2-(2,6-dichloro-4-(hydroxymethyl)phenoxy)ethyl nitrate (**5h**) aswhite solid, yield 85%, m.p. 49–51 °C; ^{1}H NMR (400 MHz, DMSO-d_6) δ = 4.27–4.38 (m, 2H), 4.74 (s, 2H), 4.86–4.93 (m, 2H), 7.62 (s, 2H); ^{13}C NMR (101 MHz, DMSO-d_6) δ = 43.9 (CH_2), 69.5 (CH_2), 72.4 (CH_2), 128.2 ($2C_q$), 129.7 ($2CH_{Ar}$), 136.3 (C_q), 149.9 (C_q); HRMS (ESI-MS) *m/z* calcd for $C_9H_8Cl_3NNaO_4$ $[M+Na]^+$: 321.9417, found: 321.9406; Rf (petroleum ether/EtOAc = 8/2) 0.70.

Cpd.	The Identificationcharacteristics (^{1}H NMR, ^{13}C NMR, MS, R_f)
6i	*2-(3-(Chloromethyl)phenoxy)ethyl nitrate* was obtained from 2-(3-(hydroxymethyl)phenoxy) ethyl nitrate **(5i)** as pale yellow oil, yield 88%; ^{1}H NMR (250 MHz, DMSO-d_6) δ = 4.26–4.37 (m, 2H), 4.72 (s, 2H), 4.83–4.95 (m, 2H), 6.94 (ddd, *J* = 8.2 Hz, 2.6 Hz, 1.0 Hz, 1H), 7.00–7.09 (m, 2H), 7.24–7.38 (m, 1H); ^{13}C NMR (101 MHz, DMSO-d_6) δ = 45.9 (CH_2), 64.0 (CH_2), 71.9 (CH_2), 114.4 (CH_{Ar}), 114.9 (CH_{Ar}), 121.6 (CH_{Ar}), 129.8 (CH_{Ar}), 139.2 (C_q), 157.9 (C_q); HRMS (ESI-MS) *m/z* calcd for $C_9H_{11}ClNO_4$ $[M+H]^+$: 232.0377, found: 232.0371; Rf (petroleum ether/EtOAc = 8/2) 0.60.
6j	*2-(5-(Chloromethyl)-2-methoxyphenoxy)ethyl nitrate* was obtained from 2-(5-(hydroxyl-methyl)-2-methoxyphenoxy)ethyl nitrate (**5j**) as yellow oil, yield 92%, ^{1}H NMR (250 MHz, DMSO-d_6) δ = 3.77 (s, 3H), 4.22–4.33 (m, 2H), 4.70 (s, 2H), 4.79–4.92 (m, 2H), 6.97 (d, *J* = 8.2 Hz, 1H), 7.02 (d, *J* = 1.9 Hz, 1H), 7.09 (d, *J* = 1.9 Hz, 1H); ^{13}C NMR (101 MHz, DMSO-d_6) δ = 46.5 (CH_2), 55.6 (CH_3), 65.1 (CH_2), 72.0 (CH_2), 112.1 (CH_{Ar}), 114.7 (CH_{Ar}), 122.5 (CH_{Ar}), 129.9 (C_q), 147.1 (C_q), 149.2 (C_q); HRMS (ESI-MS) *m/z* calcd for $C_{10}H_{12}ClNNaO_5$ $[M+Na]^+$: 284.0302, found: 284.0297; Rf (petroleum ether/EtOAc = 8/2) 0.45.
6k	*2-(5-(Chloromethyl)-2-nitrophenoxy)ethyl nitrate* was obtained from 2-(5-(hydroxymethyl)-2-nitrophenoxy)ethyl nitrate (**5k**) as brown solid, yield 91%, m.p. 51–53 °C; ^{1}H NMR (400 MHz, DMSO-d_6) δ = 4.47–4.56 (m, 2H), 4.81 (s, 2H), 4.88–4.97 (m, 2H), 7.23 (dd, *J* = 8.3 Hz, 1.6 Hz, 1H), 7.50 (d, *J* = 1.6 Hz, 1H), 7.91 (d, *J* = 8.3 Hz, 1H); ^{13}C NMR (101 MHz, DMSO-d_6) δ = 44.7 (CH_2), 66.1 (CH_2), 71.3 (CH_2), 115.6 (CH_{Ar}), 121.5 (CH_{Ar}), 125.5 (CH_{Ar}), 139.0 (C_q), 144.3 (C_q), 150.5 (C_q); HRMS (ESI-MS) *m/z* calcd for $C_9H_9ClN_2NaO_6$ $[M+Na]^+$: 299.0047, found: 299.0043; Rf (petroleum ether/CH_2Cl_2 = 3/7) 0.67.
6l	*2-(2-Bromo-3-(chloromethyl)-6-methoxyphenoxy)ethyl nitrate* was obtained from 2-(2-bromo-3-(hydroxymethyl)-6-methoxyphenoxy)ethyl nitrate (**5l**) as greenish yellow oil, yield 95%; ^{1}H NMR (400 MHz, DMSO-d_6) δ = 3.83 (s, 3H), 4.19–4.30 (m, 2H), 4.80 (s, 2H), 4.81–4.88 (m, 2H), 7.12 (d, *J* = 8.5 Hz, 1H), 7.38 (d, *J* = 8.5 Hz, 1H); ^{13}C NMR (101 MHz, DMSO-d_6) δ = 46.8 (CH_2), 56.2 (CH_3), 68.7 (CH_2), 72.7 (CH_2), 112.1 (CH_{Ar}), 119.3 (C_q), 127.3 (CH_{Ar}), 129.3 (C_q), 144.5 (C_q), 153.3 (C_q); HRMS (ESI-MS) *m/z* calcd for $C_{10}H_{11}BrClNNaO_5$ $[M+Na]^+$: 361.9407, found: 361.9401 ; Rf (petroleum ether/EtOAc = 6/4) 0.71.
6m	*2-(2-(Chloromethyl)phenoxy)ethyl nitrate* was obtained from 2-(2-(hydroxymethyl)phenoxy) ethyl nitrate (**5m**) as yellow oil, yield 83%; ^{1}H NMR (250 MHz, DMSO-d_6) δ = 4.34–4.42 (m, 2H), 4.69 (s, 2H), 4.89–4.97 (m, 2H), 6.92–7.11 (m, 2H), 7.29–7.46 (m, 2H); ^{13}C NMR (101 MHz, DMSO-d_6) δ = 40.5 (CH_2), 64.8 (CH_2), 72.0 (CH_2), 111.4 (CH_{Ar}), 114.8 (CH_{Ar}), 127.5 (CH_{Ar}), 129.5 (CH_{Ar}), 132.7 (C_q), 154.5 (C_q); HRMS (ESI-MS) *m/z* calcd for $C_9H_{10}ClNNaO_4$ $[M+Na]^+$: 254.0196, found: 254.0193; Rf (petroleum ether/EtOAc = 8/2) 0.64.
6t	*2-(4-Bromo-2-(Chloromethyl)phenoxy)ethyl nitrate* was obtained from2-(4-bromo-2-(hydroxylmethyl)phenoxy)ethyl nitrate **(5t)** as pale yellow oil, yield 89%; ^{1}H NMR (400 MHz, DMSO-d_6) δ = 4.33–4.41 (m, 2H), 4.67 (s, 2H), 4.87–4.96 (m, 2H), 7.07 (d, *J* = 8.7 Hz, 1H), 7.52 (dd, *J* = 8.8 Hz, 2.5 Hz, 1H), 7.62 (d, *J* = 2.6 Hz, 1H); ^{13}C NMR (101 MHz, DMSO-d_6) δ = 40.4 (CH_2), 65.2 (CH_2), 71.7 (CH_2), 112.3 (C_q), 114.9 (CH_{Ar}), 128.3 (C_q), 132.7 (CH_{Ar}), 133.1 (CH_{Ar}), 155.2 (C_q); HRMS (ESI-MS) *m/z* calcd for $C_9H_9BrClNNaO_4$ $[M+Na]^+$: 331.9301, found: 331.9310; Rf (petroleum ether/EtOAc = 8/2) 0.55.

Cpd.	The Identificationcharacteristics (^{1}H NMR, ^{13}C NMR, MS, R_f)
6u	*2-(2-Chloro-3-(chloromethyl)-6-methoxyphenoxy)ethyl nitrate* was obtained from2-(2-chloro-3-(hydroxymethyl)-6-methoxyphenoxy)ethyl nitrate **(5u)** as pale yellow oil, yield 96%; ^{1}H NMR (400 MHz, DMSO-d_6) δ = 3.83 (s, 3H), 4.21–4.30 (m, 2H), 4.79 (s, 2H), 4.80–4.87 (m, 2H), 7.08 (d, *J* = 8.6 Hz, 1H), 7.36 (d, *J* = 8.6 Hz, 1H);. ^{13}C NMR (101 MHz, DMSO-d_6) δ = 44.2 (CH_2), 56.2 (CH_3), 68.8 (CH_2), 72.7 (CH_2), 111.4 (CH_{Ar}), 126.9 (CH_{Ar}), 127.6 (C_q), 127.7 (C_q), 143.4 (C_q), 153.5 (C_q); HRMS (ESI-MS) *m/z* calcd for $C_{10}H_{11}Cl_2NNaO_5$ $[M+Na]^+$: 317.9912, found: 317.9906; Rf (petroleum ether/EtOAc = 7/3) 0.67.
6v	*2-(4-(2-Iodooethyl)phenoxy)ethyl nitrate* was obtained from 2-(4-(2-hydroxyethyl)phenoxy) ethyl nitrate **(5v)** as white solid, yield 79%, m.p. 57–59 °C; ^{1}H NMR (400 MHz, DMSO-d_6) δ = 3.05 (t, *J* = 7.4 Hz, 2H), 3.42 (t, *J* = 7.4 Hz, 2H), 4.23–4.31 (m, 2H), 4.81–4.91 (m, 2H), 6.89 (d, *J* = 7.4Hz, 2H), 7.18 (d, *J* = 7.6 Hz, 2H); ^{13}C NMR (101 MHz, DMSO-d_6) δ = 8.7 (CH_2), 38.4 (CH_2), 63.9 (CH_2), 72.0 (CH_2), 114.4 ($2CH_{Ar}$), 129.6 ($2CH_{Ar}$), 133.3 (C_q), 156.5 (C_q); HRMS (ESI-MS) *m/z* calcd for $C_{10}H_{13}INO_4$ $[M+H]^+$: 337.9889, found: 337.9884; Rf (petroleum ether/EtOAc = 8/2) 0.60.

7.2.1.2. Synthesis of 2-(1-(4-chlorobenzoyl)-5-methoxy-2-methyl-1H-indol-3-yl) acetohydrazide (7)

The synthesis of indomethacin hydrazide was based on chemical modulation of indomethacin at carboxylic group with the addition of hydrazine moiety.

Generally, the synthesis of alkyl and aryl hydrazides is performed by reaction of hydrazine hydrate with appropriate esters, acid halides, carboxylic anhydrides or amides [332]. It was reported the synthesis of hydrazide of *i*ndole-3-carboxylic acid hydrazine by the reaction between hydrazine hydrate and the corresponding esters in refluxing ethanol, in yields ranging from 78 to 98% [333–335]. Amir *et al*. and Al-Masoudi *et al*. have obtained the hydrazide of indomethacin with yields of 52% and 64% respectively [336,337]. For synthesis of some antibacterial hydrazones, Kamel *et al*., have obtained the intermediary hidrazides by conversion of corresponding carboxylic acids into acid chloride with thionyl chloride, followed by the reaction with hydrazine hydrate [338,339].

Alternatively, acyl hydrazines can be obtained by condensing carboxylic acids with hydrazine in the presence of coupling agents but, most of these methods provide low yields and complicated product isolation [307].

In our study the indomethacin hydrazide is an important intermediary compound so it was aimed to develop an effective synthesis that should be rapid, convenient, proceeds under mild conditions, and be suitable for large-scale application. To prepare the desired hydrazide, it was proposed two methods, according to the literature data, which were adapted to our synthesis in terms of the ratio of reagents, solvent, time of reaction, purification method: the reaction of the indomethacin ethyl ester with hydrazine hydrate (method 1) and the peptide coupling reaction between indomethacin and hydrazine hydrate (method 2).

Method 1. In order to identify the compounds presented in the crude product the flash chromatography (silicagel, petroleum ether/AcOEt) method was applied. The NMR and MS spectroscopic analysis allowed the identification the 4-chlorobenzoic acid and esterified indol acetic moiety that means that the indomethacin structure hydrolyzed. It was concluded that the high temperature and the presence of water in basic media are factors that significantly influence the stability of indomethacin structure.

According to the literature, the indomethacin is stable in neutral or slightly acidic conditions, but a linear increase in the concentration in hydroxyl ions (HO^-) causes an

exponential degradation with the formation of two acids: 4-chlorobenzoic acid and 5-methoxy-2-methyl-3-indol acetic acid [340–342].

Method 2. By applying the peptide coupling reaction between indomethacin and hydrazine hydrate (Fig. 6.6.), indomethacin hydrazide was successful obtained, in high yield (95%), as pale yellow solid, m.p. 202-204 °C. ^{1}H NMR (400 MHz, DMSO-d_6) δ = 2.26 (s, 3H), 3.46 (s, 2H), 3.78 (s, 3H), 4.25 (s, 2H), 6.71 (dd, *J* = 9.0Hz, 2.5 Hz, 1H), 6.92 (d, *J* = 9.0 Hz, 1H), 7.16 (d, *J* = 2.5 Hz, 1H), 7.61 − 7.75 (m, 4H), 9.22 (s, 1H). ^{13}C NMR (101 MHz, DMSO-d_6) δ = 13.3 (CH_3), 29.3 (CH_2), 55.4 (CH_3), 102.1 (CH_{Ar}), 111.1 (CH_{Ar}), 114.0 (C_q), 114.5 (CH_{Ar}), 129.0 ($2CH_{Ar}$), 130.2 (C_q), 130.8 (C_q), 131.1 ($2CH_{Ar}$), 134.2 (C_q), 135.2 (C_q), 137.5 (C_q), 155.5 (C_q), 167.8 (C_q), 168.8 (C_q). HRMS (ESI-MS) *m/z* calcd for $C_{19}H_{19}ClN_3O_3$ $[M+H]^+$: 372.1109, found: 372.2965; Rf (CH_2Cl_2/CH_3OH = 9.6/0.4) 0.57.

In addition to the very high yield and pure product, this method offers also numerous other advantages as follow: (i) the direct synthesis of hydrazide form indomethacin, (ii) the specificity of reaction by modulation of carboxyl group, (iii) reaction time is relatively short (3 h), (iv) mild conditions 0-5 °C and room temperature respectively, (v) product isolation by a simple filtration and (vi) facile separation of EDCI and HOBt excess by water washing of indomethacin hydrazide.

7.2.1.3. Synthesis of the nitric oxide-releasing indomethacin derivatives with 1,3-thiazolidin-4-one scaffold

The 1,3-thiazolidine-4-one scaffold serves as core for many synthetic compounds of great interest in medicinal chemistry [118]. In the literature were reported extensive research referring to the physico-chemical properties of this scaffold [118,131,134,343,344].

Thiazolidin-one represents the saturated form of the thiazole, having a carbonyl group (Fig. 7.4). The 1,3-thiazolidine-4-one is a heterocycle that has a sulphur atom in position 1, a nitrogen atom in position 3 and a carbonyl group in position 4. Different substituents could be introduced at positions *C*-2, *N*-3 and *C*-5, but the greatest differences in structure and properties are obtained by the substitution of hydrogen atoms from position *C*-2. The carbonyl group in position 4 is non-reactive.

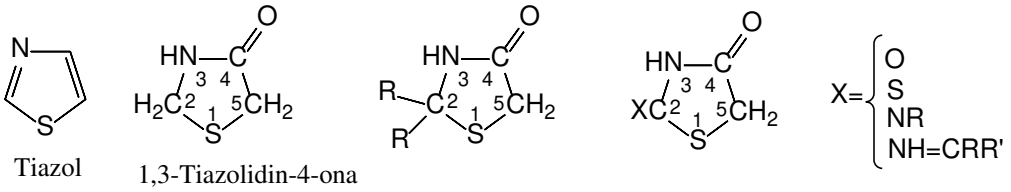

Fig 7.4. The structure of thiazolidin-4-one scaffold substituted at different positions.

There are various protocols reported in the literature for the synthesis of 1,3-thiazolidine-4-one derivatives and the main synthetic route involves a MCR (Multi Component Reaction) involving three components *i.e.* a carbonylated compound, an amine and the mercaptoacetic acid. The synthesis may be carried out either in one or two steps with the initial formation of an imine which undergoes an attack of sulfur nucleophile, followed by intramolecular cyclyzation with water elimination [345–348] (Fig. 7.5).

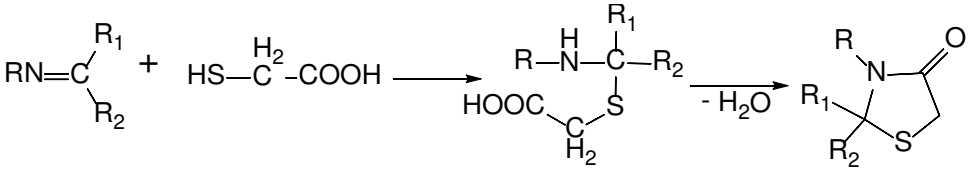

Fig. 7.5. The synthesis scheme of the thiazolidin-4-one scaffold.

For the synthesis of the 1,3-thiazolidine-4-one scaffold by an annelation with marcaptoacetic acid, various catalysts such as zinc chloride [349,350], toluene-4-sulfonic acid [351,352], magnesium sulfate [353], molecular sieves [348], dicyclohexyl-carbodiimide [354,355], could be used. Also, inert solvents such as toluene [356,357], *N,N*-dimethyl formamide [358,359], 1,4-dioxane [360,361], tetrahydrofuran [349,362] were used.

However, most of these methods present one or more drawback such as long time reaction, difficult synthesis procedures, hard reaction conditions or low yields.

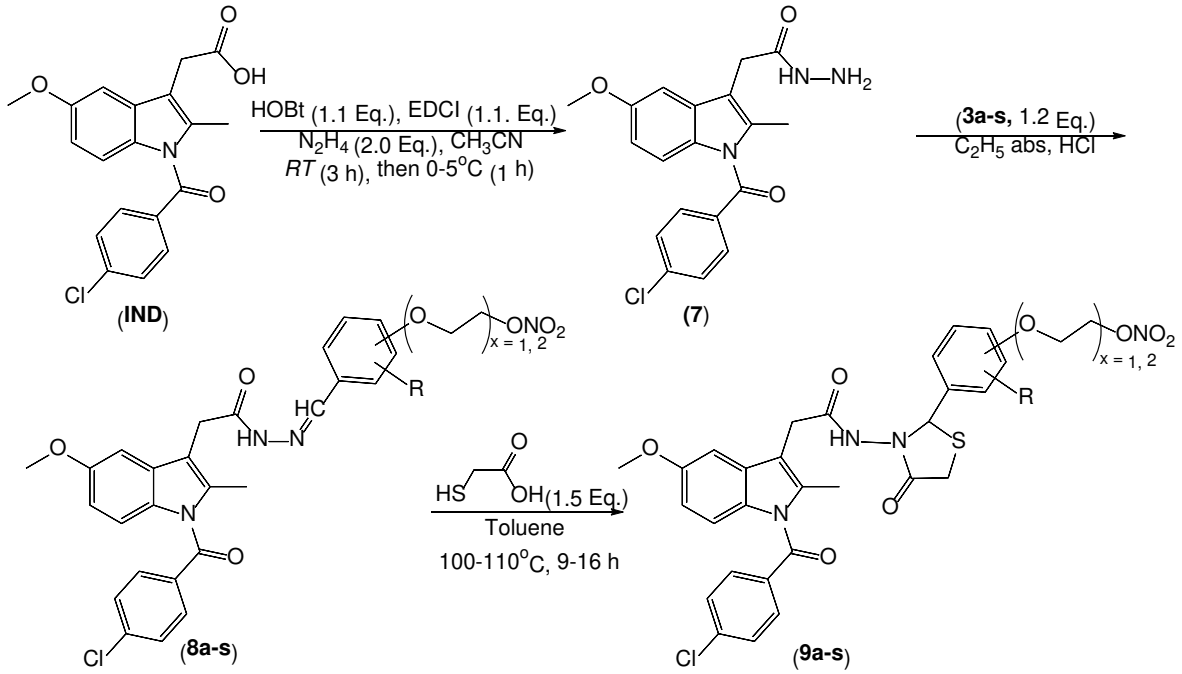

Fig. 7.6. The synthesis scheme of the NO-IND-TZDs (**9a-s**).

In our research, the desired final nitric oxide-releasing indomethacin derivatives with 1,3-thiazolidin-4-one scaffold (NO-IND-TZDs) where obtained in two steps: (i) synthesis of the indomethacin hydrazone derivatives by reaction of indomethacin hydrazide (**7**) with nitrate ester benzaldehyde derivatives **(3a-s)**, (ii) cyclization of indomethacin hydrazone derivatives (**8a-s**) with mercaptoacetic acid to afford the NO-IND-TZDs (**9a-s**) (Fig. 7.6).

The synthesis of the indomethacin hydrazone derivatives

N-Acyl-hydrazones are usually synthesized by condensation of aldehydes or ketones with hydrazides [363], which are more nucleophilic than regular amines, due to the presence of an adjacent nitrogen (Fig. 7.7).

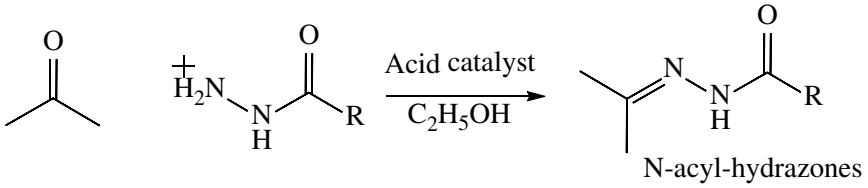

Fig. 7.7. The common synthesis route for the preparation of *N*-acyl-hydrazones.

The reaction is most rapid at pH between 4 and 5 values. Under strongly acidic condition the hidrazide becomes protonated and non nucleophilic. With no free electrons pair the nucleophilic addition from first step cannot occur [364] (Fig. 7.8).

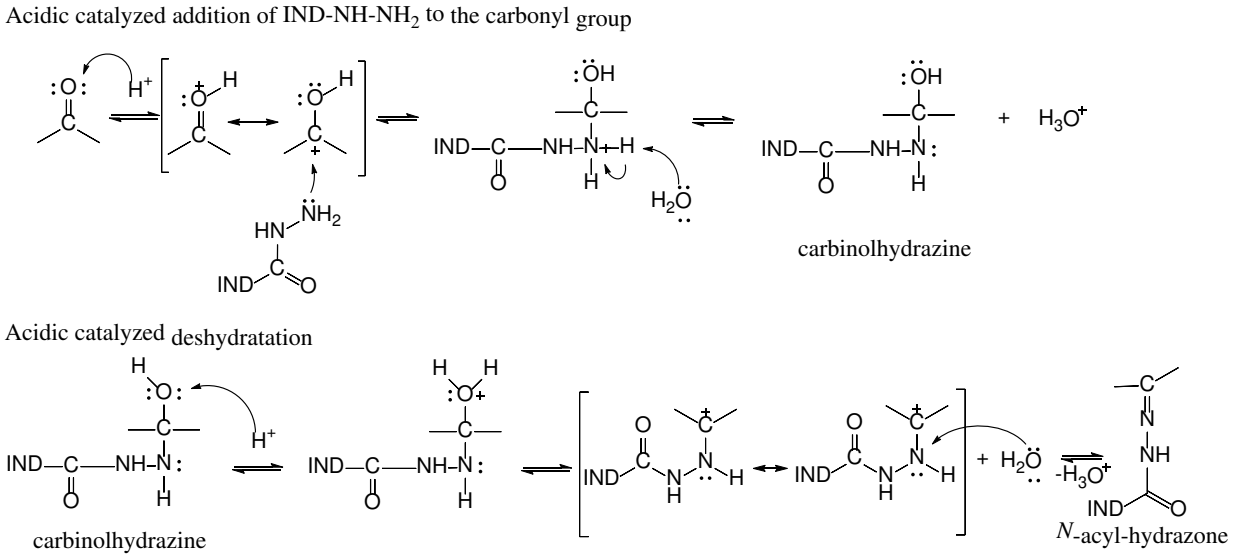

Fig. 7.8. The chemical mechanism of the formation of indomethacin-N-acyl-hydrazone.

The indomethacin hydrazone derivatives are insoluble in ethanol which made easy to separate them by simples operations of wash and filtration. These intermediaries were obtained in yields, which ranged between 90% and 98% and were used without isolation for the final step of synthesis.

The synthesis of the NO-IND-TZDs

The indomethacin hydrazone derivatives (**8a-s**) were subjected to an annelation with mercaptoacetic acid in order to obtain the NO-IND-TZDs (**9a-s**). To optimize the synthesis, the experimental conditions such as temperature, catalyst and mercaptoacetic acid amount was varied (Table 7.6).

It was noted that the use of catalyst such as $ZnCl_2$, 4-toluenesulfonic acid and molecular sieves promote synthesis of 1,3-thiazolidin-4-one scaffold, but with hydrolysis of nitrate ester group. Also long time reaction at higher temperature (120 °C) increase rate of nitrate ester hydrolysis.

Table 7.6. The variation of the experimental conditions, in order to optimize the synthesis.

Entry	Catalyst	Temp.	Mercaptoacetic acid		Conditions	Solvent	Yield
			Eq.	C% (m/v)			
1	molecular sieve	120 °C	1.5	7%	Dean-Stark 14,5 h	toluene	-
2	0.5 Eq. 4-toluenesulfonic acid	120 °C	1.5	11%	Dean-Stark 15 h	toluene	15%
3	0.1 Eq. 4-toluenesulfonic acid	120 °C	1.5	11%	Dean-Stark8.5 h	toluene	40%
4	0.5 Eq. $ZnCl_2$	110 °C	1.5	1.5%	15 h	toluene	-
5	-	120 °C	1.5	0.63%	Dean-Stark13 h	toluene	33%
6	-	120 °C	1.5	1.4%	14 h	toluene	55%
7	-	120 °C	1.5	1.3%	19 h	toluene	47%
8	-	120 °C	1.5	2%	14 h	toluene	42%
9	-	95-110 °C	1.5	1.5%	$MgSO_4$ 15 h	toluene	63%

To obtain the final NO-IND-TZDs was very important to use mercaptoacetic acid at 1.5% in final mixture reaction in presence of one spatula tip of anhydrous magnesium sulfate, to careful check the temperature (95-110 °C) and to monitor the progress of the reaction by TLC.

In the established conditions the NO-IND-TZDs were obtained in moderate yields, which ranged between 25% and 63%. Their main physico-chemical and spectral characteristics (^{1}H NMR, ^{13}C NMR, MS) are presented in Table 7.7.

Table 7.7. The identification characteristics (^{1}H NMR, ^{13}C NMR, MS, R_f) of the nitric oxide-releasing indomethacin derivatives with 1,3-thiazolidin-4-one scaffold (**9a-s**).

Cpd.	The idetification characteristics (^{1}H NMR, ^{13}C NMR, MS, R})
9a	*2-(4-(3-(2-(1-(4-Chlorobenzoyl)-5-methoxy-2-methyl-1H-indol-3-yl)acetamido)-4-oxo-thiazolidin-2-yl)phenoxy)ethyl nitrate* was obtained from *2*-(4-((2-(2-(1-(4-chlorobenzoyl)-5-methoxy-2-methyl-1*H*-indol-3-yl)acetyl)hydrazineylidene)methyl)phenoxy)ethyl nitrate **(8a)** as pale yellow *solid* in 56% yield, m.p. 169-171 °C. ^{1}H NMR (250 MHz, DMSO-d_6) δ=2.10 (s, 3H), 3.49 (s, 2H), 3.70 (s, 3H), 3.70 (d, *J* = 15.9 Hz, 1H), 3.86 (dd, *J* = 15.9 Hz, 1.7, 1H), 4.22 - 4.34 (m, 2H), 4.83 - 4.94 (m, 2H), 5.71 (s, 1H), 6.68 (dd, *J* = 9.0 Hz, 2.5 Hz, 1H), 6.88 (d, *J* = 8.7 Hz, 2H), 6.94 (d, *J* = 9.0 Hz, 1H), 7.00 (d, *J* = 2.5 Hz, 1H), 7.28 (d, *J* = 8.7 Hz, 2H), 7.65 (s, 4H), 10.35 (s, 1H). ^{13}C NMR (101 MHz, DMSO-d_6) δ=13.2 (CH_3), 28.7 (CH_2), 29.2 (CH_2), 55.3 (CH_3), 61.1 (CH), 64.1 (CH_2), 71.9 (CH_2), 101.6 (CH_{AR}), 111.6 (CH_{Ar}), 113.2 (C_q), 114.4 ($3CH_{Ar}$), 129.0 ($2CH_{Ar}$), 129.2 ($2CH_{Ar}$), 130.1 (C_q), 130.4 (C_q), 130.5 (C_q), 131.1 ($2CH_{AR}$), 134.2 (C_q), 135.2 (C_q), 137.6 (C_q), 155.5 (C_q), 158.3 (C_q), 167.8 (C_q), 168.4 (C_q), 168.7 (C_q); HRMS (ESI-MS) *m/z* calcd for $C_{30}H_{28}ClN_4O_8S$ $[M+H]^+$: 639.1316, found: 639.1311; Rf (petroleum ether/EtOAc = 2/8) 0.46.
9b	*2-(4-(3-(2-(1-(4-Chlorobenzoyl)-5-methoxy-2-methyl-1H-indol-3-yl)acetamido)-4-oxo-thiazolidin-2-yl)-2-fluorophenoxy)ethyl nitrate* was obtained from 2-(4-((2-(2-(1-(4-chlorobenzoyl)-5-methoxy-2-methyl-1*H*-indol-3-yl)acetyl)hydrazineylidene)methyl)-2-fluoro-phenoxy)ethyl nitrate **(8b)** as pale yellow *solid* in 45% yield, m.p. 154-156 °C. ^{1}H NMR (400 MHz, DMSO-d_6) δ=2.12 (s, 3H), 3.50 (s, 2H), 3.70 (s, 3H), 3.70 (d, *J* = 15.8 Hz, 1H), 3.90 (dd, *J* = 15.8 Hz, 1.8 Hz, 1H), 4.28 - 4.43 (m, 2H), 4.80 - 5.00 (m, 2H), 5.72 (s, 1H), 6.67 (dd, *J* = 9.0 Hz, 2.5 Hz, 1H), 6.92 (d, *J* = 9.0 Hz, 1H), 6.98 (d, *J* = 2.5 Hz, 1H), 7.00 - 7.10 (m, 2H), 7.29 (dd, *J* = 12.2 Hz, 1.8 Hz, 1H), 7.65 (s, 4H), 10.38 (s, 1H). ^{19}F NMR (376 MHz, DMSO-d_6) δ=133.67 (dd, *J* = 12.1 Hz, 7.4 Hz). ^{13}C NMR (101 MHz, DMSO-d_6) δ= 13.2 (CH_3), 28.7 (CH_2), 29.1 (CH_2), 55.3 (CH_3), 60.6 (CH), 65.3 (CH_2), 71.7 (CH_2) , 101.5 (CH_{Ar}), 111.5 (CH_{Ar}), 113.1 (C_q), 114.4 (C_q), 114.5 (CH_{Ar}), 115.2 (d, *J* =19.1 Hz, CH_{Ar}), 124.3 (d, *J* =3.3 Hz, CH_{Ar}), 129.0 ($2CH_{Ar}$) , 130.1 (C_q) , 130.5 (C_q), 131.1 ($2CH_{Ar}$), 131.9 (d, *J* =5.9 Hz, C_q), 134.1 (C_q), 135.3 (C_q), 137.6 (C_q), 146.1 (d, *J* =10.7 Hz, C_q), 151.4 (d, *J* =244.9 Hz, C_qF), 155.5 (C_q), 167.8 (C_q), 168.4 (C_q), 168.7 (C_q). ^{19}F NMR (376 MHz, DMSO-d_6) δ= -133.67 (dd, *J* =12.1 Hz, 7.4 Hz); HRMS (ESI-MS) *m/z* calcd for $C_{30}H_{27}ClFN_4O_8S$ $[M+H]^+$: 657.1222, found: 657.1217; Rf (petroleum ether/EtOAc = 2/8) 0.54.

Cpd.	The idetification characteristics (^{1}H NMR, ^{13}C NMR, MS, R})
9c	*2-(2-Chloro-4-(3-(2-(1-(4-chlorobenzoyl)-5-methoxy-2-methyl-1H-indol-3-yl)acetamido)-4-oxothiazolidin-2-yl)phenoxy)ethyl nitrate* was obtained from 2-(2-chloro-4-((2-(2-(1-(4-chlorobenzoyl)-5-methoxy-2-methyl-1*H*-indol-3-yl)acetyl)hydrazineylidene)methyl)phenoxy) ethyl nitrate **(8c)** as pale yellow *solid* in 40% yield, m.p. 137-139 °C. ^{1}H NMR (250 MHz, DMSO-d_6) δ=2.12 (s, 3H), 3.51 (s, 2H), 3.69 (s, 3H), 3.70 (dd, *J* = 15.9 Hz, 0.8 Hz, 1H), 3.91 (dd, *J* = 15.9 Hz, 1.8 Hz, 1H), 4.28 - 4.45 (m, 2H), 4.79 - 5.02 (m, 2H), 5.72 (s, 1H), 6.67 (dd, *J* = 9.0 Hz, 2.5 Hz, 1H), 6.94 (d, *J* = 9.0 Hz, 0.4 Hz, 1H), 6.99 (d, *J* = 2.5 Hz, 1H), 7.03 (d, *J* = 8.6 Hz, 1H), 7.23 (dd, *J* = 8.6 Hz, 2.2 Hz, 1H), 7.49 (d, *J* = 2.2 Hz, 1H), 7.65 (s, 4H), 10.40 (s, 1H). ^{13}C NMR (101 MHz, DMSO-d_6) δ=13.7 (CH_3) , 29.2 (CH_2), 29.6 (CH_2), 55.8 (CH_3), 61.0 (CH), 65.9 (CH_2), 72.0 (CH_2), 102.0 (CH_{Ar}), 112.0 (CH_{Ar}), 113.6 (C_q), 114.0 (CH_{Ar}), 114.9 (CH_{Ar}), 122.0 (C_q), 128.4 (CH_{Ar}), 129.5 ($2CH_{Ar}$), 129.6 (CH_{Ar}), 130.6 (C_q), 130.9 (C_q), 131.6 ($2CH_{Ar}$), 132.6 (C_q), 134.6 (C_q), 135.7 (C_q), 138.1 (C_q), 154.0 (C_q), 156.0 (C_q), 168.3 (C_q), 169.0 (C_q), 169.1 (C_q); HRMS (ESI-MS) *m/z* calcd for $C_{30}H_{27}Cl_2N_4O_8S$ $[M+H]^+$: 673.0927, found: 673.0921; Rf (toluene/acetonitrile = 6/4) 0.60.
9d	*2-(4-(3-(2-(1-(4-Chlorobenzoyl)-5-methoxy-2-methyl-1H-indol-3-yl)acetamido)-4-oxo-thiazolidin-2-yl)-2-methoxyphenoxy)ethyl nitrate* was obtained from 2-(4-((2-(2-(1-(4-chlorobenzoyl)-5-methoxy-2-methyl-1*H*-indol-3-yl)acetyl)hydrazineylidene)methyl)-2-methoxy-phenoxy)ethyl nitrate **(8d)** as pale yellow *solid* in 35% yield, m.p. 174-176 °C. ^{1}H NMR (400 MHz, DMSO-d_6) δ=2.09 (s, 3H), 3.51 (s, 2H), 3.69 (s, 3H), 3.70 (s, 3H), 3.71 (d, J = 15.3 Hz, 1H), 3.85 (dd, *J* = 15.9 Hz, 1.7 Hz, 1H), 4.19 - 4.29 (m, 2H), 4.83 - 4.90 (m, 2H), 5.73 (s, 1H), 6.67 (dd, *J* = 9.0 Hz, 2.6 Hz, 1H), 6.80 - 6.89 (m, 2H), 6.92 (d, *J* = 9.0 Hz, 1H), 6.99 (s, 2H), 7.65 (d, *J* = 1.4 Hz, 4H), 10.34 (s, 1H). ^{13}C NMR (101 MHz, DMSO-d_6) δ=13.2 (CH_3), 28.7 (CH_2), 29.3 (CH_2), 39.99 (CH_2) , 55.3 (CH_3), 55.5 (CH_3), 61.5 (CH), 64.9 (CH_2), 72.0 (CH_2), 101.6 (CH_{Ar}), 111.0 (CH_{Ar}), 111.5 (CH_{Ar}), 113.1 (CH_{Ar}), 113.2 (C_q), 114.4 (CH_{Ar}), 120.1 (CH_{Ar}), 129.0 ($2CH_{Ar}$), 130.1 (C_q), 130.5 (C_q), 131.1 ($2CH_{Ar}$), 134.2 (C_q), 135.2 (C_q), 137.6 (C_q), 147.8 (C_q), 149.1 (C_q), 155.5 (C_q), 167.8 (C_q), 168.4 (C_q), 168.9 (C_q); HRMS (ESI-MS) *m/z* calcd for $C_{31}H_{30}ClN_4O_9S$ $[M+H]^+$: 669.1422, found: 669.1417; Rf (petroleum ether/EtOAc = 2/8) 0.43.
9e	*2-(4-(3-(2-(1-(4-Chlorobenzoyl)-5-methoxy-2-methyl-1H-indol-3-yl)acetamido)-4-oxo-thiazolidin-2-yl)-2-ethoxyphenoxy)ethyl nitrate* was obtained from 2-(4-((2-(2-(1-(4-chlorobenzoyl)-5-methoxy-2-methyl-1*H*-indol-3-yl)acetyl)hydrazineylidene)methyl)-2-ethoxy -phenoxy)ethyl nitrate **(8e)** as pale yellow *solid* in 32% yield, m.p. 170-172 °C. ^{1}H NMR (400 MHz, DMSO-d_6) δ=1.27 (t, *J* = 6.9 Hz, 3H), 2.09 (s, 3H), 3.50 (s, 2H), 3.69 (s, 3H), 3.70 (d, *J* = 15.9 Hz, 1H), 3.80 - 4.02 (m, 3H), 4.22 - 4.29 (m, 2H), 4.83 - 4.90 (m, 2H), 5.71 (s, 1H), 6.67 (dd, *J* = 9.0 Hz, 2.5 Hz, 1H), 6.81 - 6.90 (m, 2H), 6.91 (d, *J* = 9.0 Hz, 1H), 6.97 (d, *J* = 2.0 Hz, 1H), 7.00 (d, *J* = 2.5 Hz, 1H), 7.65 (s, 4H), 10.33 (s, 1H). ^{13}C NMR (101 MHz, DMSO-d_6) δ=13.1 (CH_3), 14.6 (CH_3), 28.7 (CH_2), 29.3 (CH_2), 55.3 (CH_3), 61.4 (CH), 63.9 (CH_2), 65.3 (CH_2), 721.0 (CH_2), 101.6 (CH_{Ar}), 111.5 (CH_{Ar}), 112.5 (CH_{Ar}), 113.2 (C_q), 113.9 (CH_{Ar}), 114.4 (CH_{Ar}), 120.2 (CH_{Ar}), 129.0 ($2CH_{Ar}$), 130.1 (C_q), 130.5 (C_q), 131.1 ($2CH_{Ar}$), 131.3 (C_q), 134.1 (C_q), 135.2 (C_q), 137.6 (C_q), 148.0(C_q), 148.5 (C_q), 155.5 (C_q), 167.8 (C_q), 168.4 (C_q), 168.8 (C_q); HRMS (ESI-MS) *m/z* calcd for $C_{32}H_{32}ClN_4O_9S$ $[M+H]^+$: 683.1579, found: 683.1573; Rf (toluene/acetonitrile = 6/4) 0.58.

Cpd.	The idetification characteristics (^{1}H NMR, ^{13}C NMR, MS, R})
9f	*2-(4-(3-(2-(1-(4-Chlorobenzoyl)-5-methoxy-2-methyl-1H-indol-3-yl)acetamido)-4-oxo-thiazolidin-2-yl)-2-nitrophenoxy)ethyl nitrate*was obtained from 2-(4-((2-(2-(1-(4-chlorobenzoyl)-5-methoxy-2-methyl-1*H*-indol-3-yl)acetyl)hydrazineylidene)methyl)-2-nitro-phenoxy)ethyl nitrate **(8f)** as pale yellow *solid* in 25% yield, m.p. 165-167 °C. ^{1}H NMR (250 MHz, DMSO-d_6) δ=2.13 (s, 3H), 3.50 (s, 2H), 3.68 (s, 3H), 3.73 (d, *J* = 16.0 Hz, 1H), 3.94 (dd, *J* = 16.0 Hz, 1.8 Hz, 1H), 4.37 - 4.54 (m, 2H), 4.80 - 4.99 (m, 2H), 5.82 (s, 1H), 6.66 (dd, *J* = 9.0 Hz, 2.5 Hz, 1H), 6.90 (d, *J* = 9.0 Hz, 1H), 6.95 (d, *J* = 2.5 Hz, 1H), 7.26 (d, *J* = 8.8 Hz, 1H), 7.60 (dd, *J* = 8.8 Hz, 2.3 Hz, 1H), 7.65 (s, 4H), 7.93 (d, 2.3 Hz, 1H), 10.41 (s, 1H). ^{13}C NMR (101 MHz, DMSO-d_6) δ=13.2 (CH_3), 28.8 (CH_2), 29.1 (CH_2), 55.3 (CH_3), 60.1 (CH_2), 66.1 (CH_2), 71.2 (CH_2), 101.4 (CH_{Ar}), 111.(CH_{Ar}), 113.0 (C_q), 114.4 (CH_{Ar}), 115.2 (CH_{Ar}), 124.3 (CH_{Ar}), 129.0 ($2CH_{Ar}$), 130.0 (C_q), 130.4 (C_q), 131.1 ($2CH_{Ar}$), 131.5 (C_q), 133.7 (C_q), 134.1 (C_q), 135.3 (C_q), 137.6 (C_q), 139.1 (C_q), 150.9 (C_q), 155.5 (C_q), 167.8 (C_q), 168.5 (C_q), 168.6 (C_q); HRMS (ESI-MS) *m/z* calcd for $C_{30}H_{27}ClN_5O_{10}S$ $[M+H]^+$: 684.1167, found: 684.1162; Rf (toluene/acetonitrile = 6/4) 0.53.
9g	*2-(4-(3-(2-(1-(4-Chlorobenzoyl)-5-methoxy-2-methyl-1H-indol-3-yl)acetamido)-4-oxo-thiazolidin-2-yl)-2,6-dimethoxyphenoxy)ethyl nitrate* was obtained from 2-(4-((2-(2-(1-(4-chlorobenzoyl)-5-methoxy-2-methyl-1*H*-indol-3-yl)acetyl)hydrazineylidene)methyl)-2,6-dimethoxyphenoxy)ethyl nitrate **(8g)** as pale yellow *solid* in 42% yield, m.p. 174-176 °C. ^{1}H NMR (400 MHz, DMSO-d_6) δ=2.08 (s, 3H), 3.55 (s, 2H), 3.70 (s, 10H), 3.88 (dd, *J* = 15.9 Hz, 1.7 Hz, 1H), 4.01 - 4.17 (m, 2H), 4.62 - 4.84 (m, 2H), 5.75 (s, 1H), 6.67 (dd, *J* = 8.9 Hz, 2.5 Hz, 1H), 6.69 (s, 2H), 6.91 (d, *J* = 8.9 Hz, 1H), 7.02 (d, *J* = 2.5Hz, 1H), 7.65 (s, 4H), 10.39 (s, 1H). ^{13}C NMR (101 MHz, DMSO-d_6) δ=13.1 (CH_3), 28.8 (CH_2), 29.2 (CH_2), 55.3 (CH_3), 55.9 ($2CH_3$), 61.7 (CH), 68.5 (CH_2), 72.8 (CH_2), 101.6 (CH_{Ar}), 104.3 ($2CH_{Ar}$), 111.5 (CH_{Ar}), 113.1 (C_q), 114.5 (CH_{Ar}), 129.0 ($2CH_{Ar}$), 130.1 (C_q), 130.6 (C_q), 131.1 ($2CH_{Ar}$), 134.1 (C_q), 134.4 (C_q), 135.3 (C_q), 135.9 (C_q), 137.6 (C_q), 152.8 ($2C_q$), 155.5 (C_q), 167.8 (C_q), 168.5 (C_q), 169.1 (C_q); HRMS (ESI-MS) *m/z* calcd for $C_{32}H_{32}ClN_4O_{10}S$ $[M+H]^+$: 699.1528, found: 699.1522; Rf (petroleum ether/EtOAc = 2/8) 0.57.
9h	*2-(2,6-Dichloro-4-(3-(2-(1-(4-chlorobenzoyl)-5-methoxy-2-methyl-1H-indol-3-yl)aceta-mido)-4-oxothiazolidin-2-yl)phenoxy)ethyl nitrate* was obtained from 2-(2,6-dichloro-4-((2-(2-(1-(4-chlorobenzoyl)-5-methoxy-2-methyl-1*H*-indol-3-yl)acetyl)hydrazineylidene)methyl)phenoxy) ethyl nitrate **(8h)** as pale yellow *solid* in 53% yield, m.p. 138-140 °C. ^{1}H NMR (250 MHz, DMSO-d_6) δ =2.12 (s, 3H), 3.54 (s, 2H), 3.70 (d, *J* = 15.8 Hz , 1H), 3.72 (s, 3H), 3.98 (dd, *J* = 15.8 Hz, 1.8 Hz, 1H), 4.20 - 4.38 (m, 2H), 4.79 - 4.98 (m, 2H), 5.77 (d, *J* = 1.6 Hz, 1H), 6.67 (dd, *J* = 9.0 Hz, 2.5 Hz, 1H), 6.92 (d, *J* = 9.0 Hz, 0.4 Hz, 1H), 7.02 (d, *J* = 2.5 Hz, 1H), 7.55 (s, 2H), 7.59 - 7.70 (m, 4H), 10.45 (s, 1H). ^{13}C NMR (101 MHz, DMSO-d_6) δ=13.1 (CH_3), 28.8 (CH_2), 29.0 (CH_2), 55.3 (CH_3), 59.8 (CH), 69.4 (CH_2), 72.4 (CH_2), 101.5 (CH_{Ar}), 111.5 (CH_{Ar}), 113.0 (C_q), 114.5 (CH_{Ar}), 128.2 ($2C_q$), 128.3 ($2CH_{Ar}$), 129.0 ($2CH_{Ar}$), 130.1 (C_q), 130.5 (C_q), 131.1 ($2CH_{Ar}$), 134.1 (C_q), 135.2 (C_q), 137.5 (C_q), 137.6 (C_q), 150.1 (C_q), 155.5 (C_q), 167.8 (C_q), 168.5 (C_q), 168.7 (C_q); HRMS (ESI-MS) *m/z* calcd for $C_{30}H_{26}Cl_3N_4O_8S$ $[M+H]^+$: 707.0537, found: 707.0531; Rf (toluene/acetonitrile = 6/4) 0.64.

Cpd.	The idetification characteristics (^{1}H NMR, ^{13}C NMR, MS, R})
9i	*2-(3-(3-(2-(1-(4-Chlorobenzoyl)-5-methoxy-2-methyl-1H-indol-3-yl)acetamido)-4-oxo-thiazolidin-2-yl)phenoxy)ethyl nitrate* was obtained from 2-(3-((2-(2-(1-(4-chlorobenzoyl)-5-methoxy-2-methyl-1*H*-indol-3-yl)acetyl)hydrazineylidene)methyl)phenoxy)ethyl nitrate **(8i)** as pale yellow *solid* in 63% yield, m.p. 170-172 °C. ^{1}H NMR (400 MHz, DMSO-d_6) δ=2.09 (s, 3H), 3.52 (s, 2H), 3.70 (s, 3H), 3.71 (d, *J* = 15.8 Hz, 1H), 3.88 (dd, *J* = 15.9 Hz, 1.8 Hz, 1H), 4.25 (q, *J* = 3.8 Hz, 2H), 4.86 (t, *J* = 4.3 Hz, 2H), 5.75 (d, *J* = 1.5 Hz, 1H), 6.67 (dd, *J* = 9.0 Hz, 2.5 Hz, 1H), 6.92 (d, *J* = 9.0 Hz, 1H), 6.85 - 7.01 (m, 3H), 7.01 (d, *J* = 2.5, 1H), 7.25 (t, *J* = 7.9 Hz, 1H), 7.65 (s, 4H), 10.43 (s, 1H). ^{13}C NMR (101 MHz, DMSO-d_6) δ=13.1 (CH_3), 28.7 (CH_2), 29.1 (CH_2), 55.3 (CH_3), 61.2 (CH), 64.0 (CH_2), 72.0 (CH_2), 101.6 (CH_{Ar}), 111.6 (CH_{Ar}), 113.0 (CH_{Ar}), 113.1 (CH_{Ar}), 114.4 (C_q), 115.1 (CH_{Ar}), 120.2 (CH_{Ar}), 129.0 ($2CH_{Ar}$), 129.8 (C_q), 130.1 (CH_{Ar}), 130.5 (C_q), 131.1 ($2CH_{Ar}$), 134.1 (C_q), 135.2 (C_q), 137.6(C_q), 140.2 (C_q), 155.5 (C_q), 158.0 (C_q), 167.8 (C_q), 168.5 (C_q), 169.0 (C_q); HRMS (ESI-MS) *m/z* calcd for $C_{30}H_{28}ClN_4O_8S$ $[M+H]^+$: 639.1316, found: 6391311; Rf (petroleum ether/EtOAc = 2/8) 0.56.
9j	*2-(5-(3-(2-(1-(4-Chlorobenzoyl)-5-methoxy-2-methyl-1H-indol-3-yl)acetamido)-4-oxo-thiazolidin-2-yl)-2-methoxyphenoxy)ethyl nitrate* was obtained from 2-(5-((2-(2-(1-(4-chlorobenzoyl)-5-methoxy-2-methyl-1*H*-indol-3-yl)acetyl)hydrazineylidene)methyl)-2-methoxy-phenoxy)ethyl nitrate **(8j)** as pale yellow *solid* in 25% yield, m.p. 176-178 °C. ^{1}H NMR (400 MHz, DMSO-d_6) δ=2.07 (s, 3H), 3.50 (s, 2H), 3.70 (s, 3H), 3.71 (d, *J* = 15.8 Hz, 1H), 3.74 (s, 3H), 3.84 (dd, *J* = 15.9 Hz, 1.7 Hz, 1H), 4.04 - 4.33 (m, 2H), 4.84 (t, *J* = 4.4 Hz, 2H), 5.71 (s, 1H), 6.68 (dd, *J* = 9.0 Hz, 2.5 Hz, 1H), 6.86 (s, 1H), 6.81 - 6.93 (m, 1H), 6.93 (d, *J* = 9.0 Hz, 1H), 7.00 (d, *J* = 4.9 Hz, 1H), 7.00 (d, *J* = 4.3 Hz, 1H), 7.65 (s, 4H), 10.31 (s, 1H). ^{13}C NMR (101 MHz, DMSO-d_6) δ=13.1 (CH_3), 28.7 (CH_2), 29.3 (CH_2), 55.3 (CH_3), 55.5 (CH_3), 61.4 (CH), 64.9 (CH_2), 72.0 (CH_2), 101.6 (CH_{Ar}), 111.5 (CH_{Ar}), 111.6 (CH_{Ar}), 112.5 (C_q), 113.1 (CH_{Ar}), 114.4 (CH_{Ar}), 121.3 (CH_{Ar}), 129.0 ($2CH_{Ar}$), 130.1 (C_q), 130.1 (C_q), 130.5 (C_q), 131.1 ($2CH_{Ar}$), 134.1 (C_q), 135.3 (C_q), 137.6 (C_q), 147.3 (C_q), 149.6 (C_q), 155.5 (C_q), 167.8 (C_q), 168.3 (C_q), 168.8 (C_q); HRMS (ESI-MS) *m/z* calcd for $C_{31}H_{30}ClN_4O_9S$ $[M+H]^+$: 669.1422, found: 669.1417; Rf (toluene/acetonitrile = 6/4) 0.58.
9k	*2-(5-(3-(2-(1-(4-Chlorobenzoyl)-5-methoxy-2-methyl-1H-indol-3-yl)acetamido)-4-oxo-thiazolidin-2-yl)-2-nitrophenoxy)ethyl nitrate* was obtained from 2-(5-((2-(2-(1-(4-chlorobenzoyl)-5-methoxy-2-methyl-1*H*-indol-3-yl)acetyl)hydrazineylidene)methyl)-2-nitro-phenoxy)ethyl nitrate **(8k)** as pale yellow in 20% yield 17%, m.p. 152-154 °C. ^{1}H NMR (400 MHz, DMSO-d_6) δ=2.14 (s, 3H), 3.54 (s, 2H), 3.66 (s, 3H), 3.75 (d, *J* = 15.9 Hz, 1H), 3.95 (dd, *J* = 15.9 Hz, 1.8 Hz, 1H), 4.24 - 4.44 (m, 2H), 4.87 (t, *J* = 4.4 Hz, 2H), 5.85 (d, *J* = 1.6 Hz, 1H), 6.65 (dd, *J* = 9.0 Hz, 2.5 Hz, 1H), 6.88 (d, *J* = 9.0 Hz, 1H), 6.93 (d, *J* = 2.5 Hz, 1H), 7.17 (dd, *J* = 8.4 Hz, 1.7 Hz, 1H), 7.35 (d, *J* = 1.7 Hz, 1H), 7.65 (d, *J* = 1.4 Hz, 4H), 7.85 (d, *J* = 8.3 Hz, 1H), 10.49 (s, 1H). ^{13}C NMR (101 MHz, DMSO-d_6) δ=13.1 (CH_3), 28.8 (CH_2), 29.1 (CH_2), 55.3 (CH_3), 60.4 (CH), 66.0 (CH_2), 71.2 (CH_2), 101.6 (CH_{Ar}), 111.3 (CH_{Ar}), 113.0 (CH_{Ar}), 114.0 (CH_{Ar}), 114.4 (C_q), 119.9 (CH_{Ar}), 125.5 (CH_{Ar}), 129.0 ($2CH_{Ar}$), 130.1 (C_q), 130.4 (C_q), 131.1 ($2CH_{Ar}$), 134.1 (C_q), 135.4 (C_q), 137.6 (C_q), 139.1 (C_q), 145.6 (C_q), 150.7 (C_q), 155.5 (C_q), 167.8 (C_q), 168.6 (C_q), 168.8 (C_q); HRMS (ESI-MS) *m/z* calcd for $C_{30}H_{27}ClN_5O_{10}S$ $[M+H]^+$: 684.1167, found: 684.1162; Rf (toluene/acetonitrile = 6/4) 0.6.

Cpd.	The idetification characteristics (^{1}H NMR, ^{13}C NMR, MS, R})
9l	*2-(2-Bromo-3-(3-(2-(1-(4-chlorobenzoyl)-5-methoxy-2-methyl-1H-indol-3-yl)aceta-mido)-4-oxothiazolidin-2-yl)-6-methoxyphenoxy)ethyl nitrate* was obtained from 2-(2-bromo-3-((2-(2-(1-(4-chlorobenzoyl)-5-methoxy-2-methyl-1*H*-indol-3-yl)acetyl)hydrazineyli-dene)methyl)-6-methoxyphenoxy)ethyl nitrate **(8l)** as pale yellow in yield 52%, m.p. 184-186 °C. ^{1}H NMR (400 MHz, DMSO-d_6) δ=2.10 (s, 3H), 3.55 (d, *J* = 4.5 Hz, 2H), 3.70 (s, 3H), 3.83 (s, 3H), 3.65 - 3.96 (m, 2H), 4.04 - 4.33 (m, 2H), 4.82 (t, *J* = 4.3 Hz, 2H), 6.02 (s, 1H), 6.66 (dd, *J* = 9.0 Hz, 2.5 Hz, 1H), 6.91 (d, *J* = 9.0 Hz, 1H), 7.02 (d, *J* = 2.5 Hz, 1H), 7.21 (d, *J* = 51.3 Hz, 2H), 7.65 (d, *J* = 1.4 Hz, 4H), 10.54 (s, 1H). ^{13}C NMR (101 MHz, DMSO-d_6) δ=13.1(CH_3), 28.8 ($2CH_2$), 55.3 (CH_3), 56.2 (CH_3), 60.7 (CH), 68.7 (CH_2), 72.7 (CH_2), 101.5 (CH_{Ar}), 111.6 (CH_{Ar}), 112.5 (CH_{Ar}), 113.1 (CH_{Ar}), 114.4 (CH_{Ar}), 117.7 (C_q), 129.0 ($2CH_{Ar}$), 130.1 (C_q), 130.5 (C_q), 131.1 ($2CH_{Ar}$), 134.1 (C_q), 135.3 (C_q), 137.6 (C_q), 144.1 (C_q), 153.0 (C_q), 155.5 (C_q), 167.8 (C_q), 168.7 (C_q), 169.3 (C_q); HRMS (ESI-MS) *m/z* calcd for $C_{31}H_{29}BrClN_4O_9S$ $[M+H]^+$: 747.0527, found: 747.0522; Rf (petroleum ether/EtOAc = 2/8) 0.62.
9m	*2-(2-(3-(2-(1-(4-Chlorobenzoyl)-5-methoxy-2-methyl-1H-indol-3-yl)acetamido)-4-oxo-thiazolidin-2-yl)phenoxy)ethyl nitrate* was obtained from 2-(2-((2-(2-(1-(4-chlorobenzoyl)-5-methoxy-2-methyl-1*H*-indol-3-yl)acetyl)hydrazineylidene)methyl)phenoxy)ethyl nitrate **(8m)** as pale yellow in yield 34%, m.p. 175-177 °C. ^{1}H NMR (250 MHz, DMSO-d_6) δ= 2.11 (s, 3H), 3.54 (s, 2H), 3.65 (d, *J* = 15.8 Hz, 1H), 3.68 (s, 3H), 3.78 (dd, *J* = 15.8 Hz, 1.8 Hz, 1H), 3.99 - 4.35 (m, 2H), 4.50 - 4.88 (m, 2H), 5.99 (d, *J* = 1.5 Hz, 1H), 6.68 (dd, *J* = 9.0 Hz, 2.5 Hz, 1H), 6.93 (dd, *J* = 9.0 Hz, 0.4 Hz, 1H), 6.96 - 7.08 (m, 3H), 7.23 - 7.43 (m, 2H), 7.65 (s, 4H), 10.44 (s, 1H). ^{13}C NMR (101 MHz, DMSO-d_6) δ=13.1 (CH_3), 28.7 (CH_2), 28.8 (CH_2), 55.3 (CH, CH_3) 64.4 (CH_2), 71.8 (CH_2), 101.5 (CH_{Ar}), 111.6 (CH_{Ar}), 112.3 (CH_{Ar}), 113.2 (C_q), 114.4 (CH_{Ar}), 121.1 (CH_{Ar}), 126.8 (CH_{Ar}), 127.5 (C_q), 129.0 ($2CH_{Ar}$), 129.9 (CH_{Ar}), 130.1 (C_q), 130.5 (C_q), 131.1 ($2CH_{Ar}$), 134.2 (C_q), 135.3 (C_q), 137.6 (C_q), 155.6 (C_q), 155.6 (C_q), 167.8 (C_q), 168.6 (C_q), 169.2 (C_q); HRMS (ESI-MS) *m/z* calcd for $C_{30}H_{28}ClN_4O_8S$ $[M+H]^+$: 639.1316, found: 639.1311; Rf (petroleum ether/EtOAc = 2/8) 0.64.
9n	*2-(2-Bromo-4-(3-(2-(1-(4-chlorobenzoyl)-5-methoxy-2-methyl-1H-indol-3-yl)acetamido)-4-oxothiazolidin-2-yl)phenoxy)ethyl nitrate* was obtained from 2-(2-bromo-4-((2-(2-(1-(4-chlorobenzoyl)-5-methoxy-2-methyl-1*H*-indol-3-yl)acetyl)hydrazineylidene)methyl)phenoxy) ethyl nitrate **(9n)** as pale yellow *solid* in 38% yield, m.p. 167-169 °C. ^{1}H NMR (400 MHz, DMSO-d_6) δ=2.11 (s, 3H), 3.50 (s, 2H), 3.69 (s, 3H), 3.70 (d, *J* = 15.9 Hz, 1H), 3.91 (dd, *J* = 15.9 Hz, 1.8 Hz, 1H), 4.27 - 4.42 (m, 2H), 4.81 - 5.00 (m, 2H), 5.72 (s, 1H), 6.67 (dd, *J* = 9.0 Hz, 2.6 Hz, 1H), 6.94 (d, *J* = 9.0 Hz, 1H), 6.98 (s, 1H), 7.00 (d, *J* = 6.2 Hz, 1H), 7.27 (dd, *J* = 8.6 Hz, 2.2 Hz, 1H), 7.63 (d, *J* = 2.2 Hz, 1H), 7.59 - 7.71 (m, 4H), 10.40 (s, 1H). ^{13}C NMR (101 MHz, DMSO-d_6) δ=13.2 (CH_3), 28.7 (CH_2), 29.2 (CH_2), 55.3 (CH_3), 60.4 (CH), 65.5 (CH_2), 71.5 (CH_2), 101.5 (CH_{Ar}), 111.1 (CH_{Ar}), 111.61 (CH_{Ar}), 113.12 (C_q), 113.3 (CH_{Ar}), 114.4 (C_q), 128.6 (CH_{Ar}), 129.0 ($2CH_{Ar}$), 130.08 (CH_{Ar}), 130.5 (C_q), 131.1 ($2CH_{Ar}$), 132.1 (C_q), 132.5 (C_q), 134.2 (C_q), 135.2 (C_q), 137.6 (C_q), 154.4 (C_q), 155.5 (C_q), 167.8 (C_q), 168.44 (C_q), 168.7 (C_q); HRMS (ESI-MS) *m/z* calcd for $C_{30}H_{27}BrClN_4O_8S$ $[M+H]^+$: 717.0421, found: 717.0416; Rf (petroleum ether/EtOAc = 2/8) 0.50.

Cpd.	The idetification characteristics (^{1}H NMR, ^{13}C NMR, MS, R})
9o	*2-(3-(3-(2-(1-(4-Chlorobenzoyl)-5-methoxy-2-methyl-1H-indol-3-yl)acetamido)-4-oxo-thiazolidin-2-yl)-4-nitrophenoxy)ethyl nitrate* was obtained from 2-(3-((2-(2-(1-(4-chlorobenzoyl)-5-methoxy-2-methyl-1*H*-indol-3-yl)acetyl)hydrazineylidene)methyl)-4-nitro-phenoxy)ethyl nitrate **(8o)** as pale yellow in yield 35%, m.p. 180-182 °C. ^{1}H NMR (400 MHz, DMSO-d_6) δ=2.12 (s, 3H), 3.56 (d, *J* = 4.7 Hz, 2H), 3.64 (d, *J* = 15.8 Hz, 1H), 3.69 (s, 3H), 3.93 (dd, *J* = 15.8 Hz, 1.9 Hz, 1H), 4.44 - 4.57 (m, 2H), 4.93 (t, *J* = 4.4 Hz, 2H), 6.18 (d, *J* = 1.8 Hz, 1H), 6.67 (dd, *J* = 9.0 Hz, 2.5 Hz, 1H), 6.90 (d, *J* = 9.0 Hz, 1H), 6.98 (d, *J* = 2.5 Hz, 1H), 7.09 - 7.20 (m, 2H), 7.58 - 7.70 (m, 4H), 8.12 (d, *J* = 9.0 Hz, 1.1 Hz, 1H), 10.63 (s, 1H). ^{13}C NMR (101 MHz, DMSO-d_6) δ=13.1 (CH_3), 28.1 (CH_2), 28.9 (CH_2), 55.3 (CH_3), 57.4 (CH), 65.0 (CH_2), 71.6 (CH_2), 101.5 (CH_{Ar}), 111.5 (CH_{Ar}), 112.5 (C_q), 113.0 (CH_{Ar}), 114.5 (CH_{Ar}), 114.8 (CH_{Ar}), 128.3 (CH_{Ar}), 129.0 ($2CH_{Ar}$), 130.1 (C_q), 130.4 (C_q), 131.1 ($2CH_{Ar}$), 134.1 (C_q), 135.3 (C_q), 137.6 (C_q), 138.4 (C_q), 140.2 (C_q), 155.5 (C_q), 162.5 (C_q), 167.8 (C_q), 168.7 (C_q), 169.3 (C_q); HRMS (ESI-MS) *m/z* calcd for $C_{30}H_{27}ClN_5O_{10}S$ $[M+H]^+$: 684.1167, found: 684.1162; Rf (petroleum ether/EtOAc = 2/8) 0.73.
9p	*2-(2-Chloro-4-(3-(2-(1-(4-chlorobenzoyl)-5-methoxy-2-methyl-1H-indol-3-yl)aceta-mido)-4-oxothiazolidin-2-yl)-6-methoxyphenoxy)ethyl nitrate* was obtained from 2-(2-chloro-4-((2-(2-(1-(4-chlorobenzoyl)-5-methoxy-2-methyl-1*H*-indol-3-yl)acetyl)hydrazineyli-dene)methyl)-6-methoxyphenoxy)ethyl nitrate **(8p)** as pale yellow *solid* in 35% yield, m.p. 144-146 °C. ^{1}H NMR (400 MHz, DMSO-d_6) δ=2.10 (s, 3H), 3.54 (d, *J* = 2.3 Hz, 2H), 3.70 (s, 3H), 3.71 (d, *J* = 15.9 Hz, 1H), 3.73 (s, 3H), 3.92 (dd, *J* = 15.9 Hz, 1.8 Hz, 1H), 4.18 - 4.25 (m, 2H), 4.78 - 4.85 (m, 2H), 5.75 (s, 1H), 6.67 (dd, *J* = 9.0 Hz, 2.5 Hz, 1H), 6.91 (d, *J* = 9.0 Hz, 1H), 7.01 (d, *J* = 2.5 Hz, 1H), 7.04 (d, *J* = 2.0 Hz, 1H), 7.10 (d, *J* = 2.0 Hz, 1H), 7.60 - 7.70 (m, 4H), 10.43 (s, 1H). ^{13}C NMR (101 MHz, DMSO-d_6) δ=13.1 (CH_3), 28.7 (CH_2), 29.1 (CH_2), 55.3 (CH_3), 56.2 (CH_3), 60.7 (CH), 68.8 (CH_2), 72.6 (CH_2), 101.5 (CH_{Ar}), 110.9 (CH_{Ar}), 111.5 (CH_{Ar}), 113.1 (C_q), 114.4 (CH_{Ar}), 120.1 (CH_{Ar}), 126.9 (C_q), 129.0 ($2CH_{Ar}$), 130.1 (C_q), 130.5 (C_q), 131.1 ($2CH_{Ar}$), 134.1 (C_q), 135.3 (C_q), 135.9 (C_q), 137.6 (C_q), 143.2 (C_q), 153.2 (C_q), 155.5 (C_q), 167.9 (C_q), 168.5 (C_q), 168.8 (C_q); HRMS (ESI-MS) *m/z* calcd for $C_{31}H_{29}Cl_2N_4O_9S$ $[M+H]^+$: 703.1032, found: 703.1026; Rf (petroleum ether/EtOAc = 2/8) 0.47.
9q	*2-(2-(4-(3-(2-(1-(4-Chlorobenzoyl)-5-methoxy-2-methyl-1H-indol-3-yl)aceta-mido)-4-oxothiazolidin-2-yl)phenoxy)ethoxy)ethyl nitrate* was obtained from 2-(2-(4-((2-(2-(1-(4-chlorobenzoyl)-5-methoxy-2-methyl-1*H*-indol-3-yl)acetyl)hydrazineylidene)methyl)phenoxy) ethoxy)ethyl nitrate **(8q)** as pale yellow in yield 27%, m.p. 132-134 °C. ^{1}H NMR (400 MHz, DMSO-d_6) δ=2.09 (s, 3H), 3.49 (s, 2H), 3.70 (d, *J* = 15.9 Hz, 1H), 3.71 (s, 3H), 3.73 - 3.82 (m, 4H), 3.84 (dd, *J* = 15.9 Hz, 1.7 Hz, 1H), 3.97 - 4.28 (m, 2H), 4.56 - 4.78 (m, 2H), 5.71 (s, 1H), 6.69 (dd, *J* = 8.9 Hz, 2.5 Hz, 1H), 6.86 (d, *J* = 8.5 Hz, 2H), 6.94 (d, *J* = 8.9 Hz, 1H), 7.01 (d, *J* = 2.5 Hz, 1H), 7.27 (d, *J* = 8.5 Hz, 2H), 7.65 (s, 4H), 10.34 (s, 1H). ^{13}C NMR (101 MHz, DMSO-d_6) δ=13.2 (CH_3), 28.7 (CH_2), 29.3 (CH_2), 55.3 (CH_3), 61.2 (CH), 66.5 (CH_2), 67.1 (CH_2), 68.9 (CH_2), 72.9 (CH_2), 101.7 (CH_{Ar}), 111.5 (CH_{Ar}), 113.2 (C_q), 114.4 ($2CH_{Ar}$), 114.4 (CH_{Ar}), 129.0 ($2CH_{Ar}$), 129.1 ($2CH_{Ar}$), 129.9 (C_q), 130.1 (C_q), 130.5 (C_q), 131.1 ($2CH_{Ar}$), 134.2 (C_q), 135.2 (C_q), 137.6 (C_q), 155.5 (C_q), 158.9 (C_q), 167.8 (C_q), 168.4 (C_q), 168.8 (C_q); HRMS (ESI-MS) *m/z* calcd for $C_{32}H_{32}ClN_4O_9S$ $[M+H]^+$: 683.1579, found: 683.1573; Rf (toluene/acetonitrile = 6/4) 0.67.

Cpd.	The idetification characteristics (^{1}H NMR, ^{13}C NMR, MS, R})
9r	*2-(2-(4-(3-(2-(1-(4-Chlorobenzoyl)-5-methoxy-2-methyl-1H-indol-3-yl)acetamido)-4-oxothiazolidin-2-yl)-2-methoxyphenoxy)ethoxy)ethyl nitrate* was obtained from 2-(2-(4-((2-(2-(1-(4-chlorobenzoyl)-5-methoxy-2-methyl-1*H*-indol-3-yl)acetyl)hydrazineylidene)methyl)-2-methoxyphenoxy)ethoxy)ethyl nitrate **(8r)** as pale yellow in yield 25%, m.p. 135-136 °C. ^{1}H NMR (400 MHz, DMSO-d_6) δ=2.08 (s, 3H), 3.51 (s, 2H), 3.70 (s, 6H), 3.63 - 3.89 (m, 6H), 3.98 - 4.10 (m, 2H), 4.53 - 4.82 (m, 2H), 5.72 (s, 1H), 6.68 (dd, *J* = 8.9 Hz, 2.4 Hz, 1H), 6.83 (s, 2H), 6.93 (d, *J* = 8.9 Hz, 1H), 6.97 (s, 1H), 7.01 (d, *J* = 2.4 Hz, 1H), 7.65 (s, 4H), 10.33 (s, 1H). ^{13}C NMR (101 MHz, DMSO-d_6) δ=13.2 (CH_3), 28.7 (CH_2), 29.3 (CH_2), 55.3 (CH_3), 55.4 (CH_3), 61.5 (CH), 66.6 (CH_2), 67.8 (CH_2), 68.9 (CH_2), 72.9 (CH_2), 101.6 (CH_{Ar}), 110.9 (CH_{Ar}), 111.5 (CH_{Ar}), 112.6 (C_q), 113.2 (CH_{Ar}), 114.4 (CH_{Ar}), 120.2 (CH_{Ar}), 129.0 ($2CH_{Ar}$), 130.1 (C_q), 130.4 (C_q), 130.6 (C_q), 131.1 ($2CH_{Ar}$), 134.2 (C_q), 135.2 (C_q), 137.6 (C_q), 148.4 (C_q), 149.0 (C_q), 155.5 (C_q), 167.8 (C_q), 168.4 (C_q), 168.9 (C_q); HRMS (ESI-MS) *m/z* calcd for $C_{33}H_{34}ClN_4O_{10}S$ $[M+H]^+$: 713.1684, found: 713.1679; Rf (toluene/acetonitrile = 6/4) 0.49.
9s	*2-(2-(4-(3-(2-(1-(4-Chlorobenzoyl)-5-methoxy-2-methyl-1H-indol-3-yl)acetamido)-4-oxothiazolidin-2-yl)-2-ethoxyphenoxy)ethoxy)ethyl nitrate* was obtained from 2-(2-(4-((2-(2-(1-(4-chlorobenzoyl)-5-methoxy-2-methyl-1*H*-indol-3-yl)acetyl)hydrazineylidene)methyl)-2-ethoxyphenoxy)ethoxy)ethyl nitrate **(8s)** as pale yellow in yield 27%, m.p. 136-138 °C. ^{1}H NMR (400 MHz, DMSO-d_6) δ=1.27 (t, *J* = 6.9 Hz, 3H), 2.08 (s, 3H), 3.50 (s, 2H), 3.70 (d, *J* = 15.9 Hz, 1H), 3.70 (s, 3H), 3.77 (t, *J* = 4.7 Hz, 2H), 3.79 - 3.86 (m, 3H), 3.86 - 4.02 (m, 2H), 4.05 (t, *J* = 4.8 Hz, 2H), 4.65 - 4.72 (m, 2H), 5.70 (s, 1H), 6.67 (dd, *J* = 8.9 Hz, 2.4 Hz, 1H), 6.76 - 6.88 (m, 2H), 6.92 (d, *J* = 8.9 Hz, 1H), 6.95 (s, 1H), 7.01 (d, *J* = 2.4 Hz, 1H), 7.65 (s, 4H), 10.32 (s, 1H). ^{13}C NMR (101 MHz, DMSO-d_6) δ=13.1 (CH_3), 14.6 (CH_3), 28.7 (CH_2), 29.3 (CH_2), 55.3 (CH_3), 61.5 (CH), 63.9 (CH_2), 66.6 (CH_2), 68.1 (CH_2), 68.9 (CH_2), 72.9 (CH_2), 101.6 (CH_{Ar}), 111.5 (CH_{Ar}), 112.5 (CH_{Ar}), 113.1 (C_q), 113.2 (CH_{Ar}), 114.4 (CH_{Ar}), 120.3 (CH_{Ar}), 129.0 ($2CH_{Ar}$), 130.1 (C_q), 130.5 (C_q), 130.6 (C_q), 131.1 ($2CH_{AR}$), 134.2 (C_q), 135.2 (C_q), 137.6 (C_q), 148.3 (C_q), 148.7 (C_q), 155.5 (C_q), 167.8 (C_q), 168.3 (C_q), 168.8 (C_q); HRMS (EI-MS) *m/z* calcd for $C_{34}H_{36}ClN_4O_{10}S$ $[M+H]^+$: 727.1841, found: 727.1835; Rf (toluene/acetonitrile = 6/4) 0.55.

7.2.1.4. Synthesis of the nitric oxide-releasing indomethacin derivatives with 1,3,4-oxadiazole scaffold

1,3,4-Oxadiazole-2-thiol is a five-member heterocyclic ring which is frequently used in medicinal chemistry due to its potential multifunctional donor sites by exocyclic sulfur and endocyclic nitrogen atoms [175,189,365].

The most common strategy for the synthesis of 2-mercapto-1,3,4-oxadiazole derivatives involves the annelation reactions of acid hydrazides with carbon disulfide in the presence of an alkaline alcoholic solution, followed by acidification of the reaction mixture [313,366–369].

The synthesis of the IND-OXD derivative (**10**)

In our study, in order to avoid the basic hydrolysis of indomethacin, the method reported in the literature [311–314] was adapted to our synthesis in terms of the ratio of reagents, solvent, time of reaction, purification method. So, the indomethacin-hydrazide (**7**) was reacted with carbon disulfide, in presence of triethylamine and acetonitril to afford the

dithiocarbazate salt, which by cyclization in warming conditions, gives the (4-chlorobenzoyl)-5-methoxy-2-methyl-1*H*-indol-3-yl)methyl)-2-mercapto-1,3,4-oxadiazole, IND-OXD derivative (**10**) (Fig. 7.9) as white solid, yield 92%, m.p. 199-201 °C. ^{1}H NMR (400 MHz, DMSO-d_6) δ = 2.29 (s, 3H), 3.76 (s, 3H), 4.25 (s, 2H), 6.74 (dd, *J* = 9.0 Hz, 2.5 Hz, 1H), 6.90 (d, *J* = 9.0 Hz, 1H), 7.12 (d, *J* = 2.5 Hz, 1H), 7.56 − 7.76 (m, 4H), 14.36 (s, 1H). ^{13}C NMR (101 MHz, DMSO-d_6) δ = 13.1 (CH_3), 20.4 (CH_2), 55.4 (CH_3), 101.6 (CH_{Ar}), 111.1 (C_q), 111.6 (CH_{Ar}), 114.7 (CH_{Ar}), 129.1 ($2CH_{Ar}$), 129.9 (C_q), 130.2 (C_q), 131.2 ($2CH_{Ar}$), 133.9 (C_q), 136.1 (C_q), 137.7 (C_q), 155.6 (C_q), 162.3 (C_qS), 167.8 (C_q), 177.8 (C_q). HRMS (ESI-MS) *m/z* calcd for $C_{20}H_{17}ClN_3O_3S$ $[M+H]^+$: 414.0679, found: 414.0680; Rf (CH_2Cl_2/CH_3OH = 9.8/0.2) 0.52.

The synthesis of the NO-IND-OXDs

The final NO-IND-OXDs (**11a-m**, **t-v**) were synthesized by the condensation of the (4-chlorobenzoyl)-5-methoxy-2-methyl-1H-indol-3-yl)methyl)-2-mercapto-1,3,4-oxadiazol (**10**) with appropriate (halidealkyl)phenoxy nitrates **(6a-m**, **t-v)**, at room temperature in the presence of tryethylamine (Fig. 7.9).

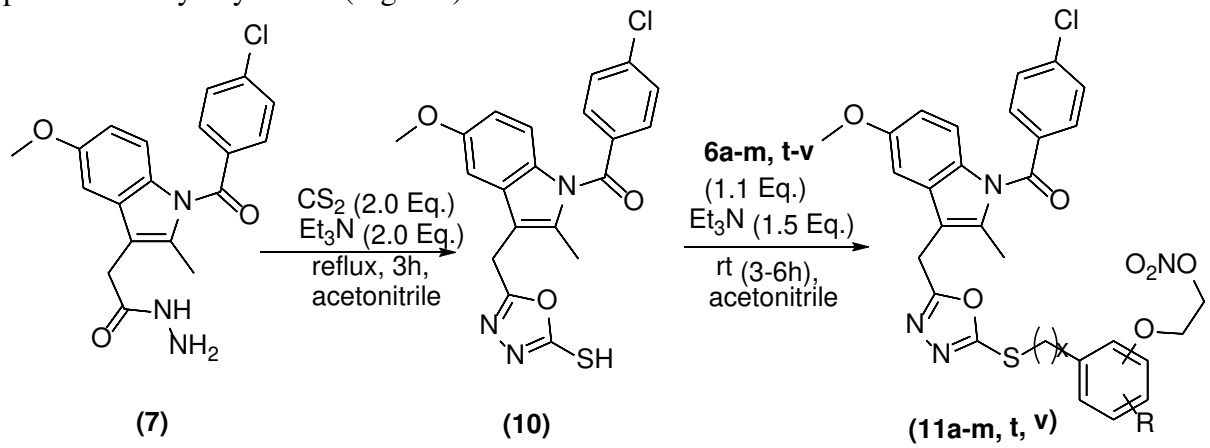

Fig. 7.9. The synthesis scheme of the NO-IND-OXDs (**11a-s, t-v**).

The final NO-IND-OXDs were obtained in good yields, which ranged between 70% and 93%. Their main physico-chemical and spectral characteristics (^{1}H NMR, ^{13}C NMR, MS) are presented in Table 7.8.

Table 7.8. The identification characteristics (^{1}H NMR, ^{13}C NMR, MS, R_f) of the nitric oxide-releasing indomethacin derivatives with 1,3,4-oxadiazole scaffold (**11a-s, t-v**).

Cpd.	The identification characteristics (^{1}H NMR, ^{13}C NMR, MS, R_f)
11a	*2-(4-(((5-((1-(4-Chlorobenzoyl)-5-methoxy-2-methyl-1H-indol-3-yl)methyl)-1,3,4-oxadiazol-2-yl)thio)methyl)phenoxy)ethyl nitrate* was obtained from 2-(4-(chloromethyl)phenoxy)ethyl nitrate (**6a**) as pale yellow solid, yield 88%, m.p. 108–110 °C; ^{1}H NMR (250 MHz, DMSO-d_6) δ = 2.29 (s, 3H), 3.74 (s, 3H), 4.19–4.28 (m, 2H), 4.36 (s, 2H), 4.37 (s, 2H), 4.79–4.91 (m, 2H), 6.74 (dd, J = 9.0 Hz, 2.5 Hz, 1H), 6.73–6.86 (m, 2H), 6.93 (dd, J = 9.0 Hz, 0.5 Hz, 1H), 7.09 (dd, J = 2.6 Hz, 0.5 Hz, 1H), 7.14–7.30 (m, 2H), 7.54–7.76 (m, 4H); ^{13}C NMR (101 MHz, DMSO-d_6) δ = 13.1 (CH_3), 20.0 (CH_2), 35.4 (CH_2), 55.4 (CH_3), 64.0 (CH_2), 71.9 (CH_2), 101.5 (CH_{Ar}), 111.6 (CH_{Ar}), 111.9 (C_q), 114.4 ($2CH_{Ar}$), 114.7 (CH_{Ar}), 128.9 (C_q), 129.1 ($2CH_{Ar}$), 129.9 (C_q), 130.3 ($2CH_{Ar}$), 131.2 ($2CH_{Ar}$), 133.9 (C_q), 135.7 (C_q), 137.8 (C_q), 155.6 (C_q), 157.3 (C_q), 163.0 (C_q), 166.1 ($2C_q$), 167.9 (C_q); HRMS (ESI-MS) m/z calcd for $C_{29}H_{26}ClN_4O_7S$ $[M+H]^+$: 609.1211, found: 609.1205; Rf (petroleum ether/EtOAc = 4/6) 0.66.

Cpd.	The identification characteristics (^{1}H NMR, ^{13}C NMR, MS, R_f)
11b	*2-(4-(((5-((1-(4-Chlorobenzoyl)-5-methoxy-2-methyl-1H-indol-3-yl)methyl)-1,3,4-oxadiazol-2-yl)thio)methyl)-2-fluorophenoxy)ethyl nitrate* was obtained from 2-(4-(chloromethyl)-2-fluorophenoxy)ethyl nitrate (**6b**) as pale yellow solid, yield 86%, m.p. 105–107 °C; ^{1}H NMR (400 MHz, DMSO-d_6) δ = 2.28 (s, 3H), 3.74 (s, 3H), 4.29–4.34 (m, 2H), 4.36 (s, 2H), 4.38 (s, 2H), 4.81–4.93 (m, 2H), 6.74 (dd, J = 9.0 Hz, 2.5 Hz, 1H), 6.92 (d, J = 9.0 Hz, 1H), 7.01 (t, J = 8.5 Hz, 1H), 7.07 (dd, J = 9.0 Hz, 2.0 Hz, 2H), 7.25 (dd, J = 12.2 Hz, 2.0 Hz, 1H), 7.59–7.73 (m, 4H); ^{13}C NMR (101 MHz, DMSO-d_6) δ = 13.0 (CH_3), 20.0 (CH_2), 34.9 (CH_2), 55.4 (CH_3), 65.2 (CH_2), 71.7 (CH_2), 101.5 (CH_{Ar}), 111.6 (CH_{Ar}), 111.8 (C_q), 114.7 (CH_{Ar}), 114.9 (d, J =1.8 Hz, CH_{Ar}), 116.6 (CH_{Ar}), 116.8 (C_q), 125.3 (d, J = 3.4 Hz, CH_{Ar}), 129.0 ($2CH_{Ar}$), 129.9 (C_q), 130.2 (d, J = 3.3 Hz, C_q), 131.2 ($2CH_{Ar}$), 133.9 (C_q), 135.7 (C_q), 137.7 (C_q), 145.2 (d, J = 10.6 Hz, C_q), 151.1 (d, J = 244.6 Hz, C_qF), 155.6 (C_q), 162.9 (C_q), 166.2 (C_q), 167.9 (C_q); ^{19}F NMR (376 MHz, DMSO-d_6) δ = -134.2 (dd, J = 12.2 Hz, 8.6 Hz); HRMS (ESI-MS) m/z calcd for $C_{29}H_{25}ClFN_4O_7S$ $[M+H]^+$: 627.1117, found: 627.1102 ; Rf (petroleum ether/EtOAc = 3/7) 0.66.
11c	*2-(2-Chloro-4-(((5-((1-(4-chlorobenzoyl)-5-methoxy-2-methyl-1H-indol-3-yl)methyl)-1,3,4-oxadiazol-2-yl)thio)methyl)phenoxy)ethyl nitrate* was obtained from 2-(2-chloro-4-(chloromethyl)phenoxy)ethyl nitrate **(6c)** as pale yellow solid, yield 78%, m.p. 95–97 °C; ^{1}H NMR (400 MHz, DMSO-d_6) δ = 2.28 (s, 3H), 3.73 (s, 3H), 4.29 – 4.37 (m, 2H), 4.35 (s, 2H), 4.38 (s, 2H), 4.84–4.92 (m, 2H), 6.74 (dd, J = 9.0 Hz, 2.5 Hz, 1H), 6.92 (d, J = 9.0 Hz, 1H), 6.99 (d, J = 8.5 Hz, 1H), 7.08 (d, J = 2.5 Hz, 1H), 7.23 (dd, J = 8.5 Hz, 2.2 Hz, 1H), 7.47 (d, J = 2.2 Hz, 1H), 7.59–7.75 (m, 4H); ^{13}C NMR (101 MHz, DMSO-d_6) δ = 13.1 (CH_3), 20.0 (CH_2), 34.7 (CH_2), 55.4 (CH_3), 65.4 (CH_2), 71.5 (CH_2), 101.5 (CH_{Ar}), 111.6 (CH_{Ar}), 111.8 (C_q), 113.8 (CH_{Ar}), 114.7 (CH_{Ar}), 121.2 (C_q), 128.9 (CH_{Ar}), 129.0 ($2CH_{Ar}$), 129.9 (C_q), 130.3 (C_q), 130.5 (CH_{Ar}), 130.6 (C_q), 131.2 ($2CH_{Ar}$), 133.9 (C_q), 135.7 (C_q), 137.8 (C_q), 152.6 (C_q), 155.6 (C_q), 162.9 (C_q), 166.2 (C_q), 167.9 (C_q); HRMS (ESI-MS) m/z calcd for $C_{29}H_{25}Cl_2N_4O_7S$ $[M+H]^+$: 643.0821, found: 643.0816; Rf (petroleum ether/EtOAc = 4/6) 0.56.
11d	*2-(4-(((5-((1-(4-Chlorobenzoyl)-5-methoxy-2-methyl-1H-indol-3-yl)methyl)-1,3,4-oxadiazol-2-yl)thio)methyl)-2-methoxyphenoxy)ethyl nitrate* was obtained from 2-(4-(chloromethyl)-2-methoxyphenoxy)ethyl nitrate **(6d)** as pale yellow solid, yield 83%, m.p. 95–97 °C; ^{1}H NMR (250 MHz, DMSO-d_6) δ = 2.29 (s, 3H), 3.69 (s, 3H), 3.74 (s, 3H), 4.14 – 4.27 (m, 2H), 4.36 (s, 2H), 4.38 (s, 2H), 4.76–4.92 (m, 2H), 6.74 (dd, J = 9.0 Hz, 2.5 Hz, 1H), 6.78 (d, J = 1.1 Hz, 2H), 6.93 (dd, J = 9.0 Hz, 0.5 Hz, 1H), 7.03 (d, J = 1.2 Hz, 1H), 7.08 (d, J = 2.5 Hz, 1H), 7.58–7.73 (m, 4H); ^{13}C NMR (101 MHz, DMSO-d_6) δ = 13.1 (CH_3), 20.0 (CH_2), 35.9 (CH_2), 55.4 (CH_3), 55.4 (CH_3), 64.9 (CH_2), 72.0 (CH_2), 101.5 (CH_{Ar}), 111.6 (CH_{Ar}), 111.9 (C_q), 113.0 (CH_{Ar}), 113.5 (CH_{Ar}), 114.7 (CH_{Ar}), 121.2 (CH_{Ar}), 129.0 ($2CH_{Ar}$), 129.6 (C_q), 129.9 (C_q), 130.3 (C_q), 131.2 ($2CH_{Ar}$), 133.9 (C_q), 135.7 (C_q), 137.7 (C_q), 146.8 (C_q), 148.9 (C_q), 155.6 (C_q), 163.1 (C_q), 166.1 (C_q), 167.9 (C_q); HRMS (ESI-MS) m/z calcd for $C_{30}H_{28}ClN_4O_8S$ $[M+H]^+$: 639.1316, found: 639.1311; Rf (petroleum ether/EtOAc = 4/6) 0.66.
11e	*2-(4-(((5-((1-(4-Chlorobenzoyl)-5-methoxy-2-methyl-1H-indol-3-yl)methyl)-1,3,4-oxadiazol-2-yl)thio)methyl)-2-ethoxyphenoxy)ethyl nitrate* was obtained from 2-(4-(chloromethyl)-2-ethoxyphenoxy)ethyl nitrate **(6e)**: as pale yellow solid, yield 91%, m.p. 122–124 °C; ^{1}H NMR (250 MHz, DMSO-d_6) δ = 1.27 (t, J = 6.9 Hz, 3H), 2.29 (s, 3H), 3.74 (s, 3H), 3.94 (q, J = 6.9 Hz, 2H), 4.14–4.27 (m, 2H), 4.36 (s, 2H), 4.37 (s, 2H), 4.75–4.91 (m, 2H), 6.74 (dd, J = 9.0 Hz, 2.5 Hz, 1H), 6.79 (d, J = 1.1 Hz, 2H), 6.93 (dd, J = 9.0 Hz, 0.5 Hz, 1H), 7.02 (d, J = 1.1Hz, 1H), 7.08 (dd, J = 2.5 Hz, 0.5 Hz, 1H), 7.57–7.73 (m, 4H); ^{13}C NMR (101 MHz, DMSO-d_6) δ = 13.1 (CH_3), 14.6 (CH_3), 20.0 (CH_2), 35.8 (CH_2), 55.4 (CH_3), 63.9 (CH_2), 65.3 (CH_2), 71.9 (CH_2), 101.5 (CH_{Ar}), 111.6 (CH_{Ar}), 111.9 (C_q), 114.3 (CH_{Ar}), 114.5 (CH_{Ar}), 114.7 (CH_{Ar}), 121.3 (CH_{Ar}), 129.0 ($2CH_{Ar}$), 129.8 (C_q), 129.9 (C_q), 130.3 (C_q), 131.2 ($2CH_{Ar}$), 133.9 (C_q), 135.7 (C_q), 137.8 (C_q), 147.1 (C_q), 148.3 (C_q), 155.6 (C_q), 163.1 (C_q), 166.0 (C_q), 167.9 (C_q); HRMS (ESI-MS) m/z calcd for $C_{31}H_{30}ClN_4O_8S$ $[M+H]^+$: 653.1473, found: 653.1459; Rf (petroleum ether/EtOAc = 4/6) 0.58.

Cpd.	The identification characteristics (^{1}H NMR, ^{13}C NMR, MS, R_f)
11f	*2-(4-(((5-((1-(4-Chlorobenzoyl)-5-methoxy-2-methyl-1H-indol-3-yl)methyl)-1,3,4-oxadiazol-2-yl)thio)methyl)-2-nitrophenoxy)ethyl nitrate* was obtained from 2-(4-(chloromethyl)-2-nitrophenoxy)ethyl nitrate **(6f**) as pale yellow solid, yield 93%, m.p. 92–94 °C;. ^{1}H NMR (400 MHz, DMSO-d_6) δ = 2.27 (s, 3H), 3.73 (s, 3H), 4.35 (s, 2H), 4.39–4.51 (m, 2H), 4.47 (s, 2H), 4.78–4.95 (m, 2H), 6.73 (dd, J = 9.0 Hz, 2.5 Hz, 1H), 6.91 (d, J = 9.0 Hz, 1H), 7.06 (d, J = 2.5 Hz, 1H), 7.24 (d, J = 8.7 Hz, 1H), 7.55–7.74 (m, 5H), 7.96 (d, J = 2.3 Hz, 1H); ^{13}C NMR (101 MHz, DMSO-d_6) δ = 13.0 (CH_3), 20.0 (CH_2), 34.2 (CH_2), 55.4 (CH_3), 66.0 (CH_2), 71.3 (CH_2), 101.5 (CH_{Ar}), 111.6 (CH_{Ar}), 111.8 (C_q), 114.7 (CH_{Ar}), 115.4 (CH_{Ar}), 125.5 (CH_{Ar}), 129.0 ($2CH_{Ar}$), 129.9 (C_q), 130.1 (C_q), 130.2 (C_q), 131.2 ($2CH_{Ar}$), 133.9 (C_q), 134.9 (CH_{Ar}), 135.7 (C_q), 137.7 (C_q), 139.0 (C_q), 150.0 (C_q), 155.6 (C_q), 162.8 (C_q), 166.2 (C_q), 167.9 (C_q); HRMS (ESI-MS) m/z calcd for $C_{29}H_{25}ClN_5O_9S$ $[M+H]^+$: 654.1062, found: 654.1053; Rf (CH_2Cl_2/CH_3OH = 9.8/0.2) 0.73.
11g	*2-(4-(((5-((1-(4-Chlorobenzoyl)-5-methoxy-2-methyl-1H-indol-3-yl)methyl)-1,3,4-oxadiazol-2-yl)thio)methyl)-2,6-dimethoxyphenoxy)ethyl nitrate* was obtained from 2-(4-(chloromethyl)-2,6-dimethoxyphenoxy)ethyl nitrate **(6g)** as pale yellow solid, yield 91%, m.p. 110–112 °C; ^{1}H NMR (250 MHz, DMSO-d_6) δ = 2.28 (s, 3H), 3.68 (s, 6H), 3.74 (s, 3H), 4.03–4.18 (m, 2H), 4.36 (s, 2H), 4.42 (s, 2H), 4.64–4.80 (m, 2H), 6.73 (dd, J = 9.0 Hz, 2.5 Hz, 1H), 6.73 (s, 2H), 6.92 (dd, J = 9.0 Hz, 0.5 Hz, 1H), 7.09 (d, J = 2.3 Hz, 1H), 7.57–7.74 (m, 4H); ^{13}C NMR (101 MHz, DMSO-d_6) δ = 13.1 (CH_3), 20.0 (CH_2), 36.3 (CH_2), 55.4 (CH_3), 55.8 ($2CH_3$), 68.5 (CH_2), 72.8 (CH_2), 101.5 (CH_{Ar}), 106.2 ($2CH_{Ar}$), 111.5 (CH_{Ar}), 111.8 (C_q), 114.7 (CH_{Ar}), 129.0 ($2CH_{Ar}$), 129.9 (C_q), 130.2 (C_q), 131.2 ($2CH_{Ar}$), 132.3 (C_q), 133.9 (C_q), 135.3 (C_q), 135.7 (C_q), 137.7 (C_q), 152.7 ($2C_q$), 155.6 (C_q), 163.1 (C_q), 166.1 (C_q), 167.9 (C_q); HRMS (ESI-MS) m/z calcd for $C_{31}H_{30}ClN_4O_9S$ $[M+H]^+$: 669.1422, found: 669.1411; Rf (petroleum ether/EtOAc = 4/6) 0.57.
11h	*2-(2,6-Dichloro-4-(((5-((1-(4-chlorobenzoyl)-5-methoxy-2-methyl-1H-indol-3-yl)methyl)-1,3,4-oxadiazol-2-yl)thio)methyl)phenoxy)ethyl nitrate* was obtained from 2-(2,6-dichloro-4-(chloromethyl)phenoxy)ethyl nitrate **(6h)** as pale yellow solid, yield 89%, m.p. 125–127 °C; ^{1}H NMR (250 MHz, DMSO-d_6) δ = 2.28 (s, 3H), 3.73 (s, 3H), 4.22–4.32 (m, 2H), 4.35 (s, 2H), 4.42 (s, 2H), 4.80–4.91 (m, 2H), 6.72 (dd, J = 9.0 Hz, 2.5 Hz, 1H), 6.91 (dd, J = 9.0 Hz, 0.5 Hz, 1H), 7.07 (dd, J = 2.5 Hz, 0.5 Hz, 1H), 7.54 (s, 2H), 7.59–7.74 (m, 4H); ^{13}C NMR (101 MHz, DMSO-d_6) δ = 13.1 (CH_3), 20.0 (CH_2), 34.0 (CH_2), 55.4 (CH_3), 69.4 (CH_2), 72.4 (CH_2), 101.5 (CH_{Ar}), 111.6 (CH_{Ar}), 111.8 (C_q), 114.7 (CH_{Ar}), 128.0 ($2C_q$), 129.0 ($2CH_{Ar}$), 129.7 ($2CH_{Ar}$), 129.9 (C_q), 130.2 (C_q), 131.2 ($2CH_{Ar}$), 133.9 (C_q), 135.7 (C_q), 135.7 (C_q), 137.7 (C_q), 149.4 (C_q), 155.6 (C_q), 162.8 (C_q), 166.3 (C_q), 167.8 (C_q); HRMS (ESI-MS) m/z calcd for $C_{29}H_{24}Cl_3N_4O_7S$ $[M+H]^+$: 677.0431, found: 677.0723; Rf (petroleum ether/EtOAc = 5/5) 0.49.
11i	*2-(3-(((5-((1-(4-Chlorobenzoyl)-5-methoxy-2-methyl-1H-indol-3-yl)methyl)-1,3,4-oxadiazol-2-yl)thio)methyl)phenoxy)ethyl nitrate* was obtained from 2-(3-(chloromethyl)phenoxy)ethyl nitrate (**6i**) as pale yellow solid, yield 80%, m.p. 98–100 °C; ^{1}H NMR (250 MHz, DMSO-d_6) δ = 2.28 (s, 3H), 3.74 (s, 3H), 4.15–4.31 (m, 2H), 4.35 (s, 2H), 4.41 (s, 2H), 4.76–4.93 (m, 2H), 6.73 (dd, J = 9.0 Hz, 2.5 Hz, 1H), 6.79 – 6.98 (m, 2H), 6.92 (dd, J = 9.0 Hz, 0.5 Hz, 1H), 6.98–7.03 (m, 1H), 7.08 (dd, J = 2.6 Hz, 0.5 Hz, 1H), 7.10–7.20 (m, 1H), 7.58–7.73 (m, 4H); ^{13}C NMR (101 MHz, DMSO-d_6) δ = 13.0 (CH_3), 20.0 (CH_2), 35.7 (CH_2), 55.4 (CH_3), 63.9 (CH_2), 71.9 (CH_2), 101.5 (CH_{Ar}), 111.6 (CH_{Ar}), 111.9 (C_q), 113.6 (CH_{Ar}), 114.7 (CH_{Ar}), 115.3 (CH_{Ar}), 121.6 (CH_{Ar}), 129.1 ($2CH_{Ar}$), 129.6 (CH_{Ar}), 129.9 (C_q), 130.2 (C_q), 131.2 ($2CH_{Ar}$), 133.9 (C_q), 135.7 (C_q), 137.7 (C_q), 138.1 (C_q), 155.6 (C_q), 157.8 (C_q), 163.0 (C_q), 166.1 (C_q), 167.9 (C_q). HRMS (ESI-MS) m/z calcd for $C_{29}H_{26}ClN_4O_7S$ $[M+H]^+$: 609.1211, found: 609.1207; Rf (petroleum ether/EtOAc = 4/6) 0.63.
11j	*2-(5-(((5-((1-(4-Chlorobenzoyl)-5-methoxy-2-methyl-1H-indol-3-yl)methyl)-1,3,4-oxadiazol-2-yl)thio)methyl)-2-methoxyphenoxy)ethyl nitrate* was obtained from 2-(5-(chloromethyl)-2-methoxyphenoxy)ethyl nitrate (**6j**) as pale yellow solid, yield 75%, m.p. 104–106 °C; ^{1}H NMR (250 MHz, DMSO-d_6) δ = 2.28 (s, 3H), 3.70 (s, 3H), 3.74 (s, 3H), 4.10 – 4.26 (m, 2H), 4.36 (s,

Cpd.	The identification characteristics (^{1}H NMR, ^{13}C NMR, MS, R_f)
	4H), 4.75–4.92 (m, 2H), 6.70–6.76 (m, 1H), 6.77 (s, 1H), 6.83 (dd, J = 8.3 Hz, 1.9 Hz, 1H), 6.93 (dd, J = 9.0 Hz, 0.5 Hz, 1H), 7.06 (d, J = 1.9 Hz, 1H), 7.08 (dd, J = 2.5 Hz, 0.5 Hz, 1H), 7.59–7.74 (m, 4H); ^{13}C NMR (101 MHz, DMSO-d_6) δ = 13.1 (CH_3), 20.0 (CH_2), 35.8 (CH_2), 55.4 (CH_3), 55.5 (CH_3), 65.0 (CH_2), 71.9 (CH_2), 101.5 (CH_{Ar}), 111.6 (CH_{Ar}), 111.9 (C_q, CH_{Ar}), 114.7 (CH_{Ar}), 114.8 (CH_{Ar}), 122.3 (CH_{Ar}), 128.5 (C_q), 129.1 ($2CH_{Ar}$), 129.9 (C_q), 130.3 (C_q), 131.2 ($2CH_{Ar}$), 133.9 (C_q), 135.7 (C_q), 137.7 (C_q), 147.0 (C_q), 148.8 (C_q), 155.6 (C_q), 163.0 (C_q), 166.0 (C_q), 167.9 (C_q); HRMS (ESI-MS) m/z calcd for $C_{30}H_{28}ClN_4O_8S$ $[M+H]^+$: 639.1316, found: 639.1313; Rf (petroleum ether/EtOAc = 4/6) 0.53.
11k	*2-(5-(((5-((1-(4-Chlorobenzoyl)-5-methoxy-2-methyl-1H-indol-3-yl)methyl)-1,3,4-oxadiazol-2-yl)thio)methyl)-2-nitrophenoxy)ethyl nitrate* was obtained from 2-(5-(chloromethyl)-2-nitrophenoxy)ethyl nitrate **(6k)** as pale yellow solid, yield 88%, m.p. 90–92 °C; ^{1}H NMR (400 MHz, DMSO-d_6) δ = 2.27 (s, 3H), 3.72 (s, 3H), 4.35 (s, 2H), 4.40–4.46 (m, 2H), 4.50 (s, 2H), 4.81–4.95 (m, 2H), 6.73 (dd, J = 9.0 Hz, 2.5 Hz, 1H), 6.90 (d, J = 9.0 Hz, 1H), 7.05 (d, J = 2.5 Hz, 1H), 7.09 (dd, J = 8.3 Hz, 1.6 Hz, 1H), 7.47 (d, J = 1.6 Hz, 1H), 7.60–7.71 (m, 4H), 7.73 (d, J = 8.3 Hz, 1H); ^{13}C NMR (101 MHz, DMSO-d_6) δ = 13.0 (CH_3), 20.0 (CH_2), 35.1 (CH_2), 55.4 (CH_3), 66.0 (CH_2), 71.2 (CH_2), 101.5 (CH_{Ar}), 111.5 (CH_{Ar}), 111.8 (C_q), 114.7 (CH_{Ar}), 115.9 (CH_{Ar}), 121.5 (CH_{Ar}), 125.2 (CH_{Ar}), 129.0 ($2CH_{Ar}$), 129.9 (C_q), 130.2 (C_q), 131.2 ($2CH_{Ar}$), 133.9 (C_q), 135.8 (C_q), 137.8 (C_q), 138.6 (C_q), 144.0 (C_q), 150.5 (C_q), 155.6 (C_q), 162.6 (C_q), 166.3 (C_q), 167.9 (C_q); HRMS (ESI-MS) m/z calcd for $C_{29}H_{25}ClN_5O_9S$ $[M+H]^+$: 654.1062, found: 654.1049; Rf (petroleum ether/EtOAc = 3/7) 0.48.
11l	*2-(2-Bromo-3-(((5-((1-(4-chlorobenzoyl)-5-methoxy-2-methyl-1H-indol-3-yl)methyl)-1,3,4-oxadiazol-2-yl)thio)methyl)-6-methoxyphenoxy)ethyl nitrate* was obtained from 2-(2-bromo-3-(chloromethyl)-6-methoxyphenoxy)ethyl nitrate **(6l)** as pale yellow solid, yield 88%, m.p. 94–96 °C; ^{1}H NMR (400 MHz, DMSO-d_6) δ = 2.29 (s, 3H), 3.74 (s, 3H), 3.77 (s, 3H), 4.16–4.24 (m, 2H), 4.37 (s, 2H), 4.46 (s, 2H), 4.75–4.87 (m, 2H), 6.74 (dd, J = 9.0 Hz, 2.5 Hz, 1H), 6.86 (d, J = 8.7 Hz, 1H), 6.93 (d, J = 8.9 Hz, 1H), 7.10 (d, J = 2.5 Hz, 1H), 7.12 (d, J = 8.6 Hz, 1H), 7.60–7.72 (m, 4H); ^{13}C NMR (101 MHz, DMSO-d_6) δ = 13.1 (CH_3), 20.0 (CH_2), 36.9 (CH_2), 55.4 (CH_3), 56.1 (CH_3), 68.6 (CH_2), 72.7 (CH_2), 101.5 (CH_{Ar}), 111.6 (CH_{Ar}), 111.7 (CH_{Ar}), 111.9 (C_q), 114.7 (CH_{Ar}), 119.2 (C_q), 126.6 (CH_{Ar}), 127.7 (C_q), 129.0 ($2CH_{Ar}$), 129.9 (C_q), 130.3 (C_q), 131.2 ($2CH_{Ar}$), 133.9 (C_q), 135.8 (C_q), 137.8 (C_q), 144.5 (C_q), 152.7 (C_q), 155.6 (C_q), 162.6 (C_q), 166.3 (C_q), 167.9 (C_q); HRMS (ESI-MS) m/z calcd for $C_{30}H_{27}BrClN_4O_8S$ $[M+H]^+$: 717.0421, found: 717.0409; Rf (petroleum ether/EtOAc = 4/6) 0.55.
11m	*2-(2-(((5-((1-(4-Chlorobenzoyl)-5-methoxy-2-methyl-1H-indol-3-yl)methyl)-1,3,4-oxadiazol-2-yl)thio)methyl)phenoxy)ethyl nitrate* was obtained from 2-(2-(chloromethyl)phenoxy)ethyl nitrate **(6m)** as pale yellow solid, yield 70%, m.p. 89–91 °C; ^{1}H NMR (400 MHz, DMSO-d_6) δ = 2.28 (s, 3H), 3.74 (s, 3H), 4.28–4.40 (m, 2H), 4.34 (s, 2H), 4.35 (s, 2H), 4.79–4.98 (m, 2H), 6.74 (dd, J = 8.9 Hz, 2.5 Hz, 1H), 6.78 (td, J = 7.5 Hz, 1.0 Hz, 1H), 6.92 (d, J = 8.9 Hz, 1H), 7.01 (dd, J = 8.4 Hz, 1.0 Hz, 1H), 7.08 (d, J = 2.5 Hz, 1H), 7.19 (dd, J = 7.5 Hz, 1.7 Hz, 1H), 7.25 (ddd, J = 8.2 Hz, 7.4 Hz, 1.7 Hz, 1H), 7.58–7.72 (m, 4H); ^{13}C NMR (101 MHz, DMSO-d_6) δ = 13.1 (CH_3), 20.0 (CH_2), 31.4 (CH_2), 55.4 (CH_3), 64.7 (CH_2), 71.8 (CH_2), 101.5 (CH_{Ar}), 111.6 (CH_{Ar}), 111.9 (C_q), 112.2 (CH_{Ar}), 114.7 (CH_{Ar}), 120.8 (CH_{Ar}), 124.3 (C_q), 129.0 ($2CH_{Ar}$), 129.6 (CH_{Ar}), 129.9 (C_q), 130.3 (C_q), 130.3 (CH_{Ar}), 131.2 ($2CH_{Ar}$), 133.9 (C_q), 135.7 (C_q), 137.7 (C_q), 155.6 (C_q), 155.7 (C_q), 163.3 (C_q), 166.1 (C_q), 167.9 (C_q); HRMS (ESI-MS) m/z calcd for $C_{29}H_{26}ClN_4O_7S$ $[M+H]^+$: 609.1211, found: 609.1195 ; Rf (petroleum ether/EtOAc = 4/6) 0.68.
11t	*2-(4-Bromo-2-(((5-((1-(4-chlorobenzoyl)-5-methoxy-2-methyl-1H-indol-3-yl)methyl)-1,3,4-oxadiazol-2-yl)thio)methyl)phenoxy)ethyl nitrate* was obtained from *2*-(4-bromo-2-(chloromethyl)phenoxy)ethyl nitrate **(6t)** as pale yellow solid, yield 87%, m.p. 91–93 °C; ^{1}H NMR (400 MHz, DMSO-d_6) δ = 2.28 (s, 3H), 3.74 (s, 3H), 4.26–4.41 (m, 2H), 4.34 (s, 4H), 4.79–4.92 (m, 2H), 6.73 (dd, J = 8.9 Hz, 2.5 Hz, 1H), 6.92 (d, J = 8.9 Hz, 1H), 7.00 (d, J = 8.8 Hz, 1H), 7.07 (d, J = 2.5 Hz, 1H), 7.44 (dd, J = 8.7 Hz, 2.5 Hz, 1H), 7.50 (d, J = 2.5 Hz, 1H), 7.59–7.72 (m, 4H); ^{13}C NMR (101 MHz, DMSO-d_6) δ = 13.1 (CH_3), 20.0 (CH_2), 30.7 (CH_2), 55.4

Cpd.	The identification characteristics (^{1}H NMR, ^{13}C NMR, MS, R_f)
	(CH_3), 65.1 (CH_2), 71.7 (CH_2), 101.4 (CH_{Ar}), 111.6 (CH_{Ar}), 111.8 (C_q), 112.0 (C_q), 114.4 (CH_{Ar}), 114.7 (CH_{Ar}), 127.1 (C_q), 129.0 ($2CH_{Ar}$), 129.9 (C_q), 130.2 (C_q), 131.2 ($2CH_{Ar}$), 131.9 (CH_{Ar}), 132.7 (CH_{Ar}), 133.9 (C_q), 135.7 (C_q), 137.7 (C_q), 155.0 (C_q), 155.6 (C_q), 163.1 (C_q), 166.2 (C_q), 167.8 (C_q); HRMS (ESI-MS) m/z calcd for $C_{29}H_{25}BrClN_4O_7S$ $[M+H]^+$: 687.0316, found: 687.0302; Rf (petroleum ether/EtOAc = 4/6) 0.70.
11u	*2-(2-Chloro-3-(((5-((1-(4-chlorobenzoyl)-5-methoxy-2-methyl-1H-indol-3-yl)methyl)-1,3,4-oxadiazol-2-yl)thio)methyl)-6-methoxyphenoxy)ethyl nitrate* was obtained from 2-(2-chloro-3-(chloromethyl)-6-methoxyphenoxy)ethyl nitrate **(6u)** as pale yellow solid, yield 87%, m.p. 117–119 °C; ^{1}H NMR (400 MHz, DMSO-d_6) δ = 2.29 (s, 3H), 3.74 (s, 3H), 3.76 (s, 3H), 4.17–4.27 (m, 2H), 4.37 (s, 2H), 4.44 (s, 2H), 4.71–4.86 (m, 2H), 6.74 (dd, J = 9.0 Hz, 2.5 Hz, 1H), 6.82 (d, J = 8.6 Hz, 1H), 6.93 (d, J = 8.9 Hz, 1H), 7.10 (dd, J = 5.5 Hz, 3.0 Hz, 2H), 7.60–7.73 (m, 4H); ^{13}C NMR (101 MHz, DMSO-d_6) δ = 13.1 (CH_3), 20.0 (CH_2), 34.3 (CH_2), 55.4 (CH_3), 56.1 (CH_3), 68.8 (CH_2), 72.7 (CH_2), 101.5 (CH_{Ar}), 111.0 (CH_{Ar}), 111.6 (CH_{Ar}), 111.8 (C_q), 114.7 (CH_{Ar}), 126.2 (C_q), 126.4 (CH_{Ar}), 127.4 (C_q), 129.0 ($2CH_{Ar}$), 129.9 (C_q), 130.2 (C_q), 131.2 ($2CH_{Ar}$), 133.9 (C_q), 135.8 (C_q), 137.8 (C_q), 143.4 (C_q), 152.9 (C_q), 155.6 (C_q), 162.6 (C_q), 166.3 (C_q), 167.9 (C_q); HRMS (ESI-MS) m/z calcd for $C_{30}H_{27}Cl_2N_4O_8S$ $[M+H]^+$: 673.0927, found: 673.0918; Rf (petroleum ether/EtOAc = 4/6) 0.53.
11v	*2-(4-(2-((5-((1-(4-Chlorobenzoyl)-5-methoxy-2-methyl-1H-indol-3-yl)methyl)-1,3,4-oxadiazol-2-yl)thio)ethyl)phenoxy)ethyl nitrate* was obtained from 2-(4-(2-iodooethyl) phenoxy)ethyl nitrate **(6v)** as yellow solid, yield 82%, m.p. 92–94 °C; ^{1}H NMR (250 MHz, DMSO-d_6) δ = 2.29 (s, 3H), 2.91 (t, J = 7.5 Hz, 2H), 3.25–3.45 (m, 2H), 3.74 (s, 3H), 4.18–4.31 (m, 2H), 4.36 (s, 2H), 4.79–4.93 (m, 2H), 6.74 (dd, J = 9.0 Hz, 2.5 Hz, 1H), 6.81–6.89 (m, 2H), 6.92 (dd, J = 9.0 Hz, 0.5 Hz, 1H), 7.04–7.16 (m, 3H), 7.56–7.73 (m, 4H); ^{13}C NMR (101 MHz, DMSO-d_6) δ = 13.1 (CH_3), 20.0 (CH_2), 33.4 (CH_2), 34.0 (CH_2), 55.4 (CH_3), 63.9 (CH_2), 72.0 (CH_2), 101.5 (CH_{Ar}), 111.5 (CH_{Ar}), 111.9 (C_q), 114.4 ($2CH_{Ar}$), 114.7 (CH_{Ar}), 129.0 ($2CH_{Ar}$), 129.7 ($2CH_{Ar}$), 129.9 (C_q), 130.2 (C_q), 131.2 ($2CH_{Ar}$), 131.7 (C_q), 133.9 (C_q), 135.7 (C_q), 137.7 (C_q), 155.6 (C_q), 156.5 (C_q), 163.4 (C_q), 165.9 (C_q), 167.9 (C_q); HRMS (ESI-MS) m/z calcd for $C_{30}H_{28}ClN_4O_7S$ $[M+H]^+$: 623.1367, found: 623.1364; Rf (petroleum ether/EtOAc = 5/5) 0.63.

7.2.2. The structure confirmation of the synthesized derivatives

The chemical structure of all synthesized compound (intermediary and final compounds) was proved on basis of spectral methods (^{1}H NMR, ^{13}C NMR, ^{1}H,^{13}C-HSQC and HRMS).

7.2.2.1. The structure confirmation of the intermediary compounds

In the ^{1}H NMR spectra of *nitrate ester benzaldehyde derivatives* (**3a-s**) it was found the characteristic multiplet signals corresponding to methylene protons close to the electron withdrawing nitrate ester group (−C$\underline{H_2}$−ONO_2) that appear more deshielded (δ 4.80-5.00, m, 2H) compared with the protons close to halide (−C$\underline{H_2}$−X) (δ 3.75 - 3.90, m, 2H) from halide-ethoxy-benzaldehyde derivatives **(2a-s)**. At the same time, ^{13}C NMR signal for −$\underline{C}H_2$−ONO_2 was observed in range of δ 71.1-72.6 ppm compared to the signal of the same carbon from derivatives (**2a-s**), which was recorded in range of δ 30.4-31.6 ppm.

The proton from corresponding carbonyl group was observed as singlet signal in range of δ 9.84-10.45 ppm and the corresponding carbon (C=O) was observed in range of δ 189.1-192.8 ppm.

For exemplification, the ^{1}H NMR and ^{13}C NMR spectra of 2-(4-formyl-2-nitrophenoxy)ethyl nitrate (**3f**) in reference with 4-(2-bromoethoxy)-3-nitrobenzaldehyde (**2f**) is presented in Fig. 7.10 and Fig. 7.11, respectively.

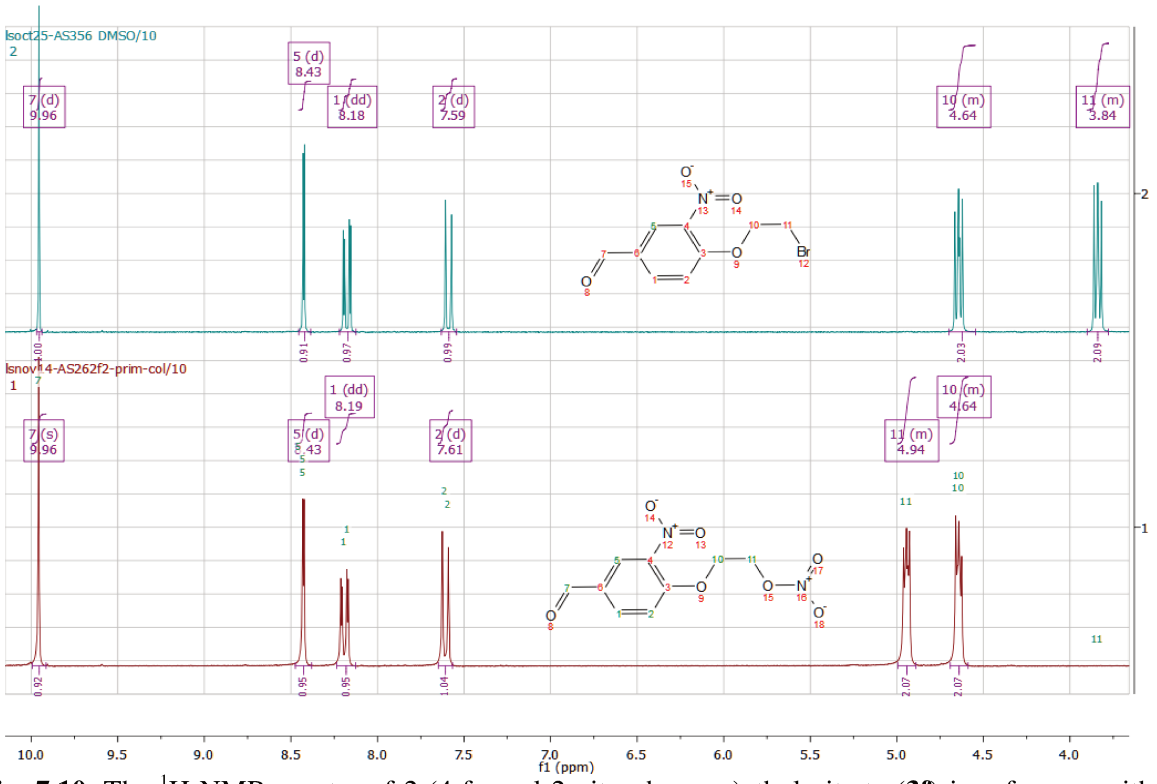

Fig. 7.10. The ^{1}H NMR spectra of 2-(4-formyl-2-nitrophenoxy)ethyl nitrate (**3f**) in reference with 4-(2-bromoethoxy)-3-nitrobenzaldehyde (**2f**), respectively.

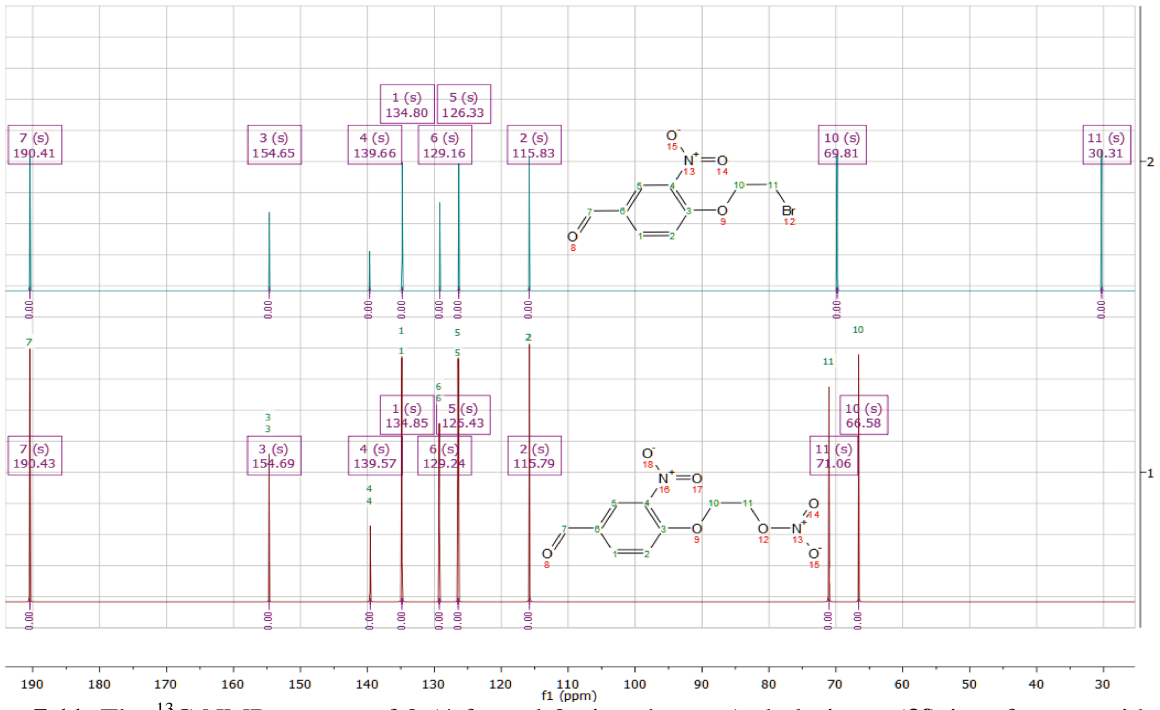

Fig. 7.11. The ^{13}C NMR spectra of 2-(4-formyl-2-nitrophenoxy)ethyl nitrate (**3f**) in reference with 4-(2-bromoethoxy)-3-nitrobenzaldehyde (**2f**), respectively.

Reduction of carbonyl group from halide-alcoxy-benzaldehyde derivatives (**2a-s**, **t**, **u**) was confirmed by some modification in the ^{1}H NMR spectra.

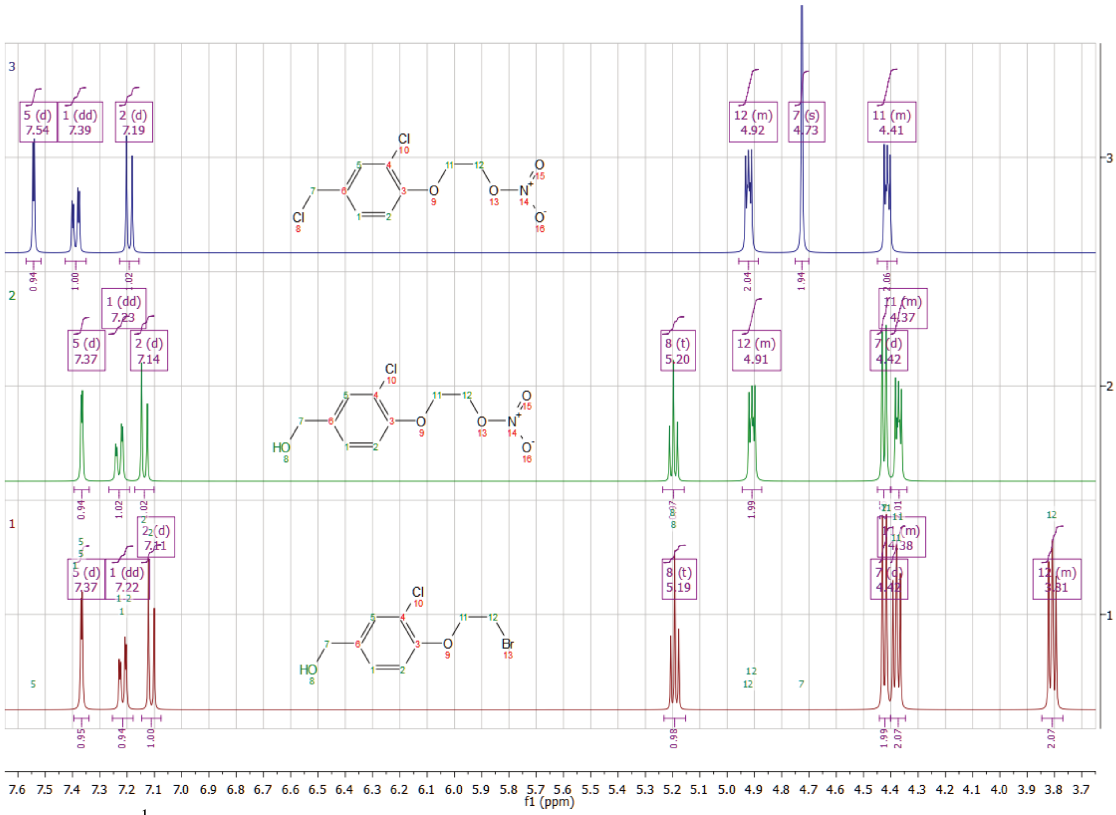

Fig. 7.12. The ^{1}H NMR spectra of (4-(2-bromoethoxy)-3-chlorophenyl)methanol (**4c**), 2-(2-chloro-4-(hydroxymethyl)phenoxy)ethyl nitrate (**5c**) and 2-(2-chloro-4-(chloromethyl)phenoxy)ethyl nitrate (**6c**), respectively.

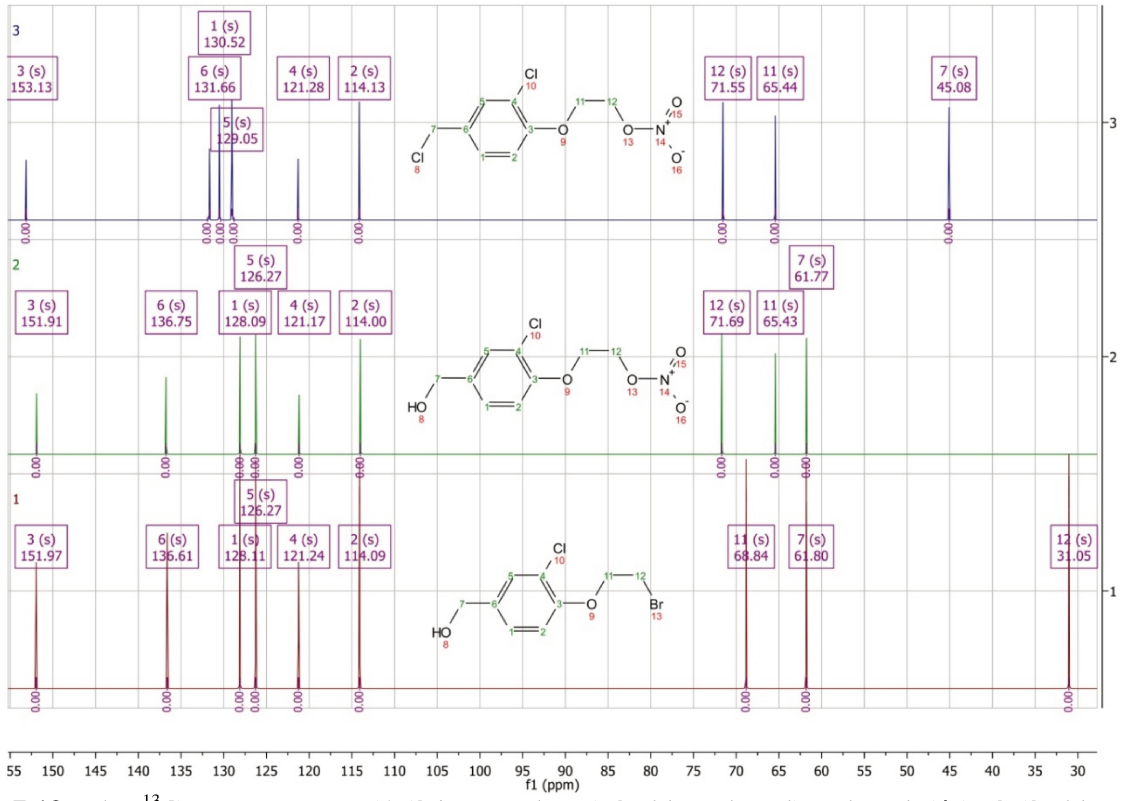

Fig. 7.13. The ^{13}C NMR spectra (4-(2-bromoethoxy)-3-chlorophenyl)methanol (**4c**), 2-(2-chloro-4-(hydroxymethyl)phenoxy)ethyl nitrate (**5c**) and 2-(2-chloro-4-(chloromethyl)phenoxy)ethyl nitrate (**6c**), respectively.

So, in the ^{1}H NMR spectra of (bromoethoxy)aromatic alcohol derivatives **(4a-m**, **t**, **u)** it was found the missing of proton signal of carbonyl group at δ 9.83 - 10.45 ppm and presence of other two signals: proton of OH appeared at δ 4.37 - 4.48 (t, *J* = 5.8 Hz, 2H) and the adjacent protons of the methylene group appeared at δ 5.01 - 5.48 (d, *J* = 5.8 Hz, 2H). Also, ^{13}C NMR signal for CH_2OH was shifted up field to δ 57.3 - 62.9 ppm from δ 189.1 - 192.8 ppm, in C=O.

For exemplification, the ^{1}H NMR and ^{13}C NMR spectra of (4-(2-bromoethoxy)-3-chlorophenyl)methanol (**4c**) is presented in Fig. 7.12 and Fig. 7.13, respectively.

After nitrate esterification of the (bromoethoxy)aromatic alcohol derivatives (**4a-m, t-v**), the corresponding (hydroxyalkyl)phenoxy nitrate derivatives (**5a-m**, **t-v**) were obtained. In their ^{1}H NMR spectra the characteristic multiplet signals corresponding to methylene protons close to the electron withdrawing nitrate ester group (−C<u>H</u>$_2$−ONO_2) appears more deshielded (δ 4.80-5.00, m, 2H) compared with the protons close to bromide (−C<u>H</u>$_2$−Br) (δ 3.75 - 3.90, m, 2H) from (bromoethoxy)aromatic alcohol derivatives (**4a-m**, **t-v**). At the same time, ^{13}C NMR signal for −<u>C</u>H_2−ONO_2 was observed in range of δ 71.3 - 72.9 ppm compared to the signal of the same carbon from derivatives **4a-m**, **t-v**, recorded in range of δ 31.0-31.8 ppm.

For exemplification, the ^{1}H NMR and ^{13}C NMR spectra of 2-(2-chloro-4-(hydroxyl-methyl)phenoxy)ethyl nitrate (**5c**) is presented in Fig. 7.12 and Fig. 7.13, respectively.

The successful conversion of (hydroxyalkyl)phenoxy nitrate derivatives (**5a-m**, **t-v**) into (halidealkyl)phenoxy nitrate derivatives (**6a-m**, **t-v**) was confirmed by weakly deshieded of aromatic protons and missing of OH proton signal in ^{1}H NMR of the **6a-m, t-v** compounds. The methylene protons close to corresponding halide were also shifted downfield, appearing at singlet at δ 4.69 - 4.81 ppm. Moreover, ^{13}C NMR signal for CH_2−X was shifted upfield to δ 43.9-46.8 ppm from δ 57.6 - 62.9 ppm, in corresponding CH_2OH.

For exemplification, the ^{1}H NMR and ^{13}C NMR spectra of 2-(2-chloro-4-(chloro-methyl)phenoxy)ethyl nitrate (**6c**) is presented in Fig. 7.12 and Fig. 7.13, respectively.

7.2.2.2. The structure confirmation of the nitric oxide-releasing indomethacin derivatives with 1,3-thiazolidin-4-one scaffold

The ^{1}H NMR spectra of the indomethacin (in DMSO-d_6) showed that the O−<u>H</u> proton of carboxylic acid is highly deshielded, appearing at 12.43 ppm and the protons of the methylene group, adjacent to carboxylic acid (−C<u>H</u>$_2$−COOH), appeared at 3.72 ppm.

In the ^{1}H NMR spectra on indomethacin hydrazide (**7**) it was found the missing of proton signal (O−<u>H</u>) at 12.43 ppm and the adjacent methylene showed an upfield shift from 3.72 ppm to 3.46 ppm. Moreover, it was observed the presence of other two signals at δ 4.25 ppm (s, 2H) and at δ 9.22 ppm (s, 1H), respectively, corresponding of hydrazine moiety (−NH−NH_2). The aliphatic and aromatic protons of the indomethacin hydrazide were observed at expected values of chemical shift, which indicated that the hydroxyl from carboxyl group was replaced by hydrazine. At the same time, ^{13}C NMR signal for −<u>C</u>O−NH−NH_2 was shifted upfield to δ 168.8 ppm from δ 172.0 ppm, in indomethacin.

Moreover, the HSQC experiment, which determines the proton-carbon single bond correlations, offered a very informative approach for signal assignments and strong support the proposed structure for indomethacin hydrazide. (Fig. 7.14)

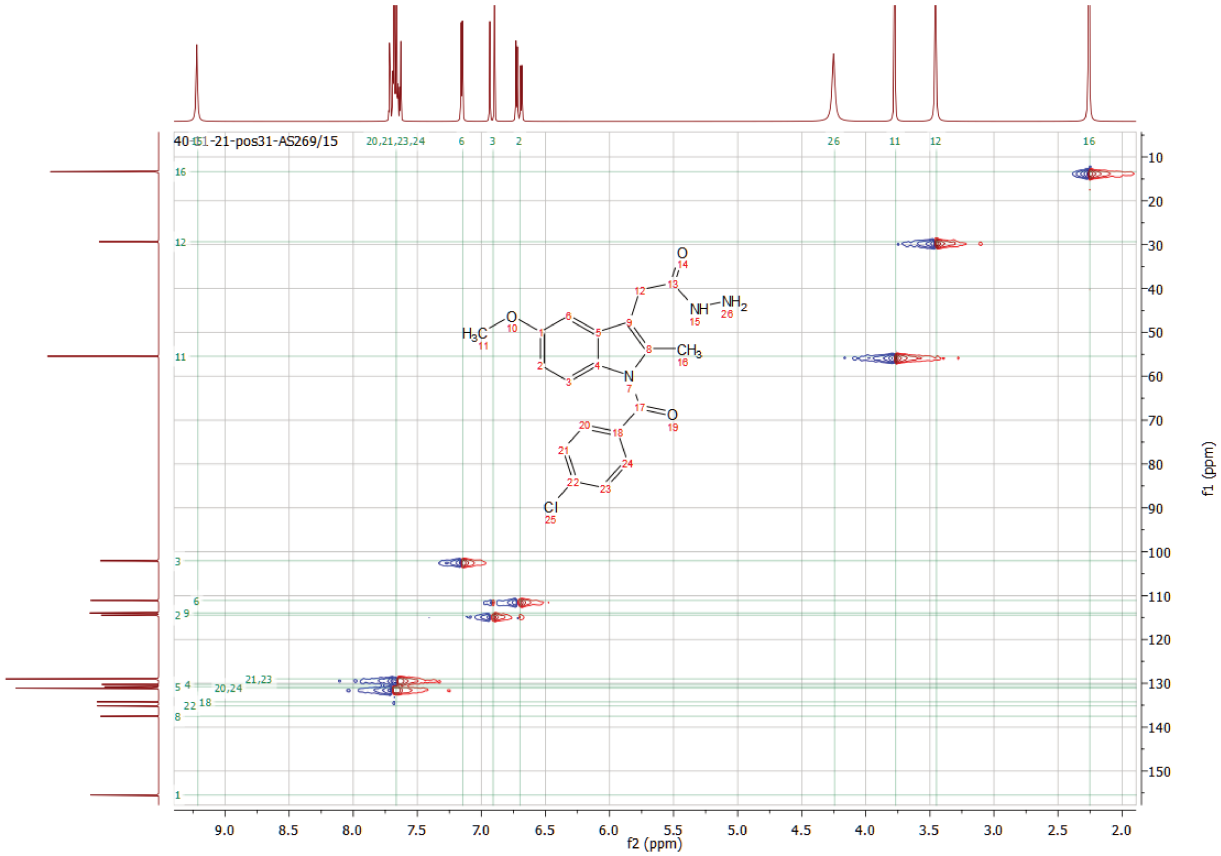

Fig. 7.14. The ^{1}H,^{13}C-HSQC spectra (250 MHz, DMSO-d_6) of indomethacin hydrazide (**7**).

The final NO-IND-TZDs (**9a-s)** showed the multiplet signals of protons and secondary carbon of methylene ($-CH_2-ONO_2$) in the range of δ 4.80-4.90 ppm and δ 64.00-69.00 ppm, respectively. The presence of 1,3-thiazolidine-4-one scaffold in the structure of NO-IND-TZDs (**9a-s)** was proved by the characteristic signals of protons and carbons corresponding to methine (=CH−) and methylene ($-CH_2-$) groups. In ^{1}H NMR spectra, the signal of =CH− was observed in the range of δ 5.70-6.00 ppm. For $-CH_2-$ there is **diastereotopic** protons, that have different chemical shifts δ 3.70 (d, J = 15.9 Hz, 1H) respectively δ 3.90 (dd, J = 15.9 Hz, 1.7 Hz, 1H) ppm. In ^{13}C NMR spectra, signal of the =CH− group was observed in the range of δ 60.0 - 61.4 ppm and of the $-CH_2-$ group at δ 28.9 - 29.6 ppm. The protons and carbon signals of other aliphatic and aromatic fragments of **9a-s** were observed at expected values of chemical shift. The presence of the signals above mentioned confirmed successful cyclization of indomethacin hydrazone derivatives (**8a-s**) to form 1,3-thiazolidine-4-one ring and preserved the nitrate ester moiety in the **9a-s**. Moreover the NMR spectral data coupled with mass spectra strong support the proposed structures of the all NO-IND-TZDs (**9a-s)**.

For exemplification, the ^{1}H NMR and ^{13}C NMR spectra 2-(2-(3-(2-(1-(4-chloro-benzoyl)-5-methoxy-2-methyl-1H-indol-3-yl)acetamido)-4-oxo-thiazolidin-2-yl)phenoxy) ethyl nitrate **(9m)** is presented in Fig. 7.15 and Fig. 7.16, respectively.

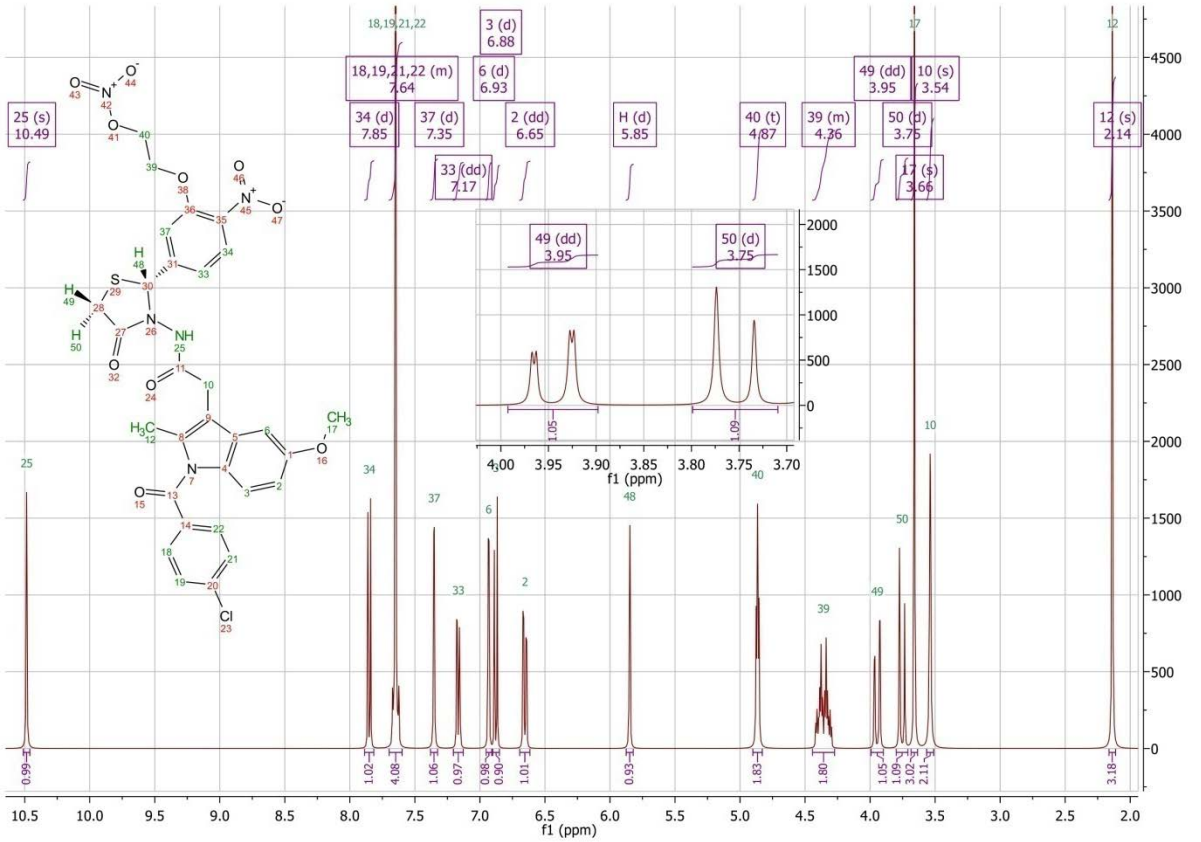

Fig. 7.15. The ^{1}H NMR spectra of 2-(2-(3-(2-(1-(4-chloro-benzoyl)-5-methoxy-2-methyl-1*H*-indol-3-yl)acetamido)-4-oxo-thiazolidin-2-yl)phenoxy) ethyl nitrate (**9m**).

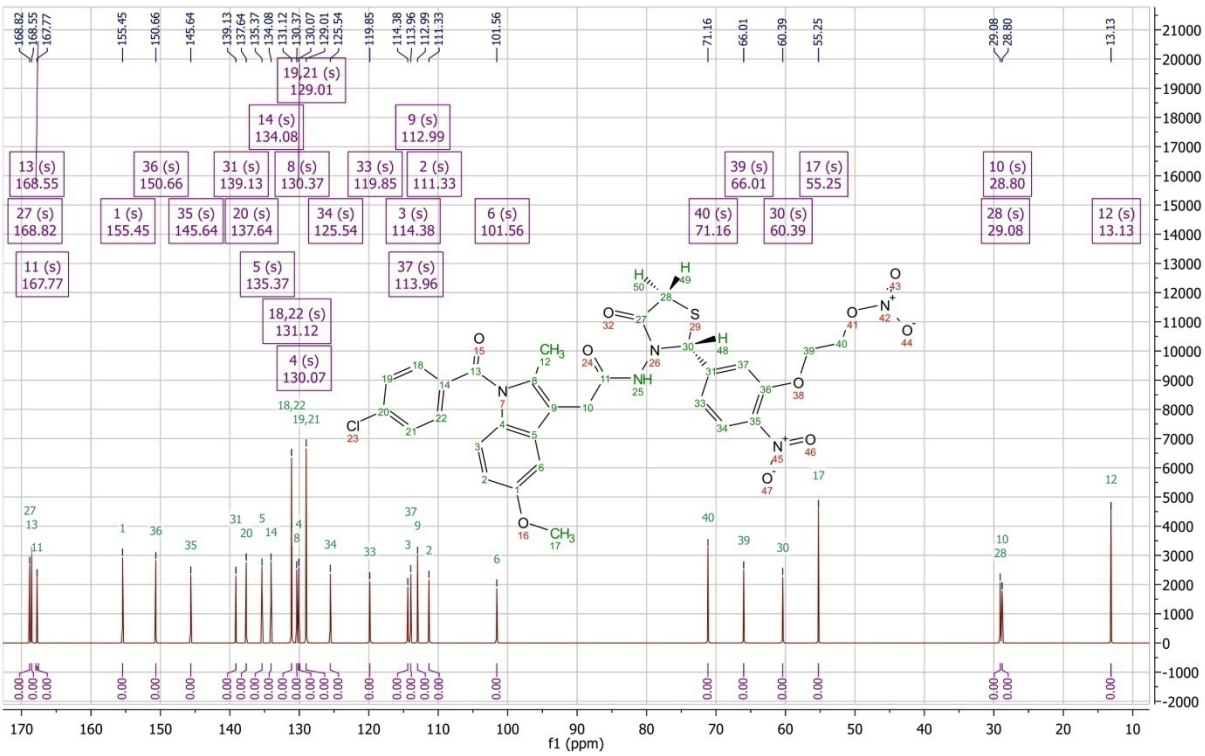

Fig. 7.16. The ^{13}H NMR spectra of 2-(2-(3-(2-(1-(4-chloro-benzoyl)-5-methoxy-2-methyl-1*H*-indol-3-yl)acetamido)-4-oxo-thiazolidin-2-yl)phenoxy) ethyl nitrate (**9m**).

7.2.2.3. The structure confirmation of the nitric oxide-releasing indomethacin derivatives with 1,3,4-oxadiazole scaffold

The ^{1}H NMR spectra of (4-chlorobenzoyl)-5-methoxy-2-methyl-1*H*-indol-3-yl)methyl)-2-mercapto-1,3,4-oxadiazole (**10**) showed that the proton of sulfhydryl group (S−H) was highly deshielded, appearing at δ 14.36 ppm and was found the missing of signals corresponding to protons of hydrazide group (CO−NH−NH_2). Moreover, the protons of the methylene group (−CH_2−), adjacent to 1,3,4-oxadiazole moiety, showed one down field shift from 3.45 ppm to 4.25 ppm, whereas the protons of other aliphatic and aromatic fragment were observed at expected values of chemical shift (Fig. 7.17). At the same time, ^{13}C NMR signal for C−S was higly deshielded, appearing at 177.8 ppm and the second carbon from oxadiazole moiety (−N=C−O−) was shifted up field to 162.3 ppm from 168.8 ppm (in reference to O=C−NH_2−NH_2) (Fig. 7.18).

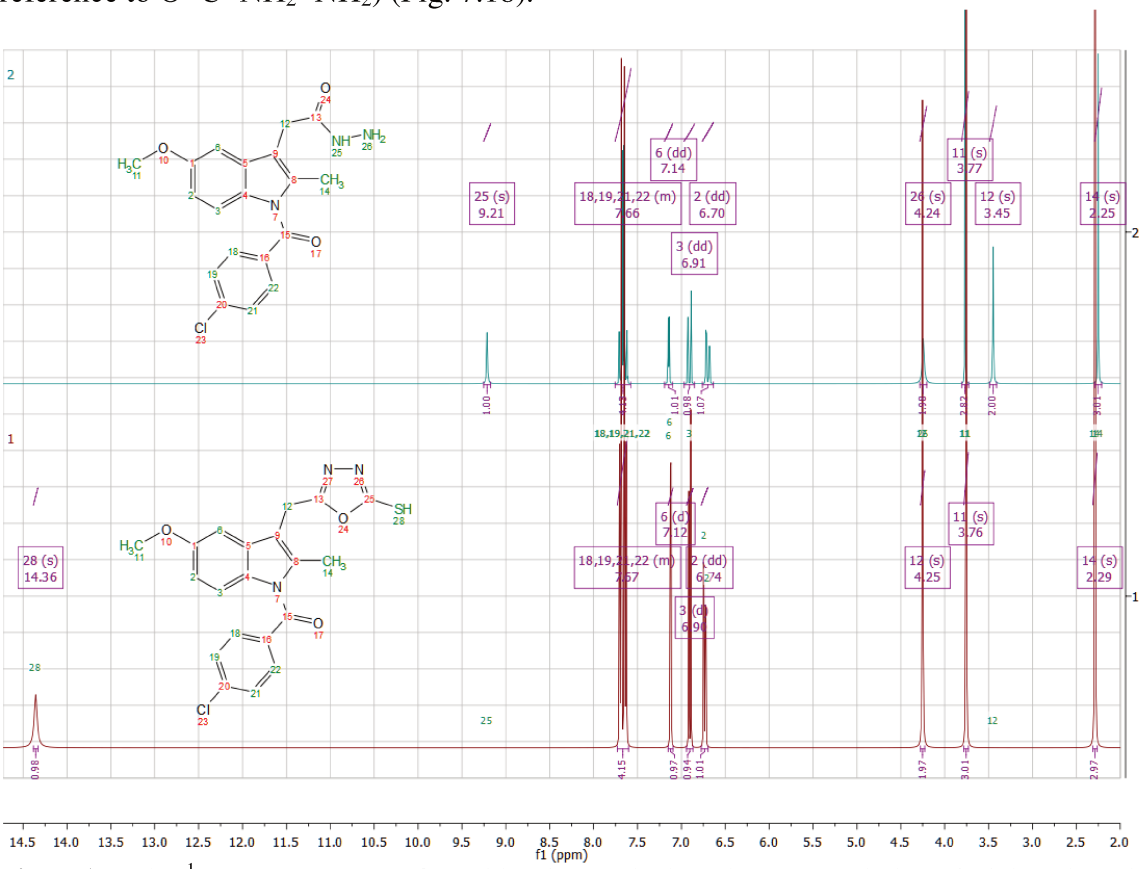

Fig. 7.17. The ^{1}H NMR spectra of (4-chlorobenzoyl)-5-methoxy-2-methyl-1*H*-indol-3-yl)methyl)-2-mercapto-1,3,4-oxadiazole (**10**) în reference with indomethacin hydrazide (**7**).

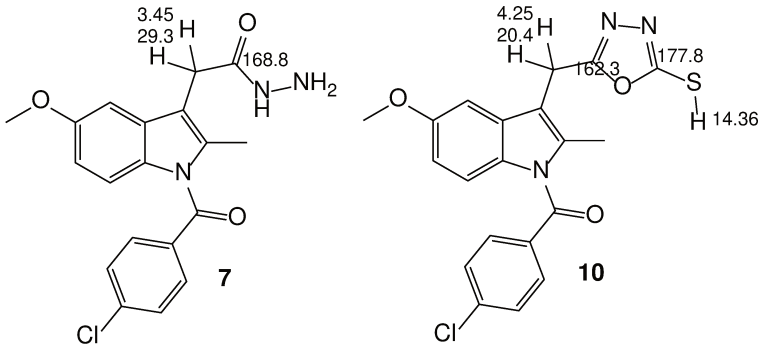

Fig. 7.18. The ^{1}H and ^{13}C signal assignments (ppm) of (4-chlorobenzoyl)-5-methoxy-2-methyl-1*H*-indol-3-yl)methyl)-2-mercapto-1,3,4-oxadiazole (**10**) în reference with indomethacin hydrazide (**7**).

The NO-INN-OXDs (**11a-m**, **t-v**) showed in ^{1}H NMR spectra the characteritics proton signals for $-CH_2ONO_2$ and $-CH_2S$ in the range of δ 4.7-4.9 ppm, and δ 4.3-4.5 ppm, respectively. In ^{13}C NMR spectra the signals for $-CH_2ONO_2$ group was observed in the range of δ 71.0-72.0 ppm, for CH_2S in the range of 34.0-36.0 ppm and for quaternary carbon from second position of *1,3,4-oxadiazole scaffold* (C_qS) was observed in range of δ 162.0-163.0 ppm (Fig. 7.19).

The aliphatic and aromatic protons and carbon signals of NO-INN-OXDs (**11a-m**, **t-v**) were observed at expected values of chemical shift. The presence of the signals above mentioned confirmed the presence of 2-mercapto-1,3,4-oxadiazole scaffold and the preserved the nitrate ester moiety in the final compounds. Moreover the NMR spectral data coupled with mass spectra support the proposed structures of the all synthesized compounds.

For exemplification, the ^{1}H,^{13}C-HSQC spectra of 2-(2,6-dichloro-4-(((5-((1-(4-chlorobenzoyl)-5-methoxy-2-methyl-1*H*-indol-3-yl)methyl)-1,3,4-oxadiazol-2-yl)thio)methyl)phenoxy)ethyl nitrate (**11h**) is presented in Fig. 7.19.

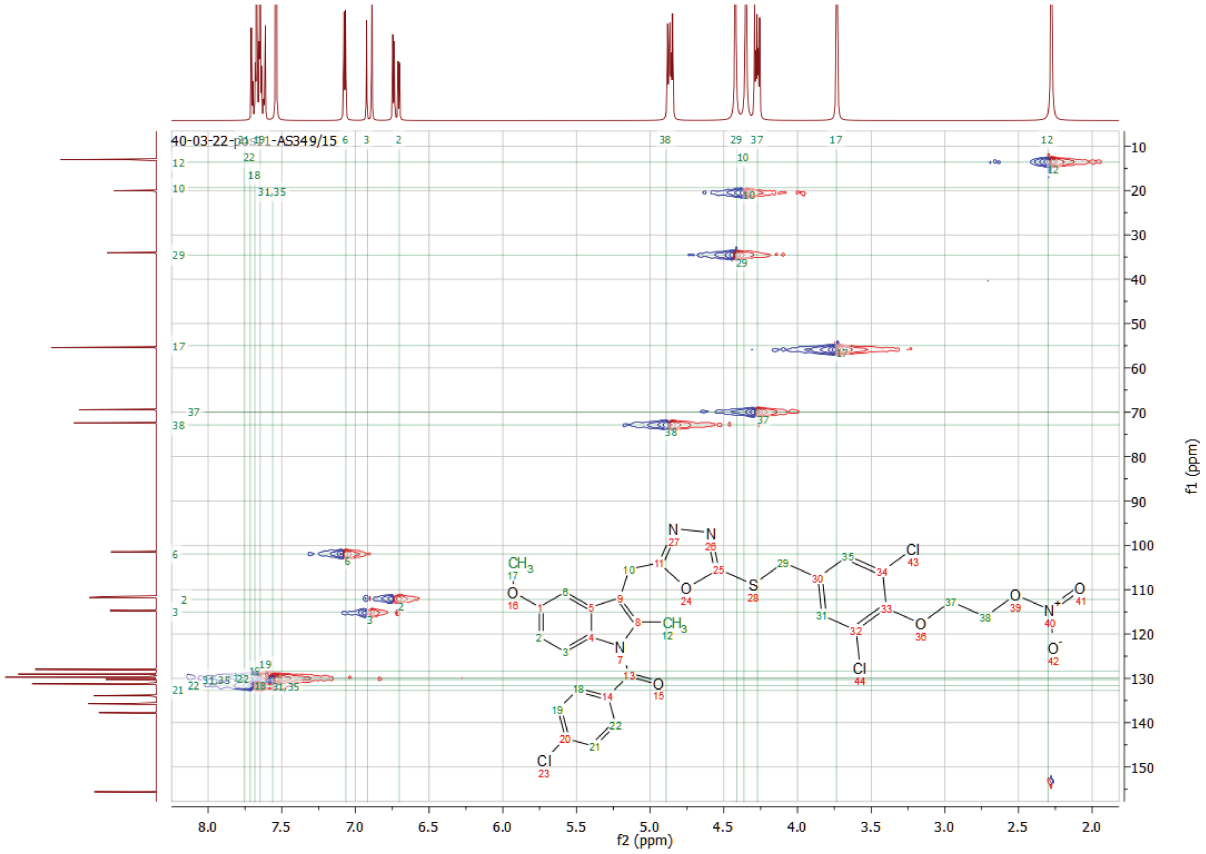

Fig. 7.19. The ^{1}H,^{13}C-HSQC spectra of (2-(2,6-dichloro-4-(((5-((1-(4-chlorobenzoyl)-5-methoxy-2-methyl-1*H*-indol-3-yl)methyl)-1,3,4-oxadiazol-2-yl)thio)methyl)phenoxy)ethyl nitrate (**11h**).

7.3. Conclusions

In this study a number of 144 compounds were synthesized, of which 109 intermediate and 35 final compounds (NO-IND-TZDs, and NO-IND-OXDs). The synthesis was performed in several steps: (i) synthesis of NO-donor linkers, which involved synthesis of halide-alcoxy-benzaldehyde derivatives (**2a-s, t, u**), of nitrate ester benzaldehyde derivatives (**3a-s**), of (bromoethoxy)aromatic alcohol (**4a-m**, **t-v**), of (hydroxyalkyl)phenoxy nitrate derivatives (**5a-m**, **t-v**) and of (halidealkyl)phenoxy nitrate derivatives (**6a-m**, **t-v**); (ii) synthesis of the nitric oxide-releasing indomethacin derivatives containing a 1,3-thiazolidin-4-one scaffold

(NO-IND-TZDs, **9a-s**), which involved synthesis of indomethacin hydrazide (**7**) and of varius indomethacin hydrazones (**8a-s**) and (iii) synthesis of the nitric oxide-releasing indomethacin derivatives containing 1,3,4-oxadiazole scaffold (NO-IND-OXDs, **11a-m**, **t-v**), which involved synthesis of indomethacin-oxadiazole derivative (IND-OXD, **10**).

The chemical structure of all synthesized derivatives (intermediaries and finals) was proved by NMR (^{1}H NMR, ^{13}C NMR, (^{1}H,^{13}C)-HSQC) and mass spectroscopic analysis (HRMS) which confirm the synthesis designed.

Chapter 8

In silico docking study for the novel nitric oxide-releasing indomethacin derivatives

The computational docking is widely used to study ligand-protein interactions and for the drug development and discovery [370,371]. This fast computing technique starts with a target of known structure (a crystallographic structure of an enzyme of medicinal interest). The docking is used to predict the binding affinity of a ligand against the target macromolecule, based on their ionic and hydrophobic interactions in simulated physiological conditions [371,372]. While single docking experiments are useful for exploring the function of the target [373], the virtual screening uses computational algorithms and models in order to identify and optimize the hit and lead compounds [372]. The virtual screening is based on a large library of compounds that are docked and ranked and may be used for identification of the novel bioactive molecules for drug development [373,374]. The *in silico* techniques used for drug design have emerged as economical, reliable, cost-effective and time saving methods as well as require fewer labor forces [370,371].

8.1. Materials and methods

For this research it was used AutoDock4.2.6 software which is a free open source software. This software offers the advantage of molecular docking at a relatively faster pace. It employs a stochastic Lamarckian type of genetic algorithm for ligands with varying conformation and minimizing the scoring function which approximate the thermodynamic stability of the ligand bound to the target protein. However, the AutoDock using in virtual screening is limited to the compounds whose characteristics can be calculated [371,373,375,376].

The selectivity of the new final developed nitric oxide-releasing indomethacin derivatives, with 1,3-thiazolidin-4-one scaffold (NO-IND-TZDs, **9a-s**) and 1,3,4-oxadiazole scaffold (NO-IND-OXDs, **11a-m**, **t-v**) was studied for COX isoenzymes (COX-1 and COX-2). The results, expressed as Gibbs free energies values (ΔG) and inhibition effect rate (Ki), docking score were compared to indomethacin (IND), diclofenac (DCF) and celecoxib (CCB), used as reference drugs.

AutoDock calculations are performed in several steps: (i) preparation of receptor and ligand coordinate files respectively, (ii) precalculation of atomic affinities maps by using a 3D grid around the receptor and ligand, (iii) defining the docking parameters of ligands and running the docking simulation, and finally (iv) analysis of results**.**

8.1.1. Generate the receptor coordinate file (RCF)

X-ray crystallographic structure of the ligand-enzyme complex were downloaded from RCSB Protein Data Bank, for COX-1 (pdb code: **4o1z**) and COX-2 (pdb code: **3nt1**) and processed prior to docking. The corresponding ligand-enzyme complexes were used to

remove the ligands, the water molecules, cofactors and ions that should not be included in the receptor by a text editor. After that, each receptor was converted to PDBQT format file using AutoDock 4.2.6 by reading the coordinates, adding charges, merging nonpolar hydrogens and assigning appropriate atom types.

8.1.2. Generate the ligand coordinate file (LCF)

Dimensional structures of the nitric oxide-releasing indomethacin derivatives (**9a-s**, **11a-m**, **t-v**) were sketched in ChemDraw and after that were converted to PDB coordinate files using Chimera 1.14. Each LCF contain special keywords recognized by AutoDock 4.2.6 like ROOT, ENDROOT, BRANCH, and ENDBRANCH that establish a rigid set of atoms and rotatable groups of atoms that are connected to the rigid root. As well, TORSDOF is used in estimating the change in free energy caused by the loss of torsional degrees of freedom upon binding. Each structure was energy minimized and converted to PDBQT format file using AutoDock4.2.6. A docking method for study the interaction between a single ligand with a single receptor, with explicit calculation of affinity maps, was applied. The receptors were kept rigid and the ligands were allowed to be flexible.

8.1.3. Preparing the grid parameter file (GPF)

The GPF specifies the PDBQT files for the receptor and the parameters for generating the atomic affinity maps. For COX-1 was used a grid box of 73×78×82 points with a spacing of 0.375 Å between grid points and the grid box center was put on x = 251.00, y = 104.00 and z = 1.364. COX-2 was enclosed in a 74×72×86 grid box having 0.375 Å spacing and −37.882, −50.853 and −21.24 as x, y and z center. The ligand binding site of COX-1 and COX-2 respectively is identified by using protein visualization software such as DSvisualizer, PyMOL and Chimera 1.14.

8.1.4. Preparing the docking parameter file (DPF)

The DPF consist of which grid map files to use, which ligand molecule to dock, what is its center and number of torsions, which docking algorithm to use and how many runs to do. For doing the conformation search, was applied the Lamarckian Genetic Algorithm (LGA) with the following parameters: number of individuals in the population (300), the maximum number of 27,000 generations simulated during each LGA run, the maximum number of evaluation at 25,000,000, a mutation rate of 0.02 and a cross over rate of 0.80, while remaining docking parameters were set to default. The ligands were allowed to move within the target proteins to achieve the lowest energy conformations and the number of runs for each docking procedure was set to 200. The selected ligands were docked against COX-1 and COX-2 using AutoDock 4.2.6 to identify their selectivity. After performing molecular docking simulation of the selected ligand molecules against the COX isoenzymes, the best ligand molecules were evaluated on the basis of their binding energy against the COX receptor. All the results obtained by molecular docking simulation were evaluated on the basis of hydrophilic and lipophilic interactions obtained between the binding residues present in the active ligand binding site of the macromolecule and ligand. The dockings experiments were clustered with a root mean square deviation (RMSD) of 0.5 Å and evaluated by PyMol software. Most energetically favored orientations were selected for next research.

8.2. Results and discussions

The X-ray crystallographic structures used in this study were selected in term of the quality of the atomic model obtained from the crystallographic data [377]. A murine COX-2 (PDB ID **3nt1**) and an ovine COX-1 (PDB ID **4o1z**) X-ray crystallographic structures were selected to study the predicted binding mode of the ligands with COX isoenzymes. The PDB **3nt1** and PDB **4o1z** were described as the COX-2 and respectively COX-1 structures with highest resolution to date, 1.7 Å and 2.4 Å respectively [378], which means that there is a more confidence in the location of atoms in the electron density map. Also the reliability factor (R-value) was less 0.16, indicating a strong agreement between the crystallographic model and the experimental X-ray diffraction data [379,380].

To validate the computational method, it was used the RSMD variation (less than 2Å) for IND, DCF and CCB individually, as reference drugs, into the active site of both COX-1 and COX-2 isoforms and we found the same binding cleft residues reported by other authors [110,381,382]. The IND and DCF are non selective COX inhibitors, inhibiting both types of the COX enzymes, whereas CCB is a preferentially COX-2 selective inhibitor. It was found also that all reference drugs have polar interactions with the catalytic site of both COX-1 and COX-2.

As expected, IND was approximately equipotent against COX-1 and COX-2, but more active against COX-2 than DCF (Table 8.1), although the both drugs belong to the same chemical class, being acetic acid derivatives. More specific, it was showed that IND and DCF bound deeply into the COX-2 active site in very similar conformation, when their corresponding carboxylate moiety forms two strong hydrogen bonds to the side chain of Arg120 (1.8 Å) and Tyr355 (2.7 Å). In addition, IND formed a extra hydrogen bond with Ser530 (3.2 Å) through benzoyl oxygen moiety, which explains why IND showed an enhancing affinity to COX isoenzymes compared to DCF.

It was noted that the free carboxylate moiety, common for IND and DCF, is responsible for non selective inhibition of the COX isoenzymes, being in accordance with the literature data [383,384]. That's why it forms a salt bridge with the basic nitrogen of Arg120, being responsible for the conformational change of COX isoenzymes.

Referring to the CCB, which is a substituted pyrazole derivative, it was showed that the most important for binding to COX are its phenyl sulfonamide substituent and pyrazole ring. Sulfonamide group forms four strong hydrogen bonds to the side chains of Gly519 (3.3 Å), His90 (2.2 Å), Gly354 (3.3 Å) and Leu352 (2.1 Å) of the enlarged polar pocket from COX-2. Moreover, pyrazole ring interacts with Tyr355 (3.3 Å) via an extra hydrogen bond, which explain high COX-2 selectivity of CCB.

In order to calculate the Gibbs free energies (ΔG) of thiazolind-4-one serie (**9a-s**) and 1,3,4-oxadiazole series (**11a-m**, **t-v**) each ligand-receptor complex was subjected to careful analysis for ideal docked poses on the basis of least binding energy scores and maximum number of cluster conformations and the results are presented in Tables 8.1 and 8.2.

8.2.1. Docking results for the nitric oxide-releasing indomethacin derivatives with 1,3-thiazolidin-4-one scaffold

In order to establish the statistical significance of the difference between the receptors while removing ligand variances from the overall error variance, a two-way ANOVA analysis was applied. In the same manner, the difference between the ligands while removing the receptor variances from the overall error variance term was also analyzed. The results established a statistically significant difference between receptors ($F(0.5, 1, 21) = 17.4616$, p

= 0.0004, Fcrit = 4.3247) and no difference between ligands (F(0.5, 21, 21) =1.3707, *p* =0.2380, Fcrit =2.0841).

Therefore, the ligand's (**9a-s**) effect over the COX-1 and COX-2 isozymes don't differ significantly (the compounds have affinity to the both receptors), but the accessibility of COX-1 and COX-2 for binding the ligands differ significantly. The estimated free binding energy of the reference drugs (IND, DCF and CCB) has a higher negative value for the COX-2 than COX-1, so less energy is needed to stabilize the drug at the ligand binding center (Table 8.1).

Table 8.1. The Gibbs free energies values (ΔG) and inhibition effect rate (Ki) of NO-IND-TZDs (**9a-s**) and of reference drugs (IND, DCF, CCB) for COX-1 and COX-2.

Ligand	COX-1		COX-2		Selectivity index $\log_{10}(Ki_{COX-1}/Ki_{COX-2})$
	ΔG(kcal/mol)	Ki (nM)	ΔG(kcal/mol)	Ki (nM)	
9a	-12.23	1.09	-8.27	872.4	-2.903
9b	-10.96	9.18	-10.07	41.59	-0.656
9c	-13.08	0.26	-11.89	1.94	-0.877
9d	-10.96	9.2	-8.73	397.62	-1.635
9e	-11.06	7.83	-11.07	7.74	0.005
9f	-10.62	16.32	-8.06	1240	-1.88
9g	-9.56	98.66	-7.68	2350	-1.376
9h	-12.43	0.77	-9.76	70.25	-1.957
9i	-13.72	0.09	-9.1	213.93	-3.387
9j	-11.87	1.98	-10.12	38.28	-1.286
9k	-10.91	10.12	-10.34	26.56	-0.419
9l	-10.34	26.52	-11.4	4.41	0.779
9m	-12.42	0.79	-8.52	568.34	-2.855
9n	-11.9	1.9	-11.07	7.74	-0.609
9o	-11.29	5.34	-9.06	229.29	-1.632
9p	-11.6	3.15	-10.45	21.85	-0.841
9q	-11.73	2.51	-10.44	22.22	-0.947
9r	-12.01	1.57	-10.07	41.36	-1.42
9s	-11.29	5.29	-8.97	266.2	-1.701
CCB	-8.37	737.59	-10.31	27.52	1.428
DCF	-8.12	1120	-8.63	468.54	0.378
IND	-9.98	48.23	-10.35	25.72	0.273

In addition, to estimate the selectivity of docked NO-IND-TZDs (**9a-s**) for COX isoenzymes a selectivity index was calculated based on logarithm of ratio between calculated inhibitory constant (Ki) for COX-1 and COX-2 ($\log_{10}Ki_{COX-1}/Ki_{COX-2}$) (Table 8.1, Fig. 8.1) [373]. It was noted that studied compounds are COX-1 selective except **9l**, which is COX-2 selective, with improved selectivity index in reference with IND and DCF (Fig. 8.1).

The COX binding pocket is a hydrophobic channel that is extended from the membrane binding domain of the COX isoezymes that comprises four α-helices that create a hydrophobic surface to the core of the catalytic domain. At the apex of the channel, both isoenzymes have two important amino acids Ser530 and Tyr385. Ser530 is the amino acid targeted by different NSAIDs and influences the COX stereochemistry in prostaglandins

synthesis. The catalytic residue Tyr385 is located at the top of the cannel and is involved in the hydroperoxidase activity. Arg120 and Tyr355 are two charged amino acids present in the COX active site of both isozymes, which form together a narrow constriction in the channel towards the bottom of the COX active site. The main difference between the active sites of both COX isoenzymes is the replacement of Ile (Ile434 and Ile523) in COX-1 by less bulky amino acid Val (Val434 and Val523) in COX-2. The loss of a single methylene group (Ile *vs* Val) is sufficient to open a secondary internal hydrophobic side pocket in COX-2 that enlarging the volume of the active site by approximately 25% and giving access to Arg513 replaced in COX-1 by a His.

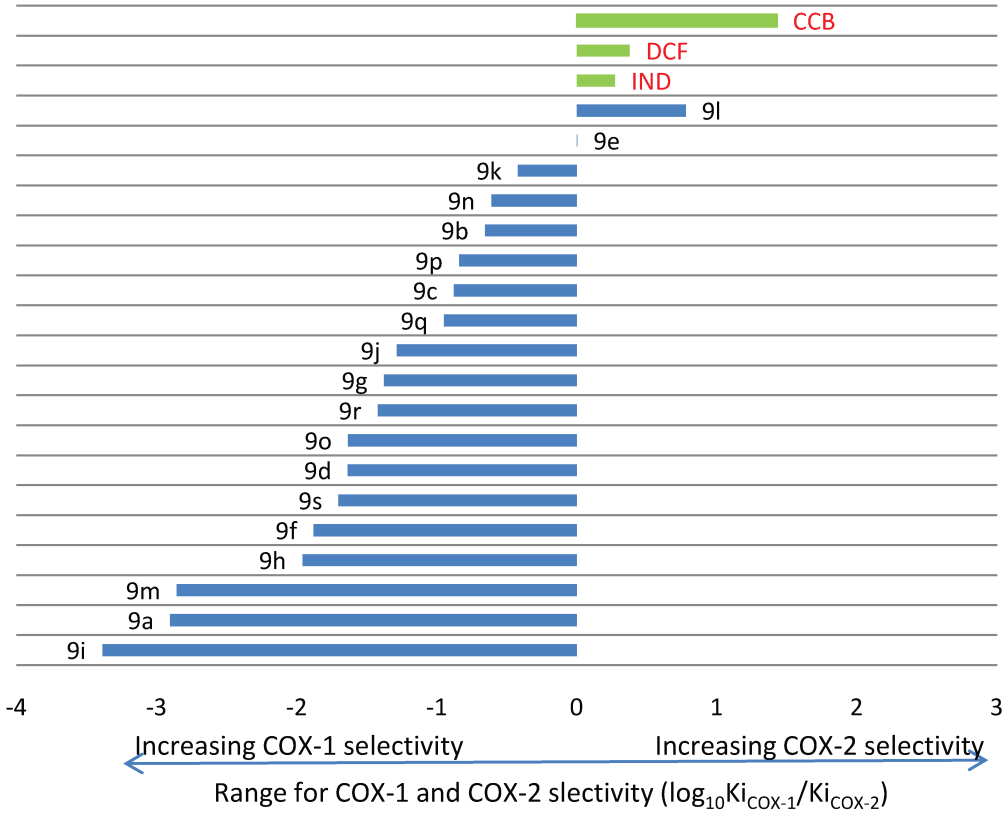

Fig. 8.1. The COX selectivity of NO-IND-TZDs (**9a-s**) in respect to references drugs (IND, DCF, CCB).

The binding mode of NO-IND-TZDs (**9a-s**) to COX-1 side pocket is quite similar (Fig. 8.2a.) for all compounds, they having affinity for hydrophobic channel. It was noted that NO releasing chain and 1,3-thiazolidine-4-one moiety interact with amino acids from entrance of the active site (Arg120, Tyr355, Glu524, Val116) while the indole structure (IND) interacts with the amino acids from inside of pocket (Ala527, Ser530, Tyr385, Ile523).

Referring to the binding of NO-IND-TZDs (**9a-s**) to COX-2 it was noted differences between compounds. However it was observed that all compounds interact with amino acids both from the narrow constriction and the inside of COX-2 active site, especially with the site pocket (delimited by Val523, Phe518, Arg513, Ala516, Gln192, His90, Tyr355) and extra space (delimited by Leu384, Leu503, Tyr385, Trp387) (Fig. 8.2b).

Based on docking results we can appreciate that NO-IND-TZDs (**9a-s**) are bulky and can block the access of arachidonic acid (physiological substrate) to the active site of COX isoenzymes.

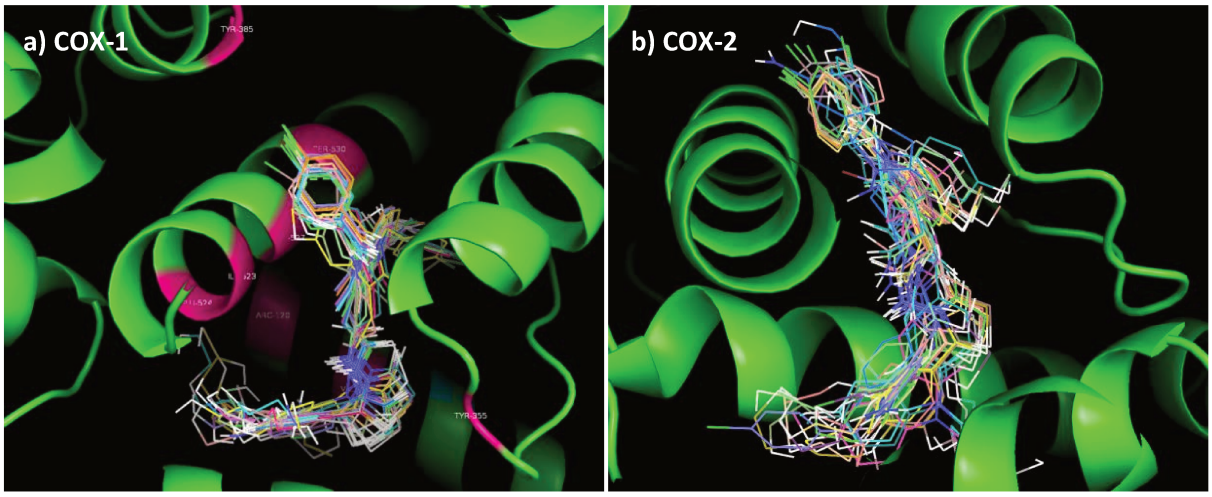

Fig 8.2. Binding mode of **9a-s** to the active site of COX-1 (a) and COX-2 (b).

8.2.2. Docking results for the nitric oxide-releasing indomethacin derivatives with 1,3,4-oxadiazole scaffold

In order to establish the statistical significance of the difference between the ligands (**11a-m**, **t-v**), while removing the receptor variances from the overall error variance term, a two way ANOVA was applied. The results (Table 8.2) established a statistically significant difference between ligands ($F(0.5, 18, 37) = 3.2648$, $p = 0.0079$, $F\text{crit} = 2.2171$).

Table 8.2. The Gibbs free energies values (ΔG) and inhibition effect rate (Ki) of NO-IND-OXDs (**11a-m**, **t-v**) and of reference drugs (IND, DCF, CCB) for COX-1 and COX-2.

Ligand	COX-1		COX-2		Selectivity index
	ΔG(kcal/mol)	Ki (nM)	ΔG(kcal/mol)	Ki (nM)	$\log_{10}(Ki_{COX\text{-}1}/Ki_{COX\text{-}2})$
11a	-12.68	0.508	-13.18	0.219	0.364
11b	-11.52	3.59	-12.32	0.925	0.589
11c	-11.15	6.71	-13.14	0.232	1.461
11d	-11.91	1.86	-10.18	34.8	-1.272
11e	-12.27	1.01	-13.84	0.072	1.146
11f	-11.5	3.7	-12.67	0.512	0.859
11g	-12.6	0.584	-11.66	2.84	-0.687
11h	-12.37	0.86	-13.45	0.137	0.796
11i	-12.76	0.442	-13.37	0.157	0.449
11j	-12.03	1.52	-12.79	0.419	0.559
11k	-11.03	8.24	-13.51	0.124	1.821
11l	-11.42	4.27	-13.58	0.11	1.587
11m	-11.85	2.05	-7.88	1680	-2.914
11t	-12.55	0.631	-13.2	0.211	0.476
11u	-10.75	13.14	-13.2	0.209	1.796
11v	-12.72	0.47	-14.27	0.034	1.129
IND	-9.98	48.23	-10.35	25.72	0.273
DCF	-8.12	1120	-8.63	468.54	0.378
CCB	-8.37	737.59	-10.31	27.52	1.428

The estimated free binding energy of the compounds **11a-m**, **t-v** was less than −10 kcal/mol and less then of the reference drugs (IND, DCF and CCB). So less energy is needed to stabilize the synthesized compounds **11a-m**, **t-v** at the ligand binding center of the COX receptor

Based on inhibitory constant (Ki) for COX-1 and COX-2 [373], a selectivity index ($\log_{10}Ki_{COX\text{-}1}/Ki_{COX\text{-}2}$) was also calculated for docked NO-IND-OXDs (**11a-m**, **t-v**) (Table 8.2. and Fig. 8.3.). It was noted that studied compounds are COX-2 selective with improved selective index in reference with IND and DCF except **11m**, **11d** and **11g** which are COX-1 selective. Also, it was observed that compound **11l**, **11u** and **11k** could be more COX-2 selective in reference with CCB (Fig. 8.3).

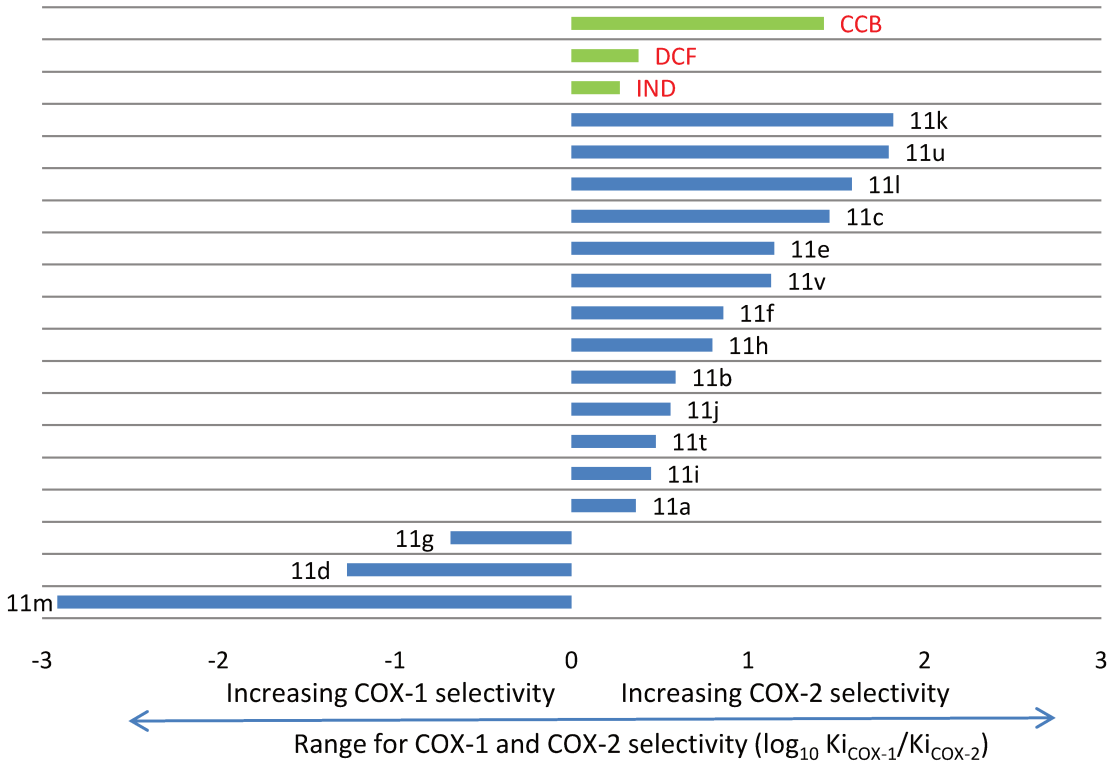

Fig. 8.3. The COX selectivity of NO-IND-OXDs (**11a-m, t-v**) in respect to references drugs.

Referring to the binding of NO-IND-OXDs (**11a-m**, **t-v**) to COX-1 it was noted differences between compounds. However it was observed that all compounds interact with amino acids both from the narrow constriction and the inside of COX-1 active site (Fig. 8.4a.).

The binding mode of NO-IND-OXDs (**11a-m**, **t-v**) to COX-2 side pocket is quite similar (Fig. 8.4b.) for all compounds, they having affinity for hydrophobic channel. It was noted that NO releasing chain interacts with the site pocket (delimited by Val523, Phe518, Arg513, Ala516, Gln192, Tyr355) and extra space (delimited by Leu384, Leu503, Tyr385, Trp387). The oxadiazole moiety interacts by hydrogen bonds with Arg120 and Tyr355 from the narrow constriction while the indole structure interacts with amino acids from entrance of active site.

The analysis of the results revealed that the COX-1/COX-2 selectivity of tested compounds is influenced by the position of nitrate ester moiety on aromatic ring and also by the number and type of the substituents on aromatic ring. The most proper positions of nitrate ester moiety are *meta* and *para*, **11i** (3-oxy-ethylnitrate) and **11a** (4-oxy-ethylnitrate)

respectively, being more active on COX-2 than **11m** (2-oxy-ethylnitrate) which is more COX-1 selective. Referring to the substitution of phenoxy-ethylnitrate moiety the presence of electron withdrawing groups (F, Cl, Br, NO_2) on aromatic ring increase the COX-2 selectivity index, in contrast with electron donating groups ($-OCH_3$, from **11g** and **11d**) which increase COX-1 selectivity. Also, it was observed that the elongation of distance between oxadiazole moiety and aromatic ring from methylene group (**11a**) to ethylene group (**11v**) seemed to be responsible for a better ligand flexibility and selectivity for COX-2 active site. So, the most active compounds, in term of COX-2 selectivity were **11l**, **11u** and **11k** which contain a nitrate ester moiety on *meta* position and electron withdrawing groups (Cl, Br and NO_2) on aromatic ring.

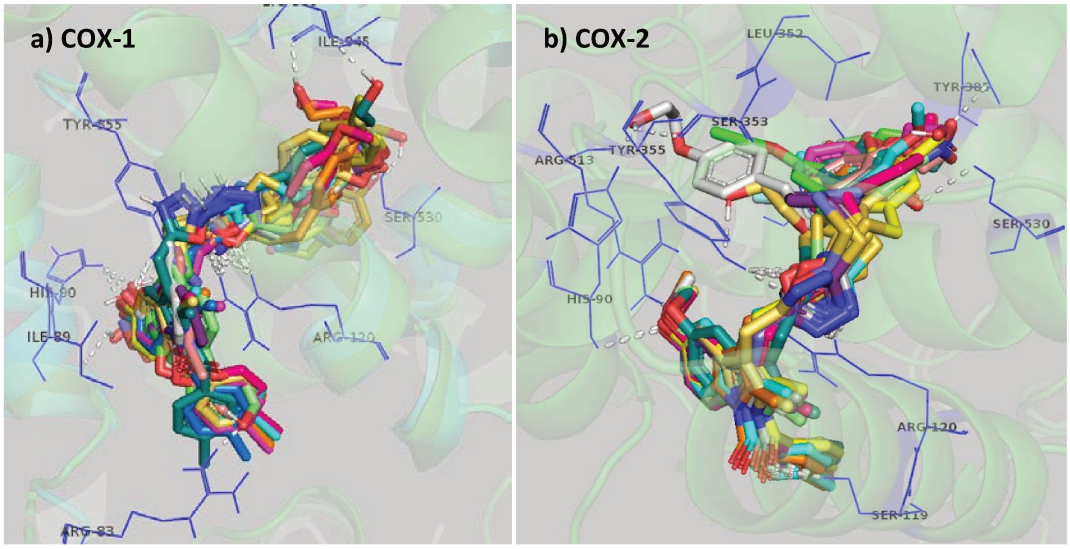

Fig. 8.4. Binding mode of **11a-m, t-v** to the active site of COX-1 (a) and COX-2 (b).

8.3. Conclusions

Based on the obtained results we can say that the synthesized nitric oxide-releasing indomethacin derivatives, with 1,3-thiazolidine-4-one scaffold (NO-IND-TZDs, **9a-s**) and 1,3,4-oxadiazole scaffold (NO-IND-OXDs, **11a-m**, **t-v**) have the theoretical premises to be promising anti-inflammatory agents. Moreover, it is know that the hybridization of different pharmacophoric molecule would result in a synergistic effect on their anti-inflammatory activity, especially the ability to inhibit COX.

Based on the COX isoenzymes selectivity index values it appreciate that NO-IND-TZDs (**9a-s**) are COX-1 selective except **9l**, which is COX-2 selective, with improved selectivity index, in reference with IND and DCF.

Refffering to the NO-IND-OXDs (**11a-m, t-v**) it was noted that they are COX-2 selective with an improved selective index in reference with IND and DCF, except **11m**, **11d** and **11g** which are COX-1 selective. Also, it was observed that compound **11l**, **11u** and **11k** are more COX-2 selective in reference with CCB.

Our results are in agreement with the literature which reported that the replacement of the free carboxylic acid group of conventional NSAIDs with different heterocycles like 1,3,4-oxadiazole 1,3-thiazolidine-4-one may provides new drugs with increased anti-inflammatory activity, improved efficiency and with fewer side effects, reducing ulerogenic potential [140,194,385].

Chapter 9

In silico ADME-Tox study

ADME-Tox (Absorption, Distribution, Metabolism, Excretion and Toxicity) study offers important data to predict the pharmacological and toxicological properties of new candidates, during the drug discovery process [386–388].

9.1. Materials and methods

The ADME-Tox profile of the new final developed nitric oxide-releasing indomethacin derivatives, with 1,3-thiazolidin-4-one scaffold (NO-IND-TZDs, **9a-s**) and 1,3,4-oxadiazole scaffold (NO-IND-OXDs, **11a-m, t-v**) was predicted using *SwissADME* (http://www.swissadme.ch) and *pkCSM-pharmacokinetics* (http://structure.bioc.cam.ac.uk/pkcsm) tools.

SwissADME provide an overall assessment of the pharmacokinetics profile of small molecules by most relevant computational methods [389,390] and *pkCSM-pharmacokinetics* is a new method based on graph signatures and experimental data [391]. The methods have been selected for robustness, but also for ease of interpretation to enable efficient translation to medicinal chemistry. For these web tools were provided in the literature the methods design description, the methods validation information and the datasets used.

The most important ADME-Tox properties provided from the ADME-Tox tools were selected to predict pharmacokinetic and toxicity profile of the synthesized compounds.

9.2. Results and discussions

Using the ADME-Tox evaluation, the pharmacokinetic properties of the synthesized NO-IND-TZDs (**9a-s**) and NO-IND-OXDs (**11a-m, t-v**) were predicted and the results are summarized in Table 9.1. and Tabele 9.2.

It is known that oral ***absorption*** (Table 9.1) of the drug is influenced by solubility, permeability (active and passive) across the gastrointestinal tract wall and by the first pass metabolism [387]. The absorption of the developed compounds was predicted using the following parameters: the lipophilicity, the water solubility, the percentage of intestinal human absorption (HIA) properties and the P-glycopretein (P-gp) inhibitor properties.

The *water solubility* was predicted using the *Silicos IT LogSw* descriptor (SwissADME) depending on which was gave a qualitative estimation of the solubility class [389]. The results established a statistically significant difference between the two series of tested compounds (NO-IND-TZDs and NO-IND-OXDs) as determined by one-way ANOVA ($F(1,33) = 82.734$ $p < 0.05$, Fcrit = 4.139). *LogSw* values for NO-IND-TZDs (**9a-s**) were predicted to range from –9.36 to –7.54, being considered poorly soluble. But for NO-IND-OXDs (**11a-m, t-v**) *LogSw* predicted values were ranged from –10.97 to –9.15, being at the border of solubility class between insoluble (log S scale < −10) and poorly soluble (log S scale < −6).

The *lipophilicity* was predicted using the *Consensus LogPo/w* descriptor (SwissADME), which is the arithmetic mean of five computational methods values [389]. Lipophilicity has a

significant influence on various pharmacokinetic properties such as the absorption, the distribution, the permeability, as well as the routes of drugs clearance [392]. The compounds with a *LogPo/w* higher than 1 or less than 4 are generally considered to have optimal physico-chemical and ADME properties for oral route [393] whereas log*Po/w* > 5 (high lipophilicity) often contributes to high metabolic turnover, low solubility and poor oral absorption [393]. For NO-IND-TZDs (**9a-s**) series, the predicted values of *LogPo/w* ranged from 2.88 to 4.74 while for NO-IND-OXDs (**11a-m, t-v**) series the *LogPo/w* varies between 4.15 and 5.55. A one way ANOVA was conducted and was noted that 1,3,4-oxadiazole scaffold enhances significantly de lipophilicity of compounds **11a-m, t-v** ($F(1,33) = 49.631$ $p < 0.05$, Fcrit = 4.139).

Table 9.1. The Absorption and Distribution profile of NO-IND-TZDs (**9a-s**) and NO-IND-OXDs (**11a-m, t-v**) predicted using pkCSM-pharmacokinetics and SwissADME tools.

	Absorption						**Distribution**	
Comp.	Cons. Log Po/w	Silicos-IT LogSw	Silicos-IT class	HIA (%)	P-gp I/II inhibitor	VDss (human)	Fraction unbound (human)	BBB permeability
9a	3.79	-8.23	Poorly soluble	100	Yes	-0.867	0.129	-1.496
9b	4.01	-8.48	Poorly soluble	100	Yes	-0.972	0.136	-1.680
9c	4.21	-8.79	Poorly soluble	100	Yes	-0.830	0.135	-1.648
9d	4.36	-8.96	Poorly soluble	100	Yes	-0.817	0.136	-1.656
9e	3.77	-8.31	Poorly soluble	100	Yes	-0.869	0.250	-2.111
9f	4.06	-8.70	Poorly soluble	100	Yes	-0.804	0.256	-2.135
9g	2.99	-7.54	Poorly soluble	96.22	Yes	-1.236	0.211	-1.924
9h	3.75	-8.39	Poorly soluble	100	Yes	-0.876	0.262	-2.340
9i	4.76	-9.36	Poorly soluble	100	Yes	-0.767	0.147	-2.267
9j	4.22	-8.88	Poorly soluble	100	Yes	-0.845	0.155	-2.327
9k	3.8	-8.23	Poorly soluble	95.01	Yes	-0.864	0.128	-1.493
9l	3.7	-8.31	Poorly soluble	91.23	Yes	-0.865	0.152	-1.708
9m	3.06	-7.54	Poorly soluble	92.26	Yes	-1.180	0.208	-1.976
9n	2.88	-7.54	Poorly soluble	97.89	Yes	-1.276	0.238	-1.915
9o	4.29	-9.04	Poorly soluble	100	Yes	-0.811	0.156	-1.868
9p	3.75	-8.23	Poorly soluble	95.13	Yes	-0.885	0.127	-1.490
9q	3.84	-8.71	Poorly soluble	95.34	Yes	-0.774	0.142	-1.713
9r	3.85	-8.80	Poorly soluble	100	Yes	-0.722	0.266	-2.386
9s	4.04	-9.18	Poorly soluble	100	Yes	-0.660	0.273	-2.410
11a	4.96	-9.83	Poorly soluble	100	Yes	-0.568	0.325	-2.073
11b	5.31	-10.09	Insoluble	98.94	Yes	-0.725	0.352	-2.271
11c	5.49	-10.40	Insoluble	100	Yes	-0.480	0.331	-2.239
11d	5.00	-9.92	Poorly soluble	96.99	Yes	-0.686	0.331	-2.288
11e	4.37	-10.30	Insoluble	97.75	Yes	-0.621	0.327	-2.307
11f	4.27	-9.15	Poorly soluble	99.48	Yes	-0.979	0.358	-2.571
11g	5.13	-10.01	Insoluble	89.03	Yes	-0.798	0.307	-2.509
11h	5.11	-10.97	Insoluble	100	Yes	-0.392	0.310	-2.403
11i	5.01	-9.83	Poorly soluble	100	Yes	-0.596	0.326	-2.067
11j	4.94	-9.92	Poorly soluble	97.03	Yes	-0.697	0.330	-2.284
11k	4.24	-9.15	Poorly soluble	100	Yes	-1.069	0.370	-2.571
11l	5.48	-10.66	Insoluble	97.83	Yes	-0.617	0.328	-2.470
11m	4.15	-9.83	Poorly soluble	100	Yes	-0.608	0.319	-2.070
11t	5.55	-10.57	Insoluble	100	Yes	-0.512	0.330	-2.266
11u	5.47	-10.49	Insoluble	98.10	Yes	-0.628	0.328	-2.462
11v	5.24	-10.22	Insoluble	100	Yes	-0.624	0.317	-2.079

The *pkCSM-pharmacokinetics* prediction showed a good human intestinal absorption for all synthesized compounds, which ranged from 89% to 100%. Obviously, with values much higher than the 30% limit, the tested molecules may show good absorption in the small intestine after oral administration. These results support their good absorption in the small intestine and predict also their capacity to inhibit *P-glycoprotein I/II transport*.

Using *pkCSM-pharmacokinetics*, the drug ***distribution*** (Table 9.1.), based on the blood brain barrier (BBB) permeability, the volume of distribution (VDss) and the fraction unbound in plasma protein descriptors, could be also predicted. For tested NO-IND-TZDs the predicted values of VDss ranged from –1.28 to –0.66 and of fraction unbound ranged from 0.13 to 0.27. Also, for tested NO-IND-OXDs the predicted values of VDss ranged from –1.07 to –0.39 and of fraction unbound ranged from 0.30 to 0.37. The lower VDss values (< −0.15) are in agreement with lower value for the fraction of drug molecules in the plasma which are unbound (free) to proteins. It is know that only the unbound fraction of the drug is active whereas the high binding to proteins can affect both the pharmacokinetics and pharmacodynamics of drugs [392,394].

The BBB permeability is assessed using two parameters, one qualitative (BBB) and other one quantitative (LogBB). Depending of the BBB parameter value, the drugs are classifies as drugs with high and low permeability respectively. More specific, a LogBB value higher 0.3 means that drug readily cross the blood brain barrier while a value less than −1, indicates a reduced permeability for this barrier [391]. The BBB permeability values of tested compounds (**9a-s, 11a-m, 11t-v**) were predicted to range from –2.57 to −1.49 which means that are poorly distributed to the brain.

The ***metabolism*** (Table 9.2) of NO-IND-TZDs and NO-IND-OXDs respectively, based on inhibition of the main cytochromes (CYP) of the P450 family (CYP1A2, CYP2C19, CYP2C9, CYP2D6 and CYP3A4) descriptors (SwissADME) was also estimated. CYP2C19 is involved in detoxifying of potential carcinogens or bio-activating environmental procarcinogens [395], CYP2C9 is the major enzyme that metabolizes drugs with a low therapeutic index [396] and CYP2D6 is very polymorphic and metabolizes ∼20% of drugs [397]. Referring to the CYP2D6 it is known that reduced or absent activity of this enzyme reduces the efficacy of the drugs or increases the occurrence of the adverse effects [397]. The tested compounds were predicted to inhibit all tested CYP enzymes, except CYP1A2 and CYP2D6 respectively.

The ***excretion*** (Table 9.2) of the drugs is measured by total clearance (CLtot) and can be achieved by either the kidney and/or the liver where drugs are eliminated in the form of urine or bile, respectively [392]. Using the CLtot descriptor of *pkCSM-pharmacokinetics* it was forecast that excretion of NO-IND-TZDs varies between –0.17 and 0.40 log(mL/min/kg) while for NO-IND-OXDs this parameter ranges from −0.02 to 0.25 log(mL/min/kg). Also, there were no statistically significant difference between the two series of tested compounds as determined by one-way ANOVA ($F(1,33) = 0.422$ $p = 0.520$, Fcrit = 4.139).

The assessment of drugs ***toxicity*** (Table 9.2.), in terms of hepatotoxicity, oral rat acute toxicity (LD_{50}) values, maximum tolerated dose (MRTD) and mutagenic potential using bacteria (AMES), was predicted by using *pkCSM-pharmacokinetics*. The hepatotoxicity descriptor predicted that all molecules could present hepatotoxicity except **11c**, **11g**, **11h**, **11l**, **11t**, **11u**. Predicted LD_{50} values ranged from 2.49 to 3.07 mol/kg. Moreover, predicted MRTD value lies in the range of 0.47 and 0.58 log(mg/kg/day). Since the values are greater than 0.47 log(mg/kg/day) it means that the tested compounds could be toxic, but many studies, including *in vivo*, must be performed in order to confirm it. Most of the tested compounds also showed negative results for AMES toxicity (excepting **9f**, **9k** and **9o**) indicating that they do not have mutagenic potential.

Table 9.2. The Metabolism, Excretion and Toxicity profile of NO-IND-TZDs (**9a-s**) and NO-IND-OXDs (**11a-m, t-v**) predicted using pkCSM-pharmacokinetics and SwissADME tools.

	Metabolism					Excretion	Toxicity			
Comp.	CYP1A2 inhibitior	CYP2C19 inhibitior	CYP2C9 inhibitior	CYP2D6 inhibitior	CYP3A4 inhibitior	Total Clearance	AMES toxicity	Max. tolerated dose (human)	Oral Rat Acute Toxicity (LD_{50})	Hepato-toxicity
9a	No	Yes	Yes	No	Yes	-0.053	No	0.509	2.674	Yes
9b	No	Yes	Yes	No	Yes	-0.096	No	0.527	2.714	Yes
9c	No	Yes	Yes	No	Yes	0.007	No	0.525	2.639	Yes
9d	No	Yes	Yes	No	Yes	-0.174	No	0.527	2.639	Yes
9e	No	Yes	Yes	No	Yes	0.086	No	0.514	2.971	Yes
9f	No	Yes	Yes	No	Yes	0.040	No	0.524	2.953	Yes
9g	No	Yes	Yes	No	Yes	0.012	Yes	0.472	2.528	Yes
9h	No	Yes	Yes	No	Yes	0.224	No	0.514	2.969	Yes
9i	No	Yes	Yes	No	Yes	0.044	No	0.493	2.656	Yes
9j	No	Yes	Yes	No	Yes	0.142	No	0.488	2.725	Yes
9k	No	Yes	Yes	No	Yes	-0.047	No	0.515	2.670	Yes
9l	No	Yes	Yes	No	Yes	0.084	No	0.530	2.733	Yes
9m	No	Yes	Yes	No	Yes	-0.048	Yes	0.473	2.523	Yes
9n	No	Yes	Yes	No	Yes	0.112	Yes	0.527	2.492	Yes
9o	No	Yes	Yes	No	Yes	0.069	No	0.545	2.719	Yes
9p	No	Yes	Yes	No	Yes	0.074	No	0.520	2.659	Yes
9q	No	Yes	Yes	No	Yes	0.261	No	0.580	2.634	Yes
9r	No	Yes	Yes	No	Yes	0.401	No	0.550	2.982	Yes
9s	No	Yes	Yes	No	Yes	0.355	No	0.557	2.962	Yes
11a	No	Yes	Yes	No	Yes	-0.034	No	0.560	3.060	Yes
11b	No	Yes	Yes	No	Yes	-0.074	No	0.567	3.037	Yes
11c	No	Yes	Yes	No	Yes	0.025	No	0.551	3.077	No
11d	No	Yes	Yes	No	Yes	0.108	No	0.518	3.029	Yes
11e	No	Yes	Yes	No	Yes	0.061	No	0.527	3.026	Yes
11f	No	Yes	Yes	No	Yes	0.030	No	0.444	2.774	Yes
11g	No	Yes	Yes	No	Yes	0.250	No	0.443	3.028	No
11h	No	Yes	Yes	No	Yes	0.060	No	0.490	3.064	No
11i	No	Yes	Yes	No	Yes	-0.027	No	0.560	3.043	Yes
11j	No	Yes	Yes	No	Yes	0.112	No	0.515	3.044	Yes
11k	No	Yes	Yes	No	Yes	0.034	No	0.422	2.676	Yes
11l	No	Yes	No	No	Yes	0.043	No	0.513	3.059	No
11m	No	Yes	Yes	No	Yes	0.087	No	0.573	3.033	Yes
11t	No	Yes	Yes	No	Yes	-0.067	No	0.554	3.077	No
11u	No	Yes	No	No	Yes	0.225	No	0.512	3.059	No
11v	No	Yes	Yes	No	Yes	-0.020	No	0.536	3.050	Yes

9.3. Conclusion

Briefly, the ADME-Tox profile predicted for NO-IND-TZDs (**9a-s**) and NO-IND-OXD (**11a-m, t-v**) consisted of optimal physico-chemical and ADME properties for oral administration, good absorption in the small intestine, low fraction unbound value and poorly distributed to the brain. Referring to the metabolism, the tested compounds do not inhibit the CYP2D6, which is determinant in biotransformation processes and could have some degree of hepatotoxicity.

Finally, ADME-Tox profile of the tested compounds showed that the proposed designed compounds are generally considered to have optimal physico-chemical and ADME properties for oral administration.

Chapter 10

Biological evaluation of the new nitric oxide-releasing indomethacin derivatives

The synthesized nitric oxide-releasing indomethacin derivatives, with 1,3-thiazolidine-4-one scaffold (NO-IND-TZDs, **9a-s**) and 1,3,4-oxadiazole scaffold (NO-IND-OXDs, **11a-m, t-v**), were biological evaluated in terms of antioxidant and anti-inflammatory effect as well as of nitric-oxide release capacity.

10.1. *In vitro* radical scavenging effects

The free radical scavenging activity of the new NO-IND-TZDs (**9a-s**) and NO-IND-OXDs (**11a-m, t-v**) was evaluated using 2,2-diphenyl-1-picrylhydrazyl radical (DPPH) assay with slight modification [398–400]. The IND and aspirin (ASP), as reference drugs, and vitamin C, as standard antioxidant, were used in the assay.

10.1.1. Materials and methods

10.1.1.1. Preparation of DPPH and test solutions

A weighed amount of DPPH (29.71 mg, 75.34 μmol) was dissolved by sonication in 50 mL methanol of analytical grade and kept in darkness. After 30 min, a sample of 10 mL was taken and made up to 100 mL with methanol. The resulted DPPH solution (150.68 μM) was stored in the darkness at room temperature and used up on the day of preparation.

The stock solutions (2600 μM) of tested derivatives (**9a-s**, **11a-m**, **11t-v**) were prepared in DMSO, then serially diluted with methanol to obtain different concentrations (2600 μM, 1500 μM, 700 μM, 620 μM, 530 μM, 440 μM, 350 μM, 260 μM and 120 μM). The concentration of tested derivatives, after addition to DPPH, covered a range from well above DPPH to eliminate possible diffusion effects to well below the DPPH concentration and to allow full reaction.

The serially diluted solutions of IND and ASP were prepared in the same manner with tested derivatives (**9a-s**, **11a-m**, **11t-v**). The serially diluted solutions of vitamin C were prepared by dilution of freshly prepared solution (2619 μM) with methanol to make different concentrations (152.2 μM, 132.7 μM, 112.2μM, 95.2 μM, 77.6 μM, 54.6 μM, 40.3 μM, 20.5 μM).

10.1.1.2. DPPH assay procedure

500 μL from each sample of the tested compounds (**9a-s**, **11a-m**, **11t-v**), reference drug (IND, ASP) and vitamin C were added to 1000 μL of DPPH solution. Two blanks (*blank 1*: 500 μL of methanol and 1000 μL of DPPH and *blank 2*: 1500 μL methanol) were also used.

The mixture was kept for 3 h in the darkness at room temperature. Thereafter, a 270 μL aliquot of each sample tube was added in a 96 well plate. The absorbance was then measured at 517 nm using Tecan Sunrise Remote Microplate Reader TW/ML-Abbott F039306. All tests were performed in quadruplicate.

The DPPH radical-inhibiting capacity (inhibition/scavenging activity) (%) was calculated using the following formula [401,402]:

$$\text{Inhibition (Scavenging activity) \%} = [(A_{CS}-A_s)/A_{CS}] \times 100 \quad (1)$$

where: A_{cs} is the difference between absorbance of *blank 1* and *blank 2* and A_s is the difference between the absorbance of tested sample and *blank 2*.

To calculate IC_{50} ($f_{(x)} = 50$) of each tested compounds, the inhibition ratios ($f_{(x)}$) were plotted against the sample concentration (x). The results for each experiment were represented by a dose-response curve and were used two types of regression lines (f(x)): a sigmoid curve and a quadratic line.

The DPPH radical scavenging activity of each tested compounds was expressed also as the vitamin C equivalent antioxidant capacity (CEAC) and was calculated using the following formula [403,404]:

$$CEAC = IC_{50(\text{vit. C})}/IC_{50(\text{sample})} \quad (2)$$

where: $IC_{50(\text{vit. C})}$ is the concentration of vitamin C required for 50% inhibition and $IC_{50(\text{sample})}$ is concentration of tested compounds (**9a-s**, **11a-m**, **11t-v)** and reference drugs, respectively, required for 50% inhibition. The higher CEAC value means the higher DPPH radical scavenging activity.

10.1.2. Results and discussions

The DPPH assay is the most used method being considered a accurate, a rapid, a simple and an economic method to evaluate the radical scavenging effect of the antioxidants compounds [405].

It is a colorimetric method based on the capacity of the antioxidant compounds to scavange the DPPH radical. DPPH is a stable free radical due to the delocalization of the odd electron over the molecule as a whole, so that the molecule does not dimerise, as most other free radicals. Due to spare electron, DPPH shows a strong absorption band at 517 nm and its alcoholic solution has a deep violet color. In the presence of a proton or electron donating agents, the absorption vanishes because the electron pairs off and DPPH becomes a stable diamagnetic molecule. The resulting decolorization is stoichiometric in term of to the number of electrons taken up, being a measure of the capacity of antioxidants to directly react with DPPH radicals [405–408].

Also, this method can be used to quantify the antioxidants in the complex biological medium and it can assay either the hydrophilic or lipophylic antioxidants, using various solvents, such us hydro alcoholic or non polar organic solvents [409,410].

The method is not standardized to date, which is why in the literature there are many working protocols and the reporting mode currently is used for rating the radical scavenging activity [408]. The data are commonly reported as IC_{50} [402] or EC_{50} [401], which represents the antioxidant concentration required for reducing the initial DPPH concentration by 50%. A lower value of EC_{50} means a stronger radical scavenging effect. Another way to report the results consists in the determination of the antiradical power ($ARP = 1/EC_{50}$), in which a higher ARP value indicates a higher scavenging capacity. Also, the antioxidant efficiency ($AE = 1/EC_{50} \times T_{EC50}$), which represent the time needed to reach the steady state to EC_{50} concentration and the percentage of remaining DPPH radical, provide also information about

stoichiometry reaction between DPPH and antioxidant (mole of DPPH reduced by mole of antioxidant), ignoring the reaction kinetics [411].

Because these approaches make it no possible to compare the results reported in the literature, new methods are need. A new approach, proposed for estimation of antioxidant activity, consists in measure of the relative DPPH scavenging effect to that of an antioxidant standard, like vitamin C or Trolox [403,404]. This method allows for comparison of antioxidant capacity results done at different concentrations and in different protocols, because it is independent of the samples or the initial DPPH concentrations in the assay system. Expression of antioxidant activity as equivalents of standard antioxidants also ignores chemistry altogether and just ranks compounds, assuming all act by the same mechanism.

In order to evaluate the scavenging effect of the nitric oxide-releasing indomethacin derivatives (**9a-s, 11a-m, 11t-v**), the concentration needed to decrease by 50% the initial DPPH concentration (IC_{50}), was calculated and the values found are showed in Table 10.1. A lower IC_{50} value means a higher antioxidant effect.

Table 10.1. The IC_{50} values of **9a-s, 11a-m, 11t-v**, referring to the DPPH radical scavenging effect.

Comp.	IC_{50} (mM)[a]	Comp.	IC_{50} (mM)[a]	Comp.	IC_{50} (mM)[a]
9a	2.63 ± 0.02	**9n**	2.21 ±0.02	**11h**	2.46 ± 0.02
9b	2.18 ± 0.01	**9o**	0.54 ± 0.01	**11i**	2.56 ± 0.01
9c	2.28 ± 0.01	**9p**	2.25 ± 0.02	**11j**	1.99 ± 0.01
9d	2.47 ± 0.06	**9q**	2.78 ± 0.12	**11k**	2.19 ± 0.01
9e	2.58 ± 0.04	**9r**	2.14 ± 0.01	**11l**	2.90 ± 0.31
9f	2.21 ± 0.01	**9s**	2.20 ± 0.01	**11m**	2.85 ± 0.06
9g	15.64 ±1.00	**11a**	2.38 ± 0.02	**11t**	4.03 ± 1.11
9h	2.32 ± 0.01	**11b**	4.35 ± 0.34	**11u**	5.29 ± 0.21
9i	2.78 ± 0.04	**11c**	2.37 ± 0.01	**11v**	2.77 ± 0.03
9j	2.22 ± 0.01	**11d**	2.42 ± 0.02	**ASP**	4.58 ± 0.09
9k	2.32 ± 0.01	**11e**	2.98 ± 0.06	**IND**	54.36 ± 7.93
9l	2.17 ± 0.02	**11f**	2.16 ± 0.03	**Vit C**	0.07 ± 0.001
9m	1.83 ± 0.05	**11g**	2.49 ± 0.02		

Moreover, the CEAC values, that represent how many times the tested compounds are more active than vitamin C, used as antioxidant standard, were also calculated and the results are presented in Figures 10.1 and 10.2.

10.1.2.1. In vitro radical scavenging effects of NO-IND-TZDs

Using one-way ANOVA test there was determined that there is a statistically significant difference ($F(20, 63) = 11891.16$, $p < 0.05$) between tested compounds (**9a-s**, **ASP**, **IND**) (Fig. 10.1.). Analysis of the results revealed that all tested compounds have improved antioxidant effect compared to reference drugs (IND, ASP), the CEAC values ranging between 0.266−0.137. It can appreciate the majority of compounds are around 23 times more active than IND (CEAC = 0.0014 ± 0.0002) and 2 times more active than ASP (CEAC = 0.016 ± 0.004). The most active compound was **9o** (CEAC = 0.137 ± 0.01), which has on the second position of 1,3-thiazolidne-4-one scaffold the 2-(4-nitrophenoxy)-ethyl nitrate as substituent, being around 100 times more active than IND. Compared to vitamin C, used as a positive control, all tested compounds were less active, the CEAC values being less than 1.

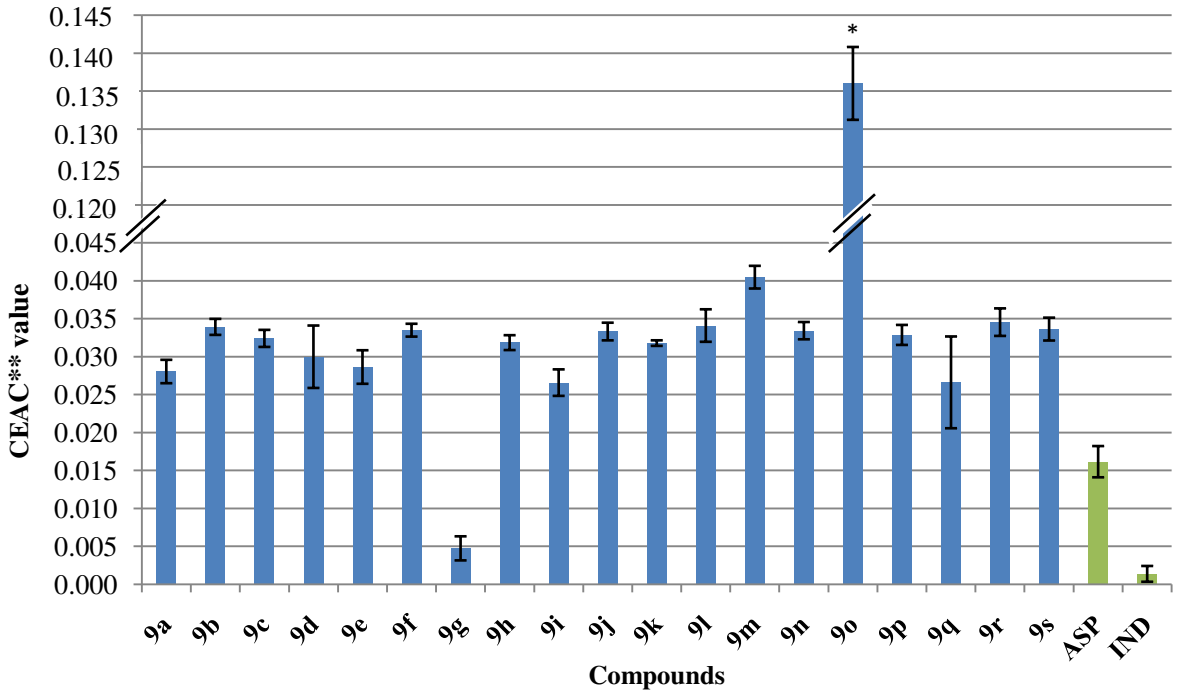

Fig. 10.1. The DPPH radical scavenging activity of NO-IND-TZDs (**9a-s**) and of reference drugs (IND, ASP) expressed as CEAC values (*significant differences ($p < 0.05$); ** mean ± SD, $n = 4$).

10.1.2.2. In vitro radical scavenging effects of NO-IND-OXDs

Using one-way ANOVA test there was determined that there is a statistically significant difference ($F(17, 71) = 164.778$, $p < 0.05$) between tested compounds (**11a-m**, **t-v**, **ASP**, **IND**) (Fig. 10.2). Post hoc comparisons using the Tukey HSD test revealed that all tested compounds have significantly improved antioxidant effect in reference with IND ($p < 0.05$). Also, it was noted that the most of the tested compound (excepting **11b**, **11t** and **11u**) are significantly more active than ASP ($p < 0.05$). It can appreciate that the majority of compounds are from 10.0 to 26.7 times more active than IND and from 1.5 to 2.3 times more active than ASP.

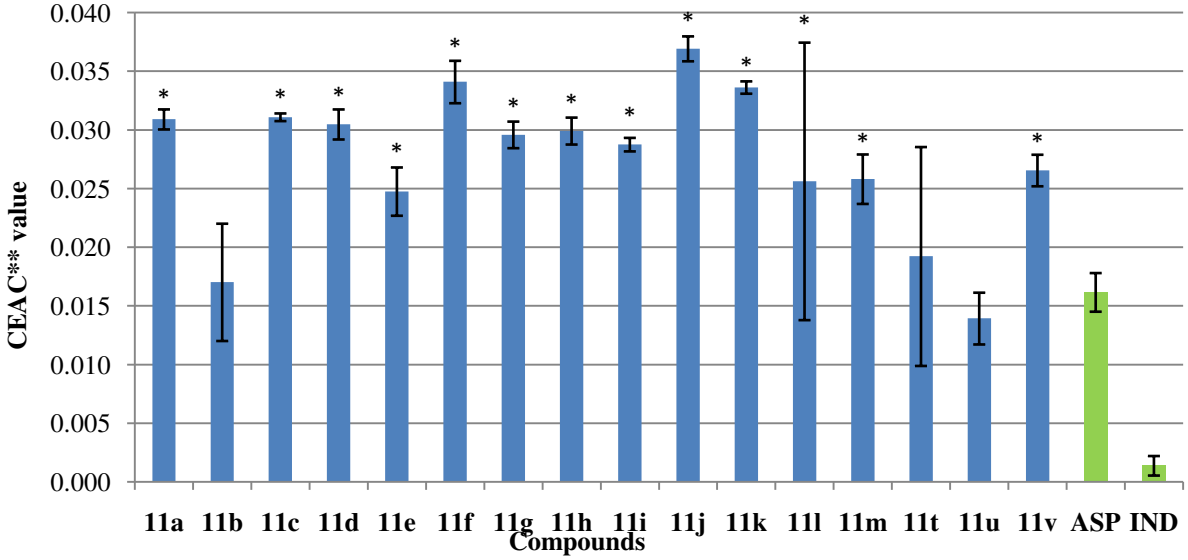

Fig. 10.2. The DPPH radical scavenging activity of NO-IND-OXDs (**11a-m**, **t-v**) and of reference drugs (IND, ASP) expressed as CEAC values (* significant differences than ASP ($p < 0.05$); ** mean ± SD, $n = 4$)

10.1.3. Conclusions

Based on DPPH radical scavenging results it can appreciate that the presence of thiazolidine-4-one and 1,3,4-oxadiazole scaffolds had a favorable influence on the antioxidant potential, all tested compounds being more active than parent compound IND.

Using one-way ANOVA test there was determined that there is a statistically significant difference ($F(1, 142) = 7.609$, $p = 0.007$) between the two series of tested compounds. It was also noted that the presence of the 1,3-thiazolidine-4-one scaffold (NO-IND-TZDs*)* improve significantly the antioxidant effect than the presence of 1,3,4-oxadiazole moiety (NO-IND-OXDs), in the final nitric oxide releasing indomethacin derivatives. Moreover, it was reported that 1,3,4-oxadiazole have been found to be a potent antioxidant pharmacophore and molecular hybridization with medicinal drugs resulted in a synergistic effect enhancing antioxidant efficiency than parent drug.

Compared to vitamin C, used as a positive control, all tested compounds (**9a-s**, **11a-m**, **t-v**) were less active, the CEAC values being less than 1.

10.2. *In vitro* anti-inflammatory effects

Mizushima's test is the most common assay cited in literature to predict the anti-inflammatory potencies of the drugs. This is a nephelometric assay based on thermal denaturation of bovine serum albumin (BSA), which assures a significant correlation between the *in vitro* and *in vivo* anti-inflamamtory effects [412].

10.2.1. Materials and methods

A solution of bovine serum albumin (BSA) 0.2% in 0.9% NaCl/DMSO = 6/4 was used to test the anti-inflammatory potential of the nitric oxide-releasing indomethacin derivatives (NO-IND-TZDs, NO-IND-OXDs). Two controls (positive and negative), as well as reference drugs (IND, ASP), were also used. The positive control consisted of the action of 0.1 M hydrochloric acid, as denaturing agent, in 0.9% NaCl, on the 0.2% BSA solution. The negative control consisted of untreated 0.2% BSA solution.

Each sample was tested at different concentration. So, the NO-IND-TZDs (**9a-s**) were tested at 50 μM, 100 μM and 150 μM respectively and the NO-IND-OXDs (**11a-m**, **t-v**) were tested at 20 μM, 50 μM and 100 μM respectively.

The test samples and controls were incubated at 38°C for 5 h. The degree of denaturation of BSA was evaluated by measuring the increase in optical density at 450 nm, recorded using Tecan Sunrise Remote Microplate Reader TW/ML-Abbott F039306. All tests were performed in quadruplicate. The maximum value of the absorbance at 450 nm of the positive control was considered as the 100% effect. Results, expressed as averages of the percentage values (% effect), were plotted versus the concentration of tested sample.

10.2.2. Results and discussions

The discovery of the new drugs is focused primary to identification of a ligand that binds to the target protein with high affinity [413–415]. It is known that NSAIDs are strong ligands to enzymatic and non-enzymatic proteins, being proved that their anionic radicals interact with the polar amino acids of proteins, whereas their lipophilic moieties are fixed into hydrophobic site of proteins [416].

Referring to the COX, different mechanisms of inhibition are known. For example, ASP has a unique therapeutic action and irreversibly inhibits COX-1 and COX-2, due to covalent

acetylation of the enzymes [5,41,417,418], while IND and other aryl acetic acid derivatives inhibits COX by the conformational change of protein [5].

In order to study the mechanism of inhibition of newly synthesized derivatives (NO-IND-TZDs, NO-IND-OXDs), IND and ASP were used as reference NSAIDs. Literature notes that ASP also induce acetylation of multiple proteins (such as human serum albumin, fibrinogen, p53, cellular protein) by *in vitro* and *in vivo* assays and extensive ASP therapy give rise of anti-acetylated serum albumin antibodies [419–421].

These interactions make changes on the native structure of the proteins as the modification of the secondary, tertiary or quaternary structure without the breaking of covalent bonds. As result, a variety of easily quantifiable physico-chemical effects are produced, which are used to predict the anti-inflammatory effects of different compounds [422].

Literature data report that the native state of the proteins is stable in hydrophobic solvents, whereas the proteins tend to lose their native structure in polar organic solvents like DMSO, DMFA or trifluoroethanol [423]. In addition, it was suggested that the effect of DMSO on the proteins stability depends on the concentration [424]. It was showed that the native structure of BSA was retained in the presence of low concentration of DMSO (<10%) while the protein starts losing its structure with increasing amount of DMSO. If at 30% DMSO, the protein is partially unfolded state, at 40% DMSO, a completely unfolded was observed BSA [423,424].

To predict the anti-inflammatory potencies of the synthesized indomethacin derivatives (**9a-s**, **11a-m**, **t-v**), a modified Mizushima's test was used [422,425]. When a chemical is incubated with an unfolded protein (BSA), an increase in optical density will occur because of protein precipitation, which is directly proportional to the amount of precipitated protein. The ability of a chemical to precipitate proteins is considered as a measure of its interaction with non enzymatic proteins.

Because the tested compounds (**9a-s**, **11a-m**, **t-v**) have poor solubility in water, DMSO (40%) was used as solvent. The our study showed that BSA, 0.2% in 0.9% NaCl/DMSO = 6/4 remained stable after incubation at 38°C for 5 h and no turbidity was observed. In similar conditions, the tested compounds (**9a-s**, **11a-m**, **t-v**) cause an intense precipitation of BSA, resulting a cloudy solution. In order to study the mechanism of inhibition of newly synthesized derivatives, IND and ASP were used as reference NSAIDs.

10.2.2.1. In vitro anti-inflammatory effects of NO-IND-TZDs

The results, expressed as denaturation effects (%), at different concentrations (50 μM, 100 μM and 150 μM) in reference with positive control (100%), are presented in Fig. 10.3. Using two-way ANOVA test there was determined that there is a statistically significant interaction ($F(40, 189) = 49644.649$, $p < 0.05$) between concentration and type of tested compounds referring to the BSA denaturation process.

It was noted that the tested compounds (**9a-s**) were able to increase the albumin denaturation in a concentration dependent manner; the higher concentrations increase the denaturation effect (Fig. 10.4). For example, the compounds **9a**, **9i** and **9m** showed a statistically significant increasing of denaturation effect ($p < 0.05$) at 150 μM but there were no difference ($p = 0.701$) at 50 μM and 100 μM respectively. At 150 μM, compound **9i** was more active (15.04 ± 0.02%) compared with **9a** (8.44 ± 0.02%) and **9m** (3.33 ± 0.02%).

Therefore, in relation with chemical structure, we can conclude that the presence of 3-phenoxy moiety on second position of thiazolidine-4-one scaffold (**9i**) enhance the anti-inflammatory activity.

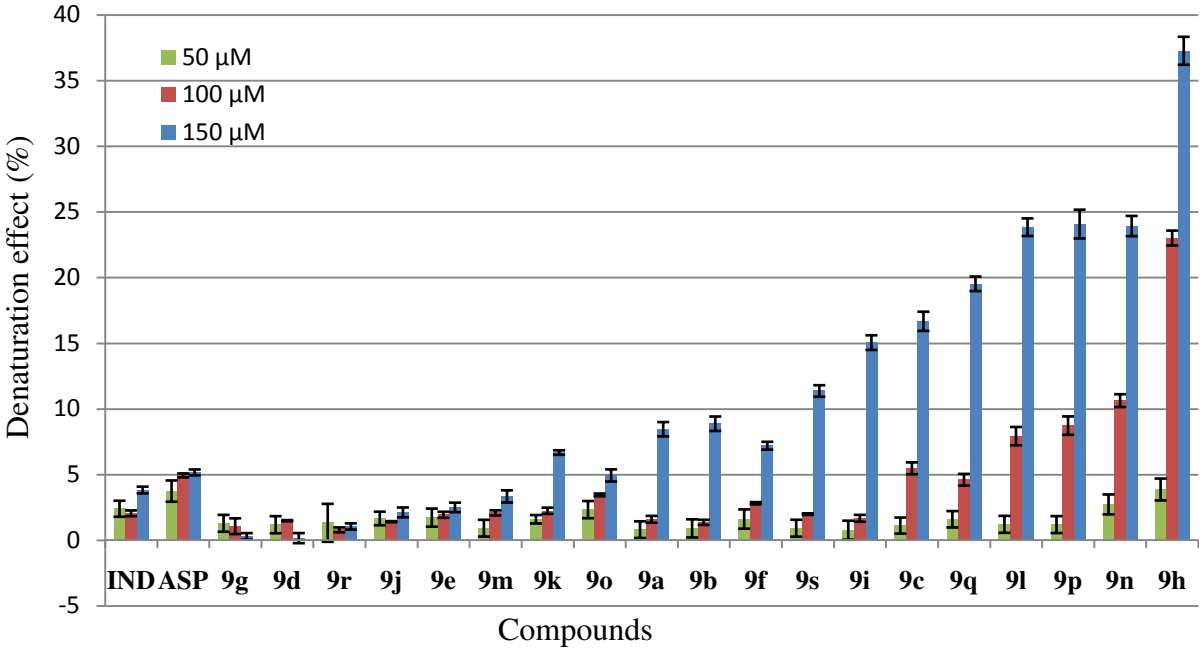

Fig. 10.3. The effects of NO-IND-TZDs (**9a-s**) and of reference drugs (IND, ASP) on BSA denaturation process.

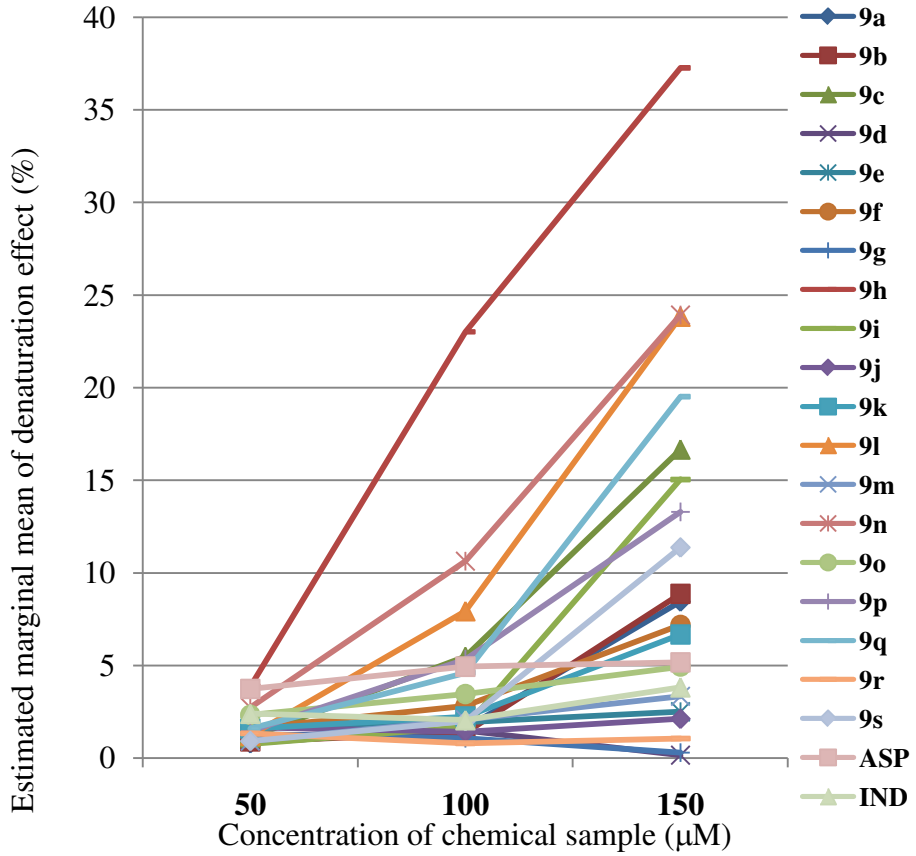

Fig. 10.4. The marginal mean of denaturation effect of NO-IND-TZDs (**9a-s**) and of reference drugs (IND, ASP).

As expected, ASP (4.78 ± 0.18 %) bonded BSA significantly stronger ($p < 0.05$) than IND (2.65 ± 0.23 %). We also noted that, comparing with the reference drugs (IND and ASP),

that have a denaturation effect less 5%, the derivatives **9i**, **9c**, **9q**, **9l**, **9p**, **9n** and **9h** showed to be more active, with a denaturation effect value between 15% and 37%.

The analysis of the results revealed that the substitution of the aromatic ring on 1,3-thiazolidne-4-one scaffold with electron withdrawing groups (like Cl, Br) as well as increase of $-O-CH_2-CH_2-$ spacer length (from 1 unit to 2 units) increase the denaturation effect and thus promote interaction with non enzymatic proteins. The most active compound, in term of anti-inflammatory effects was **9h** which contain a (2,6-dichloro-phenoxy)ethyl nitrate moiety.

10.2.2. In vitro anti-inflammatory effects of NO-IND-OXDs

The results, expressed as denaturation effects (%), at different concentrations (25 μM, 50 μM and 100 μM), in reference with positive control (100%), are presented in Fig. 10.5.

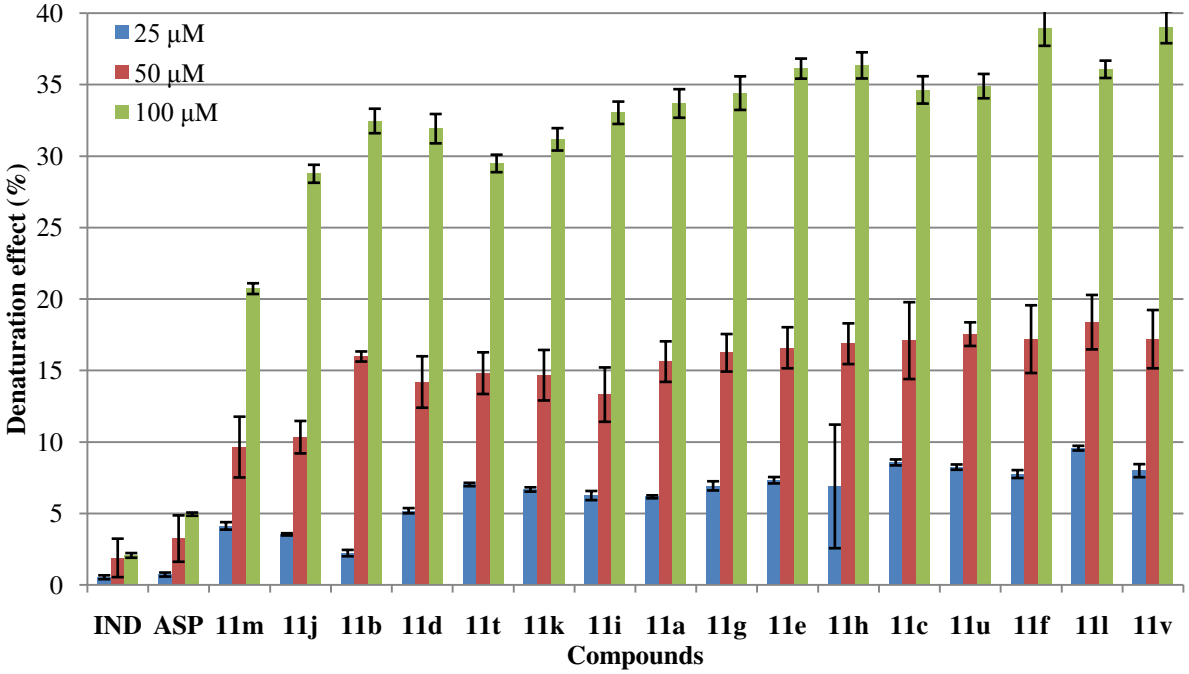

Fig. 10.5. The effects of NO-IND-OXDs (**11a-m, t-v**) and of reference drugs (IND, ASP) on BSA denaturation process.

Using two-way ANOVA test there was determined that there is a statistically significant interaction ($F(30, 144) = 2060.794$, $p < 0.05$) between concentration and structure of tested compounds referring to BSA denaturation process.

It was noted that the tested compound (**11a-m**, **t-v**) were able to increase the albumin denaturation in a concentration dependent manner, the higher concentration increasing the denaturation effect. For example, the compounds **11a**, **11i** and **11m** showed a statistically significant increasing of denaturation effect ($p < 0.05$) with concentration increasing, but at the same level of each concentration there were no difference ($p = 0.150$) between **11a** and **11i** compared with **11m**, for which the denaturation effect increase significantly less ($p < 0.05$). At 100 μM, compound **11m** was less active (20.7 ± 0.4%) compared with **11a** (33.7 ± 1.0%) and **11i** (33.0 ± 0.9%). Therefore, in relation with chemical structure, we can conclude that the presence of nitrate ester moiety in *para* and *meta*, **11a** (4-oxy-ethylnitrate) and **11i** (3-oxy-ethylnitrate) respectively enhancing the anti-inflammatory activity than **11m** (2-oxy-ethylnitrate).

We also noted that, comparing with the reference drugs (IND and ASP), that have the denaturation effect less 5%, all the tested compound showed to be more active, with a value of denaturation effects between 20% and 40% (at 100 μM).

Moreover, the analysis of the results revealed that the substitution of the aromatic ring on 1,3,4-oxadiazole scaffold with electron withdrawing groups (like Cl, Br, NO2) as well as the elongation of distance between oxadiazole moiety and aromatic ring from methylene group (**11a**) to ethylene group (**11v**) increase the denaturation effect and thus promote the interaction with non enzymatic proteins.

10.2.3. Conclusions

Referring to the overall results, one way ANOVA analysis established there was a statistically significant difference between thiazolidin-4-one (NO-IND-TZDs) and 1,3,4-oxadiazole (NO-IND-OXDs) series ($F(1, 418) = 175.2811$, $p < 0.05$). It was noted that the presence of 1,3,4-oxadiazole moiety increase significantly the denaturation effect (18.35 ± 0.8) than presence of thiazolidine-4-one moiety (5.79 ± 0.5) and thus promote the interaction with non enzymatic proteins.

Moreover, the our research revealed that the replacement of carboxyl group of IND with the thiazolidin-4-one or 1,3,4-oxadiazole moiety enhances drug-protein interactions. These measurable effects were reported [426] to be a measure for prediction of anti-inflammatory properties of the different compounds. These results are in agreement with the previous *in silico* results which showed that the synthesized compound promise to have significant anti-inflammatory properties.

10.3. *In vitro* nitric oxide release

To evaluate the nitric oxide release, the newly synthesized NO-NSAIDs (**9a-s**, **11a-m**, **t-v**) were subjected to a modified Griess colorimetric method [427,428], based on decomposition of nitrate ester moiety in presence of Hg^{2+} and thiol based compounds.

The Griess reagents consists of 0.34% (wt/v) *N*-(1-naphthyl)ethylenediamine (NED) solution in DMSO, 3.4% (wt/v*)* sulfanilamide (SULF) in 10% (wt/v*)* phosphoric acid and a mixture between of 3.4% (wt/v) SULF and 1.07% (wt/v) mercuric chloride (SULF-$HgCl_2$) in 10% (wt/v*)* phosphoric acid. The NO released from the sample is spontaneous oxidized to NO_2^-, that subsequently reacts with the Griess reagents to form an azo dye. *S*-Nitroso-N-acetyl-penicillamine (SNAP), sodium nitropruside (SNP) and nitroglycerine (NTG), were used as reference NO donors.

The experiments were carried out in neutral (phosphate buffer solution - PBS) and acidic (hydrochloric acid solution - HCl) experimental conditions, in presence or absence of L-glutathione (GSH): PBS (pH 7.5), PBS-GSH (pH 7.51), HCl (pH 1.55) HCl-GSH (pH 1.56)

10.3.1. Material and methods

10.3.1.1. Preparation of the sodium nitrite and of the test solutions

A fresh sodium nitrite stock solution (0.1 M sodium nitrite in distilled water) was prepared by dissolving 6.97 g of the reference substance in distilled water and diluting to 1000 mL. This stock solution was standardized using the standard procedure reported in the European Pharmacopoeia and Romanian Pharmacopoeia, edition X (real molarity = 0.0999, molarity factor = 0.999) [429]. Next, a solution of 100 μM sodium nitrite was prepared by diluting 1 mL of the stock solution to 1000 mL with MeOH/H_2O = 1/1 (v/v) mixture. Then,

serially diluted solutions, containing different concentrations (100 μM, 50 μM, 25 μM, 12.50 μM, 6.25 μM, 3.125 μM, 1.56 μM and 0.78 μM), were prepared by dilution with MeOH/H_2O =1/1 (v/v) mixture. The tested compounds (**9a-s**, **11a-m**, **t-v**) and reference NO donors (SNAP, SNP, NTG) were dissolved in DMSO and water, respectively, to afford a stock solution of 2600 μM.

10.3.1.2. Preparation of the sodium nitrite standard curve

To avoid the precipitation of NO-NSAIDs (NO-IND-TZDs, NO-IND-OXDs) and to allow hydrolysis of NO-releasing moiety, different co-solvents like DMSO and MeOH, which were added to water, were used. It was noted that the presence of the co-solvents interferes to measurement of the absorbance for final azo dye compound and decreases the slope of the calibration curve for NO_2^-. In view of the shortening the assessment time, the stability of the final azo dye, the low cost of solvents and the solubility of the tested NO-NSAIDs in a large range of concentrations, a modified Griess assay, using MeOH as co-solvent, was chose to be validated .

In a micro plate reader, an aliquot of 170 μL from the sodium nitrite solution (in the range of 0.78-100 μM) was added to the 50 μL solution of SULF. After 10 min, 50 μL of the NED solution was added and the absorbance of the formed pink-red azo dye was measured at 540 nm, after 20 min. A blank sample was performed under the similar conditions (170 μL PBS, 50 μL SULF and 50 μL NED). All tests were performed five times for each concentration and the average absorbance was calculated. The calibration curve was constructed by plotting the average absorbance value in relation with the corresponding sodium nitrite concentration (Fig. 10.6.).

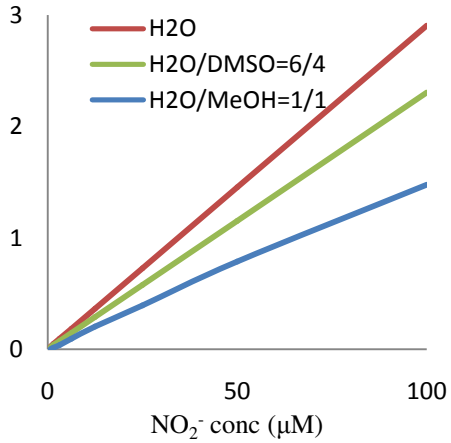

Fig. 10.6. The study of the nitrite detection by the Griess assay, using different co-solvents.

10.3.1.3. NO release assay

A solution of 100 μM of tested compounds (**9a-s**, **11a-m**, **t-v**) and reference NO donors (SNAP, SNP, NTG) was prepared by dilute 80 μL of each stock solution (2600 μM) with 2 mL of PBS, PBS-GSH, HCl and HCl-GSH. These solutions were kept at 37-38°C for 120 min, after that an aliquot of 170 μL of the each solution was measured and added to 50 μL of SULF and SULF-$HgCl_2$ respectively in a 96 well plate. After 10 min, 50 μL of NED solution was added and the absorbance of the formed pink-red azo dye was measured at 540 nm, after 20 min. A blank sample (which contains 170 μL of PBS/PBS-GSH/HCl/HCl-GSH, 50 μL of

SULF/SULF-$HgCl_2$ and 50 μL of NED solutions) was performed under the similar conditions. All tests were performed in quadruplicate.

The percentage (%) of NO release was calculated using the following formula [427]:

$$\% \text{ NO} = (C_{f\,NO} \text{x} 100)/C_{t\,NO} \qquad (3)$$

where: C_{fNO} is the found concentration of NO (μM) and C_{tNO} is the theoretical concentration of NO (μM).

10.3.2. Results and discussions

For detection and quantification of NO in complex biological systems and in physiological conditions, different methods can be used such as: chemiluminescence detection; fluorescence detection using 4,5-diaminofluorescein; conversion of Fe(II)-/oxyHb to metHb; electrochemical detection (amperometric NO-specific and porphyrinic electrodes); Griess assay of NO_2^-, NO_3^- and immunoassays using anti-nitrotyrosine antibodies. Many of these methods are indirect and have a low specificity for NO, because interfere with other components of biological systems [428,430].

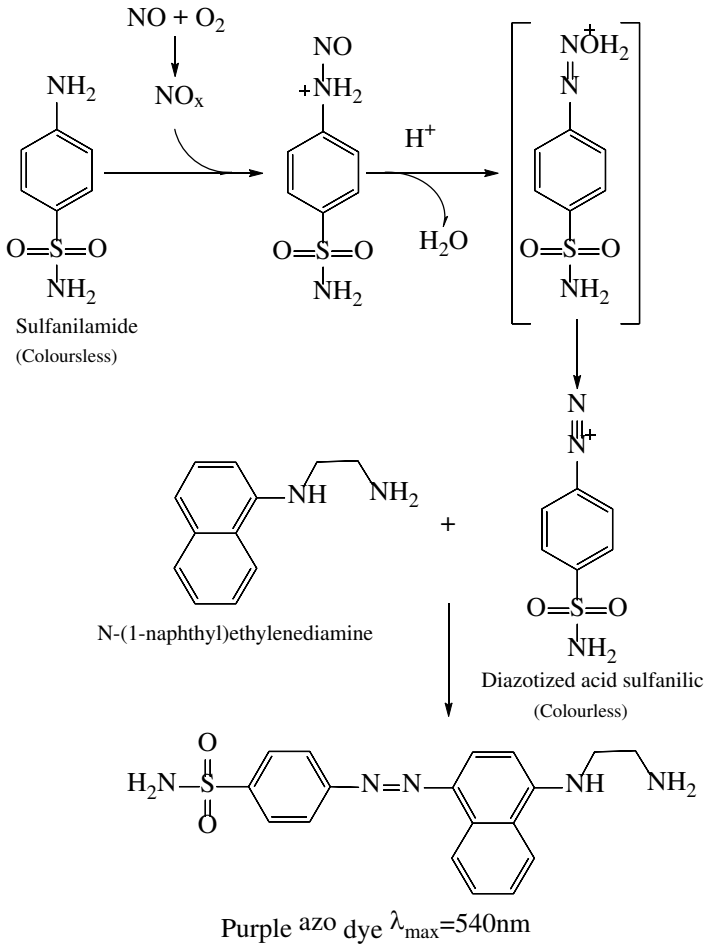

Fig. 10.7. The quantification of NO using Griess colorimetric assay.

Griess colorimetric assay represent the most commonly used method for the measurement of NO in view of the simplicity and low cost [431]. It has been used extensively

in analysis of several biological samples such as plasma (serum), urine, saliva and cell culture media.

The method is based on indirect quantification of NO *via* spectrophotometric measurement of its stable NO_2^-, using aqueous medium. Decomposition product NO is rapidly oxidized to NO_2^- by oxygen. The half-life of NO in biological matrix is very short, ranging from less than 1 sec, in the presence of hemoglobin, to ~30 sec. This method involves two steps: firstly NO_2^- reacts with SULF in acidic media to produce a diazonium ion, which in the next step reacts with NED to form a pink-red azo dye (Fig. 10.7.). The absorbance of this adduct at 540 nm is linearly proportional with the NO_2^- concentration in the sample [428,430].

It is know that the NO exerts beneficial activity (e.g. anti-inflammatory, antioxidant, wound healing processes) at low levels of NO (less 300 nM) while at high level 1000 – 3000 nM) has pro inflammatory activity in pathological condition [266,432].

10.3.2.1. The method validation

In order to be applied for determination of nitric oxide (NO) released from NO donors with poor solubility in aqueous medium, the developed method was validated in accordance with the bio analytical method validation guidelines [433,434].

The linearity of the method was studied in the 0.78-100 μM concentration range of sodium nitrite. The average value of the absorbance was calculated for each concentration (Table 10.2.) and was graphically represented in relation to the concentration (Fig. 10.8.). Statistical analysis of the experimental data leads to regression line equations. The linear regression data for the calibration curve showed good linear relationship over the concentration range. Linear regression equation was found to be $f(x)=0.0159 \times x + 0.0491$. The standard error of regression curve (SE) and the Person correlation coefficient (r^2) were also calculated.

The accuracy of the method was calculated based on the experimental absorbance data and the regression curve equation and the results are presented in Table 10.3. It was noted that recovery was between 98.34% and 101.96% (100±2%) for the studied concentration range and coefficient of variation < 2. The relative standard deviation (RSD) was also calculated. The results proved that the developed method has high degree of accuracy.

Table 10.2. The absorbance values of the samples, at different concentrations of sodium nitrite.

Conc. (μM)	Absorbance of the samples					
	Series 1	**Series 2**	**Series 3**	**Series 4**	**Series 5**	**Average**
100	1.641	1.643	1.643	1.642	1.640	1.642
50	0.852	0.854	0.854	0.854	0.856	0.854
25	0.450	0.450	0.450	0.451	0.450	0.450
12.5	0.259	0.260	0.259	0.260	0.259	0.260
6.25	0.151	0.150	0.151	0.151	0.150	0.151
3.125	0.094	0.094	0.094	0.094	0.095	0.094
1.562	0.068	0.068	0.068	0.069	0.069	0.068
0.781	0.057	0.057	0.057	0.057	0.058	0.057
Range 0.781-100 μM, Person coefficient (r^2)=0.99988						
Intercept=0.04912 / Slope=0.01598 / Standard error=0.006435						

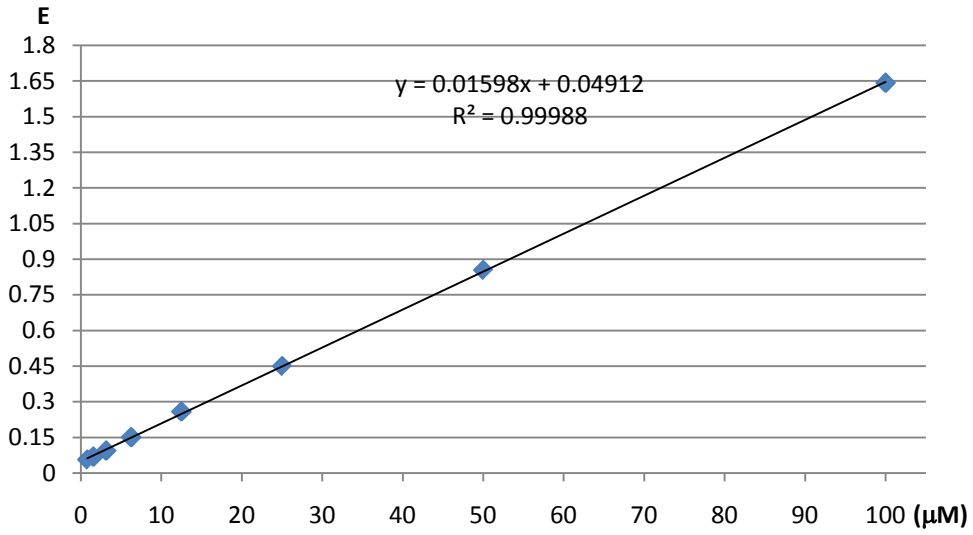

Fig. 10.8. The calibration curve for detection of NO_2^-.

Table 10.3. The results related to the accuracy of the developed method.

Conc. (µM)	Absorbance value	Calculated conc.(µM)	Recovery (%)	RSD (%)
20	0.375	20.393	101.96	1.38%
	0.365	19.767	98.84	
	0.371	20.143	100.71	
	0.367	19.892	99.46	
40	0.701	40.793	101.98	1.50%
	0.685	39.792	99.48	
	0.679	39.417	98.54	
	0.693	40.293	100.73	
60	1.017	60.568	100.95	1.53%
	0.992	59.004	98.34	
	0.999	59.442	99.07	
	1.023	60.944	101.57	

The precision of the method could be expressed as the coefficient of variation (CV) or the relative standard deviation (RSD), and the results are presented in Table 10.4. The obtained results support the reproducibility of the method. The RSD (%) values were less than 2%, which confirm that the method has a high degree of accuracy and precision and so can be applied for quantitative measurements of NO from different NO donors, such as NO-NSAIDs.

The obtained data offer all the proofs that permit the use of this method for determination of NO released from NO-NSAID, using hydro alcoholic medium, having a good sensitivity, precision and accuracy

The NO releasing from the tested compounds (**9a-s**, **11a-m**, **t-v**) was studied in different experimental conditions in order to mimics the intestinal (PBS, PBS-GSH), and gastric (HCl, HCl-GSH) environmental conditions.

The experiment included also reference NO donors, such as SNAP, SNP, NTG, which belong at different classes. So, NTG is a representative organic nitrate which requires specific thiol and/or enzymatic activation to generate NO, SNP is a metal nitrosyl compound that spontaneously releases NO at physiological pH and SNAP is an *S*-nitrosothiol which is rapidly decompose in presence of metal ions, such as Cu^{+}, Fe^{2+}, Hg^{2+} and Ag^{+}.

As expected, there was a statistically significant difference between reference NO donors, as determined by one-way ANOVA ($F(2,93) = 60.729$, $p<0.05$) (Fig. 10.9.). Post hoc comparisons using the Tukey HSD test indicated that the mean score for SNAP (52.70 ± 16.82) was significantly different from SNP (3.97 ± 1.21) and NTG (0.49 ± 0.18). Also, by two way ANOVA it was found there was not a statistically significant interaction between used Griess reagents (NED-SULF/SULF-$HgCl_2$) and experimental conditions (PBS, PBS-GSH, HCl, HCl-GSH) on NO released (($F(3,88) = 1.029$, $p = 0.384$).

Moreover, there was no statistically significant difference in mean of NO released by changing the experimental conditions ($p = 0.669$), but the presence of Hg^{2+} in Griess reagents increased significantly the quantified amount of NO ($p = 0.002$). These results suggest that the Hg^{2+}decompose the *S*-nitrosothiol from SNAP. In addition, the presence of GSH in the experimental medium can fix the free NO to form a stable *S*-nitrosothiol (GS-NO). It was noted also that the experimental pH did not influence significantly the amount of NO released from reference NO donors.

Table 10.4. The results related to the precision of the developed method.

Theoretic conc. (µM)	Intra-day precision		Inter-day precision	
	Conc. found (µM)	RSD (%)	Conc. found (µM)	RSD (%)
10	10.12	1.37%	9.87	1.69%
	9.95		10.20	
	9.85		9.97	
25	24.81	0.79%	24.76	0.80%
	24.96		24.88	
	25.20		25.15	
50	49.01	0.90%	48.95	0.75%
	48.85		49.62	
	49.68		49.55	

10.3.2.2. The NO release by NO-IND-TZDs

Using two-way ANOVA test it was found that there is no statistically significant interaction ($F(3, 600) = 1.454$, $p = 0.226$) between Griess reagents and experimental conditions applied to study the NO release by NO-IND-TZDs (**9a-s**).

Moreover, it was noted that the adding of $HgCl_2$ to SULF solution do not increase significantly the total amount of NO released from nitrate ester moiety ($F(1, 600) = 0.629$, $p = 0.428$). A statistically significant interaction between structure of **9a-s** and experimental conditions ($F(54, 532) = 29.908$, $p < 0.05$) was noted. All these results suggest that the presence of Hg^{2+} in Griess reagents do not influence de amount of NO released by NO-IND-TZDs but it is strongly influenced by the structure of tested compounds and experimental conditions (pH and GSH presence).

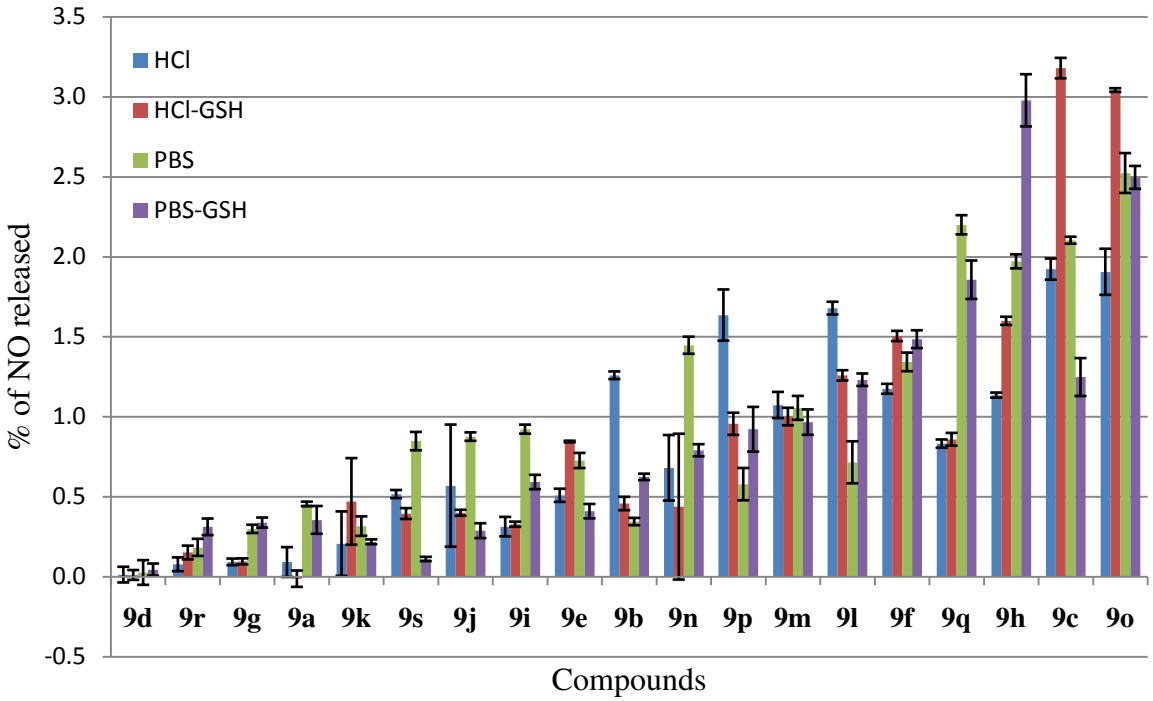

Fig. 10.9. Percentage (%) of NO released by NO-IND-TZDs (**9a-s**), in different experimental conditions (PBS, PBS-GSH, HCl HCl-GSH), relative to the theoretical maximum release of 1.0 mol NO/mol tested compound) (n = 4)

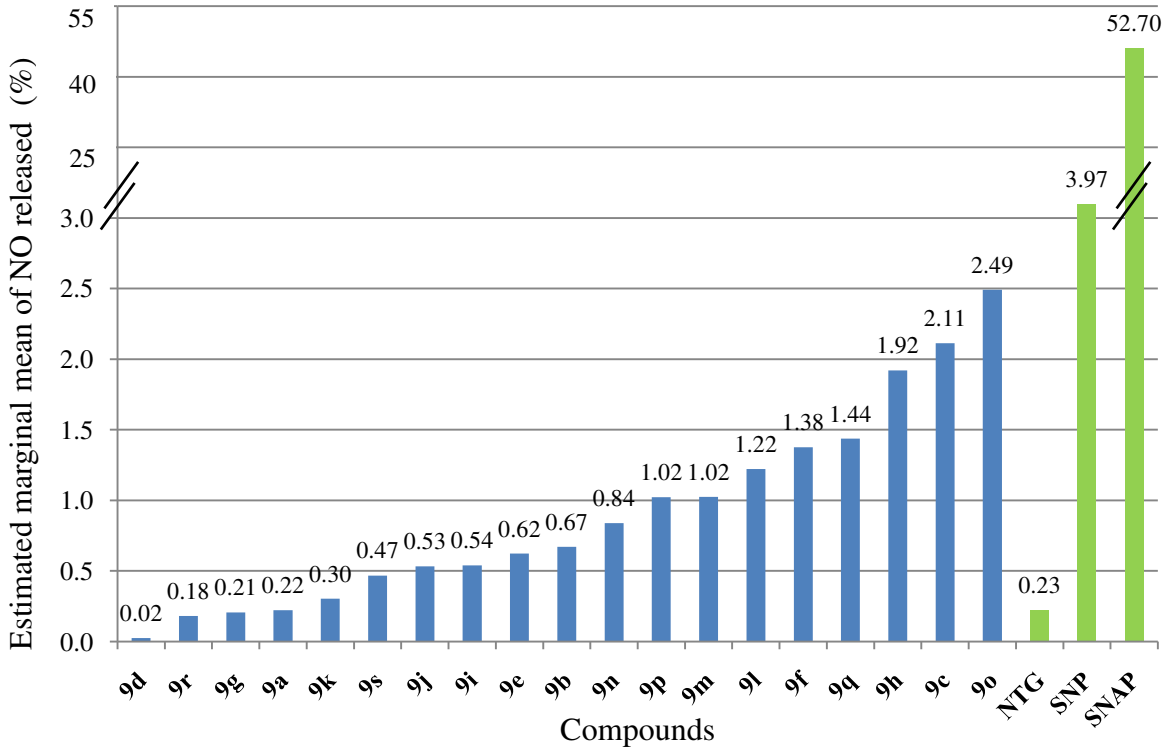

Fig 9.10. Estimated marginal means of NO (%) release by NO-IND-TZDs (**9a-s**) compared to reference NO donors (NTG, SNP, SNAP).

By estimated marginal mean of NO released it was showed that the most of **9a-s** released more NO compared with NTG (Fig. 10.10). Moreover, it can appreciate that the majority of compounds release from 4.4 to 10.8 more NO than NTG. It was also noted that

the amount of NO released is influence by the position of nitrate ester moiety on aromatic ring and also by the number and type of the substituents on aromatic ring. The most proper position of nitrate ester moiety is *ortho*, **9m** (2-oxy-ethylnitrate) being more active than **9i** (3-oxy-ethylnitrate) and **9a** (4-oxy-ethylnitrate). Referring to the substitution of phenoxy-ethylnitrate moiety, the presence of electron withdrawing groups (Cl, Br, NO_2) on aromatic ring increase the NO release, the most active compounds being **9l**, **9f**, **9q**, **9h**, **9c** and **9o** (Figures 10.9 and 10.10). Of these, the best compound was **9o** that consist of an oxy-ethylnitrate (*meta*) and nitro (*ortho*) radicals on aromatic ring.

10.3.2.3. The NO release by NO-IND-OXDs

Using two-way ANOVA test it was found that there is no statistically significant interaction ($F(3, 504) = 0.465$, $p = 0.707$) between Griess reagents and experimental conditions applied to study the NO release from by NO-IND-OXDs (**11a-m**, **t-v**). Moreover, it was noted that the adding of $HgCl_2$ to SULF solution do not increase significantly the total amount of NO released from nitrate ester moiety ($F(1, 504) = 0.122$, $p = 0.727$). A statistically significant interaction between structure of **11a-m**, **t-v** and experimental conditions ($F(45, 448) = 69.945$, $p < 0.05$) was noted. All these results suggest that the presence of Hg^{2+}in Griess reagents do not influence de amount of NO released by NO-IND-OXDs but it is strongly influenced by experimental conditions (pH and GSH presence) and the structure of tested compounds (Fig 10.11.)

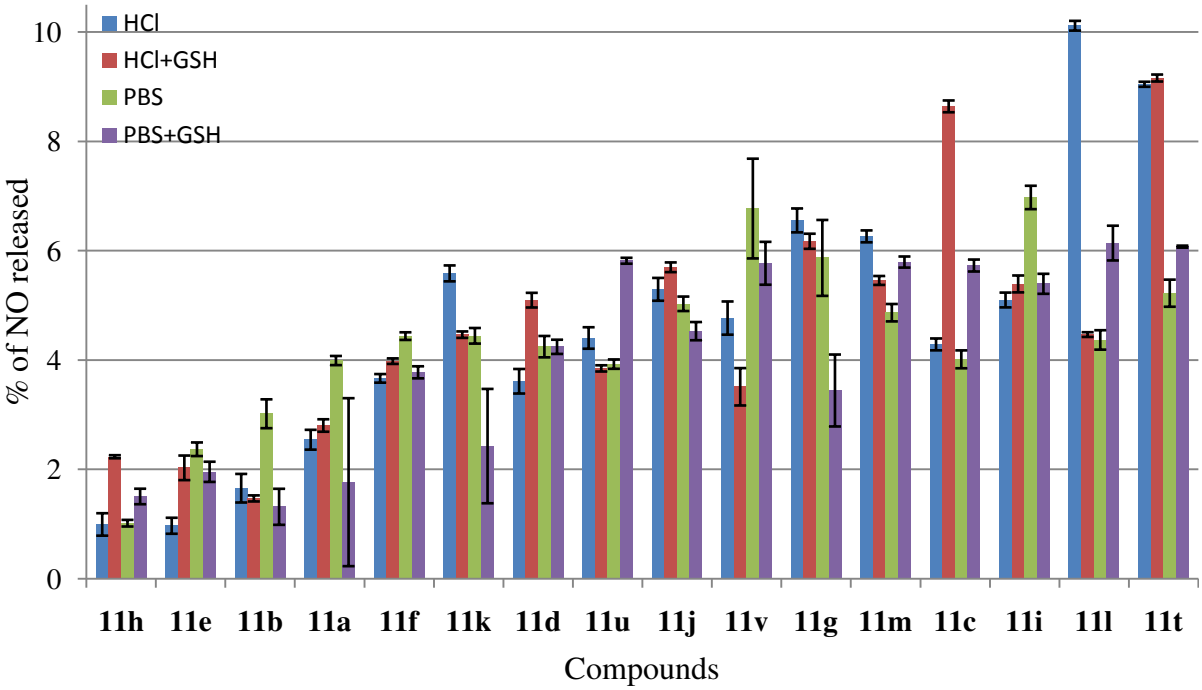

Fig. 10.11. The percentage (%) of NO released by NO-IND-OXDs (**11a-m, t-v**), in different experimental conditions (PBS, PBS-GSH, HCl, HCl-GSH), relative to the theoretical maximum release of 1.0 mol NO/mol tested compound) ($n = 4$)

By estimated marginal mean of NO released it was showed that the all of the tested compounds (**11a-m, t-v**) released more NO compared with NTG and SNP (Figure 10.12.). Using one-way ANOVA test there was determined that there is a statistically significant difference ($F(16, 255) = 33.054$, $p < 0.05$) between tested compounds. Post hoc comparisons using the Tukey HSD test revealed that **11g**, **11m**, **11c**, **11i**, **11l** and **11t** respectively released

significantly more NO than SNP ($p < 0.05$). Moreover, it can appreciate that the majority of compounds release from 1.0 to 1.9 more NO than SNP.

It was also noted that the amount of NO released is influence by the position of nitrate ester moiety on aromatic ring and by the number and type of the substituents on aromatic ring. The most proper positions of nitrate ester moiety are *meta* and *ortho*, **11i** (3-oxy-ethylnitrate) and **11m** (2-oxy-ethylnitrate) being more active than **11a** (4-oxy-ethylnitrate). Also, the elongation of distance between 1,3,4-oxadiazole moiety and aromatic ring from methylene group (**11a**) to ethylene group (**11v**) increase the percentage of NO released.

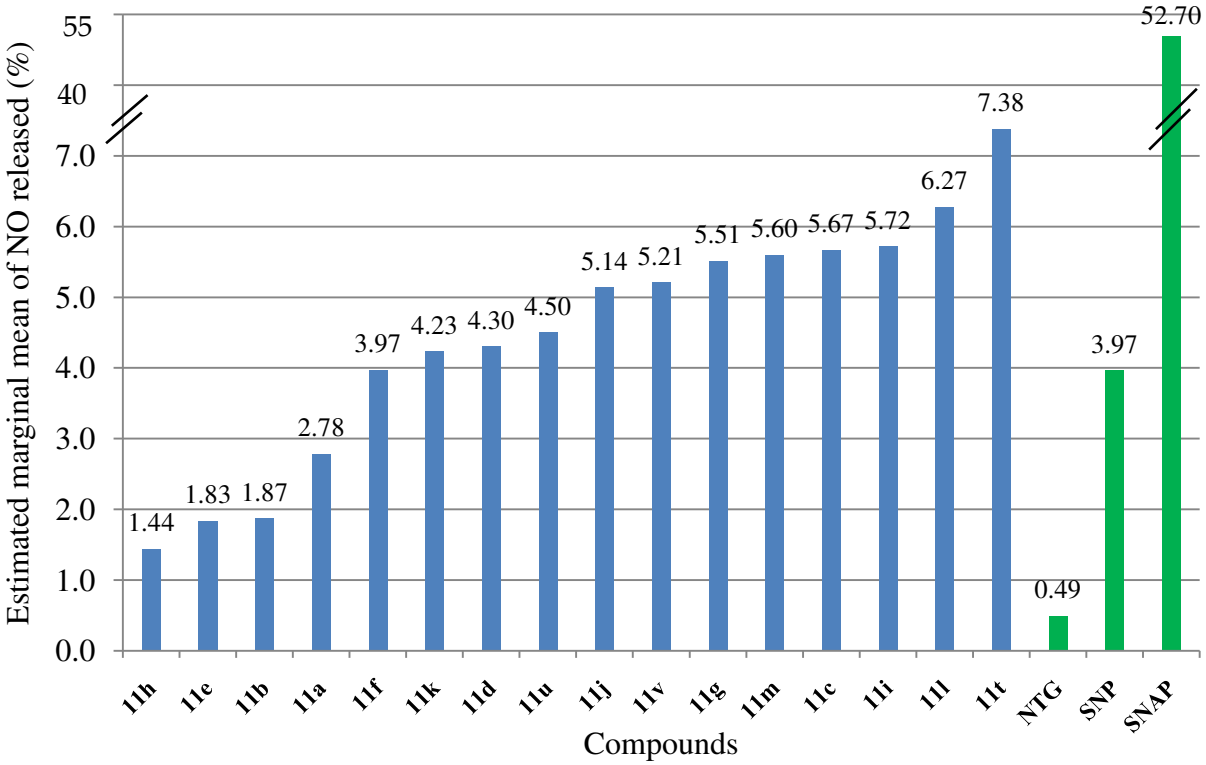

Fig. 10.12. The estimated marginal means of NO (%) release by NO-IND-OXDs (**11a-m, t-v**) compared to reference NO donors (NTG, SNP, SNAP).

10.3.3. Conclusions

Referring to the overall results, one way ANOVA analysis established there was a statistically significant difference between thiazolidin-4-one (NO-IND-TZDs) and 1,3,4-oxadiazole (NO-IND-OXDs) series ($F(1, 1086) = 25.61639$, $p < 0.05$). It was noted that the presence of 1,3,4-oxadiazole moiety enhance significantly the amount of released NO (4.28 ± 0.1%) than the presence of thiazolidine-4-one moiety (2.23 ± 0.3%).

Moreover, the NO release capacity of tested compounds was strongly influenced by the position of nitrate ester moiety and by the nature of the substituents on linker. The most proper positions of nitrate ester moiety are *meta* (3-oxy-ethylnitrate) and *ortho* (2-oxy-ethylnitrate). The presence of the electron withdrawings groups (Cl, Br, NO_2) on aromatic ring increase also the amount of NO released.

The synthesized compounds can be an entirely new chemical entity which provides balanced inhibition of COX enzymes while also being safer in terms of gastro-intestinal side effects and donating nitric oxide at sites of inflammation at physiological submicromolar concentration of NO described in literature.

Chapter 11

General conclusions

In the current context of scientific progress in the field of discovery of new compounds with therapeutic potential, the research carried out within the doctoral thesis brings original contributions in the development of new therapeutic strategies for inflammatory diseases. The research aimed to development of new indomethacin nitric oxide donors as multi-target strategy, able to improve pharmacological and safety profile of parent compound.

The objectives pursued throughout the work, such as the design and synthesis of new nitric oxide releasing indomethacin derivatives with 1,3-thiazolidine-4-one and 1,3,4-oxadiazole scaffold, respectively, as well as biological evaluation in term of COX inhibition selectivity, anti-inflammatory effect, antioxidant effect and their capacity to release NO, can be considered as fulfilled.

In the following are presented the main conclusions of the studies carried out on the new derivatives of indomethacin that are the subject of this thesis.

The synthesis performed in this study resulted to the obtaining of 144 compounds (109 intermediate and 35 final) which belong to the following series: (i) NO-donor linkers (**3a-s** and **6a-m,t-v**); (ii) indomethacin hydrazide (**7**); (iii) indomethacin hydrazone derivative (**8a-s**); (iv) IND-OXD derivative (**10**); (v) nitric oxide-releasing indomethacin derivatives containing a 1,3-thiazolidine-4-one scaffold (NO-IND-TZDs) (**9a-s**) and (vi) nitric oxide-releasing indomethacin derivatives containing a 1,3,4-oxadiazole scaffold (NO-IND-OXDs) (**11a-m,t-v**).

In order to minimize the consumption of reagents and to reduce the impact on the environment and human health, the optimization of all stages of synthesis was aimed. So, the intermediare compounds were obtained in near quantitative yields, which ranged between 85-99%. Also, the desired NO-IND-OXDs were obtained in good yield (70-93%). Due to the hard work conditions and lower stability of nitrate ester moiety, the desired NO-IND-TZDs were obtained in moderate yields, which ranged between 25% and 63%.

All synthesized compounds, intermediares and finally compounds, were characterized from a physic-chemical point of view determining the molecular formula, molecular weight, yield, melting point, retention factor as well as chromatographic characteristic.

The chemical structure of all synthesized compounds was proved on the basis of NMR and HRMS spectral methods. The protons were reveled through ^{1}H-RMN analysis, and the correlation between them was validated by the 2D-COSY spectra. DEPT experiment was used for distinguishing between a methyl group, a methyene group and a methine group from the ^{13}C-RMN spectra. The correspondence between the carbon atoms and the protons was confirmed by the HSQC experiment which determines proton-carbon single bond correlations, and HMBC experiments, which give correlations between carbon and protons that are separated by 2-4 bonds.

To study the COX isoenzymes selectivity of the new final developed nitric oxide-releasing indomethacin derivatives, with 1,3-thiazolidin-4-one scaffold (NO-IND-TZDs, **9a-s**) and 1,3,4-oxadiazole scaffold (NO-IND-OXDs, **11a-m**, **t-v**) a molecular docking analysis was performed. Based on the obtained results we can conclude that the designed compound can be a potent COX-2 inhibitors and have the theoretical premises to be promising anti-inflammatory agents.

In order to predict the pharmacological and toxicological properties of the new final developed nitric oxide-releasing indomethacin derivatives, an ADME-Tox study was performed. It was noted an optimal physico-chemical properties and a favorable pharmacokinetic profile with a good absorption in the small intestine and poorly distribution to the brain. The toxicity descriptors revealed that the tested compounds could be hepatotoxic, but many studies, including *in vivo*, must be performed in order to confirm it. ADME-Tox profile recommended the developed compound for oral administration.

The free radical scavenging activity of the new NO-IND-TZDs and NO-IND-OXDs was evaluated using a colorimetric method based on the capacity of the antioxidant compounds to scavenge the DPPH radical. The results revealed that the presence of thiazolidine-4-one and 1,3,4-oxadiazole scaffolds influence favorable antioxidant potential, all tested compounds being around 20 time more active than reference drugs (IND, ASP).

The anti-inflammatory effect was predicted by thermal denaturation of bovine serum albumin. It was noted that the NO-IND-OXDs increase significantly de denaturation effect than NO-IND-TZDs, and all of them showed to be more active comparing with the reference drugs (IND and ASP). These results are in agreement with the previous molecular docking results which showed that the replacement of carboxyl group of IND with the thiazolidine-4-one or 1,3,4-oxadiazole moiety enhances significantly the anti-inflammatory properties.

The NO release capacity of synthesized compounds was evaluated by a modified colorimetric Griess assay to appropriate simulate the body conditions. The results revealed that the amount of NO released of tested compounds was strongly favorised by the *meta* (3-oxy-ethylnitrate) and *ortho* (2-oxy-ethylnitrate) position of the nitrate ester moiety and by the presence of the electron withdrawings groups (Cl, Br, NO_2) on aromatic ring. Moreover the presence of 1,3,4-oxadiazole moiety enhance significantly the amount of released NO than the presence of thiazolidine-4-one moiety, being comparable with SNP as reference drugs. In the working conditions it can appreciate that the majority of the compounds release from 4.4 to 14.7 more NO than reference drugs NTG.

The results obtained allowed to demonstrate that synthesized compounds presented encouraging results based on a multi-target strategy that had anti-inflammatory, antioxidant and nitric oxide releasing activity when compared with the reference drugs. Also, the results of our study strongly encouraging us to appreciate that the additional effects of the synthesized compounds may reduce the side effects of the use of indomethacin.

Chapter 12

Elements of originality and research perspectives

The research performed within PhD thesis targeted the design, synthesis and biological characterization of some new indomethacin nitric oxide donors, as new therapeutic multi-targets strategy.

The major novelty of this research consists in ***the original design of the developed indomethacin derivatives***, that contain three pharmacophore elements: (i) an indol structure, (ii) a 1,3-thiazolidine-4-one/1,3,4-oxadiazole scaffold and (iii) a nitric oxide donor nitrate ester, each of them with proved important biological effects.

Indomethacin is one of the most relevant NSAID used worldwide for the treatment of acute and chronic rheumatoid arthritis and other inflammatory rheumatic diseases, but its long-term clinical use is associated with severe side effects, especially at gastrointestinal level.

The *1,3-thiazolidine-4-one and 1,3,4-oxadizole*, respectively, are important scaffolds associated with beneficial biological effects sucs as anti-inflammatory, antioxidant, anticancer, anticonvulsant, antimicrobial, antiviral and anti HIV effects.

Nitric oxide is a remarkable endogenous molecule with a key role in a wide variety of physiological and pathophysiological processes, such as inflammation, vasodilatation, platelet adhesion, thrombosis neurotransmission, neuronal communication and wound healing

Based on the designed strategy, ***35 new original nitric oxide-releasing NSAIDs*** (19 NO-IND-TZDs and 16 NO-IND-OXDs) were synthesized. Also, it was obtained ***98 intermediaries*** organic molecules, which are not cited in the literature, from a total amount of 109 intermediaries.

Moreover, to obtain the indomethacin hydrazide, which was an important intermediary derivative, it was developed a ***more effective synthesis method*** that was proved to be rapid, convenient, proceeds under mild conditions and suitable for large scale preparation, compared with the methods cited in the literature.

The results obtained by ***computational and biological evaluation*** allowed to demonstrate that the newly indomethacin derivatives presented promising results in some of the effects evaluated when compared with the reference drugs.

This encouraging us to conclude that the designed multi-target compounds has anti-inflammatory, antioxidant and nitric oxide releasing activity, respectively. So, the 1,3-thiazoldine-4-one or 1,3,4-oxadiazole unit linked to a backbone containing a nitric oxide precursor appears to be play a role of a bioisoster commonly used in modern medicinal chemistry.

Bibliography

1. Hanke T, Merk D, Steinhilber D et al. Small molecules with anti-inflammatory properties in clinical development. *Pharmacol Ther* 2016; 157:163–87.
2. Rainsford KD. Anti-Inflammatory Drugs in the 21st Century. In: Harris JR (ed.). *Subcellular Biochemistry*.Vol 42., 2007:3–27.
3. Mahmud S, Rosen N. History of NSAID Use in the Treatment of Headaches Pre and Post-industrial Revolution in the United States: the Rise and Fall of Antipyrine, Salicylic Acid, and Acetanilide. *Curr Pain Headache Rep* 2019; 23 (1):6.
4. Rao P, Knaus EE. Evolution of Nonsteroidal Anti-Inflammatory Drugs (NSAIDs): Cyclooxygenase (COX) Inhibition and Beyond. *J Pharm Pharm Sci* 2008; 11 (2):81.
5. Blobaum AL, Marnett LJ. Structural and Functional Basis of Cyclooxygenase Inhibition. *J Med Chem* 2007; 50 (7):1425–41.
6. Korbut R, Guzik TJ. Inflammatory Mediators and Intracellular Signalling. In: Parnham MJ, Nijkamp FP, Rossi AG (eds.). *Nijkamp and Parnham's Principles of Immunopharmacology*. Cham: Springer International Publishing, 2019, 139–63.
7. Medzhitov R. Origin and physiological roles of inflammation. *Nature* 2008; 454 (7203):428–35.
8. Fullerton JN, Gilroy DW. Resolution of inflammation: A new therapeutic frontier. *Nat Rev Drug Discov* 2016; 15 (8):551–67.
9. Mollaei M, Abbasi A, Hassan ZM, Pakravan N. The intrinsic and extrinsic elements regulating inflammation. *Life Sci* 2020; 260 (August).
10. Elgazzar AH. Inflammation. In: Elgazzar AH (ed.). *Synopsis of Pathophysiology in Nuclear Medicine*. Cham: Springer International Publishing, 2014:41–57.
11. Libby P. Inflammatory Mechanisms: The Molecular Basis of Inflammation and Disease. *Nutr Rev* 2008; 65 (12):140–6.
12. Ahmed AU. An overview of inflammation: Mechanism and consequences. *Front Biol China* 2011; 6 (4):274–81.
13. Furman D, Campisi J, Verdin E et al. Chronic inflammation in the etiology of disease across the life span. *Nat Med* 2019; 25 (12):1822–32.
14. Tyagi V, Singh VK, Sharma PK, Singh V. Essential oil-based nanostructures for inflammation and rheumatoid arthritis. *J Drug Deliv Sci Technol* 2020; 60 (August).
15. Fantini MC, Guadagni I. From inflammation to colitis-associated colorectal cancer in inflammatory bowel disease: Pathogenesis and impact of current therapies. *Dig Liver Dis* 2021; 53(5): 558-565.
16. Díaz-Ruiz M, Martínez-Triguero ML, López-Ruiz A et al. Metabolic disorders and inflammation are associated with familial combined hyperlipemia. *Clin Chim Acta* 2019; 490 (September):194–9.
17. Tsalamandris S, Antonopoulos AS, Oikonomou E et al. The Role of Inflammation in Diabetes: Current Concepts and Future Perspectives. *Eur Cardiol Rev* 2019; 14 (1):50–9.
18. Karunakaran D, Turner AW, Duchez AC et al. RIPK1 gene variants associate with obesity in humans and can be therapeutically silenced to reduce obesity in mice. *Nat Metab* 2020; 2 (10):1113–25.
19. Alfaddagh A, Martin SS, Leucker TM et al. Inflammation and cardiovascular disease: From mechanisms to therapeutics. *Am J Prev Cardiol* 2020; 4 (October):100130.
20. Sethwala AM, Goh I, Amerena J V. Combating Inflammation in Cardiovascular Disease. *Hear Lung Circ* 2021; 30 (2):197–206.
21. Wyss-Coray T, Mucke L. Inflammation in neurodegenerative disease - A double-edged sword. *Neuron* 2002; 35 (3):419–32.
22. Kinney JW, Bemiller SM, Murtishaw AS et al. Inflammation as a central mechanism in Alzheimer's disease. *Alzheimer's Dement Transl Res Clin Interv* 2018; 4:575–90.
23. Collins LM, Toulouse A, Connor TJ, Nolan YM. Contributions of central and systemic inflammation to the pathophysiology of Parkinson's disease. *Neuropharmacology* 2012; 62 (7):2154–68.
24. Fishbein A, Hammock BD, Serhan CN, Panigrahy D. Carcinogenesis: Failure of resolution of inflammation? *Pharmacol Ther* 2021; 218:107670.
25. Honnappa CG, Kesavan UM. A concise review on advances in development of small molecule anti-inflammatory therapeutics emphasising AMPK: An emerging target. *Int J Immunopathol Pharmacol* 2016; 29 (4):562–71.
26. Wang K, Xiao J, Liu X et al. AICD: an integrated anti-inflammatory compounds database for drug discovery. *Sci Rep* 2019; 9 (1):1–10.
27. Abdulkhaleq LA, Assi MA, Abdullah R et al. The crucial roles of inflammatory mediators in inflammation: A review. Vet World 2018; 11(5): 627-635.
28. Smith WL, Murphy RC. The eicosanoids: cyclooxygenase, lipoxygenase, and epoxygenase pathways. In:

Vance JE, Vance D (eds.) *Biochemistry of Lipids, Lipoproteins and Membranes*.Vol36. Elsevier, 2008:331–62.
29. Dhanjal JK, Sreenidhi AK, Bafna K et al. Computational Structure-Based De Novo Design of Hypothetical Inhibitors against the Anti- Inflammatory Target COX-2. Salsbury F, ed. *PLoS One* 2015; 10 (8):e0134691.
30. Koeberle A, Werz O. Multi-target approach for natural products in inflammation. *Drug Discov Today* 2014; 19 (12):1871–82.
31. Charlier C, Michaux C. Dual inhibition of cyclooxygenase-2 (COX-2) and 5-lipoxygenase (5-LOX) as a new strategy to provide safer non-steroidal anti-inflammatory drugs. *Eur J Med Chem* 2003; 38 (7–8):645–59.
32. Seo M-J, Oh D-K. Prostaglandin synthases: Molecular characterization and involvement in prostaglandin biosynthesis. *Prog Lipid Res* 2017; 66:50–68.
33. Wood I, Trostchansky A, Xu Y et al. Free radical-dependent inhibition of prostaglandin endoperoxide H Synthase-2 by nitro-arachidonic acid. *Free Radic Biol Med* 2019; 144:176–82.
34. Regulski M, Regulska K, Prukała W et al. COX-2 inhibitors: a novel strategy in the management of breast cancer. *Drug Discov Today* 2016; 21 (4):598–615.
35. Smith WL, DeWitt DL, Garavito RM. Cyclooxygenases: Structural, Cellular, and Molecular Biology. *Annu Rev Biochem* 2000; 69 (1):145–82.
36. Bhardwaj A, Kaur J, Wuest M, Wuest F. In situ click chemistry generation of cyclooxygenase-2 inhibitors. *Nat Commun* 2017; 8 (1):1.
37. Miciaccia M, Belviso BD, Iaselli M et al. Three-dimensional structure of human cyclooxygenase (hCOX)-1. *Sci Rep* 2021; 11 (1):4312.
38. Uddin MJ, Crews BC, Ghebreselasie K et al. Fluorinated COX-2 Inhibitors as Agents in PET Imaging of Inflammation and Cancer. *Cancer Prev Res* 2011; 4 (10):1536 LP – 1545.
39. Zarghi A, Arfaei S. Selective COX-2 Inhibitors: A Review of Their Structure-Activity Relationships. *Iran J Pharm Res IJPR* 2011; 10 (4):655–83.
40. Rouzer CA, Marnett LJ. Cyclooxygenases: structural and functional insights. *J Lipid Res* 2009; 50:S29–34.
41. Lucido MJ, Orlando BJ, Vecchio AJ, Malkowski MG. Crystal Structure of Aspirin-Acetylated Human Cyclooxygenase-2: Insight into the Formation of Products with Reversed Stereochemistry. *Biochemistry* 2016; 55 (8):1226–38.
42. das Chagas Pereira de Andrade F, Mendes AN. Computational analysis of eugenol inhibitory activity in lipoxygenase and cyclooxygenase pathways. *Sci Rep* 2020; 10 (1):16204.
43. Michaux C, Charlier C. Structural Approach for COX-2 Inhibition. *Mini-Reviews Med Chem* 2004; 4 (6):603–15.
44. Warner TD, Mitchell JA. Cyclooxygenases: new forms, new inhibitors, and lessons from the clinic. *FASEB J* 2004; 18 (7):790–804.
45. Tavares MT, Primi MC, Silva NATF et al. Using an in Silico Approach To Teach 3D Pharmacodynamics of the Drug–Target Interaction Process Focusing on Selective COX2 Inhibition by Celecoxib. *J Chem Educ* 2017; 94 (3):380–7.
46. Malkowski MG, Ginell SL, Smith WL, Garavito RM. The Productive Conformation of Arachidonic Acid Bound to Prostaglandin Synthase. *Science* 2000; 289 (5486):1933 LP – 1937.
47. Reddy KK, Vidya Rajan VK, Gupta A et al. Exploration of binding site pattern in arachidonic acid metabolizing enzymes, Cyclooxygenases and Lipoxygenases. *BMC Res Notes* 2015; 8 (1):152.
48. Gundogdu-Hizliates C, Alyuruk H, Gocmenturk M et al. Synthesis of new ibuprofen derivatives with their in silico and in vitro cyclooxygenase-2 inhibitions. *Bioorg Chem* 2014; 52:8–15.
49. Sae-Tang D, Kittakoop P, Hannongbua S. Roles of key residues specific to cyclooxygenase II: an ONIOM study. *Monatshefte für Chemie - Chem Mon* 2009; 140 (12):1533.
50. Goodman MC, Xu S, Rouzer CA et al. Dual cyclooxygenase–fatty acid amide hydrolase inhibitor exploits novel binding interactions in the cyclooxygenase active site. *J Biol Chem* 2018; 293 (9):3028–38.
51. Patrignani P, Sacco A, Sostres C et al. Low-Dose Aspirin Acetylates Cyclooxygenase-1 in Human Colorectal Mucosa: Implications for the Chemoprevention of Colorectal Cancer. *Clin Pharmacol Ther* 2017; 102 (1):52–61.
52. Xu S, Uddin MJ, Banerjee S et al. Fluorescent indomethacin-dansyl conjugates utilize the membrane-binding domain of cyclooxygenase-2 to block the opening to the active site. *J Biol Chem* 2019; 294 (22):8690–8.
53. Kurumbail RG, Stevens AM, Gierse JK et al. Structural basis for selective inhibition of cyclooxygenase-2 by anti-inflammatory agents. *Nature* 1996; 384 (6610):644–8.
54. Wey S-J, Augustyniak ME, Cochran ED et al. Structure-Based Design, Synthesis, and Biological Evaluation of Indomethacin Derivatives as Cyclooxygenase-2 Inhibiting Nitric Oxide Donors. *J Med Chem* 2007; 50 (25):6367–82.
55. Pergola C, Werz O. 5-Lipoxygenase inhibitors: a review of recent developments and patents. *Expert Opin Ther Pat* 2010; 20 (3):355–75.
56. Rådmark O, Samuelsson B. 5-Lipoxygenase: mechanisms of regulation. *J Lipid Res* 2009; 50

(SUPPL.):S40–5.
57. Gür ZT, Çalışkan B, Banoglu E. Drug discovery approaches targeting 5-lipoxygenase-activating protein (FLAP) for inhibition of cellular leukotriene biosynthesis. *Eur J Med Chem* 2018; 153:34–48.
58. Reddy NP, Aparoy P, Reddy TCM, et al. Design, synthesis, and biological evaluation of prenylated chalcones as 5-LOX inhibitors. *Bioorg Med Chem* 2010; 18 (16):5807–15.
59. Shang E, Liu Y, Wu Y et al. Development of 3,5-dinitrobenzoate-based 5-lipoxygenase inhibitors. *Bioorg Med Chem* 2014; 22 (8):2396–402.
60. Bruno F, Spaziano G, Liparulo A et al. Recent advances in the search for novel 5-lipoxygenase inhibitors for the treatment of asthma. *Eur J Med Chem* 2018; 153:65–72.
61. Heidenreich KA, Corser-Jensen CE. 5-Lipoxygenase-Activating Protein Inhibitors: Promising Drugs for Treating Acute and Chronic Neuroinflammation Following Brain Injury. In: Heidenreich KA (ed.) *New Therapeutics for Traumatic Brain Injury*. San Diego: Academic Press, 2017:199–210.
62. Jaismy Jacob P, Manju SL, Ethiraj KR, Elias G. Safer anti-inflammatory therapy through dual COX-2/5-LOX inhibitors: A structure-based approach. *Eur J Pharm Sci* 2018; 121:356–81.
63. Ul-Haq Z, Khan N, Zafar SK, Moin ST. Active site characterization and structure based 3D-QSAR studies on non-redox type 5-lipoxygenase inhibitors. *Eur J Pharm Sci* 2016; 88:26–36.
64. Garscha U, Voelker S, Pace S et al. BRP-187: A potent inhibitor of leukotriene biosynthesis that acts through impeding the dynamic 5-lipoxygenase/5-lipoxygenase-activating protein (FLAP) complex assembly. *Biochem Pharmacol* 2016; 119:17–26.
65. Gilbert NC, Bartlett SG, Waight MT et al. The Structure of Human 5-Lipoxygenase. *Science* 2011; 331 (6014):217 LP – 219.
66. Werz O, Steinhilber D. Therapeutic options for 5-lipoxygenase inhibitors. *Pharmacol Ther* 2006; 112 (3):701–18.
67. Hemak J, Gale D, Brock TG. Structural characterization of the catalytic domain of the human 5-lipoxygenase enzyme. *Mol Model Annu* 2002; 8 (4):102–12.
68. Brain SD, Williams TJ. Leukotrienes and inflammation. *Pharmacol Ther* 1990; 46 (1):57–66.
69. Surette ME, Koumenis IL, Edens MB et al. Inhibition of leukotriene synthesis, pharmacokinetics, and tolerability of a novel dietary fatty acid formulation in healthy adult subjects. *Clin Ther* 2003; 25 (3):948–71.
70. Srivastava P, Vyas VK, Variya B et al. Synthesis, anti-inflammatory, analgesic, 5-lipoxygenase (5-LOX) inhibition activities, and molecular docking study of 7-substituted coumarin derivatives. *Bioorg Chem* 2016; 67:130–8.
71. Shen F-Q, Wang Z-C, Wu S-Y et al. Synthesis of novel hybrids of pyrazole and coumarin as dual inhibitors of COX-2 and 5-LOX. *Bioorg Med Chem Lett* 2017; 27 (16):3653–60.
72. Engelking LR. Eicosanoids I. In: Engelking LR (ed.) *Textbook of Veterinary Physiological Chemistry*.Vol 3. Elsevier, 2015:434–8.
73. Imazio M, Maestroni S, Valenti A et al. Desirable and Adverse Effects of Antiinflammatory Agents on the Heart. In: Nussinovitch U (ed.). *The Heart in Rheumatic, Autoimmune and Inflammatory Diseases*. Academic Press, 2017:617–43.
74. Gutiérrez JM, Lewin MR, Williams DJ, Lomonte B. Varespladib (LY315920) and Methyl Varespladib (LY333013) Abrogate or Delay Lethality Induced by Presynaptically Acting Neurotoxic Snake Venoms. *Toxins (Basel)* 2020; 12 (2):131.
75. Kapoor Y, Kumar K. Structural and clinical impact of anti-allergy agents: An overview. *Bioorg Chem* 2020; 94:103351.
76. Bell RL, Harris RR. The enzymology and pharmacology of 5-lipoxygenase and 5-lipoxygenase activating protein. *Clin Rev Allergy Immunol* 1999; 17 (1):91–109.
77. Forrester SJ, Kikuchi DS, Hernandes MS et al. Reactive Oxygen Species in Metabolic and Inflammatory Signaling. *Circ Res* 2018; 122 (6):877–902.
78. Perillo B, Di Donato M, Pezone A et al. ROS in cancer therapy: the bright side of the moon. *Exp Mol Med* 2020; 52 (2):192–203.
79. Luo H, Chiang H-H, Louw M et al. Nutrient Sensing and the Oxidative Stress Response. *Trends Endocrinol Metab* 2017; 28 (6):449–60.
80. Pizzino G, Irrera N, Cucinotta M et al. Oxidative Stress: Harms and Benefits for Human Health. *Oxid Med Cell Longev* 2017; 2017:1–13.
81. Sapbamrer R, Khacha-ananda S, Sittitoon N et al. A longitudinal follow-up study of oxidative stress and DNA damage among farmers exposed to pesticide mixtures. *Environ Sci Pollut Res* 2019; 26 (13):13185–94.
82. Chelombitko MA. Role of Reactive Oxygen Species in Inflammation: A Minireview. *Moscow Univ Biol Sci Bull* 2018; 73 (4):199–202.
83. Kattoor AJ, Pothineni NVK, Palagiri D, Mehta JL. Oxidative Stress in Atherosclerosis. *Curr Atheroscler Rep*

2017; 19 (11):42.
84. Chuang YC, Chang HM, Li CY et al. Reactive Oxygen Species and Inflammatory Responses of Macrophages to Substrates with Physiological Stiffness. *ACS Appl Mater Interfaces* 2020; 12 (43):48432–41.
85. Mittal M, Siddiqui MR, Tran K et al. Reactive Oxygen Species in Inflammation and Tissue Injury. *Antioxid Redox Signal* 2014; 20 (7):1126–67.
86. Salim S. Oxidative Stress and the Central Nervous System. *J Pharmacol Exp Ther* 2017; 360 (1):201–5.
87. Aguilar TAF, Navarro BCH, Pérez JAM. Endogenous Antioxidants: A Review of their Role in Oxidative Stress. In: Morales-Gonzales JA (ed.). *A Master Regulator of Oxidative Stress - The Transcription Factor Nrf2*. InTech, 2016.
88. Khansari N, Shakiba Y, Mahmoudi M. Chronic Inflammation and Oxidative Stress as a Major Cause of Age-Related Diseases and Cancer. *Recent Pat Inflamm Allergy Drug Discov* 2009; 3 (1):73–80.
89. Chen L, Deng H, Cui H et al. Inflammatory responses and inflammation-associated diseases in organs. *Oncotarget* 2018; 9 (6):7204–18.
90. Aronson JK. Indometacin. In: Aronson JK (ed.). *Meyler's Side Effects of Drugs*. Sixteenth. Oxford: Elsevier, 2016:61–70.
91. Lucas S. The Pharmacology of Indomethacin. *Headache J Head Face Pain* 2016; 56 (2):436–46.
92. Mohamed MFA, Marzouk AA, Nafady A et al. Design, synthesis and molecular modeling of novel aryl carboximidamides and 3-aryl-1,2,4-oxadiazoles derived from indomethacin as potent anti-inflammatory iNOS/PGE2 inhibitors. *Bioorg Chem* 2020; 105 (October):104439.
93. Stachowicz K. Indomethacin, a nonselective cyclooxygenase inhibitor, does not interact with MTEP in antidepressant-like activity, as opposed to imipramine in CD-1 mice. *Eur J Pharmacol* 2020; 888 (September):173585.
94. Qandil A. Prodrugs of Nonsteroidal Anti-Inflammatory Drugs (NSAIDs), More Than Meets the Eye: A Critical Review. *Int J Mol Sci* 2012; 13 (12):17244–74.
95. Shah K, Gupta JK, Chauhan NS et al. Prodrugs of NSAIDs: A Review. *Open Med Chem J* 2017; 11 (1):146–95.
96. Kalgutkar AS, Crews BC, Saleh S et al. Indolyl esters and amides related to indomethacin are selective COX-2 inhibitors. *Bioorg Med Chem* 2005; 13 (24):6810–22.
97. Kalgutkar AS, Crews BC, Rowlinson SW et al. Biochemically based design of cyclooxygenase-2 (COX-2) inhibitors: Facile conversion of nonsteroidal antiinflammatory drugs to potent and highly selective COX-2 inhibitors. *Proc Natl Acad Sci* 2000; 97 (2):925 LP – 930.
98. Ölgen S, Nebioğlu D. Synthesis and biological evaluation of N-substituted indole esters as inhibitors of cyclo-oxygenase-2 (COX-2). *Farm* 2002; 57 (8):677–83.
99. Kalgutkar AS, Marnett AB, Crews BC et al. Ester and Amide Derivatives of the Nonsteroidal Antiinflammatory Drug, Indomethacin, as Selective Cyclooxygenase-2 Inhibitors. *J Med Chem* 2000; 43 (15):2860–70.
100. Tammara VK, Narurkar MM, Crider AM, Khan MA. Synthesis and Evaluation of Morpholinoalkyl Ester Prodrugs of Indomethacin and Naproxen. *Pharm Res* 1993; 10 (8):1191–9.
101. Arockia Babu M, Shukla R, Nath C, Kaskhedikar SG. Synthesis and biological evaluation of ester derivatives of indomethacin as selective COX-2 inhibitors. *Med Chem Res* 2012; 21 (9):2223–8.
102. Sawraj S, Bhardawaj TR, Sharma PD. Design, synthesis, and evaluation of novel indomethacin–antioxidant codrugs as gastrosparing NSAIDs. *Med Chem Res* 2012; 21 (6):834–43.
103. Sawraj S, Bhardawaj TR, Sharma PD. Design, synthesis and evaluation of novel indomethacin–flavonoid mutual prodrugs as safer NSAIDs. *Med Chem Res* 2011; 20 (6):687–94.
104. Galanakis D, Kourounakis AP, Tsiakitzis KC et al. Synthesis and pharmacological evaluation of amide conjugates of NSAIDs with L-cysteine ethyl ester, combining potent antiinflammatory and antioxidant properties with significantly reduced gastrointestinal toxicity. *Bioorg Med Chem Lett* 2004; 14 (14):3639–43.
105. Dahan A, Duvdevani R, Dvir E et al. A novel mechanism for oral controlled release of drugs by continuous degradation of a phospholipid prodrug along the intestine: In-vivo and in-vitro evaluation of an indomethacin–lecithin conjugate. *J Control Release* 2007; 119 (1):86–93.
106. Halen PK, Chagti KK, Giridhar R, Yadav MR. Substituted aminoalcohol ester analogs of indomethacin with reduced toxic effects. *Med Chem Res* 2007; 16 (3):101–11.
107. Chowdhury MA, Huang Z, Abdellatif KRA et al. Synthesis and biological evaluation of indomethacin analogs possessing a N-difluoromethyl-1,2-dihydropyrid-2-one ring system: A search for novel cyclooxygenase and lipoxygenase inhibitors. *Bioorg Med Chem Lett* 2010; 20 (19):5776–80.
108. Ikeda A, Funakoshi E, Araki M et al. Structural modification of indomethacin toward selective inhibition of COX-2 with a significant increase in van der Waals contributions. *Bioorg Med Chem* 2019; 27 (9):1789–94.

109. Blobaum AL, Uddin MJ, Felts AS et al. The 2′-Trifluoromethyl Analogue of Indomethacin Is a Potent and Selective COX-2 Inhibitor. *ACS Med Chem Lett* 2013; 4 (5):486–90.
110. Kassab SE, Khedr MA, Ali HI, Abdalla MM. Discovery of new indomethacin-based analogs with potentially selective cyclooxygenase-2 inhibition and observed diminishing to PGE2 activities. *Eur J Med Chem* 2017; 141:306–21.
111. Brunelli C, Amici C, Angelini M et al. The non-steroidal anti-inflammatory drug indomethacin activates the eIF2α kinase PKR, causing a translational block in human colorectal cancer cells. *Biochem J* 2012; 443 (2):379–86.
112. Hojka-Osinska A, Ziolo E, Rapak A. Combined treatment with fenretinide and indomethacin induces AIF-mediated, non-classical cell death in human acute T-cell leukemia Jurkat cells. *Biochem Biophys Res Commun* 2012; 419 (3):590–5.
113. Cheng YL, Zhang GY, Li C, Lin J. Screening for novel protein targets of indomethacin in HCT116 human colon cancer cells using proteomics. *Oncol Lett* 2013; 6 (5):1222–8.
114. Farrag AM. Synthesis and Biological Evaluation of Novel Indomethacin Derivatives as Potential Anti-Colon Cancer Agents. *Arch Pharm (Weinheim)* 2016; 349 (12):904–14.
115. Xie G, Zhou D, Cheng KW et al. Comparative in vitro metabolism of phospho-tyrosol-indomethacin by mice, rats and humans. *Biochem Pharmacol* 2013; 85 (8):1195–202.
116. Harras MF, Sabour R, Ammar YA et al. Design synthesis and cytotoxicity studies of some novel indomethacin-based heterocycles as anticancer and apoptosis inducing agents. *J Mol Struct* 2021; 1228:129455.
117. Kaushik NK, Kaushik N, Attri P et al. Biomedical Importance of Indoles. *Molecules* 2013; 18 (6):6620–62.
118. Sahiba N, Sethiya A, Soni J et al. *Saturated Five-Membered Thiazolidines and Their Derivatives: From Synthesis to Biological Applications*. Springer International Publishing, 2020.
119. Bockman MR, Engelhart CA, Cramer JD et al. Investigation of (*S*)-(-)-acidomycin: A selective antimycobacterial natural product that inhibits biotin synthase. *ACS Infect Dis* 2019; 5 (4):598–617.
120. Trotsko N. Antitubercular properties of thiazolidin-4-ones – A review. *Eur J Med Chem* 2021:113266.
121. Schmidt U, Utz R, Lieberknecht A et al. Amino Acids and Peptides; 59. 1 Synthesis of Biologically Active Cyclopeptides; 9. 2 Synthesis of 16 Isomers of Dolastatin 3; 3 I. Synthesis of the 2-(1-aminoalkyl)-thiazole-4-carboxylic Acids. *Synthesis (Stuttg)* 1987; 1987 (03):233–6.
122. Mishchenko M, Shtrygol S, Kaminskyy D. Thiazole-Bearing 4-Thiazolidinones as New Anticonvulsant Agents. 2020.
123. Nazeef M, Neha K, Ali S et al. Journal of Photochemistry & Photobiology A : Chemistry Visible-light-promoted C e N and C e S bonds formation : A catalyst and solvent-free photochemical approach for the synthesis of 1 , 3-thiazolidin-4- ones. 2020; 390 (December 2019).
124. Popiołek Ł, Piątkowska-Chmiel I, Gawrońska-Grzywacz M et al. New hydrazide-hydrazones and 1,3-thiazolidin-4-ones with 3-hydroxy-2-naphthoic moiety: Synthesis, in vitro and in vivo studies. *Biomed Pharmacother* 2018; 103 (April):1337–47.
125. Huber-Villaume S, Revelant G, Sibille E et al. 2-(Thienothiazolylimino)-1,3-thiazolidin-4-ones inhibit cell division cycle 25 A phosphatase. *Bioorg Med Chem* 2016; 24 (13):2920–8.
126. Pejović A, Minić A, Jovanović J et al. Synthesis, characterization, antioxidant and antimicrobial activity of novel 5-arylidene-2-ferrocenyl-1,3-thiazolidin-4-ones. *J Organomet Chem* 2018; 869 (1):1–10.
127. Agrawal N. Synthetic and therapeutic potential of 4-thiazolidinone and its analogs. *Curr Chem Lett* 2021; 10 (1):119–38.
128. das Neves AM, Berwaldt GA, Avila CT et al. Synthesis of thiazolidin-4-ones and thiazinan-4-ones from 1-(2-aminoethyl)pyrrolidine as acetylcholinesterase inhibitors. *J Enzyme Inhib Med Chem* 2020; 35 (1):31–41.
129. Bielenica A, Sanna G, Madeddu S et al. New thiourea and 1,3-thiazolidin-4-one derivatives effective on the HIV-1 virus. *Chem Biol \& Drug Des* 2017; 90 (5):883–91.
130. Ayyash AN, Hammady AO. Synthesis and Bioactivity Screening of New 1, 3-Thiazolidin-4-One Compounds Bearing (Thiadiazols/Triazoles) Moieties. *J Phys Conf Ser* 2020; 1660:012025.
131. Tripathi AC, Gupta SJ, Fatima GN et al. 4-Thiazolidinones: The advances continue. *Eur J Med Chem* 2014; 72:52–77.
132. da Silva Santos J, Junior JJ, da Silva FM. 1,3-Thiazolidin-4-ones: Biological Potential, History, Synthetic Development and Green Methodologies. *Curr Org Synth* 2018; 15 (8):1109–23.
133. Nirwan S, Chahal V, Kakkar R. Thiazolidinones: Synthesis, Reactivity, and Their Biological Applications. *J Heterocycl Chem* 2019; 56 (4):1239–53.
134. Verma A, Saraf SK. 4-Thiazolidinone – A biologically active scaffold. *Eur J Med Chem* 2008; 43 (5):897–905.
135. Rahman VPM, Mukhtar S, Ansari WH, Lemiere G. Synthesis, stereochemistry and biological activity of some novel long alkyl chain substituted thiazolidin-4-ones and thiazan-4-one from 10-undecenoic acid

hydrazide. *Eur J Med Chem* 2005; 40 (2):173–84.
136. Cunico W, Gomes C, Vellasco Jr. W. Chemistry and Biological Activities of 1,3-Thiazolidin-4-ones. *Mini Rev Org Chem* 2008; 5 (4):336–44.
137. Arora M, Choudhary S, Singh PK et al. Structural investigation on the selective COX-2 inhibitors mediated cardiotoxicity: A review. *Life Sci* 2020; 251:117631.
138. Kaur Manjal S, Kaur R, Bhatia R et al. Synthetic and medicinal perspective of thiazolidinones: A review. *Bioorg Chem* 2017; 75:406–23.
139. B. Bari S, D. Firake S. Exploring Anti-inflammatory Potential of Thiazolidinone Derivatives of Benzenesulfonamide via Synthesis, Molecular Docking and Biological Evaluation. *Antiinflamm Antiallergy Agents Med Chem* 2016; 15 (1):44–53.
140. Anekal DP, Biradar JS. Synthesis and biological evaluation of novel Indolyl 4-thiazolidinones bearing thiadiazine nucleus. *Arab J Chem* 2017; 10:S2098–105.
141. Vasincu IM, Apotrosoaei M, Constantin S et al. New ibuprofen derivatives with thiazolidine-4-one scaffold with improved pharmaco-toxicological profile. *BMC Pharmacol Toxicol* 2021; 22 (1):10.
142. Gawrońska Grzywacz M, Popiołek L, Natorska Chomicka D et al. Novel 2,3-disubstituted 1,3-thiazolidin-4-one derivatives as potential antitumor agents in renal cell adenocarcinoma. *Oncol Rep* 2018; 41 (1):693–701.
143. Sharath Kumar KS, Hanumappa A, Vetrivel M et al. Antiproliferative and tumor inhibitory studies of 2,3 disubstituted 4-thiazolidinone derivatives. *Bioorg Med Chem Lett* 2015; 25 (17):3616–20.
144. Wang S, Zhao Y, Zhu W et al. Synthesis and Anticancer Activity of Indolin-2-one Derivatives Bearing the 4-Thiazolidinone Moiety. *Arch Pharm (Weinheim)* 2012; 345 (1):73–80.
145. Holota S, Kryshchyshyn A, Derkach H et al. Synthesis of 5-enamine-4-thiazolidinone derivatives with trypanocidal and anticancer activity. *Bioorg Chem* 2019; 86:126–36.
146. Rodrigues M do D, Santiago PBGS, Marques KMR et al. Selective cytotoxic and genotoxic activities of 5-(2-bromo-5-methoxybenzylidene)-thiazolidine-2,4-dione against NCI-H292 human lung carcinoma cells. *Pharmacol Reports* 2018; 70 (3):446–54.
147. Ottanà R, Carotti S, Maccari R et al. In vitro antiproliferative activity against human colon cancer cell lines of representative 4-thiazolidinones. Part I. *Bioorg Med Chem Lett* 2005; 15 (17):3930–3.
148. Kamel MM, Ali HI, Anwar MM et al. Synthesis, antitumor activity and molecular docking study of novel Sulfonamide-Schiff's bases, thiazolidinones, benzothiazinones and their C-nucleoside derivatives. *Eur J Med Chem* 2010; 45 (2):572–80.
149. Wang S, Zhao Y, Zhang G et al. Design, synthesis and biological evaluation of novel 4-thiazolidinones containing indolin-2-one moiety as potential antitumor agent. *Eur J Med Chem* 2011; 46 (8):3509–18.
150. Elkouzi A. What is parkinsons. *Dosegljivo http//www Park org/understanding-parkinsons/what-is-parkinsons[Dostopano 258 2018]* 2020.
151. Subramnian G, Rajagopal K, Sherin F. Molecular Docking Studies, In silico ADMET Screening of Some Novel Thiazolidine Substituted Oxadiazoles as Sirtuin 3 Activators Targeting Parkinson's Disease. *Res J Pharm Technol* 2020; 13 (6):2708.
152. Sidorova-Darmos E, Sommer R, Eubanks J. The Role of SIRT3 in the Brain Under Physiological and Pathological Conditions. *Front Cell Neurosci* 2018; 12(196):1-16.
153. Ren Z, Yang N, Ji C et al. Neuroprotective effects of 5-(4-hydroxy-3-dimethoxybenzylidene)-thiazolidinone in MPTP induced Parkinsonism model in mice. *Neuropharmacology* 2015; 93:209–18.
154. Gomathy S, Antony As, Elango K et al. Synthesis and anti-Parkinson′s screening of some novel 2-(naphthalen-1-yl)-N-[2-substituted (4-oxothiazolidin-3-yl)]acetamide derivatives. *Int J Heal Allied Sci* 2012; 1 (4):244.
155. Kumar S, Kaur H, Sharma M, Vishwakarma P. Synthesis and antiparkinsonian activity of some new adamantyl thiazolidinonyl/azeti-dinonyl indole derivatives. *Indian J Chem* 2010; 49B:1398–405.
156. Natarajan A, Beena PM, Devnikar AV, Mali S. A systemic review on tuberculosis. *Indian J Tuberc* 2020; 67 (3):295–311.
157. Golli AL, Nițu MF, Turcu F et al. Tuberculosis remains a public health problem in Romania. *Int J Tuberc Lung Dis* 2019; 23 (2):226–31.
158. Nitu FM, Olteanu M, Streba CT et al. Tuberculosis and its particularities in Romania and worldwide. *Rom J Morphol Embryol* 2017; 58 (2):385–92.
159. Palomino J, Ramos D, da Silva P. New Anti-Tuberculosis Drugs: Strategies, Sources and New Molecules. *Curr Med Chem* 2009; 16 (15):1898–904.
160. Rode HB, Lade DM, Grée R et al. Strategies towards the synthesis of anti-tuberculosis drugs. *Org Biomol Chem* 2019; 17 (22):5428–59.
161. Vintonyak VV, Warburg K, Over B et al. Identification and further development of thiazolidinones spiro-fused to indolin-2-ones as potent and selective inhibitors of Mycobacterium tuberculosis protein tyrosine phosphatase B. *Tetrahedron* 2011; 67 (35):6713–29.

162. Abo-Ashour MF, Eldehna WM, George RF et al. Synthesis and biological evaluation of 2-aminothiazole-thiazolidinone conjugates as potential antitubercular agents. *Future Med Chem* 2018; 10 (12):1405–19.
163. Ekinci AS, Moncol J, Krishna VS et al. 5-Methyl-4-thiazolidinones: Synthesis and evaluation as antitubercular agents. *J Res Pharm* 2020; 24(1):30-37.
164. Aridoss G, Amirthaganesan S, Kim MS et al. Synthesis, spectral and biological evaluation of some new thiazolidinones and thiazoles based on t-3-alkyl-r-2,c-6-diarylpiperidin-4-ones. *Eur J Med Chem* 2009; 44 (10):4199–210.
165. Ethell DW, Sidhu H. Matrix Metalloproteinases in Fragile X Syndrome. In: Willemsen R, Kooy RF (eds.). *Fragile X Syndrome*. Academic Press, 2017:301–22.
166. Laronha H, Caldeira J. Structure and Function of Human Matrix Metalloproteinases. *Cells* 2020; 9 (5).
167. Panico AM, Vicini P, Geronikaki A et al. Heteroarylimino-4-thiazolidinones as inhibitors of cartilage degradation. *Bioorg Chem* 2011; 39 (1):48–52.
168. Incerti M, Crascì L, Vicini P et al. 4-Thiazolidinone Derivatives as MMP Inhibitors in Tissue Damage: Synthesis, Biological Evaluation and Docking Studies. *Molecules* 2018; 23 (2).
169. Bozdag M, Angeli A, Tanc M. Mechanisms of action of carbonic anhydrase inhibitors: compounds that anchor to the zinc-bound nucleophile. In: Supuran CT, Nocentini A (eds.). *Carbonic Anhydrases*. Academic Press, 2019:223–43.
170. Blandina P, Supuran CT. Carbonic anhydrase activators and their potential in the pharmaceutical field. In: Supuran CT, Nocentini A (eds.). *Carbonic Anhydrases*. Academic Press, 2019:477–92.
171. Genc H, Ceken B, Bilen C et al. Synthesis and Biological Evaluation of New 4-Thiazolidinone Derivatives as Carbonic Anhydrase Inhibitors. *Lett Org Chem* 2017; 14 (2):80–5.
172. Anderson RC, Newton CL, Millar RP. Small Molecule Follicle-Stimulating Hormone Receptor Agonists and Antagonists. *Front Endocrinol (Lausanne)* 2019; 9:757.
173. Siwach A, Verma PK. Therapeutic potential of oxadiazole or furadiazole containing compounds. *BMC Chem* 2020; 14 (1):70.
174. Paruch K, Popiołek L, Biernasiuk A et al. Novel 3-Acetyl-2,5-disubstituted-1,3,4-oxadiazolines: Synthesis and Biological Activity. *Molecules* 2020; 25 (24):5844.
175. Salahuddin, Mazumder A, Yar MS et al. Updates on synthesis and biological activities of 1,3,4-oxadiazole: A review. *Synth Commun* 2017; 47 (20):1805–47.
176. Glomb T, Szymankiewicz K, Świątek P. Anti-Cancer Activity of Derivatives of 1,3,4-Oxadiazole. *Molecules* 2018; 23 (12):3361.
177. Glomb T, Wiatrak B, Gębczak K et al. New 1,3,4-Oxadiazole Derivatives of Pyridothiazine-1,1-Dioxide with Anti-Inflammatory Activity. *Int J Mol Sci* 2020; 21 (23):9122.
178. Yatam S, Jadav SS, Gundla R et al. Design, Synthesis and Biological Evaluation of 2 (((5-aryl-1,2,4-oxadiazol-3-yl)methyl)thio)benzo[d]oxazoles: New Antiinflammatory and Antioxidant Agents. *ChemistrySelect* 2018; 3 (37):10305–10.
179. Chawla G, Naaz B, Siddiqui AA. Exploring 1,3,4-Oxadiazole Scaffold for Anti-inflammatory and Analgesic Activities: A Review of Literature From 2005-2016. *Mini-Reviews Med Chem* 2018; 18 (3):216–33.
180. Alisi IO, Uzairu A, Abechi SE. Free radical scavenging mechanism of 1,3,4-oxadiazole derivatives: thermodynamics of O–H and N–H bond cleavage. *Heliyon* 2020; 6 (3):e03683.
181. Jakovljević K, Joksović MD, Botta B et al. Novel 1,3,4-thiadiazole conjugates derived from protocatechuic acid: Synthesis, antioxidant activity, and computational and electrochemical studies. *Comptes Rendus Chim* 2019; 22 (8):585–98.
182. Bhutani R, Pathak DP, Kapoor G et al. Novel hybrids of benzothiazole-1,3,4-oxadiazole-4-thiazolidinone: Synthesis, in silico ADME study, molecular docking and in vivo anti-diabetic assessment. *Bioorg Chem* 2019; 83 (August 2018):6–19.
183. Wang S, Liu H, Wang X et al. Synthesis of 1,3,4-oxadiazole derivatives with anticonvulsant activity and their binding to the GABAA receptor. *Eur J Med Chem* 2020; 206:112672.
184. Mohan CD, Anilkumar NC, Rangappa S et al. Novel 1,3,4-Oxadiazole Induces Anticancer Activity by Targeting NF-κB in Hepatocellular Carcinoma Cells. *Front Oncol* 2018; 8:1–11.
185. Makane VB, Krishna VS, Krishna EV et al. Novel 1,3,4-oxadiazoles as antitubercular agents with limited activity against drug-resistant tuberculosis. *Future Med Chem* 2019; 11 (6):499–510.
186. Raval JP, Akhaja TN, Jaspara DM, Myangar KN, Patel NH. Synthesis and in vitro antibacterial activity of new oxoethylthio-1,3,4-oxadiazole derivatives. *J Saudi Chem Soc* 2014; 18 (2):101–6.
187. Gan X, Hu D, Chen Z et al. Synthesis and antiviral evaluation of novel 1,3,4-oxadiazole/thiadiazole-chalcone conjugates. *Bioorg Med Chem Lett* 2017; 27 (18):4298–301.
188. Wang S, Qi L, Liu H et al. Synthesis of 1,3,4-oxadiazoles derivatives with antidepressant activity and their binding to the 5-HT 1A receptor. *RSC Adv* 2020; 10 (51):30848–57.
189. Ajani OO, Iyaye KT. Recent advances on oxadiazole motifs: Synthesis, reactions and biological activities.

Mediterr J Chem 2020; 10 (5):418.
190. Carbone M, Li Y, Irace C et al. Structure and Cytotoxicity of Phidianidines A and B: First Finding of 1,2,4-Oxadiazole System in a Marine Natural Product. *Org Lett* 2011; 13 (10):2516–9.
191. Nayak SG, Poojary B. A Review on the Preparation of 1,3,4-Oxadiazoles From the Dehydration of Hydrazines and Study of Their Biological Roles. *Chem Africa* 2019; 2 (4):551–71.
192. Boström J, Hogner A, Llinàs A et al. Oxadiazoles in Medicinal Chemistry. *J Med Chem* 2012; 55 (5):1817–30.
193. Vaidya A, Pathak D, Shah K. 1,3,4-oxadiazole and its derivatives: A review on recent progress in anticancer activities. *Chem Biol \& Drug Des* 2021; 97 (3):572–91.
194. Khalilullah H, Ahsan M, Hedaitullah M et al. 1,3,4-Oxadiazole: A Biologically Active Scaffold. *Mini-Reviews Med Chem* 2012; 12 (8):789–801.
195. Pal S, Bhattacharjee A, Ali A et al. Chronic inflammation and cancer: potential chemoprevention through nuclear factor kappa B and p53 mutual antagonism. *J Inflamm* 2014; 11 (1):23.
196. Popov SA, Semenova MD, Baev DS et al. Lupane-type conjugates with aminoacids, 1,3,4- oxadiazole and 1,2,5-oxadiazole-2-oxide derivatives: Synthesis, anti-inflammatory activity and in silico evaluation of target affinity. *Steroids* 2019; 150:108443.
197. Abd-Ellah HS, Abdel-Aziz M, Shoman ME et al. Novel 1,3,4-oxadiazole/oxime hybrids: Synthesis, docking studies and investigation of anti-inflammatory, ulcerogenic liability and analgesic activities. *Bioorg Chem* 2016; 69:48–63.
198. Abd-Ellah HS, Abdel-Aziz M, Shoman ME et al. New 1,3,4-oxadiazole/oxime hybrids: Design, synthesis, anti-inflammatory, COX inhibitory activities and ulcerogenic liability. *Bioorg Chem* 2017; 74:15–29.
199. Sharma S, Srivastava VK, Kumar A. Synthesis of some newer indolyl-thiadiazolyl-pyrazolines and indolyl-oxadiazolyl-pyrazolines as potential anti-inflammatory agents. *Indian J Chem* 2002; 41B:2647–54.
200. Khan M, Akhtar M. Synthesis of some new 2, 5-disubstituted 1,3,4-oxadiazole derivatives and their biological activity. *Indian J Chem* 2003; 42B:900–4.
201. Iyer VB, Gurupadayya B, Koganti VS et al. Design, synthesis and biological evaluation of 1,3,4-oxadiazoles as promising anti-inflammatory agents. *Med Chem Res* 2017; 26 (1):190–204.
202. Gupta A, Rawat S. Therapeutic Importance of Benzothiazole: Review. *Asian J Reserearch Chem* 2010; 3 (4):821–36.
203. Vishwanathan BI, Gurupadayya BM, Inturi B et al. Synthesis of 1,3,4-oxadiazoles as promising anticoagulant agents. *RSC Adv* 2016; 6 (29):24797–807.
204. Paudel YN, Ali MR, Shah S et al. 2-[(4-Chlorobenzyl) amino]-4-methyl-1,3-thiazole-5-carboxylic acid exhibits antidiabetic potential and raises insulin sensitivity via amelioration of oxidative enzymes and inflammatory cytokines in streptozotocin-induced diabetic rats. *Biomed Pharmacother* 2017; 89:651–9.
205. Faizi M, Jahani R, Ebadi SA et al. Novel 4-thiazolidinone derivatives as agonists of benzodiazepine receptors: Design, synthesis and pharmacological evaluation. *EXCLI J* 2017; 16:52–62.
206. Kumar S, Rathore D, Garg G et al. Synthesis and evaluation of some 2-((benzothiazol-2-ylthio) methyl)-5-phenyl-1, 3, 4-oxadiazole derivatives as antidiabetic agents. *Asian Pac J Health Sci* 2016; 3 (4):65-74.
207. Shyma PC, Kalluraya B, Peethambar SK, Vijesh AM. Synthesis, characterization, antidiabetic and antioxidant activity of 1,3,4-oxadiazole derivatives bearing 6-methyl pyridine moiety. *Der Pharma Chem* 2015; 7 (12):137–45.
208. Nazir M, Abbasi MA, Aziz-ur-Rehman et al. New indole based hybrid oxadiazole scaffolds with N-substituted acetamides: As potent anti-diabetic agents. *Bioorg Chem* 2018; 81:253–63.
209. Beghi E, Giussani G. Aging and the Epidemiology of Epilepsy. *Neuroepidemiology* 2018; 51 (3–4):216–23.
210. Löscher W, Potschka H, Sisodiya SM, Vezzani A. Drug Resistance in Epilepsy: Clinical Impact, Potential Mechanisms, and New Innovative Treatment Options. Barker EL (ed.). *Pharmacol Rev* 2020; 72 (3):606 LP – 638.
211. Nazar S, Siddiqui N, Alam O. Recent progress of 1,3,4-oxadiazoles as anticonvulsants: Future horizons. *Arch Pharm (Weinheim)* 2020; 353 (7):1900342.
212. Prasanna Kumar BN, Mohana KN, Mallesha L. Synthesis of *N*-[{5-Aryl-1,3,4-oxadiazole-2-yl}methyl]-4-methoxyaniline Derivatives and Their Anticonvulsant Activity. Ritieni A, ed. *J Chem* 2013; 2013:121029.
213. Mashayekh S, Rahmanipour N, Mahmoodi B et al. Synthesis, receptor affinity and effect on pentylenetetrazole-induced seizure threshold of novel benzodiazepine analogues: 3-Substituted 5-(2-phenoxybenzyl)-4H-1,2,4-triazoles and 2-amino-5-(phenoxybenzyl)-1,3,4-oxadiazoles. *Bioorg Med Chem* 2014; 22 (6):1929–37.
214. Singh RB, Singh GK, Chaturvedi K et al. Design, synthesis, characterization, and molecular modeling studies of novel oxadiazole derivatives of nipecotic acid as potential anticonvulsant and antidepressant agents. *Med Chem Res* 2018; 27 (1):137–52.
215. Divekar K, Vedigounder M, Sharma R. Synthesis and characterization of some new oxadiazole derivatives as anticonvulsant agents. *Eur J Pharm Med Res* 2018; 5 (9):276–81.

216. Khatoon Y, Shaquiquzzaman M, Singh V, Sarafroz M. Synthesis, anticonvulsant and neurotoxicity screening of some novel 2,5-disubstituted-1,3,4-oxadiazole derivatives. *Int J Pharm Sci Drug Res* 2017; 9 (1):22–9.
217. Rajak H, Singh Thakur B, Singh A et al. Novel limonene and citral based 2,5-disubstituted-1,3,4-oxadiazoles: A natural product coupled approach to semicarbazones for antiepileptic activity. *Bioorg Med Chem Lett* 2013; 23 (3):864–8.
218. Botros S, Khalil NA, Naguib BH, El-Dash Y. Synthesis and anticonvulsant activity of new phenytoin derivatives. *Eur J Med Chem* 2013; 60:57–63.
219. Kontoghiorghes GJ, Kontoghiorghe CN. Prospects for the introduction of targeted antioxidant drugs for the prevention and treatment of diseases related to free radical pathology. *Expert Opin Investig Drugs* 2019; 28 (7):593–603.
220. Egbujor MC, Egu SA, Okonkwo VI et al. Antioxidant Drug Design: Historical and Recent Developments. *J Pharm Res Int* 2021; 32 (41):36–56.
221. Baunthiyal M, Singh V, Dwivedi S. Insights of Antioxidants as Molecules for Drug Discovery. *Int J Pharmacol* 2017; 13 (7):874–89.
222. Mihailovic N, Markovic V, Matic IZ et al. Synthesis and antioxidant activity of 1,3,4-oxadiazoles and their diacylhydrazine precursors derived from phenolic acids. *RSC Adv* 2017; 7 (14):8550–60.
223. Basappa VC, Penubolu S, Achutha DK, Kariyappa AK. Synthesis, characterization and antioxidant activity studies of new coumarin tethered 1,3,4-oxadiazole analogues. *J Chem Sci* 2021; 133 (2):55.
224. Ünver Y, Gökce H, Bektaş E et al. New bis 1,3,4-oxadiazole derivatives: syntheses, characterizations, computational studies, and antioxidant activities. *Can J Chem* 2018; 96 (12):1047–59.
225. Sauer AC, Leal JG, Stefanello ST et al. Synthesis and antioxidant properties of organosulfur and organoselenium compounds derived from 5-substituted-1,3,4-oxadiazole/thiadiazole-2-thiols. *Tetrahedron Lett* 2017; 58 (1):87–91.
226. Musad EA, Mohamed R, Ali Saeed B et al. Synthesis and evaluation of antioxidant and antibacterial activities of new substituted bis(1,3,4-oxadiazoles), 3,5-bis(substituted) pyrazoles and isoxazoles. *Bioorg Med Chem Lett* 2011; 21 (12):3536–40.
227. Kotaiah Y, Harikrishna N, Nagaraju K, Venkata Rao C. Synthesis and antioxidant activity of 1,3,4-oxadiazole tagged thieno[2,3-d]pyrimidine derivatives. *Eur J Med Chem* 2012; 58:340–5.
228. Swapna M, Premakumari C, Nagi Reddy S et al. Synthesis and Antioxidant Activity of a Variety of Sulfonamidomethane Linked 1,3,4-Oxadiazoles and Thiadiazoles. *Chem Pharm Bull* 2013; 61 (6):611–7.
229. Dinesha, Viveka S, Chandra S, Nagaraja GK. Synthesis, characterization, and pharmacological screening of new 1,3,4-oxadiazole derivatives possessing 3-fluoro-4-methoxyphenyl moiety. *Monatshefte für Chemie - Chem Mon* 2015; 146 (1):207–14.
230. Bondock S, Adel S, Etman HA. Synthesis and antioxidant evaluation of some new 2-benzoylamino-5-hetaryl-1,3,4-oxadiazoles. *Res Chem Intermed* 2016; 42 (3):1845–61.
231. Lancaster JR. A Concise History of the Discovery of Mammalian Nitric Oxide (Nitrogen Monoxide) Biogenesis. In: Ignarro LJ, Freeman BA (eds.). *Nitric Oxide (Third Edition)*. Third Edit. Academic Press, 2017:1–7.
232. Keeton JT. History of Nitrite and Nitrate in Food. In: Bryan NS, Loscalzo J (eds.). *Nitrite and Nitrate in Human Health and Disease*. Totowa, NJ: Humana Press, 2011:69–84.
233. Omar SA, Artime E, Webb AJ. A comparison of organic and inorganic nitrates/nitrites. *Nitric Oxide* 2012; 26 (4):229–40.
234. Anon. Commission Regulation (EU) No 1129/2011 of 11 November 2011 amending Annex II to Regulation (EC) No 1333/2008 of the European Parliament and of the Council by establishing a Union list of food additives.
235. Yetik-Anacak G, Catravas JD. Nitric oxide and the endothelium: History and impact on cardiovascular disease. *Vascul Pharmacol* 2006; 45 (5):268–76.
236. Procházková D, Wilhelmová NN, Pavlík M. Reactive Nitrogen Species and Nitric Oxide. In: Khan MN, Mobin M, Mohammad F, Corpas FJ, eds. *Nitric Oxide Action in Abiotic Stress Responses in Plants*. Cham: Springer International Publishing, 2015:3–19.
237. McCleverty JA. Chemistry of Nitric Oxide Relevant to Biology. *Chem Rev* 2004; 104 (2):403–18.
238. Toledo JC, Augusto O. Connecting the Chemical and Biological Properties of Nitric Oxide. *Chem Res Toxicol* 2012; 25 (5):975–89.
239. Clayden J, Greeves N, Warren S. Structure of molecules. In: Clayden J, Greeves N, Warren S (eds.). *Organic chemistry*. 2nd ed. New York, NY: Oxford University Press Inc, 2012:80–106.
240. Bianco CL, Toscano JP, Fukuto JM. An Integrated View of the Chemical Biology of NO, CO, H2S, and O2. In: Ignarro LJ, Freeman BA (eds.). *Nitric Oxide (Third Edition)*. Third Edit. Academic Press, 2017:9–21.
241. Hughes MN. Chemistry of Nitric Oxide and Related Species. In: Poole RK (ed.). *Globins and Other Nitric*

Oxide-Reactive Proteins, Part A.Vol 436. Methods in Enzymology. MA USA: Academic Press, 2008:3–19.
242. Roszer T. Nitric Oxide is a Bioproduct in Prokaryotes. In: Roszer T (ed.). *The Biology of Subcellular Nitric Oxide*. Dordrecht: Springer Netherlands, 2012:19–46.
243. Szabó C, Ischiropoulos H, Radi R. Peroxynitrite: biochemistry, pathophysiology and development of therapeutics. *Nat Rev Drug Discov* 2007; 6 (8):662–80.
244. Kim-Shapiro DB, Gladwin MT. Heme Protein Metabolism of NO and Nitrite. In: Ignarro LJ, Freeman BA, (eds.). *Nitric Oxide (Third Edition)*. Third Edit. Academic Press, 2017:85–96.
245. Hunt AP, Lehnert N. Heme-Nitrosyls: Electronic Structure Implications for Function in Biology. *Acc Chem Res* 2015; 48 (7):2117–25.
246. Traylor TG, Sharma VS. Why nitric oxide? *Biochemistry* 1992; 31 (11):2847–9.
247. Williams DLH. Nitric oxide in biological systems. In: Williams DLH (ed.). *Nitrosation Reactions and the Chemistry of Nitric Oxide*.Vol 18. The Netherlands: Elsevier, 2004:187–98.
248. Cantu-Medellin N, Vitturi DA, Rodriguez C et al. Effects of T- and R-state stabilization on deoxyhemoglobin-nitrite reactions and stimulation of nitric oxide signaling. *Nitric Oxide* 2011; 25 (2):59–69.
249. Broniowska KA, Hogg N. The Chemical Biology of S-Nitrosothiols. *Antioxidants & Redox Signal* 2012; 17 (7):969–80.
250. Jourd'heuil D, Jourd'heuil FL, Feelisch M. Oxidation and Nitrosation of Thiols at Low Micromolar Exposure to Nitric Oxide: Evidence For A Free Radical Mechanism. *J Biol Chem* 2003; 278 (18):15720–6.
251. Wolosker H, Panizzutti R, Engelender S. Inhibition of creatine kinase by S-nitrosoglutathione. *FEBS Lett* 1996; 392 (3):274–6.
252. Galatro A, Puntarulo S. An Update to the Understanding of Nitric Oxide Metabolism in Plants BT - Nitric Oxide in Plants: Metabolism and Role in Stress Physiology. In: Khan MN, Mobin M, Mohammad F, Corpas FJ (eds.). Cham: Springer International Publishing, 2014:3–15.
253. Lundberg JO, Weitzberg E. Nitric Oxide Formation From Inorganic Nitrate. In: Ignaro L, Freeman B (eds.). *Nitric Oxide*. Third Edit. The Netherlands: Elsevier Amsterdam, 2017:157–71.
254. Kumar S, Singh RK, Bhardwaj TR. Therapeutic role of nitric oxide as emerging molecule. *Biomed Pharmacother* 2017; 85:182–201.
255. Förstermann U, Boissel JP, Kleinert H. Expressional control of the "constitutive" isoforms of nitric oxide synthase (NOS I and NOS III). *FASEB J Off Publ Fed Am Soc Exp Biol* 1998; 12 (10):773–90.
256. Kakizawa S. Nitric Oxide. In: Gruol DL, Koibuchi N, Manto M, Molinari M, Schmahmann JD, Shen Y, (eds.). *Essentials of Cerebellum and Cerebellar Disorders: A Primer For Graduate Students*. Cham: Springer International Publishing, 2016:249–53.
257. Asakura H, Kitahora T. Antioxidants and Polyphenols in Inflammatory Bowel Disease: Ulcerative Colitis and Crohn Disease. In: Watson RR, Preedy VR, Zibadi S (eds.). *Polyphenols: Prevention and Treatment of Human Disease (Second Edition)*. Academic Press, 2018:279–92.
258. Fleming I. NO Signaling Defects in Hypertension. In: Ignarro LJ, Freeman BA (eds.). *Nitric Oxide (Third Edition)*. Academic Press, 2017:301–11.
259. da Luz PL, Favarato D, Berwanger O. Action of Red Wine and Polyphenols Upon Endothelial Function and Clinical Events. In: Da Luz PL, Libby P, Chagas ACP, Laurindo FRM (eds.). *Endothelium and Cardiovascular Diseases*. Academic Press, 2018:391–418.
260. Junho CVC, Caio-Silva W, Trentin-Sonoda M, Carneiro-Ramos MS. An Overview of the Role of Calcium/Calmodulin-Dependent Protein Kinase in Cardiorenal Syndrome. *Front Physiol* 2020; 11:735.
261. Piazza M, Guillemette JG, Dieckmann T. Dynamics of Nitric Oxide Synthase–Calmodulin Interactions at Physiological Calcium Concentrations. *Biochemistry* 2015; 54 (11):1989–2000.
262. Lundberg JO, Weitzberg E, Gladwin MT. The nitrate–nitrite–nitric oxide pathway in physiology and therapeutics. *Nat Rev Drug Discov* 2008; 7 (2):156–67.
263. Petersson J. *Nitrate, nitrite and nitric oxide in gastric mucosal defense*. Uppsala University, Sweden, 2008, 1-92.
264. Kochar NI, Chandewal AV, Bakal RL, Kochar PN. Nitric Oxide and the Gastrointestinal Tract. *Int J Pharmacol* 2010; 7 (1):31–9.
265. Zhao Y, Vanhoutte PM, Leung SWS. Vascular nitric oxide: Beyond eNOS. *J Pharmacol Sci* 2015; 129 (2):83–94.
266. Sharma JN, Al-Omran A, Parvathy SS. Role of nitric oxide in inflammatory diseases. *Inflammopharmacology* 2007; 15 (6):252–9.
267. Hirst DG, Robson T. Nitric Oxide Physiology and Pathology. In: Walker JM (ed.). *Methods in molecular biology*.Vol 704. NJ USA: Humana Press Totowa, 2011:1–13.
268. Hirst DG, Robson T. Nitric Oxide Physiology and Pathology. In: Walker JM (ed.). *Methods in molecular biology (Clifton, N.J.)*.Vol 704., 2011:1–13.
269. Lanas A. Role of nitric oxide in the gastrointestinal tract. *Arthritis Res Ther* 2008; 10 (Suppl 2):S4.

270. Santana APM, Tavares BM, Lucetti LT et al. The nitric oxide donor cis-[Ru(bpy)2(SO3)NO](PF6) increases gastric mucosa protection in mic-Involvement of the soluble guanylate cyclase/KATP pathway. *Nitric Oxide* 2015; 45:35–42.
271. Yu B, Ichinose F, Bloch DB, Zapol WM. Inhaled nitric oxide. *Br J Pharmacol* 2019; 176 (2):246–55.
272. Scatena R, Bottoni P, Martorana GE, Giardina B. Nitric oxide donor drugs: an update on pathophysiology and therapeutic potential. *Expert Opin Investig Drugs* 2005; 14 (7):835–46.
273. Liang H, Nacharaju P, Friedman A, Friedman JM. Nitric oxide generating/releasing materials. *Futur Sci OA* 2015; 1 (1).
274. Yang Y, Huang Z, Li LL. Advanced nitric oxide donors: chemical structure of NO drugs, NO nanomedicines and biomedical applications. *Nanoscale* 2021; 13 (2):444–59.
275. Brunton TL. On the use of nitrite of amyl in angina pectoris. *Lancet* 1867; 2 (2291):97–8.
276. Murrell W. Nitro-glycerine as a remedy for angina pectoris. *Lancet* 1879; 113 (2890):80–1.
277. Conaghan PG. A turbulent decade for NSAIDs: Update on current concepts of classification, epidemiology, comparative efficacy, and toxicity. *Rheumatol Int* 2012; 32 (6):1491–502.
278. Kaur G, Silakari O. Multiple target-centric strategy to tame inflammation. *Future Med Chem* 2017; 9 (12):1361–76.
279. Moore N, Duong M, Gulmez SE et al. Pharmacoepidemiology of non-steroidal anti-inflammatory drugs. *Therapies* 2019; 74 (2):271–7.
280. Arfè A, Scotti L, Varas-Lorenzo C et al. Non-steroidal anti-inflammatory drugs and risk of heart failure in four European countries: nested case-control study. *BMJ* 2016; 354:i4857.
281. Hirschfield GM, Heathcote EJ, Gershwin ME. Pathogenesis of Cholestatic Liver Disease and Therapeutic Approaches. *Gastroenterology* 2010; 139 (5):1481–96.
282. Nunes AP, Costa IM, Costa FA. Determinants of self-medication with NSAIDs in a Portuguese community pharmacy. *Pharm Pract* 2016; 14:0.
283. Aranguren I, Elizondo G, Azparren A. Safety considerations for NSAIDs. *Drug Ther Bull Navarre* 2016; 24 (2):1–13.
284. Wongrakpanich S, Wongrakpanich A, Melhado K, Rangaswami J. A comprehensive review of non-steroidal anti-inflammatory drug use in the elderly. *Aging Dis* 2018; 9 (1):143–50.
285. Spiller F, Oliveira Formiga R, Fernandes da Silva Coimbra J et al. Targeting nitric oxide as a key modulator of sepsis, arthritis and pain. *Nitric Oxide* 2019; 89:32–40.
286. Ramsay RR, Popovic-Nikolic MR, Nikolic K et al. A perspective on multi-target drug discovery and design for complex diseases. *Clin Transl Med* 2018; 7 (1):3.
287. Hada K, Suda A, Asoh K et al. Angiogenesis inhibitors identified by cell-based high-throughput screening: Synthesis, structure–activity relationships and biological evaluation of 3-[(E)-styryl]benzamides that specifically inhibit endothelial cell proliferation. *Bioorg Med Chem* 2012; 20 (4):1442–60.
288. Ortmeyer CP, Haufe G, Schwegmann K et al. Synthesis and evaluation of a [18 F]BODIPY-labeled caspase-inhibitor. *Bioorg Med Chem* 2017; 25 (7):2167–76.
289. del Carmen Gimenez-Lopez M, Räisänen MT, Chamberlain TW et al. Functionalized Fullerenes in Self-Assembled Monolayers. *Langmuir* 2011; 27 (17):10977–85.
290. Liu X, Yang Y, Wang X et al. Design, synthesis and biological evaluation of novel α-hederagenin derivatives with anticancer activity. *Eur J Med Chem* 2017; 141:427–39.
291. Liu J, Zhang C, Wang H et al. Incorporation of nitric oxide donor into 1,3-dioxyxanthones leads to synergistic anticancer activity. *Eur J Med Chem* 2018; 151:158–72.
292. Nortcliffe A, Fleming IN, Botting NP, O'Hagan D. Synthesis and anticancer properties of RGD peptides conjugated to nitric oxide releasing functional groups and abiraterone. *Tetrahedron* 2014; 70 (44):8343–7.
293. Ward DE, Rhee CK. Chemoselective reductions with sodium borohydride. *Can J Chem* 1989; 67 (7):1206–11.
294. Gisch N, Balzarini J, Meier C. Enzymatically Activated cyclo Sal-d4T-monophosphates: The Third Generation of cyclo Sal-Pronucleotides. *J Med Chem* 2007; 50 (7):1658–67.
295. Ghazy E, Zeyen P, Herp D et al. Design, synthesis, and biological evaluation of dual targeting inhibitors of histone deacetylase 6/8 and bromodomain BRPF1. *Eur J Med Chem* 2020; 200:112338.
296. Ikegashira K, Ikenogami T, Yamasaki T et al. Optimization of an azetidine series as inhibitors of colony stimulating factor-1 receptor (CSF-1R) Type II to lead to the clinical candidate JTE-952. *Bioorg Med Chem Lett* 2019; 29 (7):873–7.
297. Liu X, Yang Y, Wang X et al. Design, synthesis and biological evaluation of novel α-hederagenin derivatives with anticancer activity. *Eur J Med Chem* 2017; 141:427–39.
298. Chen Y, Sun J, Huang Z et al. Design, synthesis and evaluation of tacrine–flurbiprofen–nitrate trihybrids as novel anti-Alzheimer's disease agents. *Bioorg Med Chem* 2013; 21 (9):2462–70.
299. Lazzarato L, Donnola M, Rolando B et al. (Nitrooxyacyloxy)methyl Esters of Aspirin as Novel Nitric Oxide Releasing Aspirins. *J Med Chem* 2009; 52 (16):5058–68.

300. Liu W, Liu C, Gong C et al. Porphyrins containing nitric oxide donors: Synthesis and cancer cell-oriented NO release. *Bioorg Med Chem Lett* 2009; 19 (6):1647–9.
301. Fotopoulou T, Iliodromitis EK, Koufaki M et al. Design and synthesis of nitrate esters of aromatic heterocyclic compounds as pharmacological preconditioning agents. *Bioorg Med Chem* 2008; 16 (8):4523–31.
302. Chaudhari SS, Akamanchi KG. Thionyl Chloride-Benzotriazole in Methylene Chloride: A Convenient Solution for Conversion of Alcohols and Carboxylic Acids Expeditiously into Alkyl Chlorides and Acid Chlorides by Simple Titration. *Synlett* 1999; 1999 (11):1763–5.
303. Bandgar BP, Bettigeri SV. Efficient and Selective Halogenation of Allylic and Benzylic Alcohols under Mild Conditions. *Monatshefte für Chemie* 2004; 135 (10):1251–5.
304. Wang Q, Hu W, Wang S et al. Synthesis of new 2′-deoxy-2′-fluoro-4′-azido nucleoside analogues as potent anti-HIV agents. *Eur J Med Chem* 2011; 46 (9):4178–83.
305. Shan Y, Wang J, Si R et al. Exploring the potential intracellular targets of vascular normalization based on active candidates. *Bioorg Chem* 2021; 108:104551.
306. Sekino T, Sato S, Kuwabara K et al. Allyl 4-Chlorophenyl Sulfone as a Versatile 1,1-Synthon for Sequential α-Alkylation/Cobalt-Catalyzed Allylic Substitution. *Synthesis (Stuttg)* 2020; 52 (13):1934–46.
307. Zhang X, Breslav M, Grimm J et al. A New Procedure for Preparation of Carboxylic Acid Hydrazides. *J Org Chem* 2002; 67 (26):9471–4.
308. Chan LC, Cox BG. Kinetics of Amide Formation through Carbodiimide/*N*-Hydroxybenzotriazole (HOBt) Couplings. *J Org Chem* 2007; 72 (23):8863–9.
309. Pires Gouvea D, Vasconcellos FA, dos Anjos Berwaldt G et al. 2-Aryl-3-(2-morpholinoethyl)thiazolidin-4-ones: Synthesis, anti-inflammatory in vivo, cytotoxicity in vitro and molecular docking studies. *Eur J Med Chem* 2016; 118:259–65.
310. Abdellatif KRA, Abdelgawad MA, Elshemy HAH, Alsayed SSR. Design, synthesis and biological screening of new 4-thiazolidinone derivatives with promising COX-2 selectivity, anti-inflammatory activity and gastric safety profile. *Bioorg Chem* 2016; 64:1–12.
311. Gurenko AO, Khutova BM, Klyuchko SV et al. Synthesis of Novel Pyrazolo[3,4-d][1,2,3]Triazines. *Chem Heterocycl Compd* 2014; 50 (4):528–36.
312. Chen J, Wei C, Wu S et al. Novel 1,3,4-oxadiazole thioether derivatives containing flexible-chain moiety: Design, synthesis, nematocidal activities, and pesticide-likeness analysis. *Bioorg Med Chem Lett* 2020; 30 (8):127028.
313. Narella SG, Shaik MG, Mohammed A et al. Synthesis and biological evaluation of coumarin-1,3,4-oxadiazole hybrids as selective carbonic anhydrase IX and XII inhibitors. *Bioorg Chem* 2019; 87 (April):765–72.
314. Zabiulla, Gulnaz AR, Mohammed YHE, Khanum SA. Design, synthesis and molecular docking of benzophenone conjugated with oxadiazole sulphur bridge pyrazole pharmacophores as anti inflammatory and analgesic agents. *Bioorg Chem* 2019; 92 (August):103220.
315. Karabanovich G, Němeček J, Valášková L et al. S-substituted 3,5-dinitrophenyl 1,3,4-oxadiazole-2-thiols and tetrazole-5-thiols as highly efficient antitubercular agents. *Eur J Med Chem* 2017; 126:369–83.
316. Roh J, Karabanovich G, Vlčková H et al. Development of water-soluble 3,5-dinitrophenyl tetrazole and oxadiazole antitubercular agents. *Bioorg Med Chem* 2017; 25 (20):5468–76.
317. Münzel T, Steven S, Daiber A. Organic nitrates: Update on mechanisms underlying vasodilation, tolerance and endothelial dysfunction. *Vascul Pharmacol* 2014; 63 (3):105–13.
318. Balarini CM, Cruz JC, Alves JLB, França-Silva MS, Braga VA. Developing New Organic Nitrates for Treating Hypertension. In: Seabra AB (ed.). *Nitric Oxide Donors*. Academic Press, 2017:243–62.
319. Low SY. Application of pharmaceuticals to nitric oxide. *Mol Aspects Med* 2005; 26 (1):97–138.
320. Wang PG, Xian M, Tang X et al. Nitric Oxide Donors: Chemical Activities and Biological Applications. *Chem Rev* 2002; 102 (4):1091–134.
321. An J, Liu P, Si M et al. Practical catalytic nitration directly with commercial nitric acid for the preparation of aliphatic nitroesters. *Org Biomol Chem* 2020; 18 (34):6612–6.
322. Klimochkin YN, Yudashkin AV, Zhilkina EO, Ivleva EA, Moiseev IK, Oshis YF. One-pot synthesis of cage alcohols. *Russ J Org Chem* 2017; 53 (7):971–6.
323. Bézière N, Goossens L, Pommery J et al. New NSAIDs-NO hybrid molecules with antiproliferative properties on human prostatic cancer cell lines. *Bioorg Med Chem Lett* 2008; 18 (16):4655–7.
324. Hwu JR, Vyas KA, Patel HV, Lin CH, Yang JC. Practical Method for the Preparation of Nitrate Esters. *Synthesis (Stuttg)* 1994; 1994 (05):471–3.
325. Olah GA, Narang SC, Pearson RL, Cupas CA. Synthetic Methods and Reactions; 48: Convenient and Safe Preparation of Alkyl Nitrates (Polynitrates) via Transfer Nitration of Alcohols (Polyols) with <inline-formula>N</inline-formula>-Nitrocollidinium Tetrafluoroborate. In: *Across Conventional Lines*., :993–4.
326. Amata E, Dichiara M, Gentile D et al. Sigma Receptor Ligands Carrying a Nitric Oxide Donor Nitrate

Moiety: Synthesis, In Silico, and Biological Evaluation. *ACS Med Chem Lett* 2020; 11 (5):889–94.
327. Xie YD, Liu JP, Wang W et al. 3,4-Dihydroxyphenethyl nitrate with nitric oxide releasing, antioxidant, hypoglycemic and hypolipidemic effects. *Bioorg Med Chem Lett* 2020; 30 (15):127277.
328. Liu Y, Ho TC, Baradwan M et al. Synthesis of Functionalized Cannabilactones. *Molecules* 2020; 25 (3):684.
329. Ram RN, Soni VK. Synthesis of α-Functionalized Trichloromethylcarbinols. *J Org Chem* 2015; 80 (17):8922–8.
330. Jawabrah Al-Hourani B, El-Barghouthi MI, Al-Awaida W et al. Biomolecular docking, synthesis, crystal structure, and bioassay studies of 1-[4-(2-chloroethoxy)phenyl]-5-[4-(methylsulfonyl)phenyl]-1H-tetrazole and 2-(4-(5-(4-(methylsulfonyl)phenyl)-1H-tetrazol-1-yl)phenoxy)ethyl nitrate. *J Mol Struct* 2020; 1202:127323.
331. Itoh A, Miura T, Tada N. Oxidation of Carbon_Halogen Bonds. In: Knochel P (ed.). *Comprehensive Organic Chemistry (Second Edition)*, Amsterdam: Elsevier, 2014, 744-769.
332. Wuts PGM, Greene TW. Protection for the Thiol Group. In: Wuts PGM, Greene TW. (eds.). *Greene's Protective Groups in Organic Synthesis*. John Wiley & Sons, Ltd, 2006:647–95.
333. Gadegoni H, Manda S. Synthesis and screening of some novel substituted indoles contained 1,3,4-oxadiazole and 1,2,4-triazole moiety. *Chinese Chem Lett* 2013; 24 (2):127–30.
334. Rapolu S, Alla M, Bommena VR et al. Synthesis and biological screening of 5-(alkyl(1H-indol-3-yl))-2-(substituted)-1,3,4-oxadiazoles as antiproliferative and anti-inflammatory agents. *Eur J Med Chem* 2013; 66:91–100.
335. Kumar D, Kumar NM, Noel B, Shah K. A series of 2-arylamino-5-(indolyl)-1,3,4-thiadiazoles as potent cytotoxic agents. *Eur J Med Chem* 2012; 55:432–8.
336. Amir M, Kumar S. Anti-inflammatory and Gastro Sparing Activity of Some New Indomethacin Derivatives. *Arch Pharm (Weinheim)* 2005; 338 (1):24–31.
337. Al-Masoudi NA, Jafar NNA, Abbas LJ et al. Synthesis and anti-HIV Activity of New Benzimidazole, Benzothiazole and Carbohyrazide Derivatives of the anti-Inflammatory Drug Indomethacin. *Zeitschrift für Naturforsch B* 2011; 66 (9):953–60.
338. Metwally KA, Abdel-Aziz LM, Lashine ESM et al. Hydrazones of 2-aryl-quinoline-4-carboxylic acid hydrazides: Synthesis and preliminary evaluation as antimicrobial agents. *Bioorg Med Chem* 2006; 14 (24):8675–82.
339. Zahoor AF, Naheed S, Irfan M et al. Advances in the synthesis and reactivity of acyl azides (2005-2015). *Afinidad* 2018; 75 (583): 228-38.
340. Yi-Hung T, Min-Yung Y, Shun-Ichi N. Stability, anti-inflammatory effect and percutaneous absorption of indomethacin in absorption ointment formulations. *Int J Pharm* 1986; 28 (1):47–58.
341. Kougioumtzoglou A, Peikova L, Georgieva M, Zlatkov A. Evaluation of the stability of indomethacin substance under a model of physiological conditions, using modified and validated RP-HPLC Method. *Farmacia* 2015; 62 (2):10–7.
342. O'Brien M, McCauley J, Cohen E. Indomethacin. In: Florey K (ed.). Analytical Profiles of Drugs Substances.Vol 13. Academic Press, 1984:211–38.
343. Elkanzi NAA. Short Review on Synthesis of Thiazolidinone and beta-Lactam. *World J Org Chem* 2013; 1 (2):24–51.
344. Mashrai A, Mahmood Dar A. Strategies for the Synthesis of Thiazolidinone Heterocycles. *Med Chem* 2016; 6 (4):280–191.
345. Foroughifar N, Ebrahimi S. One-pot synthesis of 1,3-thiazolidin-4-one using Bi(SCH2COOH)3 as catalyst. *Chinese Chem Lett* 2013; 24 (5):389–91.
346. Neuenfeldt PD, Drawanz BB, Siqueira GM et al. Efficient solvent-free synthesis of thiazolidin-4-ones from phenylhydrazine and 2,4-dinitrophenylhydrazine. *Tetrahedron Lett* 2010; 51 (23):3106–8.
347. Rawal RK, Srivastava T, Haq W, Katti SB. An expeditious synthesis of thiazolidinones and tetathiazanones. *J Chem Res* 2004; 2004 (5):368–9.
348. Subhedar DD, Shaikh MH, Arkile MA et al. Facile synthesis of 1,3-thiazolidin-4-ones as antitubercular agents. *Bioorg Med Chem Lett* 2016; 26 (7):1704–8.
349. Aydin D, Karakilic E, Karakurt S, Baran A. Thiazolidine based fluorescent chemosensors for aluminum ions and their applications in biological imaging. *Spectrochim Acta Part A Mol Biomol Spectrosc* 2020; 238:118431.
350. Bade TS, Ebrahimi HP, Alsalim TA et al. A novel series of 1, 4-Dihydropyridine (DHP) derivatives bearing thiazolidin-4-one: From synthesis to structure. *J Mol Struct* 2017; 1138:136–48.
351. Barbosa VA, Baréa P, Mazia RS et al. Synthesis and evaluation of novel hybrids β-carboline-4-thiazolidinones as potential antitumor and antiviral agents. *Eur J Med Chem* 2016; 124:1093–104.
352. Saini R, Malladi SR, Dharavath N. Diversity-oriented One-pot Synthesis of Novel Imidazo[4′,5′:4,5]benzo[e][1,4]thiazepinones and Benzo[d]imidazolyl Thiazolidinones through pTSA

Promoted Cyclization and Evaluation of Antimicrobial and Anti-inflammatory Activities. *J Heterocycl Chem* 2018; 55 (7):1579–88.
353. Kuila B, Mahajan D, Singh P, Bhargava G. A facile and highly chemoselective synthesis of 1-thia-3a,6-diaza-benzo[e]azulen-3-ones by 7-exo-dig/trig halocyclizations. *RSC Adv* 2016; 6 (103):101587–91.
354. Kaur A, Kaur AP, Gautam P, Gautam D. Ultrasound-Assisted Facile Synthesis and Antimicrobial Studies of Alkanediyl-bis-thiazolidin-4-ones and Alkanediyl-bis-thiazinan-4-ones. *J Heterocycl Chem* 2019; 56 (8):2105–10.
355. Jangam SS, Wankhede SB, Chitlange SS. Molecular docking, synthesis and anticonvulsant activity of some novel 3-(2-substituted)-4-oxothiazolidine-3-yl)-2-phenylquinazoline-4(3H)-ones. *Res Chem Intermed* 2019; 45 (2):471–86.
356. Gokhale KM, Telvekar VN. Silica chloride (SiO2-Cl) catalyzed one pot synthesis of 2,3-disubstituted-thiazolidin-4-one. *Synth Commun* 2020; 50 (9):1396–403.
357. Mohammadi R, Alamgholiloo H, Gholipour B et al. Visible-light-driven photocatalytic activity of ZnO/g-C3N4 heterojunction for the green synthesis of biologically interest small molecules of thiazolidinones. *J Photochem Photobiol A Chem* 2020; 402:112786.
358. Lashkari M, Ghashang M. Preparation of thiazolidin-4-one derivatives using ZnO–NiO–NiFe2O4 nano-composite system. *Res Chem Intermed* 2021; 47 (2):589–97.
359. Rathod AS, Godipurge SS, Biradar JS. Microwave Assisted, Solvent-Free, "Green" Synthesis of Novel Indole Analogs as Potent Antitubercular and Antimicrobial Agents and Their Molecular Docking Studies. *Russ J Gen Chem* 2018; 88 (6):1238–46.
360. Bakr RB, Elkanzi NAA. Preparation of some novel thiazolidinones, imidazolinones, and azetidinone bearing pyridine and pyrimidine moieties with antimicrobial activity. *J Heterocycl Chem* 2020; 57 (7):2977–89.
361. Abu-Hashem AA, Abu-Zied KM, AbdelSalam Zaki ME et al. Design, Synthesis, and Anticancer Potential of the Enzyme (PARP-1) Inhibitor with Computational Studies of New Triazole, Thiazolidinone, - Thieno [2, 3-d] Pyrimidinones. *Lett Drug Des Discov* 2020; 17 (6):799–817.
362. Shawky AM, Abourehab MAS, Abdalla AN, Gouda AM. Optimization of pyrrolizine-based Schiff bases with 4-thiazolidinone motif: Design, synthesis and investigation of cytotoxicity and anti-inflammatory potency. *Eur J Med Chem* 2020; 185:111780.
363. Wang Z, Kang D, Chen M et al. Design, synthesis, and antiviral evaluation of novel hydrazone-substituted thiophene[3,2-d]pyrimidine derivatives as potent human immunodeficiency virus-1 inhibitors. *Chem Biol Drug Des* 2018; 92 (6):2009–21.
364. Graham S, Graig F, Scott S. *Organic Chemistry*. New York, NY: Wiley, 2014.
365. Soleiman-Beigi M, Aryan R, Yousofizadeh M, Khosravi S. A Combined Synthetic and DFT Study on the Catalyst-Free and Solvent-Assisted Synthesis of 1,3,4-Oxadiazole-2-thiol Derivatives. Mancini PM, ed. *J Chem* 2013; 2013:476358.
366. Rai G, Kenyon V, Jadhav A et al. Discovery of Potent and Selective Inhibitors of Human Reticulocyte 15-Lipoxygenase-1. *J Med Chem* 2010; 53 (20):7392–404.
367. Reddyrajula R, Dalimba U. The bioisosteric modification of pyrazinamide derivatives led to potent antitubercular agents: Synthesis via click approach and molecular docking of pyrazine-1,2,3-triazoles. *Bioorg Med Chem Lett* 2020; 30 (2):126846.
368. Patel NB, Purohit AC, Rajani DP et al. New 2-benzylsulfanyl-nicotinic acid based 1,3,4-oxadiazoles: Their synthesis and biological evaluation. *Eur J Med Chem* 2013; 62:677–87.
369. Hiremath SM, Suvitha A, Patil NR et al. Synthesis of 5-(5-methyl-benzofuran-3-ylmethyl)-3H- [1, 3, 4] oxadiazole-2-thione and investigation of its spectroscopic, reactivity, optoelectronic and drug likeness properties by combined computational and experimental approach. *Spectrochim Acta Part A Mol Biomol Spectrosc* 2018; 205:95–110.
370. Shah K, Mujwar S, Gupta JK et al. Molecular Docking and In Silico Cogitation Validate Mefenamic Acid Prodrugs as Human Cyclooxygenase-2 Inhibitor. *Assay Drug Dev Technol* 2019; 17 (6):285–91.
371. Rizvi SMD, Shakil S, Haneef M. A simple click by click protocol to perform docking: AutoDock 4.2 made easy for non-bioinformaticians. *EXCLI J* 2013; 12:831–57.
372. Schneider G. Virtual screening: an endless staircase? *Nat Rev Drug Discov* 2010; 9 (4):273–6.
373. Forli S, Huey R, Pique ME et al. Computational protein–ligand docking and virtual drug screening with the AutoDock suite. *Nat Protoc* 2016; 11 (5):905–19.
374. Cosconati S, Forli S, Perryman AL et al. Virtual screening with AutoDock: theory and practice. *Expert Opin Drug Discov* 2010; 5 (6):597–607.
375. Seeliger D, de Groot BL. Ligand docking and binding site analysis with PyMOL and Autodock/Vina. *J Comput Aided Mol Des* 2010; 24 (5):417–22.
376. Pagadala NS, Syed K, Tuszynski J. Software for molecular docking: a review. *Biophys Rev* 2017; 9 (2):91–102.

377. Gore S, Sanz García E, Hendrickx PMS et al. Validation of Structures in the Protein Data Bank. *Structure* 2017; 25 (12):1916–27.
378. Duggan KC, Walters MJ, Musee J et al. Molecular basis for cyclooxygenase inhibition by the non-steroidal anti-inflammatory drug naproxen. *J Biol Chem* 2010; 285 (45):34950–9.
379. Morris AL, MacArthur MW, Hutchinson EG, Thornton JM. Stereochemical quality of protein structure coordinates. *Proteins Struct Funct Bioinforma* 1992; 12 (4):345–64.
380. Kleywegt GJ, Alwyn Jones TBT. Model building and refinement practice. In: *Macromolecular Crystallography Part B*.Vol 277. MA USA: Academic Press: Cambridge, 1997:208–30.
381. Oniga S, Pacureanu L, Stoica C et al. COX Inhibition Profile and Molecular Docking Studies of Some 2-(Trimethoxyphenyl)-Thiazoles. *Molecules* 2017; 22 (9):1507.
382. Rowlinson SW, Kiefer JR, Prusakiewicz JJ et al. A Novel Mechanism of Cyclooxygenase-2 Inhibition Involving Interactions with Ser-530 and Tyr-385. *J Biol Chem* 2003; 278 (46):45763–9.
383. Knights KM, Mangoni AA, Miners JO. Defining the COX inhibitor selectivity of NSAIDs: implications for understanding toxicity. *Expert Rev Clin Pharmacol* 2010; 3 (6):769–76.
384. Carullo G, Galligano F, Aiello F. Structure-activity relationships for the synthesis of selective cyclooxygenase 2 inhibitors: an overview (2009-2016). *Medchemcomm* 2016; 8 (3):492–500.
385. Chawla G, Naaz B, Siddiqui AA. Exploring 1,3,4-Oxadiazole Scaffold for Anti-inflammatory and Analgesic Activities: A Review of Literature From 2005-2016. *Mini-Reviews Med Chem* 2018; 18 (3).
386. Domínguez-Villa FX, Durán-Iturbide NA, Ávila-Zárraga JG. Synthesis, molecular docking, and in silico ADME/Tox profiling studies of new 1-aryl-5-(3-azidopropyl)indol-4-ones: Potential inhibitors of SARS CoV-2 main protease. *Bioorg Chem* 2021; 106: 104497
387. Winiwarter S, Ridderström M, Ungell AL et al. Use of molecular descriptors for absorption, distribution, metabolism, and excretion predictions. In: Taylor JB, Triggle DJ (eds.). *Comprehensive Medicinal Chemistry II*.Vol 5. Elsevier, 2006:531–54.
388. Yu H, Adedoyin A. ADME-Tox in drug discovery: Integration of experimental and computational technologies. *Drug Discov Today* 2003; 8 (18):852–61.
389. Daina A, Michielin O, Zoete V. SwissADME: A free web tool to evaluate pharmacokinetics, drug-likeness and medicinal chemistry friendliness of small molecules. *Sci Rep* 2017; 7:1–13.
390. Daina A, Zoete V. A BOILED-Egg To Predict Gastrointestinal Absorption and Brain Penetration of Small Molecules. *ChemMedChem* 2016:1117–21.
391. Pires DEV, Blundell TL, Ascher DB. pkCSM: Predicting small-molecule pharmacokinetic and toxicity properties using graph-based signatures. *J Med Chem* 2015; 58 (9):4066–72.
392. Chandrasekaran B, Abed SN, Al-Attraqchi O, Kuche K, Tekade RK. Computer-Aided Prediction of Pharmacokinetic (ADMET) Properties. In: Tekade R (ed.). *Advances in Pharmaceutical Product Development and Research*. Academic Press, 2018:731–55.
393. Gao Y, Gesenberg C, Zheng W. *Oral Formulations for preclinical studies: Principle, design, and development considerations*. Elsevier Inc., 2017.
394. Shakya AK, Al-Najjar BO, Deb PK, Naik RR, Tekade RK. First-Pass Metabolism Considerations in Pharmaceutical Product Development. In: Tekade R (ed.). *Advances in Pharmaceutical Product Development and Research*. Academic Press, 2018:259–86.
395. Ghodke-Puranik YA, Lamba JK. Pharmacogenomics. In: Patwardhan B, Chaguturu R (eds.). *Inovative Approaches in Drug Discovery*, Boston: Academic Press, 2017:195–234.
396. Dasgupta A. Genetic Factors Associated With Opioid Therapy and Opioid Addiction. In: Dasgupta A (ed.) Elsevier, 2020:61–88.
397. Tirona RG, Kim RB. Introduction to Clinical Pharmacology. In: Robertson D, Williams GH (eds.). Clinical and Translational Science Principles of Human Research, Academic Press, 2017:365–88.
398. Shimamura T, Sumikura Y, Yamazaki T et al. Applicability of the DPPH Assay for Evaluating the Antioxidant Capacity of Food Additives Inter-laboratory Evaluation Study. *Anal Sci* 2014; 30 (7):717–21.
399. Abramovič H, Grobin B, Poklar Ulrih N, Cigić B. Relevance and Standardization of In Vitro Antioxidant Assays: ABTS, DPPH, and Folin–Ciocalteu. *J Chem* 2018; 2018:1–9.
400. Moualek I, Iratni Aiche G, Mestar Guechaoui N et al. Antioxidant and anti-inflammatory activities of Arbutus unedo aqueous extract. *Asian Pac J Trop Biomed* 2016; 6 (11):937–44.
401. Bondet V, Brand-Williams W, Berset C. Kinetics and Mechanisms of Antioxidant Activity using the DPPH.Free Radical Method. *LWT - Food Sci Technol* 1997; 30 (6):609–15.
402. Gamez EJC, Luyengi L, Lee SK et al. Antioxidant Flavonoid Glycosides from Daphniphyllum calycinum. *J Nat Prod* 1998; 61 (5):706–8.
403. Kim DO, Lee KW, Lee HJ, Lee CY. Vitamin C Equivalent Antioxidant Capacity (VCEAC) of Phenolic Phytochemicals. *J Agric Food Chem* 2002; 50 (13):3713–7.
404. Cheng Z, Moore J, Yu L. High-Throughput Relative DPPH Radical Scavenging Capacity Assay. *J Agric Food Chem* 2006; 54 (20):7429–36.

405. Kedare SB, Singh RP. Genesis and development of DPPH method of antioxidant assay. *J Food Sci Technol* 2011; 48 (4):412–22.
406. Pisoschi AM, Negulescu GP. Methods for Total Antioxidant Activity Determination: A Review. *Biochem Anal Biochem* 2012; 1 (1):1–10.
407. Magalhães LM, Segundo MA, Reis S, Lima JLFC. Methodological aspects about in vitro evaluation of antioxidant properties. *Anal Chim Acta* 2008; 613 (1):1–19.
408. Xie J, Schaich KM. Re-evaluation of the 2,2-Diphenyl-1-picrylhydrazyl Free Radical (DPPH) Assay for Antioxidant Activity. *J Agric Food Chem* 2014; 62 (19):4251–60.
409. Frezzini MA, Castellani F, De Francesco N et al. Application of DPPH Assay for Assessment of Particulate Matter Reducing Properties. *Atmosphere (Basel)* 2019; 10 (12):816.
410. Cao X, Yang L, Xue Q et al. Antioxidant evaluation-guided chemical profiling and structure-activity analysis of leaf extracts from five trees in Broussonetia and Morus (Moraceae). *Sci Rep* 2020; 10 (1):4808.
411. Sánchez-Moreno C, Larrauri JA, Saura-Calixto F. A procedure to measure the antiradical efficiency of polyphenols. *J Sci Food Agric* 1998; 76 (2):270–6.
412. Mizushima Y, Kobayashi M. Interaction of anti-inflammatory drugs with serum proteins, especially with some biologically active proteins. *J Pharm Pharmacol* 1968; 20 (3):169–73.
413. Gilson MK, Zhou HX. Calculation of Protein-Ligand Binding Affinities. *Annu Rev Biophys Biomol Struct* 2007; 36 (1):21–42.
414. Gohlke H, Klebe G. Approaches to the Description and Prediction of the Binding Affinity of Small-Molecule Ligands to Macromolecular Receptors. *Angew Chemie Int Ed* 2002; 41 (15):2644–76.
415. Jorgensen WL. The Many Roles of Computation in Drug Discovery. *Science* 2004; 303 (5665):1813 LP – 1818.
416. Senthil SK, Murugan PK, Selvam S et al. Fluorescence spectroscopic analysis of heavy metal induced protein denaturation. *Mater Today Proc* 2020; 33:2328–30.
417. Bienvenu J, Walzer T, Lyon U De, Inserm U. *Compendium of Inflammatory Diseases*. (Parnham MJ, ed.). Basel: Springer Basel, 2016.
418. Lei J, Zhou Y, Xie D, Zhang Y. Mechanistic insights into a classic wonder drug-aspirin. *J Am Chem Soc* 2015; 137 (1):70–3.
419. Alfonso L, Ai G, Spitale RC, Bhat GJ. Molecular targets of aspirin and cancer prevention. *Br J Cancer* 2014; 111 (1):61–7.
420. Alfonso LF, Srivenugopal KS, Bhat GJ. Does aspirin acetylate multiple cellular proteins? (Review). *Mol Med Rep* 2009; 2 (4):667–71.
421. Tatham MH, Cole C, Scullion P et al. A Proteomic Approach to Analyze the Aspirin-mediated Lysine Acetylome. *Mol Cell Proteomics* 2017; 16 (2):310–26.
422. Loukianov AS, Syomina TK, Korolev AM. Conformational Changes in Proteins In Vitro as a Means of Predicting the Acute Toxicities of Chemicals. *Altern to Lab Anim* 2007; 35 (1):123–36.
423. Pabbathi A, Patra S, Samanta A. Structural Transformation of Bovine Serum Albumin Induced by Dimethyl Sulfoxide and Probed by Fluorescence Correlation Spectroscopy and Additional Methods. *ChemPhysChem* 2013; 14 (11):2441–9.
424. Batista ANL, Batista JM, Ashton L et al. Investigation of DMSO-Induced Conformational Transitions in Human Serum Albumin Using Two-Dimensional Raman Optical Activity Spectroscopy. *Chirality* 2014; 26 (9):497–501.
425. Novillo A, Ekwall B, Castaño A. Protein Precipitation In Vitro as a Measure of Chemical-induced Cytotoxicity: An EDIT Sub-programme. *Altern to Lab Anim* 2001; 29 (3):309–24.
426. Gryglewski RJ. Screening and Assessment of the Potency of Anti-Inflammatory Drugs in vitro. In: Vane JR, Ferreira S (eds.). *Anti-Inflammatory Drugs. Handbook of Experimental Pharmacology (Continuation of Handbuch der experimentellen Pharmakologie)*. Berlin: Springer, 1979:3–43.
427. Abdel-Hafez E, Abuo-Rahma GE, Abdel-Aziz M, Radwan MF, Farag HH. Design, synthesis and biological investigation of certain pyrazole-3-carboxylic acid derivatives as novel carriers for nitric oxide. *Bioorg Med Chem* 2009; 17 (11):3829–37.
428. Aziz HA, Moustafa GAI, Abbas SH, Derayea SM. New norfloxacin/nitric oxide donor hybrids: Synthesis and nitric oxide release measurement using a modified Griess colorimetric method. *Eur J Chem* 2017; 8 (2):119–24.
429. Council of Europe. Natrii Nitris. In: *European Pharmacopoeia 10th Edition*. 10th ed. Nördlingen (Germany): Druckerei C. H. Beck, 2020:3257–8.
430. Abdelall EKA, Abdelhamid AO, Azouz AA. Synthesis and biological evaluations of new nitric oxide-anti-inflammatory drug hybrids. *Bioorg Med Chem Lett* 2017; 27 (18):4358–69.
431. Wo D, Zhuang P, Xu Z et al. A novel spectrophotometric method for indirect determination of nitric oxide (NO) in serum. *Clin Chim Acta* 2013; 424:187–90.
432. Thomas DD, Heinecke JL, Ridnour LA et al. Signaling and stress: The redox landscape in NOS2 biology.

Free Radic Biol Med 2015; 87:204–25.
433. Oprean R, Rozet E, Deve W, Boulanger B, Hubert P. *Ghid de validare a procedurilor analitice cantitative*. Cluj: Editura Medicala Universitara ”Iuliu Hatieganu”, 2007.
434. Roman L, Sandulescu R, Bojita M, Muntean DL. *Validarea metodelor analitice*. Bucuresti: Editura Medicala, 2007.

ANNEXE I

List of published scientific papers

A). Scientific articles published *in extenso* from the topic of doctoral research

A1. In impact factor journals:

1. **Sava A**, Buron F, Routier S, Panainte A, Bibire N, Constantin SM, Lupasccu FG, Focsa AV, Profire L. Design, Synthesis, In Silico and In Vitro Studies for New Nitric Oxide-Releasing Indomethacin Derivatives with 1,3,4-oxadiazole-2-thiol Scaffold. *Int J Mol Sci* 2021; 22 (13):7079 (IF=5.923).
2. **Sava A**, Buron F, Routier S, Panainte A, Bibire N, Profire L. New nitric oxide-releasing indomethacin derivatives with 1,3-thiazolidine-4-one scaffold: Design, synthesis, in silico and in vitro studies. *Biomed Pharmacother* 2021; 139:111678 (IF=6.529).

A2. In indexed BDI journals:

3. **Sava A**, Panainte A, Bibire N, Constantin S, Focsa A, Buron F, Routier S, Profire L. A Rapid, Simple And Sensitive Spectrophotometric Method For The Determination Of No From No Donors. *Med Surg J* 2020; 124 (4):678–84.

B). **Scientific articles published *in extenso* from topics related to doctoral research**

B1. In impact factor journals:

4. Focșa A, Iacob A, Vasincu A, Constantin S, Andriescu L, **Sava A**, Buron F, Routier S, Profire L. The antioxidant potential evaluation of diclofenac derivatives with hydrazones structure, *Farmacia*. 68 (2020) 329–334 (IF= **1.607**).
5. Constantin SM, Buron F, Routier S, Vasincu IM, Apotrosoaei M, Lupascu F, Confederat L, Tuchilus C, **Sava A**, Profire L. Formulation and characterization of new polymeric systems based on chitosan and xanthine derivatives with thiazolidin-4-one scaffold. *Materials*. 2019;12(4):558 (IF=2.972).
6. Lupascscu FG, Avram I, Confederat L, Constantin SM, Stan CI, Lupusoru EC, **Sava A**, Lenuta P. Biological evaluation of chitosan-antidiabetic drug formulations for the treatment of diabetes mellitus. *Farmacia*. 2017;65(4):508–14 (IF=1.507).

B2. In indexed BDI journals:

7. **Sava A**, Sava E, Panainte A, Focsa A, Bibire N. Ethics in patient counseling and pharmaceutical practice by emotions management. *RJPhP* 2021; 14 (1): 47-51.
8. Focsa A, **Sava A**, Ababei A, Apotrosoaei M. Drug interactions in gastrointestinal disorders therapy. *RJPhP* 2021; 14(1): 25-29.
9. Focsa A, Iacob A, Vasincu I, Constantin S, Andriescu L, **Sava A**, Buron F, Routier S, Apotrosoaei M, Profire L. Optimization of the synthesis of diclofenac derivatives with hydrazone structure and in vitro evaluation of the anti-inflammatory potential, *Rev Chim*. 71 (2020) 305–314.
10. Focșa A, Vasincu I, **Sava A**, Iacob A, Apotrosoaei M, Profire L. Biopharmaceutical Characteristics And In Vitro Evaluation Of The Reducing Antioxidant Power Of Some Diclofenac Derivatives, *Med. Surg. J*. 3 (2020) 124

ANNEXE II

The ^{1}H-NMR spectres of new nitric oxide–releasing indomethacin derivatives with 1,3-thiazolidin-4-one (9a-s) and 1,3,4-oxadiazole (11a-m, t-v) scafoold, respectively

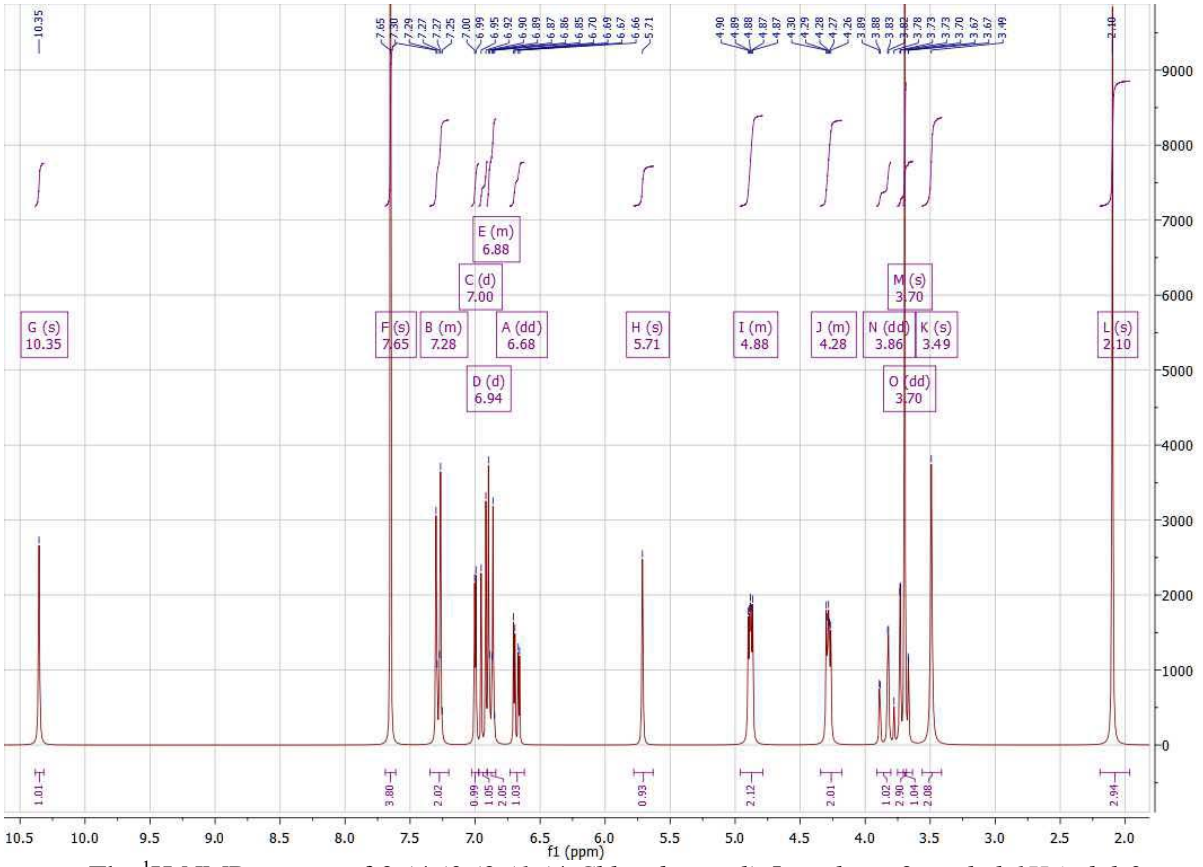

The ^{1}H-NMR spectra of *2-(4-(3-(2-(1-(4-Chlorobenzoyl)-5-methoxy-2-methyl-1H-indol-3-yl)acetamido)-4-oxo-thiazolidin-2-yl)phenoxy)ethyl nitrate* ***(9a)***

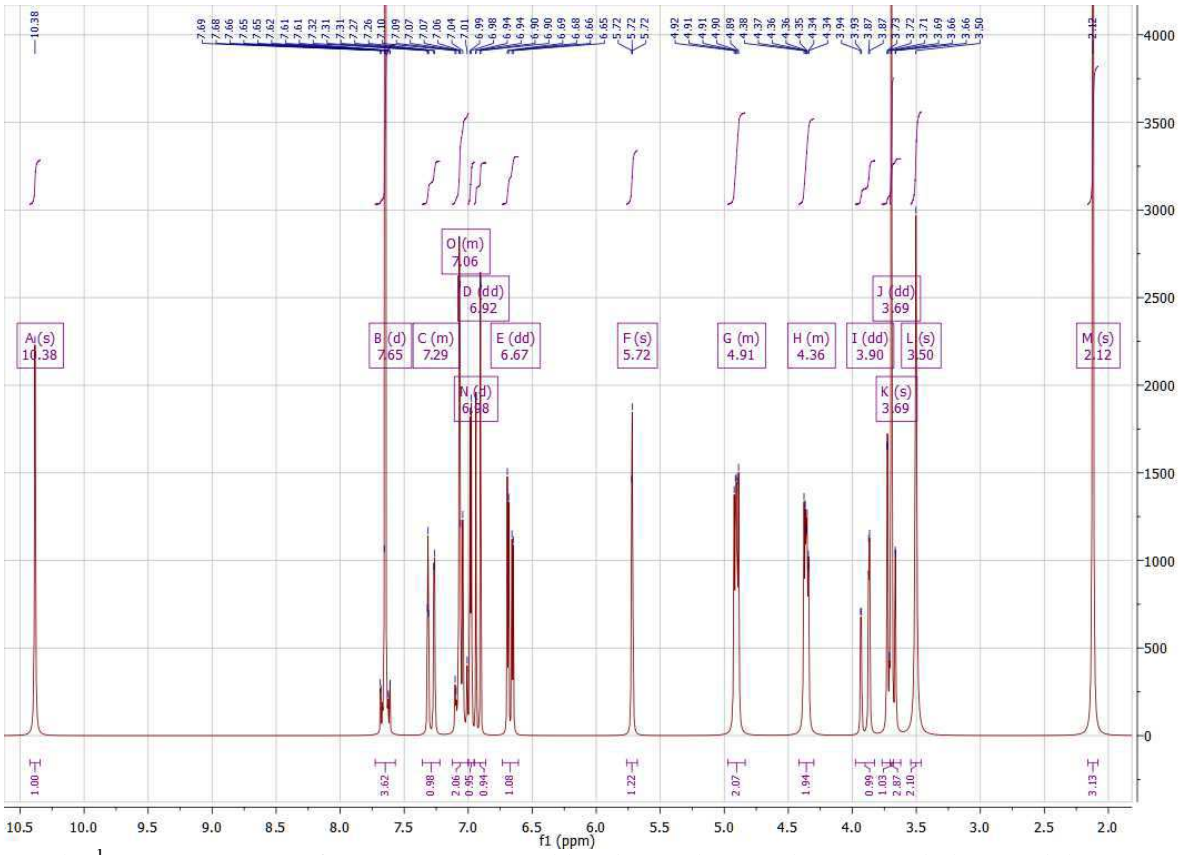

The [1]H-NMR spectra of *2-(4-(3-(2-(1-(4-Chlorobenzoyl)-5-methoxy-2-methyl-1H-indol-3-yl)acetamido)-4-oxo-thiazolidin-2-yl)-2-fluorophenoxy)ethyl nitrate* **(9b)**

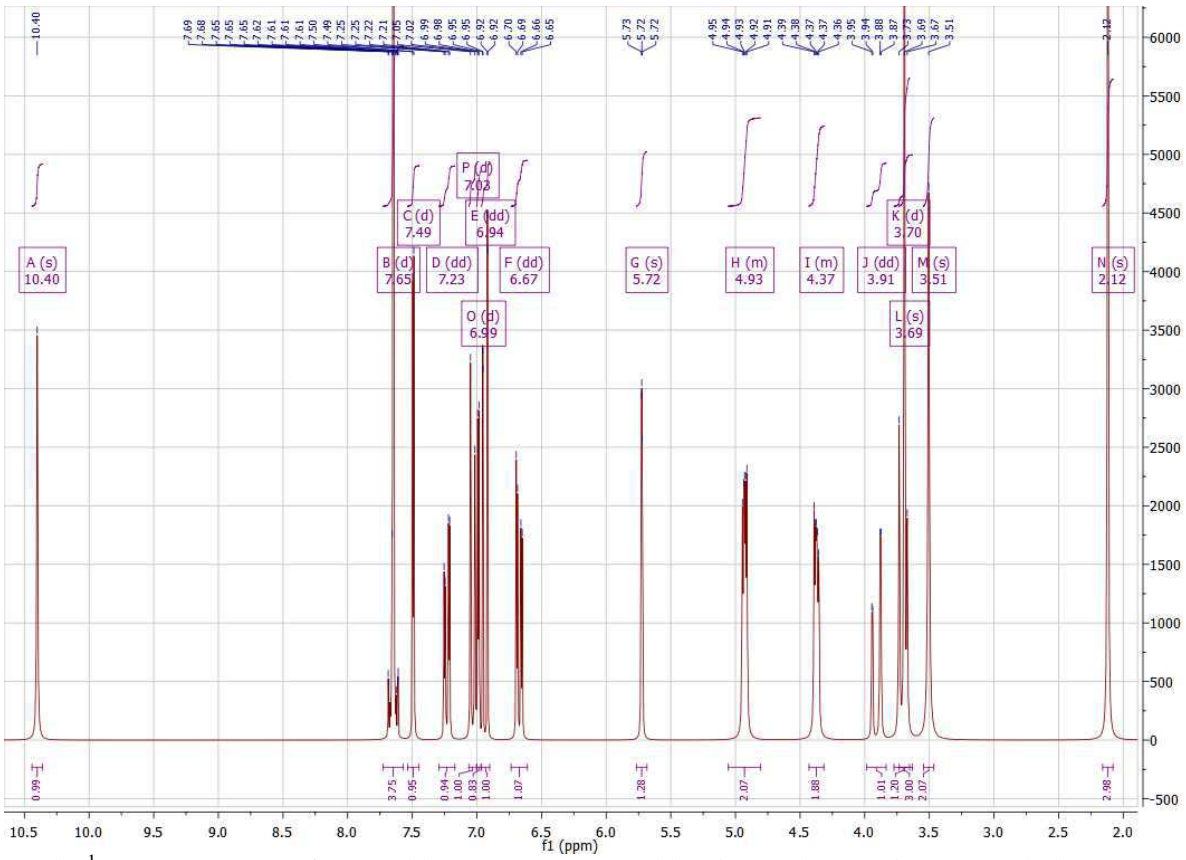

The [1]H-NMR spectra of *2-(2-Chloro-4-(3-(2-(1-(4-chlorobenzoyl)-5-methoxy-2-methyl-1H-indol-3-yl)acetamido)-4-oxothiazolidin-2-yl)phenoxy)ethyl nitrate* **(9c)**

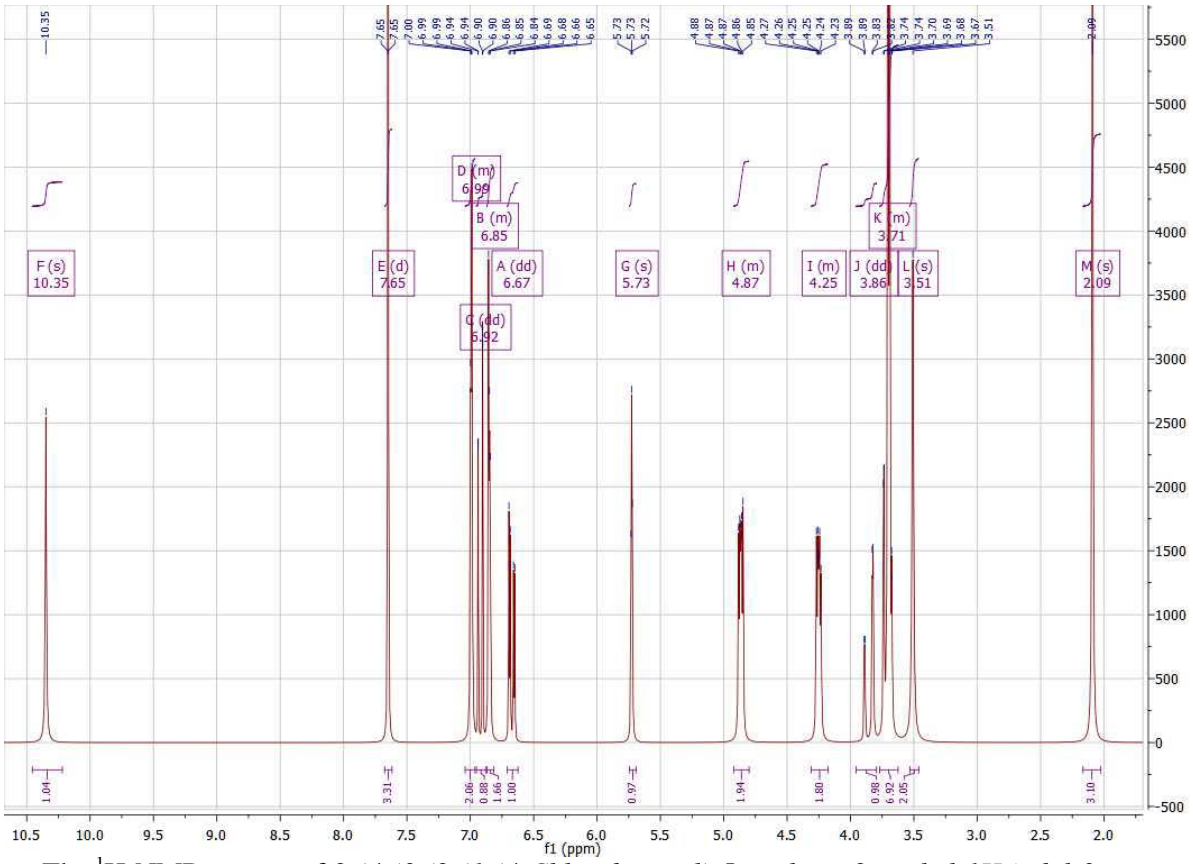

The [1]H-NMR spectra of *2-(4-(3-(2-(1-(4-Chlorobenzoyl)-5-methoxy-2-methyl-1H-indol-3-yl)acetamido)-4-oxo-thiazolidin-2-yl)-2-methoxyphenoxy)ethyl nitrate* **(9d)**

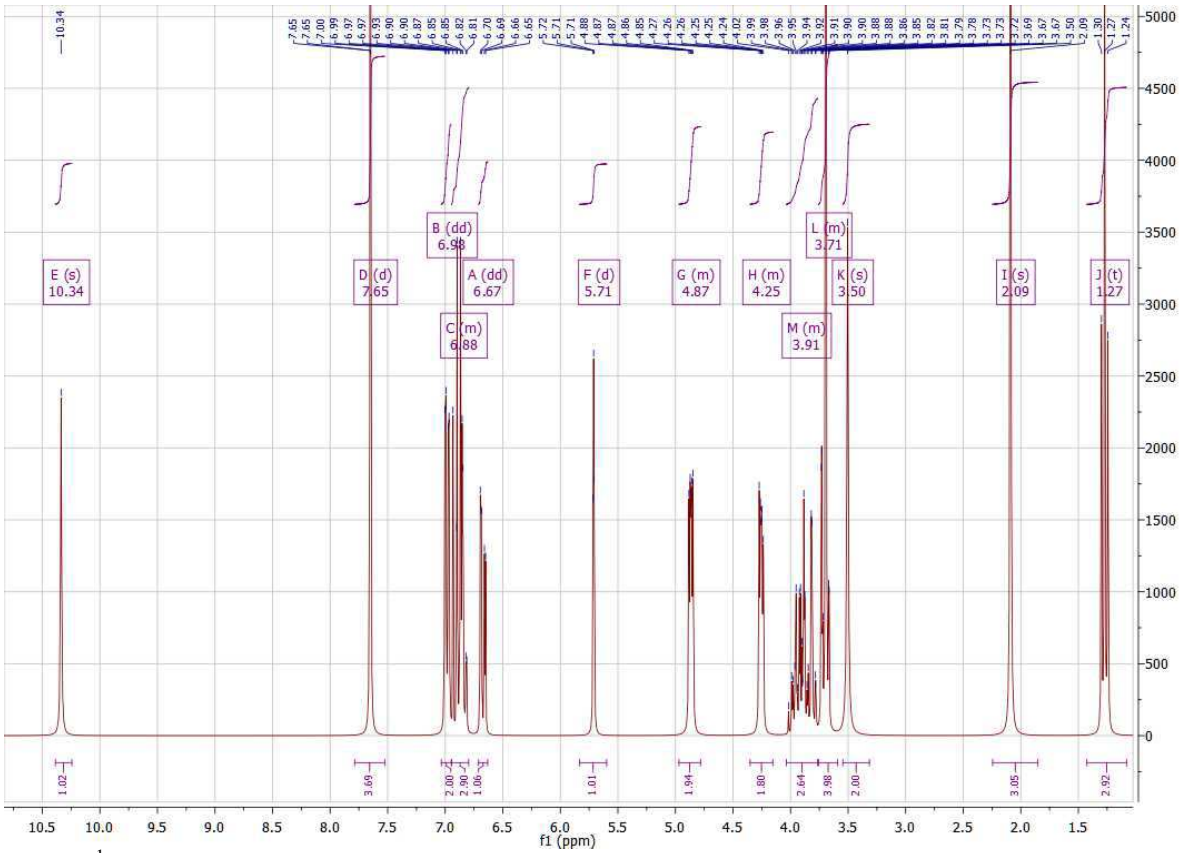

The [1]H-NMR spectra of *2-(4-(3-(2-(1-(4-Chlorobenzoyl)-5-methoxy-2-methyl-1H-indol-3-yl)acetamido)-4-oxo-thiazolidin-2-yl)-2-ethoxyphenoxy)ethyl nitrate* **(9e)**

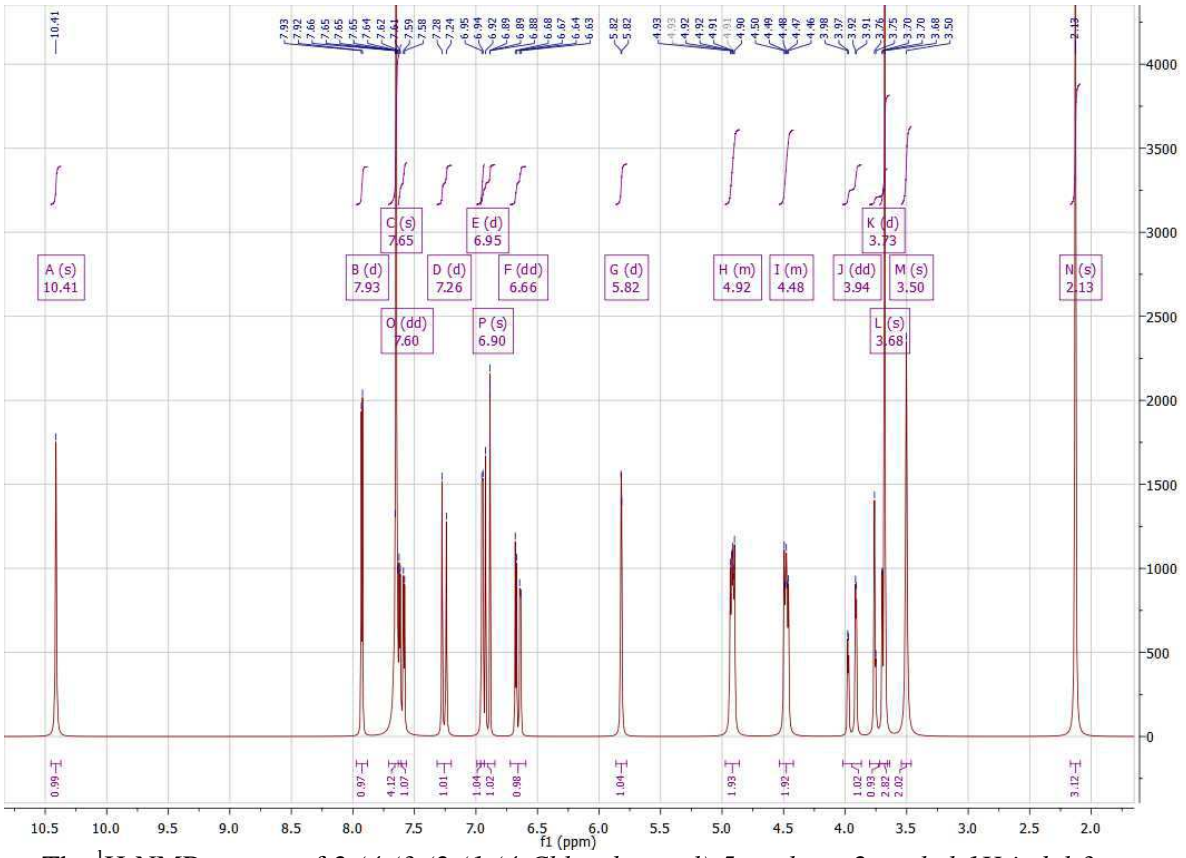

The [1]H-NMR spectra of *2-(4-(3-(2-(1-(4-Chlorobenzoyl)-5-methoxy-2-methyl-1H-indol-3-yl)acetamido)-4-oxo-thiazolidin-2-yl)-2-nitrophenoxy)ethyl nitrate* (**9f**)

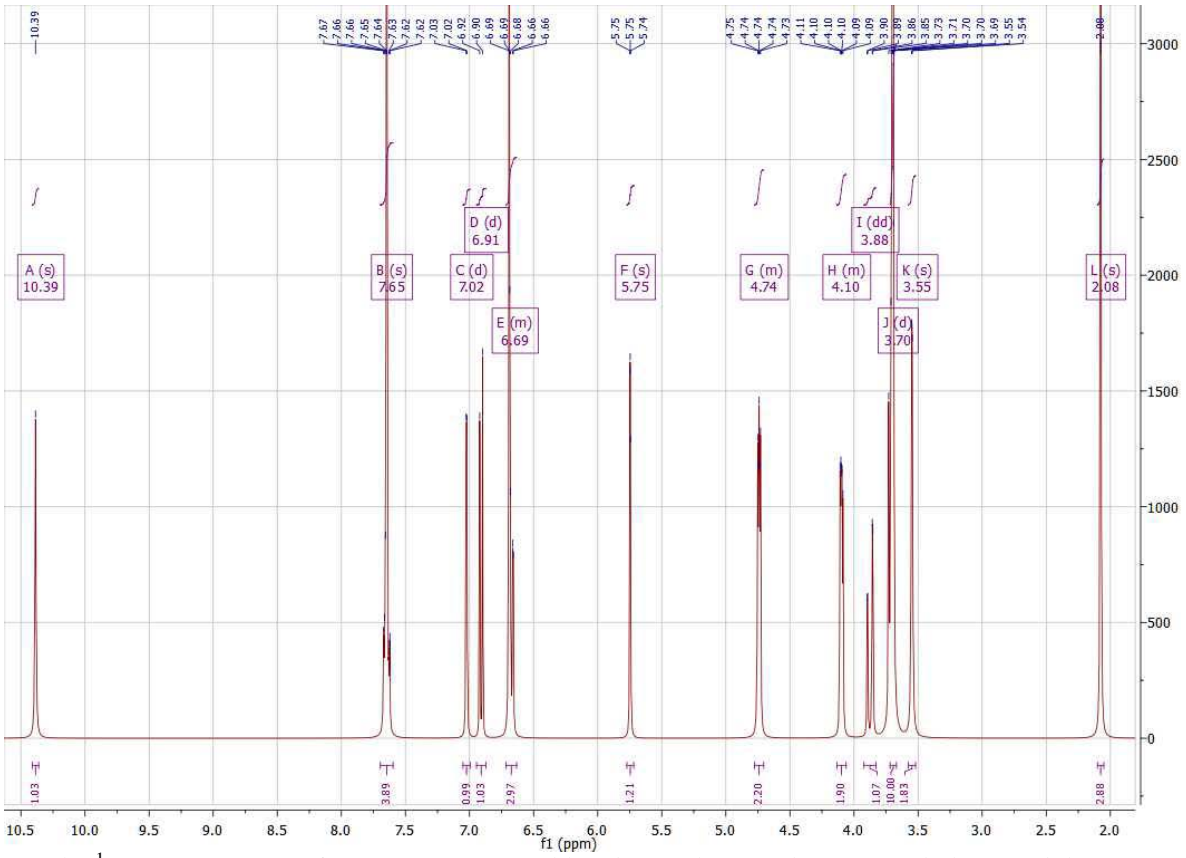

The [1]H-NMR spectra of *2-(4-(3-(2-(1-(4-Chlorobenzoyl)-5-methoxy-2-methyl-1H-indol-3-yl)acetamido)-4-oxo-thiazolidin-2-yl)-2,6-dimethoxyphenoxy)ethyl nitrate* (**9g**)

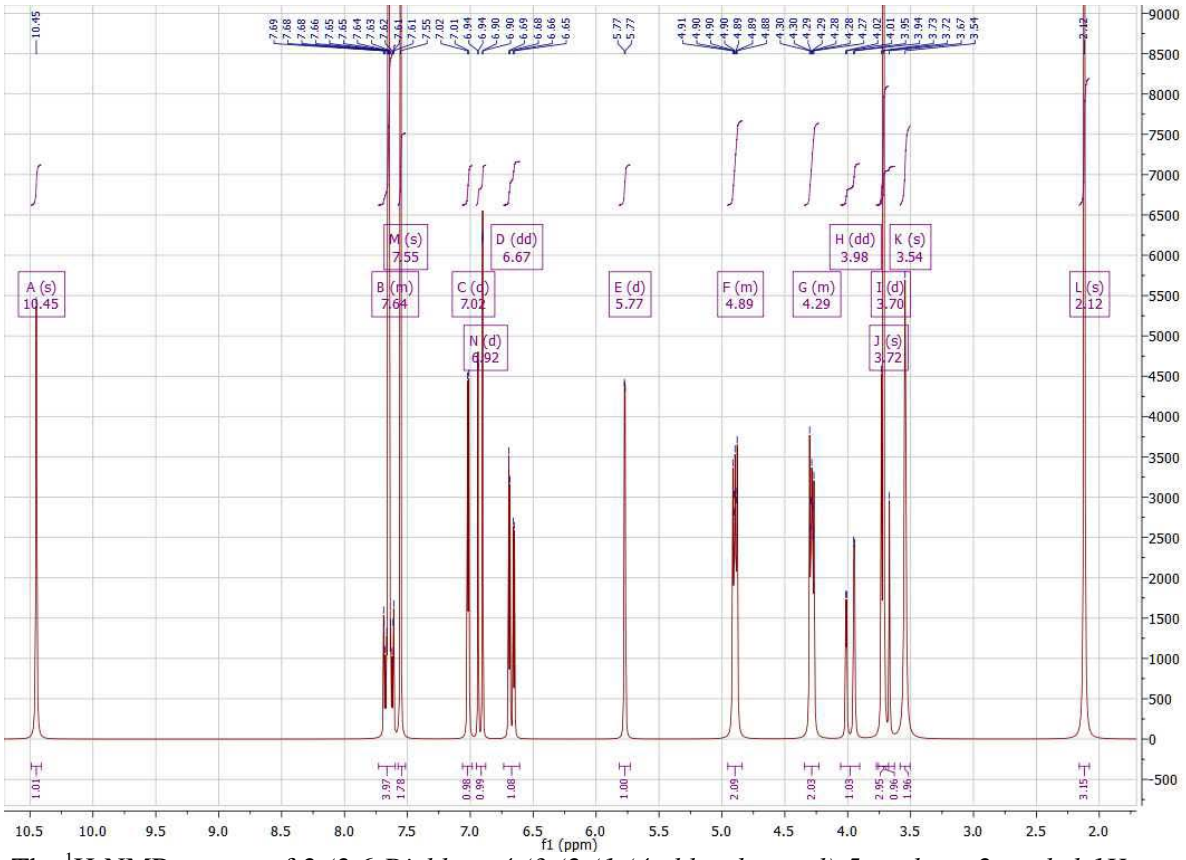

The [1]H-NMR spectra of *2-(2,6-Dichloro-4-(3-(2-(1-(4-chlorobenzoyl)-5-methoxy-2-methyl-1H-indol-3-yl)aceta-mido)-4-oxothiazolidin-2-yl)phenoxy)ethyl nitrate* **(9h)**

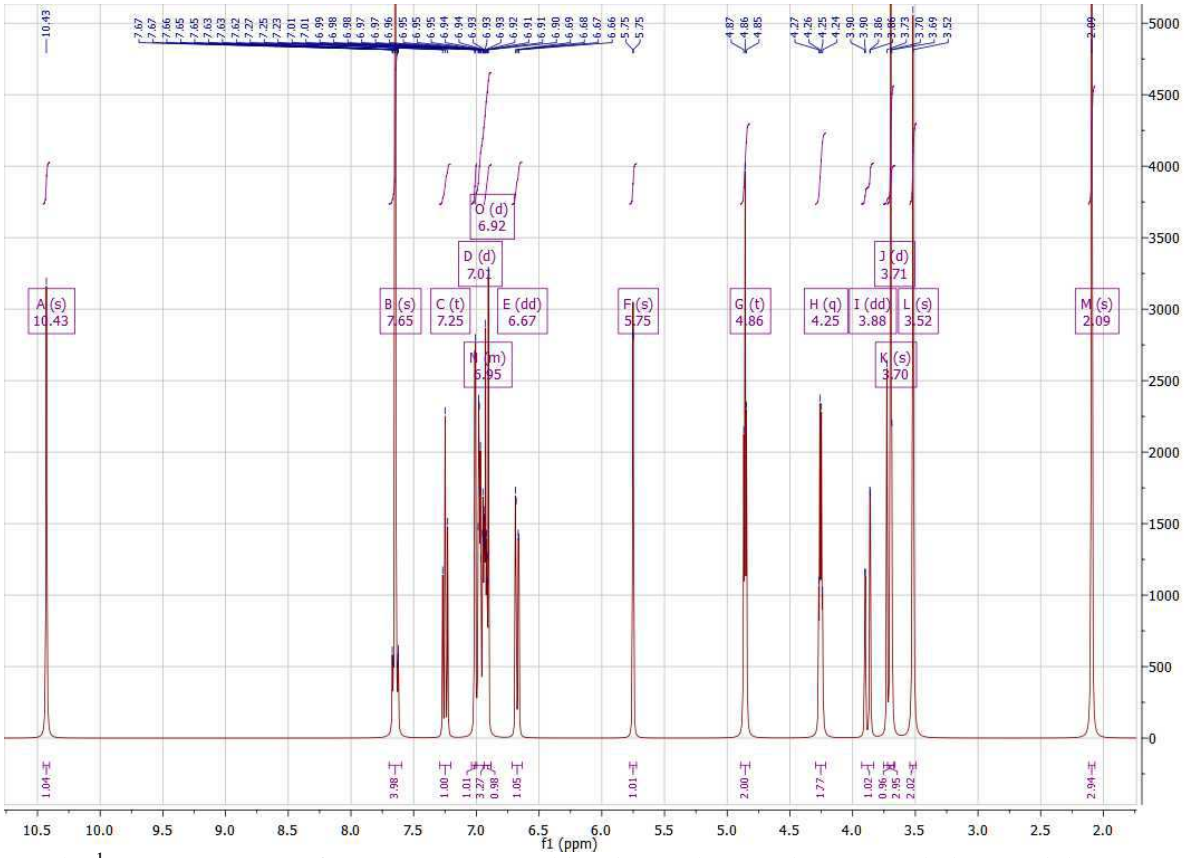

The [1]H-NMR spectra of *2-(3-(3-(2-(1-(4-Chlorobenzoyl)-5-methoxy-2-methyl-1H-indol-3-yl)acetamido)-4-oxo-thiazolidin-2-yl)phenoxy)ethyl nitrate* **(9i)**

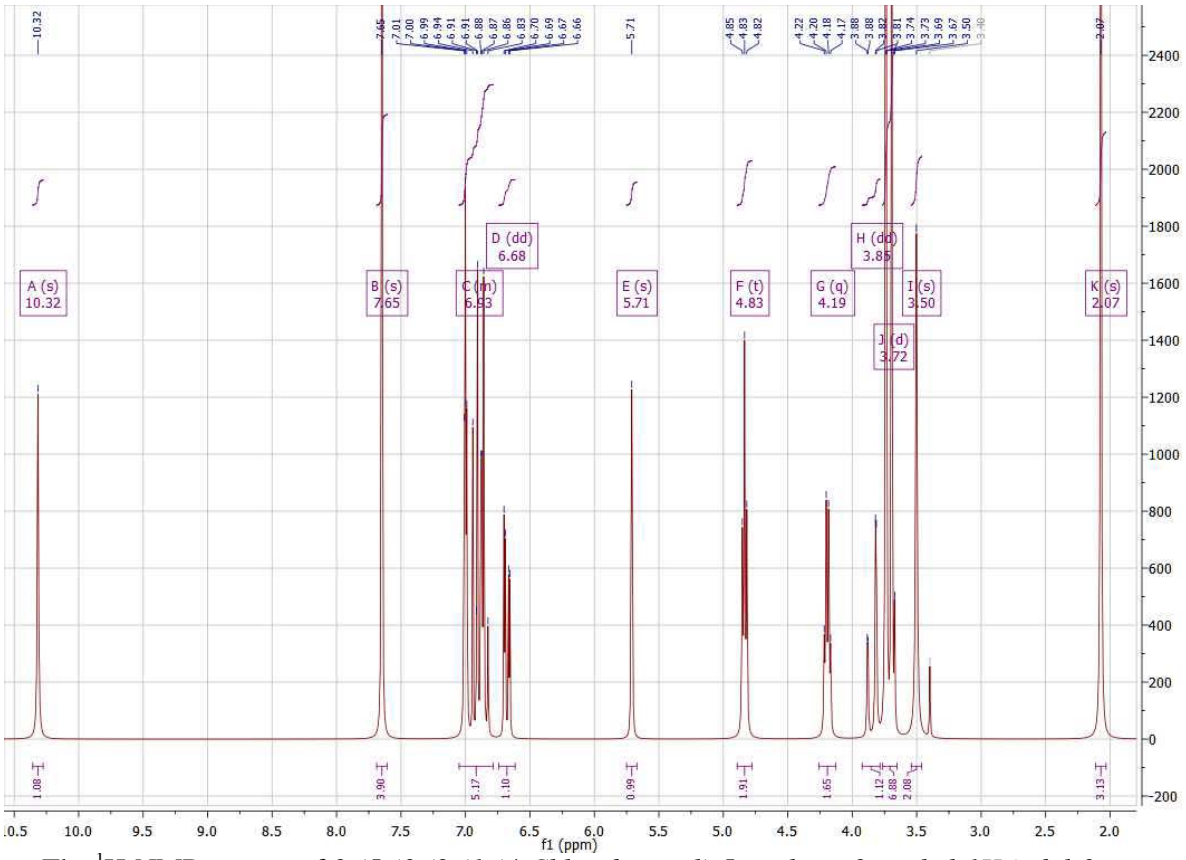

The ^{1}H-NMR spectra of *2-(5-(3-(2-(1-(4-Chlorobenzoyl)-5-methoxy-2-methyl-1H-indol-3-yl)acetamido)-4-oxo-thiazolidin-2-yl)-2-methoxyphenoxy)ethyl nitrate* **(9j)**

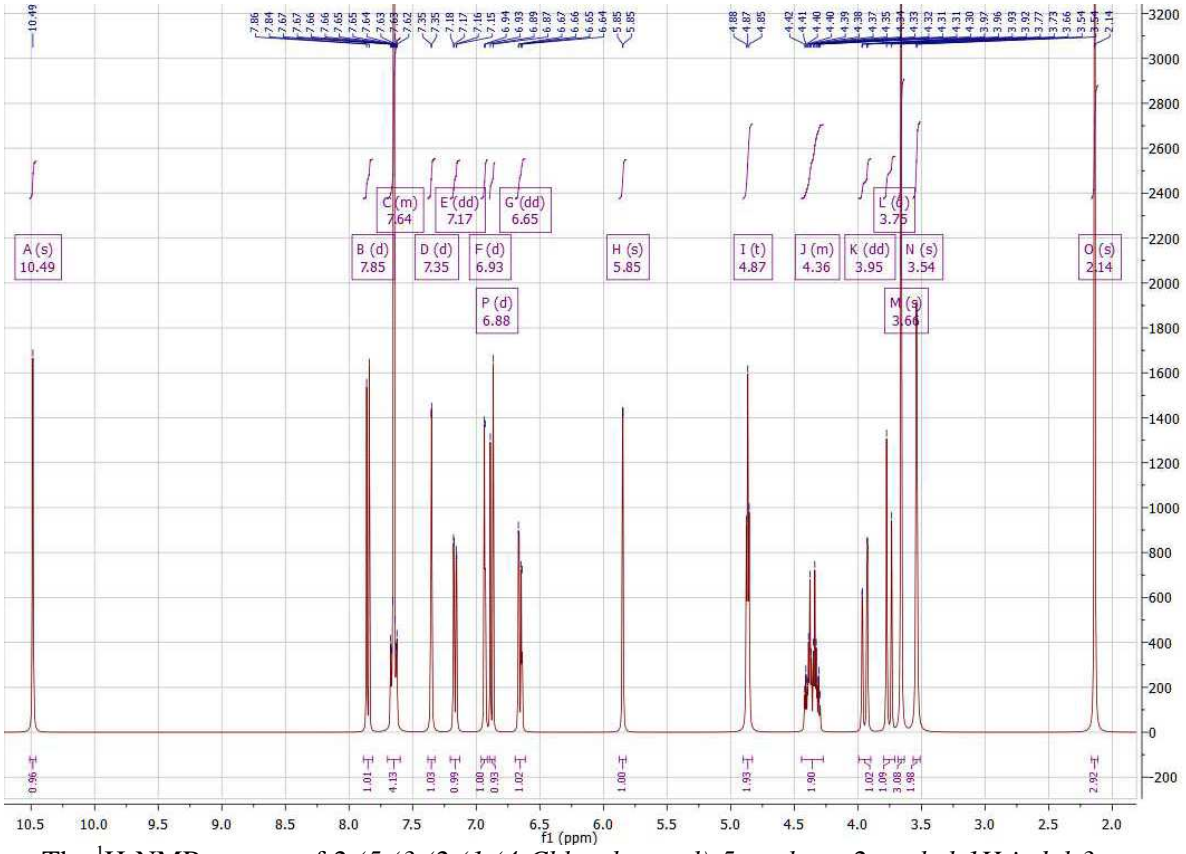

The ^{1}H-NMR spectra of *2-(5-(3-(2-(1-(4-Chlorobenzoyl)-5-methoxy-2-methyl-1H-indol-3-yl)acetamido)-4-oxo-thiazolidin-2-yl)-2-nitrophenoxy)ethyl nitrate* **(9k)**

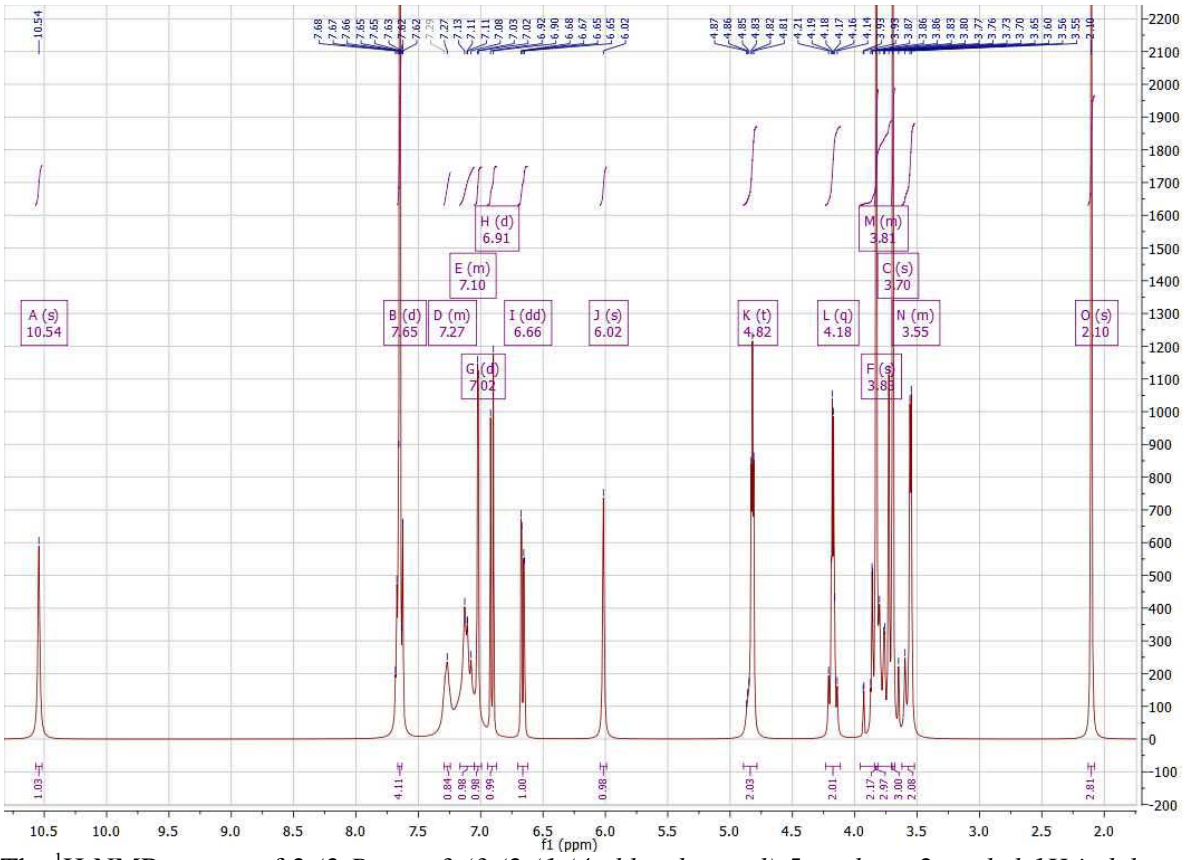

The [1]H-NMR spectra of *2-(2-Bromo-3-(3-(2-(1-(4-chlorobenzoyl)-5-methoxy-2-methyl-1H-indol-3-yl)aceta-mido)-4-oxothiazolidin-2-yl)-6-methoxyphenoxy)ethyl nitrate* **(9l)**

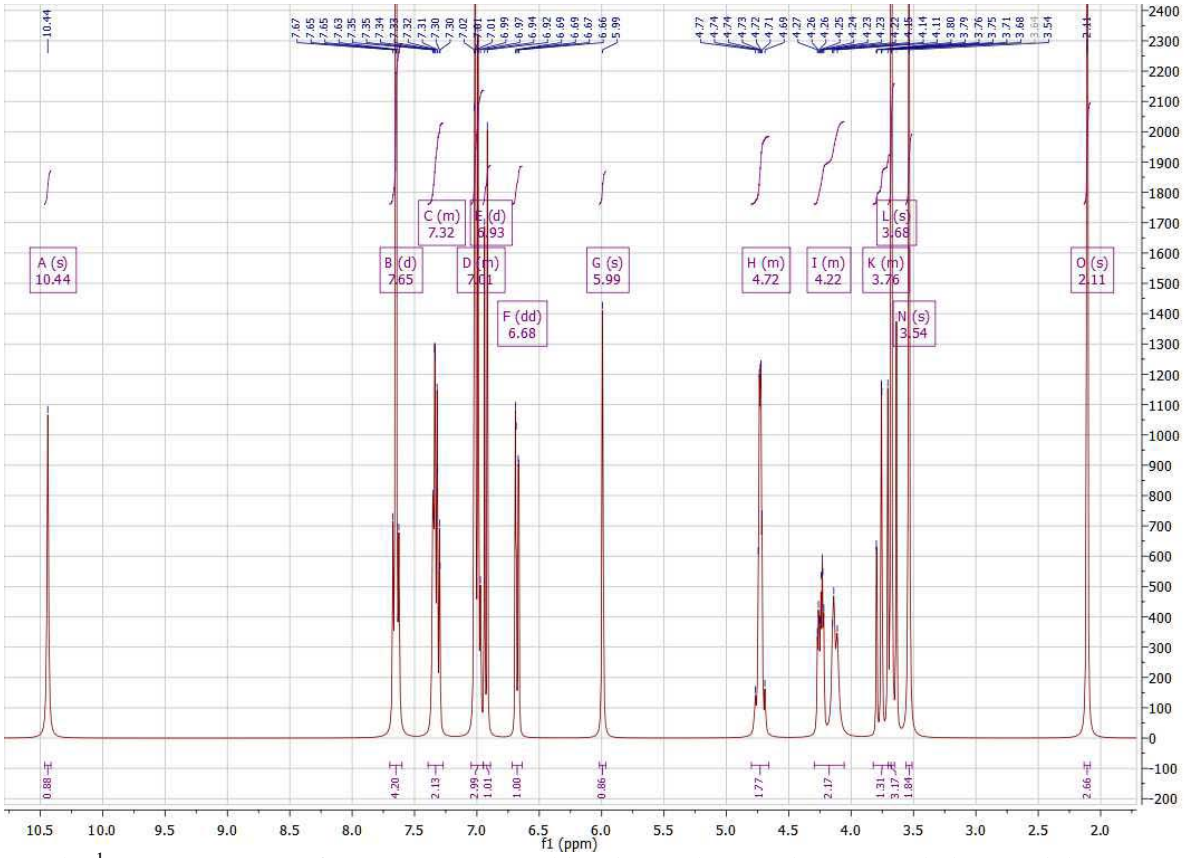

The [1]H-NMR spectra of *2-(2-(3-(2-(1-(4-Chlorobenzoyl)-5-methoxy-2-methyl-1H-indol-3-yl)acetamido)-4-oxo-thiazolidin-2-yl)phenoxy)ethyl nitrate* **(9m)**

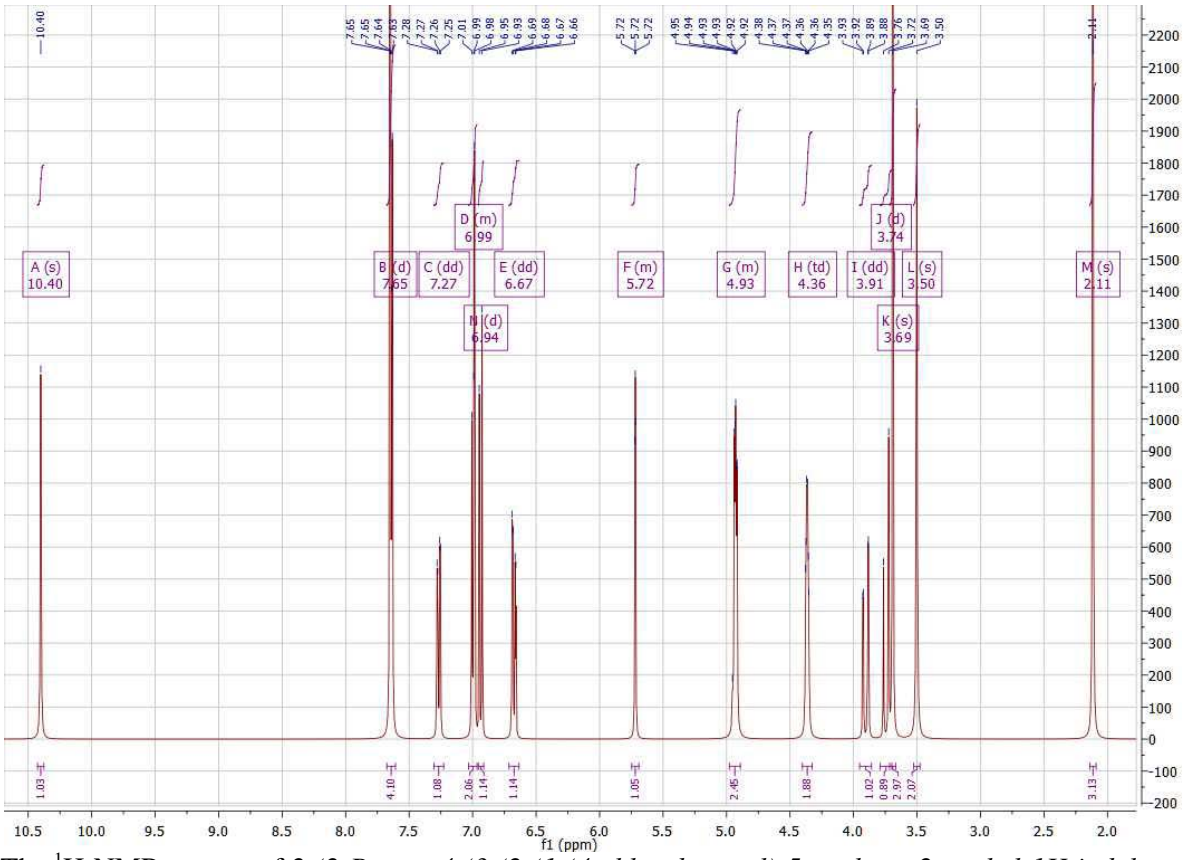

The [1]H-NMR spectra of *2-(2-Bromo-4-(3-(2-(1-(4-chlorobenzoyl)-5-methoxy-2-methyl-1H-indol-3-yl)acetamido)-4-oxothiazolidin-2-yl)phenoxy)ethyl nitrate* **(9n)**

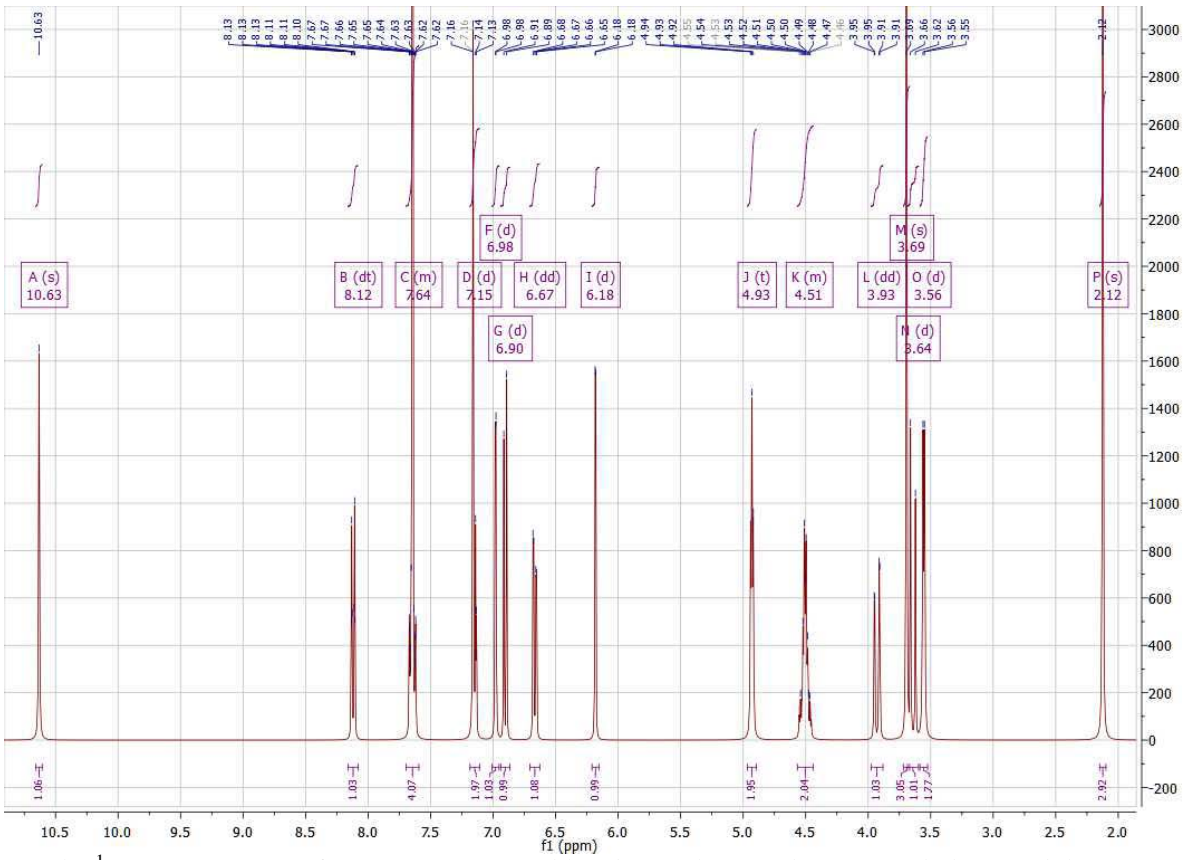

The [1]H-NMR spectra of *2-(3-(3-(2-(1-(4-Chlorobenzoyl)-5-methoxy-2-methyl-1H-indol-3-yl)acetamido)-4-oxo-thiazolidin-2-yl)-4-nitrophenoxy)ethyl nitrate* **(9o)**

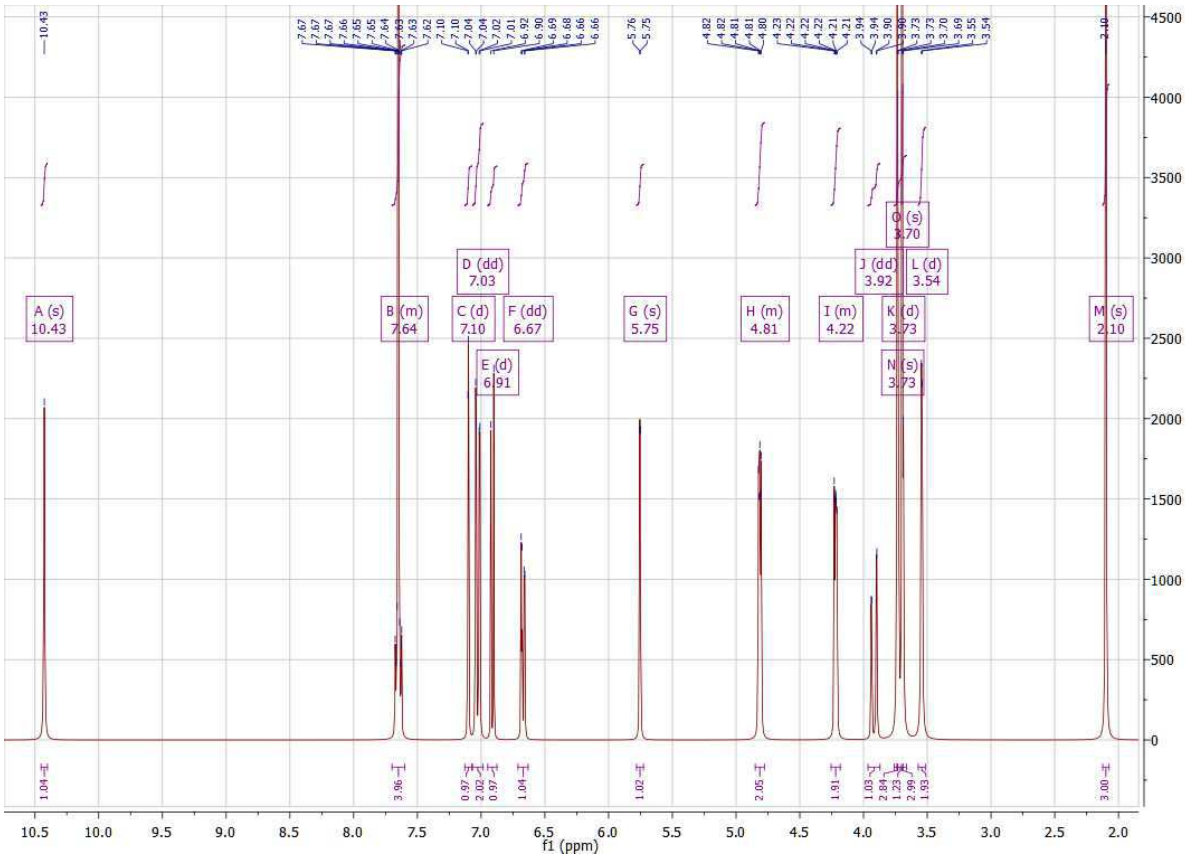

2-(2-Chloro-4-(3-(2-(1-(4-chlorobenzoyl)-5-methoxy-2-methyl-1H-indol-3-yl)aceta-mido)-4-oxothiazolidin-2-yl)-6-methoxyphenoxy)ethyl nitrate **(9p)**

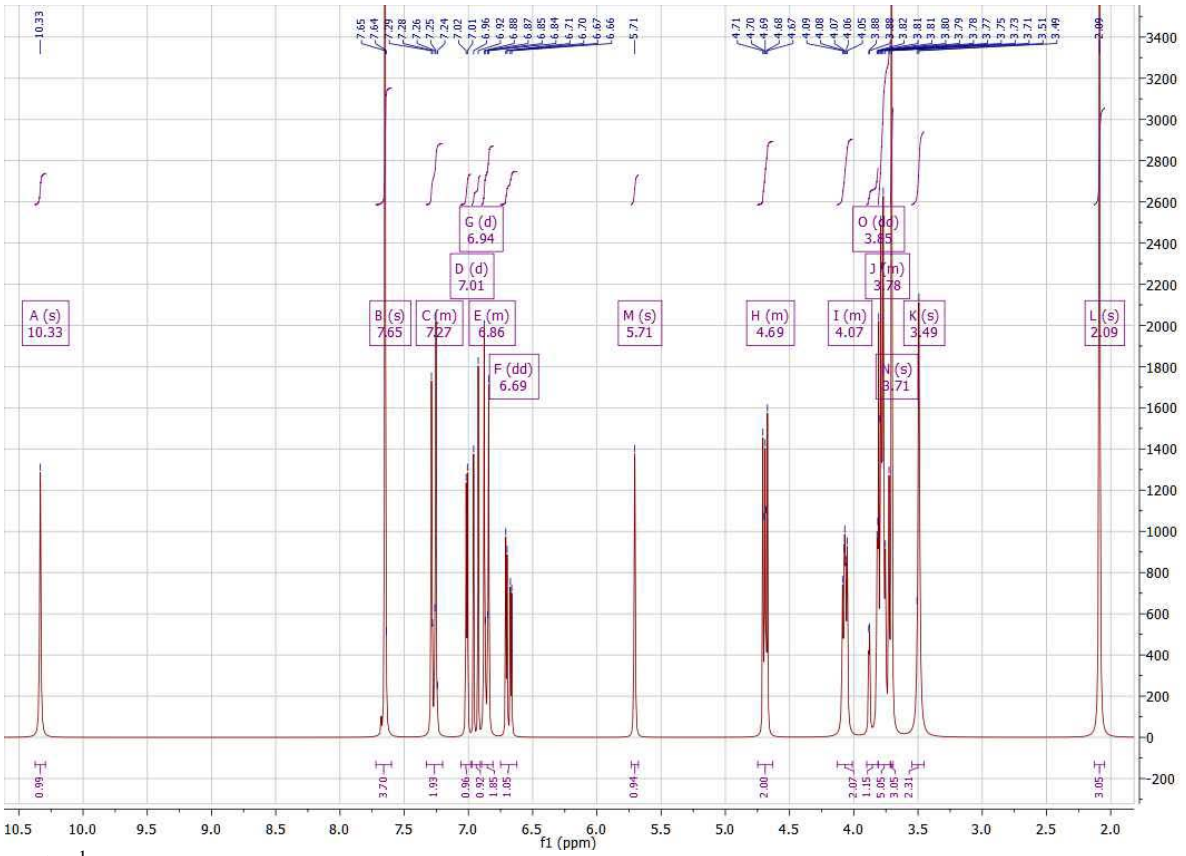

The ^{1}H-NMR spectra of *2-(2-(4-(3-(2-(1-(4-Chlorobenzoyl)-5-methoxy-2-methyl-1H-indol-3-yl)aceta-mido)-4-oxothiazolidin-2-yl)phenoxy)ethoxy)ethyl nitrate* **(9q)**

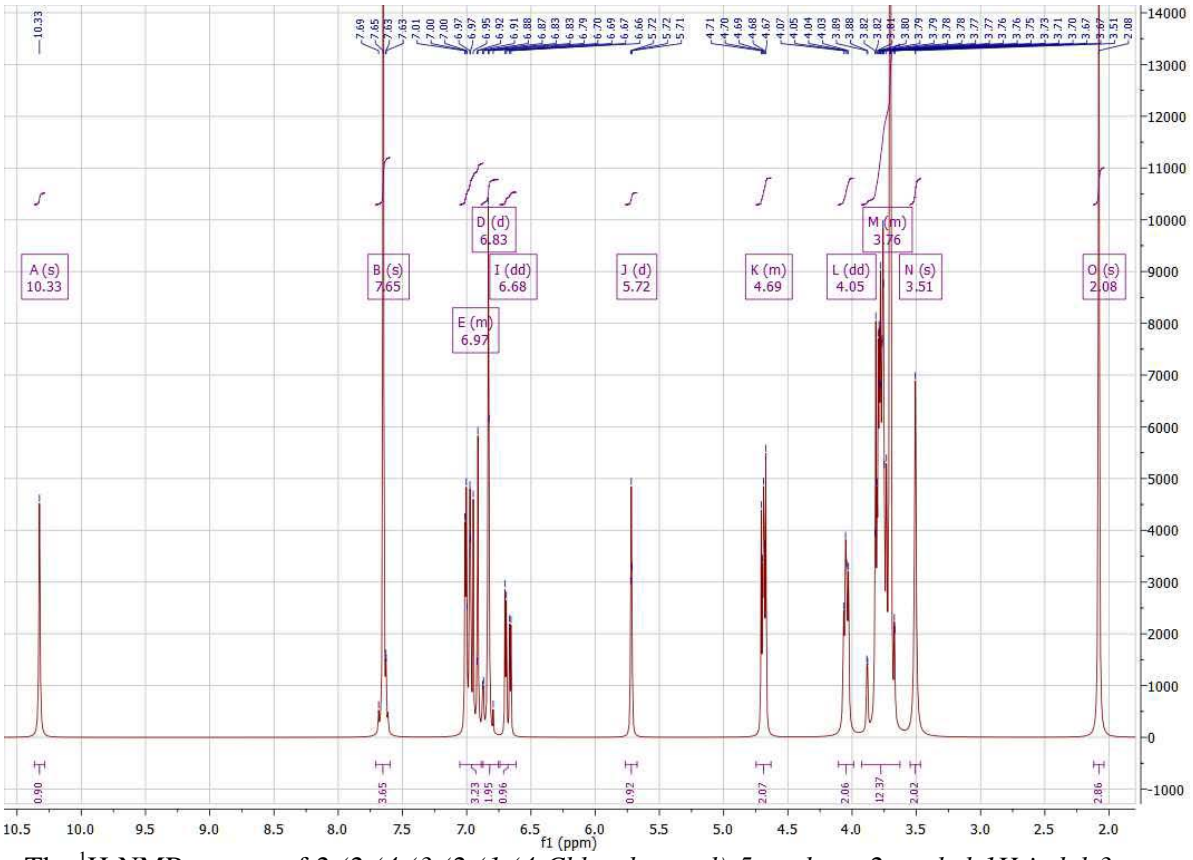

The ^{1}H-NMR spectra of *2-(2-(4-(3-(2-(1-(4-Chlorobenzoyl)-5-methoxy-2-methyl-1H-indol-3-yl)acetamido)-4-oxothiazolidin-2-yl)-2-methoxyphenoxy)ethoxy)ethyl nitrate* **(9r)**

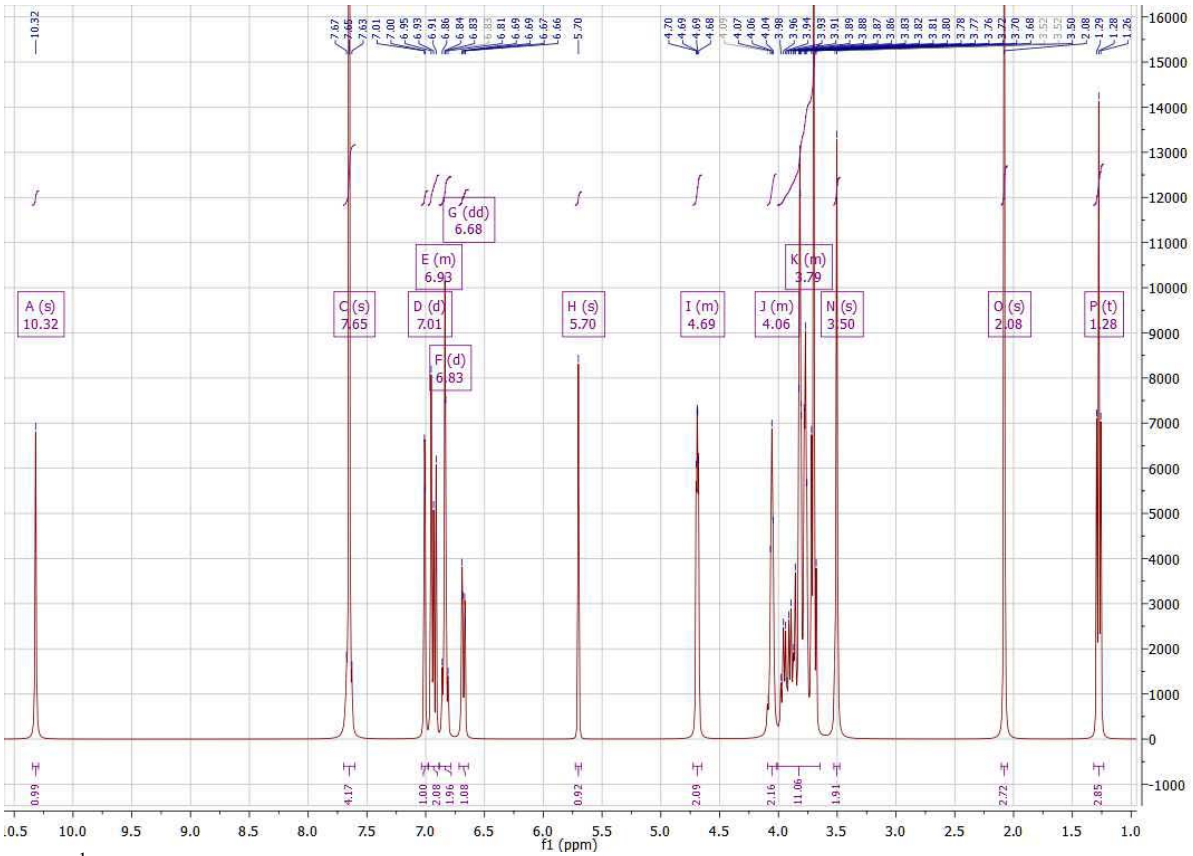

The ^{1}H-NMR spectra of *2-(2-(4-(3-(2-(1-(4-Chlorobenzoyl)-5-methoxy-2-methyl-1H-indol-3-yl)acetamido)-4-oxothiazolidin-2-yl)-2-ethoxyphenoxy)ethoxy)ethyl nitrate* **(9s)**

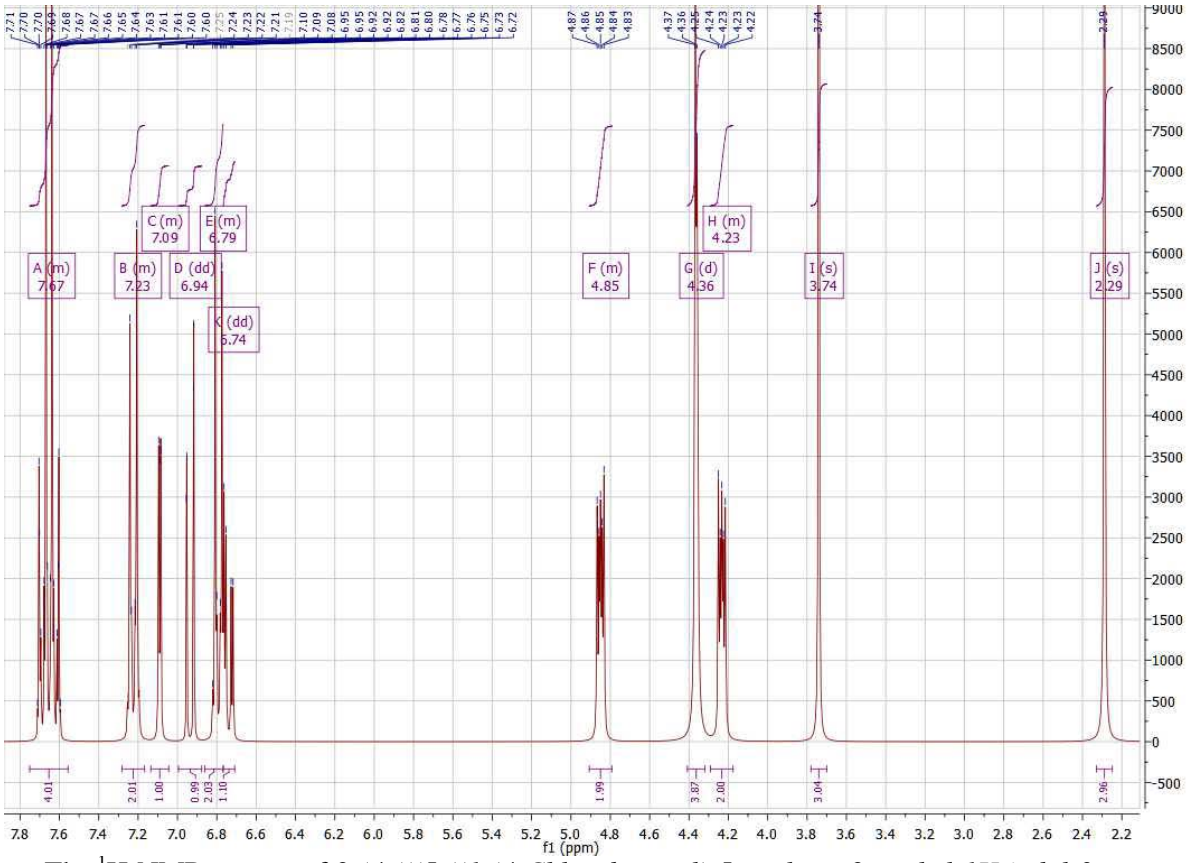

The ^{1}H-NMR spectra of *2-(4-(((5-((1-(4-Chlorobenzoyl)-5-methoxy-2-methyl-1H-indol-3-yl)methyl)-1,3,4-oxadiazol-2-yl)thio)methyl)phenoxy)ethyl nitrate* **(*11a*)**

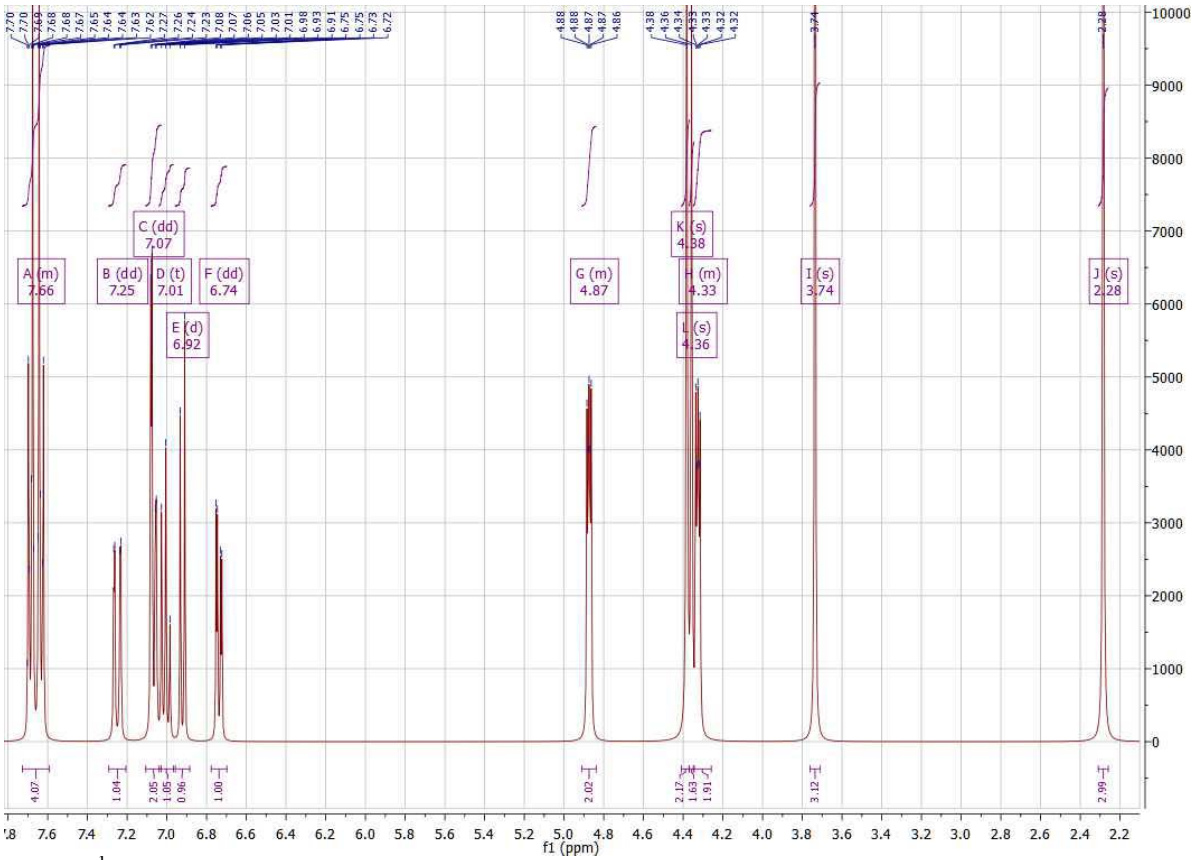

The ^{1}H-NMR spectra of *2-(4-(((5-((1-(4-Chlorobenzoyl)-5-methoxy-2-methyl-1H-indol-3-yl)methyl)-1,3,4-oxadiazol-2-yl)thio)methyl)-2-fluorophenoxy)ethyl nitrate* **(11*b*)**

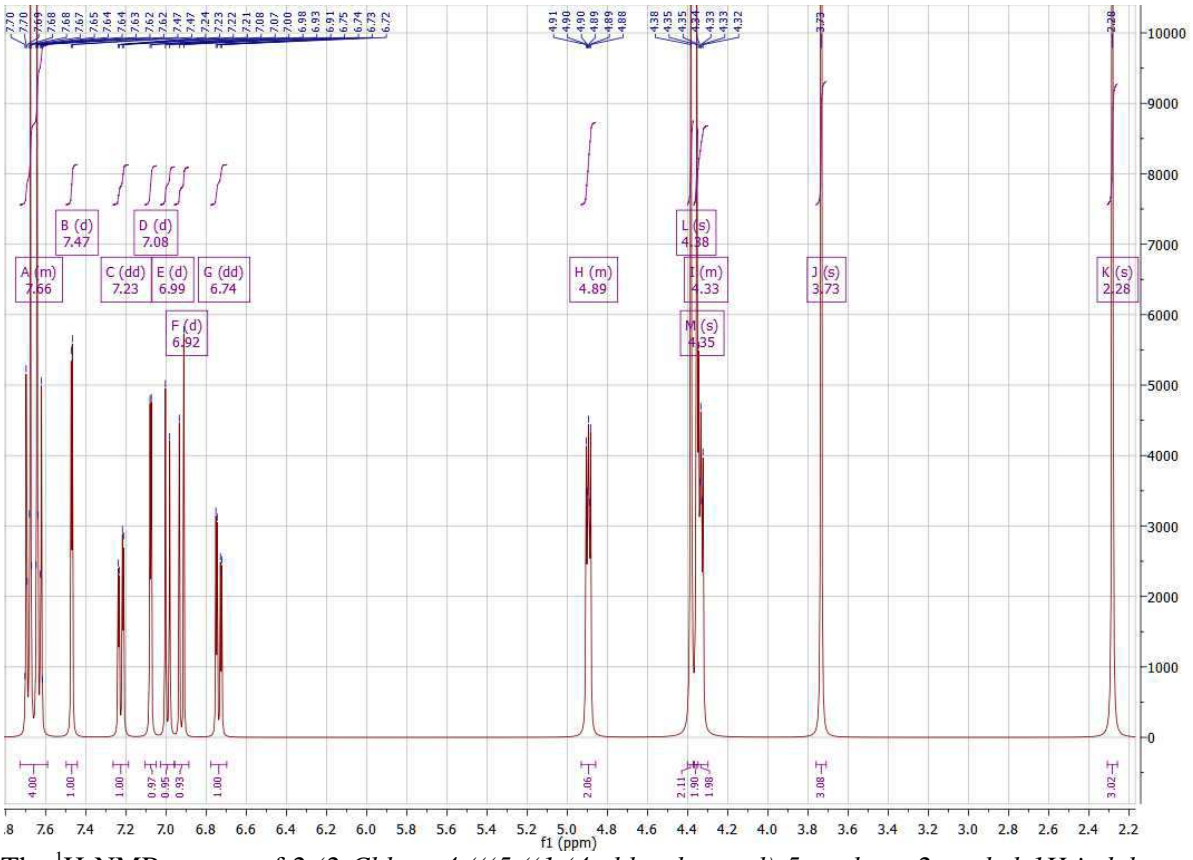

The [1]H-NMR spectra of *2-(2-Chloro-4-(((5-((1-(4-chlorobenzoyl)-5-methoxy-2-methyl-1H-indol-3-yl)methyl)-1,3,4-oxadiazol-2-yl)thio)methyl)phenoxy)ethyl nitrate* (***11c***)

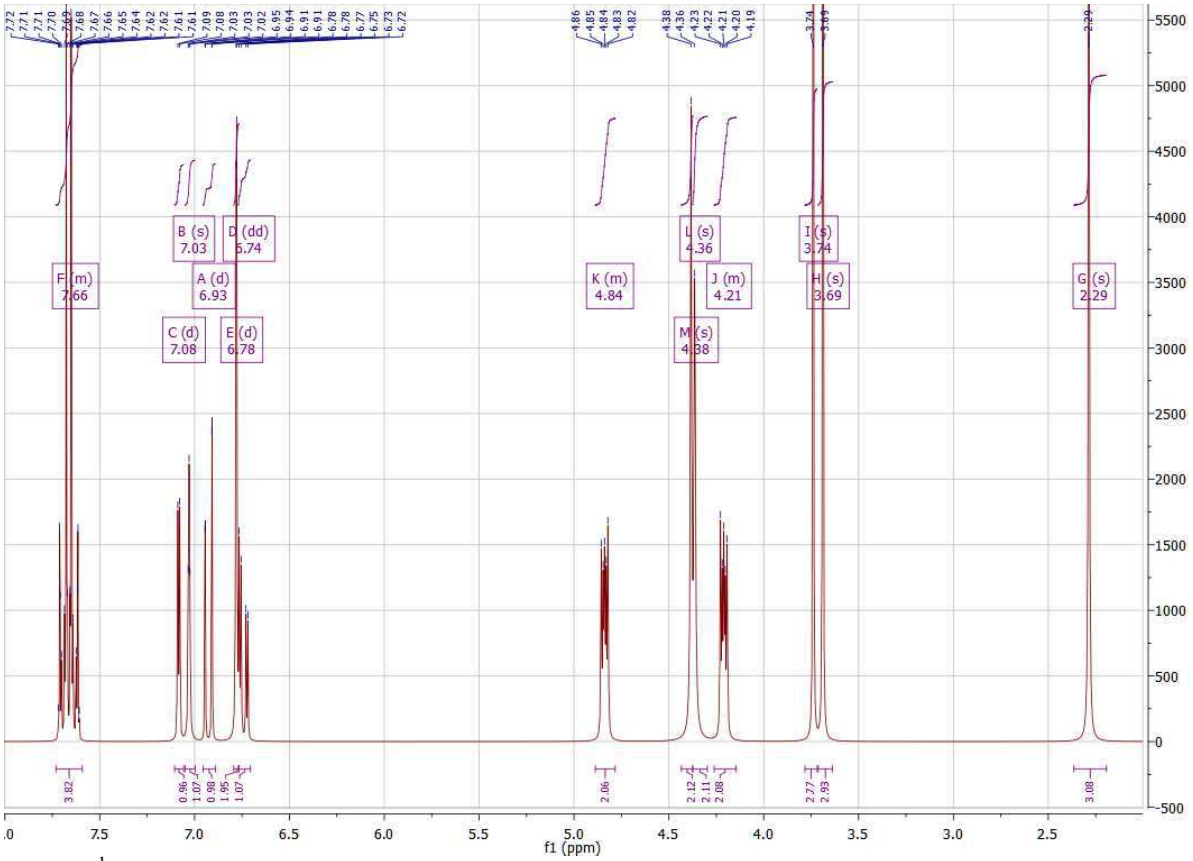

The [1]H-NMR spectra of *2-(4-(((5-((1-(4-Chlorobenzoyl)-5-methoxy-2-methyl-1H-indol-3-yl)methyl)-1,3,4-oxadiazol-2-yl)thio)methyl)-2-methoxyphenoxy)ethyl nitrate* **(11d)**

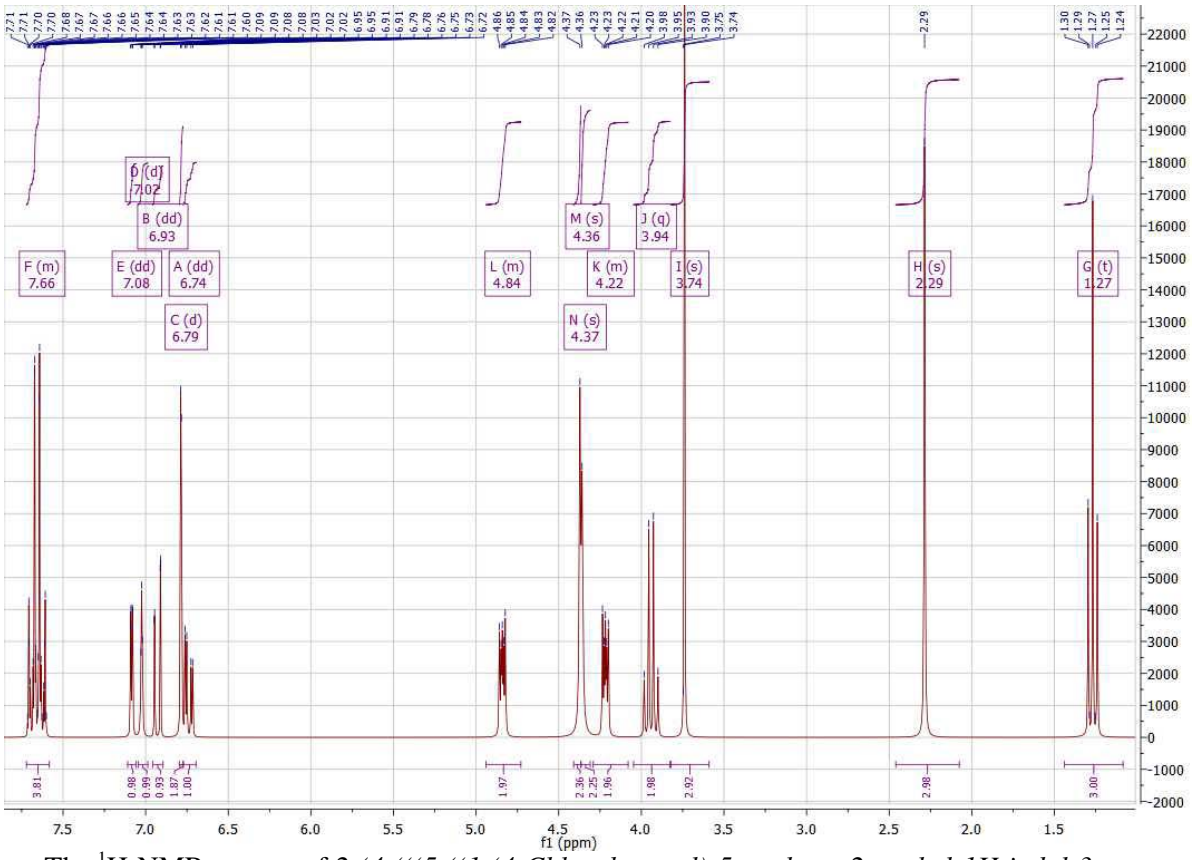

The ^{1}H-NMR spectra of *2-(4-(((5-((1-(4-Chlorobenzoyl)-5-methoxy-2-methyl-1H-indol-3-yl)methyl)-1,3,4-oxadiazol-2-yl)thio)methyl)-2-ethoxyphenoxy)ethyl nitrate* (***11e***)

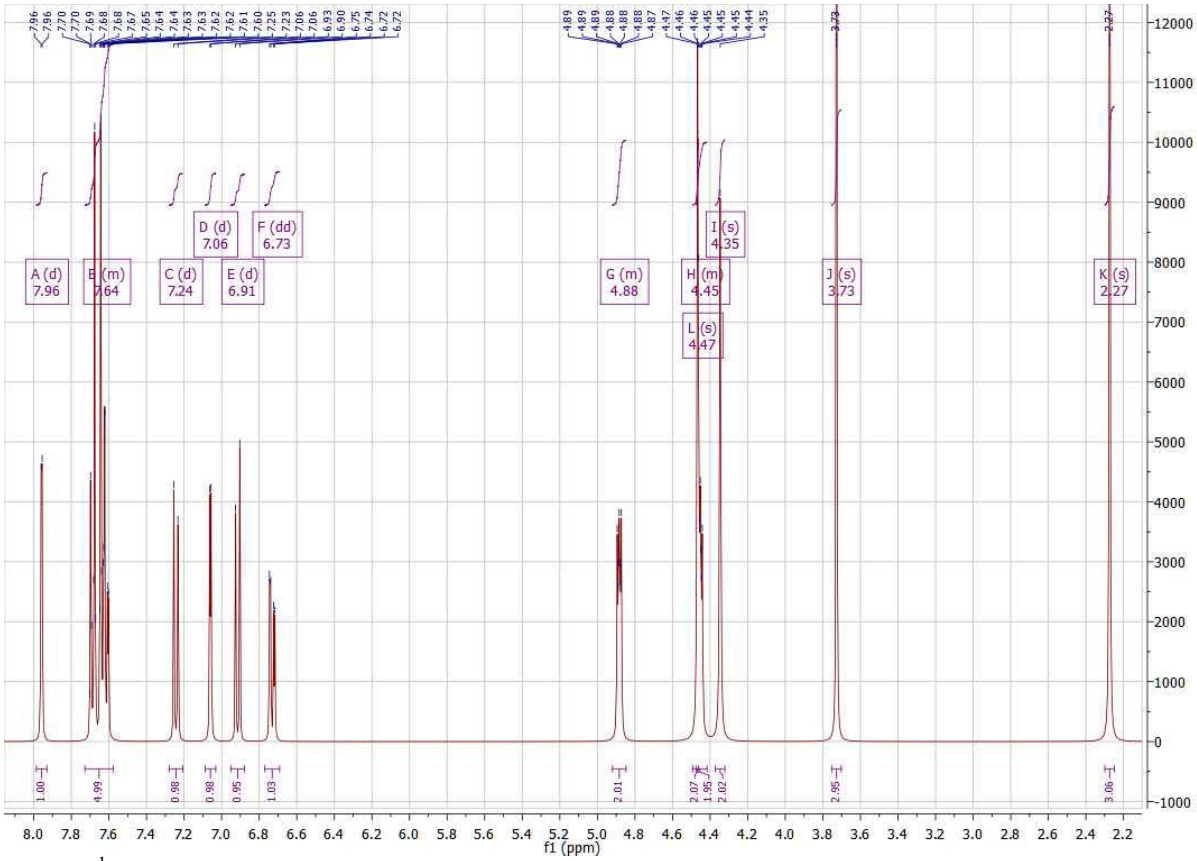

The ^{1}H-NMR spectra of *2-(4-(((5-((1-(4-Chlorobenzoyl)-5-methoxy-2-methyl-1H-indol-3-yl)methyl)-1,3,4-oxadiazol-2-yl)thio)methyl)-2-nitrophenoxy)ethyl nitrate* (***11f***)

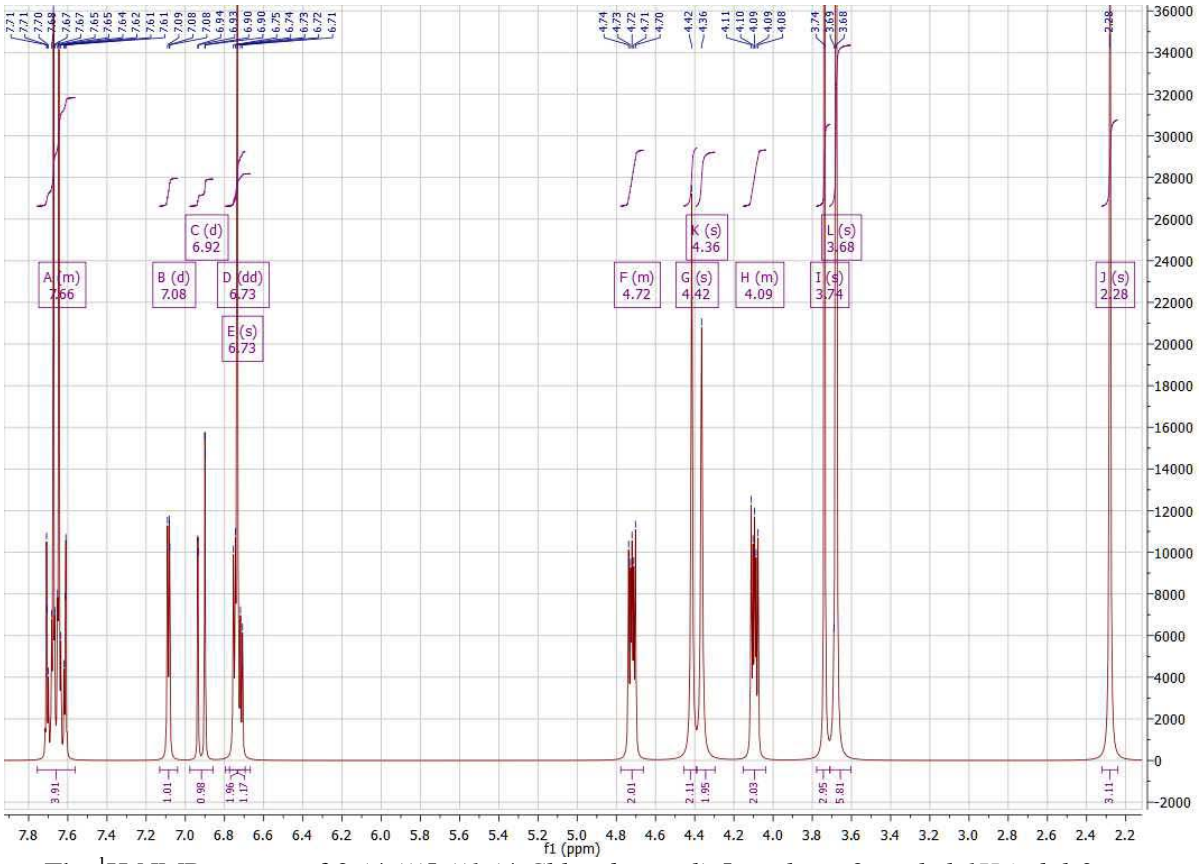

The [1]H-NMR spectra of *2-(4-(((5-((1-(4-Chlorobenzoyl)-5-methoxy-2-methyl-1H-indol-3-yl)methyl)-1,3,4-oxadiazol-2-yl)thio)methyl)-2,6-dimethoxyphenoxy)ethyl nitrate* **(*11g*)**

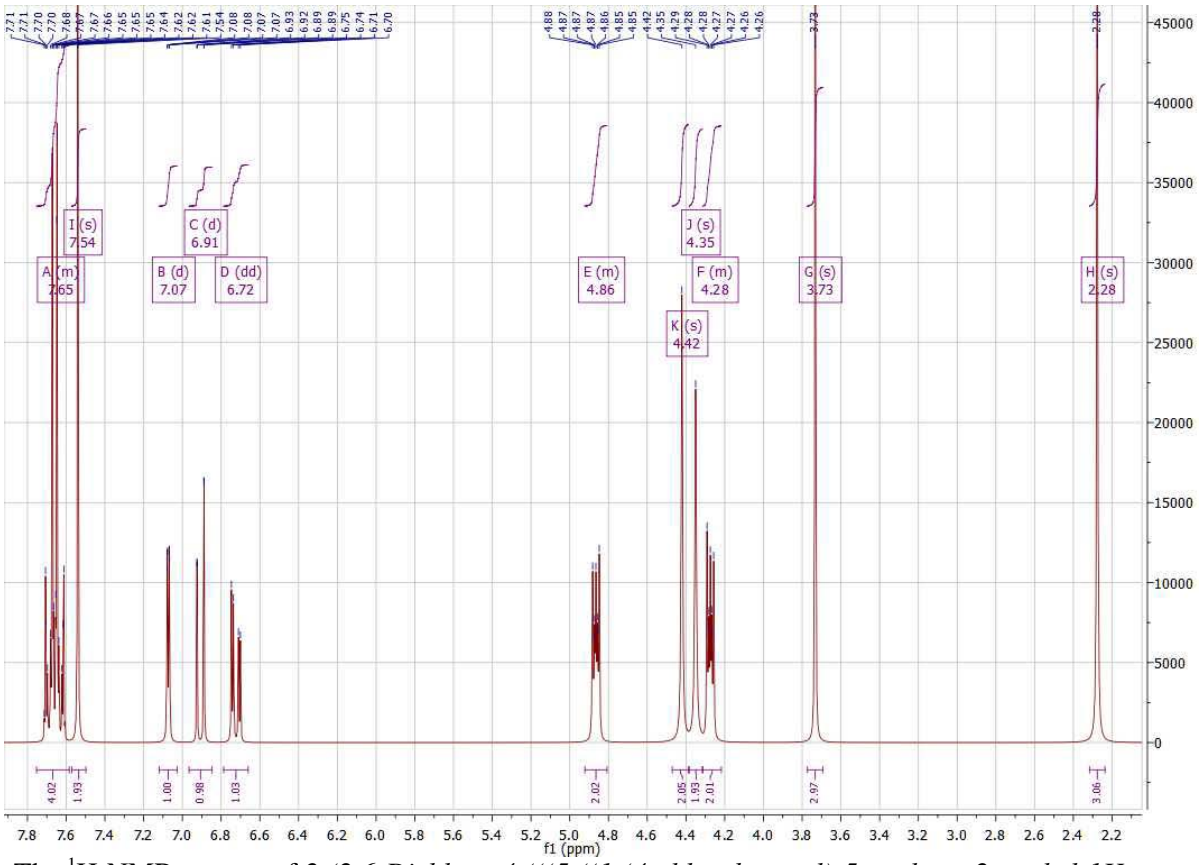

The [1]H-NMR spectra of *2-(2,6-Dichloro-4-(((5-((1-(4-chlorobenzoyl)-5-methoxy-2-methyl-1H-indol-3-yl)methyl)-1,3,4-oxadiazol-2-yl)thio)methyl)phenoxy)ethyl nitrate* **(*11h*)**

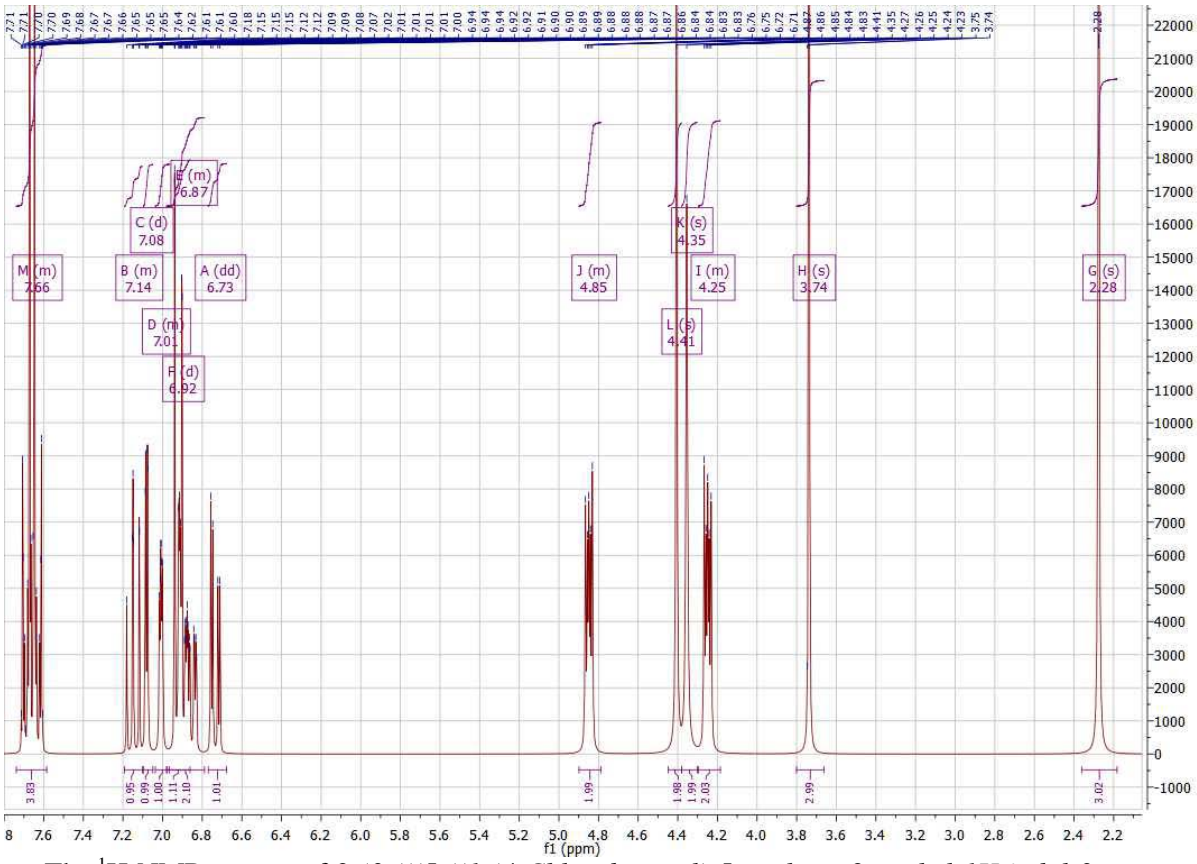

The ^{1}H-NMR spectra of *2-(3-(((5-((1-(4-Chlorobenzoyl)-5-methoxy-2-methyl-1H-indol-3-yl)methyl)-1,3,4-oxadiazol-2-yl)thio)methyl)phenoxy)ethyl nitrate* (***11i***)

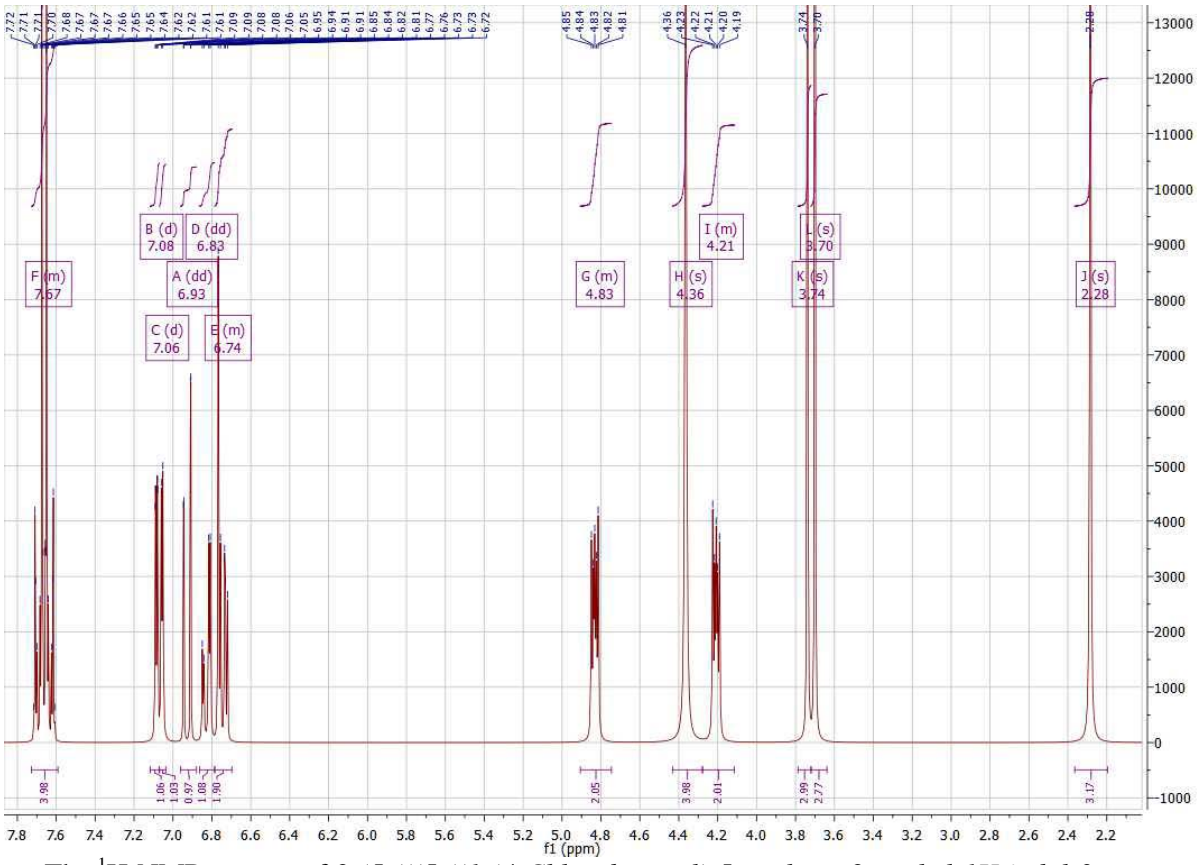

The ^{1}H-NMR spectra of *2-(5-(((5-((1-(4-Chlorobenzoyl)-5-methoxy-2-methyl-1H-indol-3-yl)methyl)-1,3,4-oxadiazol-2-yl)thio)methyl)-2-methoxyphenoxy)ethyl nitrate* (***11j***)

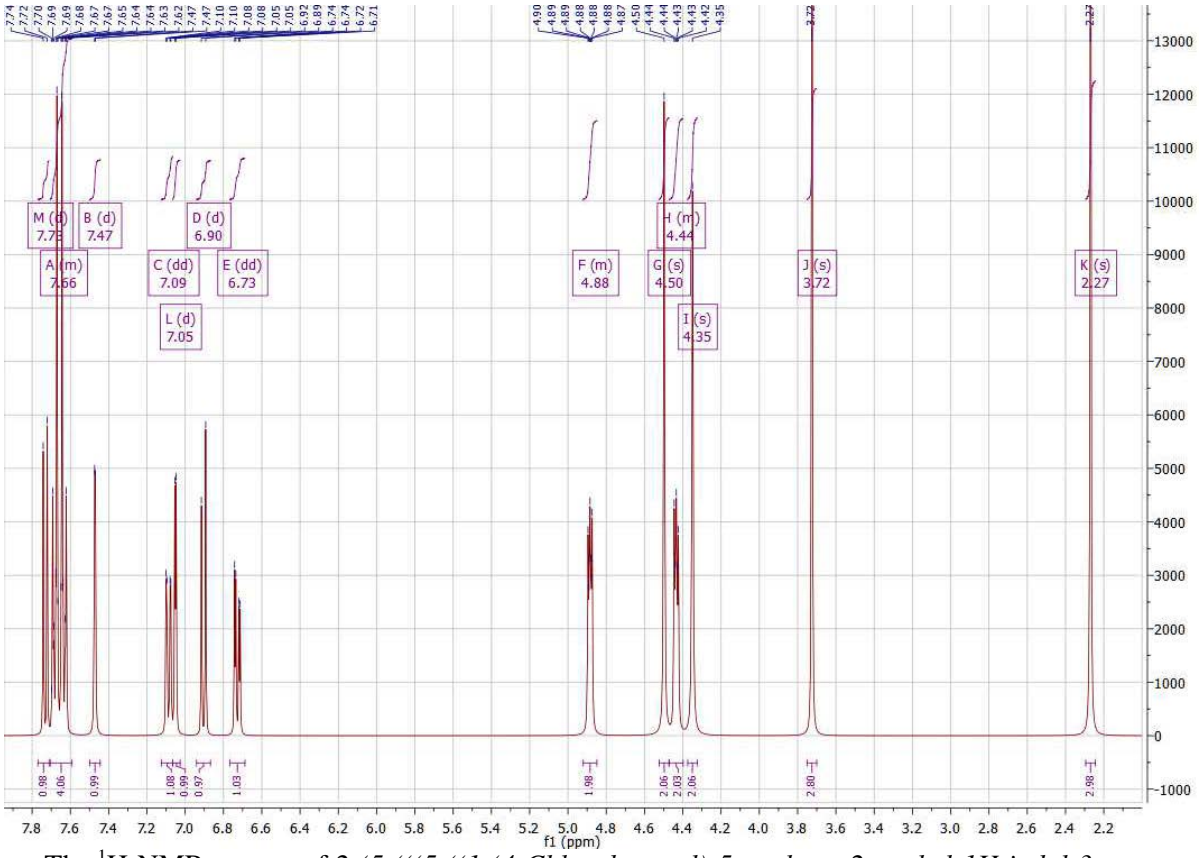

The [1]H-NMR spectra of *2-(5-(((5-((1-(4-Chlorobenzoyl)-5-methoxy-2-methyl-1H-indol-3-yl)methyl)-1,3,4-oxadiazol-2-yl)thio)methyl)-2-nitrophenoxy)ethyl nitrate* **(11*k*)**

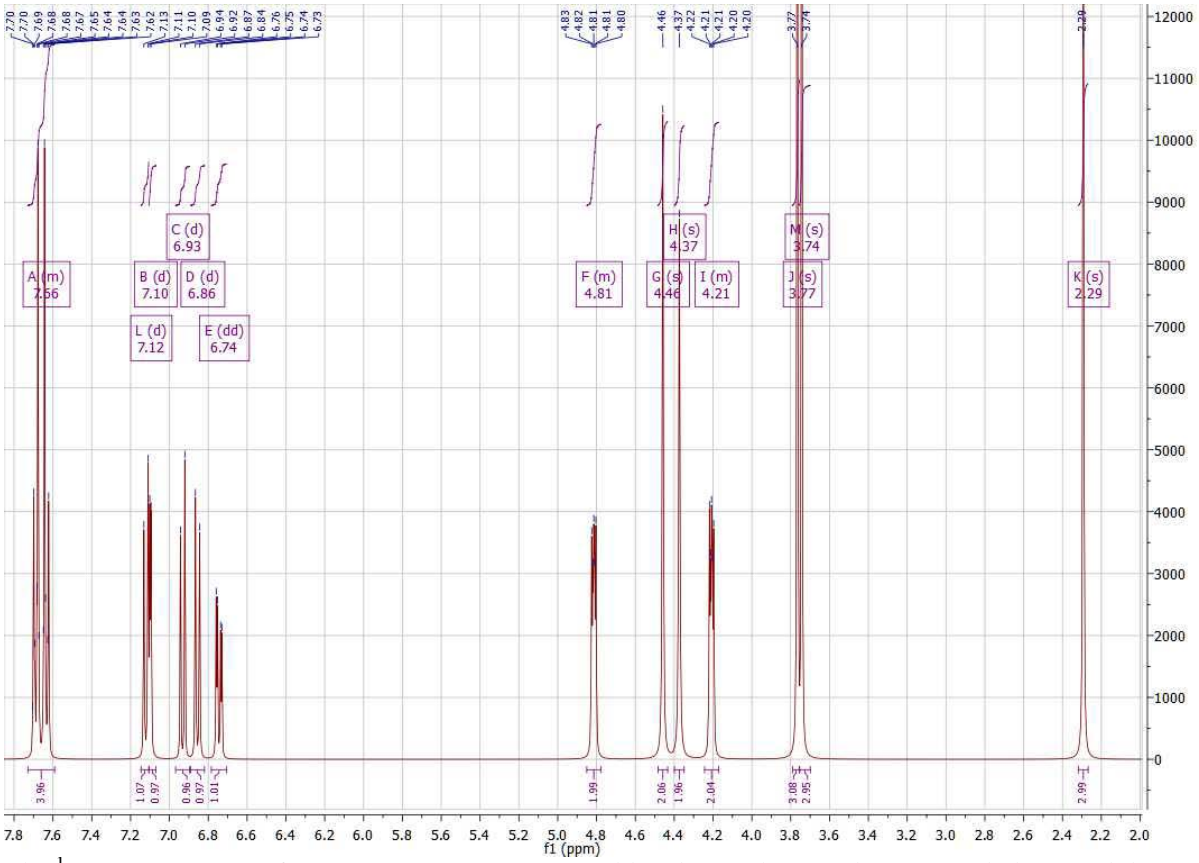

The [1]H-NMR spectra of *2-(2-Bromo-3-(((5-((1-(4-chlorobenzoyl)-5-methoxy-2-methyl-1H-indol-3-yl)methyl)-1,3,4-oxadiazol-2-yl)thio)methyl)-6-methoxyphenoxy)ethyl nitrate* **(*11l*)**

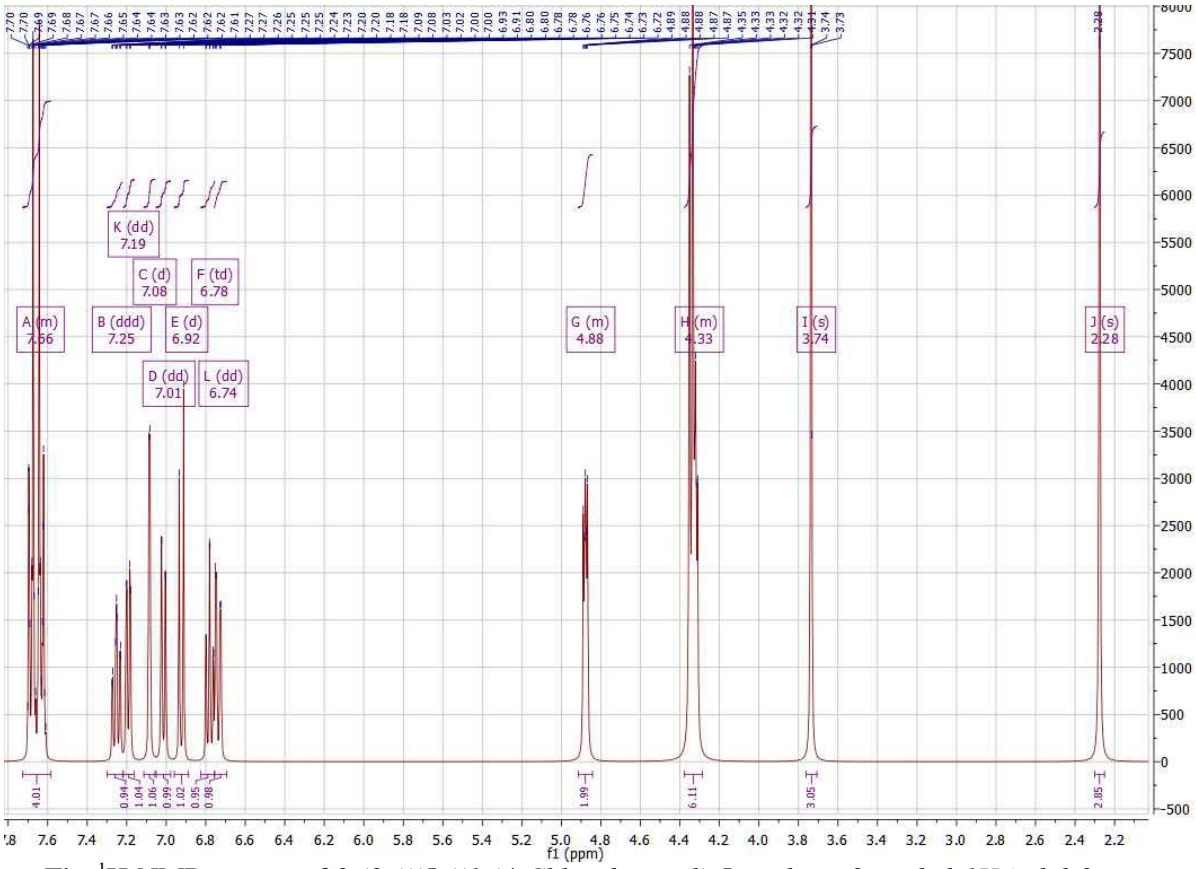

The [1]H-NMR spectra of *2-(2-(((5-((1-(4-Chlorobenzoyl)-5-methoxy-2-methyl-1H-indol-3-yl)methyl)-1,3,4-oxadiazol-2-yl)thio)methyl)phenoxy)ethyl nitrate* (***11m***)

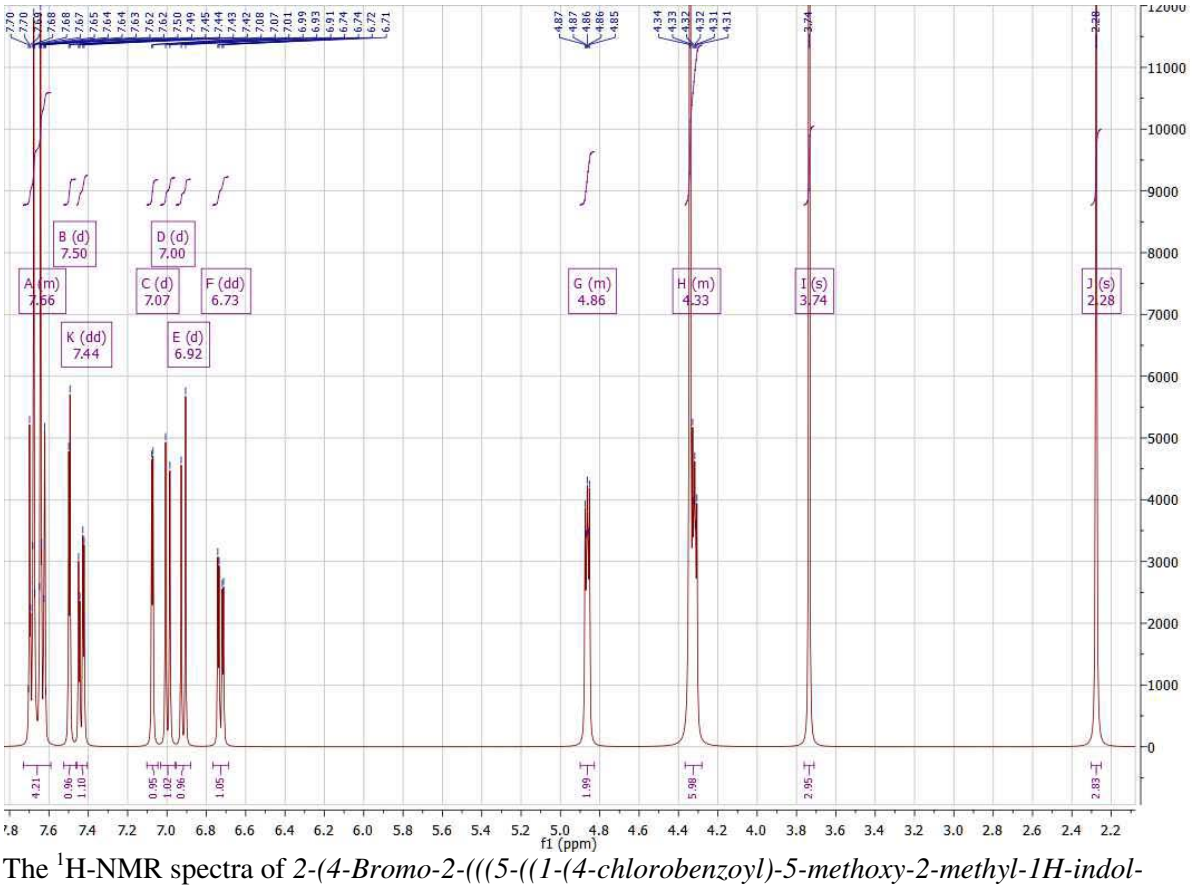

The [1]H-NMR spectra of *2-(4-Bromo-2-(((5-((1-(4-chlorobenzoyl)-5-methoxy-2-methyl-1H-indol-3-yl)methyl)-1,3,4-oxadiazol-2-yl)thio)methyl)phenoxy)ethyl nitrate* (***11t***)

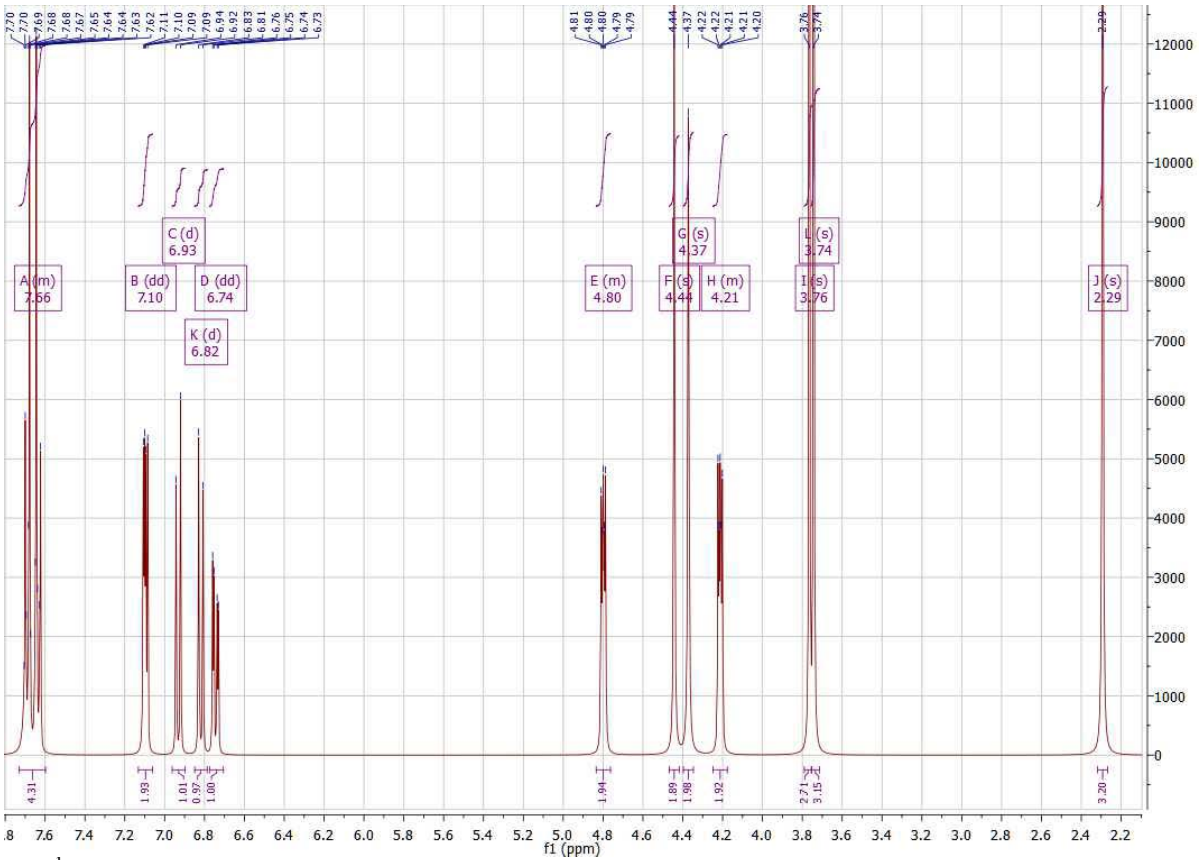

The [1]H-NMR spectra of *2-(2-Chloro-3-(((5-((1-(4-chlorobenzoyl)-5-methoxy-2-methyl-1H-indol-3-yl)methyl)-1,3,4-oxadiazol-2-yl)thio)methyl)-6-methoxyphenoxy)ethyl nitrate* **(*11u*)**

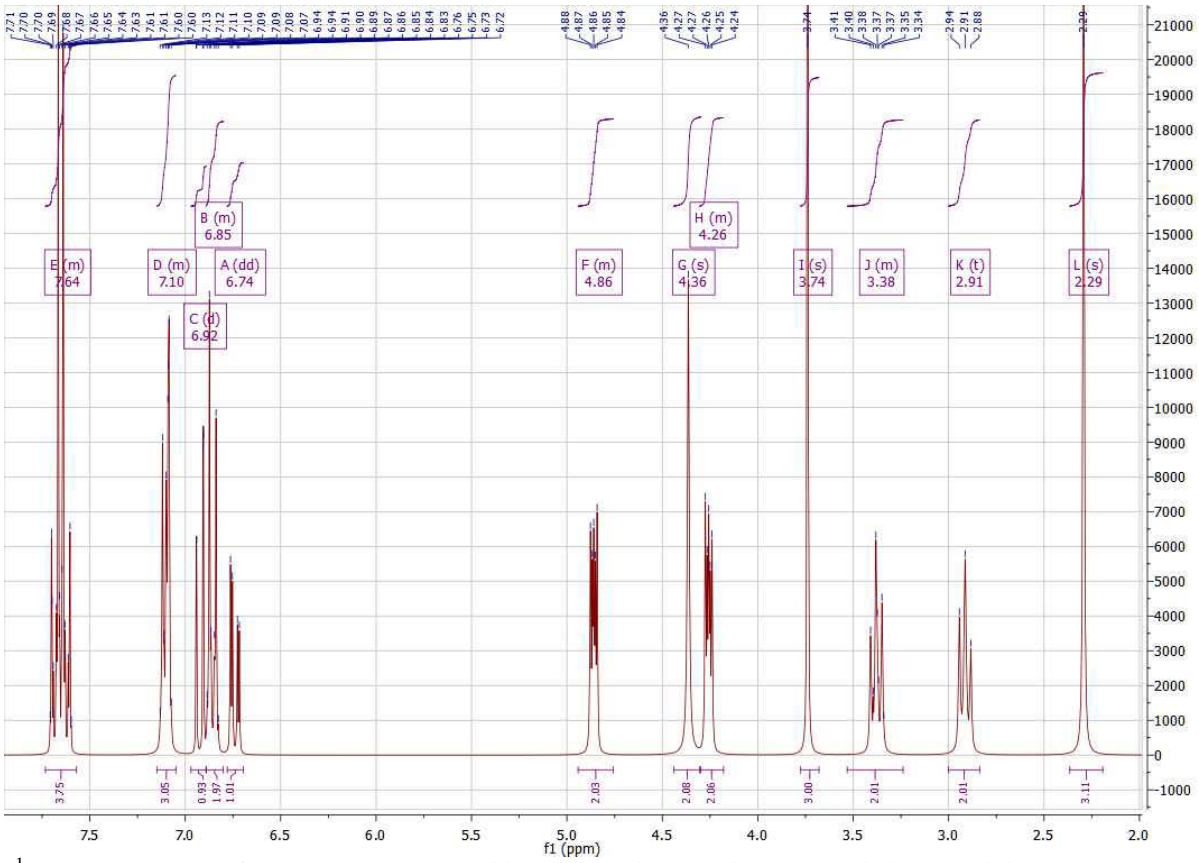

The [1]H-NMR spectra of *2-(4-(2-((5-((1-(4-Chlorobenzoyl)-5-methoxy-2-methyl-1H-indol-3-yl)methyl)-1,3,4-oxadiazol-2-yl)thio)ethyl)phenoxy)ethyl nitrate* **(*11v*)**

Alexandru SAVA

Conception, synthèse et évaluation biologique de nouveaux agents anti-inflammatoires

Les objectifs de la recherche doctorale étaient basées sur la conception de nouveaux candidats médicaments donneurs d'oxyde nitrique (NO)etsur l'évaluation puis l'amélioration du profil pharmacologique et d'innocuité de meilleurs candidats. Ces travauxont permis de développer des composés originaux basés sur un squelette de type indométacine (donneurs d'indométacine-NO) etrentrent parfaitement dans une stratégie thérapeutique multi-cibles, capables simultanément d'inhiber les voies COX et de libérer du NO dans le milieu gastrique.

Les arguments qui justifient l'importance de cette recherche sont les suivants :

- l'inflammation est un processus physiopathologique complexe qui est responsable de nombreuses maladies répandues, telles que la polyarthrite rhumatoïde, l'arthrose, l'athérosclérose, le diabète, la neuro-dégénérescence, l'allergie, l'infection et le cancer. Au cours des dernières décennies, le développement de molécules thérapeutiques a permis d'obtenir des médicaments puissants et spécifiques en se concentrant sur un nombre limité de cibles clés considérées comme cruciales pour la maladie. Les profils insatisfaisants de ces produits en termes d'innocuité et d'efficacité nécessitent le développement d'agents multi-cibles pour traiter des maladies inflammatoires complexes.
- la stratégie multi-cibles (médicaments simples-cibles multiples), qui est basée sur la conception rationnelle de nouvelles entités chimiques aux visées anti-inflammatoires potentielles, est capable d'atteindre plusieurs cibles (poly-pharmacologie) afin d'améliorer l'efficacité et/ou d'améliorer le profil de sécurité des médicaments classiques. Cette approche pourrait faire l'objet d'un transfert technologiquevers des sociétés pharmaceutiques intéressées par la détention de nouveaux médicaments innovants et de nouvelles stratégies.

Mots clés :indomethacin, 1,3-thiazolidine-4-one, 1,3,4-oxadiazole, docking study, nitric oxide, multi-target strategy

Design, synthesis and biological evaluation of novel anti-inflammatory agents

The goal of the doctoral research was to prove the improved pharmacological and safety profile of some new indomethacin nitric oxide donors (indometacin-NO donors) which were developed as new therapeutic multi-targets strategy, able to inhibit COX pathways and to release NO in the gastric medium.

The arguments that justify the importance of this research are the followings:

- the inflammation is a complex patho/physiological process which is responsible for many widespread diseases, such as rheumatoid arthritis, osteoarthritis, atherosclerosis, diabetes, neurodegeneration, allergy, infection and cancer. Drug development during the past decades made efforts to obtain potent and specific drugs focusing on a limited number of key targets considered crucial for disease. Unsatisfactory safety and efficacy profiles of them need the development of multi-target agents to treat complex inflammatory diseases.
- the multi-target strategy (single drug–multiple targets), which is based on rationale design of new chemical entities as new anti-inflammatory potential drugs, is able to hit multiple targets (polypharmacolgy) in order to enhance efficacy and/or improve safety profile of classical drugs. This approach could be subject for technogical transfer to pharmaceutical companies interested to develop new innovative drugs.

Keywords :indomethacin, 1,3-thiazolidine-4-one, 1,3,4-oxadiazole, docking study, nitric oxide, multi-target strategy

Institut de Chimie Organique et Analytique - ICOA UMR7311, Pôle de chimie, Rue de Chartres, 45100 Orléans, France